Forschungszentrum Karlsruhe
in der Helmholtz-Gemeinschaft

Wissenschaftliche Berichte
FZKA 6969

Humic Substances in Performance Assessment of Nuclear Waste Disposal: Actinide and Iodine Migration in the Far-Field

Second Technical Progress Report

G. Buckau (Editor)

Institut für Nukleare Entsorgung

Juli 2004

Forschungszentrum Karlsruhe

in der Helmholtz-Gemeinschaft

Wissenschaftliche Berichte

FZKA 6969

Humic Substances in Performance Assessment of Nuclear Waste Disposal: Actinide and Iodine Migration in the Far-Field

Second Technical Progress Report

G. Buckau (Editor)

Institut für Nukleare Entsorgung

Forschungszentrum Karlsruhe GmbH, Karlsruhe
2004

Impressum der Print-Ausgabe:

Als Manuskript gedruckt

Forschungszentrum Karlsruhe GmbH
Postfach 3640, 76021 Karlsruhe

Mitglied der Hermann von Helmholtz-Gemeinschaft
Deutscher Forschungszentren (HGF)

ISSN 0947-8620

urn:nbn:de:0005-069699

Foreword

The present report describes progress within the second year of the EC-project “Humic Substances in Performance Assessment of Nuclear Waste Disposal: Actinide and Iodine Migration in the Far-Field”. Without being a formal requirement of the Commission or co-funding bodies, this report documents results in great technical detail. It is an open report and thus makes the detailed results available to a broad scientific community.

The report contains an executive summary written by the coordinator. More detailed results are given as individual contributions in the form of 23 annexes. Not all results are discussed or referred to in the executive summary report and thus readers with a deeper interest also need to consult the annexes.

The report also reflects the successful integration of a temporary contributor via a Marie-Curie Fellowship (MCFI-2001-01983) (Annex 23). Integration of this activity extends the scope of the project to a new potential source of humic substances in clay.

Results of the first project year have already been published in a comparable Technical Progress Report*. For the final year, a comparable report is foreseen.

*: Buckau, G. (Editor) “Humic Substances in Performance Assessment of Nuclear Waste Disposal: Actinide and Iodine Migration in the Far-Field (First Technical Progress Report)”, Report FZKA 6800, Forschungszentrum Karlsruhe, Karlsruhe, 2003.

Table of contents

EXECUTIVE SUMMARY

HUMIC SUBSTANCES IN PERFORMANCE ASSESSMENT OF NUCLEAR WASTE DISPOSAL: ACTINIDE AND IODINE MIGRATION IN THE FAR-FIELD (HUPA)

SECOND TECHNICAL PROGRESS REPORT

EC Contract No.: FIKW-CT-2001-00128

Work period 11.02-10.03)

G. Buckau
(FZK/INE)

Content of executive summary

INTRODUCTION

The present project is one in a series of research activities supported by the European Commission on the role of humic substances for the long-term safety of nuclear waste disposal. These activities started in the mid eighties within the MIRAGE project (MIgration of RAdionuclides in the GEosphere) with the most recent project being “Effects of humic substances on the migration of radionuclides: Complexation and transport of actinides (HUMICS)” (FI4W-CT96-0028). The HUMICS project was conducted within the fourths framework of the European Commissions research program. It started January 1997 and had a duration of three years. The results of the HUMICS project can be found in three open technical progress reports and a final report [1-4]. In analogy with the HUMICS project, the present project makes use of annual technical progress reports where individual results are published as papers in the form of annexes. By this approach, results rapidly become available to interested parties in a compact form before their publication in various scientific journals and conference proceedings. Furthermore, some of the more preliminary and/or detailed results are not likely to appear in scientific journals and proceedings.

The present project is conducted within the fifths framework of the European Commissions research program. It started November 2001 and has a duration of three years. The first Technical Progress Report has already been published (Buckau Ed. 2002). That report covers the first project year, i.e. November 2001 to October 2002. The present Second Technical Progress Report covers the second project year, i.e. November 2002 to October 2003.

The project is divided into eight different work packages. These are (i) “Critical assessment of experimental methods”, (ii) “Generation and characterization of humic substances”, (iii) “Radionuclide humate interaction data by designed system investigations”, (iv) “Characterization of radionuclide humate complexes”, (v) “Natural chemical analogue studies”, (vi) “Radionuclide transport experiments”, (vii) “Model development”, and (viii) “Performance assessment”.

Division of work into specified work packages sometimes is not straightforward. This is also reflected in the structure of the report. The executive summary report follows the project work package structure. The annexes focus on scientific results without reference to specific work packages. Following this approach, the reader can get an overview over the overall progress by the executive summary report. Detailed information on scientific results and the respective originators is found in the annexes. It should also be noted that some results presented in the executive summary report originate from presentations and communication within the project without being presented as an annex paper. Further information on such results can be obtained through the editor.

The overall approach of the project is to provide process understanding resting on a solid scientific ground, rationalizing the developed state of knowledge in the form of models, and visualization of the impact of humic colloid mediated actinide and iodine transport via migration cases. Application of the knowledge developed within the project to specific radio-

active waste disposal strategies is the task of responsible national organizations and not within the scope of this project. The basis for application to specific disposal strategies is the models including the required background information being provided, amongst others through the technical progress reports.

The present project builds on the long foregoing development of experience and scientific basis. It distinguishes itself from previous activities by, amongst others, inclusion of iodine next to the highly radiotoxic and long-lived actinides. As the key role of kinetics became obvious, the past project experienced a strong shift in work deviating from initial intentions. This is also reflected in the present project where the main objective is clarification of interaction and transport processes, especially the question behind the wide range of dissociation kinetics observed. Another topic of key concern is the origin, stability and mobility of humic substances in natural and disposal amended far-field environments.

Access to and continuous development of advanced analytical methods is a key element in providing for the continued progress. One example is x-ray spectroscopy becoming a key element in determining the coordination of humate bound actinide ions. Clarification of the relation between the mass and size distribution is the key in a change in the overall understanding of humic substances. For this purpose, development and application of advanced mass spectroscopy techniques was the basis. It furthermore contributes by detailed information about processes and for the characterization of humic substances and their complexes. The time resolved laser fluorescence spectroscopy continues to be a corner stone in providing detailed process information.

With respect to radionuclide humic acid interaction, the main objective is to develop a thermodynamic approach reflecting the different experimental observations, contrary to the present situation where different “models” are argued for in the scientific community. Existing models reflect some aspects of available experimental data but fail to enclose other aspects and experimental observations. The project has made great steps forward in this direction. If this endeavor will be completely finished succeed within the third and final project year remains open.

1. OBJECTIVES

Nuclear energy is an important element in the energy supply in Europe. Continued use of nuclear energy contributes to a stable socio-economic development and contributes to the overall European strategic objective of lowering dependency on energy import. A key objective of the Commissions support for research in this field is providing for continued acceptance of nuclear energy by demonstrating that residues can be managed appropriately, including providing trust in the capability of safe disposal. The present project contributes to this overall objective by establishing a trustworthy scientific basis for predicting the impact of humic substances on the mobility of long-lived actinide ions and iodine in case of release from a repository in a distant future.

The direct objective of the project is to develop tools for quantification, or justification for exclusion of humic colloid mediated radionuclide migration in performance assessment (PA). It falls within the overall objective of decreasing uncertainty in long-term safety assessment of nuclear waste disposal. For this purpose, the necessary data and adequate process understanding for the radionuclide humic colloid interaction and mobility of humic colloids in natural aquatic systems is developed. The impact of humic colloid mediated radionuclide migration on PA of nuclear waste disposal is visualised by predictive modelling on real site migration cases. The project focuses on radionuclides relevant for the long-term safety of radioactive waste disposal, i.e. the actinides and iodine.

2. PARTNERS AND PROJECT STRUCTURE

The project has 9 partners from 6 European countries (Table 1). In addition, a Marie-Curie fellowship is providing for a temporary contributor, reporting through the present project. The project structure is based on eight work packages (Table 2). Six of these work packages are of experimental character. Work package No. 7 is model development where knowledge is rationalized for application to various systems and conditions. Work package No. 8 is aiming at visualizing the impact of humic colloid mediated actinide and iodine transport under three different specified conditions, defined as three different migration cases. There is no work package specifically dealing with the origin of humic substances. Analysis of natural aquifer systems and the conversion of clay organic matter show that this is an issue that still needs considerable attention. This issue is dealt with within work package No. 8.

Table 1: Project partner

Partner No.	Partner
1	Forschungszentrum Karlsruhe GmbH (FZK/INE), D (Coordinator)
2	Forschungszentrum Rossendorf (FZR-IfR), D
3	GSF-National Research Center for Environment and Health (GSF), D
4	Commissariat à l'Energie Atomique (CEA-DPC), F
5	University of Nantes - Presidence (U-Nantes), F
6	University of Manchester (U-Manch), UK
7	Technical University of Prague (CTU), Cz
8	Fodor Joszef National Center of Public Health, Frederic Joliot-Curie National Research Institute of Radiobiology and Radiohygiene (FJC), HU
9	University of Cyprus (UCY), Cy
	Temporary contributor:
	Francis Claret, FZK/INE through EC Marie-Curie Fellowship (MCFI-2001-01983)

3. OBJECTIVES OF AND PROGRESS WITHIN INDIVIDUAL WORK PACKAGES

The progress within the individual work packages is discussed below. Frequent overlap of activities between individual work packages is mirrored by the numerous cross-references between the different work packages.

Table 2: Project structure

Work package	Title	Lead contractor (Partner No. (cf. Table 1))
1	Critical assessment of experimental methods	7
2	Generation and characterization of humic material	2
3	Radionuclide humate interaction data by designed system investigations	4
4	Characterization of radionuclide humate complexes	1
5	Natural chemical analogue studies	1
6	Radionuclide transport experiments	2
7	Model development	6
8	Application to Performance Assessment	6

3.1 WP 1 (Critical assessment of experimental methods)

<Objectives>

The objectives of this work package are to provide understanding for processes involved in application of different experimental methods used for obtaining radionuclide humate interaction data. By this exercise, radionuclide humate interaction data are given a broad basis providing trust in their correctness. The knowledge generated provides the basis for judging upon the reliability of published data, thus allowing extension of the database without separate experimental investigations. In addition, identification of different processes, frequently understood as artifacts, can contribute to the understanding of processes involved, otherwise potentially ignored. One such example was recognition of kinetics as a key issue from differences in results from different experimental approaches and systems.

<Results>

Experimental methods used for complexation studies may be divided into three different types with different advantages and limitations:

-Separation of different species by size, charge, ... Examples are dialysis, ultrafiltration, (ultra-)centrifugation, size exclusion chromatography and electrophoresis. Examples of potential problems arising are shift in equilibrium, insufficient species separation and loss of species.

-Indirect speciation via additional complexing agents, ion exchange or ion selective electrodes. Examples of potential experimental problems are complexity of data analysis relying on additional input data, generation of additional unintended species and processes that may influence equilibrium.

-Direct speciation via spectroscopy has a limited sensitivity range. In the case of fluorescence spectroscopy, the behavior of excited states may deviate from that of the ground state and photodynamic processes need to be well understood.

In order to have a common basis for the intercomparison of different experimental methods, one batch of Aldrich humic acid was generated and used. Purification and the thorough characterization are documented well in order to establish a good basis for intercomparison within the exercise as well as comparison with well documented published data. Ash content is determined to be 1.8 % by weight, showing the successful purification. A broad range of additional characteristic data underlines the successful purification (cf. WP2).

Six experimental methods have been tested for their applicability. These methods are (i) dialysis, (ii) electrophoresis, (iii) ultrafiltration, (iv) acid-base titration, (v) ion exchange and (vi) GPC/HPLC. Advantages and disadvantages are identified based on the experimental results. The outcome of the work reflects the original objectives, namely to provide the basis for judging published data obtained by different methods. Results of individual methods may be summarized as follows:

Dialysis: Imperfect separation if large pore membranes are used. Slow equilibration. Loss of substances because of sorption on large surfaces involved will affect results only if uncomplexed metal ions are sorbed. Trustworthy humate complexation data can be obtained when experimental setup and conditions are well chosen.

Electrophoresis: Sorption losses on the cell may affect the results. In the radiotracer arrangement, negative effect of isotope exchange on the electrophoretic mobility measured can also influence the results, particularly at high humate ligand loadings. In other cases the method is functioning well.

Ultrafiltration: In the ideal case, an ultrafilter is used where the non-complexed metal ion shows no retention and no sorption, whereas the humate complex is fully retained. Ultrafilters are usually characterized by a nominal cut-off referring to full retention (> 95 %) of globular proteins of a given mass. Below that mass(size) retention decreases over a wide range with

decreasing mass(size). Humate complexes can be expected over the mass range of humic acid, reaching down to few hundreds of molecular mass (known from application of recently developed mass spectroscopy methods). The effective size of the metal ion humate complexes, however, is not known. Direct correlation to nominal cut-off is not possible due to different size to mass ratio compared to the ultrafilter reference substances (globular proteins). Thus, selection of a filter ensuring complete retention is not possible. This problem may be visualized by the 86 % retention of the europium oxalate complex on an ultrafilter with a nominal cut-off of 500 (Dalton globular proteins). A carboxylic acid calibration substance for FFF and HPLC with the molecular mass of 370 is basically fully retained on a 1000 Dalton ultrafilter.

Furthermore, the effective size of hydrated metal ions is not well understood. Retention of non-complexed metal ions is observed with various ultrafilters, where sorption on the membrane including the pore surfaces may further contribute to difficulties in obtaining reproducible and interpretable results. In addition, along with progression of ultrafiltration, the concentration of partially retained species is increasing. The permeation of partially retained species depends on their concentration. Consequently, prediction of the permeation behavior is difficult where significant volumes of the original solution are passed through the filter.

In summary, it is not possible to find an ultrafilter resulting in quantitative retention of the humate complex and quantitative permeation of the non-complexed metal ions. Sorption of the non-complexed metal ion may be significant. Build-up of concentrations in the retentate may further contribute to difficulties in analysis of the system behavior. Consequently, ultrafiltration based humate complexation data need to be interpreted with caution.

Acid-base titration: High humic acid and metal ion concentrations are needed to obtain measurable effects on titration data. Slow titration is required in order to ensure equilibrium. Evaluation of data is not straightforward. In summary, the applicability of results obtained by this method may be limited, particularly for environmentally relevant metal and humate concentrations.

Ion exchange: Evaluation of data has to take into account non-linear interaction isotherm of non-complexed ions with cation exchanger. If this is done, trustworthy results are obtained. With respect to making use of published data, it should be ensured that the isotherm used as input data for the distribution between non-complexed metal ions and the cation exchanger is adequately investigated.

GPC/HPLC: Problems arise with respect to sorption and ion exclusion of species. The use of high concentrations of potentially complexing buffers and high concentrations of humic acid adds to uncertainty. The method is usable only in a narrow range of experimental conditions.

<Summary of WP 1>

The investigations have provided the information aimed for in order to judge upon different experimental methods. Different experimental methods are useful for different system

windows. Furthermore, some experimental artifacts are inherent to certain methods. This provides the basis for critical evaluation of published data and design of future experiments.

3.2 WP 2 (Generation and characterization of humic material)

<Objectives>

The objectives of this work package are to ensure availability of appropriately purified and well characterized natural humic and fulvic acids and generate humic material with specified properties for certain purposes. The latter includes humic acid where specified functional groups are blocked, synthetic humic substances with designed properties and silica wafer coated with covalently bound humic acid. One reference batch of Aldrich humic acid was purified within the humate complexation intercomparison exercise (WP1).

<Results>

Humic and fulvic acids from the Gorleben groundwater Gohy-573 has been used within the EC activities in this field since the start of the MIRAGE project (MIgration of RAdionuclides in the GEosphere). A large number of complexation data has been generated over the past many years. The original material has been used up and new batches have been prepared and characterized. These two new well characterized batches will enable continuation of generation of complexation data with humic and fulvic acids from this particular source.

Lrge amounts of humic and fulvic acids have been prepared from 6 m^3 of this Gorleben groundwater. The material is characterized by a variety of methods, such as elemental composition, including inorganic impurities, spectroscopic properties (UV/Vis and IR), functional group content (potentiometric pH titration and XPS), size distribution (AF^4), and mass distribution (TOF-SIMS and ESI-MS). The mass distribution of the humic acid has its number average molecular mass in the range 500-600 mass units, with tailing up to around 3000 mass units. The corresponding numbers for the fulvic acid are 400-500 and 2000. The proton exchange behavior has been thoroughly characterized. These results verify the typical behavior of the two new humic and fulvic acid batches.

XPS has been applied to the new Gohy-573 humic and fulvic acid batches as an additional characterization method, with synthetic humic acid for reference. As expected, the humic acid is shown to be more aromatic than the fulvic acid. Nitrogen is only found in one form that may be amide or amine. Around 10 % of sulfur is found as sulfonic acids, the rest in thiophenes associated with aromatic rings. Oxygen is identified as C=O and C-O with the higher contribution in fulvic acid as expected from the elemental composition. Inorganic contaminants are not found in the humic acid, whereas the chloride ion, and Cr, Mn and Fe oxides are found in the fulvic acid.

The characterization shows that the isolation and purification was successful. Selected properties are compared to data from the previous EC reference humic and fulvic acids from this groundwater in order to provide for comparison, especially in view of future complexation

studies and the relation to results from the past almost 15 years of studies on the previous batches. The material is distributed to interested parties upon expression of interest with brief description of work to be performed.

Synthetic humic acids with a variety of designed properties have already been generated. Examples of past investigations where the added value of using such substances become clear are complexation studies with and without blocking of phenolic groups, and redox studies with various designed and natural humic acids. The results from metal ion complexation studies with and without blocking of phenolic groups show that the complex formation is not influenced by phenolic groups with respect to complex coordination (structural parameters, i.e. coordination numbers and bond lengths) and stability constants, however, the effective humate ligand concentration decreases for humic acid with blocked phenolic groups. Studies on the redox capacity show that in addition to straightforward comparison of the amount of redox sensitive groups, additional processes are involved. Present work with the synthetic humic substances with designed properties has provided further insight in, especially the redox function of humic acids. The capability of humic acid to reduce uranium(VI) to uranium(IV) has been spectroscopically verified for pH 9.

A new approach for “grafting” of humic acid on silica wafer surfaces has been developed and tested. IR and TOF-SIMS are used for characterization of individual process steps. The results show that the approach appears successful. After the final process step, a comparably homogeneous coating is found with a mass spectrum in agreement with humic acid. Results from AFM verify the findings. Final studies are still required in order to insure that the material fulfills all requirements for planned further studies on the metal ion interaction and characterization of the complexes. Additional humic acid coated silica wafers have been generated by different other approaches. These humic coated wafers are also characterized in order to provide a broader basis of such material and draw conclusions on process optimization. The material will be used for complexation studies during the final project year.

An overall important progress is made with respect to the discussion concerning the mass distribution of humic and fulvic acids with far to high numbers presented in the past. Verification that humic acid on humic wafers shows the same mass distribution as humic acid in solution (by ESI-MS) or deposited on carriers (TOF-SIMS). This shows that humic acid deposited or bound on the humic wafers are representative for the starting material. More important, given that the humic wafers show the same results as the other analytical approaches, there can be no doubt that these numbers are correct.

<Summary of WP 2>

Different humic material has been generated for a broad variety of purposes. The use of this material in below work packages is an essential part in progress of the project. Application of advanced analytical techniques on this variety of humic material (further discussed below>) also provides a main advancement in the overall understanding of humic and fulvic acids.

3.3 WP 3 (Radionuclide humate interaction data by designed system investigations)

<Objectives>

The objectives of this work package are to provide data required for predictive radionuclide transport modeling. For the latter, simplifications or in some cases restriction to kinetic parameters may be used. Without fundamental data on individual processes, however, trust in application of such data to transport modeling is missing.

<Results>

A considerable contribution to this work package is given by the work done on critical assessment of experimental methods (cf. WP 1).

The impact of humic substances on the geochemical behavior of plutonium is related to both the interaction of different species of different oxidation states as well as the influence on the plutonium redox state. According to pH/Eh conditions of the Gorleben groundwater Gohy532, the non-humate complexed plutonium ion is expected to be in the trivalent state. Addition of plutonium at different starting oxidation states results in the same end-state. The importance of humic substances for the redox process is seen by the rapid reduction of Pu(VI) to Pu(V) in the original groundwater compared to the much slower reduction in groundwater where the humic substances have been removed by ultrafiltration. The distribution between Pu(IV) and Pu(III) is dependent on pH and the redox potential. A complication in interpretation of the species distribution is the indication for coexistence of Pu(IV) humate complex and polymeric Pu(IV) hydroxide. The latter is identified in the groundwater samples by both XPS (satellite bands) and EXAFS (Pu-Pu bond distance). A further complication is the distinction between the impacts of physico-chemical conditions on the equilibrium distribution versus redox kinetics. A great deal of further studies will be required in order to provide a tool for reliable prediction of the chemical state of plutonium in reducing far-field relevant groundwater.

The complexation of the hexavalent uranyl ion with humic acid has been studied. By the use of a humic acid ligand concentration prediction, discussed under work package 7, solubility enhancement over hydroxide solid phase can be rationalized by one single interaction constant. The stepwise complexation constants from different routes to the formation of the ternary hydroxo complex indicate complexation enhancement relative to expectations by comparison with other simple complexes. A suggestion is made with respect to the possibility for hydrogen bonding with the abundant neighboring oxygen functionalities. Measurements in undersaturation, however, may be desired in order to exclude the possible formation of polynuclear complexes. A final conclusion cannot be drawn until complementary complexation data become available, including comparison with other ternary complexes.

Humic and fulvic acid from instant release under near-field cement dissolution relevant conditions is isolated and characterized. Furthermore, the Cm(III) complexation behavior is studied. Characterization and complexation studies show that humic and fulvic acids from

clay organic matter of terrestrial origin have the typical properties as found with other frequently studied humic substances. Contrary to this, fulvic acid from clay organic matter of marine origin shows a deviating behavior. Further studies will show whether this deviating behavior reflects different complexation properties depending on the functional group backbone environment or if such differences are reflected in a different photodynamic behavior.The highlight of these findings is that the clay organic matter conserves fundamental properties of the co-sedimented organic matter over millions of years and that such differences are reflected in the photodynamic/complexation behavior.

Great progress has been achieved in bringing complexation data on the humate interaction of tetravalent actinide ions together with basic input data on hydrolysis and carbonate complexation. Testing calculations with observed experimental data show that the impact of humate complexation at different pH and carbonate concentrations can be predicted with acceptable agreement for Pu(IV) and Np(IV). Problems are still there for U(IV). The overall approach and the apparent success in predicting the impact of humic substances on the species distribution of tetravalent actinide ions is a great step forward towards inclusion of the humate complexes in geochemical modeling. In order to test the plausibility of the data used and in order to provide insight in individual processes involved, individual interaction constants for the hydrolyzed tetravalent actinide ions with humic acid will be deduced and compared with expectation values.

<Summary of WP 3>

The generation of complexation data in the pH neutral range, relevant for natural groundwater conditions, is making great progress. More emphasis on comparison of stepwise constants from existing studies may help in providing confidence in the findings. The question of slow kinetics, as the main impact on the transport behavior, still needs additional attention.

3.4 WP 4 (Characterization of radionuclide humate complexes)

<Objectives>

The objectives of this work package are to ensure appropriate interpretation of the radionuclide humate interaction process and thus provide the basis for the required process understanding. A key element in this work is development and use of frontier analytical techniques. This is a key issue for providing trust in the capability to conduct predictive modeling of humic colloid mediated radionuclide transport, and thus for providing trust in the overall outcome of the project.

<Results>

Studies have been conducted on the size distribution (by AF^4) and mass distribution (by TOF-SIMS) of humic acid with and without complexation with europium. These studies are essen-

tial with respect to basic humate complexation process understanding, but especially with respect to the potential for complexation mediated humic-humic association. Interpretation of the AF^4 data is difficult because it cannot be ensured that calibration standards used reflect the mass to size ratio of humic and fulvic acids. A set of carboxylic/polycarboxylic acids shows an acceptable agreement in size to mass ratio with fulvic acid. This, however, refers to the average value between the calibration standards and the presumable mixture of molecules making up the fulvic acid. The spread in size to mass ratio in the calibration standards used clearly indicate that a unique value also cannot be expected for all individual entities of the fulvic acid.

For humic acid, the size distribution shows enhanced values evaluated with the same set of standards as the fulvic acids. Questions arising are to which extent the elevated values for humic acid reflects different properties of the humic acid entities or protonation induced association. Association of organic molecules might not lead to an increase in size comparable to the increase in mass. Alignment of organic molecules and associated dehydration in the contact surface, especially via hydrogen bonds, may lead to a marginal increase in size relative to the increase in mass. Investigations by TOF-SIMS on europium humate complexes did not show a significant increase in the mass distribution. The original mass distribution spectra were found with small modulations in the mass range between 150 and 350 in comparison to the humic acid without europium. Given the importance of the underlying question, further investigations are considered.

Synchrotron radiation based techniques have been used extensively in past years in order to provide metal ion humate complex coordination parameters. Such investigations are performed at very high substrate concentrations. The question arises to which extent data obtained under such conditions are relevant for the much more dilute conditions found in nature and used with other experimental techniques. Europium humate complexation behavior was compared from moderate to very high humic acid concentrations (2 g/L). No difference in saturation values was found for different humic acid concentrations. The results indicate that self-association of humic acid is not important for the effective humate ligand concentration and that results from synchrotron radiation spectroscopy obtained at high humic acid concentrations are applicable also in much lower concentration ranges. It furthermore supports model development according to which association is driven by charge neutralization and balancing of surface charge density versus relatively weak associative forces (cf. below, WP 7).

<Summary of WP 4>

Characterization of humic and fulvic acid complexes is making great progress, especially in conjunction with improving basic understanding of the humic and fulvic acids themselves. Nevertheless, there is a fundamental lack in understanding of a large number of individual properties and thus interpretation is still frequently contradicting. There is still a long way to go until all the characteristic properties can be adequately understood and be brought together to one consistent picture. The overall status is that humic and fulvic acids, despite their compositional range show a surprisingly narrow range in overall properties. This basic approach,

however, understanding this class of substances based on the comparably narrow range of properties and characteristics is progressing well.

3.5 WP 5 (Natural chemical analogue studies)

<Objectives>

The objectives of this work package were originally tailored towards generation of kinetic data for different metal ion inventories. The key question originated from the observation, that radionuclides added under laboratory conditions show a number of kinetic dissociation modes. The inventory of natural trace metal ions shows basically only two dissociation modes, namely one portion of the inventory with a comparably slow dissociation kinetics (slower than but in the magnitude of the bulk laboratory system kinetics) and one part of the inventory dissociating so slow that it so far has not been possible to quantify this kinetics. The key question arising from comparison of the outcome of these individual studies is to which extent actinide ions in long contact with a natural system will mimic the behavior of the natural inventory of natural actinide ions, including natural chemical analogues, or if the description of their behavior can be extrapolated from laboratory system studies. In the case of kinetics so slow that it cannot be reliably quantified, humic colloid mediated actinide transport will need to be treated as an ideal tracer in transport predictions.

<Results>

In the beginning of the project it was concluded, that dissociation data for radionuclides and trace metal ions are to a high degree available. The problem still pending is the reason for the differences observed between the different modes and inventories. This issue is presently tackled on a more fundamental level, by advanced characterization of humate complexes and fundamental development of the humate interaction process. For this reason, the emphasis of this work package has changed towards demonstration of the fundamental kinetic concept on large natural systems by analysis of anthropogenic contaminants in the Irish Sea.

The chemical behavior of americium and plutonium is studied on samples from the bank of Esk Esturia, West Cumbria, UK National Grid Reference SD113964. The anthropogenic inventory originates mainly from releases around 30 years ago. Adaptation of the K1-D model has continued for the description of kinetically governed processes describing the movement of anthropogenic actinide contaminants from the Sellafield plant to sea shore sediments of the Irish Sea. Humic matter as kinetically determined sinks and sources is of special interest and relevance for the project. The extension of the code and successful adaptation to such a large natural system provides confidence in this tool for the overall purpose of the project and the visualization of the impact of humic substances on large natural scales through work package 8.

<Summary of WP 5>

The applicability of the basic kinetic concept is demonstrated on natural anthropogenic systems. This is a key step towards trust in the capability to make predictive modeling on a real system scale over long time spans.

3.6 WP 6 (Radionuclide transport experiments)

<Objectives>

The objectives of this work package are to provide transport data for radionuclides and contribute to development of process understanding by investigations with and interpretation of these more complex natural systems. Batch and column experiments are used and results are interpreted in the light of development of general fundamental process understanding. The also provide in-put for visualization of humic colloid mediated transport via migration cases (WP 8).

<Results>

The influence of humic substances on the sorption of Np(V) was investigated for granite and its individual mineral components. The distribution of humic acid was also identified by the use of ^{14}C labeled synthetic humic acid. This approach has previously been successfully applied for U(VI). A slight decrease in the sorption of Np(V) is found with addition of humic acid. Through investigations with individual mineral components it was shown that Biotite seems to be the dominating mineral in this system. The basic approach of determining system components that govern the species distribution and transport behavior is a key element in providing for trustworthy model predictions.

Preliminary results on column experiments with plutonium with the Gorleben groundwater Gohy-532 had previously been obtained. Work on characterization of plutonium in this groundwater (cf. WP 3), shows that plutonium is present in the reduced state. If the tri- or tetravalent oxidation state is predominant could not be unambiguously determined by the characterization studies. Comparison with the transport behavior of tri- and tetravalent actinide ions revealed that plutonium shows a behavior between them. The working hypothesis is that both the reduced forms of plutonium are present, the ratio depending on the physico-chemical conditions. Furthermore, the generation of polynuclear species may be important resulting in deviation from the results of other both tri- and tetravalent actinide ions. Further work will be required in order to provide the necessary knowledge and process understanding for predictive transport modeling. This includes general progress in the field of tetravalent actinide chemistry, mostly beyond the reach of the present project.

Transport studies have been performed within the context of the uranium mining and milling rock pile migration case. Sorption/desorption studies were performed by batch and column experiments. Synthetic rock pile water was used reflecting the composition of analyzed rock-pile water. Slow kinetics was found with about two weeks required in order to obtain steady-

state conditions. The added ^{233}U was determined by liquid scintillation counting whereas the total uranium in solution, including dissolution of exchangeable sedimentary uranium (dominated by ^{238}U), was determined by ICP-MS. The combination of these two analytical results shows that the slow kinetics is related to the uranium exchange between the added uranium and the natural inventory in the sediment. The impact of humic substances is moderate and direct evidence of a solubility enhancement is statistically uncertain. Separate desorption experiments under variation of physico-chemical conditions show that the desorption can be described by a comparable kinetics. Humic acid shows no significant impact on desorption rates.

The uranium distribution data with the synthetic rock pile water is interpreted by a linear sorption isotherm where the results show acceptable consistency for different volume to mass ratios during experiments. Analysis of the sediment sorption kinetics revealed that the system can be described by two processes, one which can be treated as equilibrium for the experimental conditions/time scales, and one where the kinetics of exchange with the uranium sediment inventory needs to be regarded also for field calculations. Data for the kinetics of uranyl humate interaction is already available from other sources/experiments. There is a large number of different uranyl species in solution (several carbonate and hydroxocarbonate species). It was not possible to relate the sediment sorption data to specific species in solution. The data deduced for the transport calculations thus are specific for this system composition and cannot be used for other conditions. The column experiments performed demonstrated kinetic character of uranium desorption from the rock pile material and only a moderate influence on uranium release of humic acid presence in the leachate. The obtained results provide the required basis for predictive transport calculations within WP 8, to be conducted during the final project year.

<Summary of WP 6>

The applicability of the basic kinetic concept is demonstrated on natural anthropogenic systems. This is an important step towards trust in the capability to make predictive modeling on a real system scale over long time spans.

3.7 WP 7 (Model development)

<Objectives>

The objectives of this work package are to integrate progress in fundamental process understanding into a consistent description. The conceptual consistency is followed by mathematical description for handling and required simplifications.

<Results>

Further development has been achieved concerning a long ongoing discussion on the physico-chemical basis for the observed properties of the humate interaction. The key question is related to the successful application of complexation models where the effective humate

ligand concentration is a measured quantity. The effective humate ligand concentration is decreasing with increasing protonation and, to a lesser extent, with increasing ionic strength. The problem is that this measured quantity so far could not be brought in relation with the protonation of individual functional groups and thus empirical measured quantities are used. Furthermore, the empirical data are only accessible in the non-hydrolyzing range of interacting metal ions. In the hydrolyzing range the concentration of complexing metal ions cannot easily be varied in order to directly measure this quantity. The approach presented is based on the effective humate ligand concentration as the number concentration of entities in solution carrying reactive ionized groups. So far the approach is based on complexation data with tri- and hexavalent actinide ions showing comparable complexation strength and overall behavior.

Comparison of protonation and effective humate ligand concentration data in the non-hydrolyzing range of metal ions shows, that the effective ligand concentration decreases with one unit for the protonation of approximately 3.5 functional groups. Extrapolation of this ration to higher pH shows that the effective humate ligand concentration reaches its maximum slightly above pH 10. At this point the effective humate ligand concentration corresponds to an average molecular mass of about 550. This value corresponds well with the average mass of humic acid molecules as determined by TOF-SIMS. At this average mass, the proton exchanging group content is about 3.5. This leads to an overall consistent description of the humic acid ligand function. At high pH the effective humate ligand concentration is given by the number concentration of molecules. Protonation of the same number of functional groups as found per average molecule leads to the decrease in the effective humate ligand concentration by one unit. Analysis of the metal ion complexation data reveals that the effective humate ligand concentration decreases by one unit per metal ion complex. This is reflected in the metal ion complexation mediated humic entity association. A considerable problem with the approach is that comparable humate ligand concentrations are not obtained for metal ions with weaker interaction strength. For such ions lower humate concentrations are reported. The reason for this deviation is still subject to discussion.

The question of association of humic acid molecules as a consequence of protonation and metal ion complexation is dealt with by a modeling approach. Modeling was done of the expected behavior of organic molecules with weak associative forces and with varying anionic charge (reflecting protonation). It is shown that the organic molecules with a certain charge do not associate. With progressive protonation, the organic molecules begin to generate associates (dimers, trimers, ..). The balance between the attractive forces and the surface charge density of the molecules/associates governs the size of the associates. As the charge becomes negligible, the organic material generates a separate phase or flocculates. This reflects the observed behavior of humic acid where larger entities are generated upon protonation, finally leading to flocculation in the acidic range. The approach also provides an important visualization of the approach described above.

The humate interaction of tetravalent actinide ions has been brought into a consistent description with a separate database containing the required relevant data. The approach is an

important basis for treatment of the tetravalent actinide ions in humate systems. It furthermore provides the basis for analysis of individual processes that can be tested for plausibility and consistency. Consequently this approach provides not only data for the humate interaction of tetravalent actinides, but also a basis for ongoing development of process understanding via plausibility criteria.

<Summary of WP 7>

Modeling is progressing well by rationalization of process understanding and testing of different approaches for comparison will observations. The convergence in overall process understanding finds it way into mathematical descriptions.

3.8 WP 8 (PA)

<Objectives>

The objectives of this work package are to provide data describing the origin, stability and mobility of humic matter in natural aquifer systems and to visualize the impact of humic colloid mediated radionuclide transport for selected relevant cases. With respect to the origin of humic substances, not only natural sources are quantified, but also additional sources are dealt with originating from changes introduced via geochemical reactions of engineered structures and waste forms in a repository.

<Results>

Three migration cases are applied for visualization of the impact of humic colloid mediated actinide transport. One of these migration cases is the far-field of the Gorleben aquifer system. Over the past decades, the Gorleben aquifer system has been extensively studied by a large number of methods within the German program for disposal of high-level waste. The Gorleben migration case was formulated within the past EC-HUMICS project and preliminary calculations on the humic colloid mediated actinide transport were conducted. Some open questions, however, remained with respect to the degree/velocity of vertical groundwater exchange. Furthermore, despite the findings concerning ideal tracer behavior of humic substances in deep groundwater, additional sources could not be excluded and the mobility of aquatic humic substances in the upper part of the aquifer remained an open issue. The hydrological situation in the southeast part of the aquifer system has been investigated by a combination of chemical data, isotope-geochemical/hydrological data and historical data with respect to changes in the land-use. Furthermore, the mobility of fulvic acids has been quantified via a combination of isotope-geochemical methods, and carbon and sulfur near edge synchrotron radiation spectroscopy.

The uranium mining and milling rock pile migration case has been well documented in the first Technical Progress Report (see below, dissemination of results). The surface near sandy aquifer case (Dukovany) is documented in an working document. The same is true for the Gorleben migration case. The reason for retaining the Gorleben migration case from publica-

tion was especially the high vertical groundwater transport/exchange velocity assumed. In the first Technical Progress Report a contribution was given supporting this high groundwater mobility in this aquifer system. In the present reporting period, work has continued to provide the basis for a well justified Gorleben migration case. Carbon and sulfur near edged synchrotron radiation spectroscopy shows that the properties of the fulvic acids partly reflect the geochemical conditions of the various groundwater strata and the origin (recharge or in-situ generation). Evaluation of the carbon backbone, however, reveals that fulvic acid found in deep saline brines have an age that by ^{14}C cannot be distinguished from that of recharge groundwater. This supports the original assumption concerning a rapid vertical groundwater mobility/exchange. Consequently the Gorleben migration case is due for publication via the second Technical Progress Report.

A key question for the potential impact of humic substances on the radionuclide transport in clay media is the potential additional source via clay organic matter. In the first Technical Progress Report it was shown that high concentrations of humic and fulvic acid alike material is generated under extended time periods under alkaline conditions expected for cement dissolution in the near-field. During the present reporting period it is shown that also the initial release under alkaline conditions contains humic and fulvic acids. The properties of these humic and fulvic acids reflect the origin of the clay organic matter, i.e. marine or terrestrial as shown by biomarkers. In the past, questions have been raised to which extent these humic and fulvic acid alike substances have the same properties as commonly known ones, especially to which extent they complex and transport radionuclides. As discussed under WP 3, the complexation behavior and characteristic properties leads into more fundamental understanding of observations with respect to differences in origin and properties of this material depending on their origin.

<Summary of WP 8>

A great number of investigations have shown that the origin and mobility of humic substances in the concerned systems is well understood. The migration cases have been well defined and documented. The implementation of the state-of-the-art by these migration cases will provide for visualization of the impact of humic colloid mediated radionuclide transport.

4. OVERALL SUMMARY

The project is progressing well over the broad spectrum of investigations encompassed. In addition, incorporation of reporting from a Marie Curie mobility grant and inclusion of a new partner has widened the scope of the investigations. Progress is made in the basic understanding of the material dealt with. The different types of material generated provide the basis for investigations on systems with different and partly designed properties. Complexation studies, complex characterization, radionuclide transport experiments and analysis of anthropogenic contaminants all move in one common direction of system and process understanding. Thereby, the basis is provided for implementation of predictive modeling and determination of the relevance under different conditions.

5. REFERENCES

1. G. Buckau (Editor) "Effects of Humic Substances on the Migration of Radionuclides: Complexation and Transport of Actinides, First Technical Progress Report", Report: FZKA 6124, August 1998.

2. G. Buckau (Editor) "Effects of Humic Substances on the Migration of Radionuclides: Complexation and Transport of Actinides, Second Technical Progress Report", Report: FZKA 6324, June 1999.

3. G. Buckau (Editor) "Effects of Humic Substances on the Migration of Radionuclides: Complexation and Transport of Actinides, Third Technical Progress Report", Report: FZKA 6524, Research Center Karlsruhe, October 2000.

4. G. Buckau (Editor) "Effects of Humic Substances on the Migration of Radionuclides: Complexation and Transport of Actinides (Final Report)", Report EUR 19610 EN, 2000.

5. Buckau, G. (Editor) "Humic Substances in Performance Assessment of Nuclear Waste Disposal: Actinide and Iodine Migration in the Far-Field, First Technical Progress Report", Report FZKA 6800, Research Center Karlsruhe, 2003.

Annex 1

Vertical Exchange of Gorleben Fulvic Acids of Different Origin

T. Schäfer [1], G. Buckau [1], R. Artinger [1], J.I. Kim [1], S. Geyer [2], M. Wolf [3], W. F. Bleam [4], S. Wirick [5] and C. Jacobsen [5]

[1] Forschungszentrum Karlsruhe, Institut für Nukleare Entsorgung, PO Box 3640, 76021 Karlsruhe, Germany

[2] UFZ-Umweltforschungszentrum Leipzig-Halle, Sektion Hydrogeologie, Theodor Lieser Str., 06120 Halle, Germany

[3] GSF-National Research Center for Environment and Health, Institute of Groundwater Ecology, 85764 Neuherberg, Germany

[4] University of Wisconsin, Department of Soil Science, Madison, WI 53706-1299, USA

[5] State University of New York at Stony Brook, Department of Physics and Astronomy, Stony Brook, NY 11794, USA

Vertical Exchange of Gorleben Fulvic Acids of Different Origin

T. Schäfer[1,*], G. Buckau[1], R. Artinger[1], J.I. Kim[1], S. Geyer[2], M. Wolf[3]
W. F. Bleam[4], S. Wirick[5] and C. Jacobsen[5]

[1)] Forschungszentrum Karlsruhe, Institut für Nukleare Entsorgung, PO Box 3640, 76021 Karlsruhe, Germany

[2)] UFZ-Umweltforschungszentrum Leipzig-Halle, Sektion Hydrogeologie, Theodor Lieser Str., 06120 Halle, Germany

[3)] GSF-National Research Center for Environment and Health, Institute of Groundwater Ecology, 85764 Neuherberg, Germany

[4)] University of Wisconsin, Department of Soil Science, Madison, WI 53706-1299, USA

[5)] State University of New York at Stony Brook, Department of Physics and Astronomy, Stony Brook, NY 11794, USA

*: schaefer@ine.fzk.de

Abstract

The Gorleben aquifer system overlaying a salt dome has been under investigation for the potential to host a repository for nuclear waste in Germany for more than two decades. Groundwater in the aquifer shows a wide span of compositions, especially with respect to salt content and concentration of dissolved organic matter (DOC) with up to around 200 mgC/L. DOC originates from recharge, showing large variations depending on land-use and conditions (forest, agriculture, wet-land, …). An additional source of DOC is microbiologically mediated turn-over of lignite intercalations in sandy Miocene sediments ("in-situ generation"). The DOC consists mainly of humic and fulvic acids that are of concern for potentially enhanced transport of radionuclides in the groundwater region. A key issue in this respect is the mobility of these complexing dissolved organic acids. For this reason, a combination of isotope data and carbon as well as sulfur X-Ray absorption near edge structure (XANES) spectroscopy data is used in order to determine the mobility of fulvic acids. It is shown, that fulvic acid from the recharge zone is mobile over the entire depth, including into the salt dome influenced brines. Fulvic acid originating from in-situ generation is less hydrophilic than that originating from recharge and thus do not reach the brines but flocculate at the high ionic strength. The content of different carbon entities/functional groups correlates with the origin of fulvic acid. Contrary to this, the fulvic acid associated sulfur oxidation state also appears to be influenced by geochemical conditions/reactions. The invariance in the backbone structures of fulvic acid against high residence times and variations in geochemical conditions is in agreement with their high stability and mobility as also found in previous studies. The high mobility of fulvic acid over the broad range of chemical groundwater conditions and residence times verifies the potential for dissolved humic substances to result in radionuclide transport enhancement.

Introduction

The fate origin and mobility of aquatic fulvic acids in the Gorleben aquifer (Lower Saxony) is studied. The Gorleben aquifer extends down to 280 m below ground surface and is situated in the rock covering and surrounding a Permian salt dome. The salt content varies from fresh recharge water to saturated brines close to the salt dome. One specific feature of this aquifer is the large variety of DOC concentrations from <1 to >100 mgC/L. High DOC concentrations (>> 1 mgC/L) in deep groundwater in this part of the aquifer system result from microbiological turnover of surface near peat or Miocene brown coal (sedimentary organic carbon; SOC) in deep sandy sediments. The microbiological turnover of carbon sources is driven by reduction of sulfate originating from salt dome dissolution. Several papers dealt with the fate of aquatic humic substances in this complex aquifer system (Artinger et al., 2000; Artinger et al., 1999; Buckau et al., 2000a; Buckau et al., 2000b; Buckau et al., 2000c, Buckau et al. 2003). Humic acid is mainly found between around 50 and 200 m depth. It originates from in-.situ generation at these depths. A shown in the present paper, fulvic acid from in-situ generation does not move into the salt brines, because they are more hydrophobic than those originating from recharge. The same is expected for the rather hydrophobic humic acids. Only minor concentrations of humic acid is found in recharge groundwater. This is presumably the result of high dilution in the rather rapid groundwater exchange in the upper about 50 m recharge/fresh water zone. Contrary to humic acid, fulvic acid is found over the entire depth of the aquifer system. Elevated concentrations are found both from in-situ generation and from recharge from present and previous wet-land/marsh west and south of the salt dome, respectively (Buckau et al. 2000a, Buckau et al. 2003). In the part of the aquifer system investigated in the present study, fulvic acid in groundwater with enhanced DOC concentrations are less dominated by the in-situ origin than is the case for humic acid. Therefore, delineation of fulvic acid with different origin is very promising and thus is subject to the present study.

Fulvic acids from the Gorleben aquifer system are investigated. Groundwater origin and characteristics as well as characteristics of fulvic acids isolated from the respective groundwater is described in detail in (Artinger et al., 2000). Previous attempts to correlate different properties of fulvic acid with the origin did not lead to firm conclusions (Artinger et al., 2000). The two main problems are that, characteristic properties may vary reflecting the physico-chemical environment and that an unambiguous indicator is required for determining the respective contributions from different sources/origin. Compared to previous studies, the new approach in this paper is to analyze the recharge contribution via ^{14}C content of fulvic acid. Different characteristic properties may be invariant with changes in physico-chemical conditions, and other one not. For this reason, ten fulvic acids isolated from different parts of the Gorleben aquifer are characterized by X-Ray absorption near edge structure (XANES) spectroscopy at the Carbon and Sulfur K-edge. Structural information is deduced from the XANES spectra. Variation in characteristic properties deduced by XANES is also interpreted in view of the varying contributions from the two principle origins, namely recharge and in-situ generation.

The present paper is a short description of main results. Detailed description of experimental procedures and data evaluation is given in Schäfer et al. 2004.

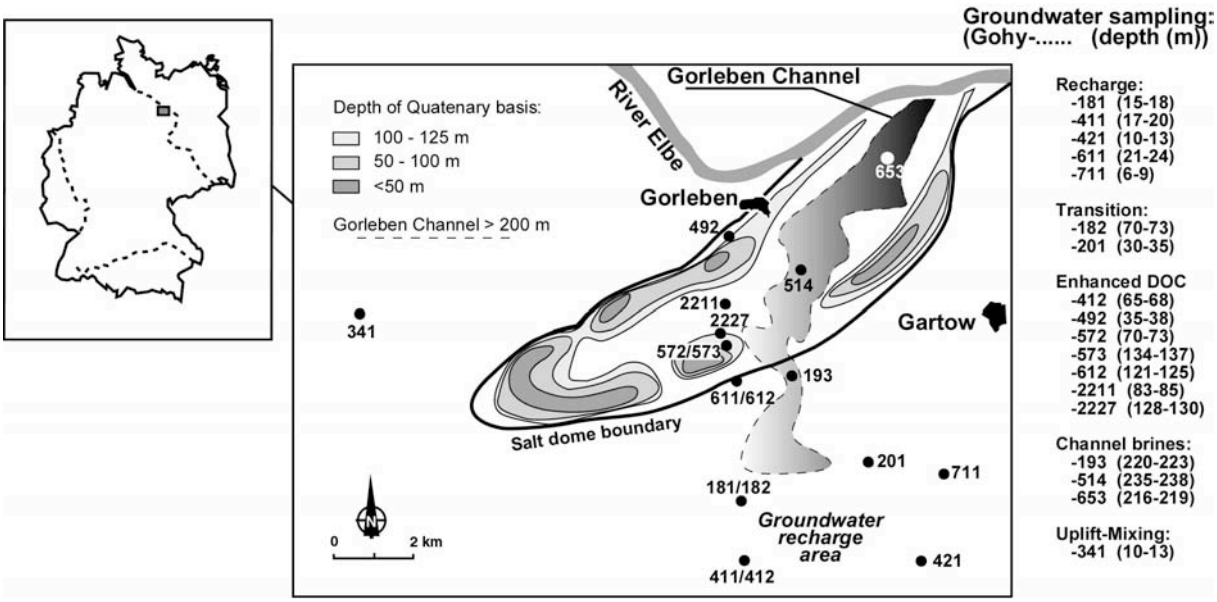

Figure 1: Gorleben sampling site with positions and grouping of investigated groundwaters.

Origin and characteristics of the fulvic acids

In Fig. 1, the Gorleben site and sampling positions for selected groundwaters is shown. Key data and description of the Gorleben aquifer system can be found in (Artinger et al., 2000). The groundwater samples are divided into five different classes, reflecting especially the chemical composition and differences in humic and fulvic acid concentrations. These different groundwater classes have the following characteristics: (i) Recharge: young groundwaters at depths down to about 25 meters situated in fluviatile quartz sands low in organic content, deposited during the most recent Weichsel/Visconsin ice age. These groundwaters have significant concentrations of tritium from nuclear atmospheric testing. The fulvic acid concentrations are low, with variations reflecting different land-use. (ii) Transition groundwaters: comparable to the recharge ones, however, with negligible tritium concentrations. (iii) Enhanced DOC groundwaters: high Dissolved Organic Carbon concentrations, including high fulvic acid concentrations. These elevated concentrations are the result from microbiologically mediated conversion of brown coal particles in these Saale, Elster and Präelster sediments driven by reduction of sulfate from dissolution of the underlying salt dome (Buckau et al., 2000c). (iv) Channel brines: the high salt content reflects the vicinity to the salt dome. The fulvic acid concentrations in these brines are comparable to those of the recharge and transition waters. (v) Up-lift-mixing (Marsh): west of the salt dome, high DOC and consequently fulvic acid concentrations are found. These high concentrations originate from the same microbiologically mediated process as found in Enhanced DOC waters. The sulfate is

assumed to originate from the neighboring “Siemen” salt dome and the organic matter being converted is relatively young peat.

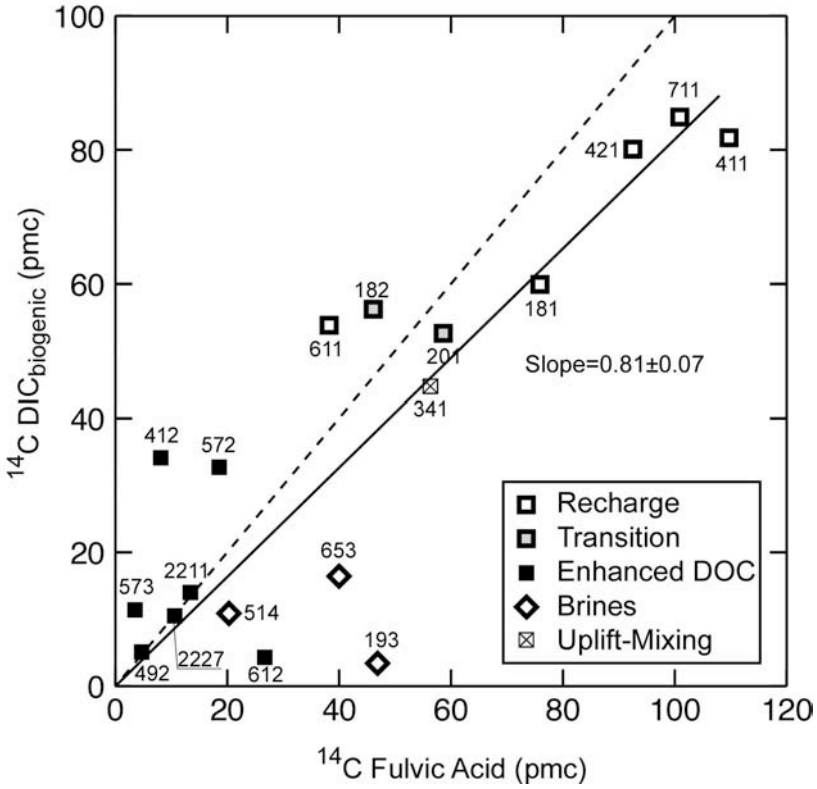

Figure 2: Co-generation of DIC of biogenic origin and fulvic acid.

Generation of fulvic acid

The generation process for the fulvic acid (and DOC) is demonstrated in Fig. 2 (cf. also Buckau et al. 2003). Fulvic acids show ^{13}C concentrations around –27 ‰ relative PDB (Kim et al., 1995). This shows that they originate from C-3 cycle plant material and do not exchange significantly with DIC (dissolved inorganic carbon). The concentration of DIC of biogenic origin is calculated via the ^{13}C value with –27 ‰ rel. V-PDB for the DIC of biogenic origin and zero for sedimentary carbonate dissolution (Buckau et al. 2003). The ^{14}C concentrations of DIC of biogenic origin and fulvic acid correlate with each other due to their common origin (microbiological turn-over of organic material of C-3 plant origin) where the absolute values reflect the ^{14}C concentrations in the different sources. Present recharge is affected by elevated ^{14}C concentrations from nuclear atmospheric testing. Recharge prior to this testing has lower ^{14}C concentrations. The organic material in old sediments (for example brown coal sand) is basically ^{14}C free. Deviations are expected where the isotopic composition of the DIC is amended via, for example carbonate precipitation and methane generation. In the former case the ^{14}C concentration of DIC is decreased. In the latter case the calculated ^{14}C concentration is too high due to incorrect ^{13}C value used in calculation of the DIC of biogenic origin. In addition, deviations due to dissolution of carbonate with unknown ^{13}C content

cannot be fully excluded. Examples may be salt dome carbonate dissolution or existence of non-marine sedimentary carbonates.

Fig. 2 verifies the common origin of DIC of biogenic origin and fulvic acid. Few samples with elevated numbers for the calculated ^{14}C concentration of DIC of biogenic origin coincide with methane in the groundwater (cf. (Buckau et al., 2000c). Few ones with particularly low^{14}C concentration of DIC of biogenic origin presumably reflect carbonate precipitation, especially in brines. The generation process is independent of the type and origin of the groundwater and source material. In average, a ^{14}C activity ratio of 0.8 is calculated for the DIC (biogenic origin) and fulvic acid. Microbiologically mediated processes show high isotopic selectivity with preference for the most common isotopes. The lower ^{14}C concentration in DIC of biogenic origin, relatively to fulvic acid, may reflect such an isotope preference for the lighter carbon in the generation of biogenic DIC.

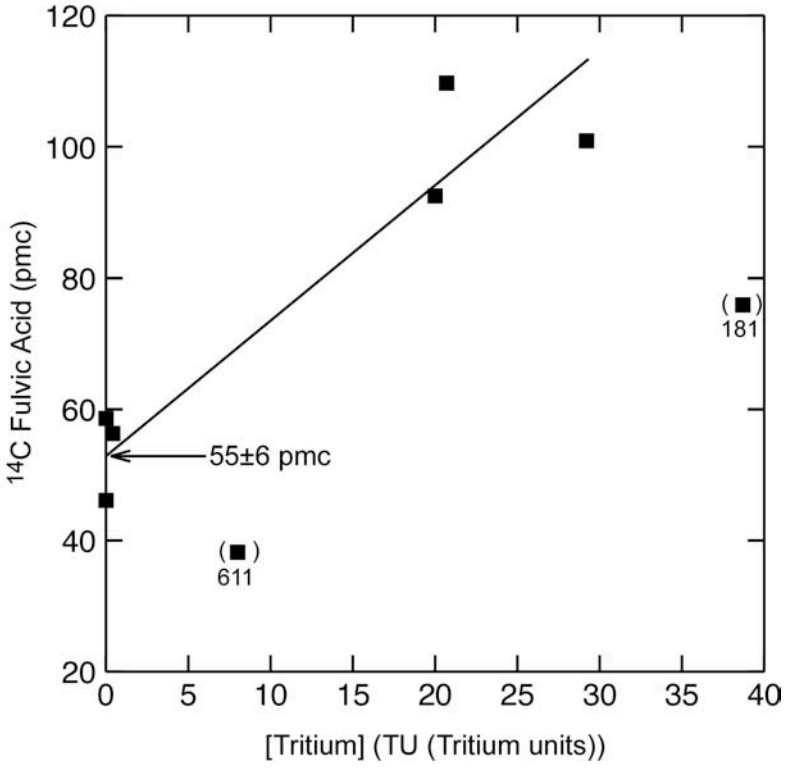

Figure 3: Impact of fall-out tritium on ^{14}C content of fulvic acid. Deviations for the two samples Gohy- 181- and –611 are also found for DIC of biogenic origin (Buckau et al. 2000b).

Source term for recharge fulvic acid

Evaluation of the ^{14}C concentration of DIC of biogenic origin for the purpose of groundwater dating revealed a value of 54 ± 2 pmc (percent modern carbon, 100 pmc = 0.23 Bq/gC) prior to nuclear atmospheric testing (Buckau et al., 2000b). The impact of nuclear atmospheric testing on the ^{14}C content was deduced from correlation with tritium from the same source.

Application of the same approach to ^{14}C of the corresponding fulvic acids is shown in Fig. 3. The groundwaters show a correlation between the ^{14}C enhancement and tritium from nuclear atmospheric testing as DIC of biogenic origin. Two groundwaters show strong deviation as also found for DIC of biogenic origin (Buckau et al., 2000b). The starting value for fulvic acid recharge prior to nuclear atmospheric testing is evaluated to be 55 ± 6 pmc (cf. 54 ± 2 for $DIC_{biogenic}$). This value is used in order to quantify the amount of fulvic acid in deep groundwaters originating from recharge under conditions prior to nuclear atmospheric testing.

Origin of fulvic acid in different groundwater

In Fig. 4, the concentrations of fulvic acid in the different groundwaters are shown as a function of sampling depth. The total fulvic acid concentrations show large variations with strongly elevated values in the depth range where in-situ generation takes place via microbiologically mediated turn-over of brown coal sand intercalations. The fulvic acid concentrations originating from recharge are in the same low range for most of the groundwaters. Exceptions are Gohy-612 and –2211 where tritium is found also at considerable depth. In the surface near up-lift mixing groundwater Gohy-341, high fulvic acid concentrations are found, all with recharge ^{14}C concentrations. Of great interest is that the fulvic acid concentrations in the brines are comparable with those of recharge groundwaters.

Groundwater from the enhanced DOC depth range will exchange with both recharge and brines. In the recharge groundwaters dilution takes place by the relatively fast groundwater transport (recharge and discharge). This will mask the inflow of elevated fulvic acid concentrations in this region. The age of the brines is difficult to determine. The fulvic acid concentrations and their fulvic acid ^{14}C content indicate that the brines are young compared to the ^{14}C half-life ($T_{1/2} \approx 5730$ years). Higher age partly indicated from ^{14}C of the DIC (Buckau et al., 2000b) is probably overestimated due to carbonate precipitation (cf. above discussion, Fig. 2). Exchange with the brines should result in inflow not only of recharge fulvic acid but also inflow of "old" ^{14}C-free ones from in-situ generation in overlaying groundwater. The latter is not the case and thus the fulvic acids from in-situ generation (from brown coal) can be expected to be less hydrophilic and precipitate at high ionic strength.

The overall picture from Fig. 4 is, that one may expect considerable exchange of groundwater over the entire depth for time-scales short compared to ^{14}C decay. This is also supported by the identification of tritium down to a depth of 125 m and the mainly exponential mixing of salt over the entire depth (Buckau et al., 2000a). Fulvic acid from recharge is transported through the various groundwaters and is found in the deep brines. In the intermediate depths, considerable amounts of fulvic acid are generated from old carbon deposits. This fulvic acid is precipitated at high ionic strength of the brines. A considerable contribution of "young" ^{14}C containing fulvic acid from wet-land/marsh is not found in the present groundwaters. In order to verify this overall picture, selected fulvic acid samples are analyzed by carbon and sulfur XANES.

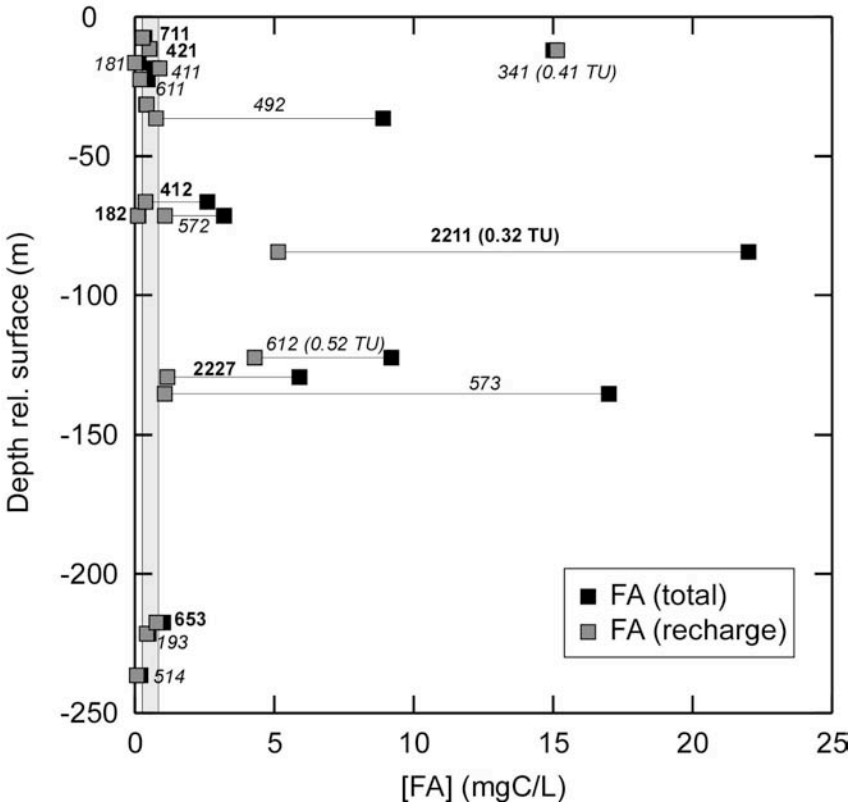

Figure 4: Concentrations of fulvic acid as a function of groundwater sampling depth. Total fulvic acid concentrations are shown together with fulvic acid originating from recharge (via ^{14}C).

C and S XANES of the fulvic acids

The general properties of the fulvic acids deduced from carbon and sulfur XANES are correlated with the fraction of fulvic acid originating from recharge (Fig. 5). Enhanced DOC fulvic acid Gohy-412(FA) is excluded because of results strongly deviating from the other ones, possibly due to contamination (the carbon content is significantly lower than in the other samples and a considerable contribution of inorganic substances, showing that purification was not very successful (Kim et al., 1995). Another possibility is that this fulvic acid originates from previous wet-land recharge (Buckau et al., 2003).

As a general trend, the carboxyl group content is increasing with the fraction of recharge fulvic acid. A corresponding decrease is seen in the C=C/aromatic content and the content of phenolic groups. The content of aliphatic groups does not change significantly with the fraction of recharge fulvic acid. Despite the uncertainty of data and the correlations shown in Fig. 5, the composition of in-situ generated fulvic acid can be estimated. Extrapolation to zero contribution of recharge fulvic acid leads to relative peak areas for different carbon entities/functionalities as follows: carboxylic groups 0.35±0.02; C=C/aromatic groups 0.19±0.02; phenolic groups 0.18±0.01, and aliphatic groups 0.08±0.02. This would lead to a rest of about 0.2 consisting from carbonyl groups, difficult to quantify.

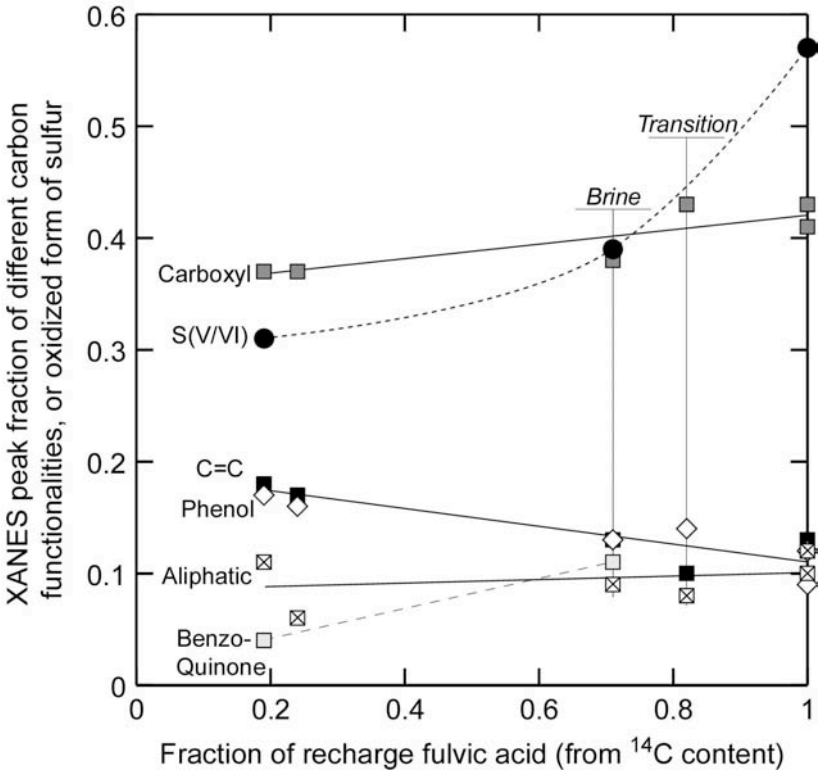

Figure 5: Peak fractions of different carbon functionalities and oxidized form of sulfur from carbon and sulfur XANES against fraction of recharge fulvic acid from ^{14}C content.

Sulfur functional groups in the oxidized form (S_{+5}/S_{+6}) show almost the double peak area for recharge fulvic acid compared to in-situ generated. The brine fulvic acid has a value in between, but more towards the in-situ generated one and less than expected from simple mixing. Deviation from direct correlation with the respective fractions of different origin leads to the conclusion, that the redox distribution of the sulfur inventory reflects also geochemical conditions and processes.

Attempts to correlate the relative peak areas for different carbon functionalities with physicochemical conditions are not successful. Therefore, the overall result is that the content of these carbon functionalities appear to reflect the respective contribution of recharge and enhanced DOC fulvic acids. The successful correlation between functionalities and the mixing between recharge and in-situ generation also verifies the high mobility of fulvic acid following relatively rapid groundwater exchange over the entire depth of the aquifer system with strong local variations. This is directly seen for the high contribution of recharge fulvic acid in the groundwater Gohy-2211 at 83-85 meters depth, verified both by the ^{14}C content and the carbon functionality distribution by carbon XANES. Not only is fall-out tritium found in this groundwater, but this groundwater also contains a surprisingly high content of recharge fulvic acid. As already discussed above, the same is found for Gohy-612, whereas other enhanced DOC groundwaters show no enhanced recharge fulvic acid content and no significant tritium concentrations.

Summary

Through a combination of thorough hydrogeological and geochemical understanding it is possible to identify the origin and mobility of fulvic acid in the Gorleben aquifer system. In analogy with previously published approach to groundwater ^{14}C dating, a relatively low ^{14}C concentration is found for recharge fulvic acid originating from conditions prior to nuclear atmospheric testing. By this approach a consistent picture is obtained for the fulvic acid generation process irrespective of the source. Furthermore, a consistent picture is obtained for the results obtained with respect to the groundwater exchange and the fulvic acid stability and mobility. A relatively rapid vertical groundwater exchange is identified with unhindered transport of recharge fulvic acid. Carbon and sulfur XANES provide a broad spectrum of structural information. This information is comparable to that obtained by for example ^{13}C-NMR, however, very small samples are required. A large number of structural entities/functionalities are shown to correlate with the origin of fulvic acid and thus remain unchanged with groundwater residence and change in physico-chemical conditions. Other functionalities (benzo-quinone and redox state of sulfur functional groups) appear to, at least partly, reflect the physico-chemical environment.

Acknowledgements

We are grateful for beamtime allotment by BNL/NSLS. Spectromicroscopic data were collected using the X1-A1 STXM developed by the group of Janos Kirz and Chris Jacobsen at SUNY Stony Brook, with support from the Office of Biological and Environmental Research, U.S. DoE under contract DE-FG02-89ER60858, and from the NSF under grant DBI-9605045. The zone plates were developed by Steve Spector and Chris Jacobsen of Stony Brook and Don Tennant of Lucent technologies Bell Labs with support from the NSF under grant ECS-9510499.

References

Artinger, R., Buckau, G., Geyer, S., Fritz, P., Wolf, M., Kim, J.I., (2000) Characterization of groundwater humic substances: influence of sedimentary organic carbon. *Applied Geochemistry*, 15, 97-116.

Artinger, R., Buckau, G., Kim, J.I., Geyer, S., (1999) Characterization of groundwater humic and fulvic acids of different origin by GPC with UV/Vis and fluorescence detection. *Fresenius J. Anal. Chem.*, 364, 737-745.

Buckau, G., Artinger, R., Fritz, P., Geyer, S., Kim, J.I., Wolf, M., (2000a) Origin and mobility of humic colloids in the Gorleben aquifer. *Appl. Geochem.*, 15, 171-179.

Buckau, G., Artinger, R., Geyer, S., Wolf, M., Fritz, P., Kim, J.I., (2000b) 14C dating of Gorleben groundwater. *Appl. Geochem.*, 15, 583-597.

Buckau, G., Artinger, R., Geyer, S., Wolf, M., Kim, J.I., Fritz, P., (2000c) Groundwater in-situ generation of aquatic humic and fulvic acids and the mineralization of sedimentary organic carbon. *Appl. Geochem.*, 15, 819-832.

Buckau, G., Artinger, R., Kim, J.I., Geyer, S., Fritz, P., Wolf, M., Frenzel, B., (2000d) Development of climatic and vegetation conditions and the geochemical and isotopic composition in the Franconian Albvorland aquifer system. *Appl. Geochem.*(15), 1191-1201.

Buckau, G., Wolf, M., Geyer, S., Artinger, R., Kim, J.I., (2003) Origin and mobility of aquatic humic substances from wetland recharge in the Gorleben aquifer system. in: Humic Substances in Performance Assessment of Nuclear Waste Disposal: Actinide and Iodine Migration in the Far-Field (First Technical Progress Report), ed. G. Buckau, Report FZKA 6800, Research Center Karlsruhe, Karlsruhe (Germany).

Kim, J.I., Artinger, R., Buckau, G., Kardinal, C., Geyer, S., Wolf, M., Halder, H., Fritz, P., (1995) Grundwasserdatierung mittels 14C-Bestimmungen an gelösten Humin- und Fulvinsäuren(Abschlußbericht). Institut für Radiochemie der Technischen Universität München, München (Germany).

Schäfer T., Buckau G., Artinger R., Kim J.I., Geyer S., Bleam W. F., Wirick S. and Jacobsen C. "Origin and Mobility of Fulvic Acids in the Gorleben Aquifer system: Implications from Isotopic Data and Carbon/Sulfur XANES", *Organic Geochemistry*, submitted.

Annex 2

Migration Case Gorleben

Buckau G., Artinger R. and Kim J.I.

Institut für Nukleare Entsorgung, Forschungszentrum Karlsruhe GmbH, Germany

Migration Case Gorleben

Buckau G., Artinger R. and Kim J.I.

Institut für Nukleare Entsorgung, Forschungszentrum Karlsruhe GmbH, Germany

Abstract

A radionuclide migration path is defined in the Gorleben aquifer system for demonstration and visualization of humic colloid mediated radionuclide migration. The scenario is release of radionuclides at the top of the salt dome, within the so-called ring-wall (at about 250 meters depth). The contaminated brine raises to 200 m depth by thermal motion. The migration case consists of vertical groundwater movement from this depth to the freshwater region at about 50 meters depth. The transport time for the vertical groundwater movement is set to 1,000 years. The document contains the definition of this migration path with respect to the hydrological and geochemical conditions as well as the rationale.

1. Introduction

For the safety assessment of a nuclear waste repository, consequences of the release of long-lived radionuclides to the surrounding/overlaying aquatic system, i.e. the far-field, needs to be investigated. Humic colloids are considered one of the most important vehicles for mobilizing multivalent radionuclides in aquatic systems. For the purpose of applying most recent advances in predictive modeling of the impact of humic colloid mediated radionuclide transport, a migration case is defined for the Gorleben aquifer system. An area is selected on top of the Gorleben salt-dome within the so called “ring-wall”. For this purpose, information is used with respect to the hydrological situation and the origin, stability and mobility of humic colloids. Various source documents and the geochemical Gorleben data-base have been used (see references).

2. Scope

The scope of the document is to define a migration path in the Gorleben aquifer system for evaluation of the influence of humic substances on the migration of radionuclides relevant for long-term safety of radioactive waste disposal. The selected migration path is considered probable and relevant for the possible migration of radionuclides from the top of the Gorleben salt-dome to the upper fresh-water aquifer. Selection of this migration path, however, does not reflect the probability of radionuclide release from the host formation, i.e. the salt dome, to different parts of the surrounding aquifer system. Thus, this document and the associated forthcoming evaluation of radionuclide migration along the selected flow-path is not a safety assessment for the Gorleben salt-dome as a possible candidate for a high-level waste repository.

3. The Gorleben site

The Gorleben salt dome is situated in the north German plain (Lower Saxony) and extends from south-west to north-east (Fig. 1). The salt dome reaches up to less than 50 meters below ground with some parts of its so-called “ring-wall“, whereas its center plateau is at approximately 250 meters depth. Due to erosion during the Elster glaciation, part of the cap-rock has been removed, resulting in a channel filled with glacial sand deposits. Consequently this “Gorleben channel“ has a relative high groundwater permeability. Due to direct contact with the rock salt it contains salt brines. Above and around the salt dome various layers of sedimentary rock have been deposited. The sediments contain local Miocene brown coal and Pleistocene peat deposits. Above the salt dome these layers are disturbed due to up-lift and by glacial events, some layers are missing and others are reworked and intermixed. More detailed information on the Gorleben salt dome and the surrounding aquifer system can be found in (BGR 1991). The hydrological situation above the salt dome is not understood in detail (BfS 1990). One may expect recharge water to enter from the south-east and run across towards north-west. Small amounts of ^{3}H is found in groundwater samples down to a depth of about 140 m (Suckow 1993, Kim et al. 1995, and Buckau et al. 2000b) High concentrations of

^{14}C are found in deep groundwater in the area south-west of the salt-dome with overlaying waters with a lower ^{14}C concentration. These high ^{14}C groundwaters are expected to reflect wet-land recharge taking place until about 250 years ago (Buckau et al. 2003). The ring-wall may to some extent hinder groundwater from entering larger depth. However, it is interrupted over large distance towards the south-eastern side of the salt dome. Unperturbed sediment layers of low groundwater permeability may also retard exchange of groundwater from different depth. In the "Gorleben Channel" a complex poorly understood brine flow-system is found.

4. The Migration Case area

4.1 Location

An area above the center plateau of the Gorleben salt dome is selected, within the so called "ring-wall" on the border to and west of the "Gorleben channel" (Fig. 1). The investigated area extends over approximately 1.5 x 2 km with a large number of drillholes and corresponding groundwater sampling locations in the center of the investigation area (Fig. 2). At the most dense cluster of drillholes, five wells are within 50 meters surface distance.

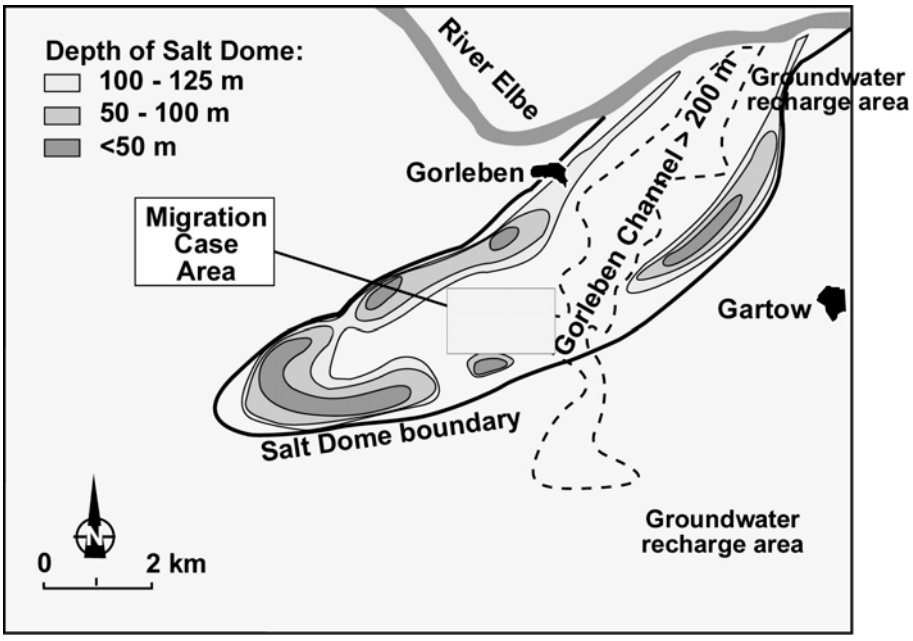

Fig. 1: The Gorleben site and the location of the Migration Case (modified from Buckau et al. 2000a).

4.2 Sediment permeability distribution

The vertical permeability distribution of drill cores from the investigation area are summarized in Fig. 3 (data from BGR 1995). At a very narrow scale layers of different permeability show some consistency. The six drill cores from the central area which are at a maximum distance of about 50 meters are comparable. However, moving only some 50

meters to the south (Gohy-2226), to the north (Gohy-2225) or to the north-east (Gohy-2224) the vertical permeability distribution is distinctly different. Over the investigation area, i.e. a maximum distance of approximately 2 km, the permeability distribution varies considerably in the upper 100 meters. The same is true for depths below 150 meters. Within the depth range of approximately 100 - 150 meters, in general, low permeabilities are found. However, also here the vertical distribution of low permeability sediments varies and several sediments also show permeabilities $>10^{-6}$ m/s. Such a permeability distribution within sediments is not expected to provide for an effective barrier against vertical groundwater flow. As seen below, this is verified from data on groundwater composition, tritium distribution and ^{14}C age.

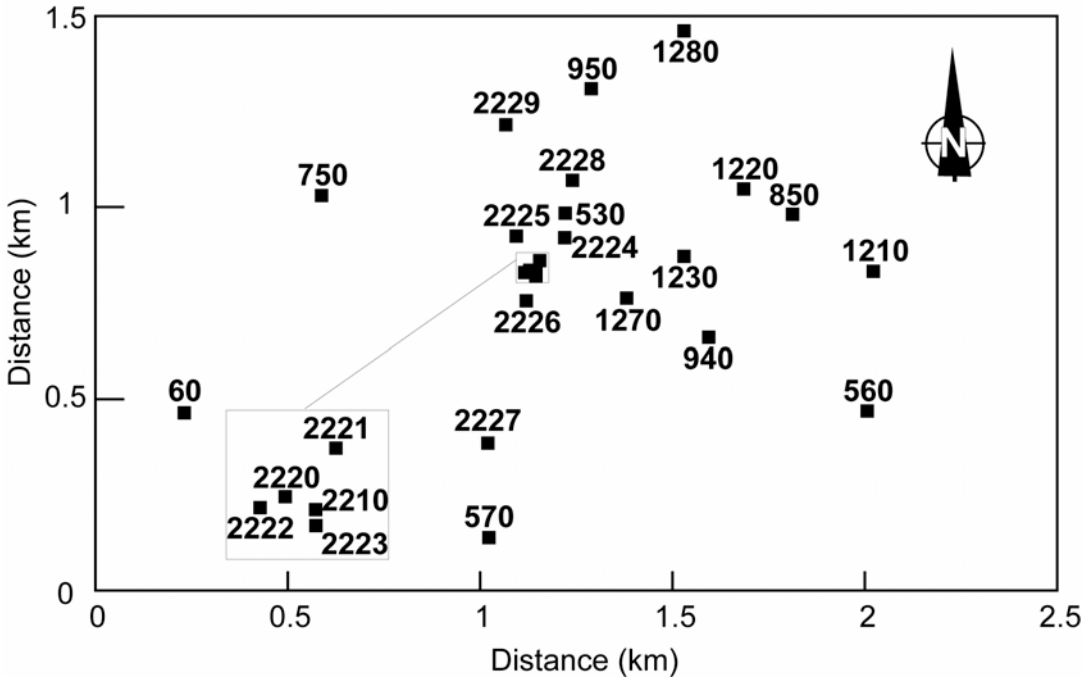

Fig. 2: Location of drill-holes and wells in the region of the Migration Case (from Buckau et al. 2000a).

4.3 Hydrological situation

The hydrological situation is investigated with emphasis to the vertical groundwater exchange. Based on the distribution of chloride and tritium and ^{14}C age, the extensive vertical groundwater exchange is shown. The velocity of groundwater exchange is estimated from ^{14}C age and the tritium concentration distribution in combination with groundwater chloride concentrations.

<Chloride distribution>

In Fig. 4, the chloride concentration is shown for different groundwater sampling depth. It has two extremes, namely saturated brines below some 230 meters; and low salinity from recharge down to some 50 meters depth. Between these two extremes, for one group of groundwaters, the logarithm of the chloride concentration shows approximately a linear

increase with decreasing depth. This is typical for exponential vertical dispersive mixing, i.e. no effective separation in different groundwater layers. Another group of groundwaters show a chloride to depth signature above this exponential mixing line. The high chloride to depth signature appears to be the result of influx of salinated groundwater from dissolution of the salt dome, including brines originating from the Gorleben channel. These results show that no effective barriers exist separating groundwater into different groundwater layers.

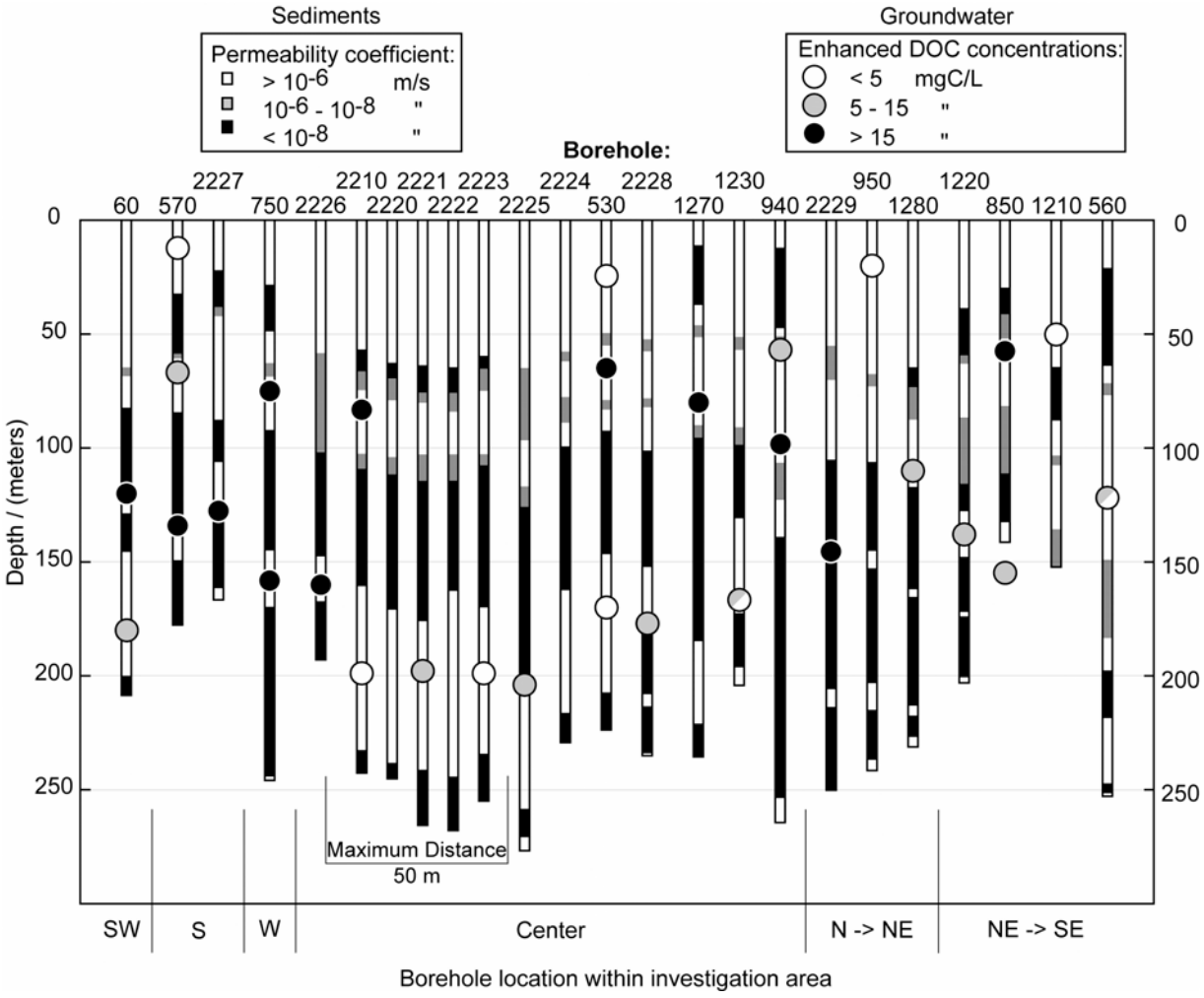

Fig. 3: Permeability distribution of sediments in the region of the Migration Case (from Buckau et al. 2000a).

The regional distribution of groundwaters with high and low chloride to depth signatures at depths between 50 and 150 meters is shown in Fig. 5. In this depth range, low chloride to depth signatures reaching down to high depth are found especially close to the ring-wall. The high chloride to depth signatures at low depth are found especially over the central area from above the Gorleben channel and towards the west but also for Gohy-1281 in the north. This indicates a flow of groundwater where relatively fresh water is sinking especially at the sides of the ring-wall. Contrary to this, in the center of the area, high chloride to depth signatures are found. This appears to be the result of inflow of highly saline water from the Gorleben channel and/or vertical uplift of salt water. Another alternative would be diffusion of salt under relatively stagnant conditions. This, however, appears unlikely in this area with highly

reworked sediments and especially the low groundwater ages of Gohy-851 and -2211 with their high chloride to depth signatures.

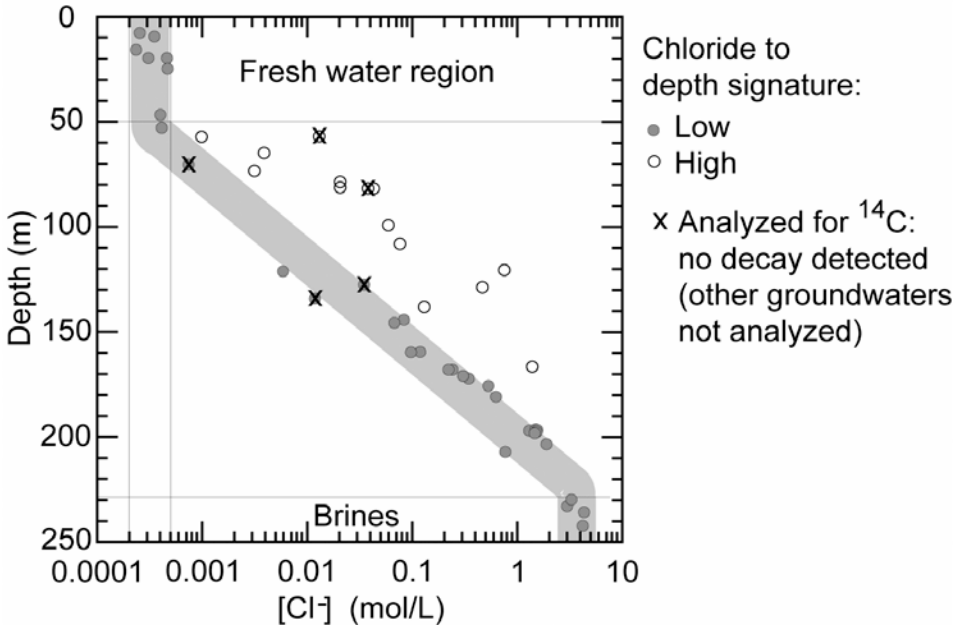

Fig. 4: Chloride concentration at different depths of groundwaters of the Migration Case (from Buckau et al. 2000a).

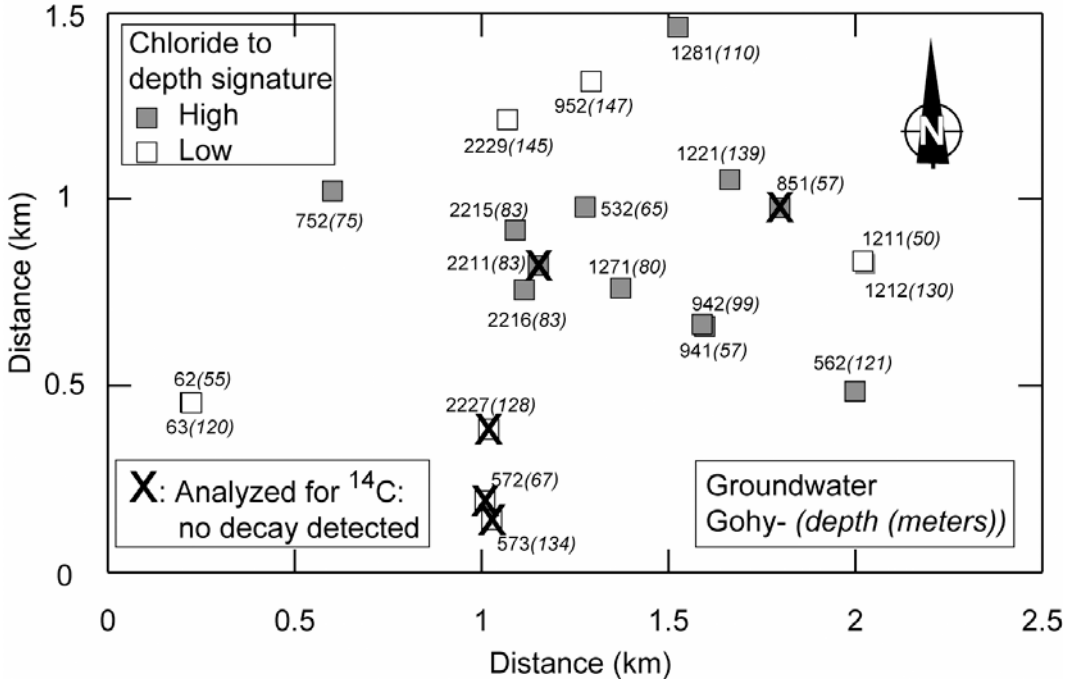

Fig. 5: Regional distribution of chloride concentration signatures between 50 and 150 m depth (from Buckau et al. 2000a).

Below 230 meters depth, vertical groundwater exchange cannot be identified by the chloride concentration as only saturated brines are found. In the upper 50 meters basically constant chloride concentrations are found reflecting groundwater recharge conditions. Slightly below

50 meters depth groundwaters with high chloride to depth signatures are found. One extreme example is Gohy-851 at 57 meters depth with approximately one and a half orders of magnitude higher chloride concentration than the recharge groundwaters, including Gohy-62 and Gohy-1211 at 55 and 50 meters depth, respectively. Gohy-851 appears to be situated under a sediment of low permeability (Fig. 3) and depending on the flow direction upwards mixing may occur at different places. Considering, however, that no significantly enhanced chloride concentrations are found in the upper 50 meters one may assume that the groundwater movement in these upper 50 meters is such that groundwater components introduced from below are rapidly diluted and dispersed.

<Tritium Distribution>

Tritium is mainly found in the upper 50 meters of the groundwater. In analogy with the chloride depth-concentration profile, however, a vertical exponential mixing of tritium can be followed down to a depth of about 140 meters (Fig. 6). This shows that vertical exponential mixing also occurs in the upper part of the groundwater, including the fresh water region where the constant chloride concentration reflects recharge conditions. It furthermore shows that the vertical groundwater mixing occurs relatively rapid (cf. also below).

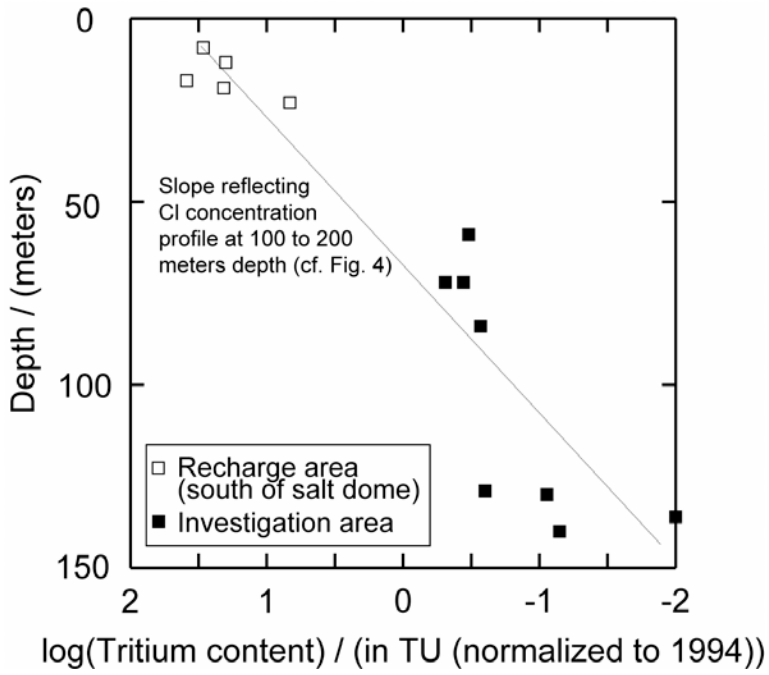

Fig. 6: Tritium concentration with depth for groundwaters in the region of the Migration Case and recharge groundwaters from the area south of the salt dome.

<^{14}C age distribution>

Down to a depth of about 140 meters, no significant decay of ^{14}C of dissolved inorganic carbon (DIC) can be detected (Buckau et al. 2000b). ^{14}C age of DIC in the brines is hampered by not fully understood chemical reactions and thus dating is not reliable (Buckau et al. 2003). ^{14}C dating of fulvic acid reveals that the fulvic acid from recharge is found in the

saturated brines with ^{14}C concentrations not affected by decay (Schäfer et al., Annex 1). This supports the rapid vertical groundwater exchange/intermixing as discussed above.

In summary, sediments in the migration case area do not have sufficiently large and homogeneous regions of low permeability to prevent rapid vertical groundwater exchange. The chloride concentration distribution shows that groundwaters also are subject to vertical exponential exchange as well as up-lift in the central part of the study area. 40 years after atmospheric nuclear testing culminated, exponential mixing of tritium can be traced down to about 140 meters depth. The same exponential mixing ratio is found for chloride down to the vicinity of the salt dome. Superimposed over this exponential mixing for the lowest chloride concentration to depth ratios, also up-lift of salinated groundwater occurs in the central part of the area. Thus, the overall vertical groundwater transport towards the freshwater horizon is not known.

4.4 Humic colloid generation and distribution

In the Gorleben aquifer system, abundant in-situ generation of dissolved organic carbon (DOC) results in highly elevated humic colloid concentrations. This process is related to the microbiologically mediated mineralization of sedimentary organic carbon (SOC) with sulfate as a dominating oxidizing agent (Buckau 2000c). One part of SOC is oxidized to dissolve inorganic carbon (DIC) and another part is released as DOC. In Fig. 7, the DOC concentrations in groundwaters from the present investigation area are shown against the sampling depth. Down to 27 meters, DOC concentrations of 1 mgC/L or less are found and at 50 meters 2 mgC/L. These values reflect typical DOC concentrations in young Gorleben recharge groundwaters (Artinger et al. 2000). Below 50 meters down to about 200 meters strongly enhanced DOC concentrations are found resulting from in-situ generation of DOC via mineralization of SOC. In the brines below 200 meters moderate to low DOC concentrations are found. In these brines and in recharge groundwaters DOC is dominated by fulvic acid. In contrary to this, in enhanced DOC groundwaters DOC is dominated by humic acid (Artinger et al. 2000).

The humic and fulvic acids generated in the enhanced DOC depth range are not found in the saturated brines. The reason is that they are less hydrophilic than the recharge fulvic acids (Schäfer at al., Annex 1). This shows that humic colloid mediated radionuclide transport in the saturated brines will only be effected by fulvic acid. Once entering into groundwater of lower salt content, the high concentrations of humic and fulvic acid from the in-situ generation is also participating in the radionuclide transport.

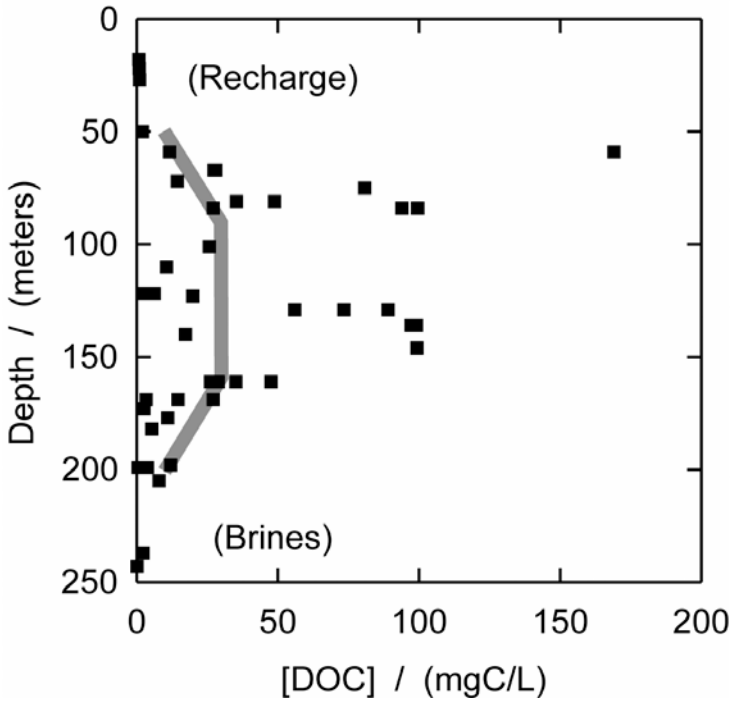

Fig. 7: DOC (dissolved organic carbon) concentration at different depths of groundwaters of the Migration Case (from Buckau et al. 2000c). The shaded line shows the values to be used for initial actinide transport calculations.

In Fig. 3, DOC concentration ranges at different groundwater sampling locations are shown. In the area where several sampling positions are within some 50 meters surface distance (magnified in Fig. 2) DOC values are available for three samples (Gohy-2210, -2221, and -2223), and some 100 meters further north Gohy-2225. All these samples from approximately 200 meters depth originate from one water bearing layer. Although the distance between the sampling locations is very low the DOC concentrations vary between < 5 mgC/L in Gohy-2211 and -2223, and 12 and 7.9 mgC/L in Gohy-2221 and -2225, respectively. This shows that the humic colloid generation has a very strong local variation and through dilution and dispersion, decreases rapidly away from the source of generation.

In summary, enhanced concentrations of DOC, and thus humic colloids, are found at depths below 50 m. These enhanced DOC concentrations are the result of microbiologically mediated mineralization of SOC. There are strong local variations in the magnitude of this process. In the salt saturated brines only fulvic acid from recharge is found.

5. Scenario

Brines containing dissolved actinide ions are released at the top of the salt dome, i.e. at the bottom of the aquifer system in the case study area (at approximately 240 m depth). This actinide contaminated brine is expected to have a higher temperature than the groundwater. Therefore, the contaminated brine will move upwards. Due to equilibration of temperature and differences in density, this upwards movement is set to cease at 200 m depth. This is the starting point for the migration case path. Once the groundwater has reached the fresh water

region (upper 50 m), the water may be attractive for extraction and usage by future generations. This defines the end point of the migration case path.

6. Definition of the Migration Case

<Migration path>

The migration path is defined by vertical groundwater movement within the case study area. In the central part of the case study area there is a groundwater up-lift movement. Therefore, the simplest approach is an upward piston flow. However, two major problems occur, namely (i) the actual main groundwater flow direction is not well known; and (ii) considerable groundwater mixing occurs. Therefore, the piston flow approach is not necessarily correct. For the purpose of simplicity, however, a vertical uplift piston flow is used. A further consequence of such a simplification is that dispersion due to exponential mixing between different parts of the groundwater body is not accounted for. In addition to this, the probably high horizontal groundwater flow velocity in fresh water region, and as a consequence high degree of dilution, is not accounted for.

<Source term>

The concentrations of actinide ions are estimated over their solubility in the humic colloid containing brines at 200 m depth. The scope of the present exercise is not to achieve dose rates to recipients but to evaluate the transport of actinide ions relative to a starting value. Therefore, the actinide concentrations in the source term are not a critical parameter for this purpose.

<Groundwater transport time>

Based on the exponential mixing of fall-out tritium that can be traced down to a depth of about 140 m, no significant ^{14}C decay in dissolved inorganic carbon at this depth and no significant ^{14}C decay of recharge fulvic acid in the saturated brinaes at 250 m depth, a groundwater transport time along the migration path of 1,000 years is chosen.

7. Geochemical conditions along the migration path

A multitude of geochemical condition may be found along the migration path. For the purpose of geochemical modeling of the actinide ions, the basic parameters are humic colloid concentration, pH and redox-potential. The distribution of humic colloid concentrations is discussed above (cf. Fig. 7).

<pH and Eh>

In Figs. 8 and 9, distributions of pH and redoxpotential with depth are shown. pH follows a relatively stable trend with basically linear increase in values from around 6.5 at 200 m depth to about 8 around 50 m depth. In Fig. 9, the mean values of the redoxpotential are shown. The original Eh values show considerable scatter. Examples are Gohy-572, 573 and 2227, with 40±22, -6±39 and –24±82, respectively. Beyond such scatter in data, however, Gohy-753, -

943, -1272 and –2225, at depth between 159 and 204 m, show very negative Eh values relative to the depth compared to the other groundwaters (Fig. 9). The reasons for these low Eh values are not yet understood. For the purpose of actinide transport calculations, pH and Eh values for different depth are chosen as indicated by shaded lines in Figs. 8 and 9.

<Chemical composition>
Depending on the scope of transport calculations and inclusion of different chemical reactions, the concentrations of different potential ligands will be evaluated from the data base, as requested.

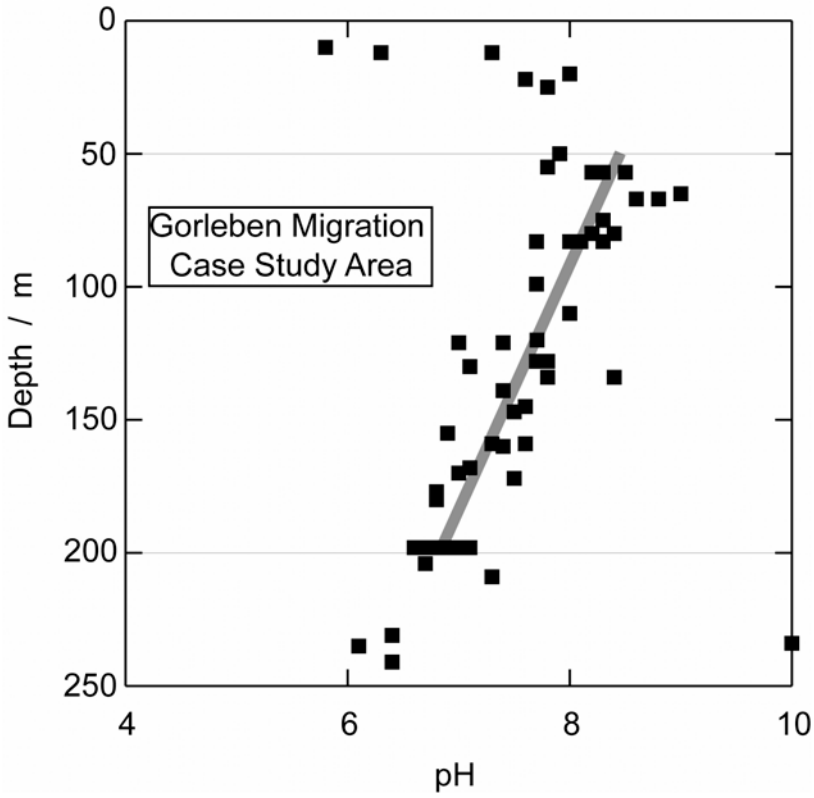

Fig. 8: Distribution of pH values in groundwater of the migration case study area. The shaded line shows the values to be used for initial actinide transport calculations.

9. The Migration Case

The migration case is defined as follows:

- The migration path is 150 m long with 1,000 years transport time for the groundwater in piston-flow. It starts at 200 m depth and stops at 50 m depth.

- Along the path, pH and Eh are as shown in Figs. 8 and 9.

- The humic colloid concentration is shown in Fig. 7. It is 10 mgC/L at the starting point; increases linearly with flow distance to 30 mgC/L at 40 m flow distance; remains 30 mgC/L for the next 70 m flow distance; decreases linearly to 10 mgC/L at the end of the flow-path.

- The concentrations of potential ligands will be deduced from the data base upon request.

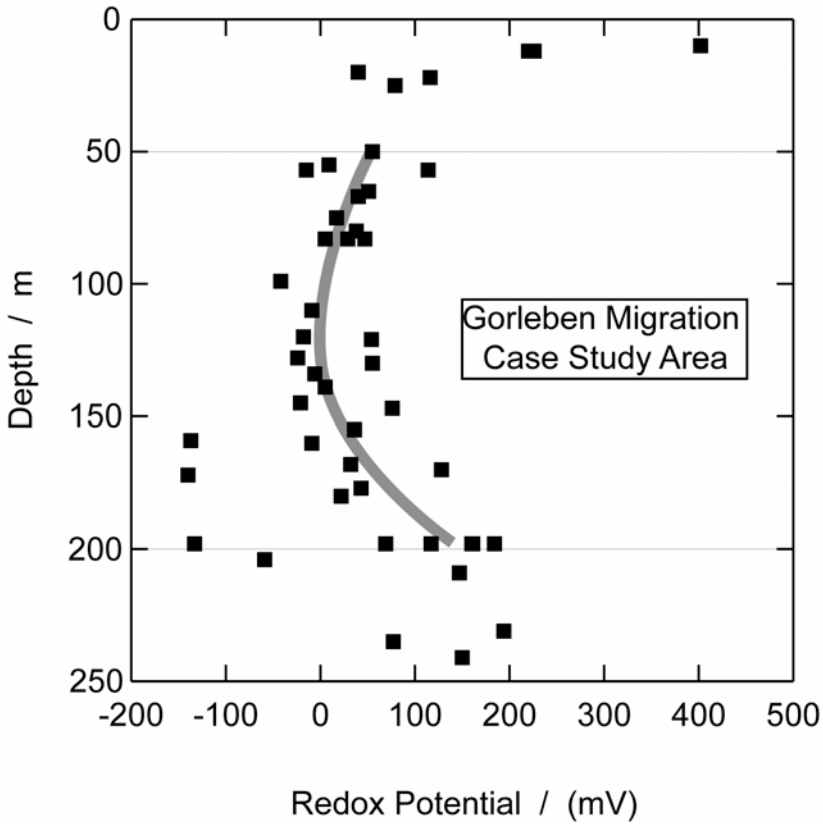

Fig. 9: Distribution of Eh values in groundwater of the migration case study area. The shaded line shows the values to be used for initial actinide transport calculations.

References

Artinger R., Buckau G., Geyer S., Wolf M., Kim J.I. and Fritz P. (2000) "Characterization of Groundwater Humic Substances: Influence of Sedimentary Organic Carbon", *Applied Geochemistry*, **15/1**, 97-116.

Buckau G., Artinger R., Fritz P., Geyer S., Kim J.I. and Wolf M. (2000a) "Origin and Mobility of Humic Colloids in the Gorleben Aquifer System", *Applied Geochemistry*, **15/2**, 171-9.

Buckau G., Artinger R., Geyer S., Wolf M., Kim J.I. and Fritz P. (2000b) "^{14}C Dating of Gorleben Groundwater", *Applied Geochemistry*, **15/5**, 583-97.

Buckau G., Artinger R., Geyer S., Wolf M., Kim J.I. and Fritz P. (2000c) "Groundwater in-situ Generation of Aquatic Humic and Fulvic Acids and the Mineralization of Sedimentary Organic Carbon", *Applied Geochemistry*, **15/6**, 819-32.

Buckau G., Wolf M., Geyer S., Artinger R. and Kim J.I. (2003) “Origin and Mobility of Aquatic Humic Substances from Wetland Recharge in the Gorleben Aquifer System “, in: Humic Substances in Performance Assessment of Nuclear Waste Disposal: Actinide and Iodine Migration in the Far-Field (First Technical Progress Report), ed. G. Buckau, Report FZKA 6800, Research Center Karlsruhe.

Kim J.I., Artinger R., Buckau G., Kardinal Ch., Geyer S., Wolf M., Halder H. and Fritz P. (1995) “Grundwasserdatierung mittels ^{14}C-Bestimmungen an gelösten Humin- und Fulvinsäuren (Abschlußbericht)“, Report RCM 00895, May 1995, Technical University Munich.

Kim J.I. and Buckau G. (1990) “Huminstoffuntersuchungen an Gorleben-Grundwässern“, Report: RCM 01590, TU München.

BfS/DB Data base of (Bundesamt für Strahlenschutz / Federal Office for Radiation Protection) for the Gorleben site.

Suckow A. (1993) Isotopenhydrologische und Edelgaspaläotemperatur-Untersuchungen im Deckgebirge über dem Salzstock Gorleben, Dissertation, Universität Heidelberg.

BGR (Bundesanstalt für Geowissenschaften und Rohstoffe) (1991) Übertägige geowissenschaftliche Erkundung des Standortes Gorleben, Report Zusammenfassender Bericht Stand 01.01.1990, Hannover.

BGR (Bundesanstalt für Geowissenschaften und Rohstoffe) (1995) Standortbeschreibung Gorleben-Süd, Hydrologie des Deckgebirges, Kentnisstand 1994, Report: BGR Archive-No. 112 693, Hannover.

BfS (Bundesamt für Strahlenschutz / Federal Office for Radiation Protection) (1990) Fortschreibung des zusammenfassenden Zwischenberichtes über bisherige Ergebnisse der Standortuntersuchung Gorleben vom Mai 1983, Bundesamt für Strahlenschutz BfS, ET-2/90, Salzgitter.

Annex 3

Approach for Physico-Chemical Interpretation of An(III) and An(VI) Humate Complexation.

G. Buckau

Institut für Nukleare Entsorgung, Rorschungszentrum Karlsruhe,
P.O. Box 3640, 76021 Karlsruhe, Germany

Approach for Physico-Chemical Interpretation of An(III) and An(VI) Humate Complexation.

G. Buckau
Institut für Nukleare Entsorgung, Rorschungszentrum Karlsruhe, P.O. Box 3640, 76021 Karlsruhe, Germany

Abstract

The humic acid complexation of trivalent and hexavalent actinide ions (Am(III), Cm(III) and U(VI)) is discussed. The complexation reaction is written with in the frequently argued for simple way with the complexation constant as the complex concentration divided by the product of the free metal ion and the free humate ligand concentrations. The concentrations of free and complexed metal ions is trivial, the problem in interpretation of the reaction is the nature of the humic acid ligand and description of this concentration. Analysis shows that the humate ligand concentration can be described by the number concentration of reactive (ionized) humic acid molecules. This concentration is given by the total number concentration of humic acid molecules, reduced by one unit for protonation of the average number of proton exchanging groups per average molecule and furthermore reduced by one unit per complex formed. This implies that individual molecules are inactivated for complexation by protonation of its proton exchanging groups. Furthermore, a reactive/ionized humic acid molecule becomes inactivated by the complexation with one metal ion. The study provides a physico-chemical explanation for the frequently used simple approach with the metal ion humic acid complexation described by an experimentally determined effective humate ligand concentration (or also binding or complexation capacity) and one associated stability constant. It thus provides the justification for application of this frequently used simple approach.

1. Introduction

As well recognized, humic and fulvic acids are not substances with molecules of a sole composition and molecular mass but a mixture of molecules with a distribution of mass and functionalities. Nevertheless, the metal ion complexation of humic and fulvic acids shows a surprisingly consistent and systematic behavior. This shows that the functional behavior towards metal ion complexation of these substances is relatively well defined and falls in a narrow range. For strongly complexing metal ions, the complexation may be described as follows.

- If a humic acid is titrated with the metal ion, progressive complexation occurs. Approaching a certain complex concentration/amount, the complex formation approaches a plateau value. The complexation may be described by a simple interaction isotherm with one interaction constant and one ligand saturation value. The observation can be summarized as a relatively simple complexation behavior with a surprisingly narrow distribution in the complexation properties.

- As the plateau value is approached, humic acid flocculates whereas fulvic acid shows strong increase in light scattering. This behavior is directly comparable with protonation. In both cases the complex shows less hydrophilic properties and can be isolated by sorption of the XAD-8 resin (used as standard isolation method). Sorption on other surfaces is also observed. The observation shows that the hydrophilic character and the charge repulsion of humic and fulvic acids is diminished with protonation as well as with complexation.

- With increasing protonation or ionic strength, the plateau value is decreasing. The problem encountered, is that the plateau value corresponding to the total humate ligand concentration does not correlate with the total concentration of proton exchanging groups in a simple fashion. Similarly, the decrease in the plateau value does not strictly follow the decrease in the degree of ionization of humic and fulvic acid proton exchanging functional groups.

This last observation is not surprising. Strictly speaking the straightforward use of the degree of ionization for proton exchanging functional groups is only allowed where this corresponds to one complex per ionized functional group and one functional group per reactive entity/molecule. In the case of humic and fulvic acids, there are more than one functional groups per molecule/reactive entity. Combination of the observation that the complexation follows a simple 1:1 interaction isotherm and the systematic decrease in the concentration of reactive entities/molecules with protonation (and to a lesser extent ionic strength) shows that the key questions are:

(i) how does the number concentration of reactive entities/molecules decrease with the progress in protonation, and
(ii) what is the concentration of reactive entities at a given progress of protonation (including full ionization).

These questions are the basis for the present paper where the interaction of one humic acid (Gohy-573(HA)) in one ionic medium (0.1 M $NaClO_4$) with the trivalent Am^{3+} and Cm^{3+} actinide ions, and the hexavalent uranyl ion (UO_2^{2+}).The latter has a comparable charge in the equatorial plane as the homogeneous charge of the Am^{3+} and Cm^{3+} ions and very comparable complexation behavior is observed.

The paper does not go into questions related to the potential for a weaker type of interaction after flocculation of humic acid, nor the potential for a stronger interaction at very low metal ion concentrations. It also does not make strong reference to the observed comparably slow kinetics of the metal ion complexation, especially rearrangements shifting the inventory of complexed metal ions to a slower dissociation mode, and the reason for the comparably slow dissociation with at least two kinetic components. The fundamental, and surprisingly simple and systematic complexation properties deduced, however, opens up for further discussion and specifically tailored investigations.

The main aim of the paper is to show that very complicated approaches frequently proposed, published and used are mainly based on false interpretation of the ligand function (specifically using the concentration of ionized groups instead of the concentration of reactive entities/molecules). In some descriptions reference is made to a polyelectrolyte character, hardly to be expected for average humic and fulvic acid molecules with around 3.5 proton exchanging groups (see below). Other approaches make use of a sequence of complexation constants, more recent models with such sequences over molecular mass distributions. This feeds a view of humic and fulvic acids as being an excessively complicated system or even beyond the reach of a systematic description. The key point about this paper is a different and very straightforward simple interpretation of existing published data. Most of the observations discussed are common knowledge in the concerned community. Consequently, there is a deliberate very restricted use of references. The present paper also reflects a progressive understanding of the mass distribution of humic and fulvic acids applying modern mass spectroscopic techniques in recent years, changing the entire understanding of humic and fulvic acid systems and functions. Last but not least, the present paper is the outcome of discussion with a large number of colleagues in the field. This is reflected in the acknowledgements.

2. Elemental composition and oxygen functional group content

Below a brief discussion of elemental composition and functional group content is given. The discussion is focused on numbers and properties important for the purpose of this document. For more detailed information on distribution of the elemental compositions, including hetero-atoms and different origins, as well as different functional groups, the literature needs to be consulted. The elemental composition of humic substances varies within limits. An overall elemental composition is well described by $CO_{0.5}H$, omitting minor contributions of sulfur and nitrogen. Interesting enough, this overall formula is also obtained by removing one half water molecule per carbon in carbohydrates. The carbon has a formal oxidation state of around zero.

Examples of the content of the most abundant oxygen containing proton exchanging groups is given in Table 1 (Kim et al. 1990, Schmeide et al. 1998). The amounts of proton exchanging functional groups obtained by different operational methods cannot be allocated to specific groups *per se*. Nevertheless, certain types of functional groups are frequently reported by the use of these operational methods. The Gohy-573(HA) at the bottom of this table is the one for which complexation data are discussed in this paper. The numbers should be compared also to the "total proton exchange capacity" by potentiometric pH titration of 6.40 meq/g for Gohy-573(HA) (cf. Fig. 1). The latter refers to the assumption that no further deprotonation occurs for increasing pH beyond about 10.25. There is an excellent agreement between the Ba exchange capacity at high pH and the total proton exchange capacity by potentiometric pH titration. The latter number is only about 3 % lower than the former one. This is in the order of experimental uncertainty. The numbers show that the total proton exchange capacity can be correctly evaluated whereas allocation of parts of this inventory to different types of groups is questionable.

Table 1: Proton exchange capacities by different operational methods with groups frequently reported to be associated with these methods: "total" (Ba exchange capacity under alkaline conditions), and "carboxylic group content" by "Ca-Acetate" (Ca exchange capacity in acetate buffer medium), "radiometric" (attachment of ^{14}C labeled methyl groups via diazomethane), and "potentiometric pH titration" (potentiometric pH titration where the proton exchanging groups are quantified as those protonated at and below titration curve turning point slightly below pH of 8).

Humic Acid	Ba-Exchange ("Total")	Ca-Exchange ("Carboxylic")	Radiometric ("Carboxylic")	Pot. pH Titration ("Carboxylic")
Aldrich(HA)[1)]				
meq/g	7.12	4.41	3.9	5.06
% of "total"	(100)	62	55	71
Aldrich(HA)[2)]				
meq/g	7.06	4.80	-	5.43
% of "total"	(100)	68	-	77
Gohy-573(HA)[2)]				
meq/g	6.61	4.75	-	5.38
% of "total"	(100)	72		81
	Average (%):	67 ± 5	55	76 ± 5

1) Schmeide et al. 1998; 2) Kim et al. 1990

The total exchange capacity for two batches of Aldrich humic acid (Aldrich(HA)) independently purified by two different groups are basically indistinguishable. The total proton exchange capacity is about 7 % higher than for the Gohy-573(HA). This shows that careful handling of humic acid leads to high reproducibility for the functional group content and that there are differences between humic acids from different sources. More important is that the presumably contents of carboxylic groups deduced from different operational methods deviate from each other. This is obvious from Fig. 1, showing that one cannot identify a sharp distinction between different proton exchanging groups along with progressive protonation. This should be kept in mind where the proton exchange behavior is represented by a distinct

number of “acidic groups” from fitting the curve in Fig. 1. It is especially surprising, when pKa values are allocated to a limited number of “proton exchanging groups” including in the lower pH range. Potentiometric titration does not allow going much further into the acidic range due to lowering of the electrode response to proton ion concentration/activity and thus the protonation endpoint cannot be determined.

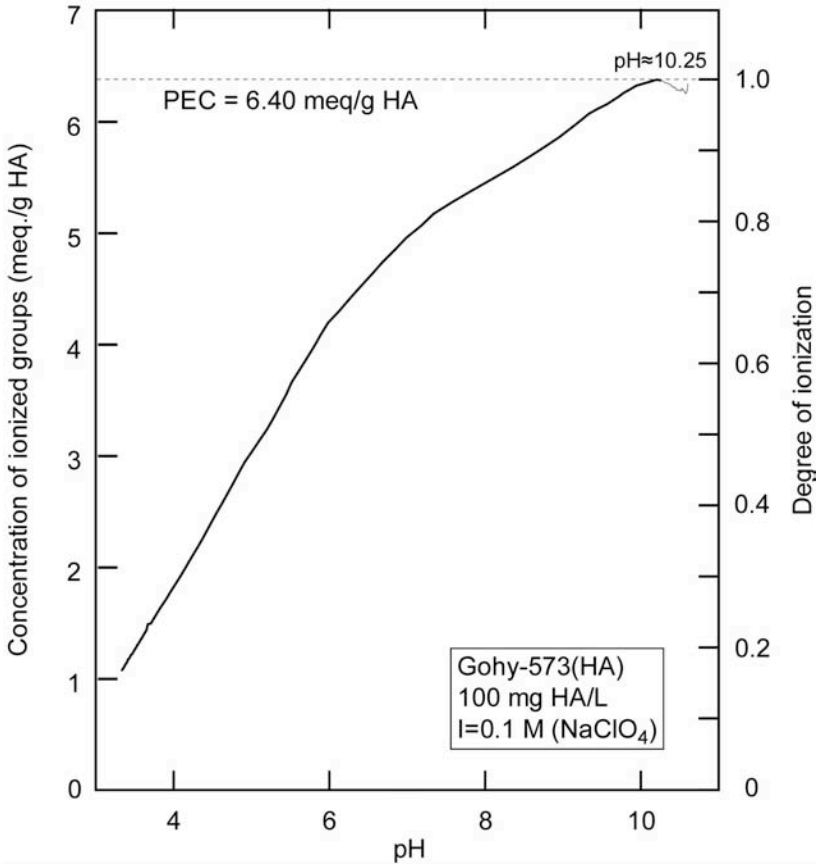

Fig. 1: Potentiometric pH titration of the humic acid Gohy-573(HA).

3. Mass distribution

The mass distribution of Aldrich humic acid and humic and fulvic acids from the groundwater Gohy-573 are shown in Table 2. The concentration of molecules in solution if no association occurs is given by the number average distribution maximum (M_n). It should be noticed that meanwhile the mass distribution as given in Table 2 represent numbers that are slowly becoming generally accepted. This is important because of the previous perception of humic and fulvic acid molecules as having much higher mass distribution numbers from misinterpretation of size measurements by gel permeation/size exclusion chromatography and field flow fractionation methods (Wolf et al. 2001). An important number for the metal ion complexation that can be deduced is the average number of proton exchanging functional groups per average molecule. For Gohy-573(HA), with 6.61 meq/g of proton exchanging functional groups (cf. Table 1) and an number average molecular mass of 521 (cf. Table 2), the average number of proton exchanging functional groups per average molecule becomes 3.44.

Table 2: Calculated distribution parameters of the distributions M_{conc} versus mass (for details, see Wolf et al., Annex 8).

Humic substance	Mass range	M_n	M_w	M_w/M_n
	(Da)	(Da)	(Da)	
Gohy-573 FA	150 – 3000 [5000]	428 [428]	609 [613]	1.42 [143]
Gohy-573 HA	150 – 3000 [5000]	521 [523]	752 [759]	1.44 [1.45]
Aldrich HA	150 – 3000 [5000]	445 [446]	626 [627]	1.40 [1.41]

Under the assumption, that the proton exchanging functional group content is equally distributed with mass for molecules of different mass, about one proton exchanging group per molecule is found at the lower end of the mass distribution. At the upper end of the mass distribution, the corresponding number is less than 20. Because the O/C ratio is decreasing with increasing molecular mass, the number of proton exchanging functional groups on the molecules with higher mass may be expected to be lower (Plancque et al. 2001). Given the relatively narrow mass distribution and the above discussed uncertainty in the allocation of different nature of the of the proton exchanging groups, the most important number to carry over for the further discussion, however, is the around 3.4 proton exchanging groups per average molecule.

4. Binding capacity, effective humate ligand concentration (EHLC)

The plateau/saturation value for complexation is frequently called the binding capacity or complexation capacity. It represents the effective humate ligand concentration (EHLC) under given physico-chemical conditions. As already mentioned above, application of this EHLC results in a simple and consistent description of the complexation reaction. In this section the relation between the EHLC and the nature of humic and fulvic acid is discussed.

4.1 Impact of pH and ionic strength

As already mentioned in the introduction, titration of humic or fulvic acid with a complexing metal ion results in a progressive increase in the amount of metal humate complex until a plateau value is reached. Approaching this plateau/saturation value, flocculation of humic acid takes place. One example is shown in Fig. 2, where the dissolved and flocculated Am(III) humic acid complex is shown together as AmHA (Kim et al. 1989). In Fig. 3, these plateau/saturation values are shown for the UO_2^{2+} and Am^{3+} complexation with Gohy-573(HA) as a function of pH in 0.1 M $NaClO_4$ (the same ionic medium as used for potentiometric pH titration in Fig. 1) (Higgo et al. 1993, Czerwinski et al. 1996, and Montavon et al. 2000). The plateau/saturation value decreases with increasing protonation of the humic acid. At pH 3 this value is only about 11 % of what is found at pH 6. At higher pH values the Am^{3+} ion shows hydrolysis and thus direct evaluation is not possible. The data for the uranyl ion are directly measured at pH 4. At higher pH values hydrolysis occurs. Data above pH 4 are deduced from

interaction data below the saturation value making use of an invariable interaction constant and accounting for the impact of hydrolysis. The straight line in the figure may not be understood as a functional relation, especially as the plateau/saturation value then would fall below zero around pH 2.6. It may, however, be used for description of the data in the concerned pH range (cf. below).

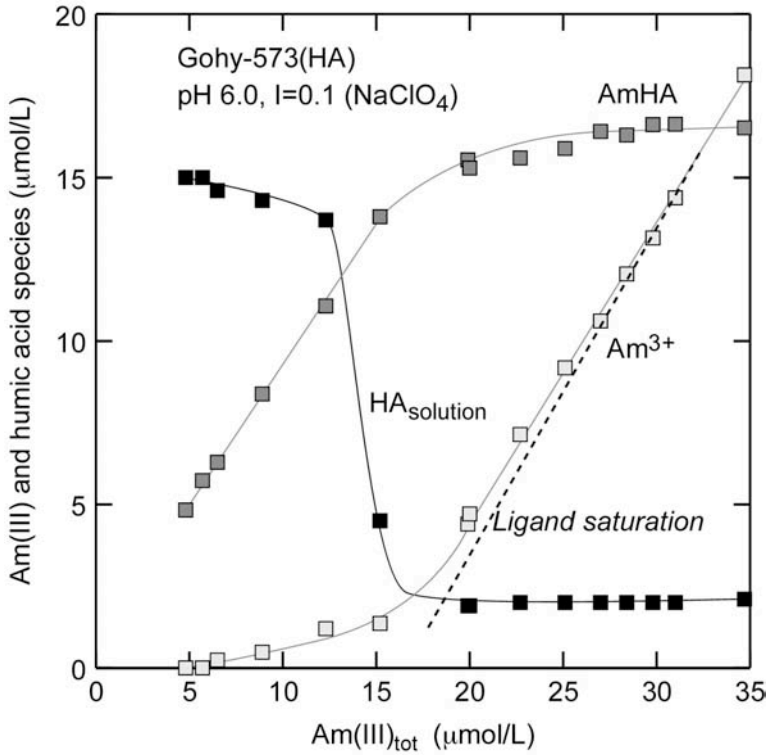

Fig. 2: Titration of the humic acid Gohy-573(HA) with the Am^{3+} ion at pH 6.0 in 0.1 M $NaClO_4$. The humate ligand saturation is given by AmHA approaching a constant value with a corresponding increase in the non-complexed Am^{3+} ion with an increase in the total Am(III) concentration. The approaching the humate ligand saturation is preceded by the flocculation of AmHA (decrease in $HA_{solution}$).

In Fig. 3, also the impact of the ionic strength on the plateau/saturation value is shown for a pH value of 6.0. For comparison with the impact of pH, a logarithmic scale is used (upper scale of Fig. 3). The principle impact of the ionic strength is the same as for pH, however, the magnitude of the impact is lower. This shows that the accessibility of humic acid i.e. the concentration of reactive entities decreases not only with increasing protonation but also with increasing cation concentration of the ionic medium. These results lead to the question how the protonation correlates with the effective humic acid ligand concentration (the plateau/ saturation value).

4.2 Relation between EHLC and pH

The relation between the EHLC and the protonation function of the humic acid Gohy-573(HA) with Am^{3+} and UO_2^{2+} in 0.1 M $NaClO_4$ is shown in Fig. 4. Without the intention of allocating functional relationships between pH and EHLC as well as the concentration of ionized groups, the respective data are rationalized/represented by straight lines. The surpris-

ing finding is a ratio between the concentration of ionized groups and EHLC of 3.41 (eq./mol). This should be compared with the number of 3.44 proton exchanging functional group per average molecule (cf. above). The outcome is that the EHLC decreases by one unit/molecule for the protonation of the same amount of proton exchanging groups as found per average molecule. As a consequence, the EHLC can be written as:

$$EHLC = PEC/n \times \alpha \quad (1)$$

where PEC is the total proton exchange capacity, n is the average number of proton exchanging groups per molecule and α is the degree of ionization.

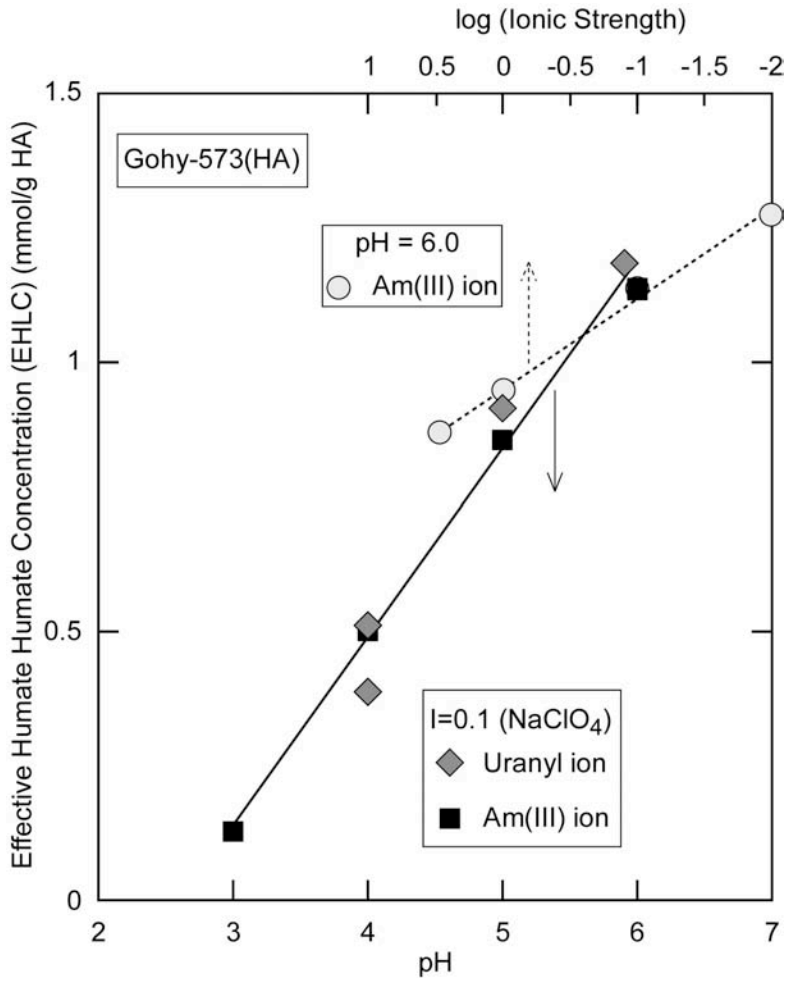

Fig. 3: Effective humate ligand concentration (EHLC) of the uranyl (UO_2^{2+}) and Am^{3+} ions with the humic acid Gohy-573(HA) as a function of pH (in 0.1 M $NaClO_4$) (lower scale), and as a function of ionic strength (at pH = 6.0) (upper scale). The EHLC values are given by the total amount of Am humic acid complex at humate ligand saturation (cf. Fig. 2) under these different physico-chemical conditions.

Consistent evaluation of experimental data is obtained for a free humate ligand concentration as follows (cf. also eq. (4):

$$[HA]_{free} = EHLC - MHA \quad (2)$$

Combination of eqs. (1) and (2) leads to:

$$[HA]_{free} = PEC/n \times \square - MHA \qquad (3)$$

This implies that for each complex formed, the number of reactive molecules decreases by one unit. If, however, there are three molecules each with an interaction probability of 2/3, formation of a complex with one molecule would leave two molecules with each 2/3 metal ion interaction/complex formation probability. Consequently the free humic acid ligand concentration after three protonations and one metal ion complexation would be 4/3 and not 1 as experimentally found and also correctly postulated from the first approach with non-random protonation. In the non-random protonation case the three protonations would lead to the decrease in one ligand unit and the metal ion complexation with one of the remaining molecules with each three ionized groups would lead to the decrease in the free humic acid concentration by another ligand unit. This is in agreement with eq. (3) reflecting experimental findings.

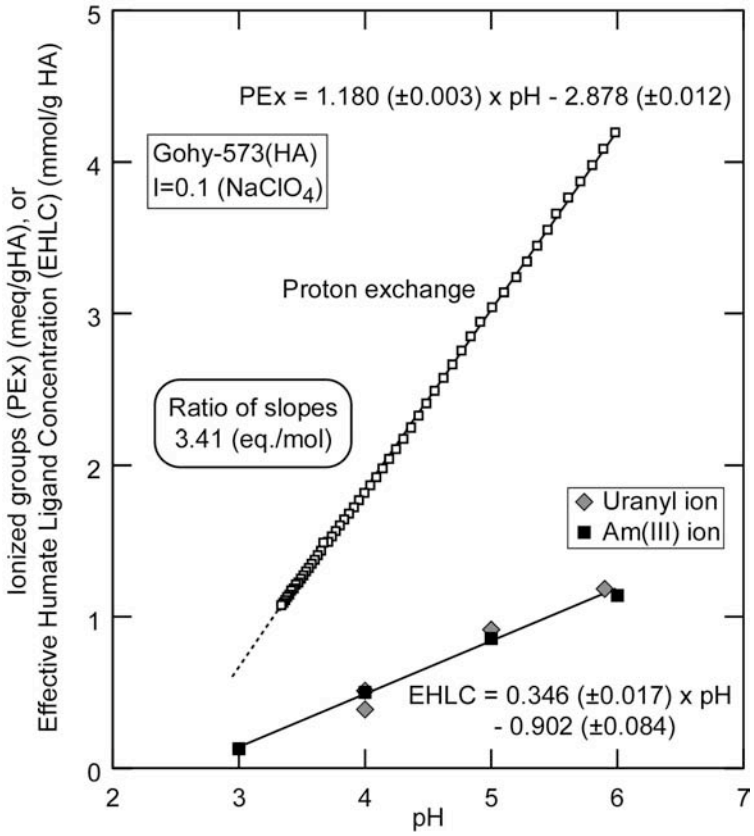

Fig. 4: Variation with pH of experimental data and representation of these data by linear regression for the concentration of ionized groups and EHLC for the UO_2^{2+} and Am^{3+} ions with the humic acid Gohy-573(HA) in 0.1 M $NaClO_4$. The ratio between the slopes of linear regression is 3.41 (eq./mol).

A final conclusion on the possibility to use a refined random protonation approach or requires further data evaluation. The simple approach of preferred consecutive protonation following the initial one (by random) is very tempting, reflects experimental findings and would be supported by neighboring impacts from the first protonation changing the overall functional groups behavior of the residual ionized ones, making them more prone to protonation. A

direct evidence for such an approach, however, is still pending. Furthermore, the impact of variation of ionic strength is still not well understood.

4.3 Extrapolation to full ionization

In the range of metal ion hydrolysis, the ligand saturation plateau values cannot be directly measured. Therefore, numbers for the EHLC of Am^{3+} beyond pH 6 needs to be indirectly deduced. In Fig. 5, the relationship between the EHLC and the protonation behavior is extrapolated to full ionization, i.e. to a pH of 10.25. For this extrapolation the constant ratio between EHLC and the protonation of 3.41 eq./mol is used (cf. Fig. 4). This extrapolation is not based on direct experimental evidence, but leads to a fully consistent description of the system and the complexation process. The reason is that the EHLC at full ionization becomes 1.88 mmol/g humic acid. The inverse value of this number is 533 g/mol humic acid. This basically identical with the number averaged molecular mass of individual molecules. This means that the EHLC at full ionization is simply the number concentration of humic acid molecules. Starting from this point, the process of protonation and complexation is then described by eq. (3), namely the decrease in humic acid ligand concentration by one unit (inactivation of one molecule) for consecutive protonation of its ionized groups, followed by the decrease by one ligand unit per complex formation (inactivation of one molecule as a consequence of one complex formation). In this discussion, the weaker impact of ionic strength is omitted.

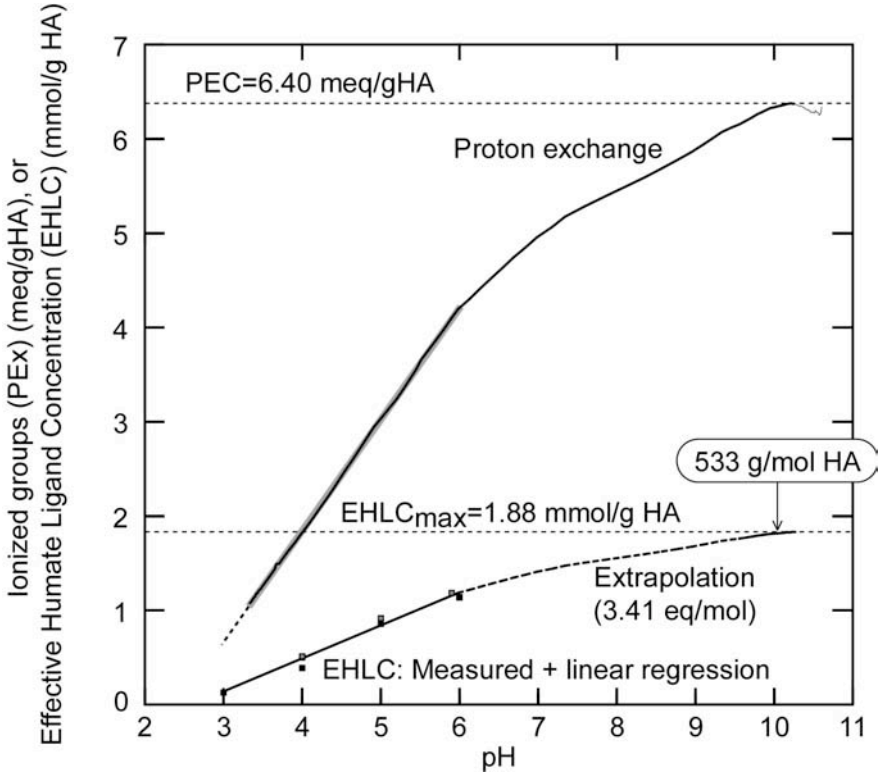

Fig. 5: Extrapolation of the concentration of ionized groups and EHLC for the UO_2^{2+} and Am^{3+} ions for pH between 6 and 10.25 by a constant ratio of 3.41 eq./mol (cf. Fig. 4). The maximum value for EHLC of 1.88 mmol/g HA is achieved at pH 10.25. This corresponds to a molecular weight of the humate ligand of 533 g/mol (inverse value of $EHLC_{max}$) and is basically identical with the number averaged mass distribution value from mass spectroscopy by TOF-SIMS (cf. Table 2).

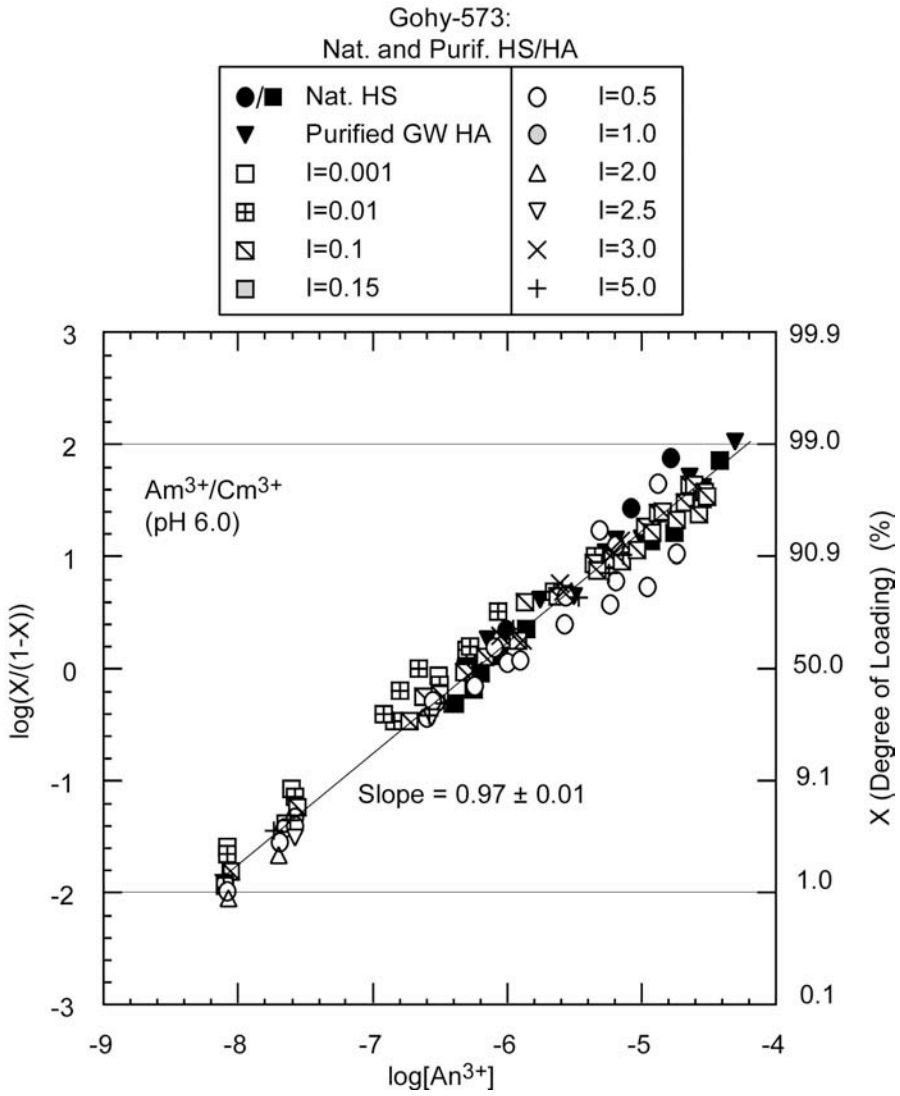

Fig. 6: Cm^{3+} and Am^{3+} complexation with different forms of humic acid from the Gorleben groundwater Gohy-573. Data on a straight line with unity slope represent one single complexation constant

4.4 Interaction constant

The interaction process is described by:

$$ß = [MHA] / (M_{free} \text{ x } [HA]_{free}) \quad (4)$$

with $[HA]_{free}$ given by eqs. (2) or (3).

Eq. (4) can be rearranged making use of the degree of saturation (X) as [MHA]/EHLC. Plotting log(X/(1-X)) against log($[M_{free}]$) results in a straight line with unity slope for one specific interaction constant (Buckau et al. 1992). In Fig. 6, this is done for a large number of complexation data for the Am^{3+} and the analogous Cm^{3+} ion with various forms of Gohy-573 humic acid. The ionic strength varies from 0.001 to 5 mol/L ($NaClO_4$) at a constant pH of 6.0. The EHLC is experimentally determined for each condition and system. The data fall on one

single straight line with the slope of unity. The same is found for variation of pH using the experimentally determined EHLC in eq. (2). This shows that the interaction process for an individual complex formation is basically invariant with respect to the ionic strength and pH. Furthermore, the complex formation strength is invariant with respect to the degree of humic acid ligand saturation (X) for values between about 0.01 and basically full saturation ([MHA] -> EHLC) (right hand scale in Fig. 6). This is also reflected in the invariant shape of absorption spectra of the comlexed Am^{3+} ion in the upper approximately 90 % of ligand saturation (Kim et al. 1989).

5. Summary, conclusions and outlook

The metal ion complexation of humic and fulvic acid is discussed. The paper restricts itself to the strongly complexing trivalent Am and Cm actinide ions and equally strongly complexing hexavalent uranyl ion (UO_2^{2+}). The reason for selecting these two ions is that a large number of complexation data are available based on especially spectroscopic investigations with one and the same batch of a well characterized humic acid. It is shown that, contrary to frequently published "models" relying on a large number of fitting parameters, the complexation can be described by an effective humate ligand concentration varying with pH and ionic strength and one single complexation constant. This is not a new concept, but has been used by some groups for a long time. The trust in this simple approach, however, has been hampered by the lack in understanding of the experimentally determined effective humate ligand concentration.

The present paper shows that the variation in the ligand behavior of humic acid can be easily related to the proton exchange behavior and the molecular mass distribution. This provides trust in the simple approach and also verifies the very narrow distribution in complexation functional properties of humic and fulvic acids.

6. Acknowledgements

The present paper is based on a general development of mass spectroscopic analytical techniques showing that humic and fulvic acids has much lower mass distribution numbers than previously thought. Towards the mid/end of the nineties it became obvious that humic and fulvic acid molecules have their mass distribution maximum in the range of around 500 mass units. The community, however, has only partly recognized this in very recent years. The author would like to acknowledge the many researchers that have worked against the accepted incorrect views of the mass distribution and provided this important key information, especially M. Wolf and W. Szyamczak (GSF) participating in the present HUPA project. The basis for the present paper was started with a meeting 10-11 January 2002, at the home institution of the author with the following participants (in addition to the author): Melissa Denecke (same institution as the author), Nick Bryan (University of Manchester), Cooper Langford (University of Calgary), Willem van Riemsdijk (Wageningen University) and Ulf Wahlgren (Albanova, Stockholm). Throughout the past years the issue has also been dis-

cussed with I. Pashalidis (University of Cyprus) providing experimental data and ideas on the complexation behavior in the upper pH range. J.I. Kim (same institution as the author) has provided a continuous support with discussions, infrastructure resources and coworkers required for this work for more than two decades. The author would like to acknowledge the input by all these persons as a pre-requisite for the present paper.

7. References

Buckau G., Kim J.I., Klenze R., Rhee D.-S., Wimmer H. (1992) "A Comparative Study of the Fulvate Complexation of Trivalent Transuranic Element Ions", *Radiochim. Acta*, **57**, 105.

Czerwinski K.R., Kim J.I., Rhee D.S., Buckau G. (1996) "Complexation of Trivalent Actinide Ions (Am^{3+}, Cm^{3+}) with Humic Acid: The Effect of Ionic Strength", *Radiochim. Acta*, **72**, 179.

Higgo, J.J.W., Kinniburgh, D., Smith, B. and Tipping, E. (1993). Complexation of Co^{2+}, Ni^{2+}, UO_2^{2+} and Ca^{2+} by humic substances in groundwaters. *Radiochimica Acta*, **61**, 91.

Kim J.I., Buckau G., Li G.H., Duschner H., Psarros N. (1990) "Characterization of Humic and Fulvic Acids from Gorleben Groundwater", *Fresenius J. Anal. Chem.*, **338**, 245.

Kim J.I., Buckau G., Bryant E., Klenze R. (1989) "Complexation of Americium(III) with Humic Acid", *Radiochim. Acta*, **48**, 135.

Montavon G., Mansel A., Seibert A., Keller H., Kratz J.V. and Trautmann N. (2000) “Complexation Studies of UO_2^{2+} with Humic Acid at low metal ion Concentrations by Indirect Speciation methods”, *Radiochim. Acta*, **88**, 17.

Plancque G., Amekratz B., Moulin V., Toulhoat P. and Moulin Ch. (2001) “Molecular Structure of Fulvic Acids by Electrospray with Quadrupole Time-Of-Flight Mass Spectrometry” *Rapid Communication in Mass Spoectrometry*, **15**, 827.

Schmeide K., Zänker H., Heise K.H. and Nitsche H. (1998) “Isolation and Characterization of Aquatic Humic Substances from the Bog “Kleiner Kranichsee””, in: "Effects of Humic Substances on the Migration of Radionuclides: Complexation and Transport of Actinides, First Technical Progress Report", Ed. G. Buckau, Report: FZKA 6124, August 1998, 161.

Wolf M., Buckau G., Geckeis H., Ngo Man T., Hoque E., Szymczak W. and Kim J.I. (2001) “Aspects of Measurement of the Hydrodynamic Size and Molecular Mass Distribution of Humic and Fulvic Acids“, In: Humic Substances: Structures, Models and Functions, Eds.: E.A. Ghabbour and G. Davies, Royal Chemical Society, 2001, 51

Annex 4

Comparison of humic colloid mediated transport of plutonium studied by column experiments with tri- and tetravalent actinide experiments

R. Artinger, B. Kuczewski*, C.M. Marquardt, Th. Schäfer, A. Seibert, Th. Fanghänel

Institut für Nukleare Entsorgung, Forschungszentrum Karlsruhe,
D-76021 Karlsruhe, Germany

***Institut für Kernchemie, Johannes Gutenberg-Universität Mainz,**
D-55099 Mainz, Germany

Comparison of humic colloid mediated transport of plutonium studied by column experiments with tri- and tetravalent actinide experiments

R. Artinger, B. Kuczewski*, C.M. Marquardt, Th. Schäfer, A. Seibert, Th. Fanghänel

Institut für Nukleare Entsorgung, Forschungszentrum Karlsruhe, D-76021 Karlsruhe, Germany

*Institut für Kernchemie, Johannes Gutenberg-Universität Mainz, D-55099 Mainz, Germany

Abstract

The mobility of plutonium was studied by column experiments with the groundwater Gohy-532 and a pleistocene sand, both from the Gorleben aquifer system. Near-natural conditions (Ar + 1% CO_2) were used for all experiments, including three months conditioning of the groundwater with the sand prior to experiments. Pu(VI) is rapidly reduced to Pu(V), followed by another fast reduction to Pu(IV). Contrary to this, the subsequent reduction of the tetravalent plutonium to Pu(III) is comparably slow. The different tri- and tetravalent actinide ions are found to distribute over a size spectrum comparable to that of groundwater humic colloids. This shows the predominance of humic colloid mediated transport. The redox state of plutonium in the investigated groundwater system can be both tri- and tetravalent, with the distribution being sensitive to small changes in the redox conditions. Whether the tri- or tetravalent oxidation state is predominant in the experiments could not be unambiguously determined. The reason is the lack in precision and/or sensitivity of different speciation methods applied and partly contradicting results. Comparison of results from column experiments with different tri- and tetravalent actinide ions shows a close resemblance in the plutonium behavior with that of other tetravalent actinide ions. In general, the recovery of plutonium (relative plutonium concentration in the column outlet) is lower than that of the trivalent americium. There are significant differences in chemical behavior between different actinide ions of the same oxidation state, including the potential for generation of polynuclear species/eigencolloids. Therefore, the findings are not sufficient for unambiguous determination of the plutonium oxidation state but further development and application of analytical methods/approaches is necessary.

Introduction

Over the last few decades, field studies and laboratory experiments proved the colloid-borne actinide migration in the subsurface aquatic environment. The assessment of the actinide migration from a nuclear waste repository to the biosphere, this requires adequate understanding of reactions involved.

Besides the solubility limits of ionic or complexed species and the occurence of eigencolloids especially of the tetravalent metal cations, humic colloids can play an important role in the interaction processes of metal ions in natural aquatic systems, additionally to inorganic colloids existent in natural waters (Buckau et al., 2000). It was found that the concentration of tri- and tetravalent trace metal ions is directly related to the content of humic substances (Kim et al., 1987) in natural waters. However, the molecular structure, the number of available complexing sites, the stereochemistry of humic substances and interactions with other naturally occuring substances like minerals and secondary phases are up to now not completely concieved.

A crucial factor determining the metal ion humic colloid interaction and the migration behaviour is the redox sensitivity of some metal ions. That redox processes play an important role in the migration behaviour was shown for the humic colloid-borne migration of neptunium (Artinger et al., 2000; Kim et al., 1995). The same is expected for the redoxsensitive plutonium which can occur in four oxidation states from trivalent to hexavalent (Pu(III-VI)). Several authors report on the reduction of Pu(VI/V) to Pu(IV) in the presence of separated, purified humic acids (Bondietti et al., 1976; Nash et al., 1981; Choppin, 1991; Jianxin et al. 1993; André et al. 2000). Although an oxidation of Pu(III) in natural waters under aerobic conditions is reported (Cleveland, 1979). The role of Pu(III) as a relevant oxidation state in natural systems under anaerobic conditions is not clear yet. The so far conducted migration experiments (Kim et al., 1995) are impaired by the lack of reliable redox speciation.

Several authors report that the migration of trivalent actinide ions in humic rich groundwater is dominated by the interaction with humic colloids (Artinger et al. 1998; Schüßler et al. 2000; Artinger et al., 2002). Also for tetravalent trace metal ions (Zr, Hf, Th) a solubility enhancement by humic colloids can be shown (Artinger et al., 2003). For trivalent cations also a considerable amount of kinetic data is available (Artinger et al. 1998; Schüßler et al. 2000; Artinger et al., 2002) showing different binding modes, mainly in slow equilibrium with each other, but also aggregation processes must be regarded for multivalent cations (Artinger et al., 2002; Artinger et al., 2003). But, unless the transferability of kinetic constants may not offhand be applicable directly in the predictive modelling of natural systems (Artinger et al., 2003)., in any case information on the principle reaction schemes can be deduced from such laboratory experiments.

Experimental

Radioisotopes

The plutonium isotopes ^{238}Pu and ^{242}Pu were used in the experiments. A stock solution of ^{242}Pu was purified via anion exchange (BIO RAD AG 1-X8) in the nitrate system, afterwards fumed with perchloric acid and stored in 1 M perchloric acid. Solutions with a single oxidation state (content > 90 %) were obtained electrolytically (Cohen, 1961) The Pu-content and isotope ratio of the stock solutions were checked with α-spectroscopy to a 99.4 wt% Pu-242, beside small amounts of Pu-238, -239, -240 and -241. Liquid scintillation counting (LSC) is used for determination of the total plutonium concentration of the solutions. Absorption spectroscopy, capillary electrophoresis and liquid-liquid-extraction were used to verify the oxidation state of the solutions added to the groundwater or humic acid solutions.

A stock solution of ^{238}Pu was fumed with perchloric acid and afterwards brought to 1 M perchloric acid solution. Solutions containing PuO_2^{2+} (content > 90 %) were obtained in the same way described for ^{242}Pu.

Migration experiments

The mobility of plutonium was studied by column experiments on natural systems under near-natural conditions. A pleistocene sand from the Gorleben region conditioned with Gorleben groundwater (GoHy-532) was used in columns with a diameter of 10 cm and a length of 50 cm. Chemical and physico-chemical parameters of the system are given in Table 1. More detailed information on the origin and sampling of the system compounds is given in (Buckau et al., 2000). Informations on similar experiments with trivalent actinides can be found in (Artinger et al. 1998; Schüßler et al. 2000).

Table 1: Chemical and physico-chemical data for the column experiments

	GoHy-532	
	original	**After conditioning**
Sampling depth (m)	65-68	
pH	8.9	6.8-7.2
Eh (mV)	-160	-30 - + 70
Conductivity (mS/cm)	0.95	
Na (mmol/L)	9.5 (3)	5.7
Ca (mmol/L)	0.047 (0.026)	0.054
Cl^-(mmol/L)	3.7 (3.87)	3.65
HCO_3^-(mmol/L)	5.5 (3)	3.3
DOC (mg C/L)	30	27
Sand	Pleistocene quartz sand	

The experiments were carried out under an atmosphere of Ar/1% CO_2 in a glove box. From a reservoir the groundwater was pumped over the sandfilled column (ID = 50 mm, L = 250 mm). To reach equilibrium conditions between groundwater and sediment and a stable microstructure with constant porosity a conditioning of the system for several months prior to the experiments was necessary, therefore the groundwater was pumped in a circular flow over the columns. During this conditioning time a sorption of humic colloids onto the sand was shown to be insignificant (Artinger et al. 1998). Radionuclides can be injected in a pulse as well as continuously onto the column. The eluate was fractionated in an automated sampling device. These fractions were investigated with LSC, CE and ultrafiltration.

For each of the three column experiments (No. 1-3, see Table 2 below) discussed below, an aliquot of an acidic plutonium stock solution, containing Pu(VI) (exp. 1 and 2) or Pu(IV) (exp. 3) respectively, was added to a 250 ml fraction of the groundwater. After adjustment of the pH and a varying contact time (29 d, 5 d and 18 h) a volume of about 160 ml is added continuously onto the column with a fast flow rate. Afterwards the system was changed again to groundwater without the plutonium spike and the elution of plutonium was observed with a slower flowrate of the groundwater (experiments No. 1-2). By this method the migration time for the plutonium species was varied in one experiment from 1 h to about 100 h. In experiment 3 the flowrate was not varied throughout the experiment so only a migration time of 5.5 h was investigated. All experiment conditions are summarised together with other plutonium experiments from literature in Table 2.

Speciation with absorption spectroscopy

A CARY-5E spectrometer (Varian) was used for the spectroscopic speciations together with quartz cuvettes (1 cm pathlength) from Hellma. The wavelength range between 400 and 870 nm was examined to cover the most intense peaks of the different oxidation states of plutonium (Cohen, 1961 b). As the molar absorption coefficients of the oxidation states Pu(III-V) are not very high, this method was limited to higher plutonium concentrations (> 10^{-5} M). For Pu(VI) a detection limit one order of magnitude higher can be obtained. Even for these higher concentrations absorption spectroscopy is affected, at unfavourable concentration ratios of the different oxidation states and in coloured or turbid samples.

Capillary electrophoresis

Also capillary electrophoresis coupled to ICP/MS (CE-ICP/MS) was used to determine the plutonium oxidation state distribution in samples with a total Pu concentration down to10^{-6} M. The CE system used throughout this work was a home made set-up with a fused silica capillary (ID 50 µm). An Elan 5000 (Perkin Elmer) adapted to a glove box was used for the measurements of alpha emitting radionuclides. A complete set-up of the CE equipment and its characteristics is found in (Kuczewski et al., 2003). By using a separation buffer system of 1 M acetic acid all four oxidation states of plutonium were separated with no significant

disturbances on the oxidation state distribution during the separation time of 12 minutes (Kuczewski et al., 2003). Usually 50µl aliquots of the Pu groundwater samples were diluted with 450 µl 1M acetic acid and were directly injected into the capillary for analysis. From the electropherograms the oxidation state distribution was obtained by evaluation of the peak areas. For samples at neutral pH values a quantification of all oxidation states was difficult. In these electropherograms the background increased, due to the presence of Pu-colloids, inorganic and organic, which were not solubilised by the acetic acid and showed enhanced interaction with the capillary wall. In this cases the background intensities were added on the Pu(IV) intensities, without distinguishing between ionic species and colloid species. Furthermore, a washing step after each separation gave the part of plutonium that was adsorbed on the capillary wall which was also counted for as Pu(IV) species.

Liquid-liquid-extraction

For the very low concentrations used in some of the experiments liquid-liquid-extraction was performed for redox speciation. As extracting agents 2-Thenoyltrifluoroacetone (TTA), 4-Benzoyl-3-methyl-1-phenyl-2-pyrazolin-5-one (PMBP) in toluene, and Phosphoric acid bis-(2-ethyl-hexyl) ester (HDEHP) in xylole were taken according to (Nitsche et al. 1988; Nitsche et al. 1994). Due to the reductive conditions in the groundwater and a very fast reduction of Pu(VI), only the tri-, tetra-, and pentavalent oxidation states have to be considered. With TTA and PMBP at pH 0 the Pu(IV) state is extracted into the organic phase, Pu (III), (V) and polymers remain in the aquatic phase. By adding $Cr_2O_7^{2-}$ to the solution, the Pu(III) is oxidised to Pu(IV) and therefore together with the initial Pu(IV) extracted into the organic phase, Pu(V) and polymers remain in the aqueous phase. Extraction of a $Cr_2O_7^{2-}$ oxidised solution with HDEHP at pH 0 leaves only the polymeric species in the aqueous phase.

Ultrafiltration

For the ultrafiltration experiments, the MicroSep™ centrifugal concentrators (PallGelman Laboratory) were used (1 kD, 3 kD, 10 kD, 30 kD, 50 kD, 100 kD, 300 kD, 1000 kD). With a 1 kD (resp. 10 kD) membrane the humic bound plutonium species were retained by the filtration membrane, whereas the free cations passed through.

XANES/EXAFS-investigations

The measurements of Pu in GoHy-532 samples by XANES/EXAFS are described in detail in (Dardenne et al. 2004) and (Marquardt et al. 2004), respectively. The XANES/EXAFS-spectra of solutions containing $1*10^{-4}$ M plutonium were measured directly in PE vials.

Table 2: Column experiments in the Gorleben system (anaerob) with Pu-238,242. Experiments 4-7 are from (Kim et al. 1995); some of the experimental parameters are not explicitly given.

Exp.No.	injection mode	Contact time	Migration time	R_f	Recovery %	GoHy	DOC mg C/L	[Pu] mol/L	Added Pu oxidation state to GoHy	Pu oxidation state introduced onto column (ratio)	Speciation method	Ref
1	Cont.	29 d (+1.5 d)	1 – 109 h	0.98	54.6-9.7	532	30	$1.8*10^{-9}$	VI	IV/III	UF	This work
2	Cont.	5 d (+5 h)	1 – 109 h	0.96	34.5-3.2	532	30	$1.2*10^{-9}$	VI	IV/III (40:60)	TTA, UF	This work
3	Cont.	18 h (+5.5 h)	5.5 h	n.d.*	3.2	532	30	$9.5*10^{-6}$	IV/(III)	IV (III < 2 %)	CE	This work
4	pulse	≈ 28 d (?)	9 h	0.96	52.5	2227	80	$8.4*10^{-8}$	VI or III	IV (?)	UF (?)	Kim et al. 1995
5	pulse	≈ 28 d (?)	9 h	0.97	63.7	2227	80	$8.4*10^{-8}$	VI or III	IV (?)	UF (?)	”
6	Cont.	4 a	9 h	1.01	40.2	2227	80	$1.3*10^{-7}$	VI or III	IV (?)	UF (?)	”
7	pulse	4 a	28 h	1.24	0.24	1011	3.2	$5.5*10^{-9}$	VI or III	IV (?)	UF (?)	”

* a slight increase in Pu activity is seen before one pore volume, because of the very low recovery the determination of an R_f value is difficult

Results and Discussion

As it is known from previous work (Bondietti et al. 1976; Nash et al. 1981; Choppin 1991; Jianxin et al. 1993; André et al. 2000; Cleveland 1979) humic substances reduce hexavalent plutonium to the pentavalent, tetravalent or both oxidation states. Our recent work (Marquardt et al. 2004) showed fast reduction of Pu(VI) to Pu(V) and a following fast reduction to Pu(IV). The reduction to Pu(III) under the same anaerobic conditions as applied in this column experiment set-up was slow. Such reduction is expected from a thermodynamical calculation of the species including the redox potential, carbonate complexation, hydrolysis and metal ion concentration. The calculated species diagrams are shown in Figure 1. The interaction with the humic substance is not considered, because there is no data available for plutonium itself and only limited data for other tetravalent actinide ions like thorium or neptunium. For low concentrations (about 10^{-9} M) the calculations reveal Pu(III) to be the main species. With increasing plutonium concentration, an increasing fraction of amorphous $Pu(OH)_4$ is expected from these calculations.

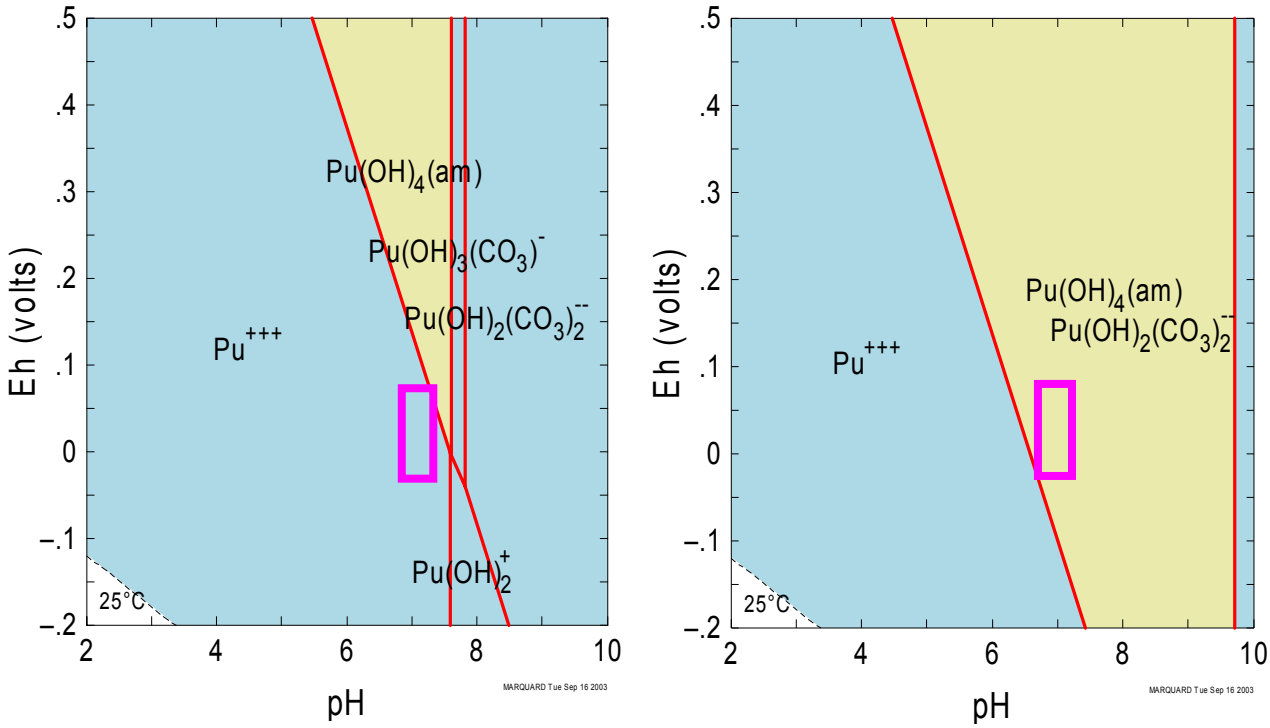

Figure 1: Species calculation with the program „Geochemical Workbench“, disregarding humic acid complexation. The squares represents the conditions for experiment 1, 2 and 3 respectively.
Left: low Pu concentration $1*10^{-9}$ M
Right: high Pu concentration $1*10^{-5}$ M

The distribution of the plutonium species over the size spectrum of the humic acid is investigated by ultrafiltration. The solution used for column experiment 2 at low Pu concentration ($1.2*10^{-9}$ M) is probed by ultrafiltration with membrane filters of pore sizes between 1 kDa and 1000 kDa after an equilibrium time of 18 hours and 5 d in addition to a representative fraction of the eluate (at R_f values about 1.1) from the column. The results of

the filtration are shown in Figure 2. Compared to the ultrafiltration of humic colloids in the original ground water and with results from earlier studies with americium (Artinger et al. 1998; Schüßler et al. 2000) no significant difference is seen between the four size patterns of the metal spiked solutions. With pore sizes smaller than 300 kDa, the plutonium is partly filtrated and with pore sizes smaller than 10 kDa the plutonium is retained almost completely on the filter. By comparison of the results of plutonium with the filtration curve of the original HS, the humic fraction between 3 kDa and 30 kDa becomes somewhat bigger after loading with the metal ion that is expressed by a higher retention of the Pu humate. This seems remarkable, because by the low Pu concentration of 1.2 $*10^{-9}$ – 1.8 $*10^{-9}$ M only a very small fraction of the carboxylate groups available for metal complexation are neutralized.

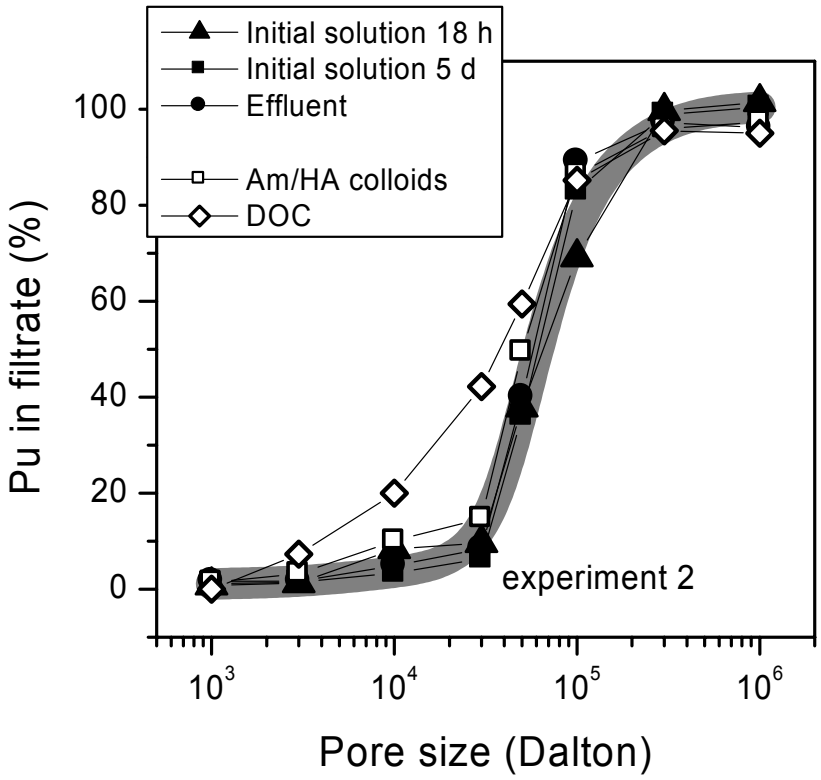

Figure 2: Data from filtration for experiment 2. For comparison data for americium and the humic colloids (represented by the DOC) are also plotted.

With the proton exchange capacity as a quantum of the carboxylates of about 3 $*10^{-4}$ M in the GoHy-532 ground water the loading of the HS is below 0.01 % at pH 7 (below 1 % for Am, respectively). Anyway the ultrafiltration experiments show clearly, that the Pu is completely bound to the HS. If the solution is acidified by hydrochloric acid to pH 1 and then filtered by 1 and 3 kDa filters, more than 80 % of the plutonium passes the filter, because the metal ions are released from the humic colloids at such low pH values. So far, neither an identification of the mechanisms of these interactions, nor a distinction whether Pu(III) or (IV) is bound to the humic substances is possible.

Therefore liquid-liquid extraction and capillary electrophoresis are tested for the determination of the oxidation state of plutonium in the groundwater solutions.

The extraction results for experiment 2 yielded in a ratio of Pu(III)/(IV) around 60:40 at the time of the introduction onto the column. But the extraction procedure was shown to influence the redox pairs of plutonium (Lit). Furthermore the fate of the humate fraction is not clear, respectively significantly lower recoveries from the two phases are obtained with humic acid containing solutions compared to simple aqueous solutions.

For column experiment 3 with a higher plutonium concentration, Pu(IV) is added directly to the groundwater; as recent experiments with EXAFS (Dardenne et al. 2004), and XPS (Marquardt et al. 2004) showed that, regardless of the oxidation state added, in this concentration range Pu colloids (eigencolloids as well as humic colloids) are the predominant species in GoHy-532 groundwater, anyway. The fourier transformed EXAFS oscillations showed features interpreted as Pu-Pu interactions. As next neighbours oxygen atoms were identified and a splitting into two shells is interpreted as an interaction with the humic/fulvic substances (Dardenne et al. 2004). For our column experiment 3 capillary electrophoresis is used for oxidation state determination in the sample solution prior to the introduction onto the column. This experiment shows that a very small part of the plutonium is in the trivalent state (< 2 %), according to the speciation result of the stock solution. Only a small fraction of ionic tetravalent plutonium exists (< 10 %), the remaining part of the plutonium must be ascribed to polymeric and colloidal species that easily adsorb on the capillary walls.

Table 3: Speciation experiments (UV/Vis and capillary electrophoresis) for experiment 3 in the Gorleben system with Pu-242

UV/Vis								
solution			Pu(III) %	Pu(IV) %	Pu(V)/(VI) %			
Pu_{stock}			2.4	97.1	0.5			
CE								
	Flush	Washing step	Cationic run			Washing step	Anionic run with pressure	Washing step
	Migrating %	Adsorbed %	Pu(III) %	Pu(IV) %	Pu(V)/(VI) %	Adsorbed %	Migrating %	Adsorbed %
Pu_{stock} 1:100			6.7	91.3	2.0			
Exp. 3	47.5	52.5	1.1	8.9	-	70.2	31.2	51.1

From the speciation results, a migration behaviour of plutonium inbetween to that observed for An(III) and tetravalent actinides (literature data available for thorium and plutonium (Kim et al. 1995; Artinger et al. 2003)) is expected for the low concentration experiments (experiments 1 and 2). Experiment 3 with high concentration of plutonium may be compared with some high concentration Np(IV) and Tc(IV) experiments (Artinger et al. 2003), except for the low contact time with the groundwater before the introduction onto the column.

The retardation factors, R_f, found for our plutonium experiments are comparable to those found in other An column experiments. Due to a size exclusion effect, the humic colloid bound plutonium shows a slightly enhanced transport compared to a conservative tracer (HTO) migrating with the groundwater velocity. R_f values in these plutonium experiments vary between 0.96 and 0.98.

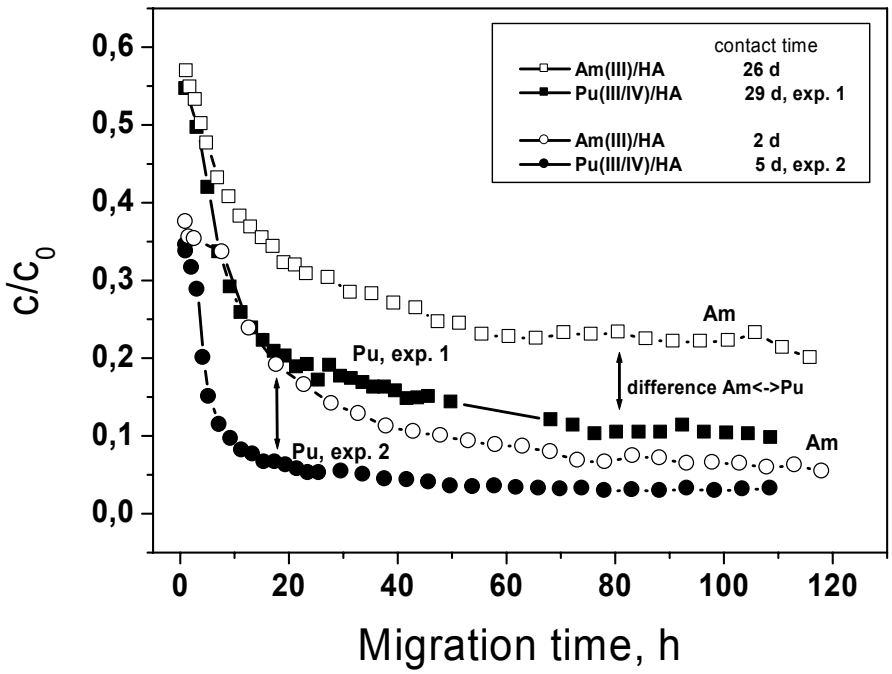

Figure 3: Comparison with Am(III) experiments of different contact times. Decreasing contact time leads to decreasing recovery as well as increasing migration time.

For experiment 1 and 2 a direct comparison with americium(III) experiments is possible, as there are experimental data under comparable hydraulic and chemical conditions available. The data compilation is shown in Figure 3. Both elements, Am and Pu, follow the trend of increasing recovery (represented by the ratio of the actinide concentration c in the eluate to the total concentration c_0) with increasing contact time (few hours up to 29 d). Furthermore the trend of a decreasing recovery in the unimpeded transport with increasing migration time is observed for both elements. The latter means, the higher the residence time in the column the higher is the amount of An sorbed onto the sand surface. That the plutonium in experiment 1 and 2 is initially completely bound to the humic colloids is corroborated by the

ultrafiltration experiments described above (Fig. 2).

As the plutonium recovery from the column is not quantitatively (<100 %), the migration behaviour should depend - similar to the "Am case" (Kim et al. 1995; Schüßler et al. 2000; Artinger et al. 2002)- on a kinetically controlled interaction of humic colloid bound plutonium with the sediment surface. In detail, at fast migration times (< 5 h) a similar Pu and Am recovery is obtained, whereas with increasing sediment contact time the recovery of the plutonium decreases faster than for the americium. So, for longer migration times a lower recovery of plutonium as for the americium is obtained. It must be emphasised that comparison can be only made for experiments at similar contact times.

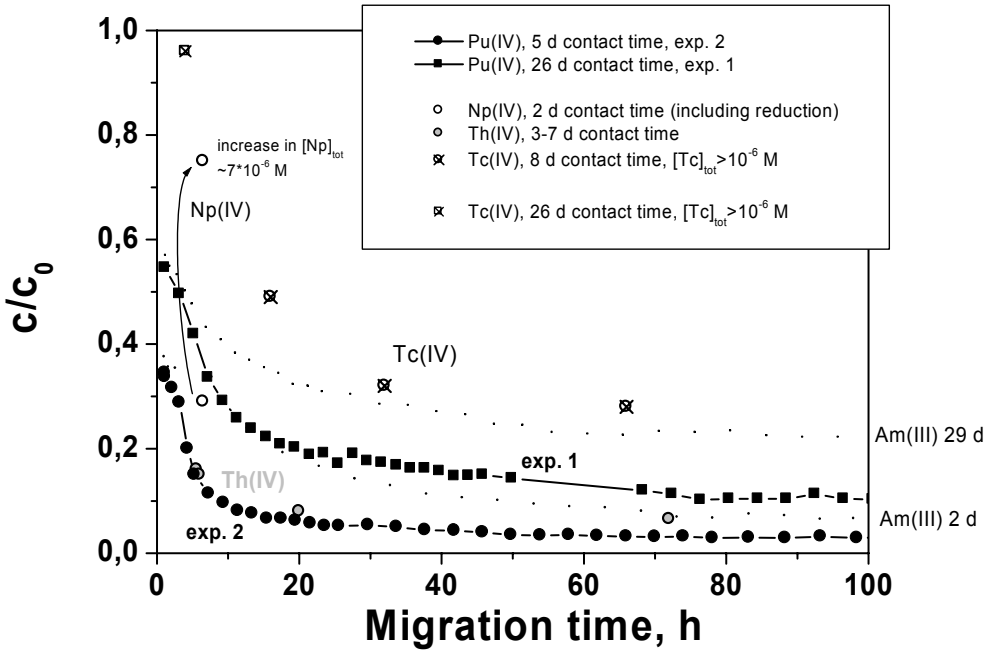

Figure 4: Comparison with An(IV) and Tc(IV) experiments. Low concentration for Pu, Th and Np (< $1*10^{-7}$ M). Tc(IV) experiments have higher concentrations but no comparable contact times to experiment 3 could be found. Circles: contact times 2 – 8 d; Squares: contact times 26 – 29 d; Dots represent the Am(III) data from Fig. 3

A direct comparison with tetravalent metal ions is more difficult, because data from the literature is only of limited comparability (different metal concentration, contact time, humic substances, different experiment operation). Nevertheless in Figure 4 some data for Th(IV), Np(IV) and Tc(IV) are plotted together with the new plutonium data. Experiment 3 is excluded because no comparable literature data could be found for the short contact time between plutonium and groundwater before the column experiment. The agreement with several Th(IV) experiments (contact time of a few days and low concentration) is quite good. Previous Pu(IV) experiments (exp. 4 and 5, Table 2) (Kim et al. 1995) with contact times of several weeks yielded recoveries of 52.5 % and 63.7 % for a migration time of 9 h (not shown in Fig. 4). So, the accordance in this case is poor, but the experimental conditions for these experiments may be different from ours with respect to sample preparation. The increased

recovery in experiments with high metal concentration (Tc(IV) and Np(IV) in Fig. 4) is discussed in detail in (Artinger et al. 2003).

Considering the other variable parameter in different column experiments with tetravalent actinides in the Gorleben system (Artinger et al. 2003) our plutonium experiments fit in some more of the general trends. Figure 5 shows the recovery of the metal ions as a function of contact time. The recovery increases with increasing plutonium (resp. thorium) groundwater contact time prior to column injection.

Experiment 3 with high plutonium concentration showed a very low recovery of plutonium. Below 5 % of the total plutonium concentration are eluted, whereas experiments with Np(IV) and Tc(IV) at higher metal ion concentrations, but also higher contact times with the groundwater, showed recoveries up to 80-100 %. The very low recovery of our column experiment is on one hand ascribed to the relatively short contact time of only 18 h between plutonium and the groundwater before the experiment; for Np(IV) and Tc(IV) the contact times vary between several days to several weeks. At the metal concentration of experiment 3 also a large fraction of polynuclear hydrolysis products is expected from EXAFS investigations on similar solutions (Dardenne et al. 2004) and the CE speciation. As it is known, that such plutonium species easily sorb on surfaces it seems to be obvious, that the plutonium also has a high affinity for sorption on the sand surface, especially for experiments with short contact time between plutonium and groundwater.

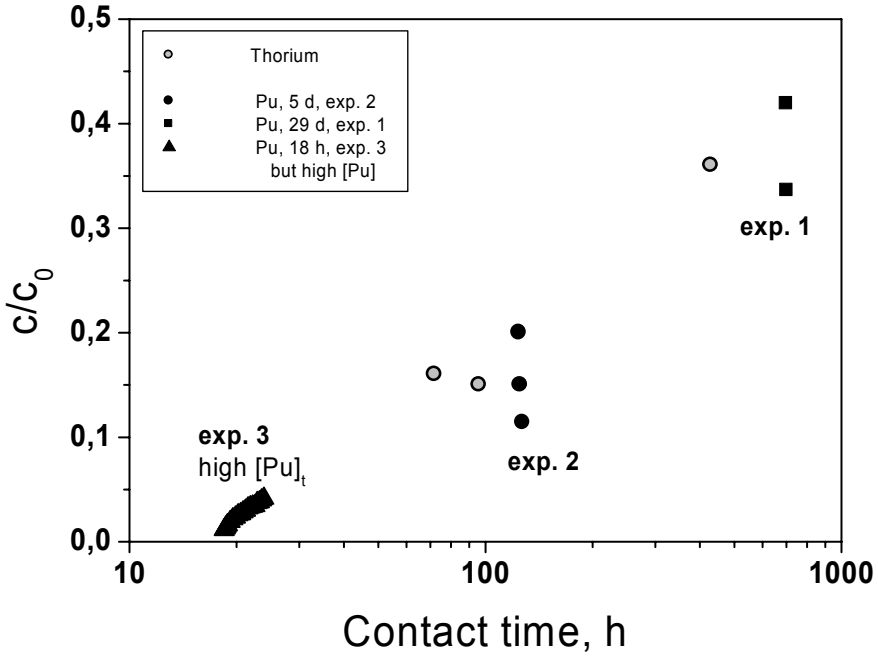

Figure 5: Comparison with An(IV), dependence on contact time. Low concentration for Pu and Th (< $1*10^{-7}$ M) and migration times between 4.3 and 7.3 h. The plutonium concentration in experiment 3 is about $1*10^{-5}$ M.

Conclusions

Experiments with different oxidation states of plutonium (Pu(IV, VI)) added to a Gorleben groundwater show migration features of plutonium similar to those of other tetravalent actinides at low concentrations. Lower recoveries than for comparable Am(III) experiments are obtained. Significant differences appear for higher plutonium concentrations and short contact times were a significant generation of polynuclear species is expected.

Several redox speciation methods were used to investigate the solutions. EXAFS/XANES experiments admit the determination of oxidation state and chemical vicinity (especially EXAFS) of the plutonium at higher concentrations. With capillary electrophoresis a tool for redox speciation of ionic plutonium species is available for metal concentrations down to $1*10^{-6}$ M. Both methods revealed Pu(IV) to be the main species in this concentration range. The redox speciation with liquid-liquid extraction for very low plutonium concentrations in the presence of humic substance is not completely convincing due to the loss of activity during the extraction which could not be quantified easily. In the future special attention will be given to the Pu(III) state and its relevance in natural systems. Here a reliable redox speciation method for very low concentrations is needed.

Several parameters for a chemically based modelling are not well understood up to now. For example a reliable model description of the Pu-migration in the Gorleben aquifer requires the inclusion of the redox behaviour of colloidal plutonium. It is also necessary elucidate the colloid formation and complexation processes in this natural groundwater systems.

References

André et al. 2000 — André, C., Choppin, G.R.: Reduction of Pu(V) by Humic Acid. Radiochim. Acta **88**, 613 (2000).

Artinger et al. 1998 — Artinger, R., Kienzler, B., Schüßler, W., Kim, J.I.: Effects of Humics Substances on the ^{241}Am Migration in a Sandy Aquifer: Column Experiments With Gorleben Groundwater / Sediment Systems. J.Contam.Hydrology **35**, 261 (1998).

Artinger et al. 2000 — Artinger, R., Marquardt, C.M., Kim, J.I., Seibert, A., Trautmann, N., Kratz, J.V.: Humic colloid-borne Np migration: influence of the oxidation state. Radiochim. Acta **88**, 609 (2000)

Artinger et al. 2002 — Artinger, R., Schüßler, W., Schäfer, T., Kim, J.I.: A Kinetic Study of Am(III)/Humic Colloid Interactions. Environ.Sci.Technol. **36**, 4358 (2002).

Artinger et al. 2003 — Artinger, R., Buckau, G., Zeh, P., Geraedts, K., Vancluysen, J., Maes, A., Kim, J.I.: Humic colloid mediated transport of tetravalent actinides and technetium. Radiochim. Acta **91**, 1 (2003).

Bondietti et al. 1976 — Bondietti, E.A., Reynolds, S.A., Shanks, M.H.: Interaction of Plutonium with Complexing Substances in Soil and Natural Waters. Transuranium Nuclides Environ., Proc.Symp.1975, 273 (1976).

Buckau et al. 2000 Buckau, G., Artinger, R., Fritz, P., Geyer, S., Kim, J.I., Wolf, M.: Origin and mobility of humic colloids in the Gorleben aquifer system. Appl. Geochem. **15**(2), 171 (2000)

Choppin 1991 Choppin, G.R.: Redox Speciation of Plutonium in Natural Water. J. Radioanal. Nucl. Chem. **147**, 109 (1991).

Cleveland 1979 Cleveland, J.M.: The Chemistry of Plutonium, American Nuclear Society, Illinois (1979).

Cohen 1961 Cohen, D.: Electrochemical Studies of Plutonium Ions in Perchloric Acid Solution. J.Inorg.Nucl.Chem. **18**, 207 (1961).

Cohen 1961b Cohen, D.: The Absorption Spectra of Plutonium Ions in Perchloric Acid Solutions. J.Inorg.Nucl.Chem. **18**, 211 (1961).

Dardenne et al. 2004 Dardenne, K., Denecke, M. A., Seibert, A., Marquardt, C. M.: EXAFS measurements of Pu(III,IV,V,VI) in humic rich Gorleben ground water, to be published.

Jianxin et al. 1993 Jianxin, T., Yaozhong, C., Zhangji, L.: A Kinetic Study of the Reduction of Plutonium With Humic Acid. Radiochim. Acta **61**, 73 (1993).

Kim et al. 1987 Kim, J.I., Buckau, G., Klenze, R.: Natural Colloids and Generation of Actinide Pseudocolloids in Groundwater. In: *Natural Analogues in radioactive Waste Disposal* (Come, B., Chapman, N., eds.) Graham + Trottman, London (1987)

Kim et al. 1995 Kim, J.I., Zeh, P., Runde, W., Mauser, C., Pashalidis, I., Kornprobst, B., Stöwer, Ch.: Nuklidmigration (99Tc, 237Np, 238Pu, 241Am) im Deckgebirge und Salzstock des geplanten Endlagerortes Gorleben (Abschlußbericht). Report: RCM 01495, Technical University Munich (1995).

Kuczewski et al. 2003 Kuczewski, B., Marquardt, C.M., Seibert, A., Geckeis, H., Kratz, J.V., Trautmann, N.: Separation of Plutonium and Nepunium Species by Capillary Electrophoresis-ICP-MS and Application to Natural Ground Water Samples. Anal.Chem. **75**, 6769 (2003).

Marquardt et al. 2004 Marquardt, C. M, Seibert, A., Artinger, R., Denecke, M. A., Kuczewski,B., Schild, D.: Redox behaviour of Plutonium in humic rich ground water, submitted to Radiochim. Acta

Nash et al. 1981 Nash, K., Fried, S., Friedman, A.M., Sullivan, J.C.: Redox Behavior, Complexing, and Adsorption of Hexavalent Actinides by Humic Acid and Selected Clays. Environ.Sci.Techn. **15**, 834 (1981).

Nitsche et al. 1988 Nitsche, H., Lee, S. C., and Gatti, R. C.: Determination of Plutonium oxidation states at Trace Levels Pertinent to Nuclear Waste Disposal. J.Radioanal.Nucl.Chem.Articles **124**(1), 171-185 (1988).

Nitsche et al. 1994 Nitsche, H., Roberts, K., Xi, R.H., Prussin, T., Becraft, K., Silber, H.B., Carpenter, S.A., Gatti, R.C., Novak, C.F.: Long-Term Plutonium Solubility and Speciation Studies in a Synthetic Brine, Radiochim. Acta **66/67**, 3 (1994).

Schüßler et al. 2000 Schüßler, W., Artinger, R., Kienzler, B., Kim, J.I.: Conceptual Modeling of the Humic Colloid-Borne Americium(III) Migration by a Kinetic Approach. Environ.Sci.Technol. **34**, 2608 (2000).

Annex 05

NIR Spectroscopic Study on the Influence of Phenolic OH Groups on the Neptunium(V) Humate Complex Formation

S. Sachs, G. Bernhard

Forschungszentrum Rossendorf e.V., Institute of Radiochemistry,
P.O. Box 510119, 01314 Dresden, Germany (FZR-IfR)

NIR Spectroscopic Study on the Influence of Phenolic OH Groups on the Neptunium(V) Humate Complex Formation

S. Sachs, G. Bernhard

Forschungszentrum Rossendorf e.V., Institute of Radiochemistry, P.O. Box 510119, 01314 Dresden, Germany (FZR-IfR)

Abstract

We investigated the influence of phenolic OH groups on the Np(V) complexation by humic acids at pH 7 and pH 8. The studies were performed by near-infrared (NIR) absorption spectroscopy applying unmodified and chemically modified humic acids with blocked phenolic/acidic OH groups. The experimental data were evaluated with the metal ion charge neutralization model. For all humic acids under investigation comparable complexation constants were determined. However, compared to the original humic acids, modified humic acids with blocked phenolic/acidic OH groups show significant lower loading capacities for Np(V) under the applied experimental. This result indicates a lower amount of maximal available humic acid ligand sites for the complexation of Np(V). Thus, it can be concluded that humic acid phenolic/acidic OH groups contribute to the interaction between humic acid and Np(V) under the studied conditions.

1 Introduction

The trustworthy modeling of the migration of actinides in the environment requires knowledge on processes and materials which can influence the transport behavior of these pollutants in the environment. Besides inorganic ligands such as sulfate, phosphate, arsenate and silicate, humic acids play an important role in the interaction processes of actinide ions due to their high complexing ability towards metal ions. There are various models describing the metal ion complexation behavior of humic acids (e.g., Kim and Czerwinski, 1996, Tipping, 1998, Torres and Choppin, 1984 and Kinniburgh et al., 1996). However, these models differ from one another, for instance in the definition of the complexation reaction and the humic acid ligand concentration. It is often assumed that only humic acid carboxylate groups act as complexing sites for metal ions (Choppin and Allard, 1985). However, other functional groups such as phenolic, enolic and alcoholic OH groups as well as amino groups, may also be involved in the complexation process, for instance, via the formation of chelate rings together with carboxylate groups (Stevenson, 1994).
In order to further improve the knowledge on the metal ion humic acid interaction, especially on the contribution of different functional groups to this interaction process, we study the influence of humic acid phenolic OH groups on the metal ion complexation. Therefore, we developed chemically modified humic acids with blocked phenolic OH groups (Pompe et al., 2000 and Sachs et al., 2002). Applying these model substances we already investigated the influence of phenolic OH groups on the U(VI) complexation by humic acids (Pompe et al., 2000 and Schmeide et al., 2003). In addition to that, we studied the influence of phenolic OH groups on the Np(V) complexation by humic acids at pH 7 by means of X-ray absorption spectroscopy (Schmeide et al., 2003a and Sachs et al., 2003). Within this investigation we obtained structural information on the near-neighbor surrounding of Np(V) in different humate complexes. In continuation of that study, we determined and compared in the present work loading capacities and complexation constants for the Np(V) complexation by unmodified and chemically modified (phenolic OH groups blocked) synthetic and natural humic acids by near-infrared (NIR) absorption spectroscopy.

2 Experimental

Humic acids

Np(V) humate solutions were prepared from natural humic acid Aldrich (AHA; Aldrich, Steinheim, Germany), synthetic humic acid type M42 (Pompe et al., 1998 and Sachs et al., 2003a), as well as from modified humic acid AHA and M42 with blocked phenolic/acidic OH groups (AHA-PB, M42-PB; Pompe et al., 2000 and Sachs et al., 2003a). Before use, AHA was purified according to (Kim and Buckau, 1988). Humic acid type M42 represents a humic acid-like product from xylose and glutamic acid, which shows a carboxyl group content comparable to most natural humic acids. Its synthesis and characterization is described in detail in (Sachs et al., 2003a).

Chemically modified humic acids with blocked phenolic/acidic OH groups (AHA-PB and M42-PB) were synthesized from AHA and M42 in a two-step modification process using diazomethane as methylation reagent. The modification process is described in (Pompe et al., 2000 and Sachs et al., 2003a). It was verified by carbon-13 NMR spectroscopy that the applied modification process causes only the intended structural changes in humic acid functional groups (Sachs et al., 2002).
Table 1 shows the functional properties of the studied humic acids. From Tab. 1 it can be concluded that 75 % and 84 % of the initially occurring phenolic/acidic OH groups of humic acid type M42 and AHA, respectively, were modified by methylation with diazomethane. A complete blocking of all phenolic/acidic OH groups was not possible. Comparing the carboxyl group content and the proton exchange capacity (PEC) of the corresponding unmodified and modified humic acids it becomes obvious that the modified humic acids, especially AHA-PB, have less carboxyl groups and a lower PEC than the corresponding unmodified humic acids. An incomplete hydrolysis of methyl ester groups formed during the methylation could be one possible reason for that (Sachs et al., 2002). Nevertheless, for both humic acids the molar ratio of phenolic/acidic OH to carboxyl groups (see Tab. 1) is smaller due to the modification. Therefore, these chemically modified humic acids can be used to study the influence of phenolic/acidic OH groups on the interaction between humic acid and Np(V).

Table 1: Functional group contents of unmodified and modified humic acid type M42 and Aldrich (AHA).

Humic acid	COOH [a] (meq/g)	PEC [b] (meq/g)	Phenolic/acidic OH [c] (meq/g)	Phenolic/acidic OH : COOH
M42 (batch M145)	3.76 ± 0.09	3.51 ± 0.07	2.0 ± 0.2	0.53
M42-PB (batch M171)	3.12 ± 0.07	3.23 ± 0.15	0.5	0.16
AHA (batch A2/98)	4.49 ± 0.14	4.60 ± 0.08	3.1 ± 0.1	0.69
AHA-PB (batch M173)	2.67 ± 0.01	3.13 ± 0.15	0.5	0.19

[a] Determined by calcium acetate exchange (Schnitzer and Khan, 1972). [b] PEC: Proton Exchange Capacity. Determined by potentiometric pH titration. [c] Radiometrically determined (Bubner and Heise, 1994).

NIR measurements

All experiments were performed under nitrogen atmosphere at room temperature. The humic acid concentration ([HA(I)], Kim and Czerwinski, 1996) was held constant at $1 \cdot 10^{-3}$ mol/L and the Np(V) concentration was varied between $5.3 \cdot 10^{-5}$ and $1.3 \cdot 10^{-3}$ mol/L. The studies were performed in 0.1 M $NaClO_4$ solutions at pH 7 for all humic acids and at pH 8 for AHA and AHA-PB. Samples were prepared from stock solutions of humic acid and NpO_2^+ (^{237}Np, $4.6 \cdot 10^{-3}$ M, 0.01 M HNO_3). The ionic strength was adjusted using 1 M $NaClO_4$ solution. The neptunium concentration in solution was determined by liquid scintillation counting (LSC, Beckman Instruments). NIR absorption spectra of the Np(V) humate solutions were measured in the wavelength range between 950 and 1010 nm with the UV-Vis-NIR spectrophotometer CARY-5G (Varian).

Neptunium(V) species distribution

The Np(V) species distribution in absence of humic acid at pH 7 and pH 8 ([NpO_2^+]: $1 \cdot 10^{-5}$ M and $1 \cdot 10^{-3}$ M, 0.1 M $NaClO_4$, 0 % CO_2) was calculated with the program EQ3/6 (Wolery, 1992) based on complex formation constants compiled in the NEA data base (Lemire et al., 2001). Under the considered conditions the NpO_2^+ ion dominates the Np(V) speciation. It occurs with a relative concentration of 100.00 % and 99.96 % at pH 7 and pH 8, respectively. From that it can be concluded that NpO_2^+ is the Np(V) species which reacts with humic acid under the studied experimental conditions.

3 Results and discussion

The measured NIR absorption spectra represent the sum of the absorption signals of the uncomplexed NpO_2^+ ion (980 nm) and the Np(V) humate complex ($NpO_2HA(I)$, 985-989 nm depending on humic acid). The measured spectra were deconvoluted into single peaks for both species in order to determine their concentration in solution. Figure 1 shows a NIR absorption spectrum of a Np(V) solution with AHA and its deconvolution.

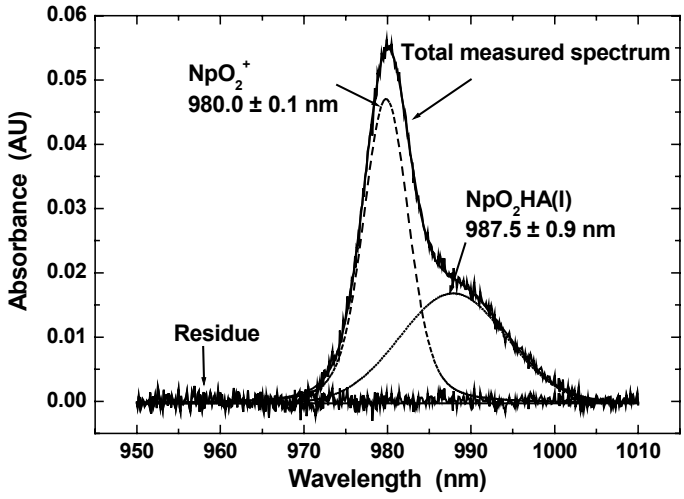

Fig. 1: Absorption spectrum of a Np(V) humate solution and its deconvoluted absorption bands (AHA, [HA(I)]: $1 \cdot 10^{-3}$ mol/L, [NpO_2^+]: $1.7 \cdot 10^{-4}$ mol/L, pH 7, 0.1 M $NaClO_4$).

The experimental data were evaluated with the metal ion charge neutralization model (Kim and Czerwinski, 1996). According to this model, NpO_2^+ occupies one proton exchanging site of the humic acid molecule [Eq. (1)]:

$$NpO_2^+ + HA(I) \leftrightarrow NpO_2HA(I) \qquad (1)$$

In Eq. (1) HA(I) represents the humic acid ligand and $NpO_2HA(I)$ stands for the neptunyl humate complex.

The stability constant β for the complexation reaction is given by

$$\beta = \frac{[NpO_2HA(I)]}{[NpO_2^+]_{free} \cdot [HA(I)]_{free}} \tag{2}$$

where $[NpO_2HA(I)]$ is the neptunyl humate complex concentration, $[NpO_2^+]_{free}$ the free NpO_2^+ concentration and $[HA(I)]_{free}$ the free humic acid ligand concentration. This model introduces the loading capacity (LC, [Eq. (3)]) which represents the mole fraction of maximal available complexing sites of humic acid under the applied experimental conditions.

$$LC = \frac{[NpO_2HA(I)]_{max}}{[HA(I)]_{tot}} \tag{3}$$

$[NpO_2HA(I)]_{max}$ is the maximal concentration of NpO_2^+ that can be complexed by functional sites of humic acid and $[HA(I)]_{tot}$ stands for the total molar humic acid concentration. Taking the LC into account the free humic acid concentration in solution can be determined according to (Kim and Czerwinski, 1996) and the stability constant (β) can be described by Eq. (4).

$$\beta = \frac{[NpO_2HA(I)]}{[NpO_2^+]_{free} \cdot ([HA(I)]_{tot} \cdot LC - [NpO_2HA(I)])} \tag{4}$$

The LC is graphically determined by linear regression after rearranging Eq. (4) for the free NpO_2^+ ion concentration. Considering the graphically determined LC, we computed a complexation constant for each experimental point.

Applying this model, the complexation behavior of humic acid can be described independently of the experimental conditions and the humic acid origin. From this it follows, that comparable complexation constants are determined for the complexation of a metal ion, e.g., Np(V), with different humic acids. Differences in the complexation behavior of various humic acids under the same experimental conditions are reflected in different LC values. A significant lower LC for humic acids with blocked phenolic/acidic OH groups should result, if the blocking of these functional groups has an influence on the complexation behavior of humic acid with Np(V) at pH 7 and pH 8.

In Tab. 2 the spectroscopically determined complexation data (LC, log β) for the investigated humic acids are listed. Figure 2 shows, exemplary for the modified and unmodified humic acid type M42, the mole ratios $[NpO_2HA(I)]/[HA(I)]_{tot}$ versus $[NpO_2^+]_{tot}/[HA(I)]_{tot}$ which illustrate the LC values.

Table 2: Complexation data (LC and log β) for the Np(V) complexation by unmodified and modified humic acid type M42 and AHA in comparison to literature data.

Humic acid	pH	LC (%) [a]	log β [a]
AHA (batch A2/98)	7.0	10.0 ± 1.5	3.87 ± 0.19
	8.0	35.3 ± 3.7	3.59 ± 0.17
AHA-PB (batch M173)	7.0	6.5 ± 2.4	3.39 ± 0.15
	8.0	12.3 ± 2.6	3.46 ± 0.22
M42 (batch M145)	7.0	11.2 ± 1.1	3.50 ± 0.15
M42-PB (batch M171)	7.0	5.3 ± 1.0	3.48 ± 0.11
GoHy-573	7	9.9 ± 0.2	3.65 ± 0.03
(Kim and Sekine, 1991)	8	14.9 ± 0.3	3.68 ± 0.08
GoHy-573	7	13.0 ± 1.0	3.53 ± 0.05
(Marquardt and Kim, 1998)	8	22.0 ± 1.5	3.61 ± 0.07
Aldrich (Seibert et al., 2001)	8	32.4	3.7

[a] ± 3 σ.

Within the experimental errors, the studied humic acids show similar Np(V) complexation constants that are close to literature data for humic acid GoHy-573 (Kim and Sekine, 1991 and Marquardt and Kim, 1998) and Aldrich (Seibert et al., 2001). However, there are differences in the LC of humic acid AHA, M42 and GoHy-573 especially at pH 8. These could be explained by the different origin of the humic acids resulting in various complexation properties. The obtained LC for AHA at pH 8 agrees with that data reported by (Seibert et al., 2001).

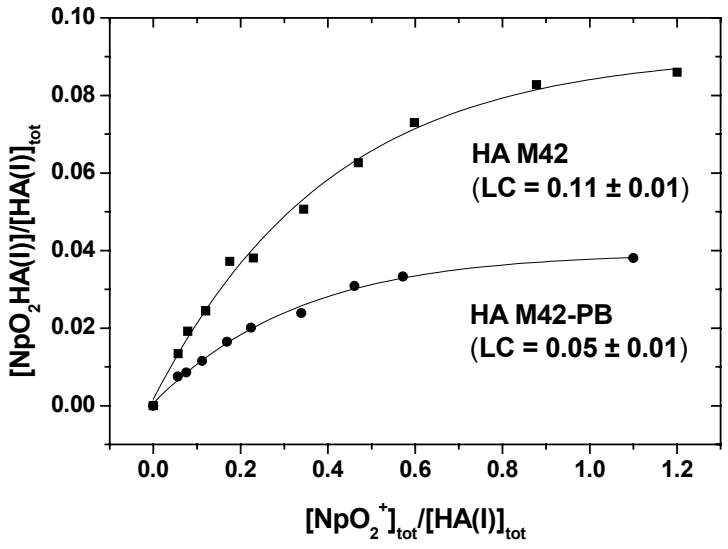

Fig. 2: Illustration of the Np(V) loading capacity of modified (M42-PB) and unmodified (M42) synthetic HA type M42 (pH 7.0).

Comparing the LC of the corresponding modified and unmodified humic acids at pH 7 and pH 8 it becomes obvious that modified humic acid AHA-PB and M42-PB have significantly lower LC than the original, unmodified humic acid AHA and M42, respectively. Due to the modification of phenolic/acidic OH groups (75 % M42 and 84 % AHA) the LC of humic acid M42 and AHA at pH 7 decreases for 53 % and 35 %, respectively. The LC of AHA at pH 8 is reduced for 65 %. These results point to a decrease of the mole fraction of humic acid binding sites for the Np(V) complexation due to the blocking of phenolic/acidic OH groups. Thus, it can be concluded that phenolic/acidic OH groups are involved into the interaction between humic acid and Np(V) in the neutral and alkaline pH range. Comparable results were already found for the uranium(VI) complexation with various humic acids at pH 4 (Pompe et al., 2000). Although the blocking of phenolic/acidic OH groups decreases the number of humic acid complexing sites, the structural parameters of Np(V) humates are not changed due to the humic acid modification, which was found by the EXAFS measurements described in (Sachs et al., 2003 and Schmeide et al., 2003a).
Increasing the pH of the studied system from pH 7 to pH 8, the LC of AHA as well as of AHA-PB increases as expected. However, the reduction of the LC due to the humic acid modification ($LC_{AHA} \rightarrow LC_{AHA\text{-}PB}$) is higher at pH 8 (65 %) than at pH 7 (35 %). That points to the fact that the influence of phenolic OH and other acidic OH groups on the Np(V) complexation by humic acids increases with increasing pH. This result can be attributed to a higher degree of deprotonated phenolic/acidic OH groups at pH 8 than at pH 7.

From our present work and our EXAFS studies described in (Sachs et al., 2003 and Schmeide et al., 2003a) we can conclude, that the Np(V) complex formation by humic acids is not influenced by phenolic/acidic OH groups with respect to the near neighbor surrounding of Np(V) in its humate complexes (coordination numbers and bond lengths) and to the complex stability constants. However, the maximal available number of humic acid complexing sites decreases for humic acids with blocked phenolic OH groups. This result indicates a contribution of humic acid phenolic/acidic OH groups to the interaction between humic acid and Np(V) in the neutral and alkaline pH range.

Acknowledgments

This study was supported by the EC Comission under contract No. FIKW-CT-2001-00128 and by the Federal Ministry of Economics and Labour (BMWA) under contract No. 02 E 9299. The authors thank R. Ruske and M. Meyer for their help in humic acid preparation and characterization and V. Brendler for speciation calculations.

References

Bubner M., Heise K.H. (1994) “Characterization of Humic Acids. II. Characterization by Radioreagent-Derivatization with [^{14}C]Diazomethane”, In: *FZR-43, Annual Report 1993* (Nitsche, H., Bernhard, G., eds.), Forschungszentrum Rossendorf, Institute of Radiochemistry, Rossendorf, Germany, 22.

Choppin G.R., Allard B. (1985) “Complexes of Actinides with Naturally Occurring Organic Compounds”, In: *Handbook on the Physics and Chemistry of the Actinides* (Freeman, A.J., Keller, C., eds.), Elsevier Science Publ., Amsterdam, 407.

Kim J.I., Buckau G. (1988) “*Characterization of Reference and Site Specific Humic Acids”,* RCM-Report 02188, TU München.

Kim J.I., Sekine T. (1991) “Complexation of Neptunium(V) with Humic Acid”, *Radiochim. Acta*, 55, 187.

Kim J.I., Czerwinski K.R. (1996) “Complexation of Metal Ions with Humic Acids: Metal Ion Charge Neutralization Model”, *Radiochim. Acta*, 73, 5.

Kinniburgh D.G., Milne C.J., Benedetti M.F., Pinheiro J.P., Filius J., Koopal L.K., Van Riemsdijk W.H. (1996) “Metal Ion Binding by Humic Acid: Application of the NICA-Donnan Model”, *Environ. Sci. Technol.*, 30, 1687.

Lemire R.J., Fuger J., Nitsche H., Potter P., Rand M.H., Rydberg J., Saphiu K., Sullivan J.C., Ullman W.J., Vitorge P., Wanner H. (2001) “*Chemical Thermodynamics of Neptunium and Plutonium. Chemical Thermodynamics Vol. 4* (OECD NEA, ed.)”, Elsevier Science B.V., Amsterdam.

Marquardt C., Kim J.I. (1998) “Complexation of Np(V) with Humic Acid: Intercomparison of Results from Different Laboratories”, *Radiochim. Acta*, 80, 129.

Pompe S., Brachmann A., Bubner M., Geipel G., Heise K.H., Bernhard G., Nitsche H. (1998) “Determination and Comparison of Uranyl Complexation Constants with Natural and Model Humic Acids”, *Radiochim. Acta,* 82, 89.

Pompe S., Schmeide K., Bubner M., Geipel G., Heise K.H., Bernhard G., Nitsche H. (2000) “Investigation of Humic Acid Complexation Behavior with Uranyl Ions Using Modified Synthetic and Natural Humic Acids”, R*adiochim. Acta,* 88, 553.

Sachs S., Bubner M., Schmeide K., Choppin G.R., Heise K.H., Bernhard G. (2002) “Carbon-13 NMR Spectroscopic Studies on Chemically Modified and Unmodified Natural and Synthetic Humic Acids”, *Talanta,* 57, 999.

Sachs S., Schmeide K., Reich T., Brendler V., Heise K.H., Bernhard G. (2003) “EXAFS Study on the Neptunium(V) Complexation by Various Humic Acids under Neutral pH Conditions”, *Radiochim. Acta*, submitted.

Sachs S., Heise K.H., Bernhard G. (2003a) “Synthetic Humic Acid Model Substances with Specific Functional Properties for the Use in Complexation and Sorption Experiments with Actinides”, In: *FZKA 6800, Wissenschaftliche Berichte* (Buckau, G., ed.), Forschungszentrum Karlsruhe, Karlsruhe, Germany, 51.

Schmeide K., Sachs S., Bubner M., Reich T., Heise K.H., Bernhard G. (2003) “Interaction of Uranium(VI) with Various Modified and Unmodified Natural and Synthetic Humic Substances Studied by EXAFS and FTIR Spectroscopy”, *Inorg. Chim. Acta*, 351, 133.

Schmeide K., Sachs S., Reich T., Heise K.H., Bernhard G. (2003a) “Determination of Structural Parameters for Th(IV), Np(IV), Np(V) and Pu(III) Humate Complexes by Means of XAFS Spectroscopy”, In: *FZKA 6800, Wissenschaftliche Berichte* (Buckau, G., ed.), Forschungszentrum Karlsruhe, Karlsruhe, Germany, 65.

Schnitzer M., Khan S.U. (1972) “*Humic Substances in the Environment”* (A.D. McLaren, ed.), Marcel Dekker, Inc., New York.

Seibert A., Mansel A., Marquardt C.M., Keller H., Kratz J.V., Trautmann N. (2001) “Complexation Behaviour of Neptunium with Humic Acid”, *Radiochim. Acta*, 89, 505.

Stevenson F.J. (1994) "*Humus Chemistry",* 2nd ed., John Wiley&Sons, New York.

Tipping E. (1998) "Humic Ion-Binding Model VI: An Improved Description of the Interactions of Protons and Metal Ions with Humic Substances", *Aquatic Geochem.*, 4, 3.

Torres R.A., Choppin G.R. (1984) "Europium(III) and Americium(III) Stability Constants with Humic Acid", *Radiochim. Acta*, 35, 143.

Wolery T.J. (1992) "EQ3/6, A Software Package for the Geochemical Modeling of Aqueous Systems", UCRL-MA-110662 Part 1, Lawrence Livermore National Laboratory.

Annex 06

Sampling and Characterization of Rock Material from Uranium Mining Waste Rocks for Study and Modeling of Release and Migration of Uranium

S. Sachs[1], P. Benes[2], D. Vopalka[2], K. Stamberg[2], J. Mibus[1], G. Bernhard[1] and A. Bauer[3]

[1] Forschungszentrum Rossendorf e.V., Institute of Radiochemistry, P.O. Box 510 119, 01314 Dresden, Germany (FZR-IfR)

[2] Czech Technical University, Department of Nuclear Chemistry, Brehova 7, 115 19 Praha 1, Czech Republic (CTU)

[3] Forschungszentrum Karlsruhe GmbH, Institute for Nuclear Waste Management, P.O. Box 3640, 76021 Karlsruhe, Germany (FZK/INE)

Sampling and Characterization of Rock Material from Uranium Mining Waste Rocks for Study and Modeling of Release and Migration of Uranium

Sachs S.[1], Benes P.[2], Vopalka D. [2], Stamberg K.[2], Mibus J.[1], Bernhard G.[1] and Bauer A.[3]

[1] Forschungszentrum Rossendorf e.V., Institute of Radiochemistry, P.O. Box 510 119, 01314 Dresden, Germany (FZR-IfR)
[2] Czech Technical University, Department of Nuclear Chemistry, Brehova 7, 115 19 Praha 1, Czech Republic (CTU)
[3] Forschungszentrum Karlsruhe GmbH, Institute for Nuclear Waste Management, P.O. Box 3640, 76021 Karlsruhe, Germany (FZK/INE)

Abstract

To study the effects of humic substances on the leaching and migration of uranium from uranium mining waste a natural rock material was sampled from a uranium rock pile situated in the mining region Schlema/Alberoda (Saxony, Germany). This report describes the sampling and characterization of the <1 mm grain size fraction of the rock material. The main focus is on the characterization of the sampled material with regard to its elemental and mineralogical composition and its content of uranium U_{ex} that is accessible to rock leaching with natural water. The content was analyzed by isotope exchange with ^{233}U and by selective leaching of the rock material. Reasons for the dependence of U_{ex} on conditions of the isotope exchange experiments are discussed.

1 Introduction

Uranium mining and milling produced large amounts of solid wastes containing uranium and other radionuclides spread over many sites of the world. These wastes represent an environmental hazard mainly due to possible release of radioactive and other contaminants into the hydrosphere and atmosphere, and to ensuing contamination of near and more distant environments of the wastes. Consequently, the release and migration of contaminants from the wastes have been rather extensively studied (see, e.g., IAEA, 1995, Merkel et al., 1995 and 2002, Baker et al., 1997, Benes, 1999, Schmeide et al., 2003).
Waste rock piles (overburden, spoils) represent the most frequently encountered wastes from uranium mining. They can release significant concentrations of uranium, together with radium and heavy metals, by leaching into percolating rain water, which is enhanced by weathering of the waste rock and possibly also by the presence of natural organic matter (mainly humic substances) in the percolating water. Such a presence may be due to the decay of plants and waste wood (from mine timbering, etc.) in the wastes. One of the aims of HUPA project has been to study the effect of humic substances on the leaching and migration of uranium from uranium mining waste by laboratory experiments and modeling. For this purpose, a typical waste rock pile was chosen as a model case representing one of the world´s largest areas of underground uranium mining, Ore Mountains (Erzgebirge) in Saxony, Germany. This paper describes the sampling of a typical waste rock material and the results of its characterization.

2 Experimental

Choice of the sample

The model sample was selected with the aim to represent a typical waste rock material for study of the effect of principal factors and conditions on the leaching and re-adsorption of uranium in the system solid phase of waste rock pile – percolating water. It should be suitable for the use in batch as well as in column experiments. Waste rock piles are known to be very heterogeneously, containing great variation of grain sizes from clay particles to large boulders, whose composition can vary as well. However, it is obvious that the release and uptake of migrating components in a solid - solution system is strongly affected by the specific surface area of the solid phase. Larger particles of the solid phase with less specific surface generally have smaller effect. Therefore, fine grained sample material is to be preferred. This sample material is more representative for the bulk composition of the dumped material and for the weathering processes within the rock pile.
The sample with grain size less than 1 mm was taken from the waste rock pile No. 66 in the mining area Schlema/Alberoda (Saxony, Germany). This pile is located in the vicinity of the former rock pile No. 250, which was studied in detail by the Forschungszentrum Rossendorf, Institute of Radiochemistry and described by (Schmeide et al., 2003). Rock pile No. 66 can be considered as a representative of other piles in the mining region Schlema/Alberoda. Some data characterizing this pile have already been published (e.g., Bernhard et al., 1996).

It was not possible to get samples typical for all the different dumped rock materials. The obtained sample is assumed to be representative. Furthermore, for the methodical aspect of this study the focus was put on one single sample.

Sampling procedure and sample treatment

A composite sample was taken from an area of approximately 20 m^2 which was excavated several days before. The samples were hand-sieved to a grain size smaller than 1 mm. The coarse-grained fraction was discarded. Then, the fraction < 1 mm was air dried in the laboratory.

Grain size analysis

Abundance of grain sizes 0.1 mm and larger was determined by sieving and weighing, smaller grain sizes were determined by sedimentation analysis in water column.

Measurement of the BET-Surface area

The N_2-BET surface areas of the material were determined after drying and out gassing for 12 hours at 100 °C under vacuum from multi-point adsorption isotherms. An Autosorb 1 MP Quantachrom surface area analyzer was applied for the measurements.

Determination of the elemental composition and the carbon content

The elemental composition of the sampled rock material was determined by inductively-coupled plasma mass spectrometry (ICP-MS, Perkin Elmer) as well as by atomic absorption spectroscopy (AAS, Perkin Elmer) after grinding (< 63 µm) and total digestion of the sample with HNO_3, HCl, HF (3:1:1) in a microwave oven (Perkin Elmer). The silicon content of the sample was also determined by ICP-MS, however, using HNO_3, HCl and HF in the mixing ratio of 3:1:2 for microwave digestion.
The total and inorganic carbon content of the sample was measured using a LECO-125 C/S analyzer.

Mineralogical investigations

A first qualitative X-ray powder diffraction (XRD) analysis of the sampled material was performed by INE using a Bruker AXS D8-Advance system. In addition to that, the mineralogical composition of the rock material was also quantitatively determined by XRD at the Institute of Mineralogy, Freiberg University of Mining and Technology (TU Bergakademie Freiberg). For quantification the Rietveld method (program BGMN/AUTOQUAN, Bergmann et al., 1997) was applied based on published data for crystal structures.

Determination of accessible (exchangeable) uranium

Accessible (exchangeable) uranium is that part of uranium contained in the sample which is adsorbed on the surface of rock grains or contained in readily soluble minerals and can be leached by percolating water due to a dissolution or an exchange with ions contained in the water. We tested two methods for its determination: isotope exchange with U-233 and selective leaching with solutions used in common analysis of metal bonding in solids by sequential leaching.

The first method is based on the assumption that the accessible uranium in the sample can fully exchange with U-233 added in a test solution. In equilibrium, specific activity of U-233 in the solution and in the accessible part of uranium in the solid sample is the same and can be used for calculation of the content of accessible (exchangeable) uranium U_{ex}:

$$U_{ex} = \frac{V \cdot ({}_1C_{233} + {}_1C_{238}) \cdot (IA_1 - IA_2)}{m \cdot IA_2}.$$

Here U_{ex} is in mg U-238 per mg of the sample, ${}_1C_{233}$ and ${}_1C_{238}$ are concentrations of U-233 and U-238 in the aqueous phase at the beginning of the experiment (in mg/mL), IA_1 and IA_2 are isotopic abundances (specific activities) of U-233 in aqueous phase at the beginning of the experiment and in equilibrium, respectively ($IA_1 = {}_1C_{233} / ({}_1C_{233} + {}_1C_{238})$), V is volume of the aqueous phase in mL and m is mass of the sample in mg.

The experiments were carried out with 3 mL of aqueous sample containing $(1.1\text{-}7.3)\times10^{-6}$ M U-233 in $(1\text{-}330)\times10^{-4}$ M HNO_3 and 30, 67, 150 and 300 mg of sample (V/m: 20-100 mL/mg). The suspension was shaken in polyethylene bottles at room temperature for 14 d until isotope equilibrium was established. The phases were separated by centrifugation and concentrations of U-233 and U-238 were determined in the aqueous phase by ICP-MS. Similar determination was carried out in the initial solution (${}_1C_{233}$ and ${}_1C_{238}$).

The method of selective leaching relies on the displacement of an adsorbed element by a suitable electrolyte and/or dissolution of a distinct solid phase (usually a mineral) with complexing, acidic or oxidizing/reducing solution (Tessier et al., 1979, Benes et al., 1981). The use of this method for determination of accessible uranium has already been described (Yanase et al., 1991, Payne et al., 2001). We tested two solutions used by the authors: (1) Morgan´s solution (1 M CH_3COONa, pH 5 adjusted with acetic acid) which dissolves carbonate minerals and adsorbed elements. (2) TAO solution (oxalic acid, 10.9 g/L and ammonium oxalate, 16.1 g/L, pH 2.7) which dissolves amorphous minerals of Fe, Al and Si and secondary minerals of uranium.

The waste rock sample was shaken with each of these solutions (separately) for 24 h at room temperature and V/m ratio of 40 mL/g (in dark for TAO solution). Then, the phases were separated by centrifugation and the leached amount of uranium was determined by ICP-MS.

3 Results and discussion

Grain size distribution and BET-surface area of the rock sample

The surface area of the grain size fraction smaller than 1 mm was found to be 11.8 m^2/g. Table 1 shows the grain size distribution of the sampled rock material.

Table 1: Grain size distribution of the rock sample.

Grain size (mm)	<0.008	0.008-0.016	0.016-0.035	0.035-0.1	0.1-0.2	0.2-0.5	0.5-1
Relative abundance (wt.-%)	1.9	8.1	19.3	3.5	18.8	35.7	12.7

Elemental composition and carbon content of the rock material

The elemental composition of the rock material which was determined by ICP-MS and AAS is summarized in Table 2. In addition to the elements listed in Table 2, the sampled rock material contains 200 mg/g silicon as main component.

Table 2: Elemental composition of the rock material (relative standard deviation: 1-5 %).

Element	(µg/g)	Element	(µg/g)	Element	(µg/g)	Element	(µg/g)
Li	108	Mn	3120	Nb	22.2	Hg	2.02
Be	4.76	Co	83	Mo	5.56	Al	29600
B	89.2	Ni	208	Ag	4.46	Tl	1.87
Na	2440	Cu	238	Cd	1.04	Pb	91.8
Mg	3120	Zn	235	In	0.29	Bi	11.2
K	20400	Ga	91.0	Sn	15.5	Th	1.91
Ca	10400	As	954	Sb	9.4	U	57.8
Ti	8310	Rb	30.4	Cs	10.9	Sc	66.6
V	280	Sr	73.5	Ba	2300	Nd	4.38
Cr	120	Y	3.72	Ce	11.0	Eu	1.16
Fe	62400	Zr	141	Ta	1.54	Ho	0.204

The total carbon and inorganic carbon content of the sampled rock material amounts to 2 % and 0.3 %, respectively. From that it can be concluded that the studied material contains 1.7 % carbon in form of organic carbon, whose chemical form was not analyzed.

Mineralogical composition of the rock material

By qualitative XRD analysis of the rock material it was determined that the sampled material mainly consists of quartz, muscovite and chlorite. Furthermore, hematite/goethite were detected as iron phases. No expandable clay minerals were found in the rock material.

The results of the quantitative analysis of the mineralogical composition of the rock material are listed in Table 3. The detection limit for the XRD analysis amounts to 0.5–5 wt.-% depending on crystal structure and matrix. The obtained results were normalized to 100 % of the crystalline content.

Table 3: Mineralogical composition of the sampled rock material.

Mineralogical component (Formula after Strunz and Nickel, 2001)		%	3 σ
Anatase	TiO_2	1.25	0.25
Ankerite Fe0.54	$CaFe^{(II)}_{0.54}Mg_{0.46}(CO_3)_2$	9.04	0.60
Barite	$BaSO_4$	0.92	0.11
Calcite	$CaCO_3$	1.43	0.29
Chlorite 2b dis	Mineral group	6.68	0.75
Cordierite [a]	$(Mg, Fe^{(II)})_2Al_4Si_5O_{18}$	0.55	0.66
Fluorapatite	$Ca_5F(PO_4)_3$	0.99	0.39
Gypsum	$CaSO_4 \cdot 2H_2O$	1.16	0.45
Hematite	Fe_2O_3	1.84	0.17
Hornblende, Iron Magnesium	$Na_{<0.5}Ca_2(Fe^{(II)},Mg)_4(Al,Fe^{(III)},Fe^{(II)})(OH)_2(Si,Al)_8O_{22}$	1.85	0.51
Muscovite 2M1 dis	$KAl_2(OH)_2AlSi_3O_{10}$	42.52	1.17
Orthoclase	$KAlSi_3O_8$	3.77	0.72
Plagioclase Albite	$NaAlSi_3O_8$	3.07	0.57
Quartz	SiO_2	21.12	0.57
Rutile	TiO_2	0.70	0.17
Siderite	$Fe^{(II)}CO_3$	3.08	0.28

[a] Detection is uncertain.

From Table 3 it becomes obvious that the mineralogical composition of the rock material is dominated by silicates and carbonates. This is in accordance with the general rock composition in the mining area Schlema/Alberoda (Schmeide et al., 2003). Rock forming minerals are muscovite, chlorite, quartz and feldspars. Vein filling material is represented by carbonates (ankerite, siderite, calcite). Secondary alterations are indicated by gypsum.
It cannot be excluded that in addition to muscovite, a small amount of partly hydrated biotite or a tri-octahedral mixed-layered mineral occurs in the rock material. However, a quantification of these minerals is not possible.

Determination of accessible (exchangeable) uranium

The results of the determination of U_{ex}, mostly by two parallel experiments, are presented in Table 4. As can be seen, the values of U_{ex} vary significantly, depending on the conditions and method of the analysis. Rather clear-cut effect of the liquid-to-solid ratio (V/m) has been found where U_{ex} increases with increasing V/m. This effect is very probably due to the partial dissolution of uranium containing minerals, which enhances accessibility of uranium for isotope exchange. Relative extent of the dissolution should increase with V/m.

Table 4: Determination of accessible (exchangeable) uranium U_{ex} in the sample of waste rock material using isotope exchange under different experimental conditions and selective leaching.

V/*m* (mL/g)	HNO_3 added (10^{-4} mol/L)	pH	U-233 added (10^{-6} mol/L)	U_{ex} (µg/mg)
100	1	8.49	1.1	23.7
100	1	8.50	1.1	22.2
45	1	8.75	1.1	22.9
45	1	8.76	1.1	19.3
20	1	8.66	1.1	20.1
10	1	8.24	1.1	17.6
20	7.7	8.35	1.1	29.7
20	7.7	8.42	1.1	25.9
20	100	7.99	1.1	24.3
20	100	8.04	1.1	22.6
20	330	7.48	1.1	26.9
20	330	7.49	1.1	37.8
20	3.3	8.38	3.7	20.6
20	3.3	8.42	3.7	22.1
20	6.7	8.40	7.3	23.1
20	6.7	8.42	7.3	23.7
40	Leaching with Morgan´s solution			24.6
40	Leaching with TAO solution			34.5

Because the dissolution should also depend on the concentration of acid added with U-233, we studied this dependence by changing the concentration in a rather broad range. The results shown in Table 4 indicate a decrease in pH and an increase in U_{ex} with added HNO_3. However, the effect on U_{ex} is not proportional to the added concentration and considerable differences between parallel experiments were found. At the same time, increasing adsorption (decreased leaching) was observed for U-233 and U-238 with the decreasing pH (increasing added HNO_3). These effects are probably due to dissolution of carbonate minerals and change in uranium speciation in solution with the change in the concentration of CO_3^{2-} ions in the solution. Variation of added amount of U-233 had only a small effect on U_{ex}, which was probably connected with the change in simultaneously added concentration of HNO_3.

From these results it can be concluded that the proportion of accessible uranium in the analyzed sample depends on the conditions under which it is determined, particularly on the *V*/*m* ratio and the initial composition (acidity) of the liquid phase used. The average value for the basic conditions studied (without the excessive acid) is 22.2 ± 2.2 µg/g (about 35 % of total U).

This value can be compared with the amount of uranium released by the selective leaching procedures. The data, expressed as U_{ex}, are also given in Table 4 and represent average values from two determinations. It is obvious that a closer value has been obtained by the leaching with Morgan`s solution, known to dissolve carbonates and adsorbed cations. This supports the abovementioned interpretation of the effect of added acid. TAO solution dissolved significantly higher amount of uranium than corresponds to the average value of U_{ex} and is clearly not suitable for the purpose. It must be emphasized, however, that selective leaching procedures generally have limited selectivity and the forms or bonding of an analyte in a solid phase determined by them are operationally defined.

Table 5: Determination of accessible (exchangeable) uranium U_{ex} in the sample of waste rock material in contact with simulated seepage water using isotope exchange.

V/*m* (mL/g)	U-nat added (10^{-6} mol/L)	U-233 added (10^{-6} mol/L)	U_{ex} (µg/mg)
10	8.6	1.1	19.9
10	0	0.33	20.8
20	0	1.1	20.2
100	8.6	1.1	19.5
100	0	0.33	19.4

Probably the most correct value for exchangeable uranium in a solid phase can be obtained if the isotope exchange is studied under conditions as close as possible to those for which the value is sought. With the aim to check this possibility we carried out similar experiments with isotope exchange of added U-233 using simulated seepage water. Based on the data presented in Table 6, the following components (with corresponding concentrations) were chosen for the preparation of a simulated Schlema/Alberoda water, SAW: $MgSO_4$ (0.0175 mol/L), $CaSO_4$ (0.0091 mol/L), $NaHCO_3$ (0.00258 mol/L). The determination of U_{ex} using SAW is summarized in Table 5. The results show that in the simulated natural medium the influence of experimental conditions, mainly of *V*/*m*, on the value of U_{ex} is weaker, probably due to the smaller changes in total composition caused by leaching of waste rock material.

Composition of a typical seepage water

The composition of a characteristic seepage water from rock pile No. 66 is shown in Table 6 and compared to literature data for the same rock pile (Bernhard et al., 1996).

Table 6: Characteristic parameters for the seepage water composition of the rock pile No. 66.

Parameter	Dimension	Average values derived from data given by (Weinert, 2002)	Literature data (Bernhard et al., 1996)
pH		7.80	8.14
Eh	mV	449.3	
Conductivity	mS/cm	3.38	
O_2	mg/L	10.84	
DOC	mg/L	0.92	
Na	mmol/L	0.535	0.572
K	mmol/L	0.396	0.465
Mg	mmol/L	17.53	16.46
Ca	mmol/L	9.98	11.45
Fe	mmol/L	0.001	
Si	mmol/L	0.07	0.064
As	mmol/L	0.007	0.012
U	mmol/L	0.011	0.011
Cl^-	mmol/L	0.166	0.121
SO_4^{2-}	mmol/L	26.6	25.5
NO_3^-	mmol/L	0.051	0.026
HCO_3^-	mmol/L	2.58	
CO_3^{2-}	mmol/L	0.343	1.933

The average values given were derived from data for one measuring point (M-013) provided by WISMUT GmbH (Weinert , 2002).
The main components of this seepage water are comparable to those of rock pile No. 250, Schlema/Alberoda (Schmeide et al., 2003). Thus, it represents a typical seepage water for the mining region.

Acknowledgements

The authors gratefully acknowledge the WISMUT GmbH for giving us the opportunity for the sampling of the rock material and providing us data for the seepage water composition. In particular, thanks are given to M. Weinert for his assistance during the sampling.
The authors would also like to thank U. Schaefer (Institute of Radiochemistry, Forschungszentrum Rossendorf) for the determination of the elemental composition of the rock material. Thanks are given to R. Kleeberg (Institute of Mineralogy, TU Bergakademie Freiberg) for the XRD analysis and to F. Sus (Nuclear Research Institute, Rez, Czech Republic) for the ICP-MS analysis of uranium solutions.

References

Baker R., Slate S., Benda G. (1997) "*Proceedings of the Sixth International Conference on Radioactive Waste Management and Environmental Remediation ICEM´97",* The American Society of Mechanical Engineers, New York.

Benes P., Sedlacek J., Sebesta F., Sandrik R., John J. (1981) "Method of Selective Dissolution for Characterization of Particulate Forms of Radium and Barium in Natural and Waste Waters", *Water Res.*, 15, 1299.

Benes P. (1999) "The Environmental Impacts of Uranium Mining and Milling and the Methods of their Reduction", In: *Chemical Separation Technologies and Related Methods of Nuclear Waste Management* (Choppin G.R. and Khankhasayev M.Kh., eds.), Kluwer Academic Publishers, Dordrecht, The Netherlands, 225.

Bergmann J., Kleeberg R., Taut T., Haase A. (1997) "Quantitative Phase Analysis Using a New Rietveld Algorithm-Assisted by Improved Stability and Convergence Behaviour", *Adv. X-Ray Anal.*, 40, 425.

Bernhard G., Geipel G., Brendler V., Nitsche H. (1996) "Speciation of Uranium in Seepage Waters of a Mine Pile Studied by Time-Resolved Laser-Induced Fluorescence Spectroscopy (TRLFS)", *Radiochim. Acta,* 74, 87.

IAEA (1995) "*Planning and Management of Uranium Mine and Mill Closures",* IAEA-TECDOC-824, International Atomic Energy Agency, Vienna, Austria.

Merkel B., Hurst S. Loehnert E.P., Struckmeier W. (eds., 1995) *"Uranium Mining and Hydrogeology, Proceedings of the International Conference and Workshop, Freiberg, Germany",* Verlag Sven von Loga, Köln, Germany.

Merkel B., Planer-Friedrich B., Wolkersdorfer C. (eds., 2002) "*Uranium in the Aquatic Environment. Proceedings of the International Conference UMH III and the IMWA Symposium Freiberg, Germany, 15-21 September 2002",* Springer, Berlin, Germany.

Payne T.E. (2001) "Comparison of Laboratory Uranium Sorption Data with 'In Situ Distribution Coefficients' at the Koongarra Uranium Deposit, Northern Australia", *J. Environ. Rad.*, 57, 35.

Schmeide K., Geipel G., Heise K.H., Bernhard G. (2003) "Uranium Mining Waste Rock Pile No. 250 in the Region Schlema/Alberoda (Saxony, Germany)", In: *FZKA 6800, Wissenschaftliche Berichte* (Buckau, G., ed.), Forschungszentrum Karlsruhe, Karlsruhe, Germany, 79.

Strunz H., Nickel E.H. (2001) "*Strunz Mineralogical Tables. Chemical Structural Mineral Classification System",* 9th edition, Schweizerbart, Stuttgart, Germany.

Tessier A., Campbell P.G.C., Bisson M. (1979) "Sequential Leaching Techniques for the Speciation of Particulate Trace Metals", *Anal.Chem.*, 51, 844.

Weinert M. (2002), written note.

Yanase N., Nightingale T., Payne T., Duerden P. (1991) "Uranium Distribution in Mineral Phase of Rock by Sequential Extraction Procedure", *Radiochim. Acta*, 52/53, 387.

Annex 7

Neptunium(V) Sorption onto Granite and its Mineral Constituents in the Absence and Presence of Humic Acid

K. Schmeide, G. Bernhard

Forschungszentrum Rossendorf e.V., Institute of Radiochemistry,
P.O. Box 510119, 01314 Dresden, Germany (FZR-IfR)

Neptunium(V) Sorption onto Granite and its Mineral Constituents in the Absence and Presence of Humic Acid

K. Schmeide, G. Bernhard

Forschungszentrum Rossendorf e.V., Institute of Radiochemistry, P.O. Box 510119, 01314 Dresden, Germany (FZR-IfR)

Abstract

The sorption of neptunium(V) onto granite and its main mineral constituents quartz, orthoclase, albite, biotite, and muscovite is studied under anaerobic conditions as a function of pH in a series of batch equilibrium experiments. Furthermore, the effect of humic acid on the neptunium(V) sorption is studied applying a ^{14}C-labeled synthetic humic acid (type M42) for the experiments. The data suggest that the neptunium sorption onto granite is affected by both the pH and the presence of organic material. In the absence of humic acid, the neptunium sorption starts between pH 7 and pH 8 and increases with increasing pH value. Due to addition of humic acid the neptunium sorption onto granite is decreased in the neutral to alkaline pH range, which is attributed to complexation of neptunium by humic acid in solution. Thus, in this pH range the neptunium mobility is increased by humic substances. The neptunium(V) sorption onto granite and onto its mineral constituent biotite is nearly equal, suggesting that the sorption of neptunium(V) is controlled by the minor amount of biotite which, however, is reactive.

1 Introduction

Besides salt and clay formations also granitic subsurface environments are taken into account as potential host formations for the deep underground disposal of radioactive waste [1,2]. The sorption of Np onto different rock materials and minerals in the absence and presence of humic substances has been described in the literature [e.g., 3-9].
For this study, granite from Eibenstock was chosen which determines as geologic formation a large area of the former uranium mining areas in the Western Erzgebirge in Saxony, Germany. It was already applied for uranium(VI) sorption studies [10,11].
In this work, the sorption of Np(V) onto granite is studied under anaerobic conditions at an ionic strength of 0.1 M as a function of pH. Furthermore, the effect of humic acid (HA) on the Np sorption is studied in order to determine whether humic material is likely to significantly influence Np sorption on granite. The minerals quartz, orthoclase, albite, biotite, and muscovite were also included in this study in order to clarify whether the Np and HA sorption on granite can be explained by Np and HA sorption on its individual main mineral constituents.

2 Experimental

2.1 Materials

The rock material granite, collected in the region Eibenstock (Germany), is composed of 46.13 wt.-% quartz (SiO_2), 11.05 wt.-% orthoclase ($KAlSi_3O_8$), 14.59 wt.-% microcline ($KAlSi_3O_8$), 19.93 wt.-% plagioclase albite ($NaAlSi_3O_8$), 4.36 wt.-% biotite ($K(Mg,Fe^{2+})_3(OH,F)_2/(Al,Fe^{3+})Si_3O_{10}$), 3.44 wt.-% muscovite ($KAl_2(OH)_2AlSi_3O_{10}$), and 0.51 wt.-% fluorapatite ($Ca_5F(PO_4)_3$) (formula after Strunz and Nickel [12]). The composition was determined by XRD analysis applying the Rietveld method (program BGMN/AUTOQUAN [13]) for quantification based on published data for crystal structures. The 63 to 200 µm grain size fractions of the solids were applied for sorption experiments. The Np(V) stock solutions were obtained by dissolving solid $^{237}NpO_2NO_3$ in 0.1 M HNO_3. As HA the ^{14}C-labeled synthetic HA type M42 (batch M170) with a specific activity of 2.38 MBq/g [14,15] was used for the experiments.

2.2 Sorption experiments

For sample preparation, all solutions were prepared with CO_2-free water in a nitrogen atmosphere glovebox. 5 mL of a 0.1 M $NaClO_4$ solution (pH 2.8) were added to 50 mg of the geomaterial in 15 mL vials (PP, Greiner). The samples were stirred for 30 min to remove adsorbed CO_2 from the mineral surface. After that, the desired pH value (pH 4 to pH 11) was adjusted by addition of carbonate-free NaOH or diluted $HClO_4$. During pre-equilibration of the samples (about 4 weeks), the samples were shaken continuously and the pH values were readjusted until they were stable. The sorption experiments in the absence and presence of HA

were started by adding 5 mL 0.1 M $NaClO_4$ solution (pH about 7) and 5 mL HA stock solution (^{14}C-M42, 0.1 M $NaClO_4$), respectively, and instantly after this about 80 µL of the Np(V) stock solution to the preconditioned minerals. The Np(V) stock solutions were prepared prior to each sorption run by passing the solutions through Dowex-50 to separate the ^{233}Pa daughter from ^{237}Np, so that the determination of the β-active nuclide ^{14}C of the ^{14}C-labeled HA by liquid scintillation (LS) counting was not interfered from the beta decay of ^{233}Pa. The oxidation state of Np in the stock solutions was spectroscopically confirmed to be pentavalent. The initial Np and HA concentration in the sample solutions was 1.3×10^{-6} M and 27 mg/L, respectively. The solid solution ratio was 50 mg/10 mL. The pH was readjusted immediately after addition of the stock solutions. Then, the samples were shaken at room temperature for about 160 hours during which the Np and HA sorption onto the solids reached equilibrium. After centrifugation of the samples (3500 rpm, 15 min), the equilibrium pH values were recorded. Subsequently, the supernatant was filtered (450 nm, Minisart RC 15, Sartorius). Prior to filtering, the filters were rinsed with 1 mL of the sample solutions.
In the filtrates, the final Np and HA concentration was determined by analyzing the LS spectra recorded with an LS counter (Wallac system 1414, Perkin Elmer) using α-β discrimination. For this, 1 mL of the filtrate was mixed with 5 mL of a Ultima Gold™ scintillation cocktail (Packard BioScience Company). The amount of Np and HA adsorbed to the mineral surface was calculated as the difference between the initial Np and HA concentrations in the sample solutions and the final Np and HA concentrations in the 450 nm filtrates. Np redox speciation in the filtrates was done by liquid-liquid extraction using TTA (4,4,4-trifluoro-1-(2-thienyl)-butane-1,3-dione) [16].

3 Results and discussion

The Np sorption in the absence of HA and the Np and HA sorption in experiments performed in the presence of HA is shown for granite and its mineral constituents muscovite, orthoclase, albite, quartz, and biotite as a function of pH in Fig. 1.
The sorption experiments, carried out in the absence of HA, show that the Np sorption essentially starts between pH 7 and pH 8 and increases with increasing pH value. Comparing the percentage of Np sorption onto the minerals, biotite shows the strongest sorption, followed by muscovite, orthoclase, albite and quartz. A comparable sharp increase of the Np sorption onto biotite in the alkaline pH region was found by Nakayama and Sakamoto [7].
For the sorption experiments performed in the presence of HA the following results were obtained. As expected, the HA sorption decreases with increasing pH value. The reason for the sudden increase of the HA sorption onto biotite between pH 9.2 and pH 11, obtained in duplicate experiments, is not clear. Compared to the Np sorption in the absence of HA, the Np sorption onto granite is decreased by HA between pH 7 and pH 11. The Np sorption onto muscovite and orthoclase is somewhat increased by HA between pH 6 and pH 9 and at higher pH values relatively strongly decreased. The Np sorption onto albite and quartz is not changed by HA up to pH 10 and pH 9, respectively. At higher pH values it is again relatively strongly

decreased. In case of biotite, the Np sorption is decreased by HA between pH 7 and pH 11, as was found also for granite.

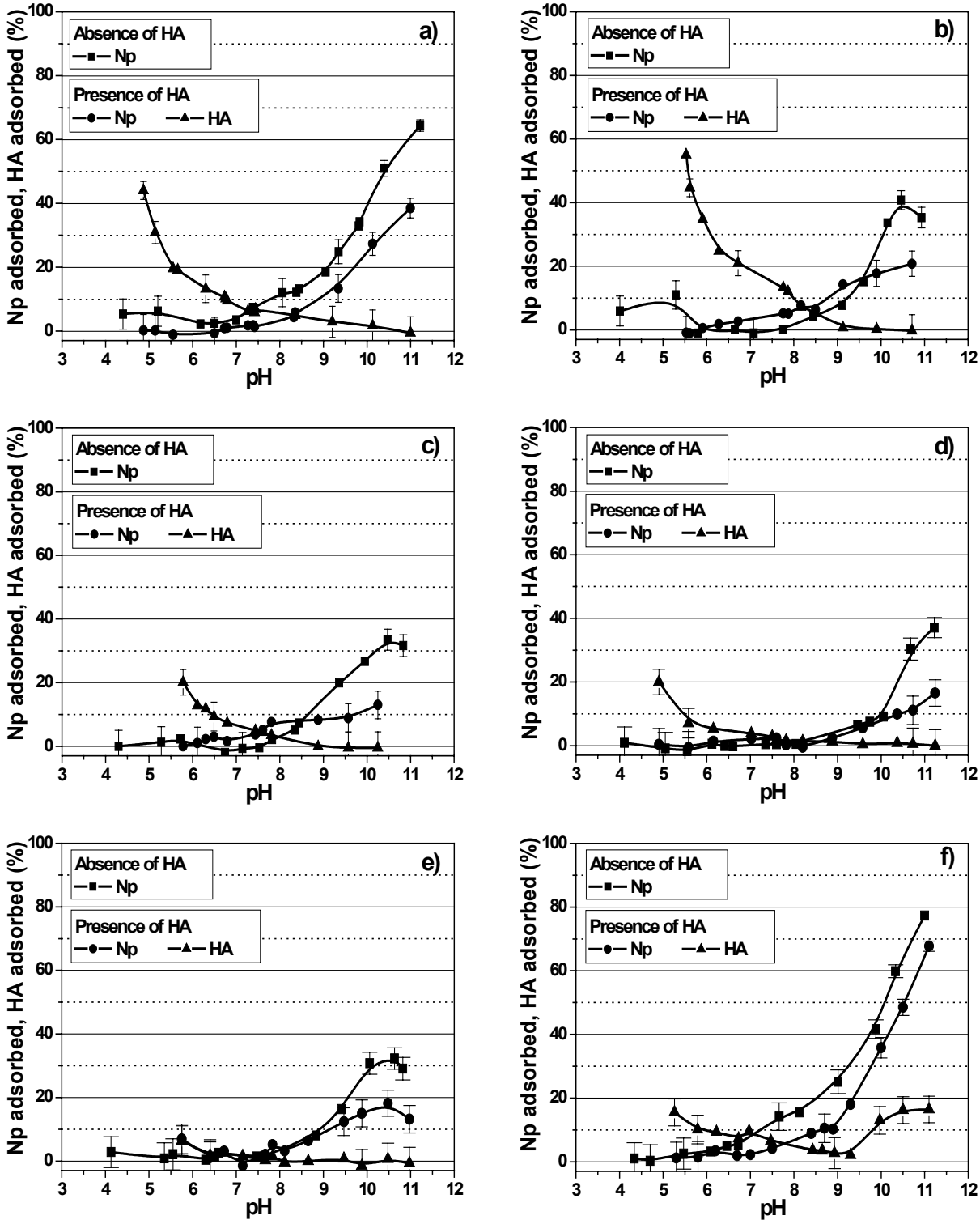

Fig. 1: Np and HA uptake by (a) granite, (b) muscovite, (c) orthoclase, (d) albite, (e) quartz, and (f) biotite ($[NpO_2^+] = 1.3\times10^{-6}$ M; [HA] = 27 mg/L; I = 0.1 M $NaClO_4$; CO_2-free).

The Np speciation for the experimental conditions applied in this study is shown in Fig. 2. It was calculated with the geochemical computer code EQ3/6 [17] applying the Np(V) hydrolysis constants compiled in the NEA data base [18], the Np(V) humate complexation constant log β = 3.6 and the pH function of the loading capacity (LC) with LC = -0.589 + 0.101 * pH [15]. The results show that the free neptunyl ion predominates the Np speciation in aqueous solution both in the absence and in the presence of HA. The neptunyl hydroxyl species $NpO_2OH_{(aq)}$ is formed increasingly in solution between pH 9.5 and pH 11. In the presence of HA, $NpO_2HA(I)$ is formed between pH 6 and pH 11 with a maximum of 13.6 % near pH 10.5. For the pH region higher than 9, the formation of the mixed complex $(NpO_2(OH)HA)_{coll.}$ is suggested by Marquardt et al. [19]. Presently, this complex cannot be quantified thermodynamically, however, this complex would explain the strong reduction of the Np sorption by HA at pH values higher than 9 and 10, respectively.

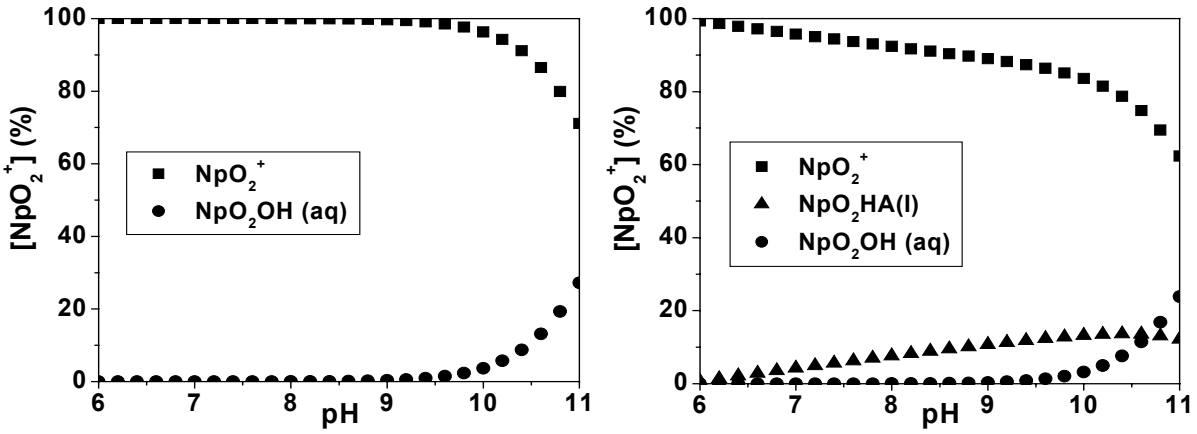

Fig. 2: Np speciation in solution ($[NpO_2^+]$ = 1.3×10^{-6} M; [HA] = 27 mg/L; I = 0.1 M $NaClO_4$; CO_2-free).

The results in Fig. 1 have shown, that both granite and biotite show a strong Np sorption in the alkaline pH region. Furthermore, compared to the Np sorption experiments in the absence of HA, the reduction of the Np sorption by HA between pH 7 and pH 11, which is attributed to the formation of soluble Np humate complexes, is similar for both materials. From this, it is concluded that biotite is the dominating mineral phase in the rock material granite for the Np sorption.

For biotite, used in this study, Mössbauer spectroscopic measurements have shown that in the un-weathered mineral 84.5 % of Fe_{total} occur as Fe(II) [20]. This Fe(II) occurring in biotite and thus, also in granite could possibly lead to a reduction of Np(V) to Np(IV).

An autoradiographic study of the Np sorption onto Climax Stock granite slabs in a synthetic groundwater [21] showed a strong sorption of Np onto Fe(II)-containing minerals biotite and pyrite on the granite surface. This was attributed to a reduction of Np(V) to the less soluble Np(IV) by Fe(II) in the Fe(II)-containing minerals. Furthermore, for magnetite it was found by Nakata et al. [22] that Np(V) is reduced to Np(IV) by Fe(II) on the surface of magnetite but not by Fe(II) ions released from magnetite into solution. In contrast, Nakayama and

Sakamoto [7] found no clear indication to Np(V) reduction in case of biotite since no significant difference was observed in the removal of Np by Fe(II)-containing minerals biotite and magnetite and by a ferric oxide of hematite.
A reduction of Np(V) to Np(IV) on the mineral surface would lead to an increase of the Np sorption. However, for Np batch and column experiments in the presence of HA it was found by Zeh et al. [23] that especially the combination of Fe(II), present at trace concentrations in solution, and HA could lead to a reduction of Np(V) to Np(IV). Compared to Np(V), Np(IV) is generally stronger complexed by HA [24,6]. The humic colloid-borne Np(IV) species is known to remain stable in groundwater and to be easily mobile in porous aquifer systems [23,6].
Thus, the decrease of the Np sorption onto granite and biotite between pH 7 and pH 11 by HA compared to the Np sorption experiments without HA, which was not observed for the other mineral constituents of granite in the neutral pH range, can be attributed to the complexation of Np(V) by HA and possibly to the complexation of Np(IV) by HA. The oxidation state of Np in the supernatant solutions of the sorption samples without and with HA was checked by liquid-liquid extraction using TTA. So far, no Np(IV) could be detected in solution.
It has to be noted, that the softer minerals biotite and muscovite in the granite 63 to 200 µm grain size fraction were, as a result of the grinding process, distinctively smaller than the harder grains quartz and albite [11]. By SEM investigations is was estimated that the grain size of biotite and muscovite in the granite powder is < 20 µm. This is also reflected by the fact, that the specific surface area determined for granite is higher than calculated from the specific surface areas of the minerals taking into account their content in the rock material. Thus, appropriate specific surface areas of the minerals biotite and muscovite have to be used in modeling the neptunium sorption onto the rock material granite.

Acknowledgements
This work was partially supported by the EC Commission under contract No. FIKW-CT-2001-00128 and by the Federal Ministry of Economics and Labour (BMWA) under contract No. 02E9299. The authors would like to thank B. Barz and R. Jander for their assistance in performing the batch experiments, V. Brendler for Np speciation calculations, S. Sachs and T. Arnold for providing the HA and the rock material, respectively, and R. Kleeberg (Institute of Mineralogy, TU Bergakademie Freiberg) for the XRD analysis.

References

[1] Papp, R.: Gegenüberstellung von Endlagerkonzepten in Salz und Hartgestein. FZKA-PTE Nr. 3, Forschungszentrum Karlsruhe GmbH, Karlsruhe, Germany, 1997.

[2] Commission of the European Communities, PAGIS: Performance Assessment of Geological Isolation Systems for Radioactive Waste, EUR 11775 EN (1988).

[3] Kohler, M., Honeyman, B.D., Leckie, J.O.: Neptunium(V) Sorption on Hematite (α-Fe_2O_3) in Aqueous Suspension: The Effect of CO_2. Radiochim. Acta 85, 33 (1999).

[4] Torstenfelt, B., Rundberg, R.S., Mitchell, A.J.: Actinide Sorption on Granites and Minerals as a Function of pH and Colloids/Pseudocolloids. Radiochim. Acta 44/45, 111 (1988).

[5] Righetto, L., Bidoglio, G., Azimonti, G., Bellobono, I.R.: Competitive Actinide Interactions in Colloidal Humic Acid-Mineral Oxide Systems. Environ. Sci. Technol. 25, 1913 (1991).

[6] Artinger, R., Marquardt, C.M., Kim, J.I., Seibert, A., Trautmann, N., Kratz, J.V.: Humic Colloid-borne Np Migration: Influence of the Oxidation State. Radiochim. Acta 88, 609 (2000).

[7] Nakayama, S., Sakamoto, Y.: Sorption of Neptunium on Naturally-Occurring Iron-Containing Minerals. Radiochim. Acta 52/53, 153 (1991).

[8] Gutierrez, M.G., Bidoglio, G., Avogadro, A., Yllera de Llano, A.: Studies on Hydro-Geochemical Controls of Neptunium and Selenium Migration in Granite Columns. Radiochim. Acta 58/59, 277 (1992).

[9] Sakamoto, Y., Nagao, S., Ogawa, H., Rao, R.R.: The Migration Behavior of Np(V) in Sandy Soil and Granite Media in the Presence of Humic Substances. Radiochim. Acta 88, 651 (2000).

[10] Krawczyk-Bärsch, E., Arnold, T., Bernhard, G.: Das Sorptionsverhalten von U(VI) am Granit von Eibenstock (Erzgebirge) und seinen mineralogischen Komponenten. European Journal of Mineralogy 13, 103 (2001).

[11] Arnold, T., Krawczyk-Bärsch, E., Bernhard, G.: Sorption of U(VI) on Granite: Comparison of Experimental and Predicted U(VI) Sorption Data. In: FZR-343, Annual Report 2001, Forschungszentrum Rossendorf, Institute of Radiochemistry, Rossendorf, Germany, 2002, p. 21.

[12] Strunz, H., Nickel, E.H.: Strunz Mineralogical Tables. Chemical Structural Mineral Classification System. 9th edition, Schweizerbart, Stuttgart, Germany, 2001.

[13] Bergmann, J., Kleeberg, R., Taut, T., Haase, A.: Quantitative Phase Analysis Using a New Rietveld Algorithm Assisted by Improved Stability and Convergence Behaviour. Adv. X-Ray Anal. 40, 425 (1997).

[14] Pompe, S., Bubner, M., Meyer, M., Nicolai, R., Heise, K.H., Bernhard, G.: Synthesis of ^{14}C-Labeled and Unlabeled Humic Acid Type M42. In: FZR-318, Annual Report 2000, Forschungszentrum Rossendorf, Institute of Radiochemistry, Rossendorf, Germany, 2001, p. 31.

[15] Sachs, S., Schmeide, K., Brendler, V., Krepelová, A., Mibus, J., Geipel, G., Heise, K.H., Bernhard, G.: Investigation of the Complexation and the Migration of Actinides and Non-Radioactive Substances with Humic Acids under Geogenic Conditions. Complexation of Humic Acids with Actinides in the Oxidation State IV Th, U, Np. Final Report, BMWA Project No. 02E9299, Rossendorf, Germany, 2003.

[16] Bertrand, P.A., Choppin, G.R.: Separation of Actinides in Different Oxidation States by Solvent Extraction. Radiochim. Acta 31, 135 (1982).

[17] Wolery, T.J.: EQ3/6. A Software Package for the Geochemical Modeling of Aqueous Systems. Report UCRL-MA-110662 Part I. Lawrence Livermore National Laboratory, California, USA, 1992.

[18] Lemire, R.J., Fuger, J., Nitsche, H., Potter, P., Rand, M.H., Rydberg, J., Spahiu, K., Sullivan, J.C., Ullmann, W.J., Vitorge, P., Wanner, H.: Chemical Thermodynamics of Neptunium and Plutonium. Elsevier, Amsterdam, 2001.

[19] Marquardt, C., Kim, J.I.: Complexation of Np(V) with Humic Acid: Intercomparison of Results from Different Laboratories. Radiochim. Acta 80, 129 (1998).

[20] Arnold, T., Forschungszentrum Rossendorf, personal communication.

[21] Beall, G.W., O'Kelly, G.D., Allard, B.: An Autoradiographic Study of Actinide Sorption on Climax Stock Granite. ORNL-5617 (1980).

[22] Nakata, K., Nagasaki, S., Tanaka, S., Sakamoto, Y., Tanaka, T., Ogawa, H.: Sorption and Reduction of Neptunium(V) on the Surface of Iron Oxides. Radiochim. Acta 90, 665 (2002).

[23] Zeh, P., Kim, J.I., Marquardt, C.M., Artinger, R.: The Reduction of Np(V) in Groundwater Rich in Humic Substances. Radiochim. Acta 87, 23 (1999).

[24] Kim, J.I., Delakowitz, B., Zeh, P., Klotz, D., Lazik, D.: A Column Experiment for the Study of Colloidal Radionuclide Migration in Gorleben Aquifer Systems. Radiochim. Acta 66/67, 165 (1994).

Annex 8

Molecular size and mass distributions of humic substances measured by AFFFF and TOF-SIMS

Wolf, M. [1], Szymczak, W. [2], Chanel, V. [1], Buckau, G. [3]

[1] GSF-National Research Center for Environment and Health, Institute of Groundwater Ecology, 85764 Neuherberg, Germany

[2] GSF-National Research Center for Environment and Health, Institute of Radiation Protection, 85764 Neuherberg, Germany

[3] Forschungszentrum Karlsruhe, Institute for Nuclear Waste Management, 76021 Karlsruhe, Germany

Molecular size and mass distributions of humic substances measured by AFFFF and TOF-SIMS

Wolf, M.[1], Szymczak, W.[2], Chanel, V.[1], Buckau, G.[3]

[1] GSF-National Research Center for Environment and Health, Institute of Groundwater Ecology, 85764 Neuherberg, Germany

[2] GSF-National Research Center for Environment and Health, Institute of Radiation Protection, 85764 Neuherberg, Germany

[3] Research Center Karlsruhe, Institute for Nuclear Waste Management, 76021 Karlsruhe, Germany

Abstract

The molecular size and mass distributions of different natural and synthetic humic substances (HSs: one fulvic acid (FA) and four humic acids (HAs)) were determined by asymmetrical flow field-flow fractionation (AFFFF) and time-of-flight secondary ion mass spectrometry (TOF-SIMS). Investigated were the following natural HSs: Aldrich HA, Gohy-573 FA and HA and synthetic HSs: M1 HA and M42 HA. The individual HSs show characteristic molecular size/mass distributions with the following trends in size (AFFFF): M42 HA > Gohy-573 HA > M1 HA > Aldrich HA > Gohy-573 FA or mass (TOF-SIMS): Gohy-573 HA > Aldrich HA > Gohy-573 FA > M42 HA ~ M1 HA. These results show that molecular size is not always correlated with molecular mass and show generally higher values. Reasons may be association in aqueous solution and/or analyte-membrane interactions, but changes in ionization probabilities and fragmentation probabilities of weak associated molecules with higher masses can also not be excluded.

1 Introduction

Humic substances (HSs) are a mixture of very complex organic molecules with mainly unknown structures and are ubiquitous in the terrestrial and aquatic environment. The chemical properties of HSs to form relatively stable complexes with heavy metals and radionuclides are important with respect to the migration of these pollutants in groundwater. To understand the physical/chemical interactions of HSs with these pollutants it is essential to elucidate not only structural information for HSs but also their molecular size/mass distribution. The measurement of molecular size/mass distribution of HSs can be done by various methods. For example the methods SEC (size exclusion chromatography), HPSEC (high-performance size exclusion chromatography) (e.g. Wolf et al. 1999, 2001; Hoque et al. 2003), FFFF (flow field-flow fractionation) (e.g. Giddings 1966; Beckett et al. 1987; Schimpf and Petteys 1997; Ngo Manh Thang et al. 2001) and AFFFF (asymmetrical flow field-flow fractionation) (Wahlund and Giddings 1987) are based on the different diffusion coefficients of molecules with different hydrodynamic sizes in solution whereas special mass spectrometrical methods (e.g. electrospray-ionization quadrupole time-of-flight mass spectrometry (Plancque et al. 2002) or TOF-SIMS (time-of-flight secondary ion mass spectrometry) (Szymczak et al. 2000, 2003) measure directly the molecular mass distribution of HSs.

The aim of this paper is to analyze the size and mass distribution of different HSs with the methods AFFFF and TOF-SIMS to get an insight into the variation of molecular size/mass distribution of natural and synthetic HSs and to get a better understanding of the chemical processes responsible for the formation and stability of HS-metal complexes generated with these HSs in further experiments.

2 Materials and methods

2.1 Chemicals and molecular mass standards

All chemicals were purchased from commercial sources (Aldrich, Fluka, Sigma-Aldrich) in the highest purity available and are used as-delivered. The aqueous solutions were prepared with high purity water (Milli-Q_{PLUS}, Millipore). Polyacrylic acid (PAA) molecular mass standards were purchased from American Polymer Standards Corporation (APSC), USA (Table 1). The chemical structures of the more complex polycarboxylic acids DMA and GA are shown in Fig. 1.

2.2 Humic substances

Five different humic substances (HSs) were investigated: The natural HSs Aldrich HA (purified and derived from Dr. J. Mizera, CTU Prague) and Gohy-573 HA and FA extracted from deep groundwater of the Gorleben aquifer (Wolf et al. 2004) and the synthetic HSs M1 HA and M42 HA (both HAs derived from Dr. S. Sachs, Research Center Rossendorf, Institute

of Radiochemistry). The synthesis and characterization of the synthetic HSs have been described elsewhere (Pompe et al. 1996, 1998).

Table1: Molecular mass data and commercial sources of used chemicals and standards.

Chemicals and standards	M_n (Da)	M_w (Da)	M_p (Da)	M_r	Commercial source
Hydrazoic acid (purchased as sodium salt)				43.03	Aldrich
Isophtalic acid				166.14	Fluka
1,2,4,5-Benzenetetracarboxylic acid				254.15	Aldrich
2-(4-(2,2-Dicarboxy-ethyl)-2,5-dimethoxy-benzyl)-malonic acid (DMA)				370.31	Sigma-Aldrich
Glycyrrhizic acid (GA) (purchased as ammonium salt)				822.94	Fluka
Polyacrylic acid (PAA) 2K	1230	1930	1250		APSC
PAA 5K	3450	5660	4100		APSC
PAA 18K	12 800	18 100	16 000		APSC

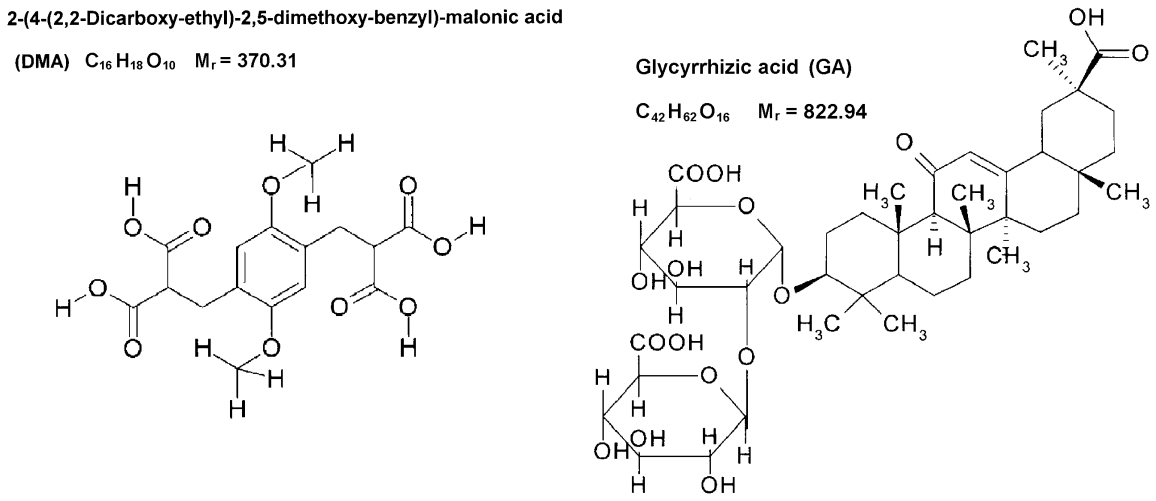

Fig. 1: Chemical structures of the used relatively complex polycarboxylic acids DMA and GA.

2.3 Asymmetrical flow field-flow fractionation (AFFFF)

Field-flow fractionation is a technique for size fractionation of macromolecules and colloids. It was first proposed in 1966 by Giddings and later also applied for humic substances (e.g. Beckett et al. 1987, Schimpf and Petteys 1997, Ngo Manh Thang et al. 2001). In this method the analyte, dissolved in a carrier medium, is pumped with constant velocity through a thin

ribbon-like channel equipped with a membrane permeable for the carrier. The flow-field is established by a cross-flow perpendicular to the channel flow and the size fractionation is a function of the diffusion coefficient. Two types of equipments are available: a) the first developed symmetrical flow field-flow fractionation (FFFF) using a symmetrical channel with constant width and two permeable walls and b) the more recently developed asymmetrical flow field-flow fractionation (AFFFF) using an asymmetrical channel with continuously reduced channel width and one permeable wall (Wahlund and Giddings 1987).

AFFFF was carried out with a system delivered from Wyatt Technology (USA) using a fractionation channel from ConSenxus (Germany) and regenerated cellulose membrane from Wyatt Technology (USA) with a cut-off of 1 kDa (related to globular proteins). The asymmetrical channel has a length of 286 mm and a spacer thickness of 0.54 mm. As mobile phase, 5 mM Tris buffer (pH ~ 9.1; cf. Ngo Manh Thang et al. 2001) was used at a channel flow of 0.6 mL min^{-1} and a cross-flow of 3 mL min^{-1}. The absorbance of the effluent was recorded with an UV/Vis detector (K-2500, Knauer, Germany) at 210 nm. The fractionated sample volume was 20 µL. Usually analyte concentrations of 3 – 30 mg/L dissolved in the mobile phase were analyzed. For calibration of the AFFFF system sodium azide, various polycarboxylic acids and polyacrylic acid (PAA) standards were used.

2.4 Time-of-flight secondary ion mass spectrometry (TOF-SIMS)

Time-of-flight secondary ion mass spectrometry (TOF-SIMS) in combination with oblique 30 keV SF_5^+ ion bombardment (Szymczak and Wittmaack 1994) produces highly reproducible mass spectra of HSs which cover up to five orders of magnitude in dynamic range without background subtraction (Szymczak et al. 2000). The recorded spectra were highly reproducible, not just with respect to characteristic spectral features but also in absolute terms. Usually the measured yields were the same to within 10% or better. Spectra in the negative ionization mode are less affected by fragmentation than in the positive mode. Therefore, spectra are presented in the negative mode.

The time-of-flight secondary ion mass spectrometer used in this work has been described elsewhere (Szymczak and Wittmaack 2002). The bombardment parameters were as follows: primary ions SF_5^+, ion source terminal voltage 30 kV, target bias -6 kV (for negative secondary ions), ion impact energy 36 kV, stationary beam current 1–2 nA, pulse width about 3 ns, repetition rate 19 kHz, $1–3 \times 10^7$ pulses per spectrum, channel width 0.5 ns/bin. The nominal angle between the primary ion beam line and the surface normal of the sample is 60°. The area of ion bombardment was ~ 0.3×0.4 mm^2. The corresponding upper limit of detectable mass was m/z 6000. Neutrals generated along the first half of the beam line were removed by tilting the second half of the drift tube by a few degrees (both sections straight). The secondary ions were directed to the detector electrostatically. Postacceleration by biasing the detector was not applied.

Solid samples for TOF-SIMS analysis were prepared by spray-deposition on cleaned silicon substrates (Szymczak et al. 1998) to produce samples with a mean coverage to about 100

monolayers. Cleaned Si-wafer with hydrophilic character was used as substrates. Solutions of 200 mg/L of HSs were dissolved in a dilute aqueous solution of NH_4OH. Typically 200 – 300 µL of solution were sprayed at a nozzle-to-substrate spacing of at least 35 mm. The area covered by the spray was a factor of about three to four larger than the area spanned by the silicon substrates (8x8 mm^2). The total amount of sprayed HSs was about 40 – 60 µg. This converts to areal densities of roughly 15 – 30 µg/cm^2.

3 Results and discussion

3.1 AFFFF results

3.1.1 Calibration of the AFFFF system

The AFFFF system was calibrated with sodium azide, various polycarboxylic acids (PCAs) and polyacrylic acid (PAA) molecular mass standards (Table 1) instead of usually used polystyrene sulfonate (PSS) standards in order to avoid overestimation of molecular sizes of HSs (cf. Wolf et al. 1999, 2001; Hoque et al. 2003). We found in accordance with Ngo Manh Thang et al. 2001 also a concentration dependency of the elution volume with the molecular mass of our used standards. To construct the calibration curve for very low concentrations (1-5 mg/L; cf. Ngo Manh Thang et al. 2001), necessary to get more realistic molecular size distributions, we measure or extrapolate the concentration dependency of the different standards down to the lowest possible measurable concentration (in our case 3 mg/L). The obtained calibration curve used for calculation of the molecular size distribution is shown in Fig. 2 and can be fitted to an exponential function expressed also in Fig. 2.

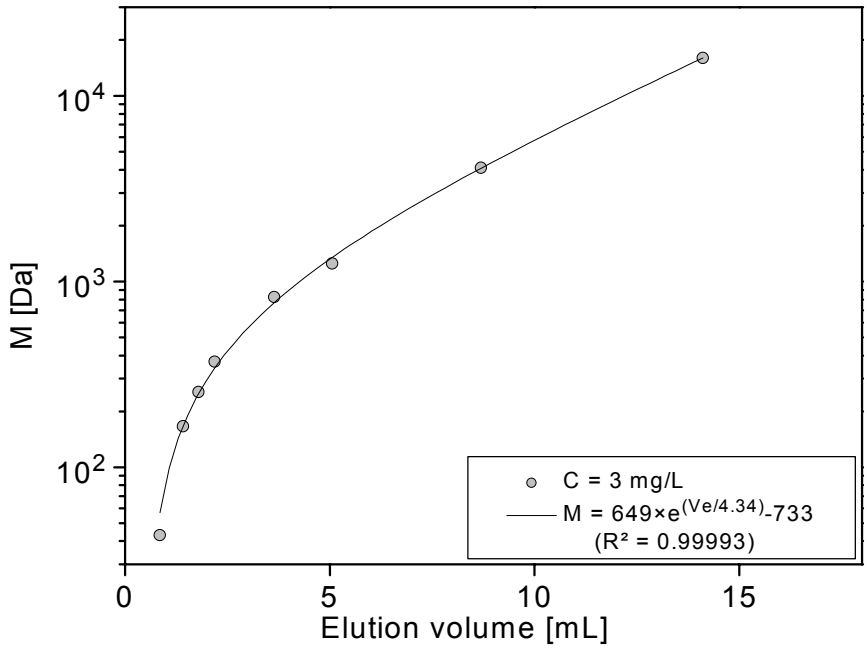

Fig.2: AFFFF calibration curve derived with sodium azide, various polycarboxylic acids and polyacrylic acid (PAA) standards.

3.1.2 Humic substances

The AFFFF fractograms were recorded simultaneously during the measurement by the software ASTRA 4.50 (Wyatt Technology). Before and after the HSs measurements blanc samples (only eluent) were measured. The derived fractogram of the blanc was subtracted from the original fractogram by using the software Corona 1.40 (Wyatt Technology). The obtained fractograms (after blanc subtraction) for the three natural HSs Aldrich HA, Gohy-573 HA and FA are shown in Fig. 3, those for the two synthetic HSs M1 HA and M42 HA are depicted in Fig. 4.

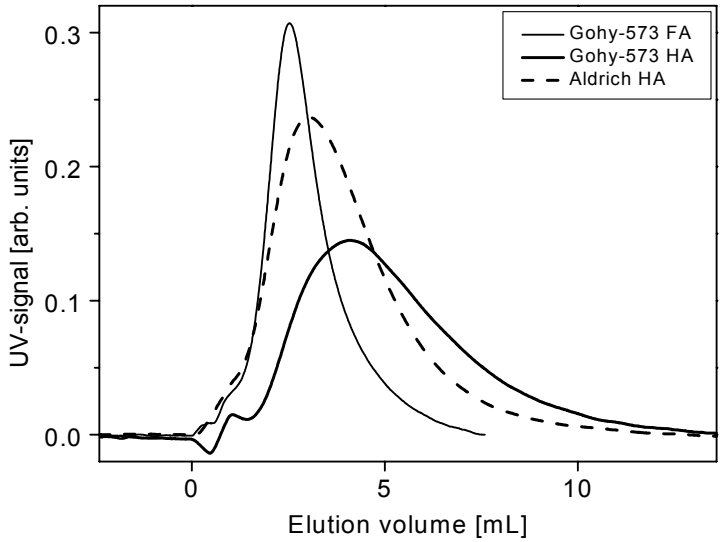

Fig. 3: AFFFF fractograms of the natural HSs Aldrich HA and Gohy-573 HA and FA.

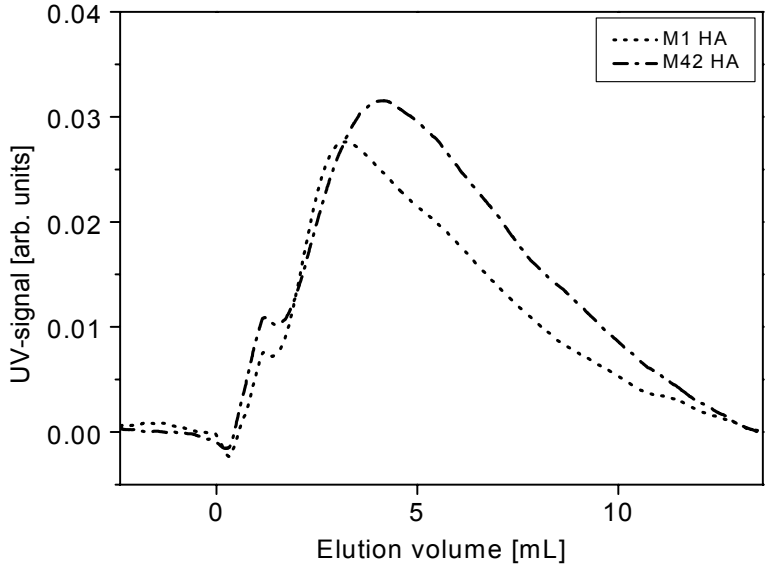

Fig. 4: AFFFF fractograms of the synthetic HSs M1 HA and M42 HA.

The transformation of the AFFFF fractograms into the size distribution (relative mass concentration related to the mass of the used polycarboxylic acid (PCA) standards) plotted on a logarithmic mass scale was done by

a) smoothing of the obtained fractogram (UV signal versus elution volume Ve)

b) calculating from Ve the corresponding molecular mass with the obtained calibration equation

$$M = 649 \times e^{(Ve/4.34)} - 733$$

c) correction of the UV signal (proportional to mass concentration) due to the nonlinearity of the calibration curve by the equation

$$H_{corr} = H_{meas}/\Delta(\log M)$$

d) transformation of the corrected UV signal in relative UV signal = relative mass concentration.

The derived molecular size distributions of all five investigated HSs are presented in Fig. 5.

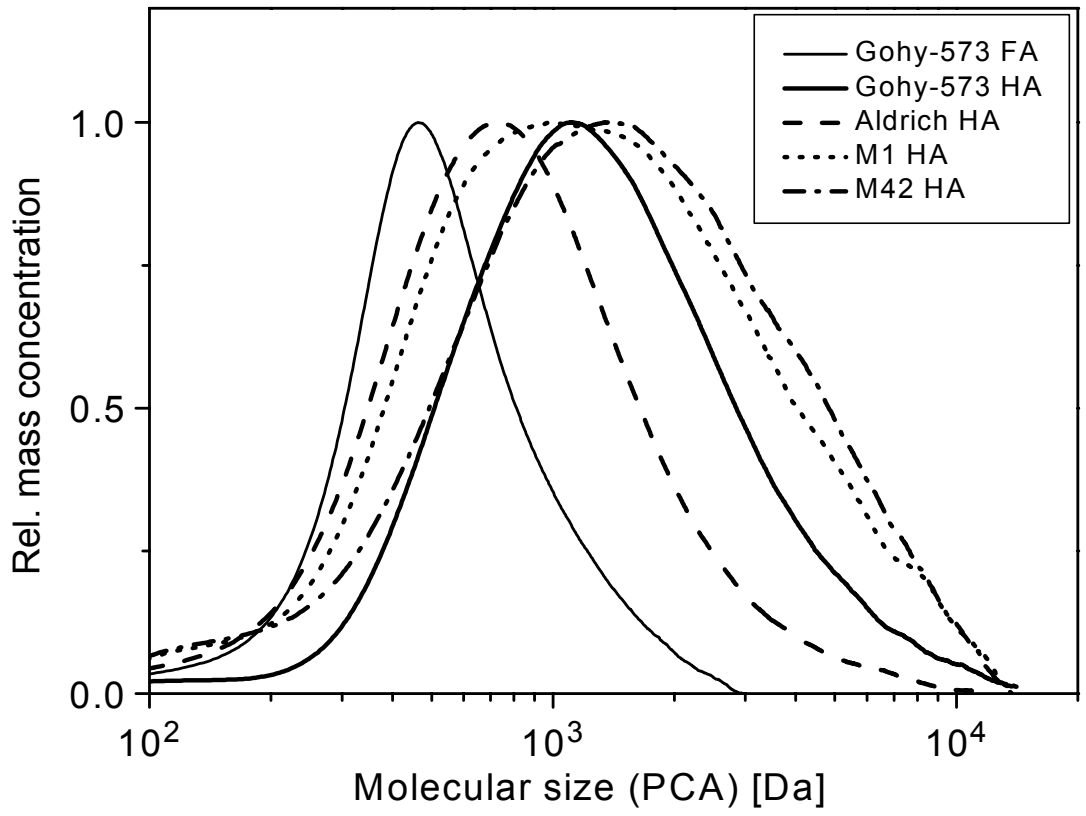

Fig. 5: Molecular size distributions related to polycarboxylic acid (PCA) standards of the investigated HSs.

Each individual HS has its own characteristic size distribution and based on the M_p' (peak value in the molecular size distribution plotted on the logarithmic molecular size scale) or M_n (number average molecular size) values (Table 2) the following trend in size is obtained: M42 HA > Gohy-573 HA > M1 HA > Aldrich HA > Gohy-573 FA. As expected the Gohy-573 FA

shows the smallest size distribution with molecular sizes up to 3000 Da whereas all HAs show larger size distributions with molecular sizes up to 10-14 kDa.

The M_n and M_w (weight average molecular size) values were calculated as usual from the AFFFF fractograms (after blanc subtraction) using the measured UV signals H_i and the corresponding molecular sizes M_i with the equations:

$$M_n = \frac{\sum_i H_i}{\sum_i (H_i / M_i)} \qquad \text{and} \qquad M_w = \frac{\sum_i (H_i \times M_i)}{\sum_i H_i}$$

The M_p' values together with the M_p values (peak value in the molecular size distribution plotted on the linear molecular size scale) and the other molecular size data M_n, M_w and M_w/M_n (polydispersity) are presented in Table 2. All M_n values fall in the range below or around 1 kDa whereas the M_w values show a range up to more than 2 kDa. As expected the polydispersity of Gohy-573 FA has a lower value (1.3) than those of the HAs (1.7 – 2.2).

Table 2: Molecular size data related to PCA standards of the investigated HSs.

Humic substance	Size range (Da)	M_p' (Da)	M_p (Da)	M_n (Da)	M_w (Da)	M_w/M_n
Gohy-573 FA	150 - 3000	460	410	470	620	1.3
Gohy-573 HA	150 - 14 000	1120	700	990	1760	1.8
Aldrich HA	150 - 10 000	730	490	640	1070	1.7
M1 HA	150 - 12 000	1100	530	890	1930	2.2
M42 HA	150 - 12 000	1400	680	1000	2150	2.1

3.2 TOF-SIMS results

3.2.1 Humic substances

Fig. 6 shows the negative TOF-SIMS spectra of the Aldrich HA sample, of the two synthetic HAs (M1 and M42) and of the natural HA and FA (Gohy-573) samples. The spectra are normalized to 2×10^7 primary ion pulses at a dc beam current of 1 nA. The mass scale is shown at the top of the graph.

Below m/z 150 all spectra are characterized by high-yield atomic ions and fragments. Above m/z > 150 the spectra show the characteristic broad, almost featureless, high-mass distribution with a long tail known from our previous work (Szymczak et al. 2000). The Aldrich HA and the two natural HSs (Gohy-573) show an observable tail up to m/z 3000 whereas the tail of both synthetic HSs disappears above m/z 1500. The broad maximum of the FA Gohy-573

distribution peaks at a lower mass and its tail declines faster with increasing mass than the HA Gohy-573 distribution.

On the lower mass side (m/z <= 100) the spectra show source specific fragments (Fig. 7). In the Aldrich HA spectrum intense sulphur based fragments, e.g. SH^-, SOH^-, SO_3^-, SO_3H^- and SO_4H^-, are present. The synthetic HA samples are dominated by intense nitrogen based fragments, e.g. CN^- and CNO^-. The yield of CN^- and CNO^-, $Y(CN^-)$ resp. $Y(CNO^-)$, of the M42 sample is roughly twice of that of the M1 sample. $Y(O^-)$ of sample M42 exceeds that of sample M1 ($Y(O^-)_{M42}$ / $Y(O^-)_{M1}$ = 1.4) whereas $Y(OH^-)$ of M1 is slightly higher than that of M42 (($Y(OH^-)_{M1}$ / $Y(OH^-)_{M42}$ = 1.09).

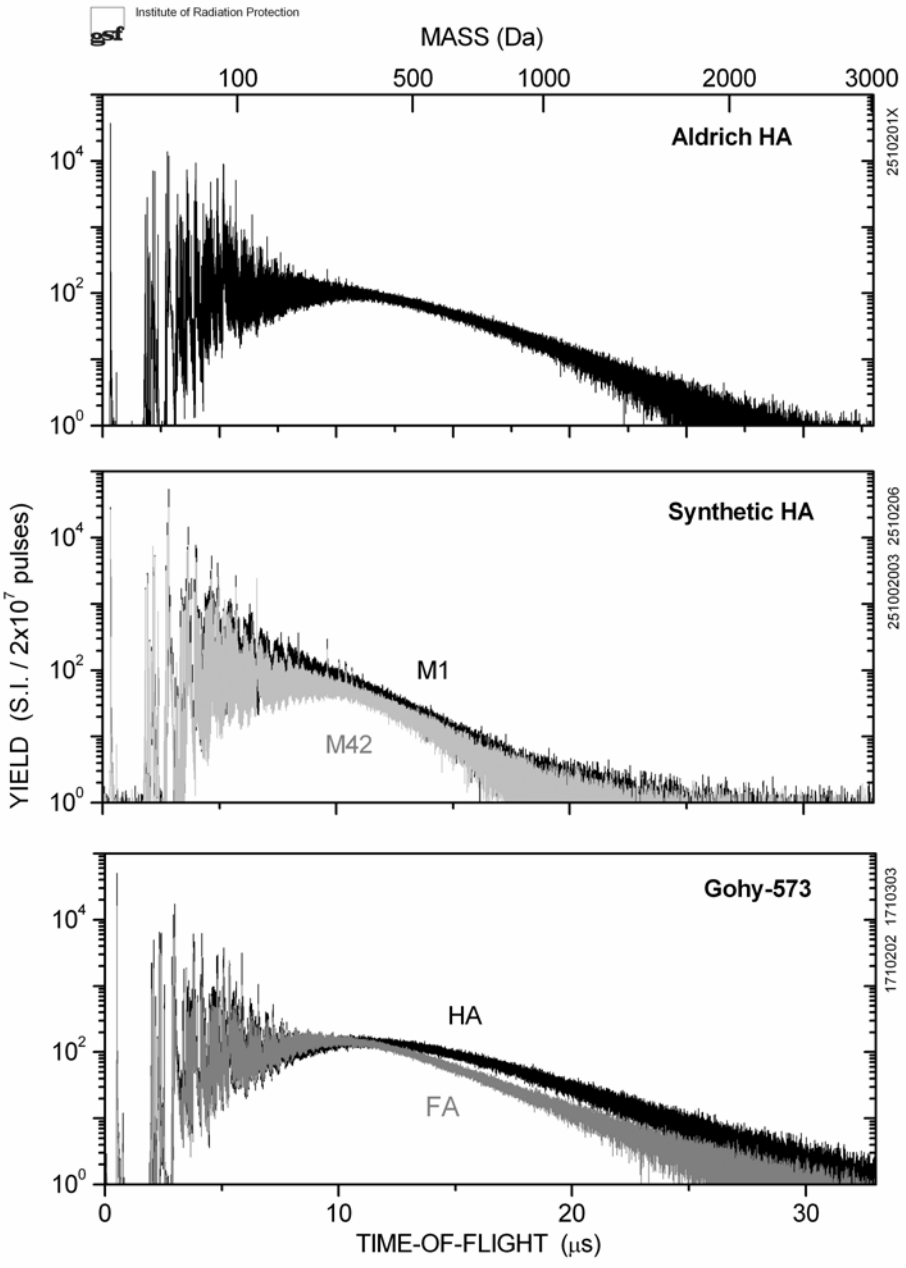

Fig. 6: Negative TOF-SIMS spectra of HSs.

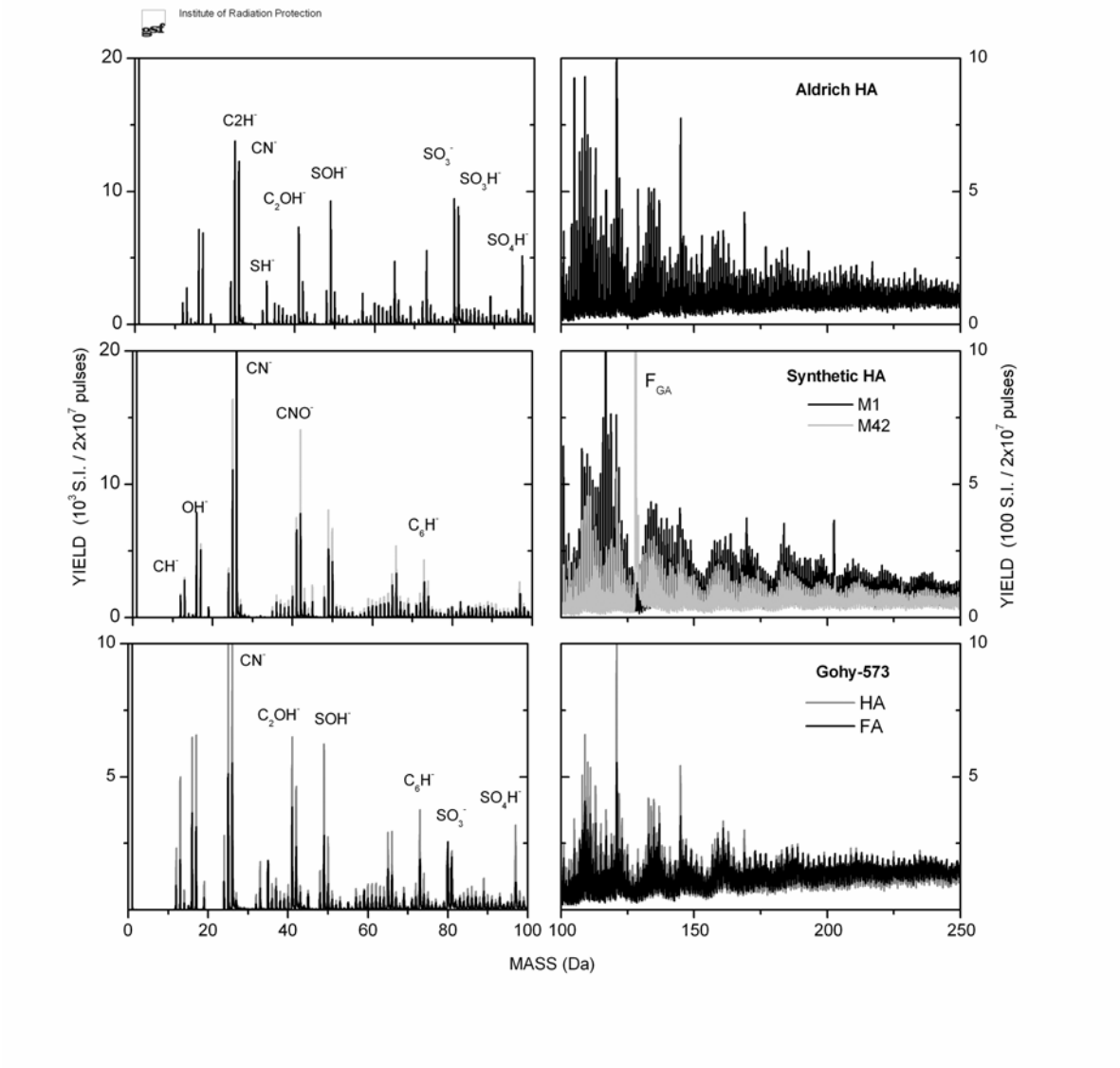

Fig. 7: Sections of negative TOF-SIMS spectra of the Aldrich HA, M1 HA and M42 HA.

The natural HSs Gohy-573 samples show nitrogen- as well as sulphur based fragments where the yield of the HA sample exceeds the yield of the FA sample mostly more than twice.
In the mid mass range (100 < m/z < 500) all spectra exhibit a dense sequence of mass lines covering every mass number. The envelope modulation around peak groups declines faster in the case of the Aldrich HA compared to the synthetic HAs. The intensity of the peak groups of M1 is higher than of the M42. The mass line at m/z 129, denoted as F_{GA} , is a fragment of the specific glutamine acid source material of M42 HA. The natural Aldrich HA denotes a weak pronounced pattern of odd-numbered mass lines in contrary to a peak group modulation with a 14-mass separation in case of the synthetic HSs.

In the mid-range mass section the FA Gohy-573 spectrum has a pronounced pattern of nearly odd-mass numbered lines. In the HA Gohy-573 the variation between odd and even numbered mass lines spectrum are less pronounced.

3.2.2 Transformation of TOF-SIMS spectrum into mass concentration versus mass

In order to compare the size distribution derived by AFFFF with the mass distribution obtained by TOF-SIMS analysis of a sample we transformed the original TOF-SIMS spectrum as follows (Fig. 8):

Based on known mass lines and the mass-TOF-relation

$$T = k \times M^{1/2} + t_o$$

the time scale was transformed individually for every spectrum into a mass scale.

The yield of the TOF-SIMS spectrum

$$Y_{TOF} = f\,(TOF), \text{ with } dT = \text{const.}$$

was transformed to the true yield Y_{true} with a constant mass interval by

$$Y_{true} \sim Y_{TOF} / (M)^{1/2}, \; dM = \text{const.}$$

Then Y_{true} was summed up over a constant log-interval, e.g. d(logM) = 0.01 and the mass concentration M_{conc} calculated by

$$M_{conc} = Y_{true} \times M$$

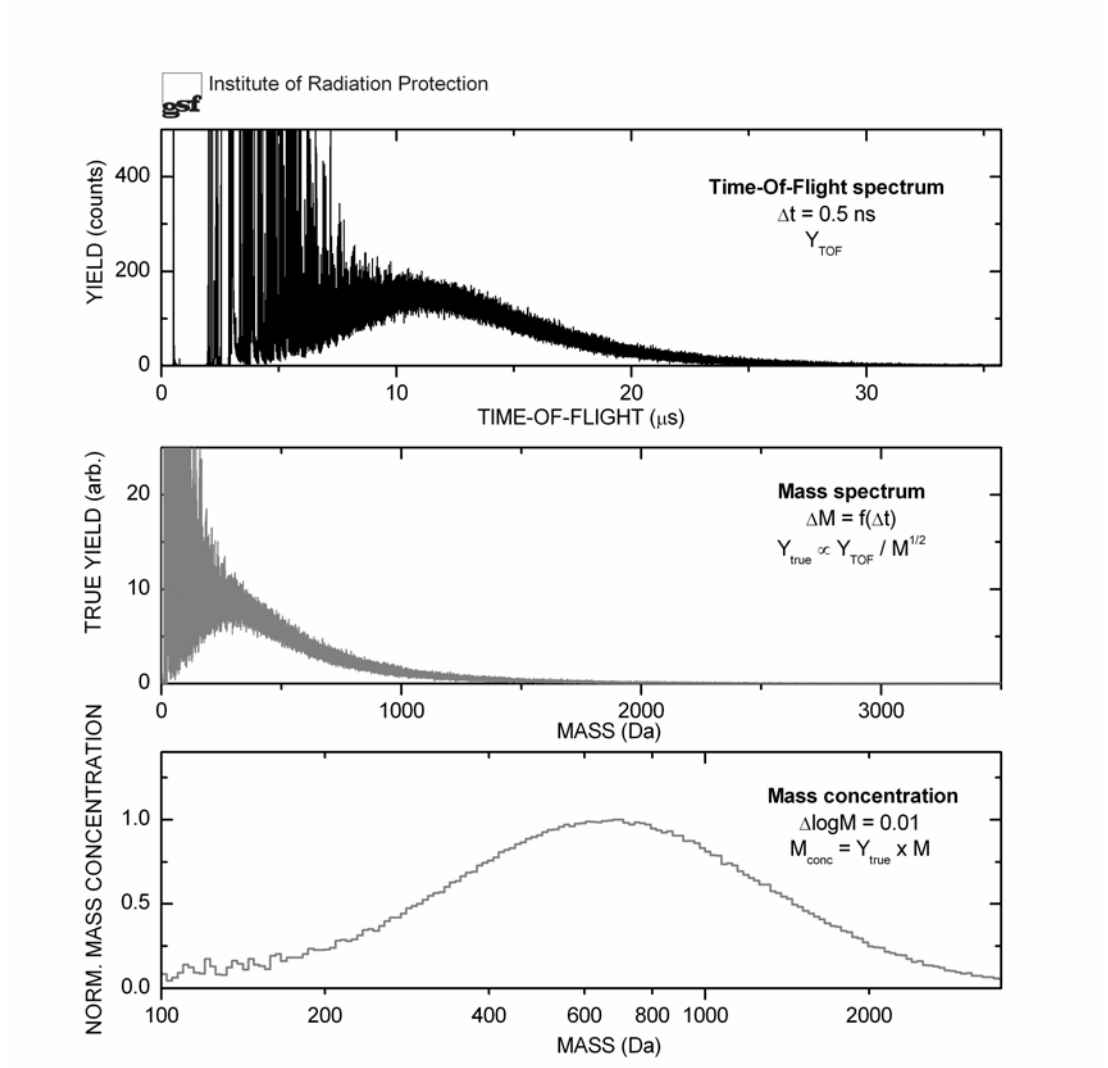

Fig. 8: Transformation of the TOF-SIMS spectrum (number of particles versus time-of-flight) into mass concentration versus mass unit.

Fig. 9 compares the transformed TOF-SIMS spectra of the different HSs. The calculated mass concentration M_{conc} was normalized to the distribution maximum. The maximum of the transformed distribution shifts to higher masses from FA Gohy-573 to HA Aldrich and HA Gohy-573. The broader HA Gohy-573 distribution is shifted as a whole whereas the high mass tail of the FA Gohy-573 distribution intersects the HA Aldrich distribution and remains comparable in mass concentration above the intersection. The distributions of the synthetic HSs M1 and M42 are comparable and both clearly shifted as a whole to lower masses. The low mass tail of the synthetic HSs is more structured than the distribution from the natural sources.

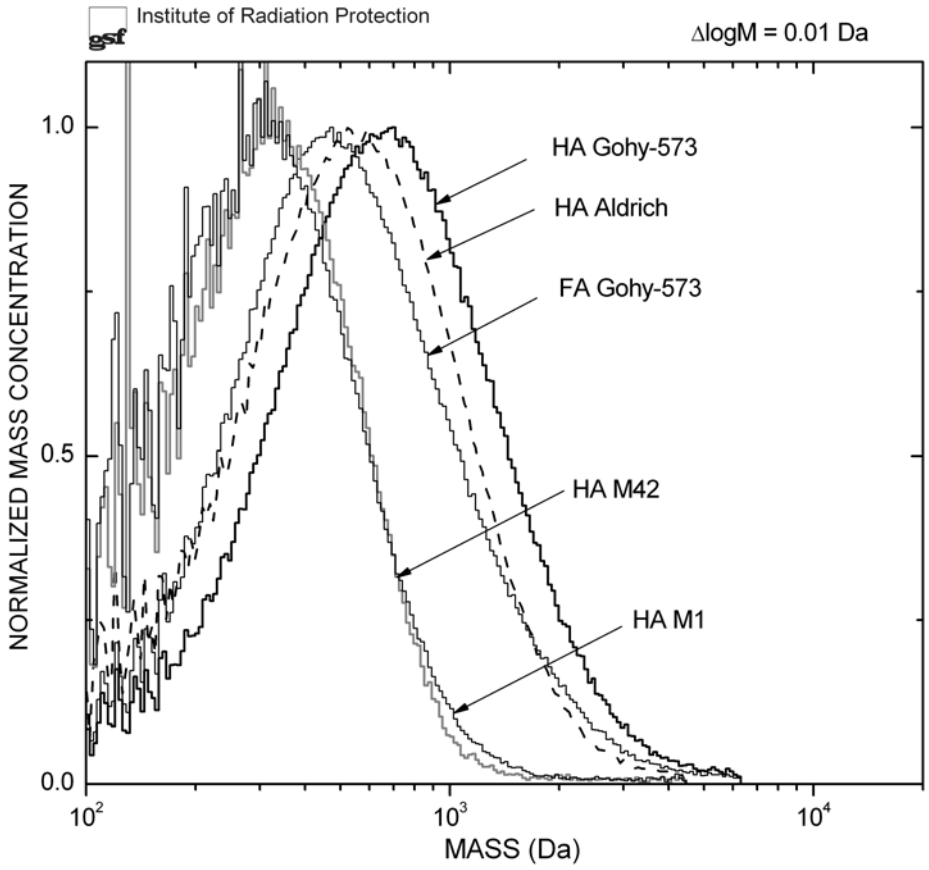

Fig. 9: Normalized mass concentration versus mass of the investigated HSs.

Table 3: Calculated distribution parameters of the distributions M_{conc} versus mass.

Humic substance	Size range (Da)	M_n (Da)	M_w (Da)	M_w/M_n
Gohy-573 FA	150 – 3000 [5000]	428 [428]	609 [613]	1.42 [1.43]
Gohy-573 HA	150 – 3000 [5000]	521 [523]	752 [759]	1.44 [1.45]
Aldrich HA	150 – 3000 [5000]	445 [446]	626 [627]	1.40 [1.41]
M1 HA	150 – 1500 [3000]	305 [306]	380 [390]	1.25 [1.27]
M42 HA	150 – 1500 [3000]	310 [312]	380 [389]	1.23 [1.25]

The distribution parameters M_n, M_w and M_w/M_n of the HSs are summarized in Table 3. The lower mass limit of integration was set to m/z 150 in order to cut the high intensity of low mass fragments. The upper limit of integration was set to the bottom out of the mass concentration versus mass (linear). Background subtraction (typically 1 - 2 counts/time bin) was applied if the mass concentration distribution increases in the highest mass range. With an extended second upper limit (values in squared brackets) the distribution parameters are nearly the same which confirms the first high mass limit. All M_n values are significant below one kDa. The M_n value as well as the polydispersity M_w/M_n is highest for the Gohy-573 HA and smallest for the synthetic HSs, in detail Gohy-573 HA > Aldrich HA > Gohy-573 FA > M42 HA ~ M1 HA.

4 Conclusions

Determination of the molecular size and mass distributions of different natural and synthetic humic substances by the methods AFFFF and TOF-SIMS shows different characteristic molecular size/mass distributions with calculated M_n values below or around 1 kDa. These results support the lower molecular size/mass range of aquatic HSs found in literature. Based on the M_n values the measured trend in size measured by AFFFF was M42 HA > Gohy-573 HA > M1 HA > Aldrich HA > Gohy-573 FA, different from that of the trend in mass measured by TOF-SIMS: Gohy-573 HA > Aldrich HA > Gohy-573 FA > M42 HA ~ M1 HA. In the case of the Gohy-573 FA there is good agreement between the size and mass derived M_n and M_w values. With both natural HSs Aldrich HA and Gohy-573 HA the TOF-SIMS based M_n values are significantly lower. But with the synthetic HSs M1 HA and M42 HA the size outnumbers definitely the mass derived distribution. These results show that molecular size is not always correlated with molecular mass. Compared to the molecular masses of the individual HSs the molecular sizes show generally higher values probably due to association of HSs in aqueous solution and/or analyte-membrane interactions, but changes in ionization probabilities and fragmentation probabilities of weak associated molecules with higher masses, particularly in the case of the synthetic HSs, can also not be excluded.

5 Acknowledgements

The authors thank Dr. J. Mizera (CTU Prague) and Dr. S. Sachs (Research Center Rossendorf, Institute of Radiochemistry) for making the purified Aldrich HA and synthetic HAs M1 and M42 available. For skilful laboratory work and technical support of this work we thank D. Jurrat and G. Teichmann.

References

Beckett R., Jue Z., Giddings J.C. (1987) “Determination of Molecular Weight Distributions of Fulvic and Humic Acids Using Flow Field-Flow Fractionation”, *Environ. Sci. Technol.*, **21**, 289.

Giddings J.C. (1966) “A New Separation Concept Based on a Coupling of Concentration and Flow Uniformities”, *Sep. Sci.*, **1**, 123.

Hoque E., Wolf M., Teichmann G., Peller E., Schimmack W., Buckau G. (2003) “Influence of ionic strength and organic modifier concentrations on characterization of aquatic fulvic and humic acids by high-performance size-exclusion chromatography”, *J. Chromatogr. A*, **1017**, 97.

Ngo Manh Thang, Geckeis H., Kim J.I., Beck H.P. (2001) “Application of the flow field flow fractionation (FFFF) to the characterization of aquatic humic colloids: evaluation and optimization of the method”, *Colloids Surf. A*, **181**, 289.

Plancque G., Amekraz B., Moulin V., Toulhoat P., Moulin Ch. (2001) “Molecular structure of fulvic acids by electrospray with quadrupole time-of-flight mass spectrometry”, *Rapid Commun. Mass Spectrom.*, **15**, 827.

Pompe S., Brachmann A., Bubner M., Geipel G., Heise K.H., Bernhard G., Nitsche H. (1998) “Determination and Comparison of Uranyl Complexation Constants with Natural and Model Humic Acids”, *Radiochim. Acta*, **82**, 89.

Pompe S., Bubner M., Denecke M.A., Reich T., Brachmann A., Geipel G., Nicolai R., Heise K.H., Nitsche H. (1996) “A Comparison of Natural Humic Acids with Synthetic Humic Acid Model Substances: Characterization and Interaction with Uranium (VI)”, *Radiochim Acta*, **74**, 135.

Schimpf M.E., Petteys M.P. (1997) “Characterization of humic materials by flow field-flow fractionation”, *Colloids Surf. A*, **120**, 87.

Szymczak W., Wessels J., Kataoka Y., Wittmaack K. (1998) “Secondary Ion Mass Spectrometry SIMS XI”, ed. By G. Gillen, R. Lareau, J. Bennett and F. Sievie, John Wiley & Sons, Chicester, p. 493.

Szymczak W., Wittmaack K. (1994) “Evidence for strongly enhanced yield of negative molecular secondary ions due to bombardment with SF_n cluster ions”, *Nucl. Instrum. Methods in Physics Res. B*, 149.

Szymczak W., Wittmaack K. (2002) “Effect of water treatment on analyte and matrix ion yields in matrix-assisted time-of-flight secondary ion mass spectrometry: the case insulin in and on hydroxycinnamic acid”, *Rapid Commun. Mass Spectrom.*, **16**, 2025.

Szymczak W., Wolf M., Wittmaack K. (2000) “Characterization of Fulvic Acids and Glycyrrizic Acid by Time-of-Flight Secondary Ion Mass Spectrometry”, *Acta hydrochim. hydrobiol*., **28**, 350.

Szymczak W., Wolf M., Wittmaack K. (2003) “Comparison of as-delivered and AFFFF-size-fractionated Suwannee River fulvic acid by time-of-flight mass spectrometry”, In: Humic Substances: Nature’s Most Versatile Materials (Eds. E.A. Ghabbour and G. Davies), Taylor & Francis, New York, 31.

Wahlund K.-G., Giddings J.C. (1987) “Properties of an Asymmetrical Flow Field-Flow Fractionation Channel Having One Permeable Wall”, *Anal. Chem.*, **59**, 1332.

Wolf M., Buckau G., Geckeis H., Ngo Manh Thang, Hoque E., Szymczak W., Kim J.I. (2001) “Aspects of Measurement of the Hydrodynamic Size and Molecular Mass Distribution of Humic and Fulvic Acids”, In: Humic Substances: Structures, Models and Functions (Eds. E.A. Ghabbour and G. Davies), Royal Society of Chemistry, Cambridge, 51.

Wolf M., Buckau G., Geyer S. (2004) “Isolation and characterization of new batches of Gohy-573 humic and fulvic acids”, In this report.

Wolf M., Teichmann G., Hoque E., Szymczak W., Schimmack W. (1999) “Copper speciation in aqueous solutions of fulvic acid and related molecular weight distributions”, *Fresenius J. Anal. Chem.*, **363**, 596.

Annex 9

Isolation and characterization of new batches of Gohy-573 humic and fulvic acids

Wolf, M. [1], Buckau, G. [2], Geyer, S. [3]

[1] GSF-National Research Center for Environment and Health, Institute of Groundwater Ecology, 85764 Neuherberg, Germany

[2] Forschungszentrum Karlsruhe, Institute for Nuclear Waste Management, 76021 Karlsruhe, Germany

[3] UFZ Centre for Environmental Research Leipzig-Halle, Department of Hydrogeology, 06120 Halle, Germany

Isolation and characterization of new batches of Gohy-573 humic and fulvic acids

Wolf, M.[1], Buckau, G.[2], Geyer, S.[3]

[1] GSF-National Research Center for Environment and Health, Institute of Groundwater Ecology, 85764 Neuherberg, Germany

[2] Research Center Karlsruhe, Institute for Nuclear Waste Management, 76021 Karlsruhe, Germany

[3] UFZ Centre for Environmental Research Leipzig-Halle, Department of Hydrogeology, 06120 Halle, Germany

Abstract

Natural aquatic humic acid (HA) and fulvic acid (FA) from 6000 L groundwater of the deep borehole Gohy-573 in the Gorleben aquifer (Lower Saxony, Germany) were isolated, purified and characterized. Characterization includes elemental composition (C,H,N,O and S), content of inorganic constituents (by ICP-MS and ICP-AES), determination of size distribution by asymmetrical flow field-flow fractionation (AFFFF), mass distribution by time-of-flight secondary ion mass spectrometry (TOF-SIMS), and proton exchange capacity by potentiometric pH titration. The results show that the isolation and purification was successful, and that the prepared humic and fulvic acids have the expected typical properties. The large batches of the substances serve the basis for a broad number of scientific investigations with the insurance that the material used is well purified and that results from different future investigations can be compared with each other.

1 Introduction

The natural humic acid (HA) and fulvic acid (FA) from groundwater of the deep borehole Gohy-573 in the Gorleben aquifer have been used for numerous studies for almost two decades. These batches were isolated, purified and characterized within the EC project MIRAGE (MIgration of RAdionuclides in the GEosphere). These two batches have been used up and therefore a new sampling campaign was started. Large new batches of humic and fulvic acids from this groundwater were isolated, purified and characterized. The borehole Gohy-573 is located in the Gorleben aquifer above the Gorleben salt dome in Lower Saxony, Germany (Fig. 1) with an inflow of groundwater from Präelster sediments in the depth range 134 – 137 m (Artinger et al. 2000, Buckau et al. 2000). The groundwater of this borehole is dark brown and has an elevated DOC (dissolved organic carbon) content of 97.2 mg C/L with the main DOC components being humic acid (60 mg C/L) and fulvic acid (17 mg C/L) (Artinger et al. 2000, Buckau et al. 2000).

This paper describes the sampling, isolation, purification and characterization of the new Gohy-573 humic and fulvic acid batches. These new batches of humic and fulvic acids will enable comparison of results from different types of experiments for many years to come. Through comparison with the characteristic properties of the old batches from the same groundwater, future results can also be compared with results from past investigations of almost two decades.

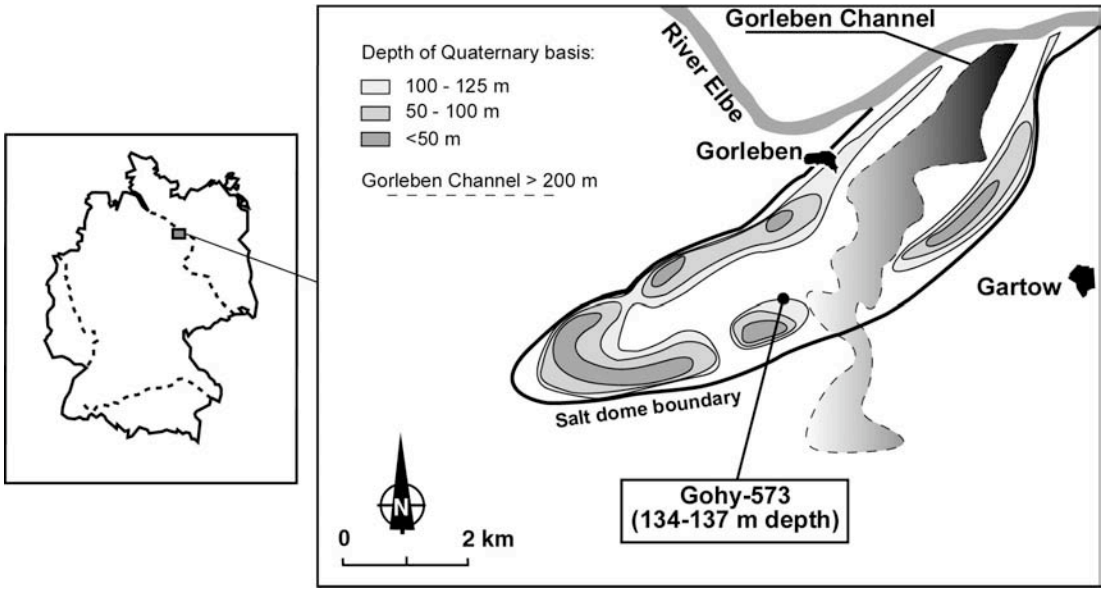

Fig. 1: Location of the borehole Gohy-573 in the Gorleben aquifer (simplified from Schäfer et al. 2004).

2 Materials and methods

2.1 Chemicals

All chemicals were purchased from commercial sources (Aldrich, Fluka, Merck) in the purity p.A. or higher and are used as delivered. The XAD-8 resin was purchased from Rohm & Haas in the purity technical grade but extensively purified (Geyer 1993) before use. The cation

exchanger AG® 50W-X8 was purchased from Bio-RAD Laboratories and used as recommended by the supplier. The aqueous solutions were prepared with high purity water (Milli-Q_{PLUS}, Millipore).

Fig. 2: Acidification of the original groundwater from borehole Gohy-573 in the tank trailer by G. Buckau (photo: S. Geyer).

2.2 Isolation of Gohy-573 humic and fulvic acids

The field sampling of Gorleben groundwater Gohy-573 was carried out in cooperation with DBE (Deutsche Gesellschaft zum Bau und Betrieb von Endlagern für Abfallstoffe mbH, Peine). After groundwater pumping until constant conditions were obtained (on-line measurement of temperature, pH and redox potential), about 6000 L of groundwater was pumped into a cleaned tank trailer (Fig. 2). The groundwater was acidified to a pH of about 4 by addition of HCl, in order to avoid calcite precipitation in the subsequent field concentration process by RO (reverse osmosis). Mixing and degassing of the groundwater sample was achieved by driving the trailer about 2 km over forest tracks to the facility area where electric power etc. was available for the subsequent RO concentration. By RO treatment (custom designed RO system from Wilhelm Werner GmbH - Reinstwassertechnik, Leverkusen; Fig. 3), the volume was reduced to about 900 L in 50 L stainless steel containers. The containers were then transported to the laboratory for further treatment.

Fig. 3: Concentration of humic and fulvic acids from the groundwater by reverse osmosis (S. Geyer (photo: G. Buckau)).

Fig. 4: View of the flow-through centrifuge (Flottweg GmbH, Vilsbiburg) together with G. Buckau and M. Wolf (photo: Flottweg GmbH).

The concentrate was acidified further to pH 2 and the flocculating humic acid was separated by flow-through centrifugation (Fig. 4) in cooperation with the company Flottweg GmbH, Vilsbiburg. The humic acid flocculate and remaining 850 L fulvic acid containing solution were transported to the laboratory for further treatment. Fulvic acid was separated/concentrated by sorption on a 10 L XAD-8 column (for details, see Geyer 1993). After desorption from XAD-8 resin, the fulvic acid was protonated with the cation exchanger AG® 50W-X8 and freeze dried with an 8 L freeze dryer (The VirTis Company, New York). Humic acid was purified as described in Buckau 1991, by NaF treatment, repeated solution/precipitation followed by freeze-drying. As a final step, traces of adsorbed HCl were removed by vacuum for two weeks at slightly elevated temperature (~ 40 °C). In total, about 130 g humic acid (Gohy-573 HA) and 52 g fulvic acid (Gohy-573 FA) were prepared.

3 Characterization

3.1 Elemental composition

The elemental composition is shown in Table 1. Different atom ratios are given in Table 2. For comparison, results for previous humic and fulvic acid batches from the same groundwater are also given. In general, the sum formula of humic and fulvic acid is close to $CO_{0.5}H$, i.e. the formal oxidation state of carbon is close to zero, comparable to for example carbohydrates.

Table 1: Elemental composition of the new prepared Gohy-573 FA and HA. Summarized are the mean values of triplicate analysis, carried out by Analytische Laboratorien, Lindlar, Germany, together with the standard deviation. For comparison, also the elemental compositions of the former charges are shown (Gohy-573 FA (one analysis) and the mean value for Gohy-573 HA I and II (see, Buckau 1991)). The data are normalized to a total CHNOS content of 100 %.

Humic substance Gohy-573	C (%)	H (%)	O (%)	N (%)	S (%)
FA	54.1 ± 0.1	4.23 ± 0.08	38.94 ± 0.04	1.38 ± 0.02	1.32 ± 0.01
HA	59.3 ± 0.1	4.57 ± 0.02	32.1 ± 0.1	2.01 ± 0.06	2.02 ± 0.09
FA (old batch)	57.18*	4.85	35.38	1.14	1.44
HA (old batch)	56.79	4.64	35.76	1.73	1.73**

* new calculated value; ** only the value of separate pre-batch (HA I) is given.

Table 2: Atom ratios of Gohy-573 humic and fulvic acids, calculated from Table 1.

Humic substance Gohy-573	O/C	H/C	N/C	S/C	O/H
FA	0.54	0.93	0.022	0.009	0.58
HA	0.41	0.92	0.029	0.013	0.44
FA (old batch)	0.46	1.02	0.017	0.009	0.45
HA (old batch)	0.48	0.98	0.026	0.011	0.49

As expected, Gohy-573 FA has a lower C content and a higher O content than Gohy-573 HA. They show relatively similar H contents, however, reflecting the higher oxygen content in fulvic acid and the comparable hydrogen contents, the O/H ratio is higher for the fulvic than the humic acid. These results are expected with the higher hydrophilicity of fulvic acid than humic acid. Contrary to this, the old humic and fulvic acid batches show very similar elemental composition, especially with respect to C, H and O, with the fulvic acid showing values rather typical for humic acid. There are minor contributions of nitrogen and sulfur. The N/C ratios are higher for humic than fulvic acid in both the new and the old batches. The S/C ratios are comparable for all four substances, with the potential for slightly higher ratios in humic than fulvic acid.

In summary, the elemental composition verifies the successful isolation and purification of the humic and fulvic acids. Reproducibility is very high between sampling and treatment about twenty years ago and now. The old fulvic acid batch, however, shows an elemental composition rather typical for humic acid. This may indicate differences in sample treatment and separation of humic and fulvic acid fractions. As seen by previous characterization, however, the old fulvic acid batch does not show the typical humic acid bi-modal size distribution and thus the difference is rather in the operationally based separation within the rather hydrophilic, small molecule overlapping humic and fulvic acid fraction.

3.2 Inorganic constituents

Inorganic constituents, analyzed by ICP-MS and ICP-AES, are given in Table 3. The purification of fulvic acid is very successful also with respect to the potentially critical step of protonation by ion exchange. The sum of Na, Ca and Mg is 0.12 meq/g FA with only 0.025 meq/g FA of the easily exchangeable Na^+ ion. To which extent Ca (and Mg) is in exchangeable positions or part of mineral constituents cannot be determined from the present data. In summary, however, the concentration of exchanging metal cations is low and need not be regarded in calculation of the proton exchange capacity (cf. below). In the case of humic acid, the concentration of the easily exchangeable Na^+ ion is very low (0.013 meq/g HA) as expected from repeated washing with hydrochloric acid prior to the final preparation steps, namely freeze-drying and HCl evaporation. Al, Ca, Ti, Cr, Fe and Cu show higher values than the fulvic acid. Furthermore, the Mg to Ca ratio is higher than in the fulvic acid. The Si/Al atom ratio is 0.57, indicating the possible presence of clay type minerals. The data indicate presence of small amounts of mineral constituents and/or process contaminants rather than residues of ions in exchangeable positions. The overall conclusion is that also preparation and purification of the humic acid is successful with no need to regard potentially exchanging cations for evaluation of proton exchange capacity.

3.3 Size distribution (by AFFFF)

Determination of size distribution by FFF or GPC/HPLC requires calibration with substances of known mass to size ratios. Another issue is the increase in size with protonation and complexation induced association, eventually leading to flocculation in the acidic range as well as with quasi saturation of complexing sites. For this reason, comparison of different size

determination results is only possible for well-defined and comparable physicochemical conditions.

Table 3: Inorganic constituents in Gohy-573 humic and fulvic acids, determined by ICP-MS and ICP-AES.

	Humic Acid		Fulvic Acid	
Element	Element concentration (□g/g HA)	Stand. dev. (%)	Element concentration (□g/g FA)	Stand. dev. (%)
Na	302	0.3	570	0.7
Mg	3.2	21	0.5	38
Al	81.8	14	13.5	18
Ca	2133	3.6	1861	5
Ti	814.8	8	92.4	9
Cr	162.6	6	77.9	4
Fe	547	9	23.8	2
Co	2.6	4	0.07	13
Ni	20.6	7	0.7	10
Cu	410.0	1	5.8	3
Y	6.6	5	0.04	3
Zr	123	3	205	2
Nb	3.8	9	1.1	3
Mo	13.8	2	8.5	2
La	3.0	3	0.01	13
Ce	9.0	4	0.02	11
Pr	1.3	3	<0.01	
Nd	6.0	6	0.01	10
Sm	1.9	5	<0.01	
Eu	0.4	6	<0.01	
Gd	1.8	7	<0.01	
Tb	0.3	9	<0.01	
Dy	1.8	3	<0.01	
Ho	0.4	3	<0.01	
Er	1.3	4	<0.01	
Tm	0.2	5	<0.01	
Yb	1.5	7	<0.01	
Lu	0.3	3	<0.01	
Hf	1.6	7	2.1	4
Ta	0.2	4	0.02	3
Pb	8.3	8	0.09	13
Th	11.2	6	0.36	3
U	2.9	5	0.01	10
Si	48.8	7	381	3

The elution behavior of the investigated substance is compared with that of the calibration standards and via mass to size ratio of the calibration standards, the size of the investigated substance can be obtained. For practical reasons, however, another procedure/nomenclature is normally used. For a given set of calibration standards, the size of the investigated substance is given as the mass-equivalent size of that particular type of standard. It therefore must be

clearly underlined, that the numbers given (as the mass of the calibration standard) will vary with the standard used. As an example, calibration with very compact globular proteins may result in a mass-equivalent size of a certain sample of 10 000 Dalton (molecular mass of this globular protein standard). If a bulky highly hydrated standard is used (for example, PSS (polystyrene sulfonate) or PAA (polyacrylic acid)), the corresponding mass-equivalent numbers will be lower for the same actual size. In the present determination of size distribution with asymmetric flow field-flow fractionation, a set of polycarboxylic acid (PCA) standards (including PAA standards) is used. Detailed results can be found in Wolf et al. 2004.

In Table 4, the size distribution is given by (in mass equivalent sizes related to PCA):

(i) The size range of elution,
(ii) M_p' (peak value in the molecular size distribution plotted on the logarithmic molecular size scale),
(iii) M_p (peak value in the molecular size distribution plotted on the linear molecular size scale),
(iv) M_n (number average molecular size),
(v) M_w (weight average molecular size), and
(vi) M_w/M_n (polydispersity).

As expected, the Gohy-573 FA shows a distribution towards smaller sizes. The size distribution reaches up to about 3000 Dalton compared to 14 000 Dalton for the humic acid Gohy-573 HA. The individual numbers for different forms of distribution maxima also show lower numbers for the fulvic acid compared to the humic acid, the difference being about a factor of two.

Table 4: Molecular size data of Gohy-573 humic and fulvic acids, related to mass-equivalent size of polycarboxylic acid (PCA) standards (data from Wolf et al. 2004).

Sample Gohy-573	Size range (Dalton/PCA)	M_p' (Dalton/PCA)	M_p (Dalton/PCA)	M_n (Dalton/PCA)	M_w (Dalton/PCA)	M_w/M_n
FA	150 - 3000	460	410	470	620	1.3
HA	150 - 14 000	1120	700	990	1760	1.8

3.4 Mass distribution (by TOF-SIMS)

Determination of the mass distribution has been a long-standing analytical problem for humic substances. The situation has changed by rather recent developments of Overhauser NMR, TOF-SIMS (time of flight – secondary ion mass spectroscopy), MALDI-TOF MS (matrix assisted laser desorption ionization time-of-flight mass spectrometry), and ESI-MS (electrospray ionization mass spectrometry). In the present work TOF-SIMS is used (for details, see Wolf et al. 2004). In Table 5, the mass distribution parameters M_n, M_w and M_w/M_n are summarized.

The lower mass limit of integration was set to m/z 150 in order to cut the high intensity of low mass fragments. The upper limit of integration was set to the bottom out of the mass concentration versus mass. Background subtraction was applied if the mass concentration distribution increases in the highest mass range. With an extended second upper limit (values in squared brackets) the distribution parameters are nearly the same, confirming the approach for setting the upper mass limit. All M_n and M_w values are significantly below 1000 Dalton. The mass distribution and the polydispersity show slightly higher values for the Gohy-573 HA than for Gohy-573 FA. The values reflect findings generally found for the mass distribution, very much lower than previously thought based upon incorrect estimates from size determination studies. The smaller difference in the mass ratio between humic and fulvic acids compared to the size ratio (cf. above) may reflect physicochemical differences between the two types of acids with a more bulky structure/higher effective hydrodynamic size per mass unit of humic acid.

Table 5: Mass distribution parameters for the Gohy-573 humic and fulvic acids by TOF-SIMS (data from Wolf et al. 2004). Values in squared brackets correspond to a higher upper limit (see text).

Sample	Mass distribution range	M_n	M_w	M_w/M_n
Gohy-573	(Dalton)	(Dalton)	(Dalton)	
FA	150 – 3000 [5000]	428 [428]	609 [613]	1.42 [1.43]
HA	150 – 3000 [5000]	521 [523]	752 [759]	1.44 [1.45]

3.5 Proton exchange capacity

The proton exchange capacity (PEC) is determined by potentiometric pH titration. The freeze-dried humic or fulvic acid is dissolved in a small amount of NaOH followed by dilution with $NaClO_4$ within few minutes. Dissolution of humic acid in alkali is necessary because the freeze-dried HA sample do not dissolve under pH neutral or acidic conditions. Dilution within few minutes is required in order to avoid alkaline hydrolysis. The samples are then kept under inert gas under exclusion of light. Storage under inert gas is important in order to exclude oxygen and carbon dioxide contamination. Exclusion of light was also shown to be important in order to avoid sample oxidation with the corresponding increase in PEC.

The amount of OH^- in the original sample is 10 meq/g humic or fulvic acid. The samples were titrated with 0.1 mol/L HCl. The sample concentration is 200 mg/L. Sample concentration of 1 g/L shows hysteresis with the corresponding error in data due to lack in reversibility (Buckau 1991). Lower sample concentrations have negative impact on the data evaluation. Titration proceeds with stepwise addition of the titrant (10 µL per addition). The time steps are set so as to insure sufficient approach to equilibrium before the subsequent titrant addition. The acid titrant is added until acid solution is obtained. Below pH around 3, data evaluation becomes difficult due to the progressively low response to titrant addition. The resulting titration curve is shown in Fig. 5 (upper part). The titration curve does not show specific features with clear indication of individual groups.

In order to evaluate the titration curve, the derivative function is generated (gray curve in Fig. 5, upper part and the lower part of this figure). Buffering of the solution (the inverse of the derivative function) has a minimum in the pH range around 7.5 - 8. This maximum in the derivative function is considered the transition between buffering groups below and above this pH range. Groups ionized below this pH range are frequently considered as "carboxylic groups". The concentration of these groups is given by the net excess of OH^- ions at this point, i.e. the number of OH^- ions that have neutralized by protons released from the originally protonated humic or fulvic acid. It should be underlined, however, that this is an operational definition without unambiguous allocation to specific functional groups. Attempts to fit such a titration curve by a number of proton exchanging functional groups is a plain fitting exercise, especially because the endpoint in the acidic range cannot be determined. Furthermore, a number of combinations of different classes of proton exchanging groups and their respective pKa values can be used in order to reproduce the curve. Finally, because of protonation induced association, the number concentration of entities decreases along with the protonation and the different proton exchanging groups are not permutable, but within a specific entity (molecule or molecule cluster/associate) they are spatially dependent from each other.

The PEC evaluated by this procedure is given in Table 6. The numbers found for the new batches are in the range expected with the higher PEC for fulvic acid compared to that of the humic acid. Compared to the old batches, the PEC of humic acid is lower and that of the fulvic acid is higher. This is in agreement with the above-discussed differences where the old batches appear to be rather similar whereas the present new batches appear to reflect higher differences in the hydrophilic nature.

Table 6: Proton exchange capacity determined by potentiometric pH titration (cf. Fig. 5) of Gohy-573 HA and FA.

	Proton exchange capacity (meq/g HA or FA)	
Gohy-573	New batches	*Old batches*
HA	4.82 ± 0.05	*5.38 ± 0.20*
FA	6.82 ± 0.04	*5.70 ± 0.09*

4 Summary and conclusions

Large new batches of humic and fulvic acids from the Gorleben groundwater Gohy-573 have been prepared and characterized. Humic acid is defined as the fraction that flocculates at low pH whereas fulvic acid is defined as the fraction that at low pH sorbs on XAD-8 resin but does not flocculate. Thus, the distinction between humic and fulvic acid is partly operational, especially reflecting the pH and separation technique/conditions used for separation of humic acid flocculate. The new batches show the typical properties of humic and fulvic acid with very low concentrations of inorganic constituents/contaminants. Due to their large amounts, properties and thorough characterization, they provide the basis for continued studies with these two humic substances, following up on almost two decades of research on the previous, meanwhile used up, batches.

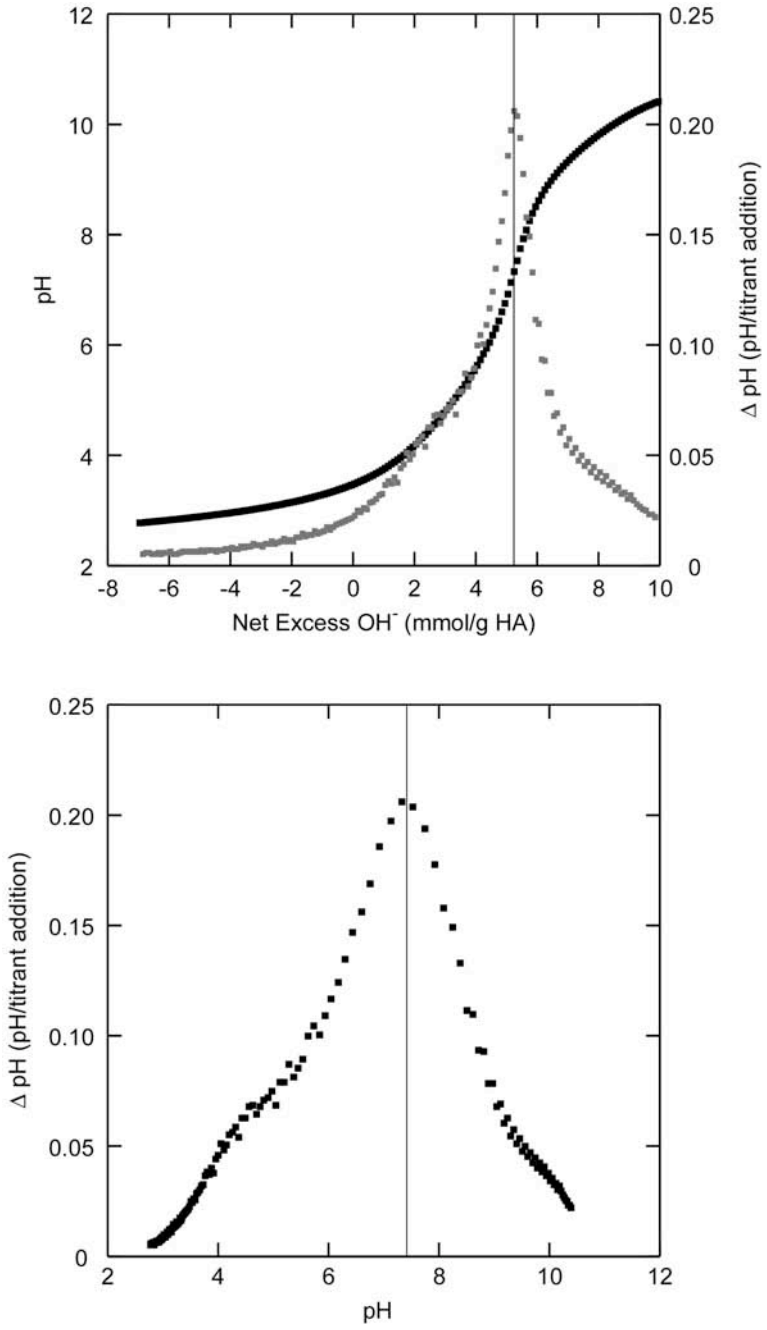

Fig. 5: Potentiometric pH titration of Gohy-573 HA. pH (black points) and the derivative function (pH variation with stepwise addition of titrant (10 µL 0.1 mol/L HCl per addition)) (gray points), both as a function of excess OH^- (upper figure). The PEC is evaluated as the excess OH^- in the turning point of the titration curve (upper figure) at around pH 7.5 (lower figure).

5 Acknowledgements

The authors thank D. Wesselow and H. Fährmann from DBE (Deutsche Gesellschaft zum Bau und Betrieb von Endlagern für Abfallstoffe mbH), Peine, for technical support in groundwater sampling and D. Jurrat for the very time-consuming extraction and purification of these large humic and fulvic acid batches in the laboratory.

References

Artinger R., Buckau G., Geyer S., Fritz P., Wolf M., Kim J.I. (2000) “Characterization of groundwater humic substances: influence of sedimentary organic carbon”, *Appl. Geochem.*, **15**, 97.

Buckau G. (1991) “Komplexierung von Americium(III) mit Huminstoffen in natürlichen Grundwässern”, PhD Thesis, Faculty of Chemistry, FU Berlin.

Buckau G., Artinger R., Geyer S., Wolf M., Fritz P., Kim J.I. (2000) “Groundwater in-situ generation of aquatic humic and fulvic acids and the mineralization of sedimentary organic carbon”, *Appl. Geochem.*, **15**, 819.

Geyer S. (1993) “Isotopengeochemische Untersuchungen an Fraktionen von gelöstem organischem Kohlenstoff (DOC) zur Bestimmung der Herkunft und Evolution des DOC im Hinblick auf die Datierung von Grundwasser”, PhD Thesis, Ludwig-Maximilians-Universität München.

Schäfer T., Buckau G., Artinger R., Kim J.I., Geyer S., Bleam W.F., Wirick S., Jacobsen C. (2004) “Vertical Exchange of Gorleben Fulvic Acids of Different Origin”, separate contribution in this report.

Wolf M., Szymczak W., Chanel V., Buckau G. (2004) “Molecular size and mass distributions of humic substances measured by AFFFF and TOF-SIMS”, separate contribution in this report.

Annex 10

X-ray Photoelectron Spectroscopy of HUPA organic substances: natural and synthetic humic compounds

Barré N. [1], Mercier-Bion F. [1] and Reiller P. [2]

[1] UMR 8587 «Analyse et Environnement» (CEA/CNRS/Université d'Evry Val-d'Essonne) Centre d'Etudes de Saclay, 91191 Gif-sur-Yvette Cedex, France

[2] CEA/DPC/SECR/LSRM Centre d'Etudes de Saclay, 91191 Gif-sur-Yvette Cedex, France

X-ray Photoelectron Spectroscopy of HUPA organic substances: natural and synthetic humic compounds

Barré N.[1], Mercier-Bion F.[1] and Reiller P.[2]

[1]UMR 8587 «Analyse et Environnement» (CEA/CNRS/Université d'Evry Val-d'Essonne) Centre d'Etudes de Saclay, 91191 Gif-sur-Yvette Cedex, France
[2] CEA/DPC/SECR/LSRM Centre d'Etudes de Saclay, 91191 Gif-sur-Yvette Cedex, France

1. Abstract

X-ray Photoelectron Spectroscopy (XPS) results on the characterisation of the HUPA organic materials, *i.e.* natural humic substances *"GOHY 573"* (Fulvic Acid FA and Humic Acid HA) extracted from the Gorleben ground waters, and synthetic humic acids *"M1"* and *"M42"* obtained from a standard melanoidin preparation from FZ Rossendorf, are presented in this paper. XPS investigations were focused on the determination of the chemical environment of the major elements as carbon, nitrogen, oxygen and sulphur, and on the identification of trace metals trapped by these organic compounds.

2. Introduction

Humic substances (HS), comprising humic acids (HA) and fulvic acids (FA), represent 40 to 60% of the dissolved carbon in natural waters. Even if the research has largely progressed in this field, the structure of HS is not perfectly well identified yet and the evidence of the functional groups constitutive of these compounds stays a real challenge. These data are of a great importance to have a better understanding of the interactions between HS and trace elements encountered in the environment and known to be associated to this organic matter, from the numerous studies reported in the literature (1-6).

The C-containing groups of HS are actually relatively well identified especially with the use of ^{13}C Nuclear Magnetic Resonance (7). On the contrary, the organic functional groups implying heteroatoms as nitrogen, oxygen and sulphur that are also major elements of humic substances, are to our knowledge, not completely evidenced. However, some publications (8, 9) report the application of X-ray Absorption Near-Edge Structure (XANES) of sulphur in humic substances and of X-ray Photoelectron Spectroscopy (XPS) of nitrogen (7) and sulphur (9, 10) in humic matter.

XPS is a powerful method to determine the chemical environment (redox state, nature of the chemical bonds) of all the elements of the periodic table. Furthermore it is a non-destructive technique, which is particularly interesting when fragile materials, as organic compounds, have to be analysed. Our preceding studies have already illustrated the applications of XPS to the study of humic substances and in particular of their physico-chemical interactions with iodine (11-13).

In this paper, XPS is carried out to determine the chemical environment of C, N, O and S and to precise if trace elements (as halogens and transition metals) are present in humic substances. Thus, this technique is applied to the investigation of two types of humic substances: natural HA and FA from the Gorleben ground waters and synthetic humic acids issued from a "standard melanoidin" preparation (14).

3. Experimental

Before XPS analyses, the powdered humic substances were mounted on double-sided carbon tape. XPS experiments were carried out at the "Surfaces and Interfaces Laboratory" of the Commissariat à l'Energie Atomique (Saclay, France),[*] with a VG Instruments® 220i spectrometer by using an unmonochromated AlK_α X-ray source (incident energy: 1486.6 eV). A source power of 15 kV and of 20 mA was used. The dimensions of the X-ray beam were approximately 8 mm per 7 mm. The analysis chamber pressure was in the range of 10^{-8} Torr. Calibration in binding energy (BE) was achieved using the Ag $3d_{3/2}$ and Ag $3d_{5/2}$ transitions (368.3 and 374.3 eV respectively). The BE resolution of the spectrometer was estimated to

[*] CEA/DPC/SCP/LRSI

0.2 eV. No charge effect compensation was achieved during the XPS analyses and so all the BE values were corrected using the C_{1s} signal of contamination carbon at 285 eV.

The survey spectra of all the samples were acquired. The core-level regions C1s, N1s, O1s and S2p, corresponding to major elements of the humic substances, were acquired and deconvoluted by using the VG Instruments® software "AVANTAGE". In addition, according to the presence of the other elements detected on the survey spectra, core-level regions were acquired: Si2p, transition metals (Cr2p, Mn2p, Fe2p), halogens (Cl2p, Br3d, I3d).

4. Results and discussion

4.1. Natural humic substances from the Gorleben site: Humic Acid (HA) and Fulvic Acid (FA) "GOHY 573"

Figure 1 displays the comparison of C1s, N1s, O1s and S2p spectra for the two humic substances samples. Apparently, the two organic fractions present the same C1s (Figure 1a) and N1s (Figure 1b) spectra in terms of BE positions, but the FA sample is poorer in nitrogen compared to the HA one.

On the contrary, notable differences are observed for the O1s (Figure 1c) and S2p (Figure 1d) regions. Firstly, the two samples do not present the same oxygenated groups since the shape of the O1s regions is clearly different (Figure 1c) for each sample. Secondly, the FA sample is largely poorer in sulphur than the HA one and the functional groups implying this element are obviously different (Figure 1d).

4.1.1. Characterisation of major elements: identification of the functional groups

- C1s region

According to the C1s signal deconvolution (Figure 2), the two fractions present the same three contributions implying similarity in terms of functional groups. A major component at 285 eV (71%) relative to carbon contamination, aromatic and aliphatic compounds; a second contribution (20%) around 286.5 eV corresponding to the C-O bond (alcohols, carboxylic acids, ethers, esters…) and a third one (9%) around 289 eV associated to the C=O bond (ketones, aldehydes, carboxylic acids, esters,…).

- N1s region

Each fraction presents a single contribution at 400.5 eV (Figure 3) relative to amides or/and amines, since these two organic functions are impossible to be discriminated by XPS.

- O1s region

As previously mentioned, the differences between the two fractions are specially marked for this region. The O1s deconvolution of the FA sample shows three contributions: a first component (32%) at 530 eV attributed to oxides, a second one (43%) at 531.5 eV assigned to

hydroxides and a last one (25%) around 533 eV relative to the C=O bond. The HA sample only displays a single contribution around 533 eV characteristic of the carbonyl group. The deconvolution of the O1s region for the FA sample is given on the Figure 4.

- S2p region

This region is notably different for the two other samples. The sulphur signal of the FA fraction is too weak to be correctly deconvoluted. The signal of the HA sample reveals the presence of two S-containing groups: a major contribution (90 %) at 164.1 eV attributed to thiophenes and a minor one at 168.6 eV (10 %) relative to sulphates (Figure 5).

4.1.2. Characterisation of trace elements: halogens and transition metals

Two types of trace elements were researched in the humic fractions: halogens such as chlorine, bromine and iodine (from the Cl2p, Br3d and I3d regions) that are often associated to the organic matter (11-15); transition metals that are complexed by humic substances.

- Halogens

The two fractions did reveal neither the presence of bromine nor iodine.

As illustrated by the Figure 6, the HA fraction does not reveal the presence of chlorine. The FA fraction displays a chlorine signal with two contributions (Figure 7): one at 198.3 eV (60%) attributed to chlorides (Cl^- ion), and another (40%) at 199.9 eV underlying the presence of metallic chloride salts (*e.g.* $AgCl_2$). No contribution revealing the presence of Cl(0) covalently associated to the organic matter was observed. These results suggest that chlorine does not react so easily than iodine with the humic matter even if the same mechanism is implied (16-18). Actually, from our previous studies (11-15), it seems that, whatever is the origin of the FA, iodine is systematically associated by covalent bonding. The behaviour of chlorine seems to be slightly different, as it can be associated as Cl^-, as it is the case for the humic substances from Gorleben ground waters, but it can also form covalent bonding with the organic matter, as it has largely been reported in the literature (16-18). The chloride present in this sample could be attributed to the treatment of the original groundwater.

- Transition metals

The two organic fractions are clearly different. Indeed, the HA fraction does not contain trace metals whereas the FA sample reveals the presence of chromium, manganese and iron, as displayed on Figure 8. These results are in agreement with those obtained from the O1s signal: the HA sample showed one single contribution of oxygen (C=O) characteristic of carbonyls whereas the FA fraction contains carbonyl groups but also oxides and hydroxides.

The absence of chloride and transition metals in the HA sample outline the quality of the separation procedure.

4.2. Synthetic humic acids from FZR: "M1" and "M42"

4.2.1. Characterisation of major elements: identification of the functional groups

As expected from the synthesis method, the two samples do not reveal the presence of sulphur. The Figure 9 illustrates the comparison of the spectral regions C1s, N1s and O1s for the two humic acids. The N1s regions are visibly similar whereas the C1s and O1s spectra are quite different for the two samples and these distinctions were evidenced by the signal deconvolutions, as discussed below in the text.

- C1s region

The two samples present the same three contributions of C-containing functions: a major component relative to the contamination carbon, aromatics and aliphatics, and in a lesser extent, two other contributions characteristic of the C-O and C=O groups. The sample M42 sample contains more pronounced contributions of C-O and C=O bonds that the sample M1.

- N1s region

The two samples display the same single contribution of nitrogen at 400 eV corresponding to amines or amides.

- O1s region

Concerning this spectral region, the two samples present marked differences. M1 is made of three O-containing groups: oxides, hydroxides (or/and silicates) and carbonyls. M42 fraction traduces the presence of only two oxygenated compounds: hydroxides (or/and silicates) and carbonyls.

4.2.2. Characterisation of trace elements: halogens and transition metals

As it was the case for sulphur, the two samples do not contain halogenated compounds. Only a weak amount of silicon was observed for the two synthetic samples, probably originated from the dissolution of vessel during the synthesis.

The transition metals were not detected in "M42". Conversely, "M1" revealed weak quantities of chromium and iron. These results concerning the presence of transition metals in "M1" and not in "M42" are perfectly in agreement with the data obtained from the O1s results: "M1" contains oxides, hydroxides and carbonyls, whereas "M42" only presents hydroxides and carbonyls. So these data suggest that transition metals in "M1" are rather associated to oxides.

5. Conclusion

Informations about the chemical environment of the major elements (carbon, nitrogen, oxygen and sulphur) of the natural humic substances from the Gorleben site and of the

synthetic humic acids were successfully obtained by XPS. Moreover, the identification of trace elements (as transition metals and halogens) was followed.

As currently observed for humic substances, the natural humic substances “GOHY 573” present three types of carbon (aromatics/aliphatics, C-O and C=O groups) and a single contribution of nitrogen attributed to amines or/and amides. The S-containing groups under the form of thiophenes and sulfates are present in the FA fraction only. Also, the two fractions distinguish from the chemical environment of oxygen and the presence or not of chlorine and transition metals.

Concerning the synthetic humic acids “M1” and “M42”, as for the natural samples, carbon is present under the same three chemical forms and nitrogen is contained in amines or/and amides. The two humic acids samples present marked differences concerning the chemical environment of oxygen and the presence of trace elements: in the opposite to the sample “M1”, the sample “M42” does not contain oxides which is in concordance with the total absence of trace elements in this sample. These results suggest that the “melanoidal” synthesis of the humic acids is particularly successful which implies that these model substances will be investigated to study their interaction with fission products or chemical analogues (transition metals, iodine) of ^{235}U, in particular in the field of nuclear waste storage studies. This approach has already been turned to good account to understand the interactions of U(VI) with synthetic humic substances (19, 20).

6. Figures

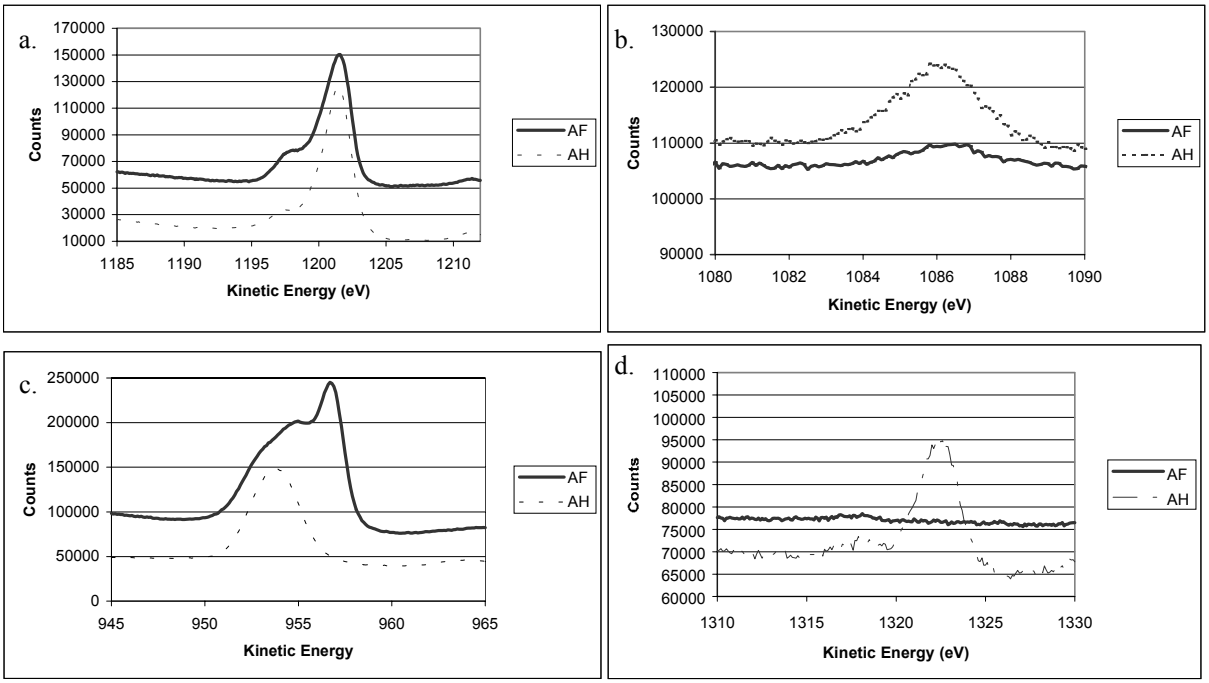

Figure 1: Comparison of C1s, N1s, O1s and S2p regions of the two samples FA and HA "GOHY 573".

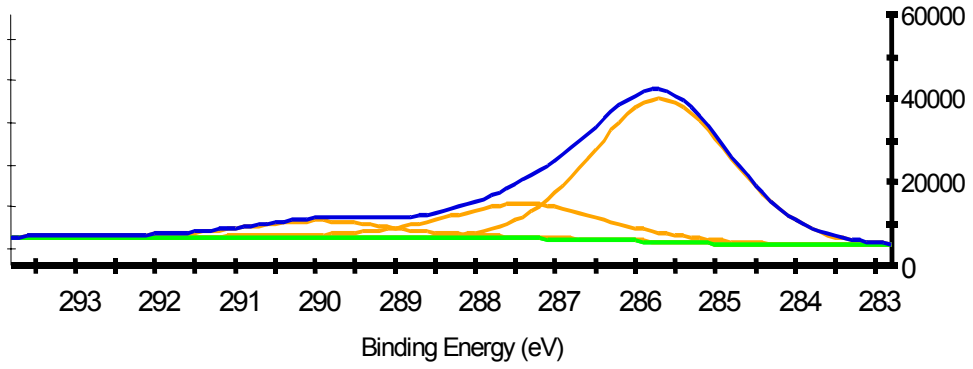

Figure 2: Deconvolution of the C1s region of the sample FA "GOHY 573, showing the presence of three contributions of carbon (285 eV, 286.5 eV and 289 eV).

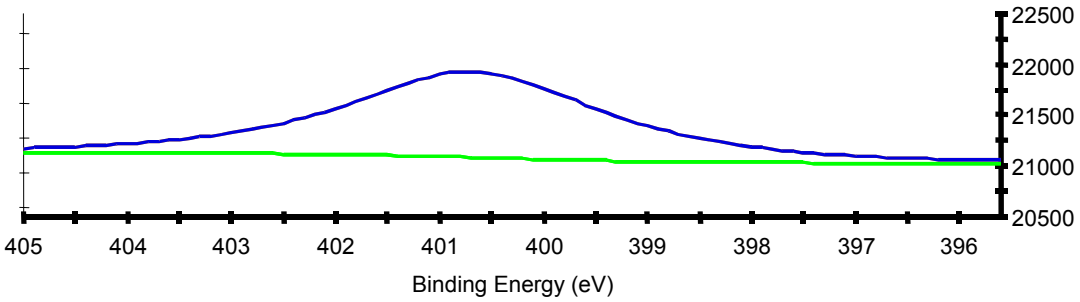

Figure 3: Deconvolution of the N1s region of the sample FA "GOHY 573, showing the presence of a single contribution of nitrogen at 400 eV.

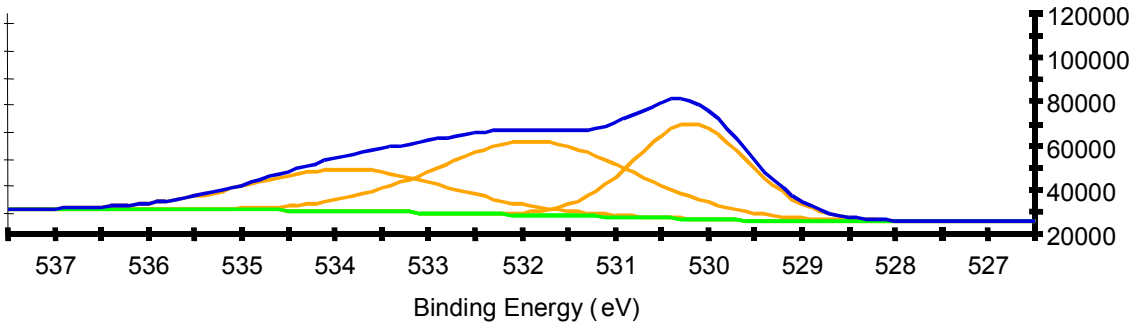

Figure 4: Deconvolution of the O1s region of the sample FA "GOHY 573", showing the presence of three contributions of oxygen (530 eV, 531.5 eV and 533 eV)

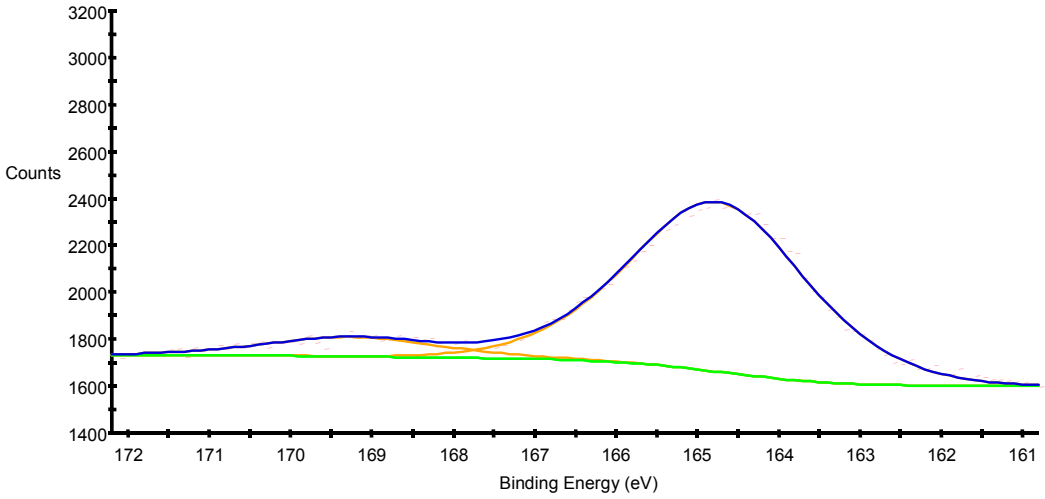

Figure 5: Deconvolution of the S2p region of the sample HA "GOHY 573, showing the presence of two contributions of sulphur (164.1 eV and 168.6 eV).

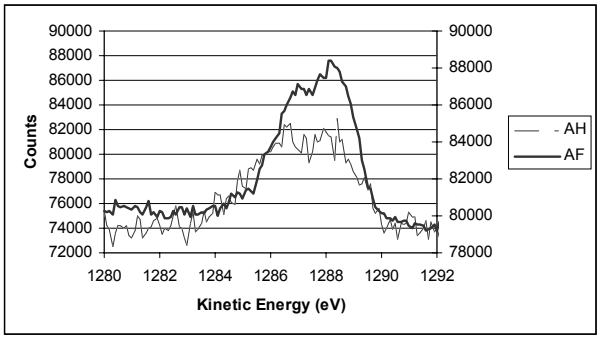

Figure 6: Comparison of the Cl2p region of the two samples FA and HA "GOHY 573

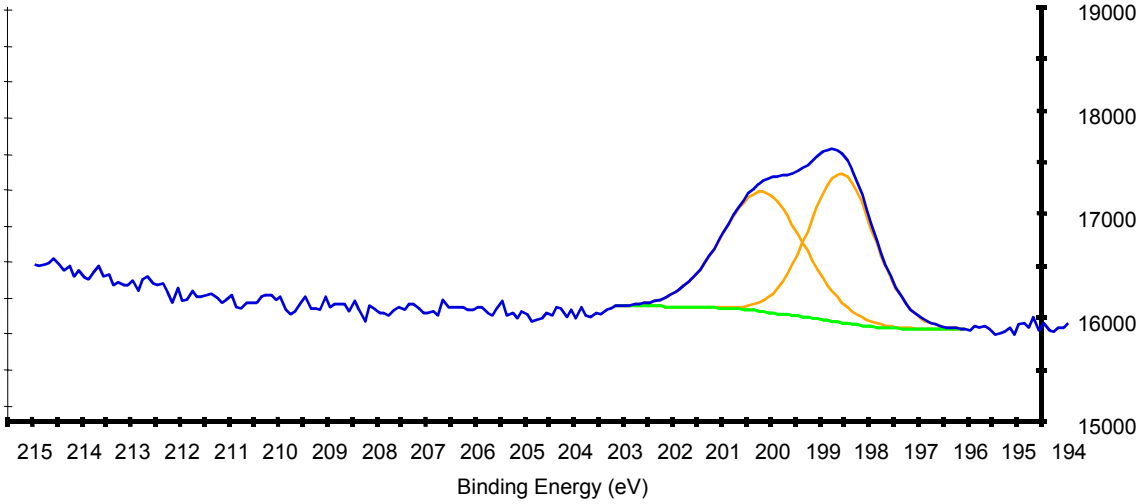

Figure 7: Deconvolution of the Cl2p region of the sample FA "GOHY 573, showing the presence of two contributions of chlorine (198.3 eV and 199.9 eV).

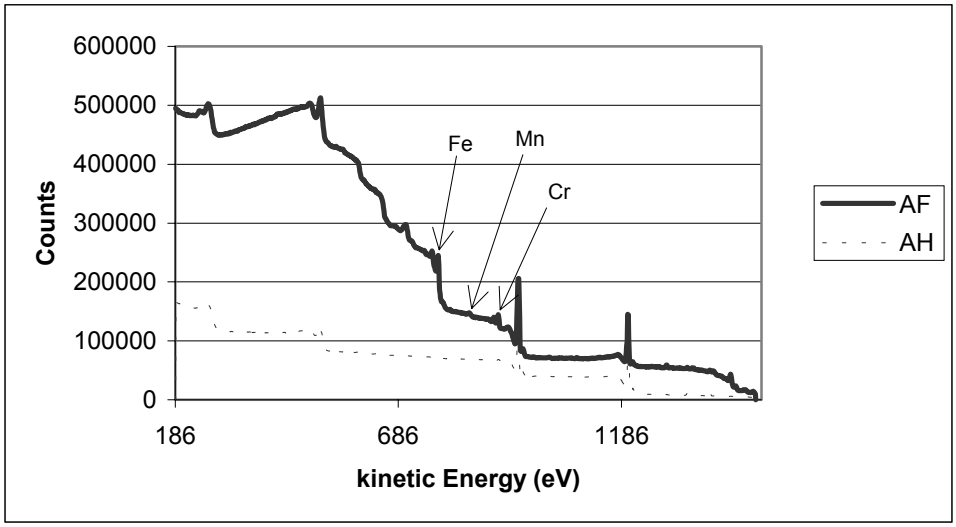

Figure 8: Comparison of the survey spectra of the two samples FA and HA "GOHY 573", showing the presence of trace elements in the FA fraction.

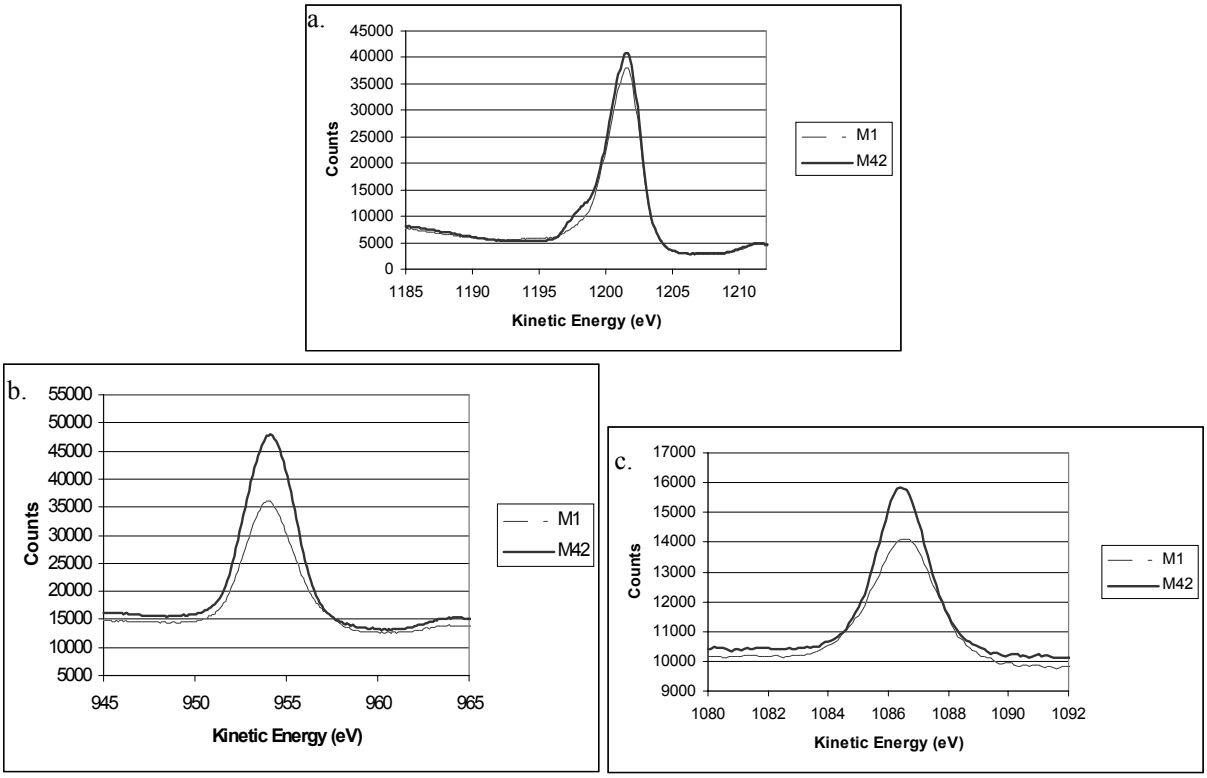

Figure 9: Comparison of C1s, N1s and O1s regions of the two synthetic humic acids "M1" and "M42".

7. References

(1) Buffle J., *Complexation Reactions in Aquatic systems* (1988) Wiley Editions.

(2) Kim J.I., Buckau G. and Zhuang W., Material Research Society Symposium Proceedings **84** (1987) 747.

(3) Longworth G., Wilkins M.A. and Ivanovitch M., Material Research Society Symposium Proceedings **127** (1988) 755.

(4) Choppin G.R. and Allard B., Handbook on the Physics and Chemistry of the Actinides (Editions A.J. Freeman and C. Keller) (1985) 407.

(5) Moulin V., Billon A., Theyssier M. and Dellis Th., *Study of the interactions between organic matter and transuranic elements*, Final Report, CEC Contract FI1W/0068, Report EUR 13651 (1991).

(6) Moulin V., Tits J., Laszak I., Moulin C., Decambox P. and de Ruty O., *Complexation behaviour of actinides with humic substances studied by Time-Resolved Laser-Induced Fluorescence and spectrophotometry* in "Effects of humic substances on the migration of radionuclides: complexation of actinides with humic substances", Final Report, CEC Contract FI2W/0083, Report EUR 16843 EN (1996).

(7) Monteil-Riveira F., Brouwer E.B., Masset S., Deslandes Y. and Dumonceau J., Analytica Chimica Acta **424** (2000) 243.

(8) Morra M.J., Fendorf S.E. and Brown P.D., Geochimica et Cosmochimica Acta **61** n°3 (1997) 683.

(9) Olivella M.A., Del Rio J.C., Palacios J., Vairavamurthy M.A., De Las Heras F.X.C., Journal of Analytical and Applied Pyrolysis **63** (2002) 59.

(10) Urban N.R., Ernst K. and Bernasconi S., Geochimica et Cosmochimica Acta **63** n°6 (1999) 837.

(11) Mercier F, Moulin V., Guittet M.J., Barré N., Toulhoat N., Gautier-Soyer M. and Toulhoat P., Radiochimica Acta **88** (2000) 779.

(12) Mercier F., Moulin V., Barré N., Trocellier P. and Toulhoat P., Nuclear Instruments and Methods in Physics Research B181 (2001) 628.

(13) Mercier F., Moulin V., Barré N., Guittet M.J., Gautier-Soyer M., Trocellier P. and Toulhoat P., Organic Geochemistry **33** (2002) 247.

(14) Enders C. and Theis K., Brennstoff Chemie **19** (1938) 360.

(15) Moulin V., Reiller P., Amekraz B. and Moulin C., Rapid Communications in Mass Spectrometry **15** (2001) 2488

(16) Gallard H. and Von Gunten U., Environmental Science and Technology **36** (2002) 884.

(17) Lee, C. F., *Kinetics of reactions between chlorine and phenolic compounds*. Principles and Applications of water chemistry proceedings. In: (S. D. Faust and J. V. Hunter eds.), Wiley, 1967, p. 54.

(18) Lee R.T., Shaw G., Wadey P. and Wang X., Chemosphere **43** (2001) 1063

(19) Pompe S., Bubner M., Denecke M.A., Reich T., Brachmann A., Geipel G., Nicolai R., Heise K.H. and Nitsche H., Radiochimiac Acta **74** (1996) 135.

(20) Schmeide K., Sachs S., Bubner M., Reich T., Heise K.H. and Bernhard G., Inorganica Chimica Acta **351** (2003) 133.

Annex 11

Prognosticating the humic complexation for redox sensitive actinides through analogy, using the charge neutralisation model.

Pascal REILLER

Commissariat à l'Énergie Atomique, CE Saclay, Nuclear Energy Division/DPC/SECR Laboratoire de Spéciation des Radionucléides et des Molécules, F-91191 Gif-sur-Yvette CEDEX, France

Prognosticating the humic complexation for redox sensitive actinides through analogy, using the charge neutralisation model.

Pascal REILLER

Commissariat à l'Énergie Atomique, CE Saclay, Nuclear Energy Division/DPC/SECR
Laboratoire de Spéciation des Radionucléides et des Molécules, F-91191 Gif-sur-Yvette CEDEX, France
pascal.reiller@cea.fr

1. Abstract

The humic complexation of redox sensitive elements, described through the charge neutralisation model (CNM) has been reviewed in order to have a comprehensive scope. The data which were acquired in HUMICS program on thorium (IV), and data available in the literature, were reinterpreted according to the CNM and adapted to uranium (IV), neptunium (IV) and plutonium (IV) through analogy. Otherwise, available data which were obtained in the framework of the CNM were used, or adapted when necessary, for other redox state when the analogy is justified, *i.e.* Am^{3+}-Cm^{3+} for Pu^{3+}, NpO_2^+ for PuO_2^+ and UO_2^{2+} for PuO_2^{2+}.

The resulting speciation diagrams indicate that, when (HA) = 100 mg/L, redox sensitive actinides should be reduced to their +IV state when $E_H \leq 650$ mV for plutonium, $E_H \leq 150$ mV for neptunium and $E_H \leq 20$ mV for U. Plutonium could be present as mixtures of plutonium (III) and (IV) depending on the pH value in reducing groundwater $-150 \leq E_H$ (mV) ≤ 150, but the known association of plutonium (VI) in marine systems are not satisfactorily represented. The known reduction of neptunium in Gorleben groundwater seems to be also well represented. The stability of uranium (VI) in humic solution when $E_H \geq 100$ mV is also represented, but these values do not represent the data obtained under reducing conditions. Experiments under well-controlled conditions are still needed to ascertain the comportment of uranium in the presence of humic substances.

2. Introduction

The aqueous chemistry of actinides is one of the most intricate and interesting chapters of the general chemistry of these elements. In particular, uranium, neptunium and plutonium are redox sensitive in aqueous solution, and the study of their complexation properties has been a challenging puzzle for generations of scientists. As the reduced states are difficult to stabilise in solution, there is a large discrepancy between the different published values of complexation constants. Therefore, the use of analogies is a convenient way to estimate unknown complexation constants [1], knowing the limitation of the approach [2].

The complexation of actinides by humic substances (HS), which represent about 40-60 % of the natural organic matter (NOM), is not an exception in that matter. Humic substances are the alkaline extracted fraction of the NOM. From this primary fraction are extracted three sub-fraction namely: humine that is insoluble at whatever pH; humic acids (HA) that are not retained on a hydrophobic resin and insoluble at acidic pH; fulvic acids (FA) that are retained on a hydrophobic resin and are soluble at whatever pH.

A lot of works have been undertaken on "stable" redox states, *i.e.* uranium (VI), neptunium (V) and americium/curium/europium (III). Experimental difficulties have often prevented from obtaining reliable results on reduced states of uranium, neptunium or plutonium. Furthermore, the redox properties of humic substances [3-5] have led to confusing results for protactinium [6], neptunium [7, 8], plutonium [9-12] and other elements [13-19], even if the use of ligands to stabilise redox state is well known in the nuclear industry [20-23]. Otherwise, the reduction of uranium (VI) by HS has not been clearly observed up to now [24-26].

The complexation of metals by humic substances has been a subject of extensive works in the past decades. Three types of models can be identified: discrete models that consider HS as a mixing of indistinct ligands [25, 27], polyelectrolytic models that consider HS as a macromolecular polyelectrolyte [28] and more or less continuous models that consider HS as a distribution of ligands [29-32]. The latter type of model could be seen as more representative of the intricate structure of HS, as it was illustrated in recent studies [33-35], and could take competition with other metals more accurately [31, 32, 36]. Nevertheless, the more operational first type of description has been widely applied to actinides and a large number of validated "constants" are available in literature. From the discrete models, the charge neutralisation model (CNM) [27, 37] has been applied to a lot of relevant actinides namely uranium (VI) [24, 38], neptunium (V) [39-41], americium, curium and europium (III) [42-45]. The variation of the number of available sites can be seen as a continuous term. Only few attempts have been reported up to now in the intricate cases of actinides (IV) and plutonium [46]. Even if the strong interaction of actinide (IV) with HS is known [38, 47-51], the available data on humic complexation are scarce.

Nash and Choppin, more than twenty years ago in the framework of a polyelectrolytic model, succeeded in obtaining high interaction parameters for thorium (IV) between pH 3.9 and 5 for different humic and fulvic acids [52]. Recently, data has been obtained under neutral pH conditions [46, 53].

The interactions with neptunium and plutonium are more confusing as HS induce redox reactions [6, 9-11]. Nevertheless, the complexing properties of HS towards almost all of the redox analogues of these elements have received great attention.

The aim of this exercise is to reinterpret and adapt the available data in the literature in the framework of the CNM in order to define the scope of humic complexation of redox sensitive elements.

3. Treatment of data

Only the complexing properties of HS will be considered here, since their reducing properties have not totally been clarified.

3.1. CNM model

The description of the CNM has been done elsewhere and will not be completely developed here [27]. Through this model, the increase of the HS interaction with metal *vs.* pH is managed through a varying parameter LC, the loading capacity, which represents the maximum fraction of the humic sites $[HA(z)]_T$, that can be involved in a complexation reaction. Hence the complexation is described by a "real constant".

$$M^{z+} + HA(z) \rightleftarrows MHA(z) \qquad \beta_z = \frac{[MHA(z)]}{[M^{z+}]_F\,[HA(z)]_F} \qquad (1),$$

where $[HA(z)]_F$ and $[M^{z+}]_F$ are respectively the concentrations of free humic sites and M^{z+} in solution. The total concentration of humic sites available to complex a metal M^{z+} is written:

$$[HA(z)]_T\ (\text{eq/l}) = \frac{(\text{HA})\ (\text{g/l}) \times \text{PEC}\ (\text{eq/g})}{z} \qquad (2),$$

where (HA) is the concentration of HA in g/l, PEC is the proton exchange capacity (eq/g) determined by titration.

The free humic site concentration $[HA(z)]_F$ is defined as the difference between the maximum concentration of humic sites available for the metal LC × $[HA(z)]_T$, and the actual concentration of humic sites that are involved in the complexation [MHA(*z*)].

$$[HA(z)]_F = LC \times [HA(z)]_T - [MHA(z)] \qquad (3)$$

The complexation constant is thus written as:

$$\beta_{1.z} = \frac{[MHA(z)]}{[M^{z+}]_F \left(LC \times [HA(z)]_T - [MHA(z)]\right)} \qquad (4).$$

Nevertheless, in the case of moderately hydrolysed actinides (*e.g.* Am^{3+} or UO_2^{2+}), the authors have managed the metal-HA interaction increase with pH by postulating the formation of mixed complexes [54-56]:

$$M^{z+} + n\ OH^- + HA(z\text{-}n) \rightleftarrows M(OH)_nHA(z\text{-}n) \qquad \beta_{1.n.z} = \frac{[M(OH)_nHA(z\text{-}n)]}{[M^{z+}]_F\ [OH^-]^n\ [HA(z\text{-}n)]_F} \qquad (5).$$

Panak *et al.* [54] have also noticed spectroscopic modifications of Cm(III) in the presence of HA with increasing pH and carbonate concentration. They postulated the occurrence of mixed carbonato species through the reaction:

$$M^{z+} + m\ CO_3^{2-} + HA(z\text{-}2m) \rightleftarrows M(CO_3)_mHA(z\text{-}2m) \beta_{1.m.z} = \frac{[M(CO_3)_mHA(z\text{-}2m)]}{[M^{z+}]_F\ [CO_3^{2-}]^m\ [HA(z\text{-}2m)]_F} \qquad (6).$$

In these cases, LC is not easy to determine and the authors postulated that LC ≡ 1 due to the pH value close to the total ionisation of the HS (pH ≥ 6) [54, 55].

3.2. Reinterpretation of thorium (IV) literature data through CNM

3.2.1. Formation of ThHA(IV)

The hydrolysis and carbonation of thorium (IV) in solution is still a matter of debate [57-63]. Nevertheless, it is commonly accepted that Th^{4+} is less prone to hydrolysis than other actinides (IV). The humic complexation* of thorium (IV) in acidic media has been studied by Nash and Choppin [52] using liquid-liquid extraction from water.† From the complexation constants available in [52] taken from [57, 64], it can be calculated that the chemistry of thorium (IV) is dominated by acetate complexation.

The reaction between Th^{4+} and HA(*IV*) can be written:

$$Th^{4+} + HA(IV) \rightleftarrows ThHA(IV) \qquad \beta_{1.IV} = \frac{[ThHA(IV)]}{[\ Th^{4+}]_F\ [HA(IV)]_F} \qquad (7).$$

The available data can be used to calculate $\log \beta_{1.IV}$. Using the Schubert formalism [65, 66], and under the conditions that thorium is present at trace concentration, the distribution coefficient of thorium between organic and aqueous phase is written as:

$$D° = \frac{[Th]_{org}}{[Th]_{aq}} \equiv \frac{[Th]_{org}}{[Th^{4+}] \times \left(1 + \sum_{i=1}^{n} \frac{{}^*\beta_i}{[H^+]^i} + \sum_{j=1}^{m} \beta_j^{AcO} \left(\frac{[AcOH]_T}{1 + \beta^H\ [H^+]} \right)^j \right)} = \frac{[Th]_{org}}{[Th^{4+}] \times \alpha} \qquad (8).$$

were ${}^*\beta_i$ are the thorium (IV) cumulative hydrolysis constants, β_j^{AcO} are the cumulative constants for acetate complexation and β^H is the protonation constant for acetate ion and α is the complexation coefficient.

---

* Humic acid from Lac Bradford

† Sodium acetate 0.05 M - sodium perchlorate 0.05 M in toluene with di-2-ethyhexyl phophoric acid

Assuming that humic complexes are not extracted in the organic phase, the distribution coefficient is thus written:

$$D \equiv \frac{[Th]_{org}}{[Th^{4+}]\left(\alpha + \beta_{1.IV}\,[HA(IV)]_F\right)} \tag{9}$$

From equation (8) and (9), comes the expression of $\beta_{1.IV}$:

$$\beta_{1.IV} = \left(\frac{D^\circ}{D} - 1\right)\frac{\alpha}{[HA(IV)]_F} \tag{10}.$$

Knowing that ^{230}Th is used as a tracer, the balance of humic sites is not significantly modified by the complexation and $\beta_{1.IV}$ can be expressed as:

$$\beta_{1.IV} \equiv \left(\frac{D^\circ}{D} - 1\right)\frac{\alpha}{LC \times [HA(IV)]_T} \tag{11}.$$

The LC parameter cannot be determined straightforwardly from the available data because Th^{4+} saturation experiment was not, or rather could not be undertaken in [52]. Hence, only the product $LC \times \beta_{1.IV}$ could be calculated.

The pH, D and $[HA]_T$ (eq/L) values from Nash and Choppin [52] are reported in table 1. $[HA(IV)]_T$ is calculated as $[HA]_T/4$, according to the model. The values of the complexation coefficient α are obtained from the thorium acetate complexation constants β_j^{AcO} available in [52, 64], pK_a (AcO^-) = 4.5 and the thorium hydrolysis constants $*\beta_i$ in [57] (Table 2).* A mean value of log ($LC \times \beta_{1.IV}$) = 11.7 ± 0.3 is obtained (Figure 1) with a 95% confidence interval.† It is to be noted that the use of other constant sets [59, 61, 63] induces only minor changes, since the speciation of thorium (IV) is controlled by acetate complexation.

---

* One should note that the strict application of SIT should require the knowledge of Th^{4+}/CH_3COO^- interaction parameter since the ionic medium is a mixture of CH_3COONa and $NaClO_4$.

† $t_{0.95} = 2.201$

Table 1: Estimation of log $\beta_{1.IV}$ using CNM, from experimental data in Nash and Choppin [52].

pH	D	$[HA]_T$	$[HA(IV)]$	$[AcO^-]$	α	$\frac{D^\circ}{D} - 1$	$\beta_{1.IV} \times LC$	$\log (\beta_{1.IV} \times LC)$
3.98	31.48			$1.16\ 10^{-2}$	$9.46\ 10^{3}$			
3.98	33.75							
3.937	2.170	$1.48\ 10^{-6}$	$3.58\ 10^{-7}$	$1.07\ 10^{-2}$	$7.60\ 10^{3}$	13.51	$2.87\ 10^{11}$	11.46
3.937	2.195					14.38	$3.05\ 10^{11}$	11.48
3.939	1.446	$1.98\ 10^{-6}$	$4.77\ 10^{-7}$	$1.08\ 10^{-2}$	$7.68\ 10^{3}$	20.77	$3.34\ 10^{11}$	11.52
3.939	1.423					22.71	$3.65\ 10^{11}$	11.56
3.93	1.120	$2.47\ 10^{-6}$	$5.97\ 10^{-7}$	$1.06\ 10^{-2}$	$7.34\ 10^{3}$	27.11	$3.33\ 10^{11}$	11.52
3.93	1.086					30.08	$3.70\ 10^{11}$	11.57
3.961	0.362	$4.95\ 10^{-6}$	$1.20\ 10^{-6}$	$1.12\ 10^{-2}$	$8.59\ 10^{3}$	85.91	$6.17\ 10^{11}$	11.79
3.961	0.380					87.90	$6.31\ 10^{11}$	11.80
3.928	0.219	$7.38\ 10^{-6}$	$1.78\ 10^{-6}$	$1.06\ 10^{-2}$	$7.26\ 10^{3}$	142.42	$5.80\ 10^{11}$	11.76
3.928	0.218					154.06	$6.28\ 10^{11}$	11.80
3.922	0.147	$9.88\ 10^{-6}$	$2.39\ 10^{-6}$	$1.05\ 10^{-2}$	$7.04\ 10^{3}$	212.61	$6.27\ 10^{11}$	11.80
3.922	0.155					217.07	$6.40\ 10^{11}$	11.81
								$\log(\overline{\beta_{1.IV} \times LC}) \pm s_{95\%} = 11.7 \pm 0.3$

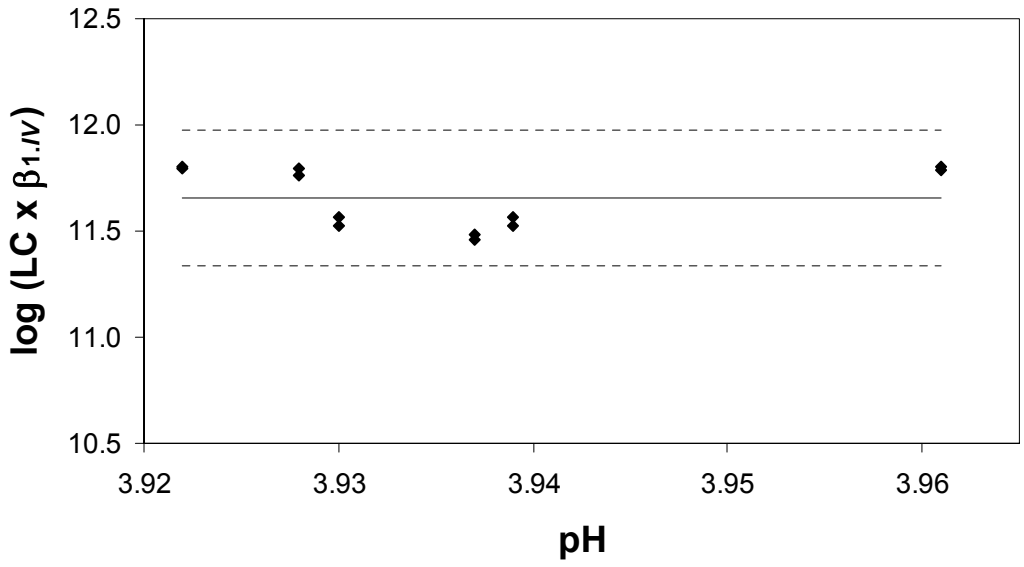

Figure 1: Values of log (LC × $\beta_{1.IV}$) in the case of thorium (IV) from the results in table 1 [52].

Table 2: Complexation constant used in this study. Extrapolation at 0.101 *m* $NaClO_4$ with SIT [67], using the parameters stated in the reference.

Equilibrium	log K [67]	Th		U [67, 68]	Np [69]	Pu [69]
$CO_2(aq) + H_2O \rightleftarrows HCO_3^- + H^+$	–6.15					
$HCO_3^- \rightleftarrows CO_3^{2-} + H^+$	–9.90					
$H_2O \rightleftarrows H^+ + OH^-$	–13.80					
$M^{3+} + H_2O \rightleftarrows MOH^{2+} + H^+$					–7.24	–7.34
$M^{3+} + 2H_2O \rightleftarrows M(OH)_2^+ + 2H^+$						–15.66
$M^{3+} + CO_3^{2-} \rightleftarrows MCO_3^+$						6.21 [69, 70]
$M^{3+} + 2CO_3^{2-} \rightleftarrows M(CO_3)_2^-$						10.69 [69, 70]
		[64]				
$M^{4+} + AcO^- \rightleftarrows MOAc^{3+}$		4.04				
$M^{4+} + 2AcO^- \rightleftarrows M(OAc)_2^{2+}$		7.33				
$M^{4+} + 3AcO^- \rightleftarrows M(OAc)_3^+$		9.47				
$M^{4+} + 4AcO^- \rightleftarrows M(OAc)_4$		11.00				
		[63]	[59, 60]			
$M^{4+} + H_2O \rightleftarrows MOH^{3+} + H^+$		–2.85	–3.79	–1.18	–0.93	–1.45
$M^{4+} + 2H_2O \rightleftarrows M(OH)_2^{2+} + 2H^+$		–7.08				
$M^{4+} + 3H_2O \rightleftarrows M(OH)_3^+ + 3H^+$		–12.30	–10.38			
$M^{4+} + 4H_2O \rightleftarrows M(OH)_4 + 4H^+$		–18.80	–15.16	–6.00	–11.09	–8.27
$M^{4+} + 5CO_3^{2-} \rightleftarrows M(CO_3)_5^{6-}$			32.27	33.94	35.58	34.07
$M^{4+} + CO_3^{2-} + 3H_2O \rightleftarrows MCO_3(OH)_3^- + 3H^+$			–2.18			
$M^{4+} + 2CO_3^{2-} + 3H_2O \rightleftarrows M(CO_3)_2(OH)_3^{3-} + 3H^+$						7.22 [71]
$MO_2^+ + H_2O \rightleftarrows MO_2OH + H^+$					–11.29	–9.72
$MO_2^+ + CO_3^{2-} \rightleftarrows MO_2CO_3^-$					4.58	4.72
$MO_2^+ + 2CO_3^{2-} \rightleftarrows MO_2(CO_3)_2^{2-}$					6.61	6.39
$MO_2^{2+} + H_2O \rightleftarrows MO_2OH^+ + H^+$				–5.38		–5.71
$MO_2^{2+} + 2H_2O \rightleftarrows MO_2(OH)_2 + 2H^+$				–10.53		–13.40
$MO_2^{2+} + 3H_2O \rightleftarrows MO_2(OH)_3^- + 3H^+$				–19.19		–19.19 [71]
$MO_2^{2+} + CO_3^{2-} \rightleftarrows MO_2CO_3$				8.80		10.76
$MO_2^{2+} + 2CO_3^{2-} \rightleftarrows MO_2(CO_3)_2^{2-}$				16.16		13.66
$MO_2^{2+} + 3CO_3^{2-} \rightleftarrows MO_2(CO_3)_3^{4-}$				21.66		17.76
$MO_2^+ + ½\ H_2 + 4H^+ \rightleftarrows M^{4+} + 2H_2O + \mathit{H^+}$					11.41	
$MO_2^+ + \mathit{H_2(g)} + 4H^+ \rightleftarrows M^{3+} + 2H_2O + \mathit{2H^+}$					14.14	
$MO_2^{2+} + ½\ H_2 \rightleftarrows MO_2^+ + \mathit{H^+}$						15.52
$MO_2^{2+} + \mathit{H_2} + 4H^+ \rightleftarrows M^{4+} + 2H_2O + \mathit{2H^+}$				9.94		34.13
$MO_2^{2+} + \mathit{3/2\ H_2} + 4H^+ \rightleftarrows M^{3+} + 2H_2O + \mathit{3H^+}$						51.12

Following the recommendation in [67], H^+ issued from the hydrogen oxidation are not taken into account in Δz^2 and $\Delta\varepsilon$, and are thus written in italic.

From the determination of LC in the case of neptunium (V), it has been observed that HAs from Gorleben (Gohy 573), Aldrich or Lac Bradford follow the same pattern [Fig. 8 in 72], yielding to the following expression:

$$\log LC = (0.26 \pm 0.03)\ pH - (2.72 \pm 0.02) \quad (12).$$

Otherwise, LC seems to increase with the charge of the metal (*e.g.* Am^{3+} - pH = 4, LC = 0,216 ± 0,007 [27]; UO_2^{2+}- pH = 4, LC = 0,186 ± 0,003 [24]; NpO_2^+, pH = 7, LC = 0.13 ± 0.01 [72]). Unfortunately, the extrapolation to z = 4 seems to be unreasonable because of the residual charges greater that z carried by the metals in actinyl (V) and (VI) molecular ions [73]. Furthermore, it is known that UO_2^{2+} behave like a trivalent cation regarding to the humic complexation [24, 37, 74, 75] and micellar exchange [76]. We propose to use LC = 0.2 in a first approximation as in the case of Am^{3+}. This leads to a value of log $\beta_{1.IV}$ = 12.4 ± 0.3 with a 95% confidence interval. Under these particular conditions, the value of LC does not seem to be as crucial as in the case of Am^{3+} [Fig. 7 in 27], as a value of LC = 0.3 would lead to a value of log $\beta_{1.IV}$ = 12.2, and log $\beta_{1.IV}$ = 12.7 when LC = 0.1. The experimental uncertainty (2.6%) is without a doubt underestimated regarding to our approximations and possible systematic errors. Consequently, a 5% uncertainty should be a better estimate, leading to log $\beta_{1.IV}$ = 12.4 ± 0.6.

The speciation of thorium (IV) using the specific interaction theory (SIT) [67], referring to the parameter in [63] (constants in Table 2) in 0.101 mol/kg water (m) (0.1 M $NaClO_4$), could be proposed on figure 2 when $[HA(IV)]_T$ = 1.85 10^{-5} eq/L,* close to the value for a the Gorleben site Gohy 2227 [77]. The importance of humic complexation would then be limited to pH ≤ 6.5, which is not in agreement with several environmental observations [38, 47-51].

In the framework of the CNM, the formation of a mixed hydrolysed complex could be postulated.

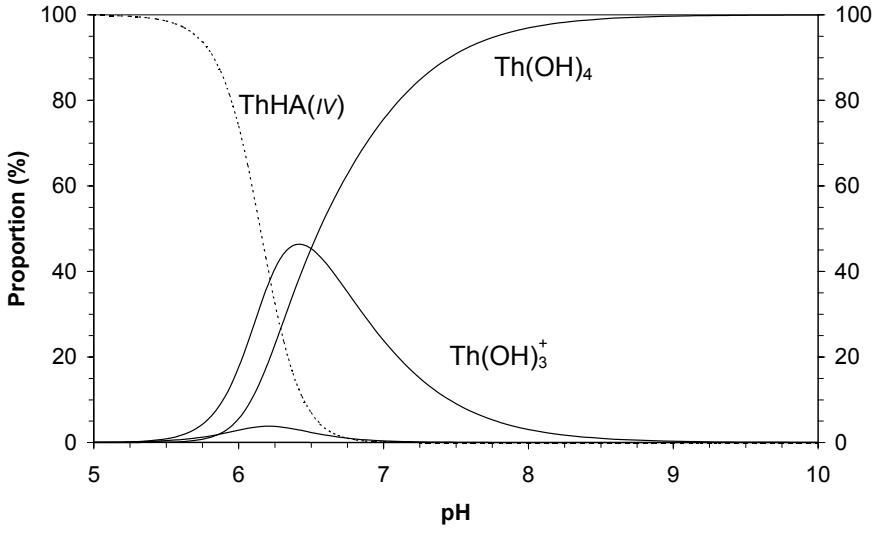

Figure 2: Speciation of thorium (IV) *vs.* pH taking into account ThHA(*IV*) log $\beta_{1.IV}$ = 12.4 referring to [63]: [Th] = 10^{-10} *m*, [$NaClO_4$] = 0.101 *m*, (HA) = 140 mg/l or [HA(*IV*)] = 1.85 10^{-5} eq/L; initial experimental data from [52].

* (HA) = 140 mg/L, PEC = 5.4 meq/g.

3.2.2. Mixed complexes formation

Up to now only few studies considering mixed complexes of tetravalent actinides have been published. The first estimation was proposed in the case of plutonium (IV) in [78] considering the fact that more than 90% of tetravalent elements were complexed by HS in natural waters. The authors proposed the formation of $Pu(OH)_3HA(I)$ through:

$$Pu^{4+} + 3OH^- + HA(I) \rightleftarrows Pu(OH)_3HA(I) \qquad \log {}^{HA}\beta_{1.3.I} = 56{,}4 \qquad (13).$$

Up to now no validation of this estimate was done.

Recently, we studied the interaction of thorium (IV) with HS in a neutral pH range in competition with the silica surface [53]. These data could also be interpreted in the framework of the CNM. Adapting the equation (8) and (9) to this particular problem leads to the following relations:

$$\beta_{1.3.I} = \frac{\alpha}{LC \times [HA(I)]_T \times [OH^-]^3}\left(\frac{K_d^o}{K_d} - 1\right) = \frac{\alpha}{LC \times [HA(I)]_T \times 10^{(pH-3pK_w)}}\left(\frac{K_d^o}{K_d} - 1\right) \qquad (14).$$

As in the case of Am^{3+}-Cm^{3+} mixed complexes, we will consider that LC ≡ 1 [54, 55]. The experimental results and estimated constants are reported in table 3.

Contrary to $\log \beta_{1.IV}$, $\log \beta_{1.n.I}$ directly depends upon the hydrolysis constant set since this phenomenon controls the aqueous speciation. Mean values of $\log \beta_{1.3.I}$ of 35.1 ± 0.7 [63] (Figure 3), 36.7 ± 0.8 [57] to 38.7 ± 0.8 [59] are obtained depending on the origin of the constants with 95% confidence interval.

The speciation with $[HA]_T = 7.8\ 10^{-4}$ eq/L,* *i.e.* close to the Gorleben Gohy 2227 case, referring to [63] is proposed on figure 4a under these assumptions. Compared with figure 2, the predominance of humic complexes of thorium (IV) is clearly shifted by more than two pH units as $Th(OH)_4(aq)$ only impede the humic complexation. When pH ≥ 9 the proportion of humic complex is still as high as 33%. If the HA concentration is reduced to $[HA]_T = 6.00\ 10^{-6}$ eq/L,† close to estimated value in Mont-Terri and Benken Swiss site [79] (Figure 4b), then humic complexes would represent 20% at pH = 7 and around 3% at pH = 8.

* (HA) = 140 mg/L, PEC = 5.4 meq/g, $[HA(I)] = 7.4\ 10^{-4}$ eq/L, $[HA(IV)] \approx 1.9\ 10^{-4}$ eq/L.

† (HA) = 0.6 mg/L, PEC = 5.4 meq/g, $[HA(I)] = 3.23\ 10^{-6}$ eq/L, $[HA(IV)] \approx 1.08\ 10^{-6}$ eq/L

Table 3: Estimation of the stability constants for $Th(OH)_3HA(I)$ and $Th(OH)_4HA(I)$ from experimental data in [53] referring to [63]. Uncertainties are 95% confidence interval[a]

pH	[HA(*I*)]	R	K_d	α	log $\beta_{1.3.I}$	log $\beta_{1.4.I}$
7.91	0	0.857	$2.395\ 10^4$			
8.02	$1.14\ 10^{-5}$	0.842	$2.133\ 10^4$	$1.97\ 10^{13}$	34.7	40.4
7.97	$2.27\ 10^{-5}$	0.744	$1.165\ 10^4$	$1.25\ 10^{13}$	35.3	41.1
7.87	$3.41\ 10^{-5}$	0.578	$5.469\ 10^3$	$5.00\ 10^{12}$	35.5	41.4
7.89	$4.55\ 10^{-5}$	0.511	$4.184\ 10^3$	$6.00\ 10^{12}$	35.5	41.4
7.86	$5.68\ 10^{-5}$	0.430	$3.012\ 10^3$	$4.57\ 10^{12}$	35.6	41.5
7.86	$6.54\ 10^{-5}$	0.368	$2.331\ 10^3$	$4.57\ 10^{12}$	35.6	41.6
7.86	$7.67\ 10^{-5}$	0.347	$2.122\ 10^3$	$4.57\ 10^{12}$	35.6	41.5
7.84	$8.53\ 10^{-5}$	0.332	$1.986\ 10^3$	$3.81\ 10^{12}$	35.6	41.5
7.81	$1.14\ 10^{-4}$	0.207	$1.042\ 10^3$	$2.90\ 10^{12}$	35.7	41.7
7.83	$1.71\ 10^{-4}$	0.176	$8.549\ 10^2$	$3.47\ 10^{12}$	35.7	41.6
					35.5 ± 0.7	41.4 ± 0.8
7.31	0	0.756	$1.243\ 10^4$			
7.22	$1.14\ 10^{-5}$	0.630	$6.825\ 10^3$	$1.44\ 10^{10}$	34.8	41.3
7.20	$2.27\ 10^{-5}$	0.377	$2.420\ 10^3$	$1.20\ 10^{10}$	35.1	41.7
7.14	$3.41\ 10^{-5}$	0.298	$1.698\ 10^3$	$7.10\ 10^9$	35.1	41.8
7.17	$4.55\ 10^{-5}$	0.242	$1.279\ 10^3$	$9.24\ 10^9$	35.1	41.8
7.18	$5.68\ 10^{-5}$	0.187	$9.221\ 10^2$	$1.01\ 10^{10}$	35.2	41.8
7.14	$6.54\ 10^{-5}$	0.182	$8.920\ 10^2$	$7.10\ 10^9$	35.1	41.8
7.10	$7.67\ 10^{-5}$	0.149	$7.012\ 10^2$	$5.00\ 10^9$	35.1	41.8
7.14	$8.53\ 10^{-5}$	0.140	$6.513\ 10^2$	$7.10\ 10^9$	35.2	41.8
7.21	$1.14\ 10^{-4}$	0.137	$6.348\ 10^2$	$1.31\ 10^{10}$	35.1	41.7
7.22	$1.71\ 10^{-4}$	0.129	$5.917\ 10^2$	$1.44\ 10^{10}$	35.0	41.5
					35.1 ± 0.3	47.7 ± 0.4
6.72	0	0.937	$5.909\ 10^4$			
6.76	$1.13\ 10^{-5}$	0.855	$2.355\ 10^4$	$2.31\ 10^8$	34.7	41.7
6.73	$2.27\ 10^{-5}$	0.662	$7.844\ 10^3$	$5.34\ 10^8$	35.1	42.0
6.74	$3.41\ 10^{-5}$	0.690	$8.888\ 10^3$	$2.12\ 10^8$	34.8	41.8
6.78	$4.55\ 10^{-5}$	0.673	$8.236\ 10^3$	$5.71\ 10^7$	34.6	41.8
6.76	$5.68\ 10^{-5}$	0.555	$4.982\ 10^3$	$3.50\ 10^8$	34.9	41.9
6.74	$6.53\ 10^{-5}$	0.560	$5.085\ 10^3$	$3.50\ 10^8$	34.8	41.8
6.76	$7.67\ 10^{-5}$	0.504	$4.067\ 10^3$	$3.22\ 10^8$	34.8	41.8
6.72	$8.53\ 10^{-5}$	0.502	$4.039\ 10^3$	$1.80\ 10^8$	34.7	41.8
6.76	$1.14\ 10^{-4}$	0.364	$2.289\ 10^3$	$2.51\ 10^8$	34.9	41.9
6.74	$1.71\ 10^{-4}$	0.311	$1.804\ 10^3$	$2.72\ 10^8$	34.8	41.9
					34.8 ± 0.3	41.9 ± 0.2
					35.1 ± 0.7	41.6 ± 0.6

[a] $\log\ \overline{\beta}\ \pm t_{0.95}.\sigma$, with $t_{0.95} = 2.262$ for 10 values (9 degrees of freedom), and $t_{0.95} = 2.045$ for 30 values (29 degrees of freedom).

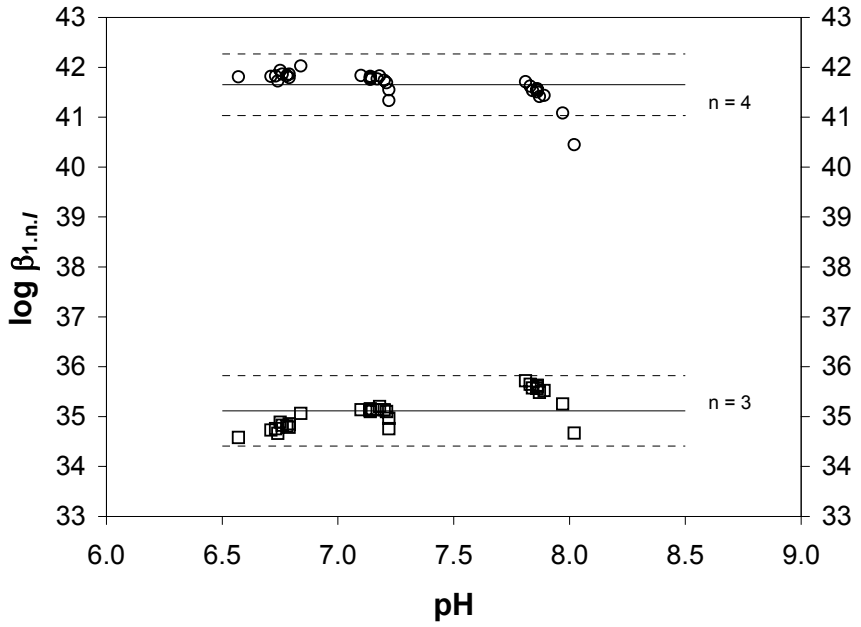

Figure 3: Determination of log $\beta_{1.3.I}$ (Eq. 14) and log $\beta_{1.4.I}$ (Eq. 16) from experimental data in [53], referring to auxiliary data in [63] (see table 3).

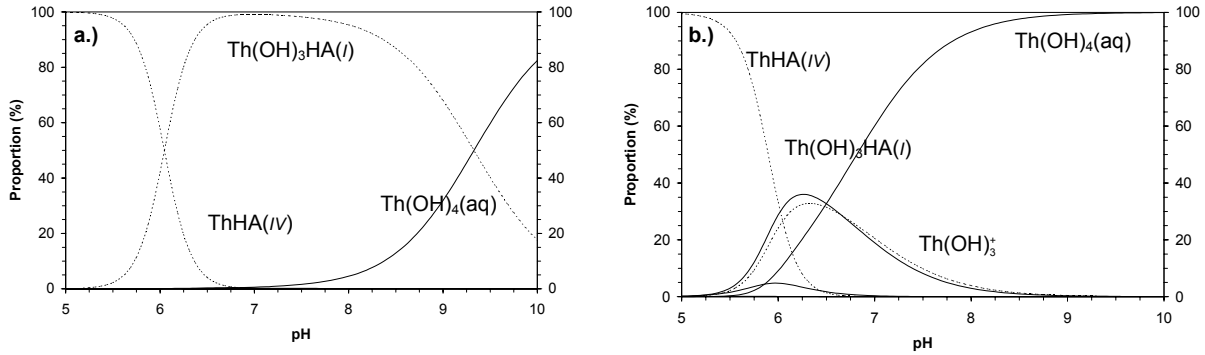

Figure 4: Speciation of thorium (IV) *vs.* pH taking into account ThHA(*IV*) (log $\beta_{1.IV}$ = 12.4 from experimental data in [52]) and $Th(OH)_3HA(I)$ (log $\beta_{1.3.I}$ = 35.1 from experimental data in [53]) referring to auxiliary data in [63]: a. $[NaClO_4]$ = 0.101 *m*, [HA(*I*)] = 7.8 10^{-4} eq/L, $[HA(IV)]_T$ = 1.95 10^{-4} eq/L; b. $[NaClO_4]$ = 0.101 *m*, [HA(*I*)] = 1.48 10^{-6} eq/L, [HA(*IV*)] = 3.7 10^{-7} eq/L.

Using a 95% confidence interval, the determinations at different pH values are not significantly different. Nevertheless, a slight increase could be mentioned (Figure 3). Two hypothesis could be made in the framework of the model: the occurrence of one less hydrolysed or one more hydrolysed species: *e.g.* $Th(OH)_2HA(II)$ and $Th(OH)_4HA(0)$ respectively. The former hypothesis is impossible to assess using these experimental data since $Th(OH)_2^{2+}$ would be predominant in solution when pH ≤ 5.5 [63]. The latter hypothesis needs an adaptation of the model. Through equation (2), if $z = 0$ then $[HA(0)] \rightarrow \infty$. Hence, the boundary condition is when $z = 0$ then $[HA(0)] = [HA(I)]$.

The following equilibrium could then be proposed:

$$Th^{4+} + 4\ OH^- + HA(I) \rightleftarrows Th(OH)_4HA(I) \qquad \log \beta_{1.4.I} = \frac{[Th(OH)_4HA(I)]}{[Th^{4+}]_F\ [OH^-]^4\ [HA(I)]_F} \tag{15}$$

The equation (14) is then rewritten as:

$$\beta_{1.4.I} = \frac{[Th(OH)_4HA(I)]}{[Th^{4+}]_F\ [OH^-]^4\ [HA(I)]_F} \equiv \frac{\alpha}{[HA(I)]_T \times 10^{(pH-4.pK_w)}} \left(\frac{K_d^o}{K_d} - 1\right) \tag{16}$$

The calculated values of log $\beta_{1.4.I}$ are also reported in table 3, and no increase with pH could be noted (Figure 3). Like in the case of log $\beta_{1.3.I}$, log $\beta_{1.4.I}$ directly depends on the hydrolysis constant set. Mean values of log $\beta_{1.4.I}$ of 41.6 ± 0.6 [63], 43.2 ± 0.6 [57] and 45.2 ± 0.6 [59] are obtained depending on the origin of the constants. The speciation could be proposed with $[HA]_T = 7.4\ 10^{-4}$ eq/L on figure 5a, where HA totally controls the thorium chemistry when pH ≤ 10. The proportion of humic complex is still important when (HA) is lowered to 0.3 mg/L or $[HA]_T = 1.48\ 10^{-6}$ eq/L (Swiss site, Figure 5b). This result does not seem to be in agreement with the results of the study of Glaus *et al.* [79]. One must remind that the carbonate complexation has not been taken into account.

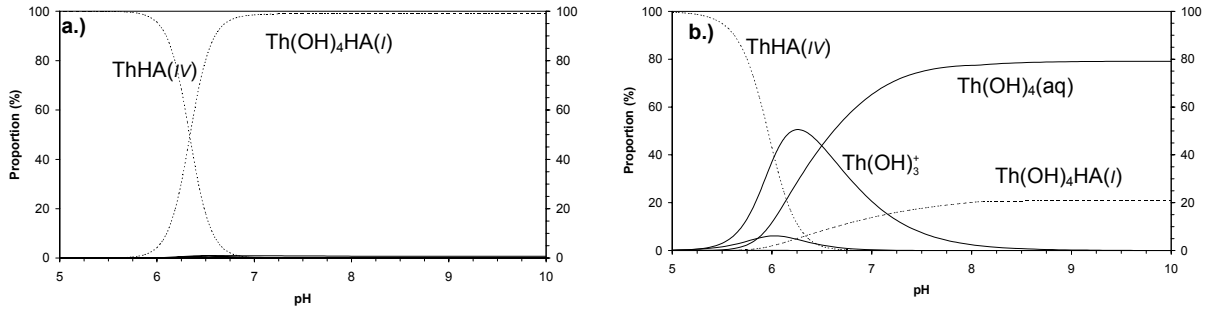

Figure 5: Speciation of thorium (IV) *vs.* pH taking into account $Th(OH)_4HA(I)$ with log $\beta_{1.4.I}$ = 41.6 referring to [63]: a. $[NaClO_4]$ = 0.101 *m*, $[HA(I)] = 7.8\ 10^{-4}$ eq/L, $[HA(IV)] = 1.95\ 10^{-4}$ eq/L; b. $[NaClO_4]$ = 0.101 *m*, $[HA(I)] = 1.48\ 10^{-6}$ eq/L, $[HA(IV)] = 0.3\ 10^{-6}$ eq/L.

The original sorption results in [53] could help us to opt for an hypothesis. Both K_d^o and K_d values of thorium (IV) in the systems Th-SiO_2-HA are very similar at the three pH values (*i.e.* 6.75, 7.2, 7.9). This fact may indicate that the complexation properties of HA towards thorium (IV) are rather constant in the pH range. This may be in favour of the $Th(OH)_4HA(I)$ option, which implies a rather constant proportion of humic complex when pH ≥ 6.7.

3.2.3. Application to solubility prediction and on independent data

One could calculate the enhancement of the "theoretical" solubility of ThO_2(cr) referring to the values in [63] in the case of Gohy 2227 (Figure 6). A fairly high enhancement of thorium solubility could be prognosticated. In the case of the Swiss sites the enhancement is lower than the uncertainty of the ThO_2 solubility (data not shown). Like it has already been observed in the case or Fe, [80, 81], Al [82] and Pd [83], an increase of more than one order of magnitude could be expected. The same trend could be observed for the other actinide oxides. An experimental validation of this hypothesis is needed.

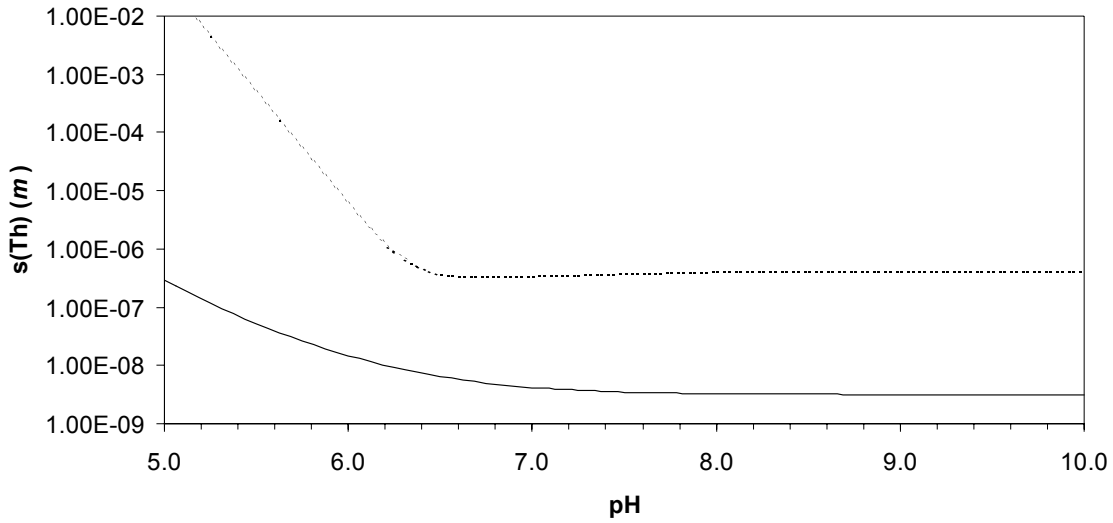

Figure 6: Calculated solubility of ThO_2(cr) [$NaClO_4$] = 0.101 *m* using ThHA(*IV*) (log $\beta_{1.IV}$ = 12.4) and $Th(OH)_4HA(I)$ (log $\beta_{1.4.I}$ = 41.6), referring to auxiliary data in [63]; plain line $[HA]_T$ = 0 eq/L, dashed line $[HA]_T$ = 7.4 10^{-4} eq/L (HA = 140 mg/L).

The formation of carbonate complexes of thorium is a matter of debate. Some authors proposed the limiting carbonate complex $Th(CO_3)_5^{6-}$ [58, 60], as it is the case for uranium (IV) [67], plutonium (IV) [84] and neptunium (IV) [69]. From solubility experiments of ThO_2 in carbonate media, the formation of $ThCO_3(OH)_3^-$ was also proposed [60]. Even if the formation of mixed complexes is also a matter of debate [85-87], we can use these constants in order to appreciate the effects of carbonate complexation of thorium (IV) on the stability of humic complexes. A speciation could be proposed with a total inorganic carbon concentration, [TIC] = 8.2 10^{-3} *m*, $[HA]_T$ = 7.4 10^{-4} eq/L, using the Th^{4+} hydrolysis and carbonation constants in [59, 60] extrapolated to 0.101 *m* (0.1 M $NaClO_4$) using the SIT parameters in [67], the associated humic constants log $\beta_{1.IV}$ = 12.4, log $\beta_{1.3.I}$ = 38.7 (Figure 7a) or log $\beta_{1.4.I}$ = 45.2 (Figure 7b). When $Th(OH)_3HA(I)$ is taken into account, the mixed carbonato complex limits the domain where the humic complexation controls thorium chemistry. Nevertheless, the humic complex represents 60% of total thorium (IV) at pH = 8 (Figure 7a). Conversely, when $Th(OH)_4HA(I)$ is considered, $ThCO_3(OH)_3^-$ only decrease the proportion of $Th(OH)_4HA(I)$ to 90% (≈ 100% without carbonate, Figure 7b). This latter result seems to be more relevant of natural situations where thorium is associated to natural organic matter in the presence of carbonate ions [44, 53, 77]. Furthermore, an application to the works of Glaus *et al.* [79] leads now to the same weak interaction of thorium (IV) with Mont-Terri and Benken organic matter as already calculated in [53] ($Th(OH)_4HA(I) \leq$ 3 %), Figure 7c).*

These reinterpretations of the literature data provide a consistent view of the environmental behaviour of thorium (IV). Nevertheless, further works are needed in order to assess these points experimentally.

* 12.5 mg/l ≤ (NOM) ≤ 5.5 mg/l, comprising around 5% HA

In the following we will use the complexes MHA(*IV*) with log $_{1.IV}$ = 12.4 and $M(OH)_4HA(I)$ with log $\beta_{1.4.I}$ adapted to the hydrolysis constants sets.

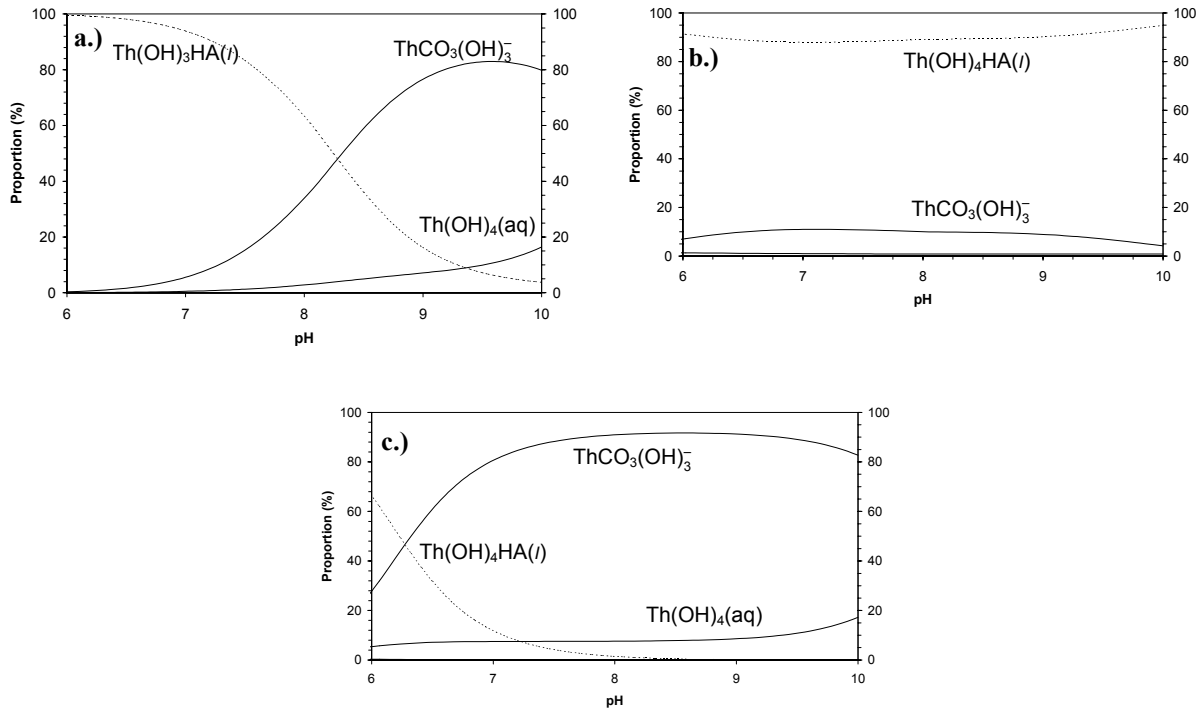

Figure 7: Speciation of thorium (IV) *vs.* pH referring to [59, 60], log $\beta_{1.IV}$ = 12.4, [$NaClO_4$] = 0.101 *m*, [TIC] = 8.2 10^{-3} *m*, [HA(*I*)] = 7.8 10^{-4} eq/L, $[HA(IV)]_T$ = 1.9 10^{-4} eq/L; log $\beta_{1.IV}$ = 12.4; a. log $\beta_{1.3.IV}$ = 38.7; b. log $\beta_{1.4.IV}$ = 45.2; c. (HA) = 0.6 mg/L, PEC = 5.4 10^{-3}, [HA(*I*)] = 3.23 10^{-6} eq/L, [HA(*IV*)] = 1.08 10^{-6} eq/L.

4. Application to other redox sensitive actinide elements

The use of analogy between elements is useful when it is a matter of estimating data on difficult systems like uranium, neptunium or plutonium [1, 71, 88]. In deep geological media, these elements are supposed to be stable in their reduced form *i.e.* neptunium (IV), uranium (IV) and plutonium (IV) - plutonium (III) [69, 89]. If data on americium (III) or curium (III) and uranium (VI) exist in the literature [24, 37], there is only one communication up to now on neptunium (IV) complexation by HA in neutral pH through CNM [46]. Using CNM, the authors report an "increasing" constant in the case of $Np(OH)_3HA(I)$ and log $\beta_{1.4.I}$ = 52 independent of pH ($6 \leq pH \leq 9.5$). The neptunium (IV) hydrolysis data are not referred in this abstract.

If one assumes that the results obtained with thorium (IV) [53] can mimic those that may be acquired in the case of uranium (IV), neptunium (IV) or plutonium (IV), then using equation (11) and (16), with the proper α values and the hydrolysis constant extrapolated to 0.101 *m* $NaClO_4$ [67, 69], would give a reasonable estimates of $\beta_{1.IV}$ and $\beta_{1.4.I}$. The value of log $\beta_{1.4.I}$ = 49.3 could be proposed in the case of neptunium (IV). This value is in fair

agreement with the results of [46]. In as much, log $\beta_{1.4.z}$ values of 54.4 referring to [67] and 52.1 referring to [69 page 323]* could be proposed in the case of uranium (IV) and plutonium (IV) respectively. One could note that these proposed constants agree with the order of affinity proposed in [90]. Furthermore, thorium (IV) and plutonium are known to have the same comportment in presence of natural organic matter [91]. Nevertheless, readers should bear in mind that these constants are only estimates and should be used with caution.

An exercise on the chemistry of uranium, neptunium and plutonium in waters that contains high HA concentration could be proposed. The complexation constants from $Am^{3+}/Cm^{3+}/Eu^{3+}$ are very similar to one another [37, 45]. Then using log $\beta_{1.III} = 6.2$ seems to be a fair approximation in the case of Pu^{3+} or Np^{3+}. The constants of the mixed complexes evidenced in [54, 55] can also be used without modification for Pu^{3+}, *i.e.* log $\beta_{1.1.II} \approx 13$ and log $\beta_{1.2.I} \approx 17.6$. In the case of the carbonato complex, the estimation of $Pu(CO_3)_m^{3-2m}$ in [70], very close to the values recommended for Am^{3+} [68], and the mixed complex postulated in [54], will be applied without any modification. The upper limit constant for the formation of mixed carbonato complex $Pu(CO_3)_2(OH)_3^{3-}$,† used by Vitorge and Capdevila [71] to fit the $PuO_2(s)$ solubility in carbonate media from literature was also included.

For actinyl (V) and (VI) ions, the values for NpO_2^+ obtained at low level [25, 40, 41], and UO_2^{2+} [24, 56], could be directly applied to PuO_2^+ and adapted to PuO_2^{2+}. The constants calculated from the original data at 0.101 *m* $NaClO_4$ referring to PuO_2^{2+}, NpO_2^+ and UO_2^{2+} are also reported in Table 4. These constants were used in the analytical resolutions of the systems.

It is also reminded to the reader that the reducing capacity of HS is not taken into account in these calculations, as this behaviour is still difficult to assess [3-5] and is dependant on light exposure [9, 92].

The speciation for plutonium (Figure 8), neptunium (Figure 9) and uranium (Figure 10) can be calculated when $E_H = -30$ mV, with [TIC] = $8.2\ 10^{-3}$ *m*, $6 \le pH \le 10$, $[HA]_T = 0$ and $5.4\ 10^{-4}$ eq/L,‡ and assuming that LC = LC(Am^{3+}) for all humic complexes [Fig. 3 in 37] except for $MO_2HA(I)$ [Eq. 14 in 72]. As expected, under these particular conditions, mixes of redox species could be observed. For every actinide, a shift in the predominance of M(III) and M(IV) towards higher pH values in the presence of HA could be observed, due to the formation of the mixed complexes. The formation of NpHA(*III*) or NpOHHA(*II*) only occurs below the reduction limit of water and are not reported.

---

* log $*\beta°(Pu(OH)_4(aq)) = -6.9$

† $Pu^{4+} + CO_3^{2-} + 3OH^- \rightleftarrows Pu(CO_3)_2(OH)_3^{2-}$, log $\beta < 50.5$

‡ (HA) ≈ 100 mg/L

Table 4: Stability constants for humic complexes used in this study. The constants that takes into account the reduction of M(VI) are calculated using the data from table 2.

Equilibrium	log $\beta_{n.m.z}$		
	Pu	**Np**	**U**
M^{3+} + HA(*III*) ⇄ MHA(*III*)	6.2		
MO_2^{2+} + *3/2* H_2 + $4H^+$ + HA(*III*) ⇄ MHA(*III*) + 2 H_2O + *3* H^+	57.3	20.3	
M^{3+} + OH^- + HA(*II*) ⇄ MOHHA(*II*)	13		
MO_2^{2+} + *3/2* H_2 + $3H^+$ + HA(*II*) ⇄ MOHHA(*II*) + H_2O + *3* H^+	50.3	13.3	
M^{3+} + 2 OH^- + HA(*I*) ⇄ $M(OH)_2HA$(*I*)	17.6		
MO_2^{2+} + *3/2* H_2 + $2H^+$ + HA(*II*) ⇄ $M(OH)_2HA$(*II*) + *3* H^+	41.1		
M^{3+} + CO_3^{2-} + HA(*I*) ⇄ MCO_3HA(*I*)	12.4		
MO_2^{2+} + *3/2* H_2 + $4H^+$ + CO_3^{2-} + HA(*I*) ⇄ MCO_3HA(*I*) + 2 H_2O + *3* H^+	63.5		
M^{4+} + HA(*IV*) ⇄ MHA(*IV*)	16.0	13.2	18.2
MO_2^{2+} + H_2 + $4H^+$ + HA(*IV*) ⇄ MHA(*IV*) + 2 H_2O + 2 H^+	50.1	24.6	28.1
M^{4+} + 4 OH^- + HA(*I*) ⇄ $M(OH)_4HA$(*I*)	52.0	49.3	54.4
MO_2^{2+} + H_2 + 2 H_2O + HA(*I*) ⇄ $M(OH)_4HA$(*I*) + *2* H^+	30.9	5.5	9.0
MO_2^+ + HA(*I*) ⇄ MO_2HA(*I*)	4.6	4.6	
MO_2^{2+} + *½* H_2 + HA(*I*) ⇄ MO_2HA(*I*) + H^+	20.0		
MO_2^{2+} + HA(*II*) ⇄ MO_2HA(*II*)	6.2		6.2
MO_2^{2+} + OH^- + HA(*I*) ⇄ MO_2OHHA(*I*)	14.05		14.7

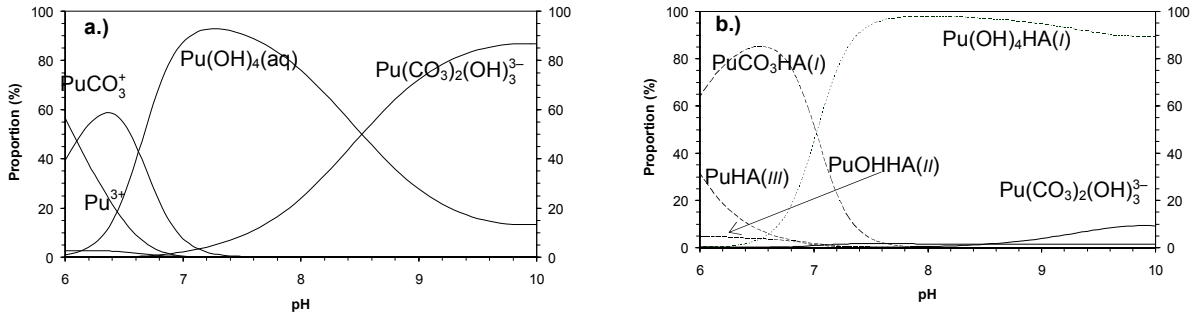

Figure 8: Speciation of plutonium *vs.* pH referring to [69], log $\beta_{1.4.IV}$ = 52, E_H = – 30 mV, [TIC] = 8.2 10^{-3} *m*; a. $[HA]_T$ = 0; b. $[HA]_T$ = 5.4 10^{-4} eq/L

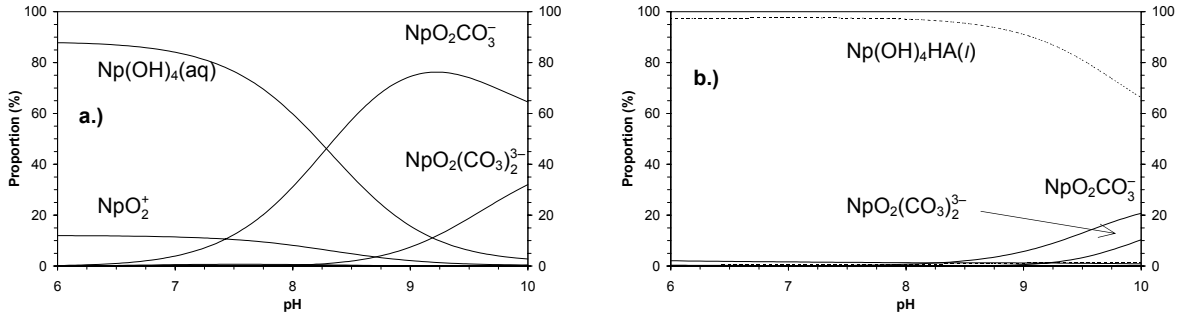

Figure 9: Speciation of neptunium *vs.* pH referring to [69], log $\beta_{1.4.IV}$ = 49.3, E_H = – 30 mV, [TIC] = 8.2 10^{-3} *m*; a. $[HA]_T$ = 0; b. $[HA]_T$ = 5.4 10^{-4} eq/L

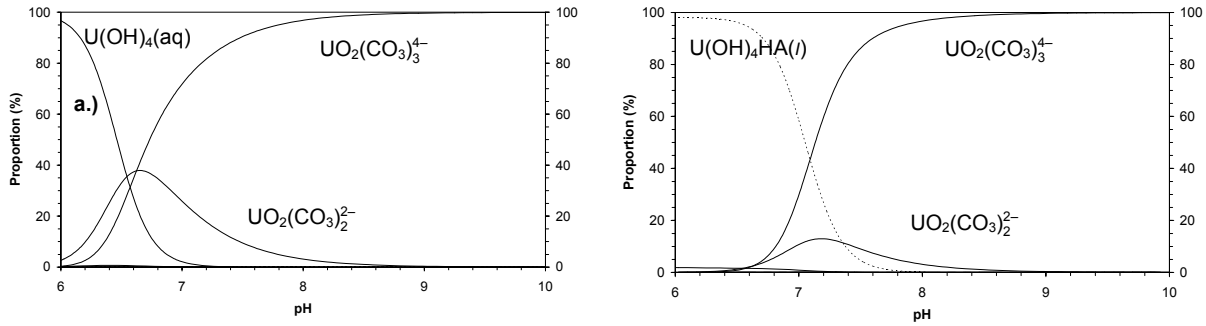

Figure 10: Speciation of uranium vs. pH referring to [67, 68], log $\beta_{1.4.IV}$ = 54.4, E_H = – 30 mV, [TIC] = 8.2 10^{-3} *m*; a. $[HA]_T$ = 0; b. $[HA]_T$ = 5.4 10-4 eq/L.

The theoretical speciation *vs.* E_H (V) at pH = 7, [TIC] = 8.2 10^{-3} *m* and $[HA]_T$ = 5.4 10^{-4} eq/L (HA) = 100 mg/L) for neptunium, plutonium and uranium (Figure 11) can also be calculated. It can be seen that neptunium could coexist as $NpO_2HA(I)$ and $Np(OH)_4HA(I)$, and that it could be totally reduced in $Np(OH)_4HA(I)$ when $E_H \leq 0$ mV (Figure 11a). This can be related with the observation from Gorleben ground waters [56]. Furthermore, the formation of $NpHA(IV)$ would impede the reduction to neptunium (III) when pH ≤ 5 (data not shown).

In the case of Pu (Figure 11b), plutonium (III) humic complexation could be significant when $E_H \leq 100$ mV and may lead to mixes of plutonium oxidation states in solution, as it has already been reported [93, 94]. The other redox behaviour of plutonium reported in [10, 11] are more difficult to assess with these data. Nevertheless, different authors have measured E_H for different humic acid solutions at pH = 7: $E_H \approx +230$ mV [4]; $E_H \approx +260$ mV [95]; $300 \leq E_H$ (mV) ≤ 400 [96]; $438 \leq E_H$ (mV) ≤ 407 [97]. Under these conditions, plutonium is stable as $Pu(OH)_4HA(I)$, and plutonium (VI) or plutonium (V) introduced could be reduced and then complexed by HA.

In the case of uranium (Figure 11c), the formation of $U(OH)_4HA(I)$ could also imply a shift in the predominance of uranium (IV) towards higher pH values. The negative carbonato complexes of uranium (VI) would impede the formation of the humic complex [56, 75]. The reduction of uranium (VI) would only be possible when $E_H \leq 80$ mV. This value is higher that the measured ones [4, 95-97] and gives a plausible explanation for the absence of reaction noted by several authors [24, 25]. One should note that the comportment of $UO_2OHHA(I)$ and $PuO_2OHHA(I)$ are not the same due to the highest constant for $PuO_2CO_3(aq)$ [68, 69], probably due to systematic uncertainty [Vitorge, Pers. Comm.]. This cannot be considered as representative of plutonium (VI) comportment in sea water [12]. Furthermore, one can notice that there is a marked difference between the experimental data form different authors for uranium (VI) under low $CO_2(g)$ partial pressure.* Zeh *et al.* [56] did not evidenced relevant humic interaction when pH ≥ 9, while Glaus *et al.* [74, 75] and Laszak [98] quantified a significant interaction up to pH = 10. The humic interaction of M(VI) cations could therefore

* $\log(pCO_2) = -6$

be underestimated in neutral to alkaline media. Further works are needed to ascertain this point.

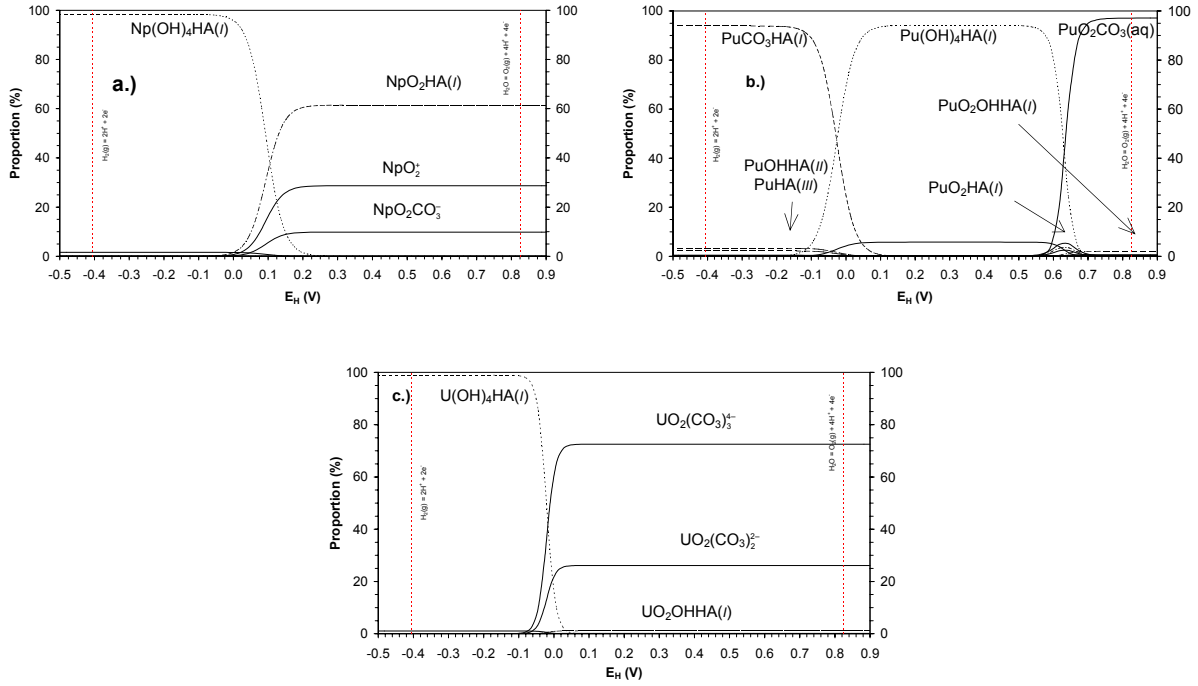

Figure 11: Speciation of actinides 10^{-10} *m vs.* E_H (V), pH = 7, [$NaClO_4$] = 0.101 *m*, [TIC] = 8.2 10^{-3} *m* and $[HA]_T$ = 5.4 10^{-4} eq/L; a. neptunium; b. plutonium; c. uranium.

Nevertheless, in the case of uranium, neither the results of Li *et al.* [99], nor those from Artinger *et al.* [26] could be assessed. In the latter study, the authors did not observe any difference in the comportment of uranium, introduced as uranium (VI) or uranium (IV), neither with purified HA [99], nor with Gorleben groundwater in the presence of natural organic matter at varying E_H [26].* Under these conditions, the uranium speciation would predict $U(OH)_4HA(I)$ as predominant species up to E_H = –20 mV, and carbonate uranium (VI) complexes for higher potentials (data not shown). More results on the actual interaction of uranium (IV) with natural organic matter under well-controlled redox conditions are thus required in order to assess this point.

E_H-pH diagrams could also be proposed in a closed system consisting of 10^{-10} mole actinide/kg water, 8.2 10^{-3} mole total carbonate/kg water and 100 mg HA/L (PEC = 5.4 meq/L). Here again we must recall that these diagrams are only the results of speciation calculations and does not take into account the redox properties of HS, and cannot be considered as strict representation of actinide comportment in the presence of HS. The most striking example is the lack of plutonium (VI) humic complexation when pH ≥ 4.5 as it has been observed in sea water [12].

* $-200 \leq E_H\,(V) \leq +150$, pCO_2 = 1%, pH = 7.2.

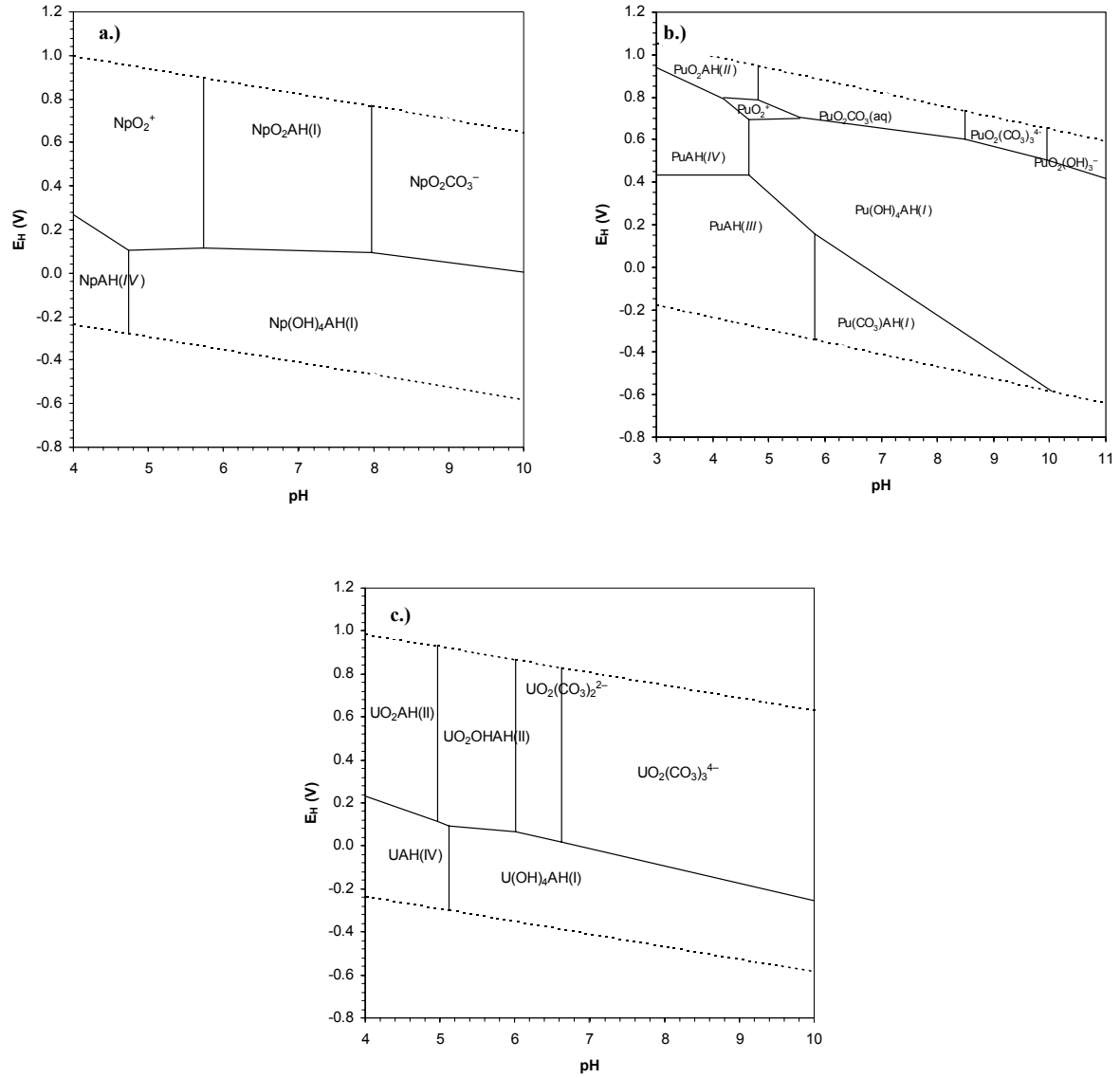

Figure 12: E_H-pH diagrams for a. neptunium, b. plutonium and c. uranium species drawn with data from table 2 for inorganic complexes and table 4 for humic complexes. Redox properties of HS are not taken into account; [M] = 10^{-10} *m*, total carbonate = 8.2 10^{-3} *m*, (HA) = 100 mg/l, PEC = 5.4 meq/g, [$NaClO_4$] = 0.101 *m*.

5. Conclusions

Through this exercise, we tried to outline that the use of analogy could permit to estimate the missing interaction constants for redox sensitive elements, namely uranium, neptunium and plutonium. Reinterpretations of thorium (IV) data available in the literature allowed us to have consistent data sets for this element and to represent independent environmental data. The adaptation of these data through analogy for uranium (IV), neptunium (IV) and plutonium (IV), permitted us to propose humic interaction constant that could be used for prognosticating the chemical form of redox sensitive actinides in environmental systems. The transposition of available data on uranium (VI), neptunium (V) and americium-curium-

europium (III) helped us to appreciate the humic complexation of the different redox states of plutonium, neptunium and uranium. We have shown that the use of these data and analogies could permit to understand some puzzling behaviour of these elements. Nevertheless, some results still cannot be represented as in the case of marine systems for plutonium and deep groundwater systems for uranium, enhancing the fact that more experiments are needed to ascertain the influence of natural organic matter onto the redox chemistry of this element.

6. Acknowledgement

The author would like to thank Drs Valérie Moulin and Pierre Vitorge, and Christophe Moulin for their critical reading of the manuscript.

7. References

1. Choppin, G. R.: Utility of oxidation state analogs in the study of plutonium behavior. Radiochim. Acta **85**, 89 (1999).
2. David, F.: Thermodynamic properties of lanthanides and actinides ions in aqueous solution. J. Less Common Metals **121**, 27 (1986).
3. Wahlberg, O., Ågren, S.: Studies of fulvic and humic acids .1. Determination of the steady states for slow processes in 0.1M NaCl aqueous solution at 25 degrees C. Acta Chem. Scand. **50**, 561 (1996).
4. Österberg, R., Shirshova, L.: Oscillating, nonequilibrium redox properties of humic acids. Geochim. Cosmochim. Acta **61**, 4599 (1997).
5. Aguer, J.-P., Richard, C., Andreux, F.: Comparison of the photoinductive properties of commercial, synthetic and soil-extracted humic substances. J. Photochem. Photobiol. A **103**, 163 (1997).
6. Kim, J. I., Delakowitz, B., Zeh, P. D., Koltz, D., Lazik, D.: A column experiment for the study of colloidal radionuclide migration in Gorleben aquifer systems. Radiochim. Acta **66/67**, 165 (1994).
7. Zeh, P., Kim, J. I., Marquardt, C. M., Artinger, R.: The reduction of Np(V) in groundwater rich in humic substances. Radiochim. Acta **87**, 23 (1999).
8. Artinger, R., Marquardt, C. M., Kim, J. I., Seibert, A., Trautman, N., Kratz, J. V.: Humic colloid-borne Np migration: influence of the oxidation state. Radiochim. Acta **88**, 609 (2000).
9. André, C., Choppin, G. R.: Reduction of Pu(V) by humic acid. Radiochim. Acta **88**, 613 (2000).
10. Sanchez, A. L., Murray, J. M., Sibley, T. H.: The adsorption of Plutonium IV and V on goethite. Geochim. Cosmochim. Acta **49**, 2297 (1985).
11. Nash, K. L., Fried, S., Friedman, A. M., Sullivan, J. C.: Redox behavior, complexing, and adsorption of hexavalent actinides by humic acid and selected clays. Stiring marine disposal of high-level radioactive waste. Environ. Sci. Technol. **15**, 834 (1981).
12. Garcia, K., Boust, D., Moulin, V., Douville, E., Fourest, B., Guillaumont, R.: Multiparametric investigation of the reactions of plutonium under estuarine conditions. Radiochim. Acta **74**, 165 (1996).
13. Miles, C. J., Brezonik, P. L.: Oxygen consumption in humic-colored waters by a photochemical ferrous-ferric catalytic cycle. Environ. Sci. Technol. **15**, 1089 (1981).
14. Skogerboe, R. K., Wilson, S. A.: Reduction of ionic species by fulvic acid. Anal. Chem. **53**, 228 (1981).
15. Liang, L., McNabb, J. A., Paulk, J. M., Gu, B., McCarthy, J. F.: Kinetics of Fe(II) oxygenation at low partial pressure of oxygen in the presence of natural organic matter. Environ. Sci. Technol. **27**, 1864 (1993).
16. Liang, L., McCarthy, J. F., Jolley, L. W., McNabb, J. A., Mehlhorn, T. L.: Iron dynamics: transformation of Fe(II)/Fe(III) during injection of natural organic matter in a sandy aquifer. Geochim. Cosmochim. Acta **57**, 1987 (1993).
17. Spokes, L. J., Liss, P. S.: Photochemically Induced Redox Reactions in Seawater .1. Cations. Mar. Chem. **49**, 201 (1995).
18. Lu, X., Johnson, W. D., Hook, J.: Reaction of vanadate with aquatic humic substances: an ESR and ^{51}V NMR Study. Environ. Sci. Technol. **32**, 2257 (1998).
19. Nakayasu, K., Fukushima, M., Sasaki, K., Tanaka, S., Nakamura, H.: Comparative studies of the reduction behavior of chromium(VI) by humic substances and their precursors. Environ. Toxicol. Chem. **18**, 1085 (1999).
20. Al Mahamid, I., Becraft, K. A., Nitsche, H.: Complexation of Plutonium(V) with Nitrilotriacetic Acid. Radiochim. Acta **68**, 63 (1995).

21. Al Mahamid, I., Becraft, K. A., Hakem, N. L., Gatti, R. C., Nitsche, H.: Stability of various plutonium valence states in the presence of NTA and EDTA. Radiochim. Acta **74**, 129 (1996).
22. Bion, L., Moisy, P., Vaufrey, F., Meot-Reymond, S., Simoni, E., Madic, C.: Coordination of U^{4+} in the complex $U(P_2W_{17}O_{61})_2^{16-}$ in solid state and in aqueous solution. Radiochim. Acta **78**, 73 (1997).
23. Reed, D. T., Wygmans, D. G., Aase, S. B., Banaszak, J. E.: Reduction of Np(VI) and Pu(VI) by organic chelating agents. Radiochim. Acta **82**, 109 (1998).
24. Czerwinski, K. R., Buckau, G., Scherbaum, F., Kim, J. I.: Complexation of the uranyl ion with aquatic humic acid. Radiochim. Acta **65**, 111 (1994).
25. Moulin, V., Tits, J., Laszak, I., Moulin, C., Decambox, P., de Ruty, O.: Complexation behaviour of humic substances studied by Time-Resolved Laser-Induced Fluorescence and Spectrophotometry. Commission of the European Communities, Report EUR 16843 EN, Brussels (1996).
26. Artinger, R., Rabung, T., Kim, J. I., Sachs, S., Schmeide, K., Heise, K. H., Bernhard, G., Nitsche, H.: Humic colloid-borne migration of uranium in sand columns. J. Contam. Hydrol. **58**, 1 (2002).
27. Kim, J. I., Czerwinski, K. R.: Complexation of metal ions with humic acid: metal ion charge neutralization model. Radiochim. Acta **73**, 5 (1996).
28. Choppin, G. R., Kullberg, L.: Protonation thermodynamics of humic acid. J. Inorg. Chem. **40**, 651 (1978).
29. Tipping, E.: Humic ion-binding model VI: An improved description of the interactions of protons and metal ions with humic substances. Aquat. Geochem. **4**, 3 (1998).
30. Kinniburgh, D. G., van Riemsdijk, W. H., Koopal, L. K., Borkovec, M., Benedetti, M. F., Avena, M. J.: Ion binding to natural organic matter: competition, heterogeneity, stoichiometry and thermodynamic consistency. Colloid Surf. A-Physicochem. Eng. Asp. **151**, 147 (1999).
31. Kinniburgh, D. G., Milne, C. J., Benedetti, M. F., Pinheiro, J. P., Filius, J., Koopal, L. K., van Riemsdijk, W. H.: Metal ion binding by humic acid: application of the NICA-Donnan model. Environ. Sci. Technol. **30**, 1687 (1996).
32. Pinheiro, J. P., Mota, A. M., Benedetti, M. F.: Lead and calcium binding to fulvic acids: salt effect and competition. Environ. Sci. Technol. **33**, 3398 (1999).
33. Leenheer, J. A., Rostad, C. E., Gates, P. M., Furlong, E. T., Ferrer, I.: Molecular resolution and fragmentation of fulvic acid by electrospray ionization/multistage tandem mass spectrometry. Anal. Chem. **73**, 1461 (2001).
34. Plancque, G., Amekraz, B., Moulin, V., Toulhoat, P., Moulin, C.: Molecular structure of fulvic acids by electrospray with quadrupole time-of-flight mass spectrometry. Rapid Commun. Mass Spectrom. **15**, 827 (2001).
35. McIntyre, C., McRae, C., Jardine, D., Batts, B. D.: Identification of compound classes in soil and peat fulvic acids as observed by electrospray ionization tandem mass spectrometry. Rapid Commun. Mass Spectrom. **16**, 1604 (2002).
36. Tipping, E.: Modelling the competition between alkaline earth cations and trace metal species for binding by humic substances. Environ. Sci. Technol. **27**, 520 (1993).
37. Czerwinski, K. R., Kim, J. I., Rhee, D. S., Buckau, G.: Complexation of trivalent actinides ions (Am^{3+}, Cm^{3+}) with humic acids: the effect of ionic strength. Radiochim. Acta **72**, 179 (1996).
38. Zeh, P., Kim, J. I., Buckau, G. Aquatic colloids composed of humic substances, Binding models concerning natural organics in performance assessment. OECD NEA Proceedings, (1995).
39. Kim, J. I., Sekine, T.: Complexation of neptunium(V) with humic acid. Radiochim. Acta **55**, 187 (1991).
40. Marquardt, C., Herrman, G., Trautmann, N.: Complexation of neptunium(V) with humic acids at very low concentrations. Radiochim. Acta **73**, 119 (1996).
41. Seibert, A., Mansel, A., Marquardt, C. M., Keller, H., Kratz, J. V., Trautmann, N.: Complexation behaviour of neptunium with humic acid. Radiochim. Acta **89**, 505 (2001).
42. Buckau, G., Kim, J. I., Klenze, R., Rhee, D. S., Wimmer, H.: A comparative spectroscopic study of the fulvate complexation of trivalent transuranium ions. Radiochim. Acta **57**, 105 (1992).
43. Kim, J. I., Rhee, D. S., Wimmer, H., Buckau, G., Klenze, R.: Complexation of trivalent actinide ions (Am^{3+}, Cm^{3+}) with humic acid: a comparison of different experiment methods. Radiochim. Acta **62**, 35 (1993).
44. Kim, J. I., Rhee, D. S., Buckau, G., Morgenstern, A.: Americium(III)-humate interaction in natural groundwater: Influence of purification on complexation properties. Radiochim. Acta **79**, 173 (1997).
45. Shin, H. S., Lee, B. H., Choi, J. G., Moon, H.: Complexation of soil humic-acid with trivalent curium and europium ions: a comparative study. Radiochim. Acta **69**, 185 (1995).
46. Pirlet, V., Delécaut, G. Complexation of Np(IV) with humic acids at hydrolysis pH range: determination of complexation constants. 9th International Conference on Chemistry and Migration Behavior of Actinides and Fission Products in the Geosphere, Migration '03. September 21-26, 2003, Gyeongju, Korea (2003).
47. Miekeley, N., Vale, M. G. R., Tavares, T. M., Lei, W.: Some aspects of the influence of surface and ground water chemistry on the mobility of thorium in the "Morro do Ferro" - environment. Mat. Res. Soc. Symp. Proc. **11**, 725 (1982).
48. Miekeley, N., Dotto, R. M., Kuchler, I. L., Insalta, P.: The importance of organic compounds on the mobilization and bioassimilation of thorium in the Morro do Ferro environment. Mat. Res. Soc. Symp. Proc. **44**, 591 (1985).

49. Niven, S. E. H., Moore, R. M.: Effect of natural colloidal matter on the equilibrium adsorption of thorium in seawater. In: *Radionuclides: A tool for Oceanography* (Guary, J. C. ed.) Elsevier, (1988) p. 111.
50. Nordén, M., Albinsson, Y., Ephraim, J. H., Allard, B.: A comparative study of europium, thorium and uranium binding to an aquatic fulvic acid. Material Research Society Symposia Proceeding **294**, 759 (1993).
51. Dai, M. H., Benitez-Nelson, C. R.: Colloidal organic carbon and ^{234}Th in the Gulf of Maine. Mar. Chem. **74**, 181 (2001).
52. Nash, K. L., Choppin, G. R.: Interaction of humic and fulvic acids with Th(IV). J. Inorg. Nucl. Chem. **42**, 1045 (1980).
53. Reiller, P., Moulin, V., Casanova, F., Dautel, C.: On the study of Th(IV)-humic acid interactions by competition sorption studies with silica and determination of global interaction constants. Radiochim. Acta **91**, 513 (2003).
54. Panak, P., Klenze, R., Kim, J. I.: A study of ternary complexes of Cm(III) with humic acid and hydroxyde or carbonate in neutral pH range by time resolved laser fluorescence spectroscopy. Radiochim. Acta **74**, 141 (1996).
55. Morgenstern, M., Klenze, R., Kim, J. I.: The formation of mixed-hydroxo complexes of Cm(III) and Am(III) with humic acid in the neutral pH range. Radiochim. Acta **88**, 7 (2000).
56. Zeh, P., Czerwinski, K. R., Kim, J. I.: Speciation of uranium in Gorleben groundwaters. Radiochim. Acta **76**, 37 (1997).
57. Baes, C. F., Mesmer, R. E.: *The hydrolysis of cations*. Wiley Interscience Publication, New-York (1976).
58. João, A., Bigot, S., Fromage, F.: Étude des carbonates complexes des éléments IVB I - Détermination de la constante de stabilité du pentacarbonatothorate (IV). Bull. Soc. Chim. France 42 (1987).
59. Grenthe, I., Lagerman, B.: Studies on metal carbonate equilibria. 23. Complex formation in the Th(IV)-H_2O-CO_2(g) system. Acta Chim. Scand. **45**, 231 (1991).
60. Östhols, E., Bruno, J., Grenthe, I.: On the influence on mineral dissolution: III. The solubility of microcrystalline ThO_2 in CO_2-H_2O media. Geochim. Cosmochim. Acta **58**, 613 (1994).
61. Ekberg, C., Albinsson, Y., Comarmond, M. J., Brown, P. L.: Studies on the complexation behavior of thorium(IV). 1. Hydrolysis equilibria. J. Solut. Chem. **29**, 63 (2000).
62. Moulin, C., Amekraz, B., Hubert, S., Moulin, V.: Study of thorium hydrolysis species by electrospray-ionization mass spectrometry. Anal. Chim. Acta **441**, 269 (2001).
63. Neck, V., Kim, J. I.: Solubility and hydrolysis of tetravalent actinides. Radiochim. Acta **89**, 1 (2001).
64. Portanova, R., diBernardo, P., Traverso, O., Mazzochin, A., Magon, L.: Thermodynamic properties of actinide complexes. 2. Thorium(IV)-acetate system. J. Inorg. Nucl. Chem. **37**, 2177 (1975).
65. Schubert, J.: J. Phys. Coll. Chem. **52**, 340 (1948).
66. Schubert, J., Richter, J. W.: J. Phys. Coll. Chem. **52**, 350 (1948).
67. Grenthe, I., Fuger, L., Konings, R. G. M., Lemire, R. J., Muller, A. B., Nguyen-Trung, C., Wanner, H.: *Chemical thermodynamics of uranium*. North Holland, Amsterdam (1992).
68. Silva, R. J., Bidoglio, G., Rand, M., Robouch, P., Wanner, H., Puigdomènech, I.: *Chemical thermodynamics of americium with an appendix on Chemical thermodynamics of uranium (Grenthe, I., Sandino, M.C.A., Puigdomenech, I., Rand, M.H.)*. North Holland, Amsterdam (1995).
69. Lemire, R. J., Fuger, J., Nitsche, H., Potter, P., Rand, M., Rydberg, J., Spahiu, K., Sullivan, J. C., Ullman, W. J., Vitorge, P., Wanner, H.: *Chemical thermodynamics of neptunium and plutonium*. North Holland, Amsterdam (2001).
70. Cantrell, K. J.: Actinide (III) carbonate complexation. Polyhedron **7**, 573 (1988).
71. Vitorge, P., Capdevila, H.: Thermodynamic data for modelling actinide speciation in environmental waters. Radiochim. Acta **91**, 623 (2003).
72. Marquardt, C., Kim, J. I.: Complexation of Np(V) with humic acid: Intercomparison of results from different laboratories. Radiochim. Acta **80**, 129 (1998).
73. Choppin, G. R., Rao, L. F.: Complexation of pentavalent and hexavalent actinides by fluoride. Radiochim. Acta **37**, 143 (1984).
74. Glaus, M. A., Hummel, W., Van Loon, L. R.: Trace metal-humate interactions. I. Experimental determination of conditional stability constants. Appl. Geochem. **15**, 953 (2000).
75. Hummel, W., Glaus, M. A., Van Loon, L. R.: Trace metal-humate interaction. II. The conservative roof model and its application. Appl. Geochem. **15**, 975 (2000).
76. Reiller, P., Moulin, C., Beaucaire, C., Lemordant, D.: Dual use of micellar enhanced ultrafiltration and time-resolved laser-induced spectrofluorometry for the study of uranyl exchange at the surface of alkylsulfate micelles. J. Colloid Interface Sci. **163**, 81 (1994).
77. Kim, J. I., Marquardt, C. M.: Chemical reaction of Np(V) with humic colloids in groundwater: Influence of purification on the complexation behaviour. Radiochim. Acta **87**, 105 (1999).
78. Czerwinski, K., Kim, J. I.: Complexation of transuranic ions by humic substances: application of laboratory results to the natural system. Mat. Res. Soc. Symp. Proc. **465**, 743 (1997).

79. Glaus, M. A., Baeyens, B., Lauber, M., Rabung, T., van Loon, L. R.: Water-extractable organic matter from opalinus clay: effect on sorption and speciation of Ni(II), Eu(III) and Th(IV). Paul Scherrer Institut, Report 01-14, Villigen (2001).

80. Rose, J., Vilge, A., Olivie-Lauquet, G., Masion, A., Fréchou, C., Bottero, J. Y.: Iron speciation in natural organic matter colloids. Colloid Surf. A-Physicochem. Eng. Asp. **136**, 11 (1998).

81. Vilgé-Ritter, A., Rose, J., Masion, A., Bottero, J. Y., Laine, J. M.: Chemistry and structure of aggregates formed with Fe-salts and natural organic matter. Colloid Surf. A-Physicochem. Eng. Asp. **147**, 297 (1999).

82. Masion, A., Vilge-Ritter, A., Rose, J., Stone, W. E. E., Teppen, B. J., Rybacki, D., Bottero, J. Y.: Coagulation-flocculation of natural organic matter with Al salts: Speciation and structure of the aggregates. Environ. Sci. Technol. **34**, 3242 (2000).

83. Wood, S. A., Tait, D. C., Vlassopoulos, D., Janecky, D. R.: Solubility and spectroscopic studies of the interaction of palladium with simple carboxylic acids and fulvic acid at low temperature. Geochim. Cosmochim. Acta **58**, 625 (1994).

84. Capdevila, H., Vitorge, P., Giffaut, E., Delmau, L.: Spectrophotometric study of the dissociation of the Pu(IV) carbonate limiting complex. Radiochim. Acta **74**, 93 (1996).

85. Bruno, J., Stumm, W., Wersin, P., Brandberg, F.: On the influence of carbonate in mineral dissolution: I. The thermodynamics and kinetics of hematite dissolution in bicarbonate solution at T = 25 °C. Geochim. Cosmochim. Acta **56**, 1139 (1992).

86. Hummel, W.: Comment on "On the influence of carbonate in mineral dissolution: 1. The thermodynamics and kinetics of hematite dissolution in bicarbonate solutions at T=25 degrees C" by J. Bruno, W. Stumm, P. Wersin, and F. Brandberg. Geochim. Cosmochim. Acta **64**, 2167 (2000).

87. Bruno, J., Duro, L.: Reply to W. Hummel's comment on and correction to "On the influence of carbonate in mineral dissolution: 1. The thermodynamics and kinetics of hematite dissolution in bicarbonate solutions at T=25 degrees C" by J. Bruno, W. Stumm, P. Wersin, and F. Brandberg. Geochim. Cosmochim. Acta **64**, 2173 (2000).

88. Guillaumont, R., Adloff, J. P.: Behaviour of environmental plutonium at very low concentration. Radiochim. Acta **58/59**, 53 (1992).

89. Vitorge, P.: Chimie des actinides. Techniques de l'ingénieur 630 (1999).

90. Tipping, E.: Modelling the binding of europium and the actinides by humic substances. Radiochim. Acta **62**, 141 (1993).

91. Santschi, P. H., Roberts, K. A., Guo, L. D.: Organic mature of colloidal actinides transported in surface water environments. Environ. Sci. Technol. **36**, 3711 (2002).

92. Aguer, J. P., Richard, C., Andreux, F.: Effect of light on humic acid substances: production of reactive species. Analusis **27**, 387 (1999).

93. Schild, D., Marquardt, C., Seibert, A. Analysis of Pu-Humate by XPS. 9th International Conference on Chemistry and Migration Behavior of Actinides and Fission Products in the Geosphere, Migration '03. September 21-26, 2003, Gyeongju, Korea (2003).

94. Artinger, R., Denecke, M. A., Kuczewski, B., Marquardt, C., Schild, D., Seibert, A., Fanghänel, T. Redox behaviour of Pu ions in a natural ground water rich in humic substances. 9th International Conference on Chemistry and Migration Behavior of Actinides and Fission Products in the Geosphere, Migration '03. September 21-26, 2003, Gyeongju, Korea (2003).

95. Zauzig, J., Stepniewski, W., Horn, R.: Oxygen concentration and redox potential gradient in unsaturated model soil aggregates. Soil Sci. Soc. Am. J. **57**, 908 (1993).

96. Matthiessen, A.: Evaluating the redox capacity and the redox potential of humic acids by redox titrations. In: *Humic substances in the global environment and implications on human health* (Senesi, N. and Miano, T. M. eds.). Elsevier, (1994) p. 187.

97. Struyk, Z., Sposito, G.: Redox properties of standard humic acids. Geoderma **102**, 329 (2001).

98. Laszak, I.: Étude des interactions entre colloïdes naturels et éléments radiotoxiques par spectrofluorimétrie laser à résolution temporelle. étude chimique et spectroscopique. Université Pierre et Marie Curie - Paris VI, Paris (1997).

99. Li, W. C., Victor, D. M., Chakrabarti, C. L.: Effect of pH and uranium concentration on interaction of uranium(VI) and uranium(IV) with organic ligands in aqueous solutions. Anal. Chem. **52**, 523 (1980).

Annex 12

Characterisation of fulvic acids by
Electrospray with Quadrupole / Time-of-Flight Mass Spectrometry

Gabriel PLANCQUE

Commissariat à l'Energie Atomique, Centre de Saclay, Direction de l'Energie Nucléaire / DPC / SECR /Laboratoire de Spéciation des Radionucléides et des Molécules, Bât. 391, 91191 Gif-sur-Yvette Cedex, France.

Characterisation of fulvic acids by Electrospray with Quadrupole / Time-of-Flight Mass Spectrometry

Gabriel PLANCQUE

Commissariat à l'Energie Atomique, Centre de Saclay, Direction de l'Energie Nucléaire / DPC / SECR / Laboratoire de Spéciation des Radionucléides et des Molécules, Bât. 391, 91191 Gif-sur-Yvette Cedex, France.
plancque@carnac.cea.fr

Abstract

Characterisation of fulvic and humic acids (FA and HA) – synthetic model substances M1 and M42 from FZR, FA and HA Gohy 573 from the Gorleben groundwaters from FZK and purified Aldrich HA from CTU – has been performed using a quadrupole time-of-flight (Q-TOF) mass spectrometer equipped with an electrospray ionisation interface. The same conclusions as for Mol fulvic acids, previously studied in the laboratory, can be drawn: molecular masses centred around 350 Da, sinusoidal spectral distributions, even and odd integral masses distributions and presence of dimmers (and possible trimmers) in negative-mode experiments have been observed for all humic substances. Tandem mass spectrometry (MS/MS) has also been used and experiments showed losses of 18 Da (H_2O), 28 Da (CO) and 44 Da (CO_2) as for Mol FA. No obvious differences, in terms of molecular structure, are observed compared to Mol FA.

1 Introduction

Humic substances (HS) have, for a long time, thought to be macromolecules with molecular masses around 10000-20000 Da for humic acids (HA) and 2000-3000 Da for fulvic acids (FA). However, recent studies have shown that humic substances have a supra-molecular nature in which relatively small heterogeneous molecules (masses around 500 Da) are self-assembled by hydrogen bonds and also by weaker forces such as Van der Waals, π-π, and CH-π interactions into large conformations of only apparently high molecular size [Conte and Piccolo, 1999; Simpson et al., 2001; Plancque et al., 2001].

HS have the ability to form rather stable complexes with cations. In order to better understand the complexation properties of HS, it seems necessary to obtain insights into the molecular structure of these molecules. For this purpose, Electrospray Ionisation Mass Spectrometry has been chosen to characterise several FA and HA of interest for HUPA project. These acids were obtained from HUPA partners: synthetic HA model substances from FZR, Rossendorf (M1 and M42), Aldrich HA purified by CTU, Prague and natural FA and HA from the Gorleben groundwaters from FZK, Karlsruhe (FA and HA Gohy 573). Their characterisation can then be compared with characteristics of HA and FA already studied at CEA.

Electrospray Ionisation Mass Spectrometry (ESI-MS) has been developed in the eighties for organic material analysis and is mainly characterised by its soft ionisation process (non alteration of the studied molecules) and by the formation of multi-charged ions (allowing the study of molecules of high molecular mass) [Yamashita and Fenn, 1984; Cole, 1997; Gaskell, 1997].

This technique has been, for several years, more and more used to study humic substances [Brown and Rice, 2000; Plancque et al., 2001; Leenheer et al., 2001; McIntyre et al., 2002; Stenson et al., 2003]. For example, studies on FA have been performed by high resolution electrospray ionisation mass spectrometry (ESI-Q-TOF-MS) which demonstrate directly the supra-molecular nature of FA and which allow to obtain the molecular structure by tandem mass spectrometry [Plancque et al., 2001]. Interaction between humic substances and cations can also be studied: for example, a tandem mass spectrometry study has shown the covalent nature of the interactions between iodine and aromatic rings presents in FA [Moulin et al., 2001].

2 Experimental

Samples

Solutions of the different fulvic and humic acids were prepared in water or in H_2O/MeOH (1/1) at different concentrations (cf. Table 1). For positive mode experiments, a few amount of formic acid is added to the solution to favour cationisations. For humic acids, dissolution was difficult as waited and so, concentrations are overestimated which is not disturbing for qualitative studies. Millipore water was used throughout the procedure. Formic acid used in the sample preparation was used without further purification.

Electrospray Ionisation Mass spectrometry

Mass spectrometry experiments were conducted using a Q-TOF hybrid mass spectrometer (Q-TOF II, Micromass, Manchester, U.K.) equipped with an electrospray source (Z-spray) operated in both positive and negative ion modes. The samples were introduced into the source with a syringe pump (Harvard Apparatus Cambridge, MA) with a flow rate set to 10 µl/min. [Glu]-fibrinopeptide B was used for mass calibration checks, and optimal parameter tuning was performed for each compound. Both MS and MS/MS spectra were recorded.

Conditions optimised for sensitivity were: ESI capillary voltage ± 3000V. Nitrogen was employed as both the drying and nebulisation gas. For full scan MS-analysis, Q1 was operated in RF-only mode with all ions transmitted into the pusher region of the TOF analyser. Spectra were recorded over the range *m/z* 50 to 2000 with 6s integration time. All TOF measurements were performed at high-resolution settings (4000 FWHM at *m/z* 500), and data were always recorded in continuum mode. Cone voltages were optimised in both modes and are given in Table 1.

In MS/MS mode, the transmission window of the quadrupole was set up to about 3 Th (FWMH) and was used to select precursor ions for fragmentation in the hexapole collision cell (using argon as collision gas). Product ion spectra were acquired with the TOF analyser. Source parameters were the same as above, and the collision energies were optimised for maximised product ion yield. Data were integrated for a total time of about 3-5 minutes for each precursor.

3.1 ESI-Q-TOF mass spectra of fulvic and humic acids

The MS spectra of FA from Gorleben (FA Gohy 573), in both negative and positive ion mode, are shown in Figures 1 and 2, respectively. Both spectra are similar to those obtained for Mol fulvic acids [Plancque et al., 2001] and similar comments can be made.

The direct analysis of FA from Gorleben in negative ion mode appears to yield distributions of abundant series of peaks with 0.5 Th inter-peak spacing. The FA solution is a complex mixture of several hundred molecular structures as seen in Figure 1, where several hundred peaks are present in the range of *m/z* 100-1000. The distribution has a sinusoidal shape with a periodicity of 14 Da corresponding to the mass of a CH_2 group and is centred around 340 Da, which supports the hypothesis that fulvic acids are supra-molecules (for comparison, mass spectrum for Mol FA was centred around 350 Da (see Figure 3)). Two main families of peaks, representing singly-charged ions, can be observed in the negative ion spectra. One series is constituted of odd integral masses and the other less intense series is constituted of even integral masses. Doubly-charged ions, which are indicative of non-covalent dimmers, can also be observed at every half-mass in the mass spectrum (see zoom in Figure 1).

The spectrum in Figure 2 shows that ESI (+) also produces ions which are useful in a qualitative sense, as in negative ion mode. The distribution shape is sinusoidal with a periodicity of 14 Da and a peak every 1 Th and the *m/z* values are centred around 450 Da. Compared to the negative spectrum, the positive-ion spectrum seems to be shifted to higher

m/z values, probably due to metal ion adduction (for example, sodium or potassium which are ubiquitous in such natural materials).

The MS spectrum, in negative ion mode, of HA from Gorleben (HA Gohy 573) is shown in Figure 4. Same comments can be made as for FA: sinusoidal distribution centred around 380 Da, two families of peaks, representing singly-charged ions (odd integral and even integral masses) and presence of doubly and even triply-charged ions (dimmers and trimmers) which can be observed in the mass spectrum (see zoom in Figure 4).

The MS spectra, in negative ion mode, of synthetic HA model substances (M1 and M42) are shown in Figures 5 and 6, respectively. Spectra are less defined than for FA from Gorleben but same comments can be made: peak distributions are centred around 300 Da and 450 Da for M1 and M42 respectively and there is one peak every 0.5 Th. The main difference is that there is no differences between the odd integral masses distribution and the even integral masses one.

The MS spectrum, in positive ion mode, of purified Aldrich HA is shown in Figure 7. The spectrum seems more complicated than those for the other substances, each peak seems to be doubled. Nevertheless, the two peak families are present and the distribution is centred around 400 Da.

3.2 Tandem mass spectrometry studies of fulvic acids from Gorleben

The mass spectrometric methodology currently used for structural analysis is tandem mass spectrometry (MS/MS). Spectra presented above (Figures 1 and 2) show that FA produce complex ion-distributions in ESI which make interpretation difficult. This implies to use a high-resolution mass spectrometer, such as the hybrid quadrupole-time of flight (Q-TOF) tandem mass spectrometer which offers an enhanced full-scan sensitivity and an improved resolution.

The Q-TOF mass spectrometer produces negative-ion mass spectra with sufficient resolution to permit daughter ion-analysis. In the mass spectrum (Figure 1), several peaks were chosen in the low range (peaks at *m/z* 191, 193, 205, 207, 221), in the medium range 300 – 400 (peaks at *m/z* 325, 339, 340, 341, 353, 355, 367, 369) and in the high range (peaks at *m/z* 409 and 617). The high peak density of the mass spectrum implies that the MS-MS spectra record mainly the fragment ions derived from the dominant odd mass-number ions since they always correspond to the most intense peak within the 3 Th transmission window of the quadrupole. Peaks adjacent to the selected parent ion, that may be inside the window, produce only limited interferences and no anomalous mass values in the MS-MS spectrum. All MS-MS experiments demonstrated losses of 18 Da (H_2O), of 28 Da (CO) and of 44 Da (CO_2), which indicate the presence of carboxylic functions and confirm that the precursor-ion peaks

correspond to singly-charged ions (for doubly-charged ions, losses of 22 Th should be observed for expulsion of CO_2).
As for Mol FA, at the end of the fragmentation (MS/MS on the peak at 193 Da), a fragment ion at *m/z* 105 is finally obtained, corresponding to the benzaldehyde anion ϕ-CO^-. It seems also that the molecular structure of the molecules present in FA from Gorleben do not differ significantly from molecules present in FA from Mol [Plancque et al., 2001]. A representative molecular structure of the molecules, which are likely to be self-assembled in the FA samples, is given in Figure 8. It is obvious that the proposed structure is only one possible isomer since the mass spectrometry does not give the relative positions of the substituents on the aromatic ring.

Conclusion

The characterisation of various fulvic and humic acids (FA and HA) used in the HUPA project has been performed using a quadrupole time-of-flight (Q-TOF) mass spectrometer equipped with an electrospray ionisation interface. AS for Mol FA previously studied at CEA, the same tendencies can be drawn: molecular masses centred around 350 Da, sinusoidal spectral distributions, even and odd integral masses distributions and presence of dimmers (and possible trimmers) in negative-mode experiments have been observed for all humic substances. Tandem mass spectrometry (MS/MS) has also been used, no obvious differences, in terms of molecular structure, are observed compared to other humic substances (Mol FA).

Acknowledgement

The author would like to thank Badia Amekraz for her help in the experimental work and Valérie Moulin and Christophe Moulin for their critical readings.

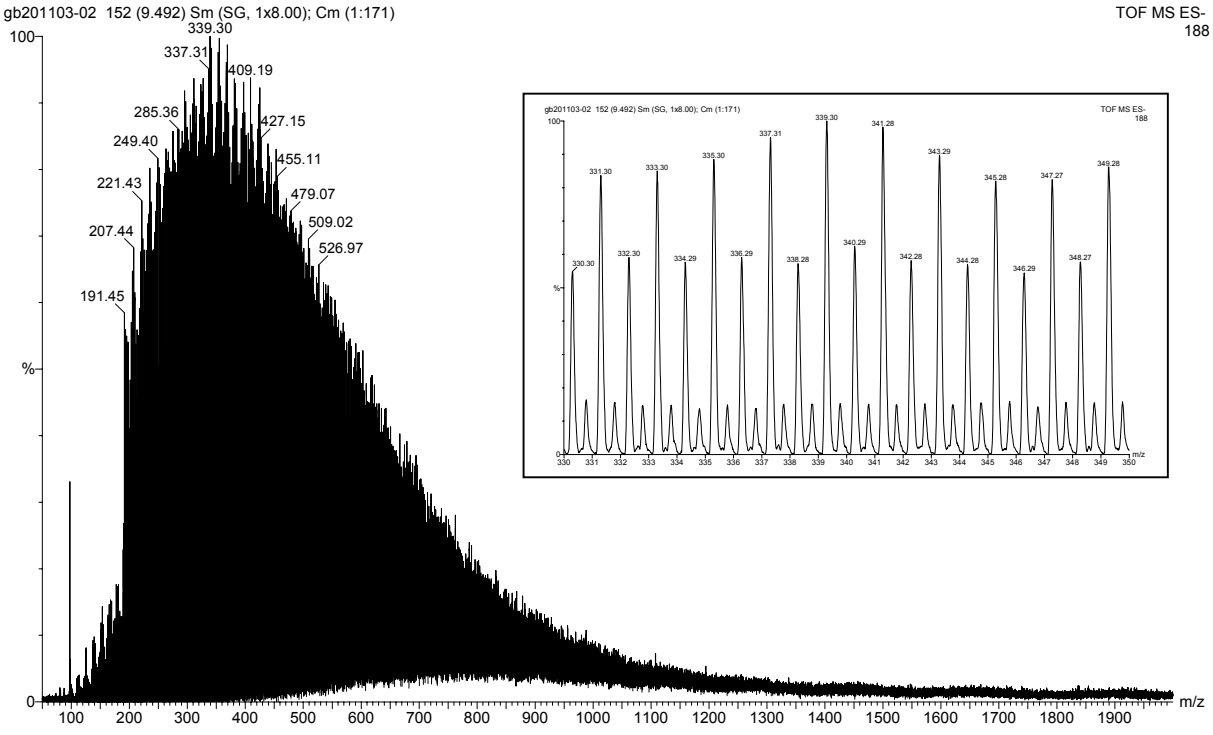

Fig. 1: Mass spectra in negative mode of fulvic acids Gohy 573 from Gorleben. Insert: zoom, *m/z* 330-350.

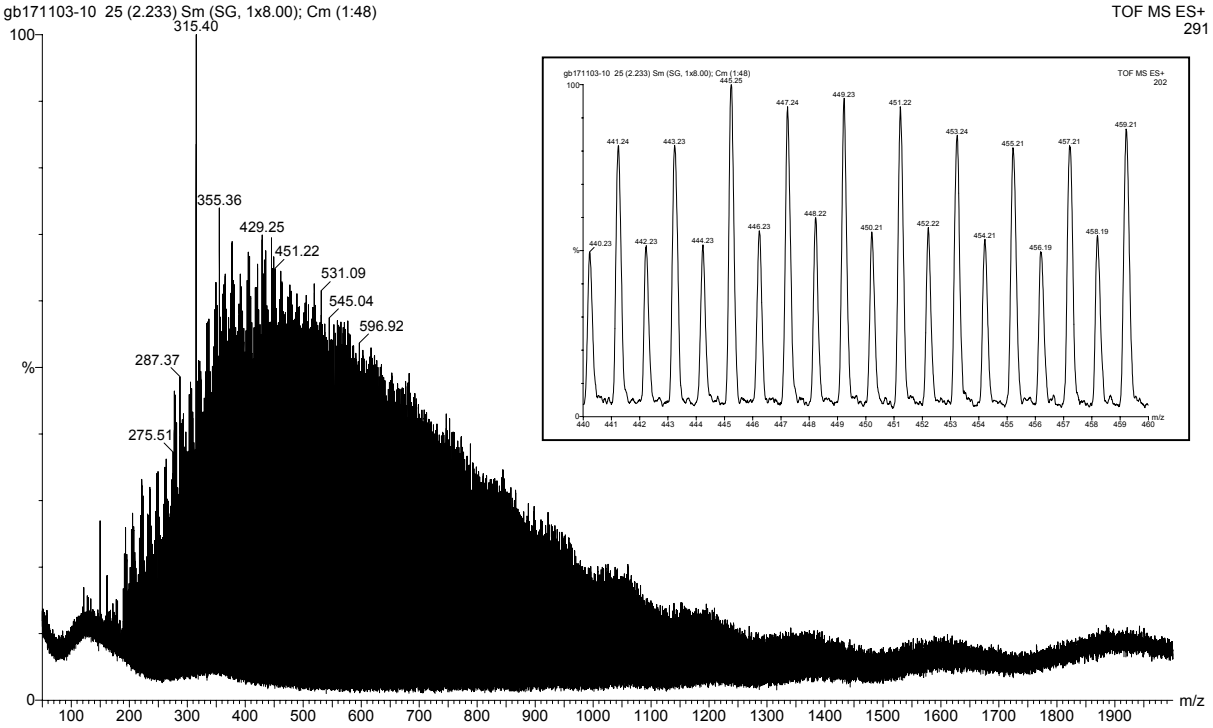

Fig. 2: Mass spectra in positive mode of fulvic acids Gohy 573 from Gorleben. Insert: zoom, *m/z* 440-460.

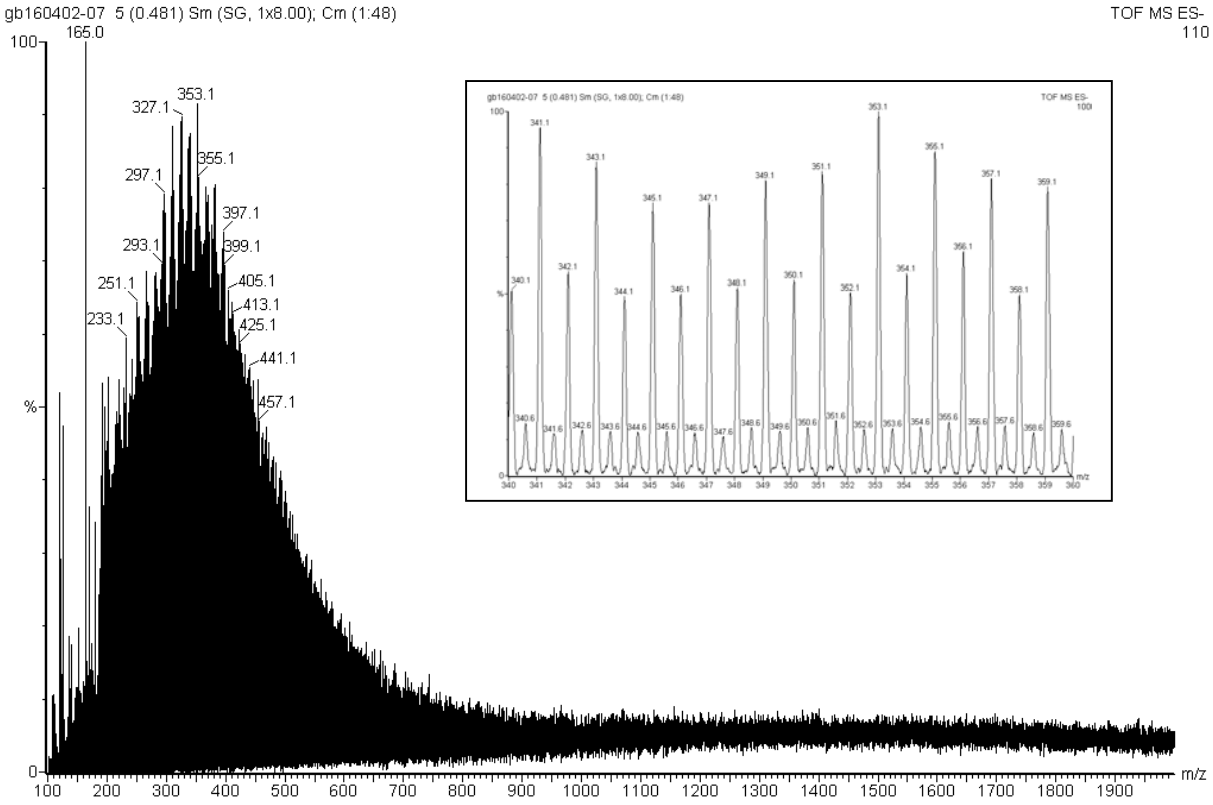

Fig. 3: Mass spectra in negative mode of fulvic acids from Mol. Insert: zoom, *m/z* 340-360.

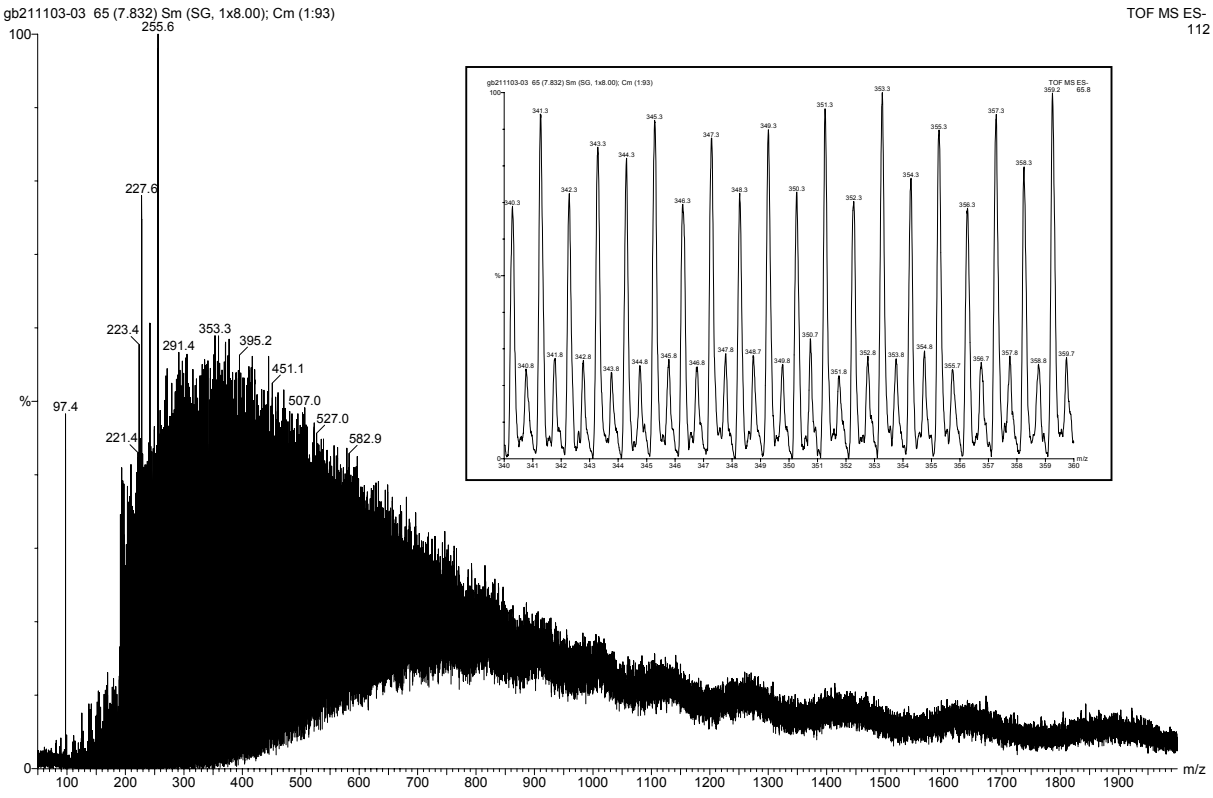

Fig. 4: Mass spectra in negative mode of humic acids Gohy 573 from Gorleben. Insert: zoom, *m/z* 340-360.

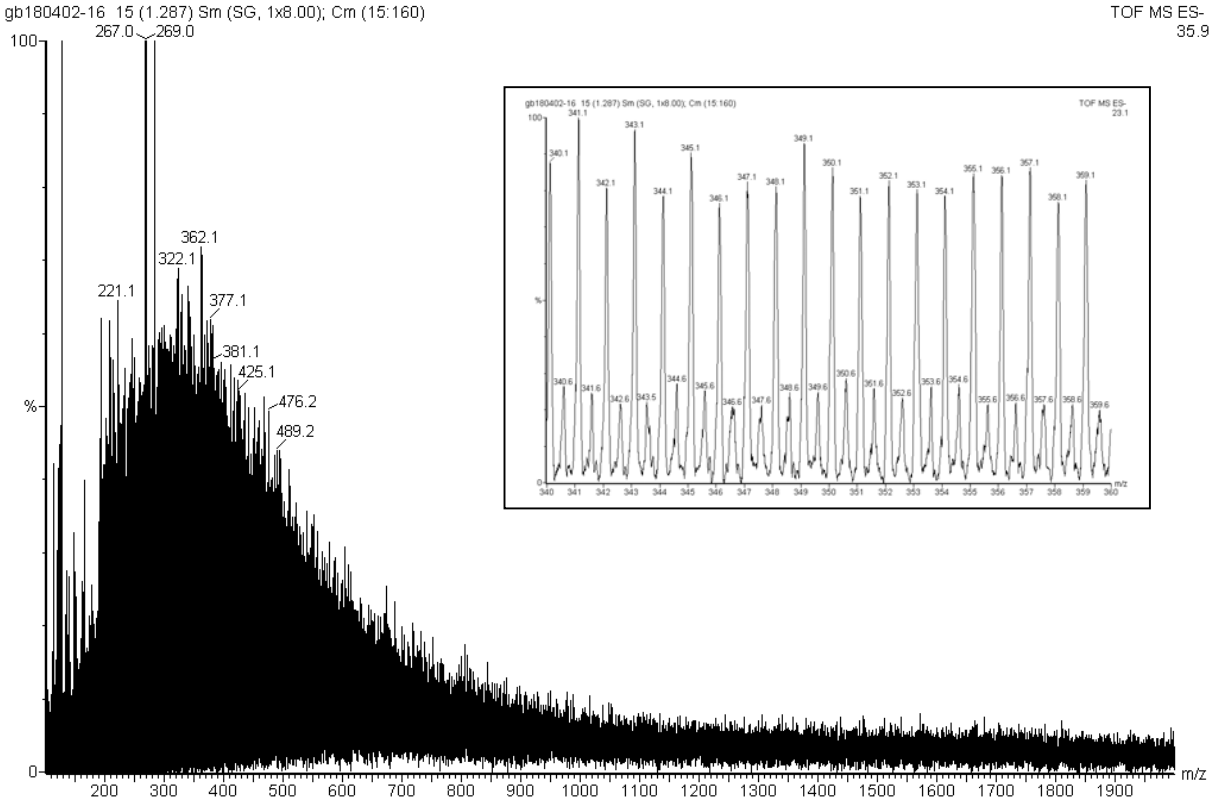

Fig. 5: Mass spectra in negative mode of humic acids M1 (FZR). Insert: zoom, *m/z* 340-360.

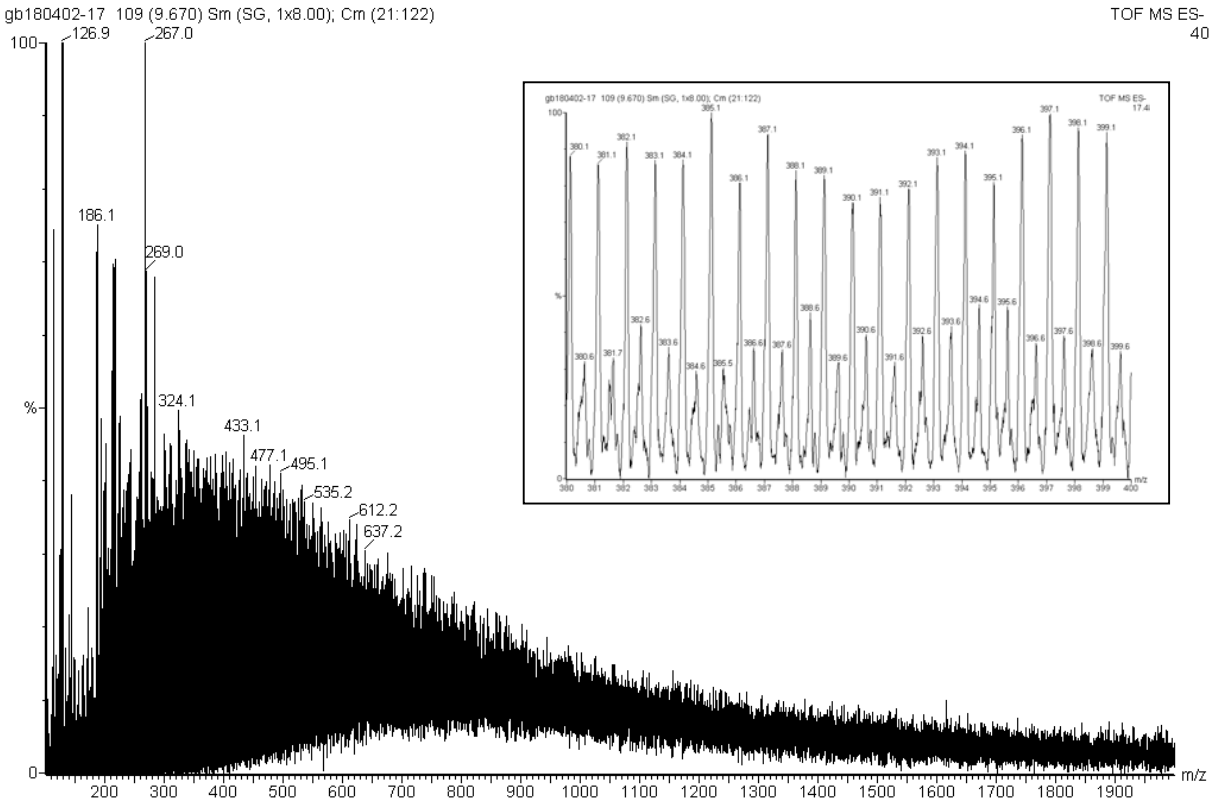

Fig. 6: Mass spectra in negative mode of humic acids M42 (FZR). Insert: zoom, *m/z* 380-400.

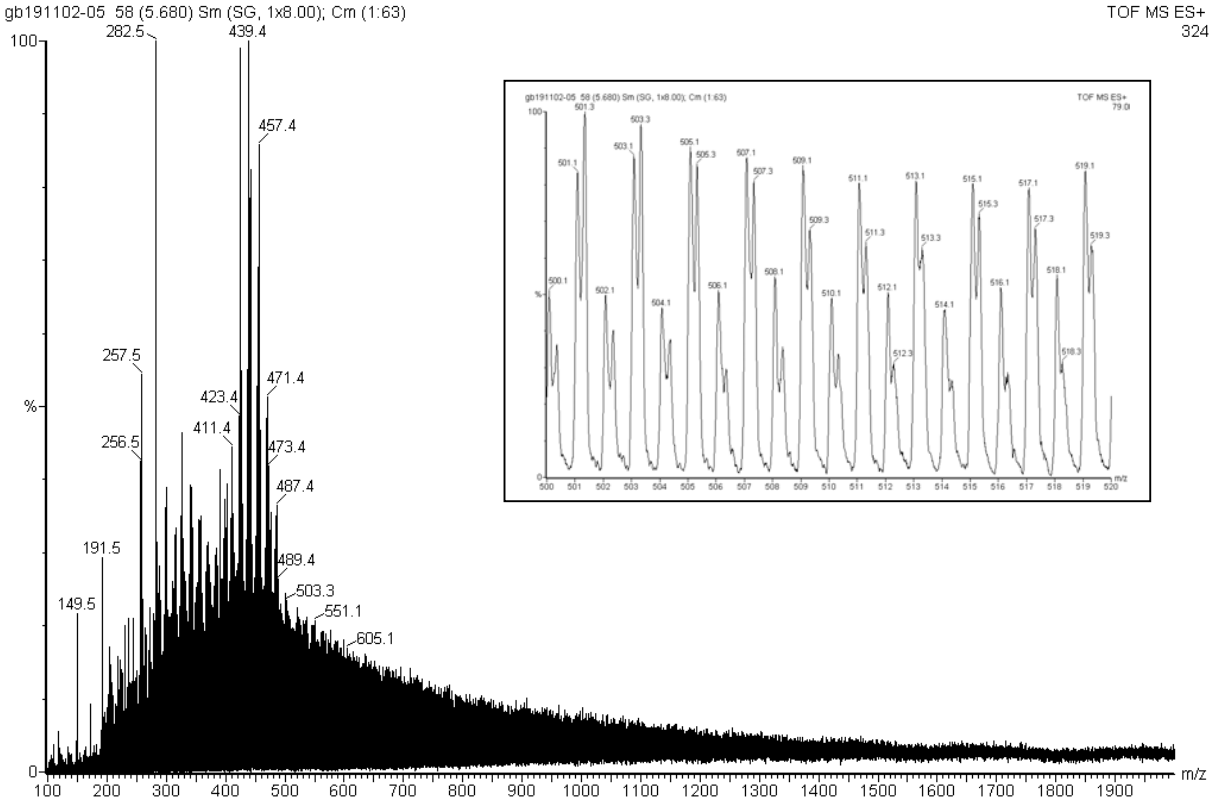

Fig. 7: Mass spectra in positive mode of humic acids from Aldrich (CTU). Insert: zoom, *m/z* 500-520.

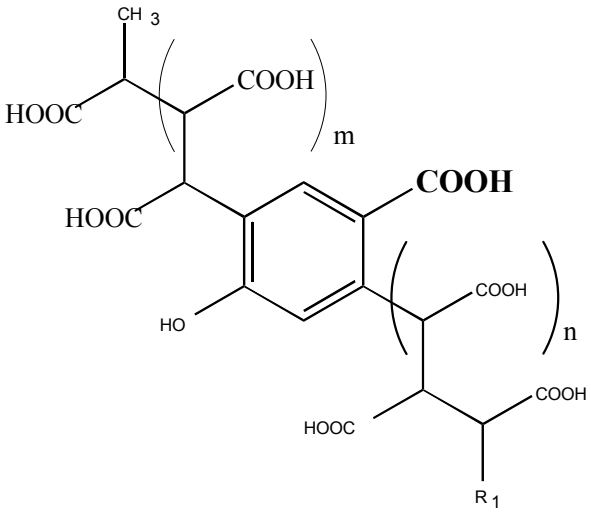

odd $[M-H]^-$ family, $R_1 = CH_3$

even $[M-H]^-$ family, $R_1 = NH_2$

Fig. 8: Representative molecular structure proposed for Mol fulvic acid.

Table 1: Experimental conditions for mass spectra for the different compounds

Humic substances	ESI (-)		ESI (+)	
	Solution concentrations	Cone voltage	Solution concentrations	Cone voltage
FA Mol	150 ppm, H_2O	55 V		
HA M1	120 ppm *, H_2O	55 V	-	-
HA M42	104 ppm *, H_2O	55 V	-	-
HA Aldrich	-	-	166 ppm *, H_2O/MeOH, 0.2 % HCOOH	60 V
FA Gohy 573	546 ppm, H_2O	50 V	182 ppm, H_2O, 1% HCOOH	55 V
HA Gohy 573	552 ppm *, H_2O	50 V	-	-

* overestimated concentration due to problems of dissolution.

References

Brown T.L., Rice J.A (2000) “Effect of experimental parameters on the ESI FT-ICR mass spectrum of fulvic acid”, *Anal. Chem.* **72**, 384.

Cole R.B. (1997) “Electrospray Ionisation Mass Spectrometry – Fundamentals, instrumentation and applications”, John Wiley & sons, New-York, 577 pages.

Conte P., Piccolo A. (1999) “Conformational arrangement of dissolved humic substances. Influence of solution composition on association of humic molecules”, Environ. Sci. Technol. **33**, 1682.

Gaskell S.J. (1997) “Electrospray: principles and practice”, J. Mass Spectrom. **32**, 677.

Leenheer J.A, Rostad C.E, Gates P.M., Furlong E.T., Ferrer I. (2001) “Molecular resolution and fragmentation of fulvic acid by electrospray ionisation/multistage tandem mass spectrometry”, *Anal. Chem.* **73**, 1461.

McIntyre C., McRae C., Jardine D., Batts B.D. (2002) “Identification of compounds classes in soil and peat fulvic acids as observed by electrospray ionisation tandem mass spectrometry”, *Rapid Commun. Mass Spectrom.* **16**, 1604.

Moulin V., Reiller P., Amekraz B., Moulin C. (2001) “Direct characterisation of covalently bound iodine to fulvic acids by electrospray mass spectrometry”, *Rapid Commun. Mass Spectrom.* **15**, 2488.

Plancque G., Amekraz B., Moulin V., Toulhoat P., Moulin C. (2001) “Molecular structure of fulvic acids by electrospray with quadrupole time-of-flight mass spectrometry”, *Rapid Commun. Mass Spectrom.* **15**, 827.

Simpson A.J., Kingery W.L., Spraul M., Humpfer E., Dvortsak P., KerssebaumR. (2001) “Separation of structural components in soil organic matter by diffusion ordered spectroscopy”, Environ. Sci. Technol. **35**, 4421.

Stenson A.C., Marshall A.G., Cooper W.T. (2003) “Exact masses and chemical formulas of individual Suwannee river fulvic acids from ultrahigh resolution electrospray ionisation Fourier transform ion cyclotron resonance mass spectra”, *Anal. Chem.* **75**, 1275.

Yamashita M., Fenn J.B. (1984) “Electrospray ion source. Another variation on the free-jet theme”, *J. Phys. Chem.* **88**, 4451.

Annex 13

Self-Assembled Monolayers of Aminosilanes Chemically Bonded onto Silicon Wafers for Immobilization of Purified Humic Acids

Cécile BARBOT, Jacques PIERI, Jean-Pierre DURAND, Françoise GOUDARD [1]

Markus PLASCHKE, Gunnar BUCKAU [2]

Wilfried SZYMCZAK [3]

Othman BOULOUSSA [4]

[1] GERMETRAD Laboratory, Université de Nantes, 2, Rue de la Houssinière, BP 92208, 44322 Nantes Cedex 03

[2] Forschungszentrum Karlsruhe, Institut für Nukleare Entsorgung, PO Box 3640, 76021 Karlsruhe, Germany

[3] GSF-National Research Center for Environment and Health, Institute of Radiation Protection, 85764 Neuherberg, Germany

[4] Curie institute, 26 rue d'Ulm, 75248 Paris Cedex 05

Self-Assembled Monolayers of Aminosilanes Chemically Bonded onto Silicon Wafers for Immobilization of Purified Humic Acids

Cécile BARBOT, Jacques PIERI, Jean-Pierre DURAND, Françoise GOUDARD
GERMETRAD Laboratory, Université de Nantes, 2, Rue de la Houssinière, BP 92208, 44322 Nantes Cedex 03

Markus PLASCHKE, Gunnar BUCKAU
Forschungszentrum Karlsruhe, Institut für Nukleare Entsorgung, PO Box 3640, 76021 Karlsruhe, Germany

Wilfried SZYMCZAK
GSF-National Research Center for Environment and Health, Institute of Radiation Protection,
85764 Neuherberg, Germany

Othman BOULOUSSA
Curie institute 26 rue d'Ulm, 75248 Paris Cedex 05

Abstract

Self-assembled monolayers of functionalized Br $(CH_2)_{11}SiCl_3$ have been prepared on oxide silicon substrates. By *in situ* modification of these monolayers the bromo end groups were transformed to amino end groups. These substrates were used to immobilize humic acids via a diazotization procedure. Characterization of these surfaces was done by different methods: ATR-FTIR, ellipsometry, AFM, TOF-SIMS and quantification of amino groups by UV/Vis modified for surface application. These different methods confirmed the immobilization of humic acids on the substrates forming a relatively homogeneous layer, necessary for further application to determination of radionuclide complexation constants with immobilized humic acid.

Introduction

In this paper the covalent attachment of humic acids on silicon wafers is reported. Humic acids are ubiquitous organic compounds present in terrestrial and aquatic systems. They interact with organic pollutants, metals and radionuclides via their numerous functional groups. In the aquatic environment they are encountered in the form of colloids, increasing the solubility and mobility of pollutants. Associated to mineral surfaces they contribute to accumulation and retention of pollutants. In order to study the organic coated mineral surfaces, covalent attachment/binding is preferred.

Humic acids have been grafted on porous silica (Barbot 2001, Barbot et al. 2002, Szabó et al. 1992) and interaction constants evaluated by the charge neutralization model (Czerwinski et al. 2000). With the porous silica system the verification/quantification of surface organic coating is difficult and selective, surface specific methods are not easy to apply. The present work shows a route for surface attachment of humic acid on silica wafer in order to provide well characterized material for studies:

- to understand the role of humic acid coated natural mineral surfaces in the retention of pollutants,
- to evaluate complexation constants between radionuclides and humic acid surface coated minerals, especially tetravalent ions where solution techniques are difficult to apply, and
- to characterize humic acid complexes by application of selective, sensitive and surface specific methods.

The aim of the present paper is to generate organic coating of silica wafer surface with chemical and physically robustness, homogeneity and full surface coating. The first overall step is attachment of a spacer by binding a functional silane in the form of a self-assembled monolayer. This self-assemble monolayer needs terminal group compatible with the subsequent immobilization of humic acids. The second overall step is humic acids "grafting" via a diazotization method. Each of the many individual steps has been accompanied by characterization by different methods. This is necessary in order to verify the assumed processes of individual steps and in order to verify the overall outcome.

Organosilanes are extensively used as coupling agents acting at the interface between an inorganic hydroxylated surface and an organic substrate. General formula of organosilanes is $RSi(OR'_3)$ (Mittal, 1992), with R an organofunctional group (vinyl, amino, epoxy, mercapto) and R' an hydrolyzable group (alkoxy, acetoxy, chloro function…).

Many authors have undertaken chemical immobilization of aminosilanes. Moon et al. (1996, 1997) immobilized different aminosilanes with short chains on fused silica plates characterizing the uniformity of the layer formed by ellipsometry. Snelling and Mottola (1987) attached also reactive amino groups on silica surfaces. These authors developed a quantification method of the amount grafted via an imine formation by the way of a chromophore as 4-

nitrobenzaldehyde or p-dimethylaminocinnamaldehyde, subsequent hydrolysis and UV-visible measurements. Haller (1978) immobilized aminopropylsilyl groups and studied changes in ellipsometric results that occurred upon reversible adsorption of dodecyl sulfate ions. Meanwhile, these authors used reactions modifying amino groups in various functionalities. For immobilization of humic acids, we have also used amino functionality, appropriate for binding humic acids by diazotization procedure.

Different coupling reactions are used depending on the aim. In general, short chain organosilanes result in multilayers formation whereas long-chain organosilanes may generate self-assembled monolayers (SAMs) with robust chemical and physical properties (Barbot et al. 2003, Kurth and Bein 1993, Navarre et al. 2001). The reason for the latter is that long-chain silanes attach alongside to each other into ordered films through Van der Waals interaction. These self-assembly monolayers are also physically and chemically robust due to the covalent bonds that anchor the silane at the surface (Balachander and Sukenik 1990, Bierbaum et al. 1995a,b, Brzoska et al. 1994, Heise et al. 1997). Such a SAM approach is chosen for the present study.

In this study, we have chosen to make a SAM by siloxane-anchored films with bromo functionality, successively modified into an alcohol, an amino and diazonium functionality. The terminal group need not compete with the surface active headgroups for adsorption to the surface or react with it but must be sterically small enough to allow a close-packed, well-ordered SAM. Thus, even if amino long alkyl-chain silanes are stable, once immobilized, amino-terminated long-chain alkyl silanes are disordered due to chemical interactions of the amino groups with the substrate. For that reason, amino and trichlorosilyl groups are not compatible. Acid-base reactions between surface silanol and silane amino groups take place because the surface silanol groups are acidic enough to protonate the amine group. Repulsive dipole-dipole interactions between the amino groups due to non-negligible moments brought by amino functionalities, over 1D, are also possible as noted by Bierbaum et al. (1995a,b). Consequently, alcohols, carboxylic acids, amines, thiols, phosphines, enamines, enols, ethers etc., must either be protected in non-nucleophilic form or introduced subsequent to molecular assembly (Fryxwell et al. 1996). For this purpose, we have used the method of Balachander and Sukenik (1990). Amino-terminated monolayer has been obtained by deposition of bromo-terminated alkyltrichlorosilane and subsequent in situ modification of the substrate (Heise et al. 1997; Fryxwell et al. 1996) into amino groups. At each step of the grafting, characterizations have been done by ATR-FTIR, UV-visible measurements, AFM and TOF-SIMS.

Experimental section

<Materials>

4-Nitrobenzoyl chloride, triethylamine, chloroform, ethylene glycol dimethyl ether, anhydrous hexane were purchased from Aldrich chemical Co. $SnCl_2$, 2-propanol, absolute ethanol were from Merck and $HClO_4$ from Prolabo. Humic acids on the sodium form were purchased from Aldrich (Aldrich Co., n°1201816, Fp >300°F). 1-bromo-11-(trichlorosilyl)undecane was

synthesized at the Curie Institute. The water used throughout the experiment was purified with a milli-Q system from Millipore Co.

Humic wafer preparation was conducted following scheme 1 (see Annex).

<*Humic acid purification*>

Humic acid in the sodium salt form was purified by the method of Kim et al. (1997), described by Barbot et al. (2002). In brief, humic acid was dissolved in 0.1 M NaOH together with NaF in the ratio 1/5 (w/w). After 10 min incubation, pH was decreased to 7 with 6 M HCl, to prevent autooxidation of the humic acid. The solution was then left overnight, followed by flocculation of humic acid by acidification to pH 1 with 6 M HCl. The supernatant was removed by centrifugation at 10 000g for 30 min. The humic acid flocculate was then redissolved in 0.1 M NaOH and acid-flocculated in three cycles. The humic acid flocculate was then washed several times with 0.1 M HCl and finally freeze-dried.

<*Surfactant synthesis*>

1-bromo-11-(trichlorosilyl)undecane was synthesized from undecyl-10-enyl bromide and trichlorosilane. Undecyl-10-enyl bromide (10 mmol) (Balachander and Sukenik, 1990) was placed in heavy walled vessel containing about 2 mg of H_2PtCl_6 (hydrogen hexachloroplatinate) hexahydrate dissolved in 200 μL of isopropanol. A three molar excess of trichlorosilane was added with stirring. The flask was sealed and heated for 6 hours at 60°C. After removal of excess trichlorosilane, the residue was isolated by Kugelrohr distillation and identified by ^{1}H NMR.

<*Substrate preparation*>

Silicon wafers were used in their oxide layer form. They were cleaned by the following method. They were first degreased by an acetone/methanol (50/50 (v/v)) mixture, followed by treatment with methanol. Each treatment was repeated four times in ultrasonic bath. Substrates were finally placed in a freshly prepared “piranha” solution (70/30 (v/v), concentrated sulfuric acid, 30% hydrogen peroxide) for 1h at 80-100°C. The procedure was repeated until the surface was perfectly hydrophilic. Subsequently substrates were rinsed with large amounts of distilled water, dried under nitrogen stream and used immediately.

<*Silanization*>

Monolayers were prepared by immersing dry substrates under nitrogen atmosphere into a cold hexane solution containing 1 % of the freshly distilled 1-bromo-11-(trichlorosilyl)undecane. The solution was stirred with a rod and vials were capped and placed at 4°C for 3 hours (reflecting findings by Brzoska et al. (1994), showing that an optimized temperature of the reaction bath is between 0°C for n=10 to 38°C for n=22, with a T_c shift of 3.5 ± 0.5°C per additional methylene groups). Subsequently, the SAM were removed from the solution and immersed in $CHCl_3$. They were sonicated 3×10 minutes in $CHCl_3$ and then 2×10 minutes in

ethanol. This cycle was repeated another two times. Finally, the substrates were dried in a nitrogen stream.

<Amino-terminated SAMs>

Bromo-terminated SAMs were hydrolyzed, at 50°C, in a 20 mL-solution of ethylene glycol dimethyl ether containing HgO (2.5 g)-$HClO_4$ 70 % (3 mL)-water (2 mL). This solution was gently heated until all the HgO was dissolved. After 24 h the SAM was rinsed with ethanol in an ultrasonic bath. Subsequently, wafers were sonicated in water and ethanol and washed with $CHCl_3$ followed by introduction of an aromatic amine, as a spacer for the diazotization procedure.

The alcohol-terminated SAM was refluxed in a chloroform solution (20-30 mL) of p-nitrobenzoyl chloride (4 g), at 50°C. After 5 hours, the nitro-terminated SAM was rinsed in chloroform, sonicated in ethanol four times, washed with 0.1 M Na_2CO_3 solution and ethanol, and finally dried in a nitrogen stream. Reduction of the nitro-terminated SAM was done with a solution containing 1 g $SnCl_2$, 2 H_2O in 2-propanol (20 mL), refluxing at 85°C for 15 h. Finally, wafers were washed with 2-propanol, sonicated in ethanol and dried under a nitrogen stream.

<Diazotization>

Amino-formed substrates were sonicated and placed in a 0.5 N HCl solution in ice. $NaNO_2$ (50 g/L) was dropwise added to this solution and the mixture was incubated at 4°C for 5 hours.

<Humic acid coupling>

Purified humic acid was diluted in a 0.1 M borate buffer at pH 9. Then diazotizated wafers were washed with 0.5 N HCl, water and borate buffer. Subsequently, wafers were dipped immediately in the humic solution at 4°C and incubated for 72 h. Subsequently, the humic acid grafted wafers were sonicated in borate buffer, distilled water and dried under a nitrogen stream.

<Verification of the bromosilane immobilization>

Br displacement by N_3 and reduction of RN_3 by $LiAlH_4$ was done by the method of Balachander and Sukenik, 1990 (scheme 2, Annex). The Br displacement by N_3 was verified by ATR-FTIR analysis.

<ATR-FTIR analysis>

This method was applied at Curie Institute. A Nicolet OMNIC 850 spectrophotometer was used for characterization of the layers. ATR-FTIR has numerous advantages over FTIR spectrometers. Sensitivity is increased by the principle of total internal reflection in which an evanescent wave probes several times an attenuated total reflection crystal. Generally, 20-40 total

internal reflections occur at the top surface of the crystal. This technique is generally used for characterizing functional groups immobilized on surfaces. Wu et al. (1997) followed the surface coverage by n-octadecyltrichlorosilane or 4-aminobutyldimethylmethoxysilane, detecting the appearance of CH_2 bands (ν_{as} CH_2 = 2920 cm^{-1}, ν_s CH_2 = 2950 cm^{-1}, N_3 chromophore at 2098 cm^{-1} (Navarre et al. (2001), Balachander and Sukenik (1990)), NH_2 bands being too weak to be observed, or monolayers containing 11-carbonyl alkyl chains, ν_{as} = 2922-2924 cm^{-1}. The broad band at 3300 cm^{-1} is assigned to Si-OH vibrations.

<Ellipsometry>

Ellipsometry was conducted at Curie Institute. Ellipsometric measurements were carried out on a PLASMOS SD 2300 ellipsometer with a rotating analyzer and a He-Ne laser (lambda: 632.8 nm) at an incidence angle of 68°. Ellipsometry is used for measuring layer thicknesses. In this technique, polarized light is reflected from a surface and the resulting polarization changes are measured. Fraction of the E-fields of p- and s-polarized light reflected from the surface and the induced phase angle difference between p- and s-polarized light gives information on the layer thickness. Ellipsometry has been conducted on SAMs of thienyl-functionalized n-alkyltrichlorosilane for measuring the film thickness obtained (Appelhans et al. 2000). The method has also been used for studying bimolecular films made on OH-terminated primer layers, showing that the thicknesses increases linearly with the hydrocarbon chain length (Brunner et al. 1996).

<NH_2 quantification by UV-visible spectrometry>

Amino groups titration was performed by a modified method adapted from Moon et al. (1997) using dimethylaminobenzaldehyde instead of 4-nitrobenzaldehyde (scheme 3, Annex). This aldehyde has a higher extinction coefficient making detection more sensitive.

- Formation of the imines

Amino-terminated SAMs were placed in absolute methanol under nitrogen atmosphere in a sealed flask containing 50 mg of 4-dimethylaminobenzaldehyde, 30 µL acetic acid and 1 g of 4 Å molecular sieve. After heating 3 hours at 50°C, the wafers were washed with absolute methanol for 2-3 minutes and dried under nitrogen.

- Hydrolysis

The imine-terminated substrates were immersed in a 10 mL-water solution containing 20 µL acetic acid and placed for 1 hour in a hood at 37 °C. Wafers were then washed with 3 mL water. Spectra of the sample solution, containing wafers with and without amino groups, were recorded and compared by measuring their absorbance at 350 nm. The aminosilylated layers were recovered by rinsing in water and sonication.

<TOF-SIMS experiments>

Time-of-flight secondary ion mass spectrometry (TOF-SIMS) is a powerful tool for obtaining chemical information on surfaces (molecular and structural, and in some cases quantitative

information). TOF-SIMS uses a pulsed primary ion beam to desorb and ionize species from the pure or covered silicon from the wafer. The outcoming secondary ions (positively or negatively charged ions) are accelerated into a field free region of a TOF-mass analyzer (flight tube) in which they are separated according to their mass-dependant time-flight from the surface to the detector. Molecular parent ions and fragmentation patterns are characteristic of the surface molecules as well as of the silicon surface itself or crystalline structure of the surface. TOF-SIMS has been a method of choice to prove that the silane is well-grafted at the surface. Quinton and Dastoor (2000) used it to study the chemical sorption of aminopropylsilane on an iron oxide surface. Other authors used TOF-SIMS to characterize organosilane at the surface of aluminium oxide (Houssiau and Bertrand 2001, Rattana et al. 2002), glass surfaces (Wang and Jones 1993), zinc or steel substrates (Van Ooij and Sabata 1991 and 1993), polymer surfaces (O'Toole et al. 1992) and particularly of γ-GPTMS (Abel et al. 2000a,b).

The SIMS measurements were performed using a time-of-flight (TOF) instrument developed at the GSF. In our study the bombarding parameters were as follows: primary ions SF_5^+, ion source terminal voltage 30 kV, target bias 6 kV (ion impact energy 36 keV for negative secondary ions, 24 keV for positive secondary ions), stationary beam current 1–2 nA, bunched pulse width about 3 ns, repetition rate 19 kHz, 2 x 10^7 pulses per spectrum. The angle between the primary ion beam line and the surface normal of the sample is 60° and the area of ion bombardment 0.3 x 0.4 mm^2. The beam was deflected strongly in the electric field between the sample and the acceleration electrode. Under these conditions the actual angle of beam incidence is estimated to 75.5° in the case of positive target bias, and 52° with a negative target bias. The beam was realigned by electric means to hit the sample on axis of the TOF analyzer. Moving the sample under the beam was used for changing the sample position.

Neutral species generated along the first half of the drift tube were removed by tilting the second half of the drift tube by 3°. The secondary ions were directed to the detector by an electrostatic field. With a target bias of 6 kV, the mass resolution in the low mass range ($u \leq 100$) is about 600. Applying deconvolution techniques in the low mass region improves the mass resolution to 3000. Mass calibration is based on the same selected peaks on each spectrum. TOF-SIMS has been conducted on the different samples in positive and negative mode, eliminating the wafer supporting diazonium group due to its instability.

<AFM measurements >

Atomic force microscopy (AFM) is a scanning probe technique. It probes the surface with a sharp tip. Tips are made from Si_3N_4 and are located at the free end of a cantilever 100 to 200 μm long. Van der Waals forces between the surface sample and the tip cause the cantilever to bend or deflect. A detector measures the tip deflection as the sample is scanned under the tip and the surface topographical data are obtained. Therefore, by the image structures information is obtained about small colloids, colloid aggregation and adsorption onto surfaces. AFM characterization has been employed by several authors to study the structural organization of organosilanes (Navarre et al. 2001, Bierbaum 1995a). Recent work has been performed by several authors to understand the aggregation of humic substances layers adsorbed on

muscovite (Plaschke et al. 1999) and mica (Liu et al. 2000) and the influence of Eu on the formation of agglomerates in aqueous solutions containing the trivalent ion (Plaschke et al. 2002).

Experiments have been conducted on a Topometrix Explorer, Si-cantilever (type 1660, Freq. 113 kHz, tapping mode, dry) at INE. Other investigations have been done with DI-AFM on a Digital Instruments Dimension 3100 (Si-cantilever (Freq. 290 kHz), tapping mode, dry). All images are topography images.

Experimental results

<ATR-FTIR results>

ATR-FTIR has been conducted respectively on bromosilane wafer (Fig. 1a), N_3 wafer (Fig. 1b) and NH_2 (Fig. 1c) wafer with bare silicon as a blank. Results are similar to those obtained by Balachander and Sukenik (1990). In case of bromosilane wafer, ATR-FTIR analysis in the range 4000-1500 cm^{-1} shows the presence of ν_s symmetric and ν_{as} antisymmetric CH_2 bands due to the long-chain bromosilane at 2859 and 2930 cm^{-1}. Displacement of Br by N_3 is observed by the appearance of the expected chromophore N_3 band at 2100 cm^{-1}. This experiment shows that the reaction was successful and consequently that bromosilane was well grafted on the silicon wafer. Reduction of azide functionality into NH_2 showed the complete disappearance of N_3 band.Immobilization of aminophenylsilane on silicon wafer has also been conducted in order to test some NH_2 quantification methods (Moon et al. 1996, 1997). Analysis of the grafting by ATR-FTIR (Fig. 2) shows the presence of C=C from phenyl groups at 1624 cm^{-1}, ν_s symmetric and ν_{as} antisymmetric CH_2 at 2851 and 2928 cm^{-1}, CH from phenyl groups at 3045 cm^{-1} and aromatic NH at 3485 cm^{-1}. These results confirm the presence of aminophenylsilane on the silicon wafer.

ATR-FTIR has been conducted also on a humic ATR crystal (Fig. 3). Characteristic bands at 2924.7 and 2847.06 cm^{-1} of CH_2 and CH_3 and C=O functionality at 1721.99 cm^{-1} are also visible (aromatic ester and aliphatic COOH-COO^-). Other bands at 2670.57 (O-H from COOH), 2218.34 ($-N^+ \equiv N$, medium frequency), 2047.37 cm^{-1} ($-C=N^+=N^-$, very strong) are also present in the spectrum. Humic acids immobilization is shown by the presence of the two vibration bands attributed to COOH functionality.

<Ellipsometry>

Ellipsometry measurements on bromosilane wafer were carried out for measuring the layer thickness. A thickness of 18 ± 2 Å was found, in agreement with the calculated thickness of a monolayer (17.4 Å) assuming a fully extended chain (Heise et al. 1997, Wasserman et al. 1989). The length of a methyl-terminated monolayer with n methylene units is calculated to be L=1.26n+4.78. Consequently, it is assumed that the layer is a homogeneous one. After grafting of humic acids, the thickness layer increased by 60 Å ± 4 Å, presumably due to immobilization of humic acids.

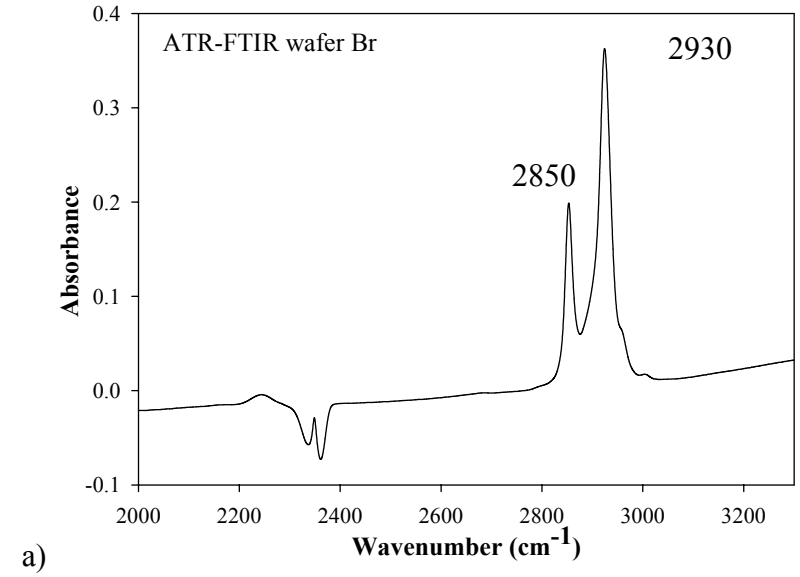

a)

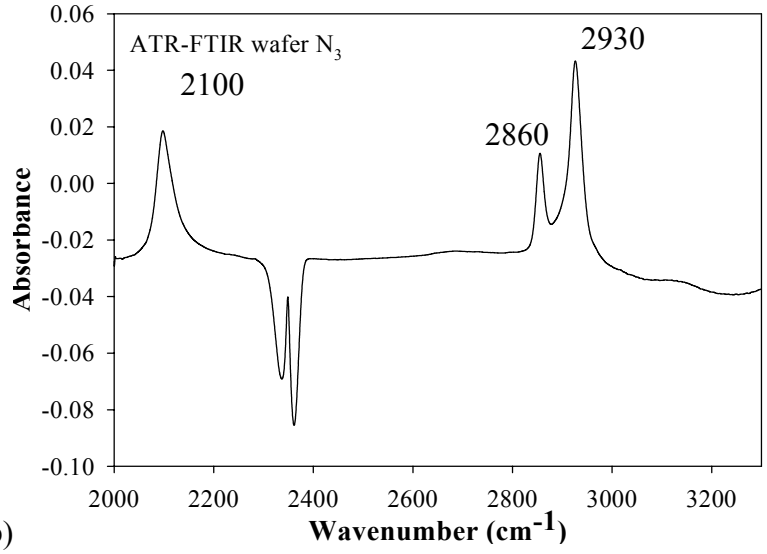

(b)

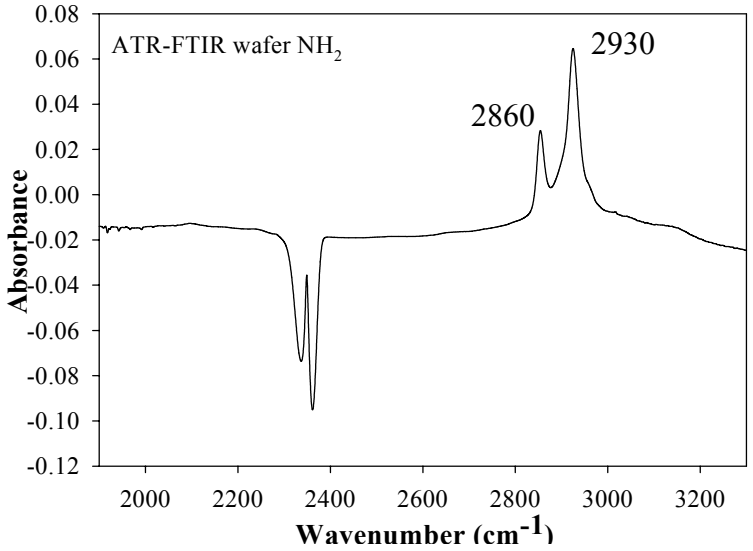

(c)

Fig.1 ATR-FTIR spectra from (a) bromosilane wafer, (b) N_3 wafer, and (c) amino wafer.

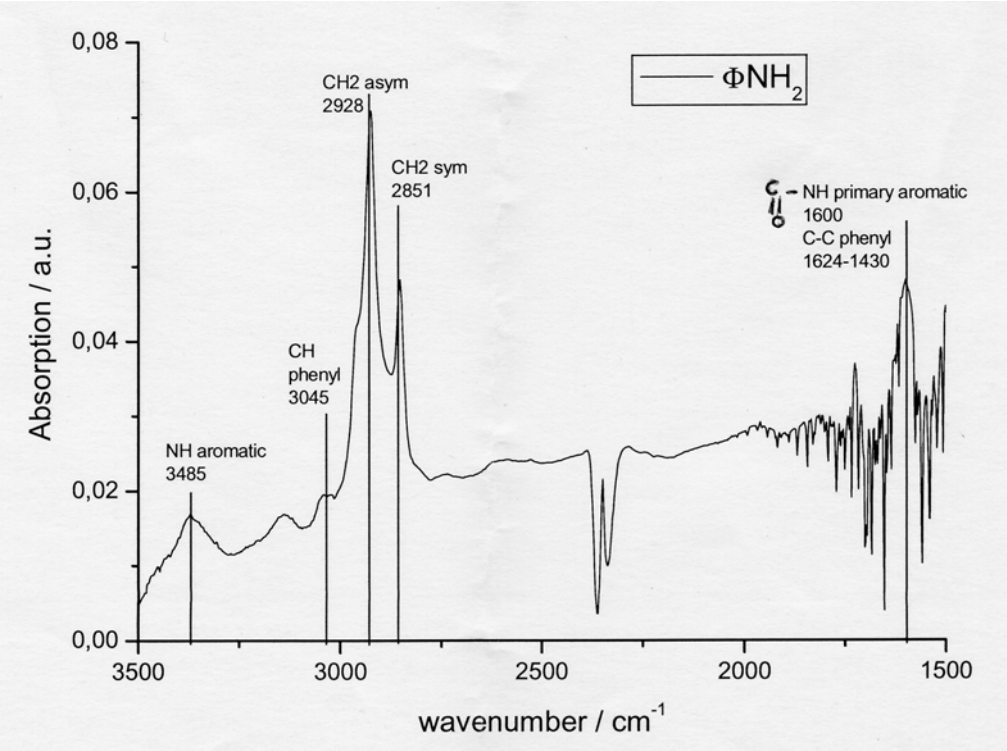

Fig.2: ATR-FTIR of aminophenylsilane immobilized on silicon wafer.

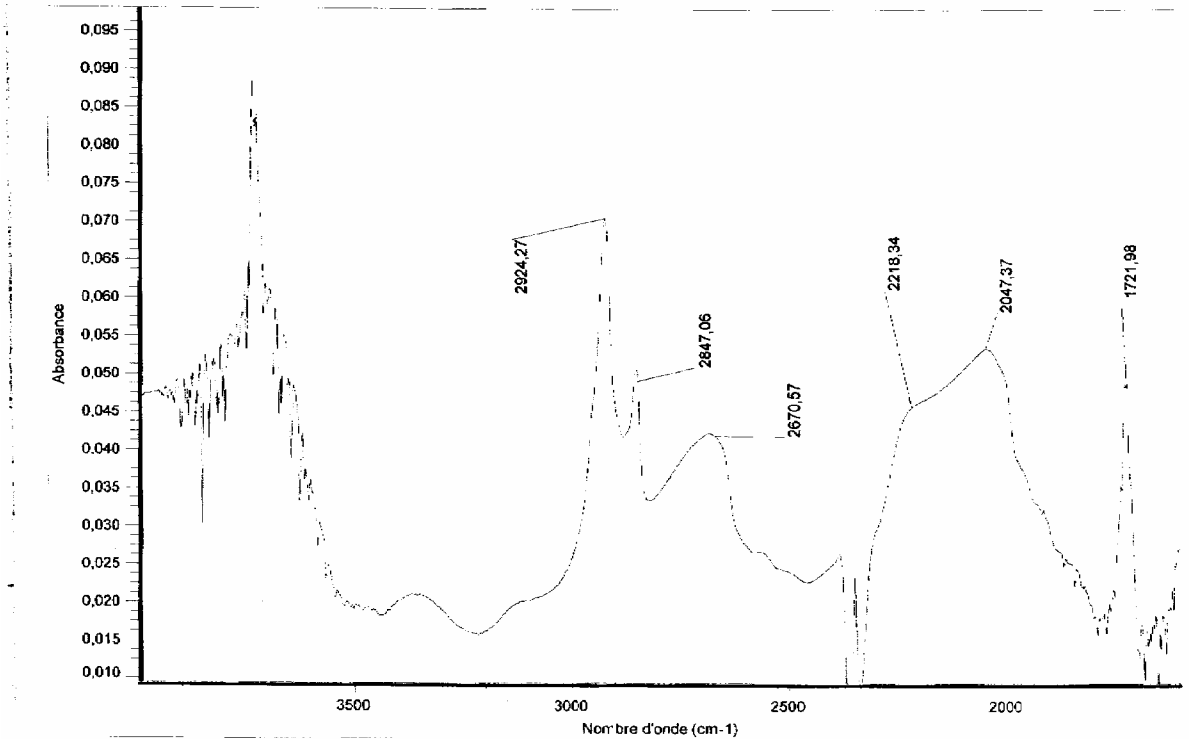

Fig. 3. ATR of humic wafer.

<UV-Visible quantification of NH_2>

NH_2 quantification was performed by the method of Moon et al. (1997) using dimethylamino-benzaldehyde instead of 4-nitrobenzaldehyde. The latter compound has a lower extinction coefficient and thus its detection is more difficult. Measuring the amount of dimethylamino-benzaldehyde at (λ_{max} = 350 cm^{-1}, ε = 23937 L mol^{-1} cm^{-1}) liberated from the hydrolysis of the imine, it is possible to evaluate the amount of amino groups per unit area (Fig. 4). This amount represents 5 NH_2/nm^2 in accordance with values obtained by Moon et al. (1997).

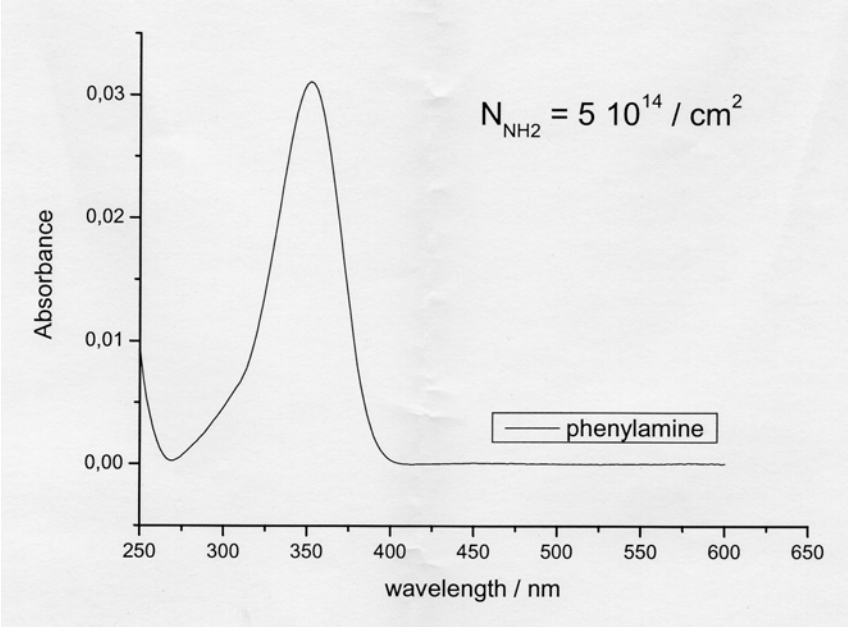

Fig. 4: UV-visible NH_2 quantification of aminophenylsilane immobilized on silicon wafer.

TOF-SIMS results

<TOF-SIMS of Silicon wafer>

TOF-SIMS spectra of silica wafer are given in Fig. 5. The spectra show the presence of fragments characteristic of silicon oxide substrate in particular on the form of $Si_nO_mH_l^-$ ($(SiO_2)_mH^-$ and $(SiO_2)_nOH^-$) with peaks at m/z=16 (O), 59.90 (SiO_2), 60.90 (SiOOH), 75.88 (SiO_3), 76.88 (SiO_2OH), 120.78 ($(SiO_2)_2H$), 136.77 ($(SiO_2)_2OH$), 180.63 ($(SiO_2)_3H$), 196.62 ($(SiO_2)_3OH$)), 240.48 $(SiO_2)_4H$, 256.44 $(SiO_2)_4OH^-$ and additional peaks present at 104.79 (Si_2O_2OH) and 152,79 (Si_2O_5OH), buried in a complex pattern of adsorbates e.g. hydrocarbon peaks $(C_nH)^-$ due to ambient contamination. Hydrocarbon peaks $(C_nH)^-$ are observed in all negative spectra at m/z= 13, 25, 37, 49, 61, 73, 85, 97 and in positive spectra $(C_xH_y)^+$ at m/z=15, 27, 29, 41, 43, 55, 69, 91 (CH_3^+, $C_2H_3^+$, $C_2H_5^+$, $C_3H_5^+$, $C_3H_7^+$, $C_4H_7^+$, $C_5H_9^+$, $C_7H_7^+$) and carbon peaks $(C_n)^-$ at m/z=12, 24, coming also from saturated aliphatic and aromatic species present as impurities in solvent. Some other peaks come from washing procedures introducing carbon containing fragments as m/z=40.979 characteristic of $SiCH^-$ or $CH{\equiv}CO^-$.

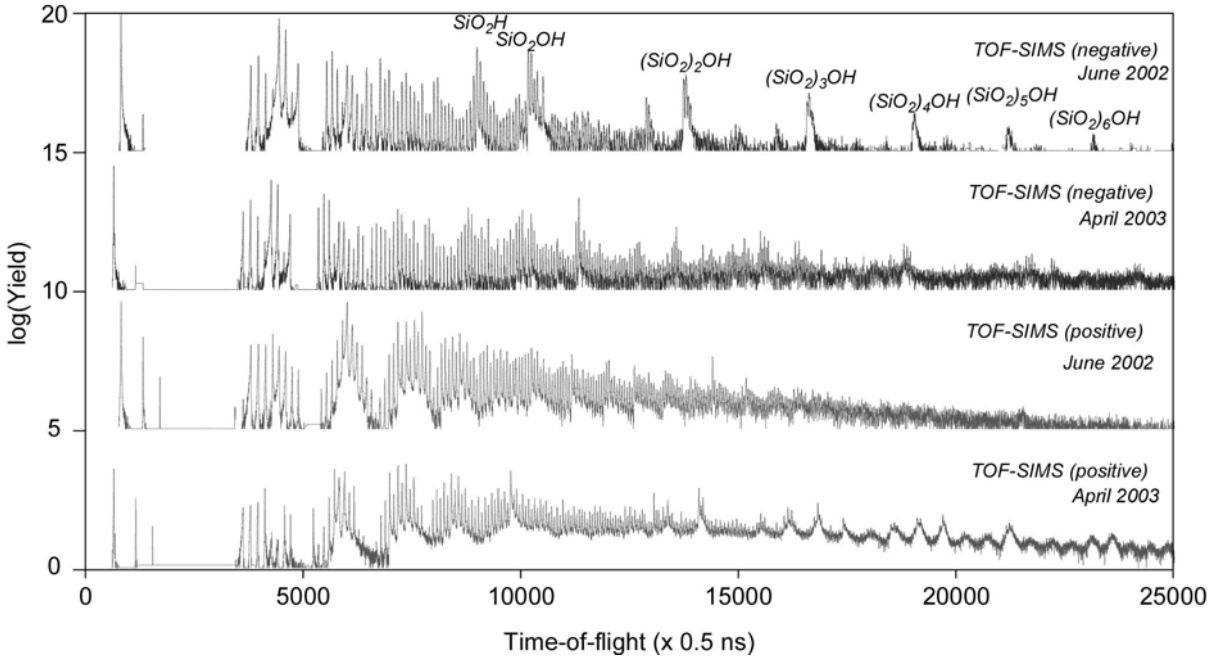

Fig. 5: TOF-SIMS spectra of silicon wafer.

At m/z=148.79, 162.76, 222.73, 236.68 very weak peaks, coming from linear or cyclic fragment of polydimethylsiloxane. This is a major frequent contaminant in TOF-SIMS measurements. This contaminant at metal surfaces occurs because PDMS has a very low surface free energy compared to the metal one (Poleunis et al., 2002). This shows that our sample is not very clean.

The positive spectrum of the current silicon-wafer exhibits a dominant contamination pattern that can be attributed to cyclic fragments, eg. C_6H^+, $(C_6H)_2H^+$ and $(C_6H)_m(CH_3)_nH^+$. This contamination pattern is present at all stages of the grafting whereas the intensity is more pronounced at the bare silicon wafer. It is open whether the contamination comes from the transport in a closed box with no additional protection of the wafer surface or from grafting facility itself. Generally, more polar surfaces, such as amino-terminated SAMs, are easily contaminated in ambient conditions, and these organic contaminations can be the main cause of thickness increase observed by AFM methods. Other cyclic and linear fragments of PDMS are also observed on positive spectra in four distinct series $[nR+73]^+$ $[(CH_3)_3Si[OSi(CH_3)_2]_n^+]$; $[nR+117]^+$ $[(CH_3)_3Si[OSi(CH_3)_2]_nOSi]^+$; $[Rn-15]^+$ $[[Si(CH_3)_2O]_n\text{-}CH_3]^+$ formed by the loss of methyl groups from cyclic fragments and $[Rn-29]^+$ coming from bicyclic fragments (Dong et al. 1997).

In our study, positive spectra were not very useful for identification of nitrogen containing compound, except for the presence of oxygen in case of alcohol wafer. Consequently, structures are mainly deduced from negative spectra and other analytical techniques. The reason of the difficulty to interpret positive spectra could be the fully packing of the hydrocarbon chains tightly held together via hydrophobic interactions and Van der Waals forces. It is more difficult for longer hydrocarbon chains to be emitted from the surface and as the layer assem-

bles, intensities of short hydrocarbon fragments increase due to clipping of the monolayer chains by the SIMS primary ion or energetic secondary ions.

<TOF-SIMS of Bromosilane wafer>

The negative TOF-SIMS spectrum of the Bromosilane wafer is given in Fig. 6. The same fingerprint as bare silicon oxide characterizes this spectrum, however, with lower yield due to surface coverage by the silane layer. The presence of this bromosilane layer is detected by the presence of Br^- monomer at m/z=78.92 and 80.91 with yields in accordance with isotopic abundance (^{81}Br representing 97.3% of ^{79}Br). Weaker peaks are observed at m/z=157.84, 159.85, 161.84 corresponding respectively to Br^- dimer $^{79}Br_2^-$, $[^{79}Br\text{-}^{81}Br]^-$, $^{81}Br_2^-$(50.5% of $^{79}Br_2^-$, 100% of $[^{79}Br\text{-}^{81}Br]^-$, 49.5% of$^{81}Br_2^-$). In addition the Br_2H^- pattern interferes with the pure Br_2^- one at m/z=158.55, 160.55, 162.53 identified as $^{79}Br_2\text{-}H^-$, $[^{79}Br\text{-}^{81}Br]\text{-}H^-$, $^{81}Br_2\text{-}H^-$. Characteristic fragments are identified as bromo containing compounds $SiO^{79}Br$ and $SiO^{81}Br$, (m/z=122.92 and 124.91), $SiO_2{}^{79}Br$ and $SiO_2{}^{81}Br$ (m/z=138.91 and 140.88) and $Si_2O_2O^{79}Br$ and $Si_2O_2O^{81}Br$ (m/z=182.86 and 184.83). There are also weak signals from the bromosilane, e.g. $Br(CH_2)_9O^-$, $Br(CH_2)_{10}OH_2^-$ and $H_2SiO_2(CH_2)_{11}Br$ at m/z = 221.17, 237.18 and 295.22, respectively.

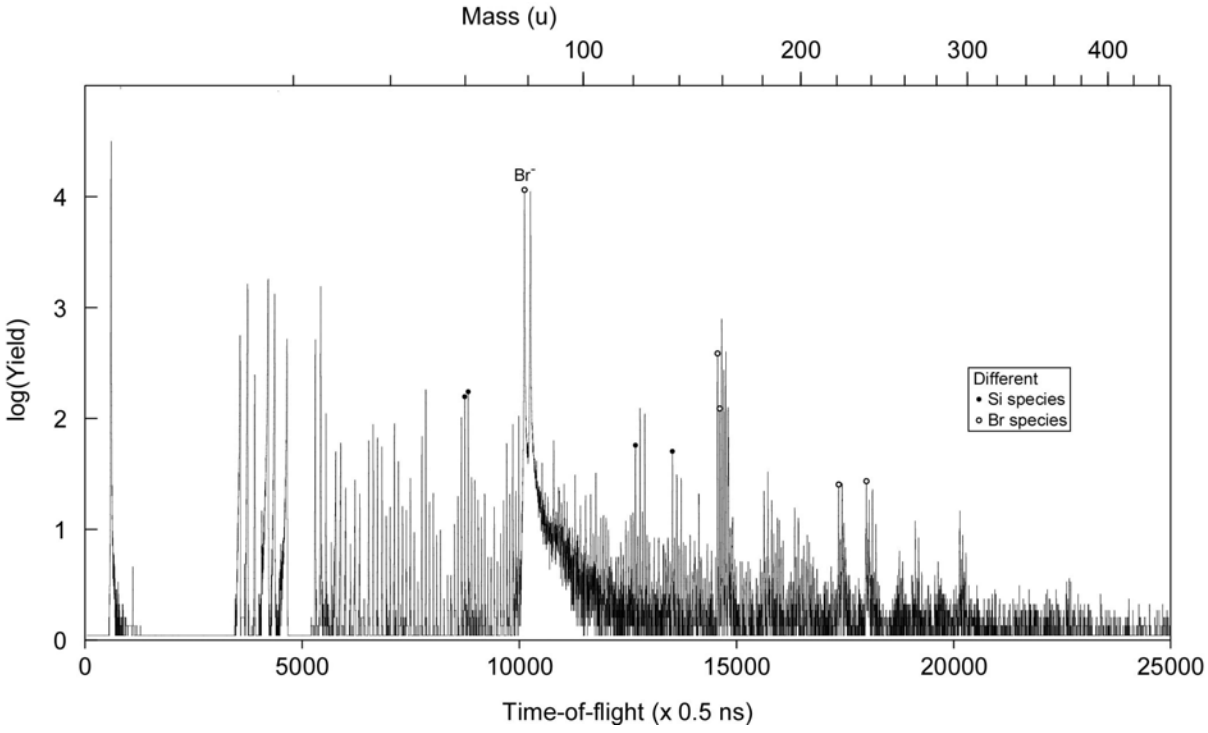

Fig. 6: Negative TOF-SIMS spectra of bromosilane wafer.

The fingerprint of the bare silicon oxide and the hydrogenocarbon peaks in the mass range below 100 u are reduced by at least a factor five due to more or less dense surface coverage by the silane. The coverage is homogeneously across the wafer (Fig. 7). The unspecific H^- peak intensity is constant as a function of the position of the beam spot, the specific Br^- peak intensity varies about a factor of 2 from the center to the border of the Si-wafer.

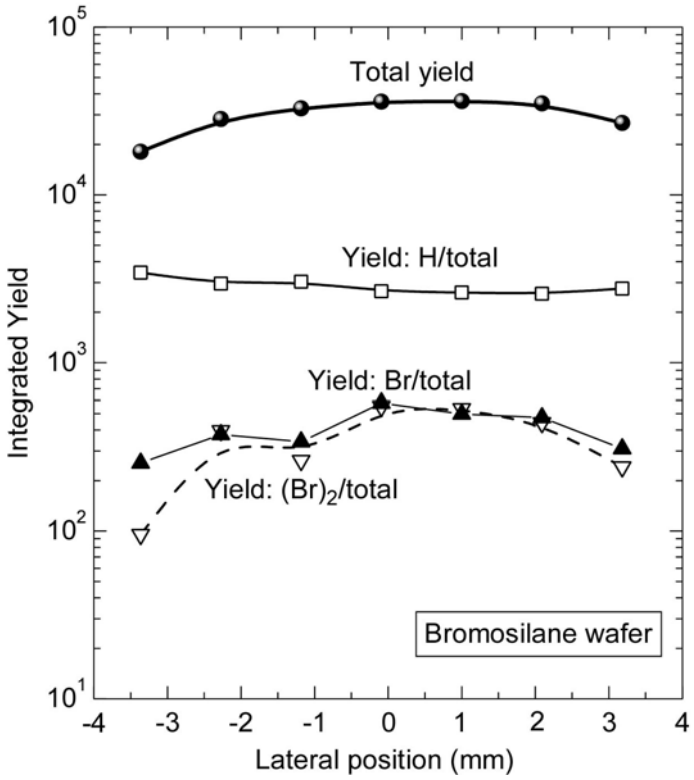

Fig. 7: Lateral distribution of Br by negative TOF-SIMS of bromosilane wafer.

<TOF-SIMS of Alcohol wafer>

The negative spectrum of the alcohol wafer obtained by reduction of the bromosilane wafer shows that the displacement of bromo functionality by alcohol functionality was successful (Fig. 8). Even if the results obtained are not quantitative, the peaks corresponding to ^{79}Br and ^{81}Br decreased considerably by a factor of 30, showing that the reaction was sufficiently complete. The peaks at m/z=122.7 and 124.7 identified as $SiO^{79}Br$ and $SiO^{81}Br$ in case of the boromosilane wafer and at m/z=138.65 and 140.62 identified as $SiO_2{}^{79}Br$ and $SiO_2{}^{81}Br$ (Fig. 6) have disappeared in the alcohol wafer (Fig. 8).

Below m/z = 100 the intensity of small fragments is increased as the carbon hydrogen chain is now exposed to the beam. The OH^- peak is elevated in comparison to the bromosilane wafer as well as short fragments of the carbon chain with C_2HO^- (m/z=41.15) and CHO_2^-, $C_2H_5O^-$ (m/z=45.15) indicating the presence of alcohol functionality. The silicon oxide pattern is still present at comparable level and short chain fragments attached to SiO_2-cluster, e.g $(SiO_2)_2(CH_2)_2H$ are increasing. The positive spectrum proves the conversion of bromo functionalities into OH groups by the presence of fragments characteristic of alcohol groups at m/z=31, 45, 59 representative of $CH_2{=}^+OH$, $CH_3\text{-}CH{=}^+OH$ and $C_2H_5\text{-}CH{=}^+OH$.

<TOF-SIMS of Nitrobenzoyl wafer>

In comparison to the alcohol wafer, the negative spectrum of the nitrobenzoyl wafer presents new peaks characteristic of the nitrobenzoyl moiety (Fig. 9). In particular, at m/z=45.99, 105.97, 121.96, 165.88 identified as NO_2^-, $C_6H_4NO^-$, $C_6H_4NO_2^-$ and $^-OOC\text{-}C_6H_4NO_2^-$. A pattern from the whole molecule $SiO_2(CH_2)_{11}OCOC_6H_4NO_2$ down to NO_2^- can be interpreted as the cleavage sequence starting from the whole molecule.

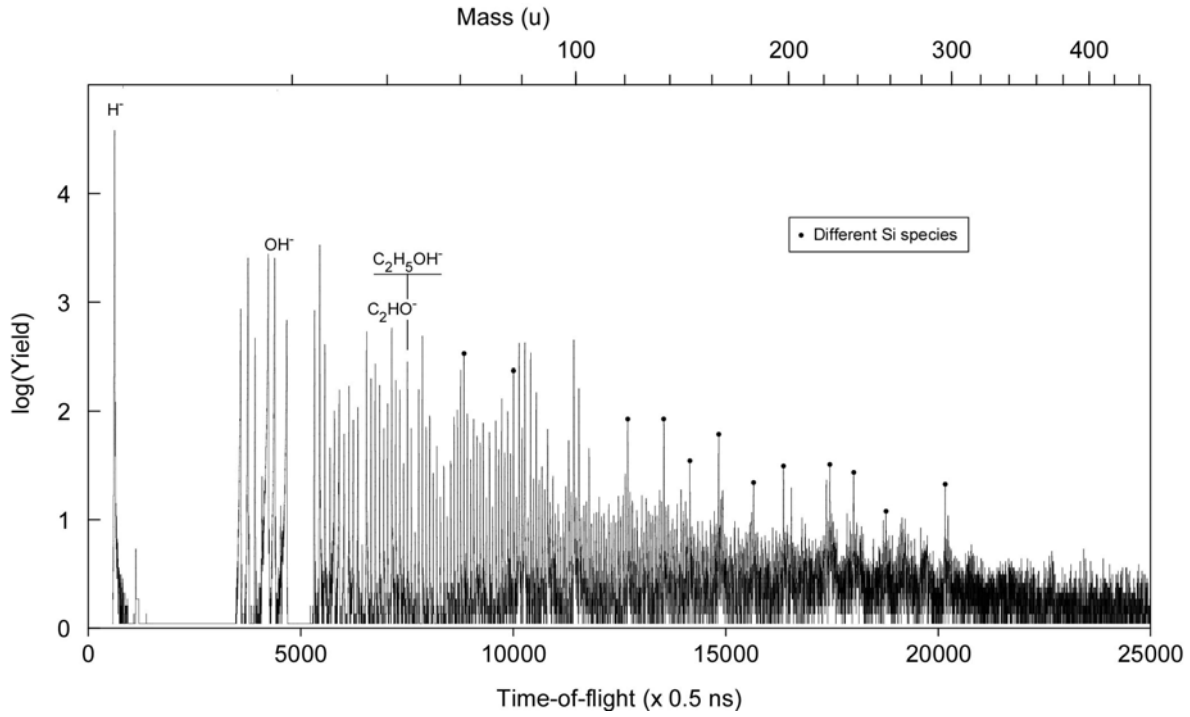

Fig. 8: Negative TOF-SIMS spectra of alcohol wafer.

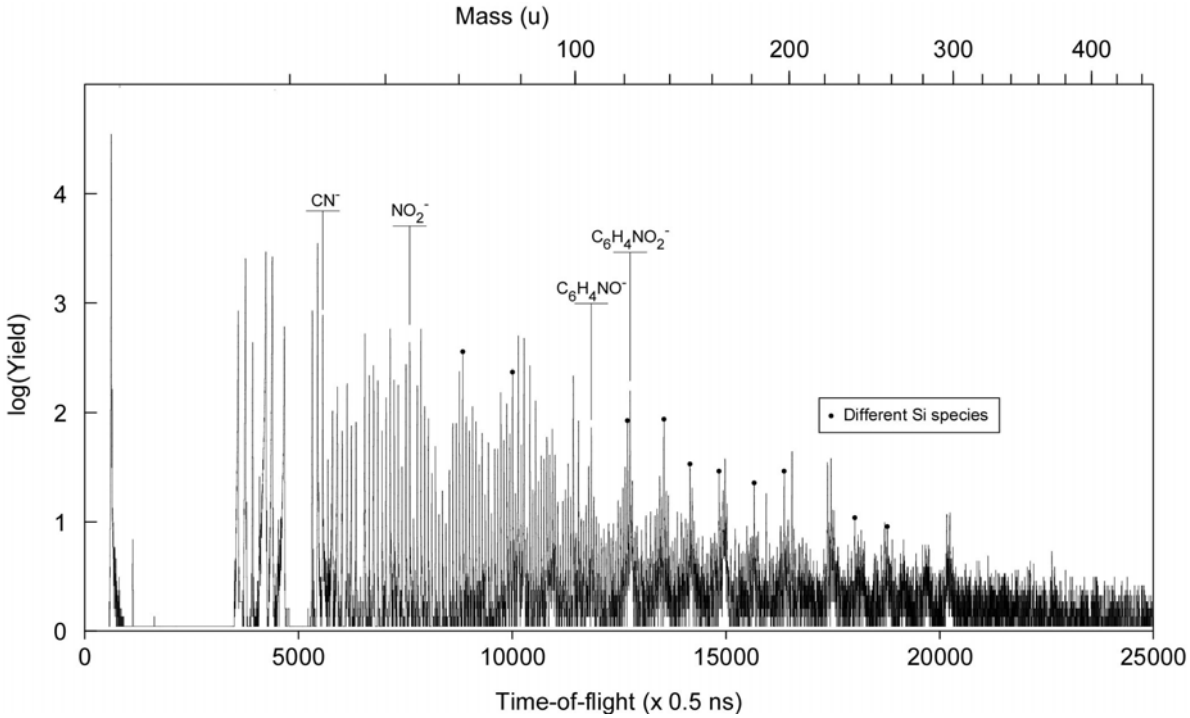

Fig. 9: Negative TOF-SIMS spectra of nitrobenzoyl wafer.

<TOF-SIMS of Aminobenzoyl wafer>

Amino groups are electron donating by resonance. This increases the electron density on the benzene ring, intensifying the negative charge. Contrary to this, nitro groups are electron withdrawing. This decreases the electron density on the benzene ring, lowering the negative charge. For these reasons, fragments from aminobenzoyl moieties and nitrobenzoyl moieties are expected to be to be different, as also found in this study.

With this preparation step, the spectrum in the mass range above m/z > 100 the spectral feature are more complex (Fig. 10). We observe that peak at m/z=46 (NO_2^-) is reduced in comparison to nitrobenzoyl wafer and C_6H^- and C_6HO^-, $C_6H_5N^-$ becomes prominent. In addition an increase in the PDMS contamination peaks (m/z=75, 89) compared to the nitrobenzoyl wafer is found. A new pattern is identified which belongs to a cleavage sequence from $C_6H_4OOCONH_2(CH_2)_8H^-$ down to C_6H^-. The spectral features in the mass range above m/z > 250 may be contributed to $(SiO_2)_m(CH_2)_n^-$ cluster. This cluster may also contribute to the complex peak groups in the mass range below m/z = 250.

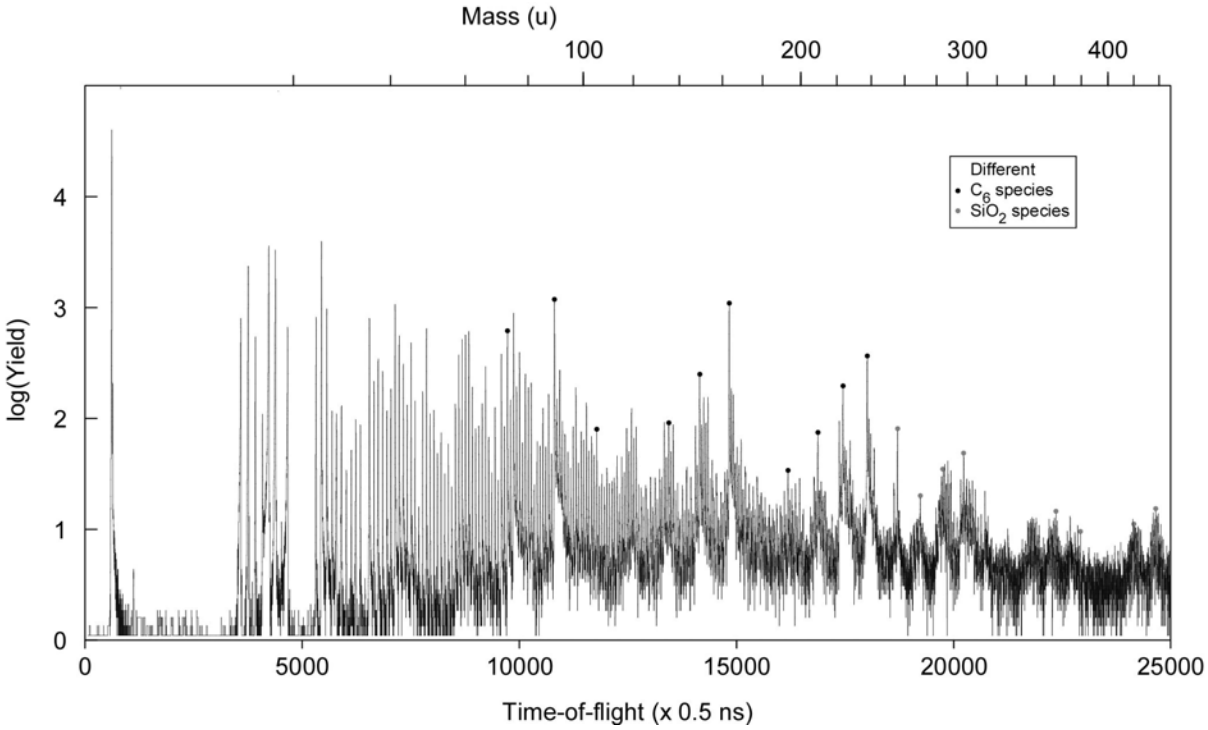

Fig. 10: Negative TOF-SIMS spectra of aminobenzoyl wafer.

<TOF-SIMS of Humic wafer>

The negative TOF-SIMS spectrum of humic wafer is shown in Fig 11 and the negative logarithmic TOF-SIMS spectra are shown in Fig. 12 for the different steps in the overall grafting. Differences occur between humic wafer and amino wafer. A peak forest can be seen which covers the entire mass domain with emphasis on elevation in the upper mass range. This is particularly true for humic acids that possess a large mass dispersion. Humic acids deposited

by jet-spray deposition gives the same mass repartition as humic acids immobilized by covalent binding (not shown here).

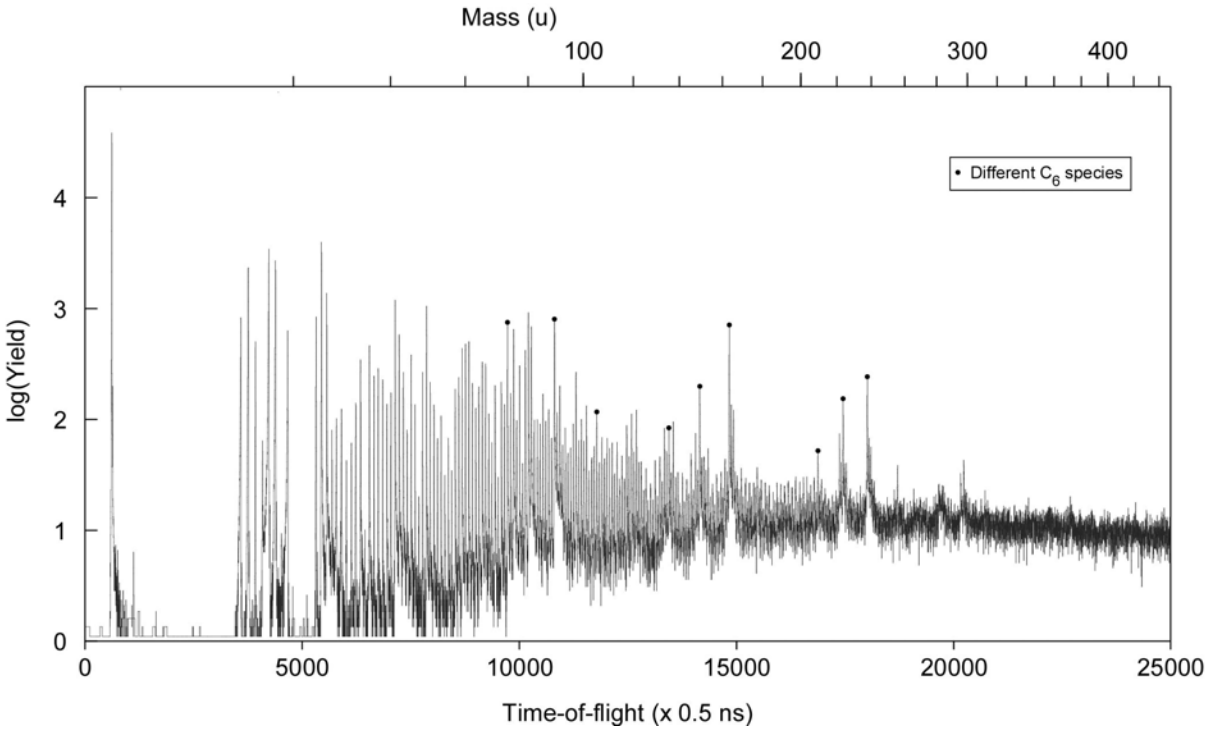

Fig. 11: Negative TOF-SIMS spectra of humic wafer.

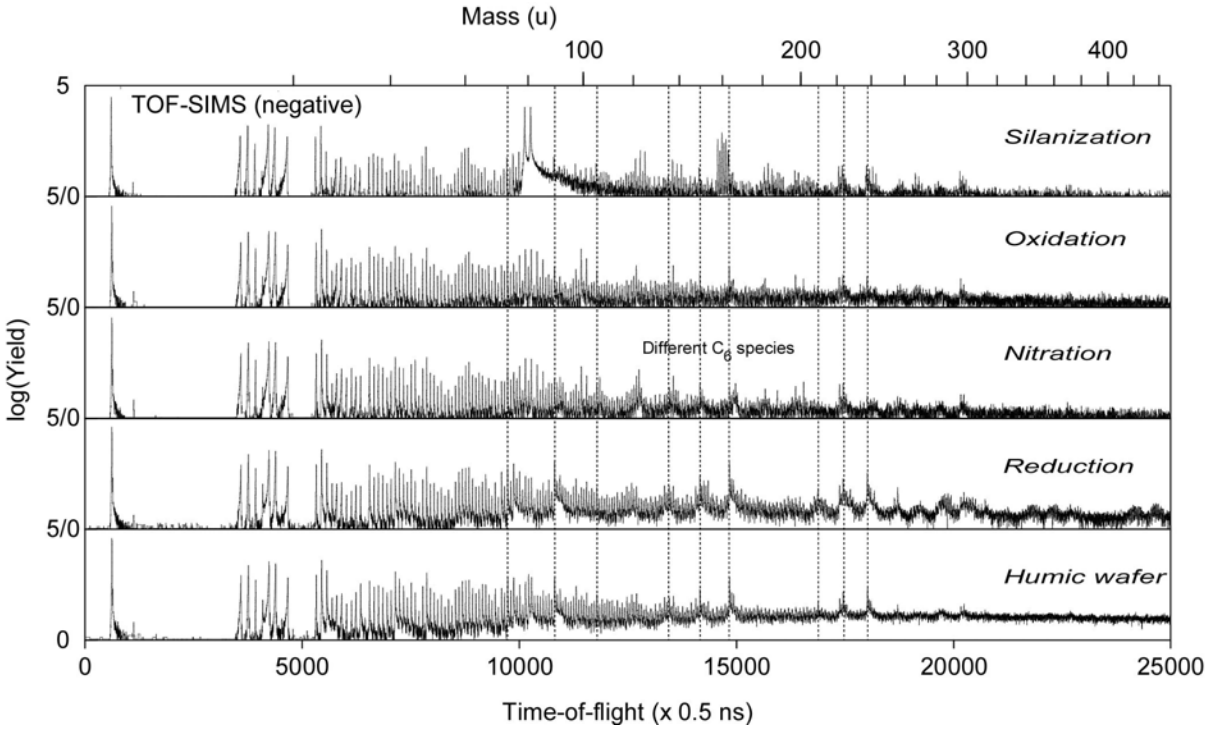

Fig. 12: Negative TOF-SIMS spectra of the wafers over different process steps.

The negative TOF-SIMS spectrum of the humic wafer (Fig. 13) shows the same dominant spectral peak pattern but on top of a smooth mass distribution over a wide mass range. This is a fingerprint of the humic acid. The complex peak distributions of the aminobenzoyl wafer are

somehow cleaned up which may reflect the masking of the surface due to the humic acids. No prominent signal related to the covalent binding of the humic acid to the aminobenzoyl-wafer can so far identified.

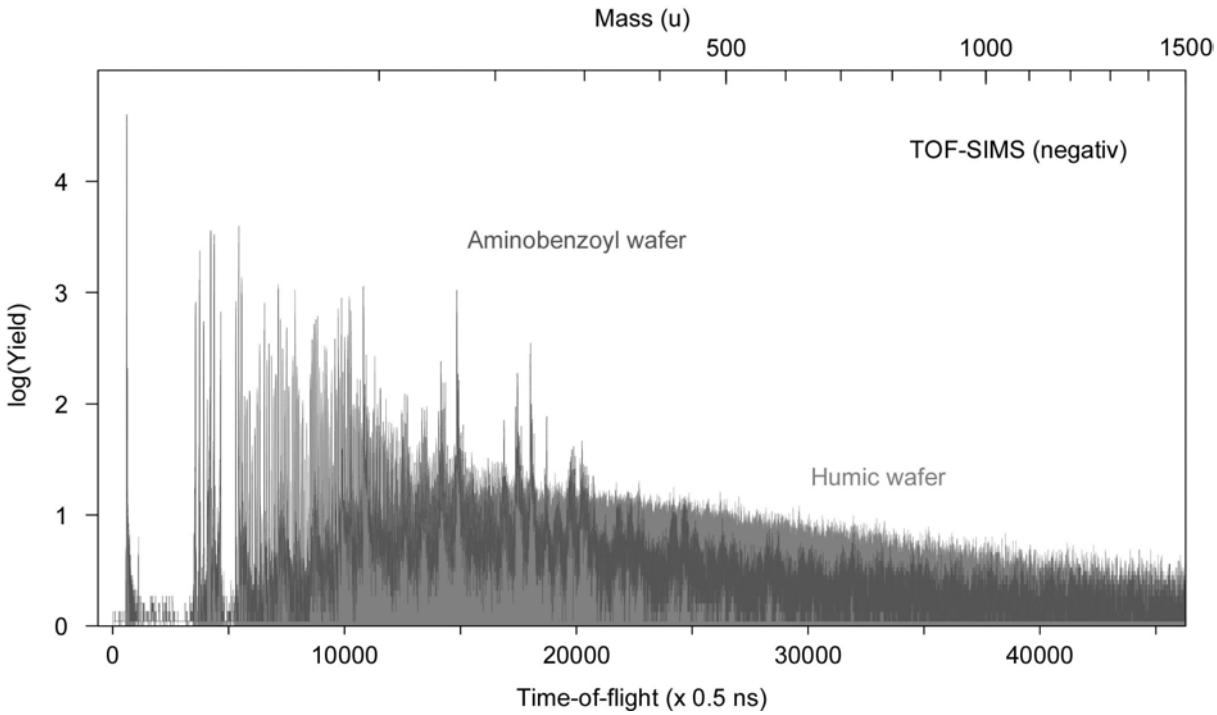

Fig. 13: Negative TOF-SIMS spectra of aminobenzoyl and humic wafers.

<TOF-SIMS: Peak maximum of selected species as a function the stage of grafting>

Fig. 14 shows the peak maximum of selected peaks as a function of the grafting stage. The total yield Y_{total}, e.g. summing up the yield drops little from stage 2 to stage 4 (Fig. 14(a)). With stage 5, Y_{total} increases more than 60% in combination with an increase in the complexity of the spectrum. Adding of humic acid to the aminibenzoyl wafer gives a higher Y_{total} but the increase is due to the smooth humic acid background. The fingerprint peaks of the silicon $(SiO_2)_mH$- and $(SiO_2)_nOH$- show a flat maximum at the medium stages. The lower values at the bromo-silane and at the humic wafer reflect the masking with bromine and humic acid (Fig. 14(a)).

The monomer and dimer bromine peak maximum decreases from the bromosilane to the alcohol wafer and remains at a very low level (Fig. 14(b)).

The specifics of the aminobenzoyl and nitrobenzoyl functionality are shown in Fig. 14(c). NO_2^- shows a sharp peak at the nitrobenzoyl wafer whereas $C_6HNH_2^-$, (C_6HO^-) and $C_6H_3O_2(CH_2)_4^-$ peaks at the aminobenzoyl wafer. Due to the medium mass resolution of our TOF-SIMS facility we can't resolve NH_2 from an O attachment.

Fig. 14(d) shows the dependence of small fragments on the stage of grafting. Removing the bromine from the wafer exposes a more sensitive surface in respect to small fragments, cov-

ering the surface with amino groups reduces the contribution of small fragments. The masking of the surface with humic acids is no additional source of small fragments. Fragments from within the long chain molecule have the same level after the removing of the bromine.

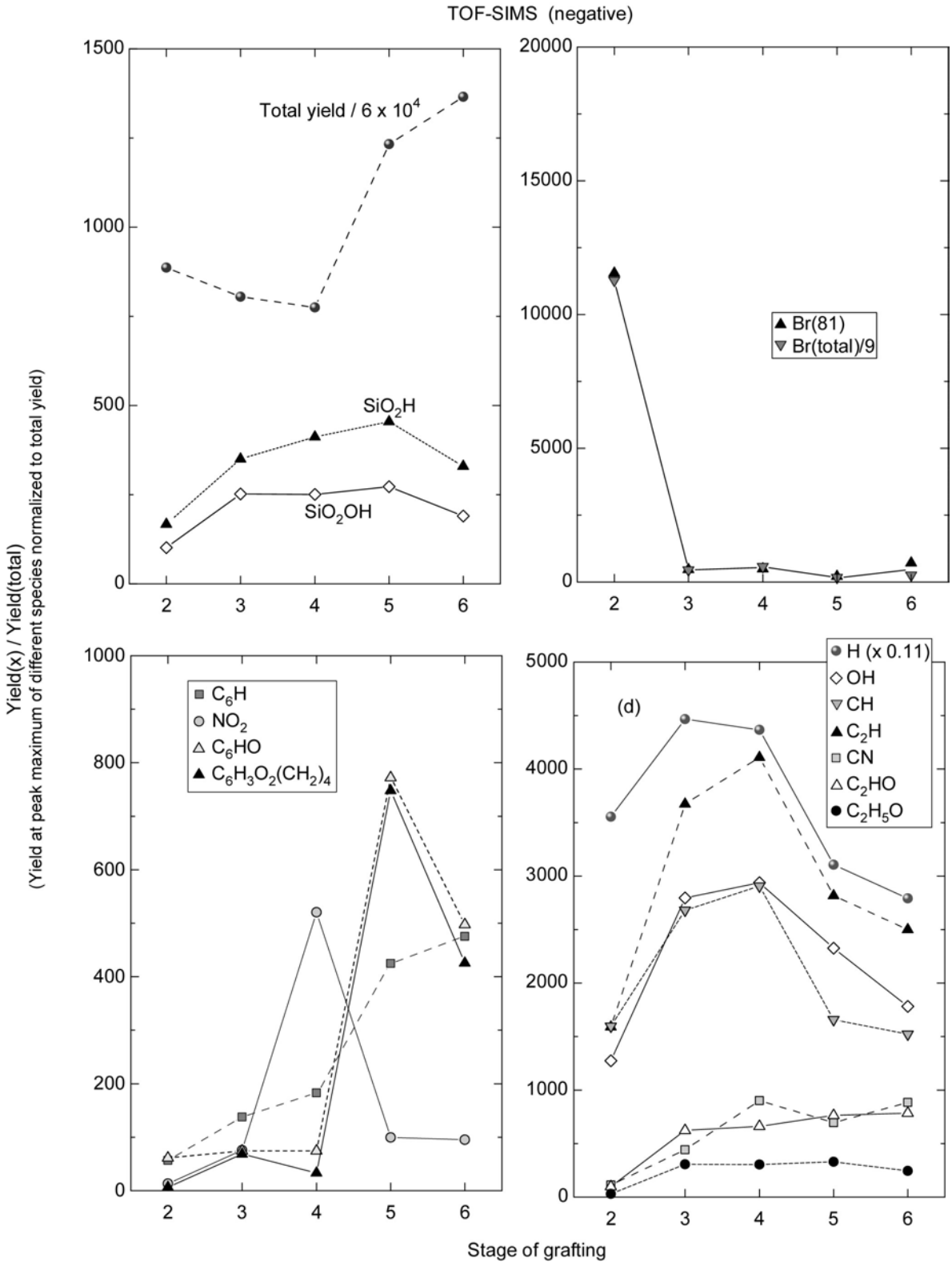

Fig. 14: Maximum of selected peaks at different grafting stages by negative TOF-SIMS. The grafting stages are (2): Bromolilane wafer, (3): Alcohol wafer, (4): Nitrobenzoyl wafer, (5): Aminobenzoyl wafer, and (6): Humic wafer.

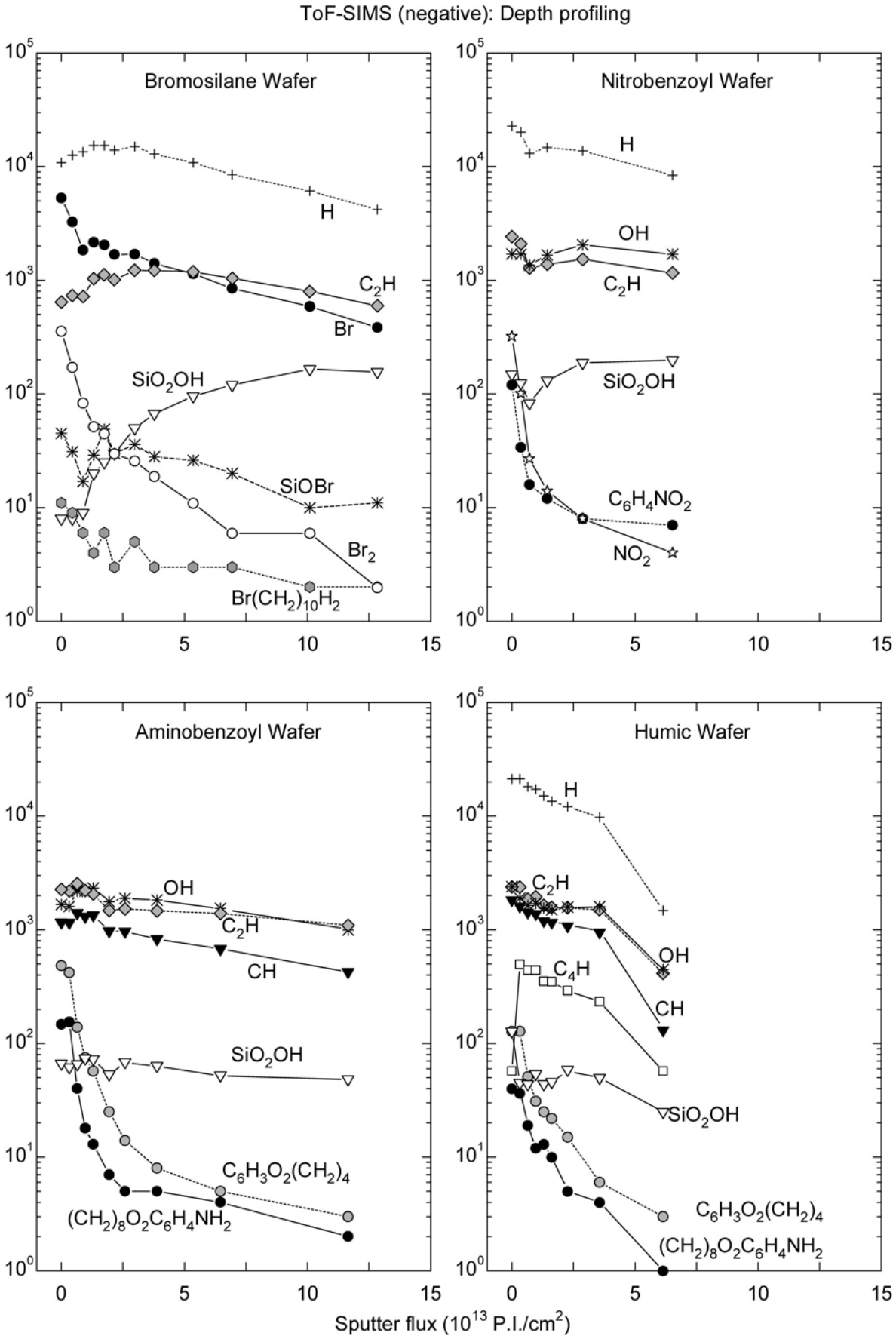

Fig. 15: Depth profiling of wafers at different stages of the grafting process.

<TOF-SIMS depth-profiles>

Depth-profile mode (sequence of static and dynamic SIMS) is applied in order to obtain information on the stability of characteristic molecules at each stage of the grafting process. With increasing sputter flux the current surface layers will be damaged and partly removed. Due to the sensitivity of the molecules on the sputter process the yield of complex molecules should decrease in more elevated manner. The results are summarized in Fig. 15.

Bromosilane wafer: With increasing sputter flux the bromine monomer and dimer peak intensities decrease whereas the silicon-cluster intensity increases at low flux and saturate above 10^{14} P.I./cm^2. Unspecific peak intensities, e.g. of H^- and C_2H^- show a maximum at about 0.5 x 10^{14} P.I./cm^2. With the removal of Br the underlying carbon hydrogen chain is exposed to the beam and results in an intermediate increase in short carbon chain fragments. At higher flux most of the spot area is damaged and the number of available chain fragments decreases. As the slope of Br^- and C_2H^- is nearly the same above 0.5 x 10^{14} P.I./cm^2 the source of CH_2^- fragments is coupled to the removal of Br from the uppermost surface.

Nitrobenzoyl wafer: There is a very steep decrease of the specific nitrobenzoyl species NO_2^- and $C_6H_4NO_2^-$ at low flux. This reflects the damage and removal of the uppermost part of the grafting molecule.

Aminobenzoyl wafer: The intensity of aminobenzoyl specific fragments decreases rapidly with increasing flux up to 0.5 x 10^{14} P.I./cm^2. This decrease in intensity suggests that these are fragments of the grafting molecule and not a series like $(SiO_2)_m(CH_2)_n^-$ which should behave like SiO_2H^-.

Humic wafer: Again the intensity of aminobenzoyl specific fragments decreases rapidly with increasing flux up to 0.5x10^{14} P.I./cm^2. All selected peak intensities decrease slightly with increasing flux reflecting the damage and removal of the humic acid layer on top of the grafting molecules.

<Summary of TOF-SIMS results>

The negative TOF-SIMS spectra change with every grafting step showing the modification of the surface in expectation with the applied chemical modification. The surfaces are homogenously covered and closed. The complexity of the spectra increases with the aminobenzoyl wafer. The immobilization of humic acid results in a peak forest characteristic for the numerous fragments generated by humic acids.

AFM results

AFM Topometrix Explorer

<Silicon wafer>

The surface is relatively smooth with an average roughness (RMS) of 0.33 nm (Fig. 16). Typical height differences measured in a line scan (not shown) are in the range of <1 nm. The maximum height range is 3.96 nm due to the contamination of the surface with a few particles. To our knowledge, the observed surface structure is typical for an oxidized Si-surface.

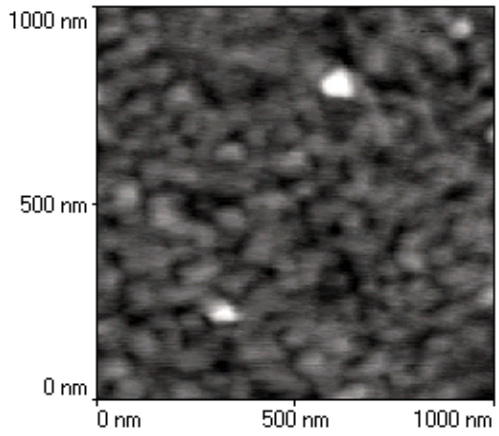

Fig.16: AFM of oxidized silicon wafer (topography)

<Bromosilane wafer>

Topographical (17a,c) and phase contrast (17b,d) images of the surface at two magnifications (scan size 1000 nm, 500 nm) can be seen on Fig. 17a,c and 17b,d, respectively. Darker color in the phase images indicates stronger tip-sample interactions. The average roughness (RMS) of the surface is in the range of 0.47 nm and thus slightly increased compared with step 1. The maximum range in image (a) is 9.3 nm due to a larger particle. Typical height differences measured in a line scan (not shown) are in the range of <1 nm. The surface structure can be described as "network-like" as we better see in the 500 nm-images. We also see a phase-contrast pattern, partly corresponding with the topography pattern. This means that tip-sample interactions slightly vary between dark and light regions in the phase image (d). This may be an indication that the surface modification is not fully homogeneous (light color might indicate interaction with hydrophobic bromoalkyl silane, dark color with the hydrophilic Si-wafer or not fully covered regions, but this is only an assumption). This silanization step is more successful than the immobilization with 3-glycidoxypropyltrimethoxysilane, where we found granular structures with height differences of 10-40 nm.

<Alcohol wafer>

Roughness (RMS) markedly increases to 2 nm (Fig. 18). Typical height differences of the major part of the surface are in the range between 2-4 nm. Maximum height differences are in

the range of 25 nm due to particulate structures onto the surface. In the bottom of the right image we see a larger region with particles. The marked increase of surface roughness might be due to formation of Si-O-Si-networks. The particulate structures on top of the functionalized surface might originate from the hydroxylation reagent (there is some indication from phase contrast images) and in particular could come from HgO residues.

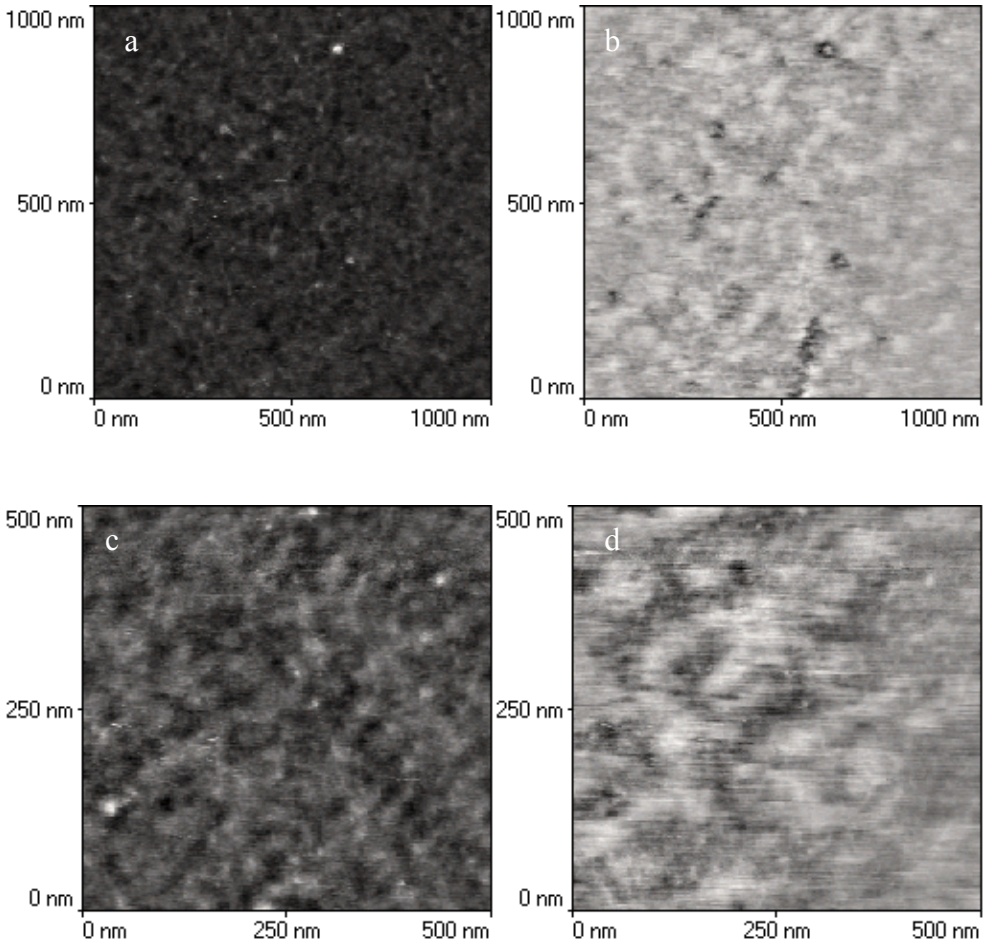

Fig. 17: Topographical phases (Figures a and c) and contrast images (Figures b and d) by AFM of silica wafer after silanization.

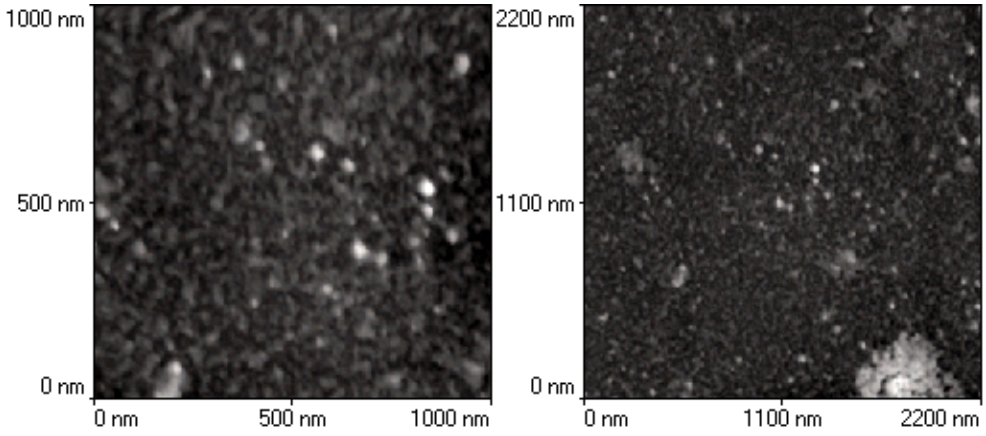

Fig.18: Topographical phases at two resolutions (left and right) by AFM of alcohol wafers after solvolyse of bromosilane wafer.

<Nitrobenzoyl wafer>

In the 2.2 μm images the roughness (RMS) slightly decreases to 1.6 nm (compared with step 3), the maximum height range is 19.8 nm (again due to some particulate structures) (Fig. 19). The surface structure appears more homogeneous than in the last step probably due to the removal of particulate contaminations. The structure again appears as a surface network.

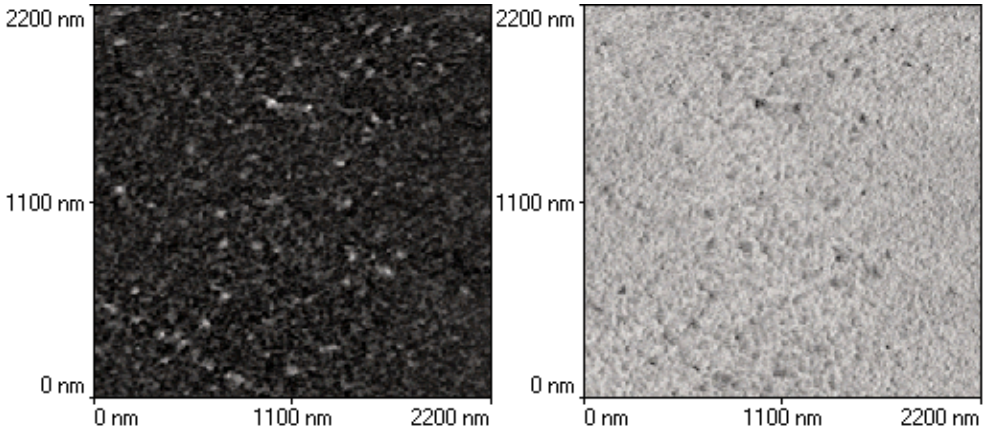

Fig.19: Topographical phases (left) and contrast images (right) of nitrobenzoyl wafers by AFM of wafers after reaction with p-nitrobenzoylchloride.

<Aminobenzoyl wafer>

Roughness (RMS) drastically increases to 2.9 nm (compared with step 4), the maximum height range is 25 nm (Fig. 20). The surface morphology markedly changes towards a granular structure. Surface coverage with this material seems to be relatively complete. It seems that the reduction step is relatively drastic.

<Humic wafer>

Going from step 5 to step 7 no principal change in surface topography is observed (Fig. 21). In step 7 the surface structure appears "smeared" which might indicate humic acid surface binding. This might also come from the contamination of the tip with attached humic acid that would reduce the image resolution. As these are the essential steps for humic acid surface binding, these steps are investigated with our new DI-AFM, presumably providing better image resolution (below).

<DI-AFM>

Again, there is no principal structural change going from step 5 to step 7 (Fig. 22). On top of the grains in step 7 some fine structure is seen that may indicate humic acid molecules. The roughness (RMS) slightly increases from 2.6 nm (step 5) to 3.0 nm (step 7).

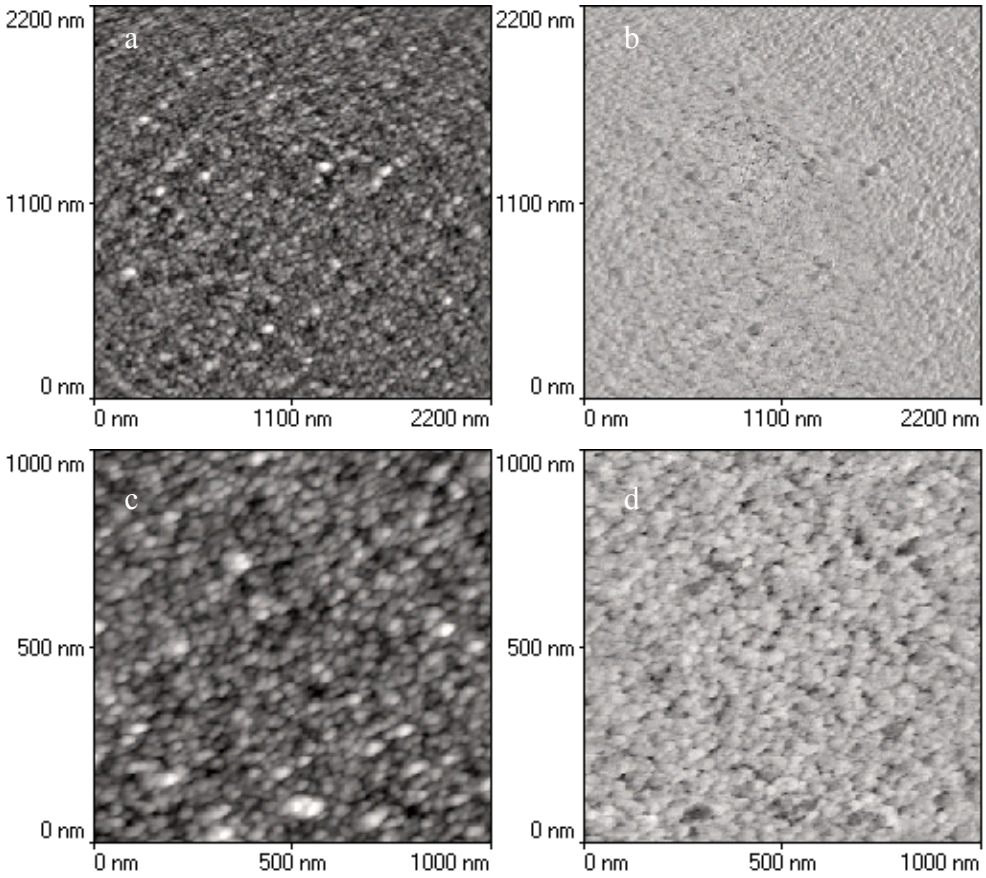

Fig.20: Topographical phases (Figures a and c) and contrast images (Figures b and d) by AFM of nitrobenzoyl wafer after reduction of the amino group.

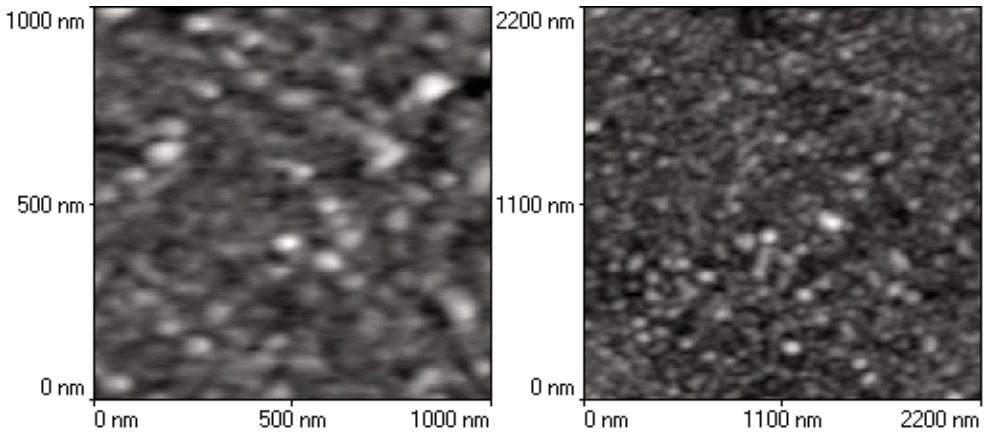

Fig.21: Topographical phases at two resolutions (left and right) by AFM of humic wafers after reaction with the diazonium spacer.

<Summary of AFM measurements>

From AFM analysis it can be conclude, that the functionalized surface is characterized by a granular morphology. The surface morphology appears more homogeneous than in the approach with 3-GPTMS (i.e., step 2). Generally, surface roughness increases from step 2 to step 7. An explanation for this observation may be the slow polymerization of the chlorosilane

compared with alkoxysilanes which is ongoing after step 2. The surface structures change in the different experimental steps from a "network-like" (step 2) towards a granular (or particular) morphology (step 5). Particle diameters do not vary significantly between step 5 and 7 and thus adsorbed or covalently bound humic acid molecules are not distinguishable from the granular surface. Therefore, a binding of humic acid to the functionalized surface cannot be confirmed.

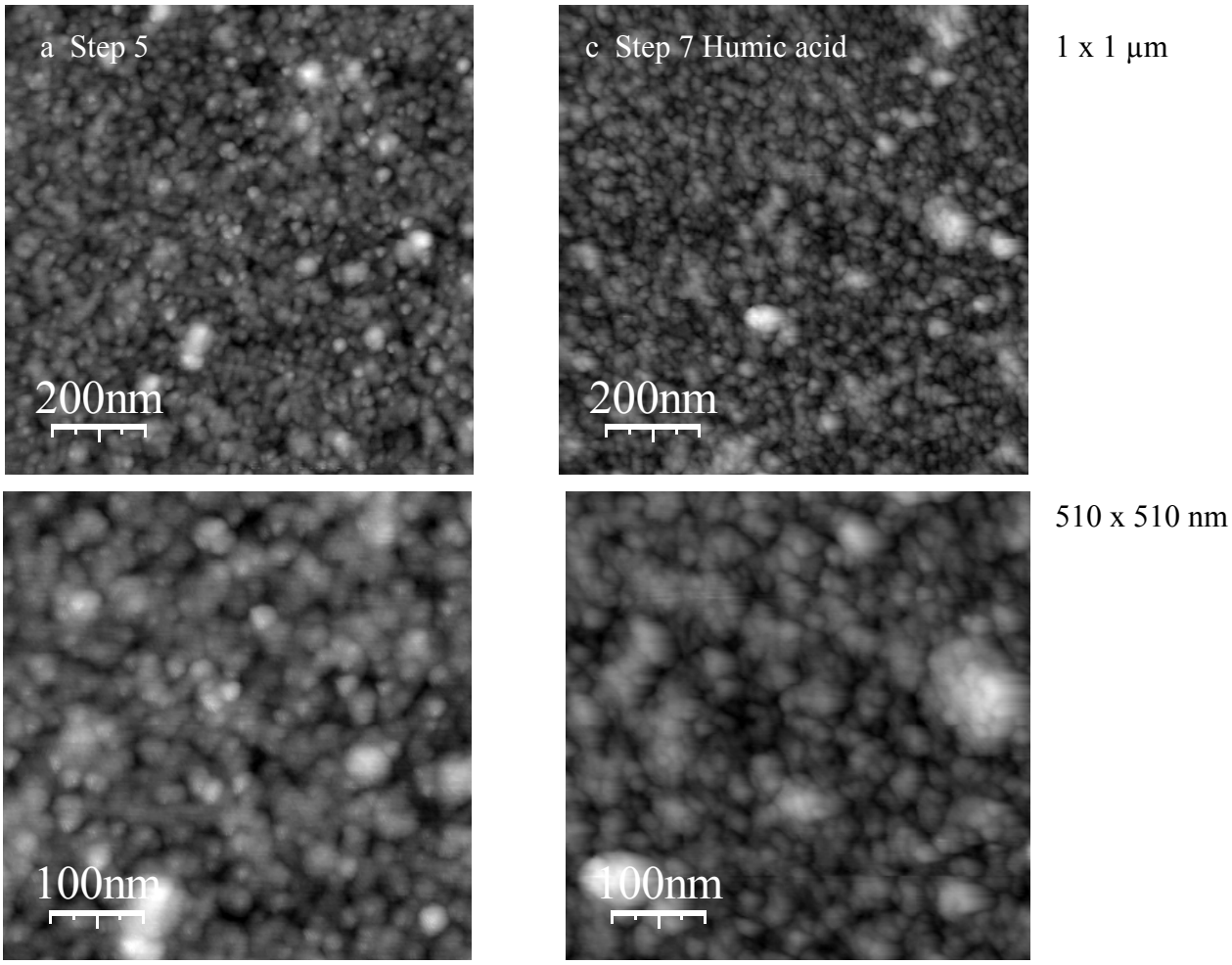

Fig. 22:Topographical phases at two different resolutions of silicon wafers before (left) and after (right) reaction with humic acids by DI-AFM.

Brief discussion

For generation of self-assembled monolayers it is important to control mainly three parameters, namely (i) silane chain length, (ii) reaction time, and (iii) temperature. A chain length of 11 carbon silanes was chosen in order to provide sufficient freedom to the terminal functional group to react in a sterically unhindered fashion maintaining enough interaction energy between the chains to ensure a strong adsorption as noted by Bierbaum et al. (1995) and Brzoska et al. (1994). Reaction time for bromosilane grafting on silicon wafer was fixed to 3 hours to efficiently cover the surface in order to prevent aggregates at the surface, as is the

case with longer reaction time. The optimal temperature depends on the chain length and varies from 0°C for n= 10 to 38°C for n=22, with a Tc shift of 3.5 ± 0.5 °C per additional methylene groups (Brzoska et al. 1994). For a chain length of 11 methylene groups, as used in this work, the optimal temperature is 4 °C. Consequently, this temperature was used in the present work. In the next step, displacement of bromide by hydroxide, mercury-assisted solvolyse was used. By this method, the bromine from 16-bromohexadecylsiloxane monolayers was basically quantitatively removed. Contact angle decreased due to displacement of bromine by more polar groups and Br quantification by TOF-SIMS both verify the success in this process step. Thereafter, alcohol-terminated SAMs reacted with p-nitrobenzoylchloride to introduce a benzene ring. This step is necessary for subsequent immobilization of humic acids by diazotization method. The basis is that arene diazonium is a weak electrophile and is expected to react with highly reactive aromatic compounds (such as phenolic groups or tertiary amines) to give azoic compounds. Therefore, humic acids with its phenolic groups is expected to be bound to the nitrobenzoyl moietie by an azoic coupling. Reaction between arene diazonium cation and phenol occurs rapidly in weakly alkaline solution, where the phenolic functionality is on the form of a phenoxide ion. The phenoxid ion is more reactive with respect to electrophilic substitution than phenol, i.e. the protonated form. Nevertheless, pH must be maintained below 10 in order to prevent the formation of diazohydroxyde or unreactive diazotate (reaction between arene diazonium salt and hydroxide ion).

Surface coverage with humic acid was verified in the final grafting step. A clear evidence for covalent attachment, however, is still pending.

References

ABEL M.-L., DIGBY R.P., FLETCHER I., WATT J.F. (2000a) “Evidence of specific interaction between γ-glycidoxypropyltrimethoxysilane and oxidized aluminum using high-mass resolution TOF-SIMS”, *Surface and interface analysis*, **29**, 115-125.

ABEL M.-L., RATTANA A., WATTS J.F. (2000b) “Theinteraction of γ-glycidoxypropyltrimethoxysilane with oxidised aluminum substrates : the effect of drying temperature”, *Journal of adhesion*, **73**, 313-340.

APPELHANS D., FERSE D., ADLER H.-J.P., PLIETH W., FIKUS A., GRUNDKE K., SCHMITT F.-J., BAYER T., ADOLPHI B. (2000) “Self-assembled monolayers prepared from ω-thiophene-functionalized n-alkyltrichlorosilane on silicon substrates”, *Colloids and surfaces. A: Physicochemical and engineering aspects*, **161**, 203-212.

BALACHANDER N. and SUKENIK C.N. (1990) “Monolayer transformation by nucleophilic substitution: Applications to the creation of new monolayer assemblies”, *Langmuir,* **6**, 1621-1627.

BARBOT C. (2001) “Etude des systèmes organo-minéraux dans leur rapport avec les métaux lourds et les radioéléments, PhD Thesis, Université de Nantes, 9 octobre 2001.

BARBOT C., CZERWINSKI K., BUCKAU G., KIM J.I., MOULIN V., VIAL M., PIERI J., DURAND J.-P., GOUDARD F. (2002) “Characterization of a humic gel synthesized from an activated epoxy silica gel”, *Radiochimica Acta*, **90**, 211-218.

BARBOT C., PIERI J., DURAND J.P., GOUDARD F., PLASCHKE M., BUCKAU G., KIM J.-I., SZYMCZAK W., WOLF M., BOULOUSSA O. (2003) “Characterization of humic wafers by AFM, TOF-SIMS, ATR-FTIR. Development of new synthesis routes”, Annex 7, pp 115-144, *In: Humic substances in performance assessment of nuclear waste disposal: actinide and iodine migration in the far field. First technical progress report*, Editor G. Buckau. FZKA 6800, April 2003.

BIERBAUM K., GRUNZE M. BASKI A.A., CHI L.F., SHREPP W., FUCHS H. (1995a) “Growth of self-assembled n-alkytrichlorosilane films on Si(100) investigated by atomic force microscopy”, *Langmuir*, **11**, 2143-2150.

BIERBAUM K., KINZLER M., WÖLL CH., GRUNZE M., HÄHNER G., HEID S., EFFENBERGER F. (1995b) “A near edge X-ray absorption fine structure spectroscopy and X-ray photoelectron spectroscopy study of the film properties of self-assembled monolayers of organosilanes on oxidized Si(100)”, *Langmuir*, **11**, 512-518.

BRUNNER H., VALLANT T., MAYER U., HOFFMANN H. (1996) “Molecular structure of self-assembled bimolecular films on gold and silicon surfaces studied by external reflection infrared spectroscopy”, *Surface science*, **368**, 279-291.

BRZOSKA J.B., BEN AZOUZ I., RONDELEZ F. (1994) “Silanization of solid substrates: a step toward reproducibility”, *Langmuir*, **10**, 4367-4373.

CZERWINSKI K.R., CEREFICE G.S., BUCKAU G., KIM J.I., MILCENT M.C., BARBOT C., PIERI J. (2000) “Interaction of europium with humic acid covalently bound to silica beads”, *Radiochimica Acta*, **88**, 417-424.

DONG X., PROCTOR A., HERCULES D.M. (1997) “Characterization of poly(dimethylsiloxane)s by time-of-flight secondary ion mass spectrometry”, *Macromolecules*, **30**, 63-70.

FRYXWELL G.E., RIEKE P.C., WOOD L.L., ENGELHARD M.H., WILLIFORD R.E., GRAFF G.L., CAMPBELL A.A., WIACEK R.J., LEE L., HALVERSON A. (1996) “Nucleophilic displacements in mixed self-assembled monolayers”, *Langmuir*, **12**, 5064-5075.

HEISE A., MENZEL H., YIM H., FOSTER M.D., WIERINGA R.H., SCHOUTEN A.J., ERB V., STAMM M. (1997) “Grafting of polypeptides on solid substrates by initiation of N-carboxyanhydride polymerization by amino-terminated self-assembled monolayers”, *Langmuir*, **13**, 723-728.

HALLER I. (1978) “Covalently attached organic monolayers on semiconductor surfaces”, *Journal of the american chemical society*, **100(26)**, 8050-8055.

HOUSSIAU L. and BERTRAND P. (2001) “TOF-SIMS study of organosilane self-assembly on aluminum surfaces”, *Applied surface science*, **175-176**, 351-356.

KIM J.I., RHEE D.S., BUCKAU G., MORGENSTERN A. (1997) “Americium(III)-humate interaction in natural groundwater: Influence of purification on complexation properties”, *Radiochimica acta*, **79**, 173-181.

KURTH D.G. and BEIN T. (1993) “Surface reactions on thin layers of silane coupling agents”, *Langmuir*, **9**, 2965-2973.

LIU A., WU C.H., ESCHENAZI E., PAPADOPOULOS K. (2000) “AFM on humic acid adsorption on mica”, *Colloids and surfaces A: Physicochemical and engineering aspects*, **174**, 245-252.

MITTAL K.L. (Ed.) (1992) “Silane and other coupling agents”, VSP, Utrecht.

MOON J.H., SHIN J.W., KIM S.Y., PARK J.W. (1996) “Formation of uniform aminosilane thin layers: an imine formation to measure relative surface density of the amine group”, *Langmuir*, **12**, 4621-4624.

MOON J.H., KIM J. H., KIM K., KANG T.-H., KIM B., KIM C.-H., HAHN J.H., PARK J.W. (1997) “Absolute surface density of the amine group of the aminosilylated thin layers: ultraviolet-visible spectroscopy, second harmonic generation and synchrotron-radiation photoelectron spectroscopy study”, *Langmuir*, **13**, 4305-4310.

NAVARRE S., CHOPLIN F., BOUSBAA J., BENNETAU B., NONY L., AIME J.-P. (2001) “Structural characterization of self-assembled monolayers of organosilanes chemically bonded onto silica wafers by dynamical force microscopy”, *Langmuir*, **17**, 4844-4850.

O’TOOLE L., SHORT R.D., BOTTINO F.A., POLLICINO A., RECCA A. (1992) “The surface photo-oxidation of polystyrene: Part I-The application of TOF-SIMS to monitor changes in polymer chain length”, *Polymer degradation and stability*, **38**, 147-154.

PLASCHKE M., RÖMER J., KLENZE R., KIM J.I. (1999) “In situ AFM study of sorbed humic acid colloids at different pH”, *Colloids and surfaces A: Physicochemical and engineering aspects*, **160**, 269-279

PLASCHKE M., ROTHE J., SCHÄFER Th., DENECKE M., DARDENNE K., POMPE S., HEISE K.-H. (2002) “Combined AFM and STXM in situ study of the influence of Eu(III) on the agglomeration of humic acid”, *Colloids and surfaces A: Physicochemical and engineering aspects*, **197**, 245-256.

POLEUNIS C., COMPERE C., BERTRAND P. (2002) “Time-of-flight secondary ion mass spectrometry: Characterization of stainless steel surfaces immersed in natural seawater”, *Journal of microbiological methods*, **48**, 195-205.

QUINTON J.S. and DASTOOR P.C. (2000) “Conformational dynamics of γ-APS on the iron oxide surface: an adsorption kinetic study using XPS and TOF-SIMS”, *Surface and interface analysis*, **30**, 21-24.

RATTANA A., HERMES J.D., ABEL M.L., WATTS J.F. (2002) “The interaction of a commercial dry film adhesive with aluminum and organosilane treated aluminum surfaces: a study by XPS and TOF-SIMS”, *International Journal of Adhesion and Adhesives*, **22**, 205-218.

SNELLING R.E. and MOTTOLA A. (1987) “On/Off chemical determination of reactive amino groups immobilized on silica surfaces”, *Analytica chimica acta*, **200**, 503-514.

SZABÓ G., FARKAS G., BULMAN R.A. (1992) “Evaluation of silica-humate and alumina-humate HPLC stationary phases for estimation of the adsorption coefficient, Koc, of soil for some aromatics”, *Chemosphere*, **24**, 403-412.

VAN OOIJ W.J. and SABATA A. (1991) “Characterization of films of organofunctional silanes by TOF-SIMS and XPS. Part I. Films of N-[2-(vinylbenzylamino)-ethyl]-3-aminopropyltrimethoxysilane on zinc and γ-aminopropyltriethoxysilane on steel substrates”, *Journal of adhesion science technology*, **5(10)**, 843-863.

VAN OOIJ W.J. and SABATA A. (1993) “Characterization of films of organofunctional silanes by TOF-SIMS. Part II. Films of γ-APS, AEAPS and FPS on cold-rolled steel and cold-rolled zinc substrates”, *Surface and interface analysis*, **20**, 475-484.

WANG D. and JONES F.R. (1993) “TOF-SIMS and XPS studies of the interaction of silanes and matrix resins with glass surfaces”, *Surface and interface analysis*, **20**, 457-467.

WASSERMAN S.R., TAO Y.-T., WHITESIDES G.M. (1989) “Structure and reactivity of alkylsiloxane monolayers formed by reaction of alkyltrichlorosilanes on silicon substrates”, *Langmuir*, **5**, 1074-1087.

WU B., GUANGZHAO M., Ng K.Y.S. (1997) “Stepwise adsorption of a long trichlorosilane and a short aminosilane”, *Colloids and surfaces. A: physicochemical and engineering aspects*, **162**, 203-213.

ANNEX

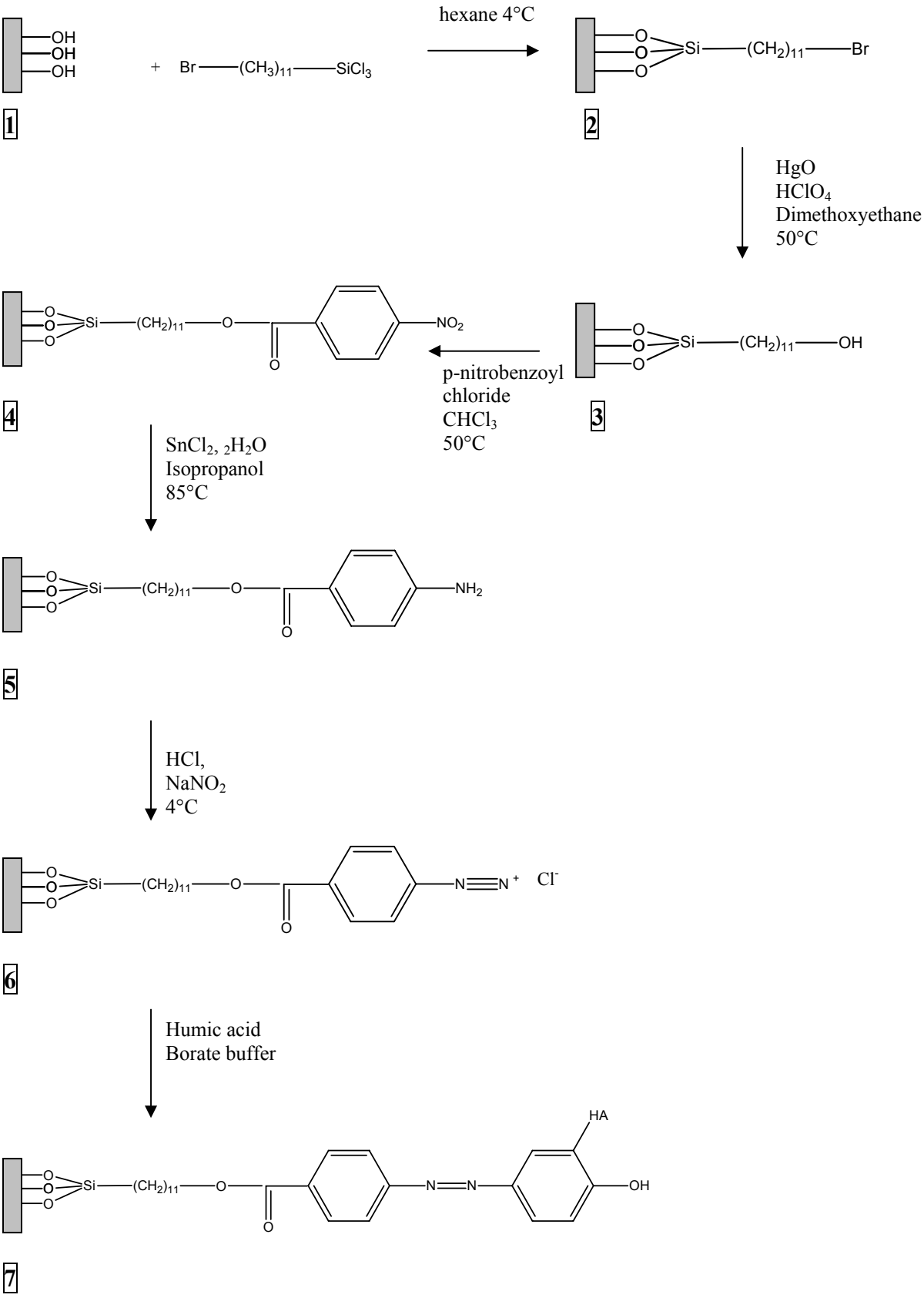

Scheme1: The different steps of humic acids immobilization on silicon wafers

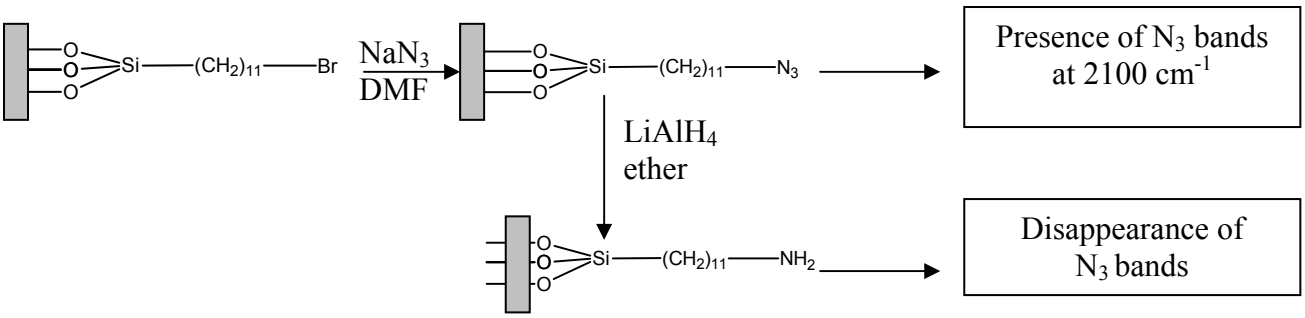

Scheme 2: Reaction steps involving the transformation of bromosilane immobilized on silicon wafer to prove its existence by ATR-FTIR.

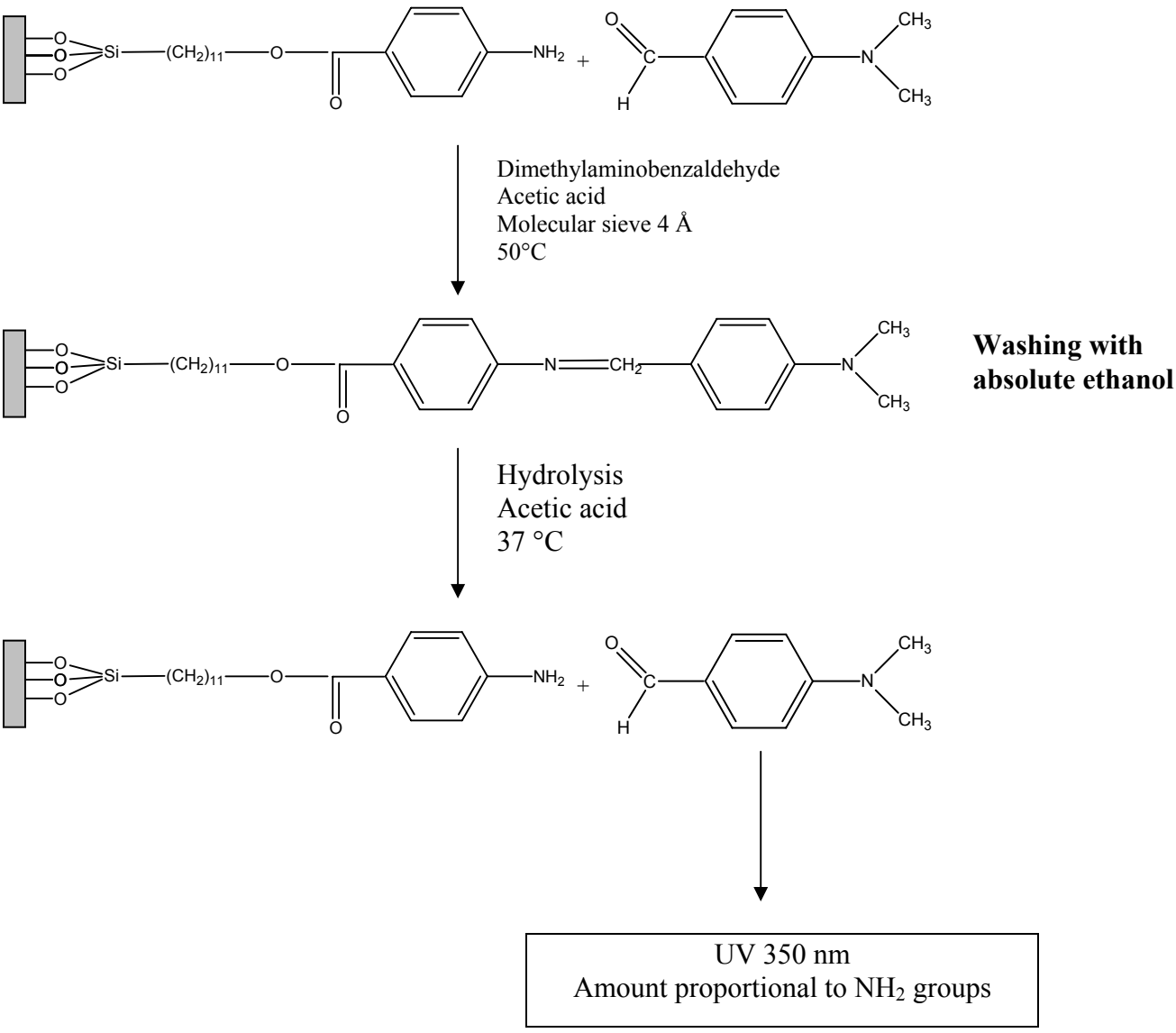

Scheme 3: Quantification of the NH_2 groups immobilized on silicon wafers.

Annex 14

Determination of Chemical Parameters for the Schlema-Alberoda Uranium Tailings Pile Migration Case Study

N. Bryan [1] , D. Vopalka [2], P. Benes [2], K. Stamberg [2], K. Doubravova [2]

[1] University of Manchester, Manchester, U.K.

[2] Czech Technical University, Prague, Czech Republic

Determination of Chemical Parameters for the Schlema-Alberoda Uranium Tailings Pile Migration Case Study.

N. Bryan
University of Manchester, Manchester, U.K.

D. Vopalka, P. Benes, K. Stamberg, K. Doubravova
Czech Technical University, Prague, Czech Republic.

Introduction

A central aim of environmental chemistry is to develop an understanding of processes at the microscopic level, and to develop speciation models to simulate that behaviour, which may be used with transport codes to predict the fate of pollutants on the field scale. In fact, one objective of this HUPA project is to develop a coupled chemical transport computer code, which includes the effects of humic substances, and then apply it to three field scale test cases:

1. a deep hypothetical repository in a salt formation;
2. a shallow, sandy hypothetical repository;
3. a large pile of uranium mine tailings.

This work concerns the third case study (U-tailings), which is based upon a real U-tailings pile at Schlema-Alberoda, near Dresden, Saxony, Germany.

Environmental problems are inherently complex, and even apparently simple systems, such as a single metal ion interacting with a 'single' surface may be extremely complex. There have been considerable advances in computing power over the last few decades, unfortunately, in order to make calculations solvable in a reasonable time, the models used to simulate the chemistry of the system must be as simple as possible. The interaction between uranium and humic substances has been studied previously (e.g. Czerwinski et al 1994). However, the details of the interaction of uranyl cations with the material of the pile have not been modelled. Therefore, the objective here is to develop a simple model of this interaction, ready to use in the migration case study. Experiments were performed at the Czech Technical University, Prague and the data modelled at the University of Manchester.

Background Speciation

The seepage water that permeates the tailings pile contains concentrations of simple inorganic species, in addition to uranium and humic materials. The experiments were performed in simulated Schlema-Alberoda Water (SAW, Table 1), which contains the major components. Therefore, their effect has been taken into account.

Table 1: Composition of simulated Schlema-Alberoda Water, SAW.

Component	Concentration mol dm^{-3}
$MgSO_4$	0.0175
$CaSO_4$	0.0091
$NaHCO_3$	0.00258

Speciation calculations were performed using PHREEQE97 (developed as part of the previous E.U. HUMICS project for the UK Environment Agency) with the CHEMVAL VI database; the results are shown in Table 2. There are a number of species that have significant concentrations, in addition to the free uranyl itself. One approach would be to include all of these simple inorganic species 'explicitly' using the relevant CHEMVAL equilibrium constants. However, this would make the transport calculations prohibitively long. However,

given that the simple inorganic species have large total concentrations compared to uranium, the fractional composition of the solution will be a constant. Therefore, we may treat the effect of this background speciation as constant. Hence, if the experimental data (that include the effects) are fitted without explicitly treating the simple inorganics, then the resulting parameters will include the effect implicitly. If these surface sorption parameters are used to make transport predictions, then the effects of the background speciation will be included, but without making the calculations very 'expensive'. In effect, this approach will treat all of the non-humic, solution phase uranium as $UO_2^{2+}{}_{(aq)}$. Given that the object of the case study is to examine the effect of humic substances, this will be acceptable.

Table 2: Results of PHREEQE97 speciation calculations on SAW, showing the major species.

SPECIES	$[U_{TOTAL}]$ = $9.7x10^{-06}$ mol dm^{-3}
$UO_2^{2+}{}_{(aq)}$	$2.198x10^{-09}$
$(UO_2OH)^{+}{}_{(aq)}$	$2.387x10^{-08}$
$(UO_2(OH)_2)_{(aq)}$	$5.299x10^{-07}$
$(UO_2(OH)_3)^{-}{}_{(aq)}$	$2.614x10^{-09}$
$(UO_2CO_3)_{(aq)}$	$9.154x10^{-07}$
$(UO_2(CO_3)_2)^{2-}{}_{(aq)}$	$7.446x10^{-06}$
$(UO_2(CO_3)_3)^{4-}{}_{(aq)}$	$7.636x10^{-07}$
$(UO_2SO_4)_{(aq)}$	$1.314x10^{-08}$
$(UO_2(SO_4)_2)^{2-}{}_{(aq)}$	$2.819x10^{-09}$

Experimental Details

Both experiments were performed using solid material from the Schlema-Alberoda Uranium Tailings pile. Both Equilibrium and time-series (kinetic) experiments have been considered here. Uranium solutions, mixtures of $^{235/238}U$ and ^{233}U tracer, of various concentrations were added to samples of Schlema-Alberoda material at various solution volume to mass ratios (V/M). However, there is also uranium already associated with the solid phase. Experiments have shown that the amount of this available/exchangeable uranium is about $1x10^{-4}$ mol kg^{-1}, and this must be taken into account during the modelling. In the description below, unless otherwise stated, 'total uranium' or 'U_T' refers only to the uranium added in the solutions during the experiments, and excludes that already associated with the solid.

Equilibrium Model

The equilbrium uptake of uranium after 335 hours equilibration time on Schlema-Alberoda Material, SAM, from the tailings pile was measured as a function of solid to solution volume ratio (V/M). The data for V/M = 20 ml g^{-1} are shown in Table 3.

Table 3: Equilibrium uptake data for V/M = 20 ml g^{-1} (%age uptake as a function of added uranium conentration).

$[U_{TOTAL}]$ (mol dm^{-3})	$1.1x10^{-06}$	$2.82\ x10^{-06}$	$4.54\ x10^{-06}$	$6.26\ x10^{-06}$	$7.98\ x10^{-06}$
Uptake (%)	51.1	48.7	45.25	44.65	44.3

The simplest equilibrium approach is to use a single equilibrium constant, K,

$$K = \frac{[MS]}{[M].[S]} \qquad (1)$$

where [M], [S] and [MS] are the concentrations of free metal ion, free surface binding sites and metal ion bound to surface sites, respectively. If $[S_T]$ is the total surface site concentration, free and occupied,

$[S_T] = [S] + [MS]$

then equation 1 may be rearranged to give,

$$\frac{1}{[MS]} = \left(\frac{1}{K[S_T]}\right)\frac{1}{[M]} + \frac{1}{[S_T]} \qquad (2)$$

and hence, if this is a suitable model, then a plot of (1/[MS]) vs (1/[M]) will be a straight line, with intercept ($1/[S_T]$) and slope ($1/K[S_T]$). Figure 1 shows this plot for the experimental data given in Table 3. Note: during these calculations, the total amount of metal ion that must be considered is the sum of that added in the solution **plus** the exchangeable uranium already associated with the solid, since at equilibrium, the two sources of uranium will be equally distributed in solution and on the solid. Clearly, the simple model simulates the behaviour adequately, for this data set at least. Linear regression provides values of $[S_T] = 1.20 \times 10^{-5}$ mol dm^{-3} and $K = 1.16 \times 10^5$ dm^3 mol^{-1}. Given that V/M = 20 ml g^{-1}, the site concentration of the solid is 2.38×10^{-7} mol g^{-1}. The values calculated at V/M = 20 ml g^{-1} and an equilibration time of 336 hours were compared with other data at different V/M and times. The site concentration, $[S_T]$ was calculated for each system using the value obtained at V/M = 20 ml g^{-}

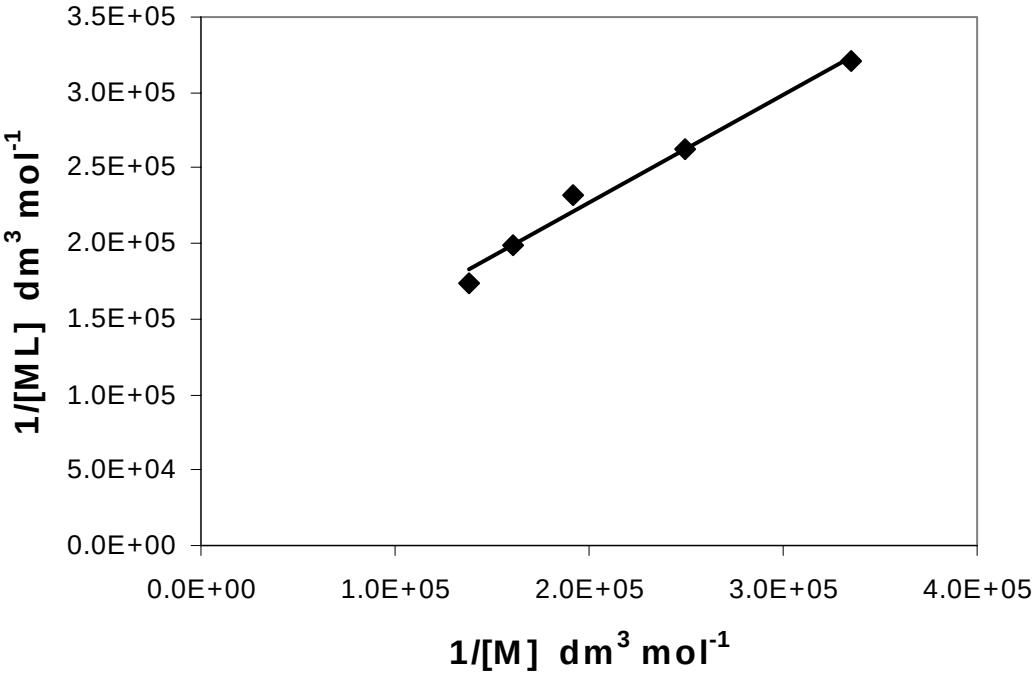

[1], and new values of K calculated. The results are shown in Table 4.

Figure 1: Plot of (1/[MS]) vs (1/[M]) for the experimental data in Table 3, V/M = 20 ml g^{-1}. For each point, the total uranium is the sum of that added in the solution plus the exchangeable uranium already associated with the solid.

Table 4: experimental data and calculated values of K.

Conditions	Equilibration time hr	Experimental uptake (%)	[MS] mol dm^{-3}	[M] mol dm^{-3}	[S] mol dm^{-3}	K dm^3 mol^{-1}
V/M = 10 mg dm^{-3}, $[U_{TOTAL}]$ =3.3x10^{-7} mol dm^{-3}	48	52.7	5.44E-06	4.89E-06	1.86E-05	5.98E+04
	168	59.4	6.13E-06	4.19E-06	1.79E-05	8.16E+04
V/M = 10 mg dm^{-3}, $[U_{TOTAL}]$ = 9.7x10^{-6} mol dm^{-3}	48	47.7	9.40E-06	1.03E-05	1.47E-05	6.22E+04
	168	51.1	1.01E-05	9.63E-06	1.40E-05	7.46E+04

The variation in the value of K, from 5.98x10^4 to 1.16x10^5 dm^3 mol^{-1} may seem large, but given the complexity of the system and the necessary simplicity of the model, this sort of variation is to be expected. In fact, the data in Table 4 give a clue to the origin of the discrepancy: the values of K increase with time (48 and 168 hours) for the V/M = 10 ml g^{-1} systems, and the highest value, obtained at V/M = 20 ml g^{-1}, corresponds to an equilibration time of 336 hours. This suggests that the 48 and 168 hour data may not repesent a fully equilibrated system, and there are slow processes operating here.

Kinetic Model

A series of kinetic uptake experiments measured the sorption of uranyl as a function of exposure time (Table 5). These data were used to formulate a second, mixed equilibrium and kinetic description of the system.

Table 5: Experimental kinetic data, uranium sorbed onto the SAM surface as a function of time, which were used in formulation of the kinetic model. The sorbed concentrations correspond only to the uranium added in the solution, excluding the exchangeable solid phase uranium, although this uranium was taken into account in the calculations. All V/M have units of ml g^{-1} and all concentrations, mol dm^{-3}

Time (hr)	V/M = 10 $[U_T]$ = 9.7x10^{-6}	V/M = 100 $[U_T]$ = 9.7 x10^{-6}	V/M = 44.8 $[U_T]$ = 9.7 x10^{-6}	V/M = 20 $[U_T]$ = 9.7 x10^{-6}	V/m=44.8 $[U_T]$ = 3.3 x10^{-7}	V/m=10 $[U_T]$ = 3.3 x10^{-7}
1	3.07x10^{-06}	5.51x10^{-07}	1.02x10^{-06}	1.82x10^{-06}	5.89x10^{-08}	1.42x10^{-07}
2	3.53x10^{-06}	5.95x10^{-07}	1.3x10^{-06}	2.05x10^{-06}	6.77x10^{-08}	1.45x10^{-07}
4	3.65x10^{-06}	6.23x10^{-07}	1.39x10^{-06}	2.16x10^{-06}	6.68x10^{-08}	1.49x10^{-07}
24	4.1x10^{-06}	9.8x10^{-07}	1.48x10^{-06}	2.94x10^{-06}	8.05x10^{-08}	1.52x10^{-07}
96	4.89x10^{-06}	1.11x10^{-06}	1.93x10^{-06}	3.59x10^{-06}	8.98x10^{-08}	1.85x10^{-07}
168	5.49x10^{-06}	1.21x10^{-06}	2.32x10^{-06}	3.62x10^{-06}	9.41x10^{-08}	1.94x10^{-07}
336	5.92x10^{-06}	1.36x10^{-06}	2.17x10^{-06}	4.48x10^{-06}	1.16x10^{-07}	1.88x10^{-07}

Inspection of the data reveals that there must be at least two components, one fast and another slower. The transport code that will be used to make the migration case study predictions, k1D, is able to cope with mixed systems of equilibria and rate equations. Therefore, a simple two reaction mixed model was used to fit the kinetic data.

The fast component was simulated using a simple equilibrium approach, i.e.

$$M + S \Leftrightarrow MS_{FAST}$$

Where M and S are the free metal ion and surface site, and MS_{FAST} represents the concentration of metal bound in this 'fast' fraction. The concentration of MS_{FAST} is calculated using a simple equilibrium constant, K_{FAST},

$$K_{FAST} = \frac{[MS_{FAST}]}{[M][S]}$$

The more slowly sorbing component was simulated with a simple, first order kinetic approach, i.e.

$$M + S \rightleftarrows MS_{SLOW}$$

where MS_{SLOW} respresents the 'slow' fraction. The change in the concentration of MS_{SLOW} with time is caculated using two first order rate constants, k_f and k_b,

$$\frac{d[MS_{SLOW}]}{dt} = k_f[M][S] - k_b[MS_{SLOW}]$$

For mathematical simplicity, the same surface site has been used for both fractions. In reality, they may be very different. However, this one surface site, two fraction approach is able to simulate the data adequately. The value of $[S_T]$ is not well defined by the kinetic data, since equilibrium has not yet been reached, but the data were consistent with the same value as for the simpler, equilibrium model, 2.38e-07 mol/g, and this value was used here. The values of k_f and k_b were obtained first, by fitting of the raw data. Data at the lowest added uranium concentration (3.3e-07 mol dm^{-3}) were not used during the fitting of the parameters, because in these systems the amount of added uranium is small compared to that already associated with the solid, and hence, might be more prone to error. However, once the fitting was completed, the model was used to simulate all the systems, to test its range of validity. Figure 2 shows the experimental data for the $[U_T]$ = 9.7x10^{-6} mol dm^{-3}, V/M = 10 ml g^{-1} system plotted as the natural log of the percentage of free added metal left in solution vs time. If there were only a single, slow reaction, then this plot would be a straight line. However, the presence of at least one fast component results in a curve, especially at short times. However, it was found that at longer times, the data could be fitted with a straight line.

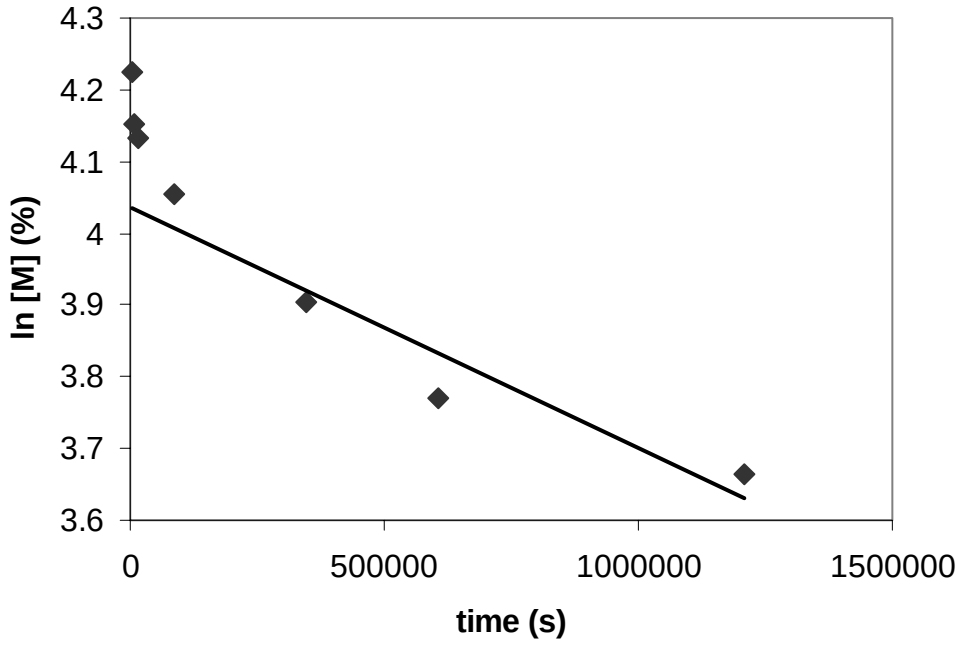

Figure 2: Experimental data (points) and model fit to longer time data (line) for $[U_T]$ = 9.7x10^{-6} mol dm^{-3}, V/M = 10 ml g^{-1} system

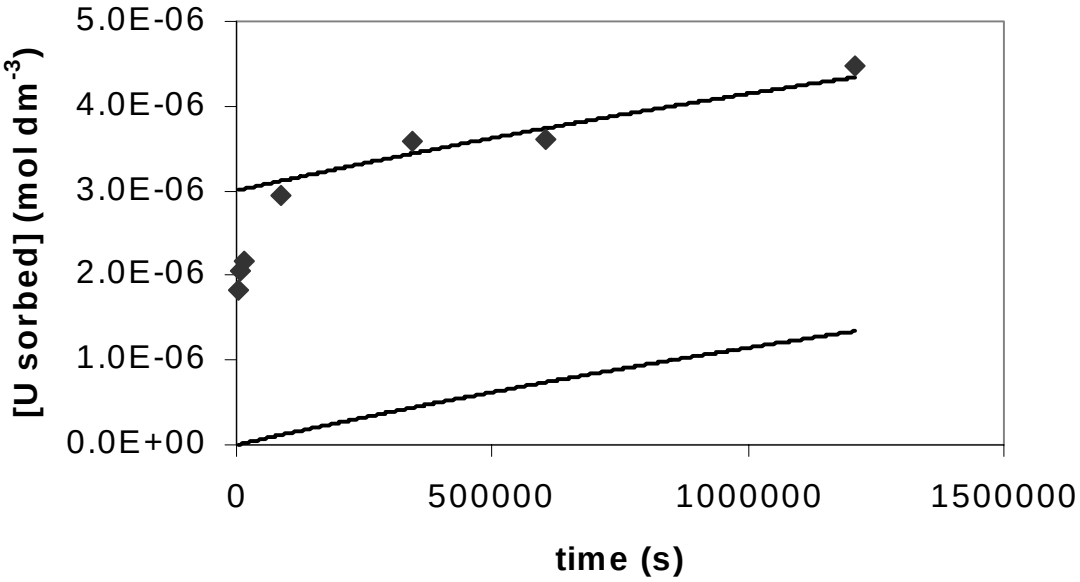

Figure 3: Experimental data (points) and model fit to longer time data (lines) for $[U_T] = 9.7x10^{-6}$ mol dm^{-3}, V/M = 20 ml g^{-1} system.

One set of constants were able to simulate all of the longer time data: $k_f = 2x10^{-2}$ mol^{-1} dm^3 s^{-1}; $k_b = 1x10^{-7}$ s^{-1}. During all of the model calculations, the starting point, time=0, condition was that all of the added uranium was free in solution, and all the solid phase derived, exchangeable uranium was sorbed on the surface. Using a series of time steps, and the equations given above, these two sources of uranium sorb and desorb, respectively. In all the figures that follow, the $[U_{sorbed}]$ concentrations correspond to the sorbed uranium from the initial solution only, excluding the initial, exchangeable uranium, although this fraction was taken into account during the calculations. Figures 3 and 4 show the fit obtained with these values of k_f and k_b for two other systems, this time the data are plotted as the concentration of (added) uranium sorbed vs time. Two model lines are plotted, the lower one represents the model predicted concentration of (added) U in the slow fraction, and the upper line represents the same data plus some arbitrary constant offset, to allow comparison of the fit with the long time data. In both cases, the fit is good, even in the case of the low uranium concentration ($3.3x10^{-7}$ mol dm^{-3}) system (Figure 4), which was not used during the fitting. Hence, the model appears to work for all of the uranium concentrations.

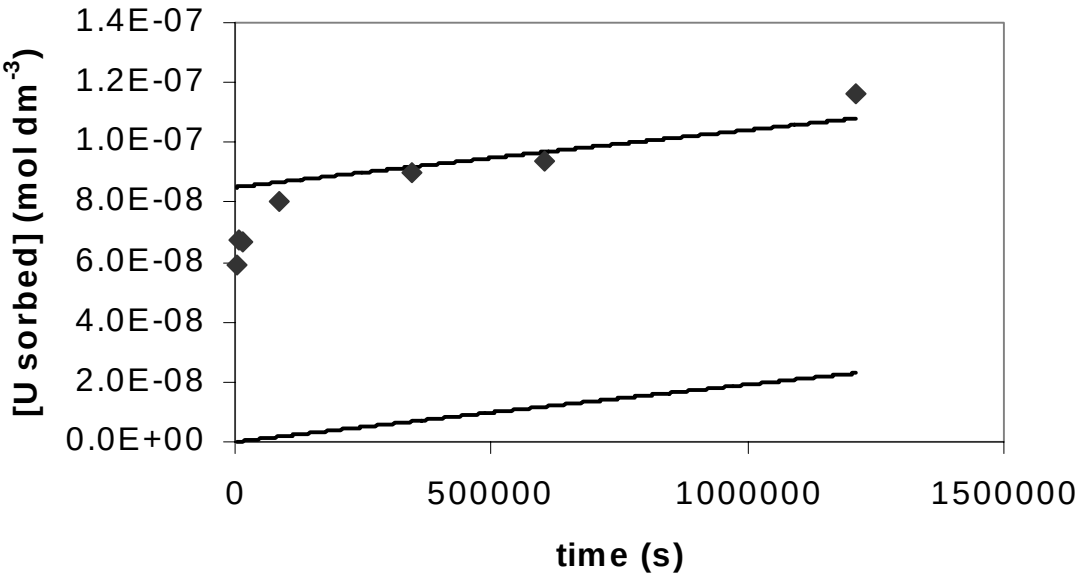

Figure 4: Experimental data (points) and model fit to longer time data (lines) for $[U_T] = 3.3x10^{-7}$ mol dm^{-3}, V/M = 44.8 ml g^{-1} system.

The arbitrary vertical offsets in Figures 3 and 4 represent the fast fraction, MS_{FAST}. It was found by a process of trial and error that an equilibrium constant, K_{FAST}, of $1.42x10^5$ dm^3 mol^{-1} gave the best fit to the data. Finally, the values of K_{FAST}, k_f and k_b were used together to produce an overall model fit to the experimental data (Figure 5). Given the inherent complexity of this system, the fit between model and experiment is good.

Conclusions

The two reaction kinetic model will be used to describe the interaction of the uranyl with the tailings material for the Schlema-Alberoda migration case study. Two components have been defined, one represented as an instantaneous equilibrium process and the other as a first order kinetic process. This is the simplest possible description of a very complex system. Certainly, the data do suggest that there are intermediate fractions between the fast and slow fractions defined in the model (see curve in plot at short times in Figure 2). However, the model is sufficient for the purposes of the transport calculations, since it is able to simulate the system adequately for reaction times in excess of 24 hours, and the transport calculations consider time periods of years.

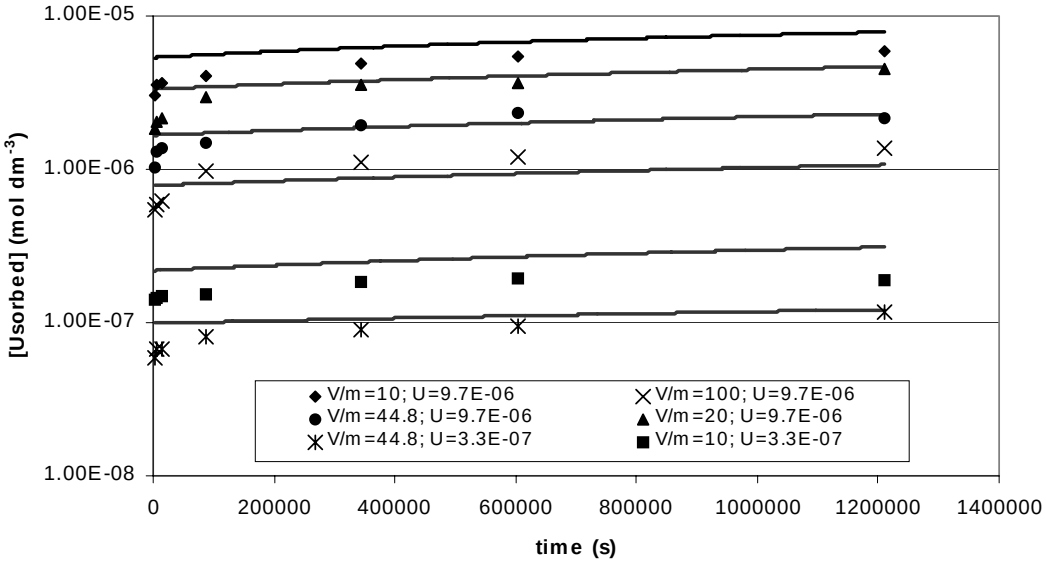

Figure 5: Experimental data (points) and model fit (lines) for kinetic data: all V/M have units of ml $g^{-1}$and all concentrations, mol dm^{-3}; sorbed concentrations expressed as effective solution concentrations (mol dm^{-3}).

To summarise, the following reactions, equations and parameters will be used in the migration case study:

Fast component

$$M + S \Leftrightarrow MS_{FAST}$$

$$K_{FAST} = \frac{[MS_{FAST}]}{[M].[S]} = 1.42x10^{5}\ dm^{3}\ mol^{-1}$$

Slow component

$$M + S \rightleftarrows MS_{SLOW}$$

$$\frac{d[MS_{SLOW}]}{dt} = k_f[M][S] - k_b[MS_{SLOW}]$$

$k_f = 2x10^{-2}$ mol^{-1} dm^3 s^{-1}; $k_b = 1x10^{-7}$ s^{-1}.

There will be a single surface site for both components, $S_T = S + MS_{FAST} + MS_{SLOW} = 2.38x10^{-7}$ mol g^{-1}

Reference

Czerwinski K.R., Buckau G., Scherbaum F., Kim J.I. (1994) Complexation of the uranyl-ion with aquatic humic-acid, *Radiochimica Acta*, 65, 111-119.

Annex 15

Mechanistic Modelling of Humic Substance Aggregation Processes

R.E. Keepax, D.M. Jones, N.D. Bryan

University of Manchester, Manchester, U.K.

Mechanistic Modelling of Humic Substance Aggregation Processes

R.E. Keepax, D.M. Jones, N.D. Bryan
University of Manchester, Manchester, U.K.

Introduction

Humic substances control the biological and chemical availability of many pollutants, and particularly metal ions (Piccolo 2002). Metallic pollutants are amongst the most serious ecological issues; for example, weapons testing and releases from civil programmes have deposited $16x10^{15}$ Bq (≈ 6 tonnes) of Pu into the environment. 'Heavy metal' pollution (e.g. Hg, Cd) is also a serious issue. Because they coordinate metal ions so readily, it has been clear for some time that humic substances can affect transport and bioavailability. However, it has been shown that, as well as binding metals exchangeably, like any simple ligand (e.g. EDTA, citrate), they also have a non-exchangeable binding mode. Initial uptake is into the exchangeable fraction but, over time, a significant proportion is transferred into the non-exchangeable. Transfer between exchangeable and non-exchangeable may be described with first order rate constants. In fact, there is a range of first order rate constants, ranging from instantaneous to very slow, and in particular, there is a clearly defined fraction, at the slow end of the spectrum of rates that may be described with a single first order desorption rate constant (King et al 2001). Metal bound in the exchangeable fraction might be transported with the humic, but will desorb instantaneously, if a sink (e.g. mineral surface) of sufficient affinity or concentration is encountered, i.e. it may be stripped from the humic and immobilised. However, once a metal ion is bound non-exchangeably, then it will remain entrapped within the humic structure, regardless of the affinity of any competing sinks, and will effectively transport with the humic (Keepax et al 2002). In fact, the only controls on the transport of the non-exchangeable metal will be any sorption of the humic itself and the metal ion desorption rate. Transport calculations have shown that the non-exchangeable fraction is the most significant contributor to environmental impact, and that, in many systems, only this fraction will be transported to any significant extent (Keepax et al 2002). Humic kinetics also affect bioavailability. It has been shown that Cu and Pb become less available with time, and Halim et al (2003) have attributed this to the movement of metal ions into ‘inner humic domains’.

Clearly, humic kinetics and non-exchangeable binding are important issues. However, the vast majority of studies have addressed only the exchangeable interaction, and hence, we know more about its origin. Exchangeable binding strength is dependent upon metal ion identity; those of high charge density having the greatest affinity. Bryan et al (2000) have shown that this interaction is driven by the entropy change, which derives from the relaxation of the double layer, and most importantly, the dehydration of the metal ion. In the case of the non-exchangeable interaction, however, the range of first order (sorption/desorption) rate constants is fairly narrow, even for a wide range of solution conditions (Table 1). This behaviour would suggest that the kinetic effect is controlled by some property of the humic itself. Previous studies have identified likely contiguous metal binding sites on humic molecules, and these would appear to be largely bidentate: higher coordination numbers are only likely if there is rearrangement of the skeleton to bring functional groups from other parts of the humic (Bryan et al 1997). The binding sites are thought to be dominated by carboxylic acids, and in the case of copper (II), nitrogen (Jones and Bryan 1998). It seems unlikely that it is the specific, chemical interaction that is responsible for the kinetic effect,

since other polydentate carboxylate ligands, such as EDTA and citrate, do not show this behaviour. Also, the lack of variation in rate constant from metal ion to metal ion would suggest that it not the local interaction between metal ion and humic that is responsible. In fact, the only significant difference between humics and simple ligands is their large size in solution.

Table 1: values of first order desorption rate for some systems (Keepax et al 2002)

Metal Ion (and conditions)	k_b (s^{-1})
Eu(III), pH 4.5	1.2×10^{-6}
Eu(III), pH 6.5	5.0×10^{-7}
Co(II)	1.3×10^{-6}
Am(III)	1.2×10^{-6}

Unfortunately, humic substances are very complex, polydisperse materials (Jones and Bryan 1998). Their molecular weight and size distributions and their conformations are not well understood, and before reliable predictions of humic behaviour will be possible, it is essential to have at least a basic understanding of their structure (Clapp and Hayes 1999, Piccolo 2002). One of the biggest uncertainties (Clapp and Hayes 1999) is the true size of humic molecules: are humics macromolecular, or are they associations of smaller species?

There are two, fairly contradictory conceptual models of humic structure in solution (Clapp and Hayes 1999): (1) Random Coil; (2) Self Association.

The Random Coil Model

Strictly speaking, the Random Coil Model treats the humic as a single contiguous molecular strand, which coils randomly with respect to time and space. This strand carries, along its length, charged and hydrated functional groups. It assumes a conformation, which is roughly spherical in shape and in which the distribution of mass is Gaussian about its centre. The solvent penetrates throughout the structure, and at the periphery exchanges freely with the bulk solvent. The colloid may be tightly or loosely coiled, depending upon several factors: the nature of the solvent; the extent of the solvent penetration; the charge of the colloid; the concentration of counterions; the surrounding pH (Hayes and Swift, 1978; 1990). At neutral to alkaline pH, the charged sites will be dissociated, giving rise to electrostatic repulsion within the colloid. In an attempt to reduce its electrostatic free energy, it will expand (and rearrange). Intramolecular expansion and solvation, together with intermolecular repulsion will keep these species in solution. Increasing I will reduce the repulsion and will lead to contraction. Adding specifically bound metal ions will reduce the magnitude of the charge, and hence, will also lead to contraction, as will protonation at lower pH. The colloid will shrink until the point where all the solvent is expelled and the flexible colloid has shrunk to its most collapsed state. In its original form, the Random Coil approach does treat the humic as a single molecular chain. However, given the complex and chaotic mechanisms of humic formation, it seems unlikely that humic colloids really have a single, contiguous chain (Clapp and Hayes 1999). In fact, Schulton and Schnitzer (1993) have found experimental evidence for significant cross-linking. Hence, it might be more realistic to think of the humic as having

a sponge like structure, which is cross-linked, but is still able to expand and contract to allow penetration by the solvent and small ions. The net effect is a penetrable, gel-like structure (Benedetti et al 1996).

The Self-Association Model

This hypothesis holds that the humic species observed in solution are actually aggregates of smaller monomers (Wershaw 1986, 1993; Piccolo et al 1996; Piccolo 1997; Conte and Piccolo 1999). The 'Self-Association' model (Piccolo 2002) treats humic substances as relatively small, but heterogeneous, molecules that reversibly self-associate into supramolecular aggregates, which are held together by weak interactions, such as van der Waals forces, π-π, CH-π and hydrogen bonds (Buurman et al 2002). Within these associations, the random and heterogeneous nature of the material leads to adjacent hydrophilic and -phobic regions (Buurman et al 2002). Originally, it was proposed that humics form aggregates with micelle-like properties, with hydrophilic parts on the outside and hydrophobic in the interior (Wershaw 1993), but Yates and von Wandruska (1999) have suggested that 'pseudo-micelles' may be formed, i.e. spontaneous aggregates that are not necessarily ordered, but which have hydrophilic and hydrophobic parts. It is likely that the aggregates would be loose and the solvent and small molecules would be able to penetrate in the same way as for a large 'Random Coil' macromolecule, and one can envisage that these associates too could have a penetrable, gel-like structure. The most important difference between the Random Coil and the Self Association models is that in the former the humic species are true, single macromolecules

Evidence

Given the big difference between these models, one might expect that one or the other could easily be ruled out. However, various authors claim evidence for both. A number of techniques have been used to probe humic structure, although heterogeneity means that the results are often inconclusive (Jones and Bryan 1998). In fact, it is characteristic of humics that different techniques give very different measures of molecular weight, and these differences are large (Piccolo 2002). Some techniques, such as ultracentrifugation, suggest that the average weights are of the order of thousands for fulvic acids and tens of thousands for humic acids (Jones and Bryan 1998), and humic acids certainly display many characteristics (e.g. flocculation and double layer properties) of macromolecular polyelectrolytes (Swift 1999). On the other hand, over the last decade, soft ionisation mass spectrometry, such as matrix assisted laser desorption/ionisation (MALDI) and electrospray ionisation (ESI), have seemed to support the self-association model. Both MALDI and ESI mass spectrometries give low average masses, with a distribution that has largely tailed off by M=2000, indicating that intrinsically high molecular weight material does not form a significant part of humic substances in solution (Stenson et al 2002). However more recently, Reemtsma and These (2003) and Stenson et al (2002) have found that much of the signal in the spectra is due to fragments, rather than 'true' molecular ions. Reemtsma and These (2003) have also found that the presence of small molecules may prevent the ionisation and detection of very large species. Given these recent developments, it is still possible that some part of

humic substances is, after all, truly macromolecular, and it is entirely possible that true macromolecules and associates coexist in solution. The fact that, despite decades of research, there can still be such fundamental disagreement about the nature of humic substances is indicative of their gross complexity. The only certainty is that large species do exist in solution, but their origin is unclear.

Possible mechanisms for the origin of non-exchangeable binding

For the Random Coil/Penetrable Gel Model, the humic has an open structure, which is penetrated by solvent and small ions. Therefore, metal ions could migrate into the interior and become hidden. Now, the exact mechanism by which they could become trapped is unclear. Choppin (1988) describes the metal ion moving from exchangeable (weaker) to non-exchangeable (stronger) sites, i.e., the metal is required to move from one place on the humic to another. An alternative is illustrated in Figure 1: the metal binds at an exchangeable site within the humic, and initially, is available for further reaction. However, with time, the humic rearranges its structure, completely surrounding the metal ion. The metal is now surrounded by the humic organic skeleton, and a hydrophobic zone has been formed, isolating the metal from aqueous solution phase chemistry, and rendering it non-exchangeable.

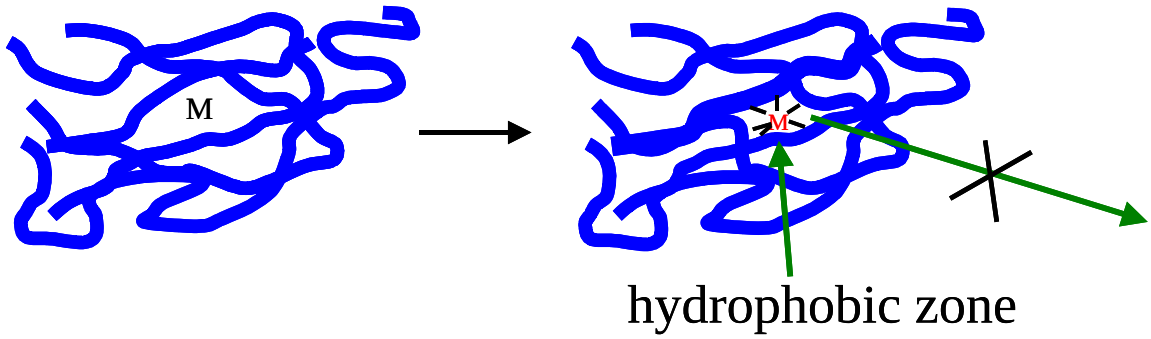

FIGURE 1: Possible 'Random Coil' mechanism for non-exchangeable binding.

In the case of Self Association, metals could bind at a site on one of the smaller units, which make up the larger aggregates. Initially, that metal would remain exposed to the solution, and available for removal by surfaces or competing ligands. However, rearrangement of the humic aggregate could trap the metal within the structure of the aggregate, hiding it from the solution (Figure 2). If this is true, then one would expect a direct relationship between the rates of humic aggregation/disaggregation, and the observed metal ion non-exchangeable binding rates.

Of course, self-association may just provide large, penetrated aggregates, which could entrap metal ions via a similar mechanism to that proposed for the Random Coil approach. If this is the case, then there would be no automatic relationship between the rates of aggregation/disaggregation and the metal ion rates themselves.

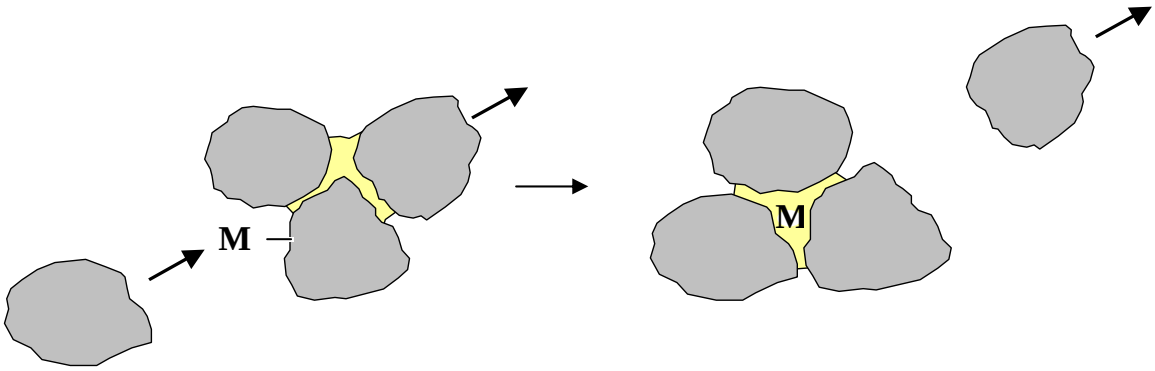

FIGURE 2: Possible 'Self-Association' mechanism for non-exchangeable binding

Aims

Although experimental evidence has been cited for and against self-association, there has been no quantitative theoretical investigation to determine whether or not humic species are likely to aggregate to any significant extent, let alone the likely rates of any such aggregation. The aim of this work is to examine the mechanism of aggregation of humic molecules in solution, and to develop a mathematical model to calculate their rates of aggregation and disaggregation The rates will be used to predict changes in the mass distributions of humic substances with time. In this way, the model will test whether a self association mechanism could explain the presence of large aggregates in solution.

A second aim of this work is to search for a mechanism for the non-exchangeable binding of metal ions by humics. The aggregation predicted by the model will be compared with non-exchangeable binding data to see if any link is apparent.

Theoretical potential energy curves and aggregation rates

To estimate the rates of aggregation or disaggregation, one must calculate the form of the potential energy curve as the two particles either approach to contact, or separate. There will be two forces acting on the pair of particles:

(1) the repulsive Coulombic interaction that will tend to retard or prevent aggregation;
(2) the attractive, Van der Waal's interaction that will promote aggregation.

The first step in calculating the Coulombic interaction is to calculate the potentials at the surfaces of the two particles. There are two approaches to calculating the potential at the surface of a particle. One can treat the particle as an impenetrable sphere with charge arranged uniformly on the surface, or one can treat the structure as penetrable with the charge distributed across the structure, which is open to solvent molecules and small ions. It is thought that the large humic species in solution are penetrated, and hence the penetrable approach is more appropriate. However, mass spectrometry suggests that the small molecules that make up any aggregates probably have masses of only a few hundred. In this case, the impenetrable model is more realistic. Both methods have been used here. Whichever approach is to be used, the first steps are the same.

The potential around a charged colloid particle, ψ, will be governed by Poisson's equation (Tanford 1961):

$$\nabla^2\psi = \frac{-\rho}{\varepsilon} \qquad (1)$$

where ∇^2 is the Laplacian operator, ρ is the charge density, and ε is the permitivity. ρ will vary with distance from the centre of the colloid, and will depend upon both the humic and counterion charges (Bartschat et al 1992). The concentration of any counterion, i, will be governed by a Boltzmann equation (Tanford 1961),

$$[X_i^{z_i+}]_r = [X_i^{z_i+}]_{BULK}\, e^{-\left(\frac{\psi_r z_i e}{kT}\right)} \qquad (2)$$

where ψ_r is the potential at a distance r from the centre of the colloid, k is Boltzmann's constant, T is absolute temperature, e is the charge of an electron, and $[X_i^{zi+}]_r$ and $[X_i^{zi+}]_{BULK}$ are the counterion charges at r and in the bulk solution, respectively. Combining equations 1 and 2 gives the '*Poisson-Boltzmann*' equation (Bryan et al 2000),

$$\nabla^2\psi = -\frac{N_A e}{\varepsilon}\left(\sum_{i=1}^{N_{IONS}} z_i [X_i^{z_i}]_{BULK} \exp^{-\left(\frac{\psi_r z_i e}{kT}\right)}\right) \qquad (3)$$

where N_A is Avogadro's number and N_{IONS} is the number of ion types, i, in the solution. This equation will describe the variation in ψ around any particle. At this point, the impenetrable and penetrable methods diverge.

Impenetrable Method

For the impenetrable approach, only one Poisson-Boltzmann equation is solved (eqn 3). According to Gauss' law, for a charged surface the potential gradient, dψ/dr, at the surface (r=R) is given by,

$$\left.\left(\frac{\partial\psi}{\partial r}\right)\right|_{r=R} = -\frac{\sigma}{\varepsilon} \qquad (4)$$

Here, equation 3 actually describes the variation in ψ from the radius of gyration, not the surface itself. The radius of gyration, B, is the distance of closest approach for small ions (Stern Layer). However, the charge density within the Stern layer is zero, and so there equation 1, becomes,

$$\nabla^2\psi = 0 \qquad (5)$$

and hence,

$$\left.\left(\frac{\partial\psi}{\partial r}\right)\right|_{r=B} = \left.\left(\frac{\partial\psi}{\partial r}\right)\right|_{r=R} = -\frac{\sigma}{\varepsilon} \qquad (6)$$

Equation 6 forms the first boundary condition. The second is given by,

$$\psi_r \to 0 \quad \text{as} \quad r \to \infty$$

Penetrable Method

In the case of the penetrable method, electrolyte penetrates the structure, and so a second Poisson-Boltzmann equation is required to describe the variation in ψ across the particle

itself. If β is the fraction of the particle volume accessible to solvent and small ions, then the potential in the interior, $\psi_{INTERIOR}$, is determined by,

$$\nabla^2 \psi_{INTERIOR} = -\frac{1}{\varepsilon}\left[\rho_{HUMIC} + \beta N_A e\left(\sum_{i=1}^{N_{ions}} z_i [X_i^{z_i}]_{BULK} \exp\left(-\left(\frac{\psi_r z_i e}{kT}\right)\right)\right)\right] \qquad (7)$$

where ρ_{HUMIC} is the charge density of the humic. In this case, the boundary conditions are (Bartschat et al 1992, Bryan et al 2000),

$$\left(\frac{\partial \psi}{\partial r}\right)\Bigg|_{r=0} = 0 \qquad (8)$$

and,

$$\psi_r \to 0 \quad \text{as} \quad r \to \infty$$

In either case, penetrable or impenetrable, the equations are solved by a 'shooting' method using Runge-Kutta and modified Adam's numerical integration routines (Bryan et al 2000). From this point on, the method is the same, regardless of whether the particles are penetrable or impenetrable. In both cases, the magnitude and shape of the potential is dependent upon the humic charge: the potential at any point increases with increasing humic charge, but decreases with increasing ionic strength. In addition, the extent of the double layer is affected, shrinking or compressing as ionic strength increases. Using these equations, the potential generated by the humic charge as a function of distance from the center of each particle was calculated, although only the potential at the colloid/diffuse layer boundary, ψ_R, was carried forward.

The methods of Hogg et al (1966) and Wiese and Healy (1970) were used to calculate the Coulombic interaction energy, Φ_{Coul}, as a function of d, the surface-surface separation of the two particles (labelled 1 and 2; Figure 3).

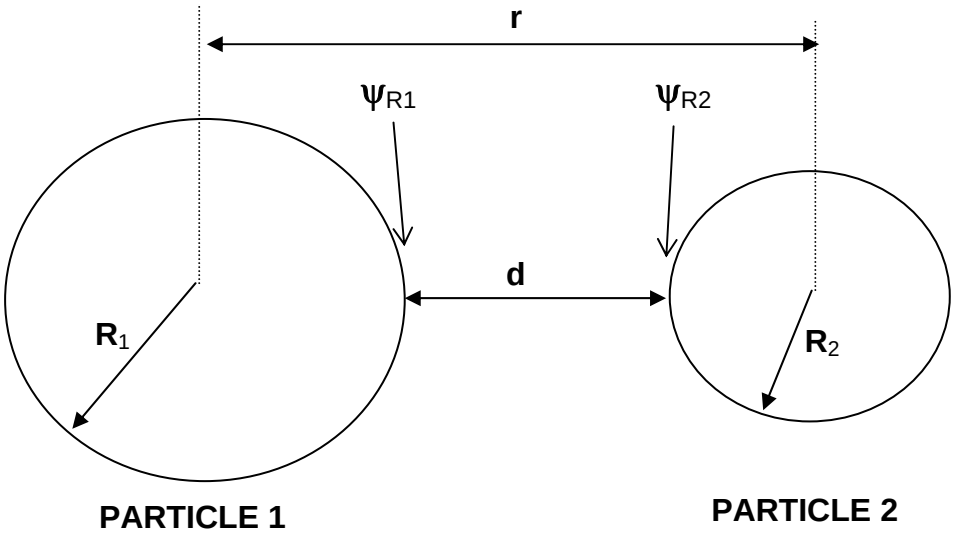

FIGURE 3: parameters used to calculate Φ_{Coul}. Note, the particles may be dissimilar.

If R_1 and R_2 are the radii of particles 1 and 2 respectively, and ψ_{R1} and ψ_{R2} are their surface potentials, then the Coulombic interaction energy will be given by,

$$\Phi_{Coul} = \pi\varepsilon R_1 R_2 \left(\frac{(\psi_{R1})^2 + (\psi_{R2})^2}{R_1 + R_2} \right) \left[\left(\frac{2\psi_{R1}\cdot\psi_{R2}}{(\psi_{R1})^2 + (\psi_{R2})^2} f(d) \right) - \ln(1 - \exp(-2\kappa d)) \right] \quad (9)$$

where the function, f(d), is defined by,

$$f(d) = \ln\left(\frac{1 + \exp(-\kappa d)}{1 - \exp(-\kappa d)} \right) \quad (9a)$$

and κ is the ionic strength dependent Debye-Huckel parameter,

$$\kappa = \sqrt{\frac{2e^2 N_A I}{\varepsilon k T}} \quad (10)$$

The attractive, Van der Waals interaction energy, Φ_{ATT}, will be given by (Hiemenz and Rajagopalan 1997)

$$\Phi_{ATT} = -\frac{A}{6}\left[\frac{2R_1R_2}{d^2 + 2R_1 d + 2R_2 d} + \frac{2R_1R_2}{d^2 + 2R_1 d + 2R_2 d + 4R_1R_2} + \ln\left(\frac{d^2 + 2R_1 d + 2R_2 d}{d^2 + 2R_1 d + 2R_2 d + 4R_1R_2} \right) \right] \quad (11)$$

Combining the repulsive, Coulombic and attractive, Van der Waals energies provides the total interaction energy, Φ_T,

$$\Phi_T = \Phi_{Coul} + \Phi_{ATT} \quad (12)$$

which may now be calculated as a function of particle separation.

Figure 4 shows examples of total interaction energy plots along with the corresponding Coulombic and Van der Waals contributions. There are 3 general shapes of interaction profile. In the case where the Coulombic term dominates over the Van der Waals for all values of d, for example where the particles have high surface potentials, then the total interaction energy becomes increasingly positive (repulsive) as the particles approach (Figure 4A). Under these conditions, it is not possible for a stable doublet to form when the two particles come into contact. Alternatively, in the case of low surface potentials, where the Van der Waals interaction dominates, then the interaction becomes steadily more negative (attractive) as the separation decreases (Figure 4B). In this case, a stable doublet will form and the process will be diffusion limited (fast). Finally, when the Coulombic and Van der Waals contributions are more evenly balanced, then the characteristic shape shown in Figure 4C is obtained. The Coulombic interaction is a longer range effect than the Van der Waals, and therefore, initially the total interaction energy increases as the particles get closer, but at very short separations, the attractive contribution dominates, and the total becomes more negative. The result is that a potential well forms at small d, which is preceded by a 'Coulomb barrier'. In these cases, the particles may form a doublet when they come into contact, the stability of which will depend upon the depth of the potential well. However, the particles first must overcome the Coulomb barrier. The effect is that the aggregation process will be slow, and the rate will depend directly upon the height of the barrier.

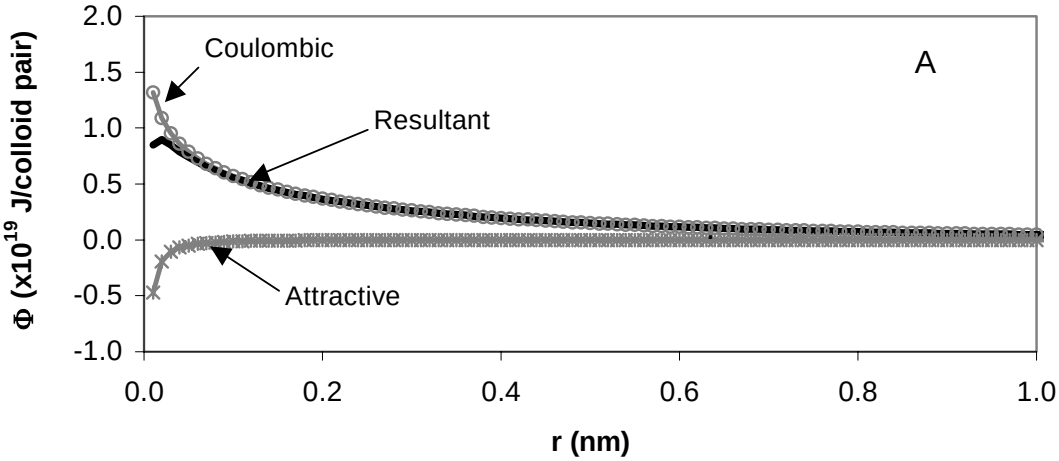

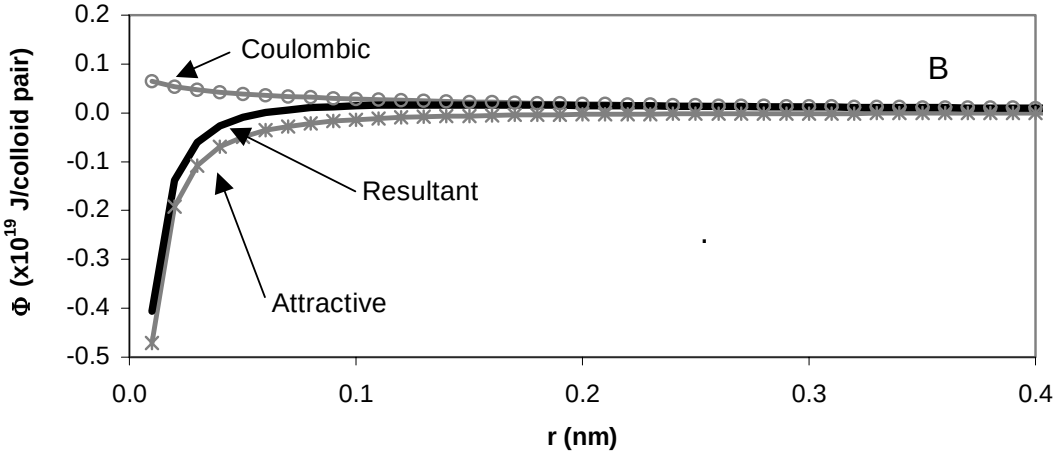

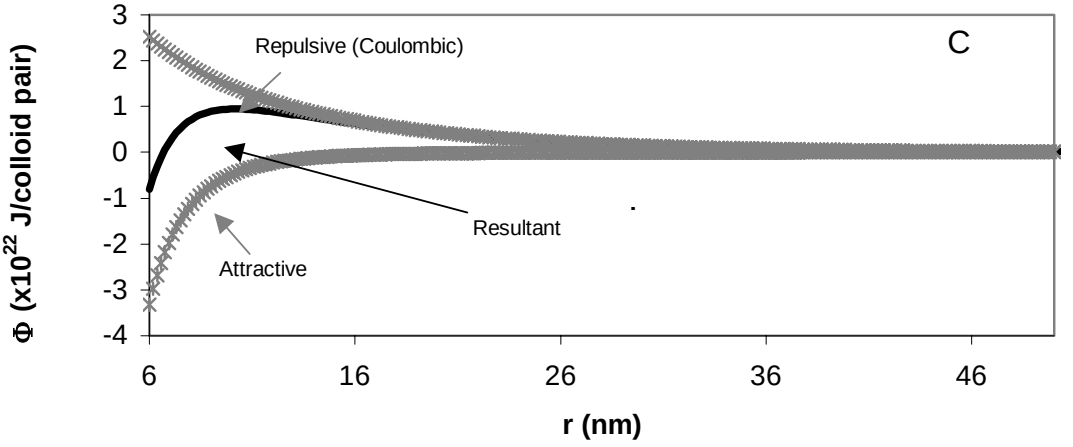

FIGURE 4: the three types of potential energy profile: A - Coulomb dominated; B - Van der Waals dominated; C - balanced, giving a Coulomb barrier and a potential well.

For a system containing two distinct particle populations, 1 and 2, with particle concentrations (particles/m^3) of N_1 and N_2 respectively. The rate of loss of particle type 1, via aggregation with particles of type 2 will be given by,

$$\frac{dN_1}{dt} = -k_f N_1 N_2 \approx k' N_1 \qquad (13)$$

where k_f is the forward, aggregation rate constant, its value depending upon the form of the total interaction energy profile. While the particle concentrations do not change significantly, k_f and N_2 may be combined to produce a pseudo first order rate constant, k'.

Fast aggregation (diffusion limited)

In the case of a profile of the type shown in Figure 4B (attractive interaction dominated), the rate of aggregation will be diffusion limited. In this case, k_f, will be given by (Hiemenz and Rajagopalan 1997),

$$k_f = 4\pi(R_1 + R_2).\left(\frac{kT}{6\pi\eta R_1} + \frac{kT}{6\pi\eta R_2}\right) \qquad (14)$$

Slow aggregation (Coulomb barrier limited)

In the case of a significant Coulomb barrier, k_f, is given by (Hiemenz and Rajagopalan 1997),

$$k_f = \frac{4\pi\left(\frac{kT}{6\pi\eta R_1} + \frac{kT}{6\pi\eta R_2}\right)}{\int_0^{\infty} \frac{\exp\left(\frac{\Phi_{Coul}(r) + \Phi_{ATT}(r)}{kT}\right)}{r^2} dr} \qquad (15)$$

where r is the separation of the particle centres (Figure 3, note $r \neq d$), and $\Phi_{Coul}(r) + \Phi_{ATT}(r)$ are the Coulomb and Van der Waals interaction energies at r respectively.

Backward (Disaggregation) rates

Once the forward rates have been calculated, they are used to calculate the backward rates.The depth of the potential well, ΔG_{AGG} (Figure 5), is the free energy change associated with the aggregation process and ($-\Delta G_{AGG}$ will be that associated with disaggregation). It is determined at the same time as the potential energy profile. Consider a generalised aggregation reaction between two particles, X_1 and X_2, to give a third, X_3,

$X_1 + X_2 \Leftrightarrow X_3$,

The equilibrium constant, K_{AGG}, is determined by ΔG_{AGG},

$$K_{AGG} = \frac{N_3}{N_1 N_2} = \exp^{-\left(\Delta G_{AGG} / RT\right)} \qquad (16)$$

where N_1, N_2 and N_3 are the concentrations of X_1, X_2 and X_3, respectively. On the way to equilibrium, the change in N_3 with time is given by,

$$\frac{dN_3}{dt} = k_f N_1 N_2 - k_b N_3 \qquad (17)$$

where k_f and k_b are the forward and backward rate constants: k_f has been determined by the method above and may be determined by,

$$K_{AGG} = \frac{k_f}{k_b} \qquad (18)$$

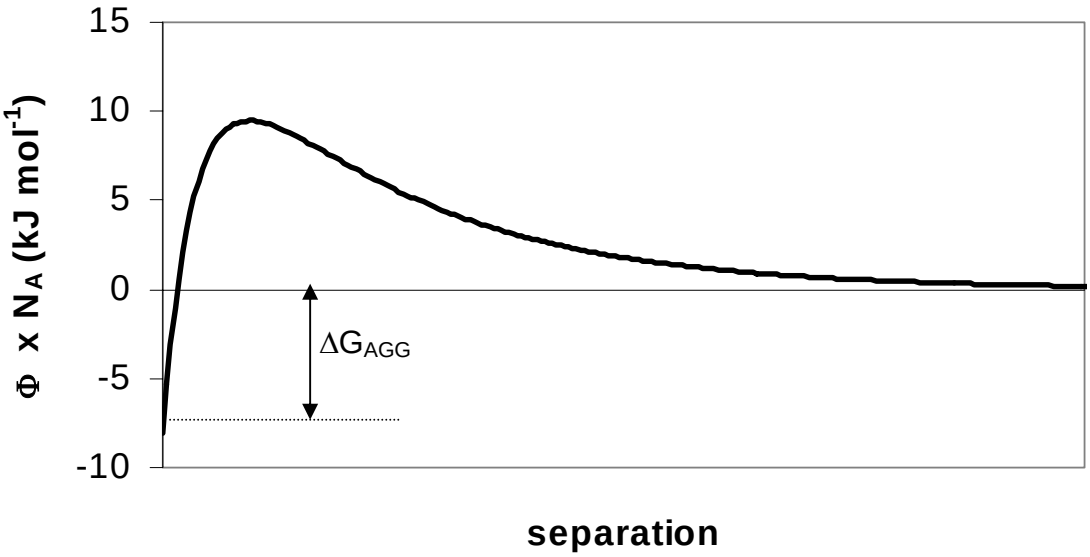

Figure 5: Example of a potential profile, showing the depth of the potential well, ΔG_{AGG}

Values of Rate Constants

All real humic samples are highly polydisperse, and therefore, it is not possible to define a single value of k_f that describes all the aggregation reactions that might take place. Rather, there will be a unique value of k_f for each possible combination of particle types. The values of the rate constants that are obtained if typical humic parameter values (charge density etc.) are used have been discussed previously (Bryan et al 2003). Figure 6 shows the results for WBPHA2, a peat humic acid at pH 6 and I=0.1. In order to calculate a particular value of k_f, it is necessary to define the two particle types, 1 and 2. The procedure adopted here was to define particle 1 (M_1) first and then, in series, define each of the species in the distribution as particle 2 (M_2). The figure shows the results of two such series of calculations, the first for a particle 1 mass (M_1) of 500, and the second for M_1 = 123,000. It is clear that the identity of particle 1 does have an impact upon the distribution of k_f values. The k_f profiles in Figure 6 are examples of the two general types. For M_1 = 500, the values increase with increasing particle 2 masses, because the small particles have very low surface potentials, and hence lower Coulomb terms. As the mass of particle 2 increases, the attractive, Van der Waals, term increases more rapidly than the Coulomb, and hence, k_f and the rate of aggregation increases. When M_1 = 123,000, however, because of the higher surface potential, the Coulomb term increases more rapidly than the Van der Waals, and k_f generally decreases. That said, there is a slight increase in k_f for very large values of M_2, because, although there is an increase in surface potential with mass, the rate of increase is much lower at high mass, which is due to

the reduction in particle charge density. Therefore, the Van der Waals term becomes more significant.

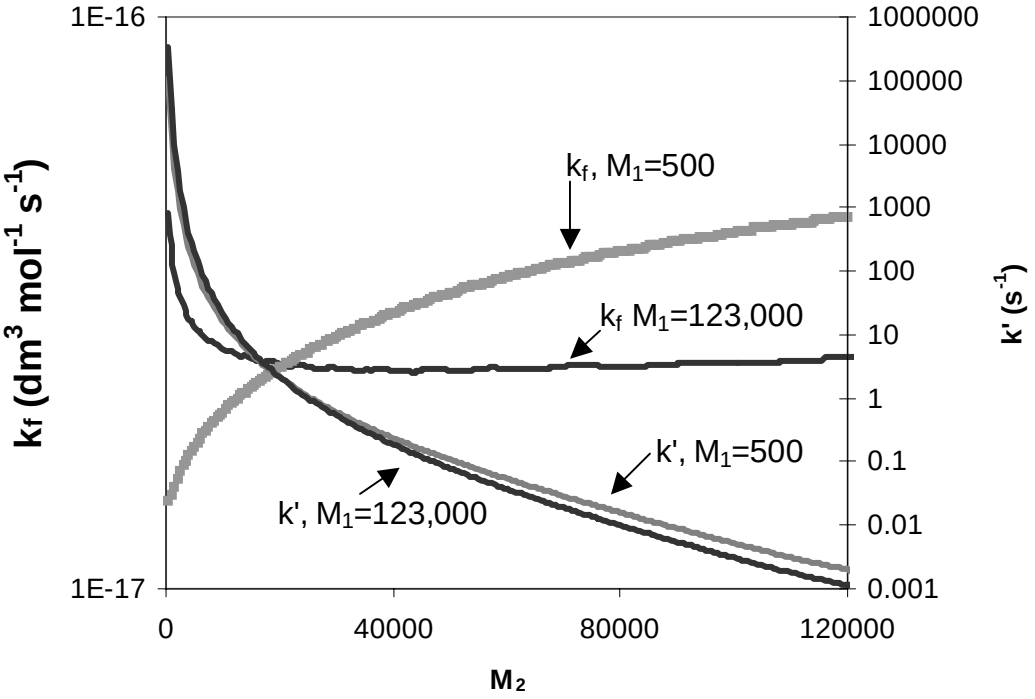

FIGURE 6: calculated k_f and k' distributions for two particle 1 masses, 500 and 123,000 for WBPHA2, [HA]=10ppm, pH=6, I=0.1.

Figure 6 also shows the corresponding distribution of pseudo first order rate constants, k' ($k'=k_fN_2$, eqn. 13). These values have been calculated using the particle mass distributions measured by ultracentrifugation (Bryan et al 2001a,b). Although the k_f distributions are radically different, there appears to be much less difference for k'. The particle concentrations (N_2) decrease very significantly with particle mass, in the case of WBPHA2 by a factor of 10^4 between M=2000 and 123,000. Hence, this variation, which will be the same for both series, dominates over the much more modest changes in k_f.

There are certain characteristics of the metal ion-humate non-exchangeable interaction that any proposed mechanism must be able to explain (Keepax et al 2002; King et al 2001; unpublished data). Although there is a distribution of fast and intermediate desorption rates, there is a distinct, long lived fraction that accounts for a significant amount of the non-exchangeable metal, and which has a discrete, single first order desorption rate constant. All metal ions show very similar rates of transfer from exchangeable to the longest lived non-exchangeable fraction and similar rates of desorption. The rates are insensitive to pH, total metal ion concentration, humic concentration and humate/metal ion ratio.

In some cases, the behaviour predicted for the self-association mechanism is consistent with the experimental facts. For example, very little effect of pH is predicted by the model. Further, the origin of the rates is entirely 'physical' in nature and the chemical identity of any

bound metal ion would not have any effect, and therefore, at least for metal ions of the same charge, there would be no difference in predicted rates. However, there are a number of discrepancies between the predicted rates and experiment. The calculations predict that the first order rates of aggregation will vary greatly across the distribution of particle masses. There is certainly no evidence for a single, consistent aggregation rate, or a distinct long lived fraction with a single, first order desorption rate. The effect of humic concentration on the predicted rates is also anomalous: the model predicts increases in rates, where none is observed. The ionic strength effect is also problematic. A very large effect is predicted for aggregation rates, but no significant change is observed in experiments. The final problem is that the predicted association rates are too high. Only at the lowest ionic strength do the self-association rates start to approach those of the real non-exchangeable fraction. Therefore, in some ways, the self association rates predicted by the model are consistent with the metal ion non-exchangeable fraction rates. However, in other ways they are not. In order for the self-association mechanism to be responsible for the non-exchangeable behaviour, at least in the absence of some other, additional mechanism, then it must be consistent with **all** of the experimental data. In fact, even when the input parameters are allowed to vary, regardless of the charge or size selected, the mechanism was still unable to produce a single distinct fraction, or the correct ionic strength behaviour.

Therefore, it seems unlikely that the self-association mechanism can be responsible for the metal ion non-exchangeable behaviour. However, it is important to appreciate that although the modelling suggests no link between aggregation and non-exchangeable behaviour, it certainly does not imply that the self-association process itself will not take place. On the contrary, the model predicts that aggregation of the 'monomer' units within the mass distribution should take place. Hence, if the non-exchangeable behaviour occurs as a result of the collapse of the humic structure around a metal ion and the formation of a hydrophobic zone, then it may be that self-association provides the large species for this mechanism.

Calculating Mass Distributions

The aggregation of a population of monomers is a complex process. Even for an initial population of monomers all of the same mass, as aggregation proceeds, a large number of species of different masses develop. It is necessary to keep track of the concentrations of all of these species while the aggregation is taking place. Thus far, two methods for calculating mass distributions have been attempted: 'single monomer' and 'four monomers'.

Method 1: Single Monomer

In this method the initial, completely disaggregated, population is monodisperse; i.e. all of the individual molecules have the same mass and charge. Hence, at zero time, there is no aggregation, and all of the mass exists as isolated monomers, X_1. The first step is for these monomers to aggregate to produce dimmers, X_2,

$$X_1 + X_1 \rightarrow X_2$$

which in turn will undergo a further aggregation to produce trimers, X_3,

$$X_2 + X_1 \rightarrow X_3$$

This process continues, producing further aggregates, X_n, where n is the number of monomer units making up the aggregates. In this way, the model only allows aggregation steps where one of the reactants is a monomer; i.e. all aggregations take the form,

$$X_n + X_1 \xrightarrow{k_f(n)} X_{n+1}$$

where n can take any whole number value, greater than 0, and $k_f(n)$ is the forward rate constant. A rate constant is also defined for the disaggregation steps,

$$X_n \xrightarrow{k_b(n)} X_{n-1} + X_1$$

where this time n takes any value greater than 1. If N_n is the concentration of species X_n, then we may write down equations to describe the change in these concentrations with time.

$$\frac{dN_1}{dt} = \sum_{n=2} k_b(n).N_n - 2k_f(1)N_1^2 - \sum_{n=2} k_f(n)N_n N_1 \qquad (19)$$

$$\frac{dN_n}{dt} = k_f(n-1)N_{n-1}N_1 - k_f(n)N_n N_1 - k_b(n)\,N_n + k_b(n+1)\,N_{n+1} \qquad (20)$$

The model uses these equations to calculate the change in all concentrations, N_n, with time. The model splits the total simulation time into discrete steps, the length of which it calculates such that no species will change by more than 5% over the step. In addition, the equations are not linearised, and the integrated forms are used to prevent the introduction of even small errors in the concentrations, which could be magnified over a large number of steps.

Results

The results obtained with method 1 are shown in Figures 7 to 10: in all cases, the mass distributions are plotted as particle concentrations, rather than mass concentrations; i.e. these are 'number distributions'. Figures 7 and 8 show the effect of time on the distribution for a monomer mass of 500 and a charge of 5 meq/g at I=0.1. The most significant result of the whole work is that the model **does** predict that aggregation will take place amongst a population of small molecules with realistic humic properties. The value of the Hamaker constant used in these calculations is 5.4×10^{-21} J, which is at the lower end of the range that might be expected for organic materials, such as humics. This value was chosen for the initial calculations, because it makes the predictions of aggregation conservative; i.e. the aggregation observed here is not an artefact caused by the selection of optimistic input parameters. The value of humic charge is also realistic, and is what would be expected at neutral pH. Therefore, it would seem that there is no reason why these small molecules may not self-associate to give larger species. Of course, the size of the aggregates predicted here are still relatively small; significant concentrations only extend to approximately mass 5000, which is much smaller than some of the species that have been observed in real humic samples, which can be as large as 60,000, even in the absence of multi-valent cations (Bryan et al 2001a,b). However, these are only initial calculations for a single monomer mass.

The model predicts that an equilibrium will be established relatively quickly, and within a few hundred seconds, a stable distribution has been produced. In fact, the log scale in the figures, necessary to show all the data, is slightly misleading. The majority of the aggregation, certainly in terms of the loss of free monomer happens very quickly, within the first second. The move from dimers and trimers to the final distribution takes longer. The shape of the final distribution is interesting, a maximum in the distribution is predicted, which shifts to an equilibrium position at an aggregate number of 4, or a mass of 2000. This may suggest that the balance between the repulsive forces and attractive forces, results in a most stable configuration: the repulsive forces will increase faster than the attractive with particle mass. However, this result must be treated with caution, since it may be a product of the fact that only free monomer is allowed to aggregate to increase particle mass. The effect is that in the model, the free monomer becomes highly reactive, compared with other species, and this may be responsible for the large depletion of very low mass material.

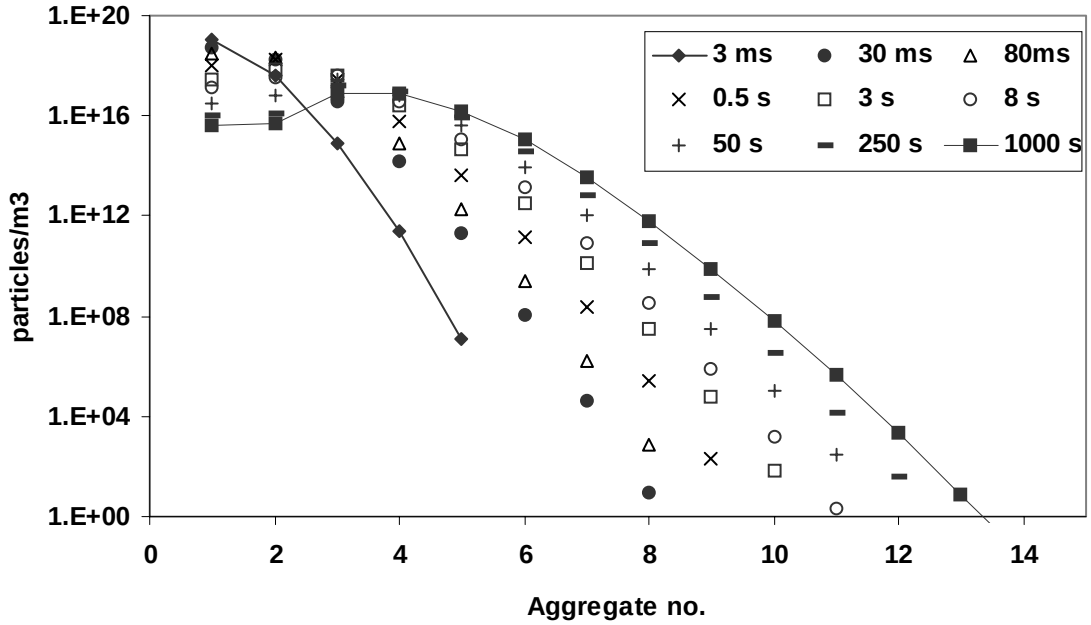

Figure 7: The effect of time on aggregation of monomers; monomer mass = 500, charge = 5 meq/g, [HA] = 10ppm, I=0.1.

Figure 9 shows the effect of monomer mass on the distribution. The main figure shows the data plotted versus aggregate mass, whilst the inset shows the same result plotted versus aggregate number. The results show that aggregation is predicted regardless of monomer mass; i.e. there is nothing special about a mass of 500. Also, both monomer masses yield a maximum, but in different places. The larger mass monomer yields more massive aggregates, but the degree of aggregation (the number of monomers in an aggregate) is much smaller. This makes sense, because for a constant charge density, there will be lower repulsive forces between the smaller monomers, and so they will find it 'easier' to aggregate. However, the greater mass of the larger monomer means that it still produces more massive aggregates. The difference in the position of the maximum suggests that if this effect is not an artefact, then

the process will not always select a particular 'magic', most stable aggregate size. This is reassuring, because the distributions of large humic species in solutions have broad, featureless distributions, without peaks.

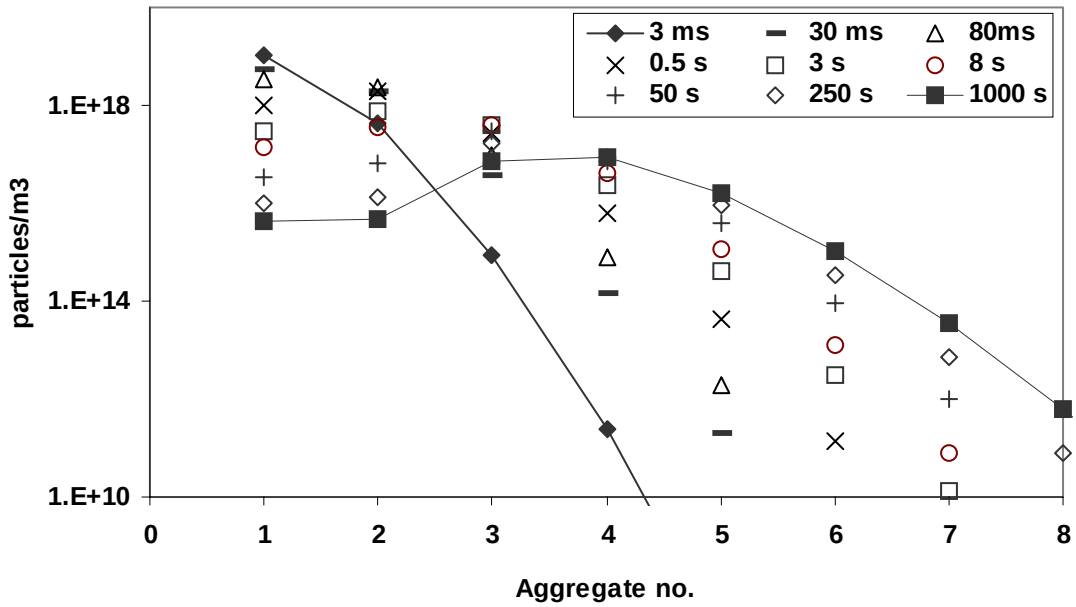

Figure 8: The effect of time on aggregation of monomers; close up of low mass region.

Figure 10 shows the effect of reducing humic charge on aggregation. It has been shown that the sizes of humic species in solution increase as their charge is neutralised; for example, by the addition of multi-valent cations (Bryan et al 2001a,b). As the charge is neutralised, species of higher and higher mass are produced, but small species still remain, and in fact, make up a very significant part of the distribution, even when the charge has been almost completely neutralised. The net effect is that the distribution is 'pulled' to higher mass. The model shows a small shift in the maximum, from M=2000 to M=3000, however, the most significant change is in the concentration of the larger species, which increase significantly, though concentrations of the smaller aggregates have been maintained. There has been a very significant reduction in the concentration of the monomer, which has virtually disappeared from solution. This is almost certainly an artefact caused by the fact that all aggregations must involve it. That said, the general behaviour predicted by the model does seem to match qualitatively the real behaviour, although once again, the masses of these aggregates are much lower than for real samples.

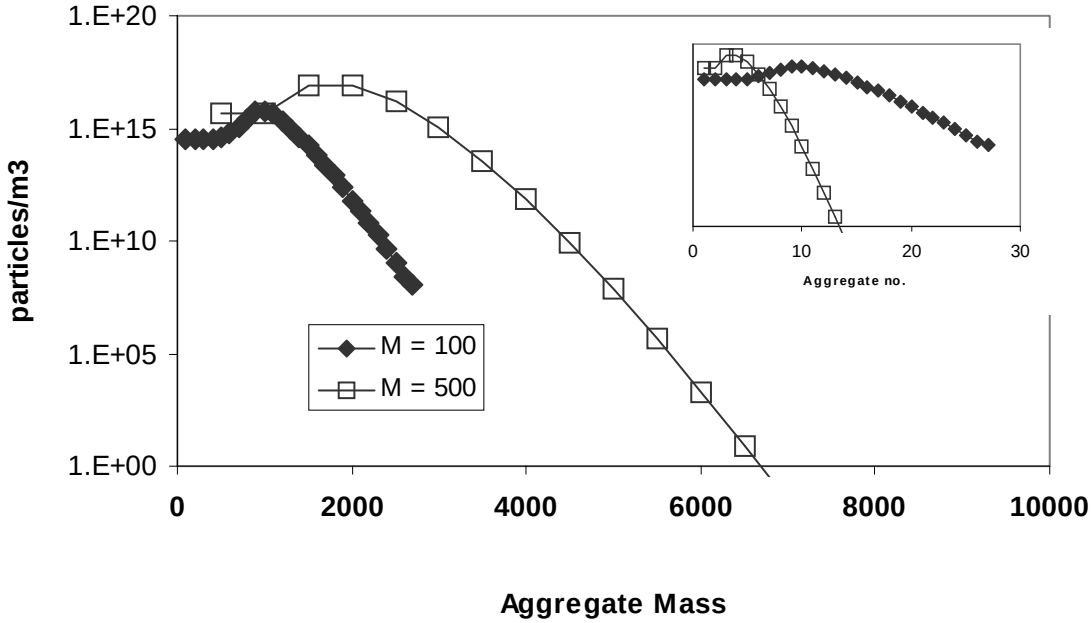

Figure 9: The effect of monomer mass,M, charge = 5 meq/g, I=0.1, [HA]=10 ppm. Main figure distribution plotted versus aggregate mass; inset plotted versus no of monomers in the aggregate.

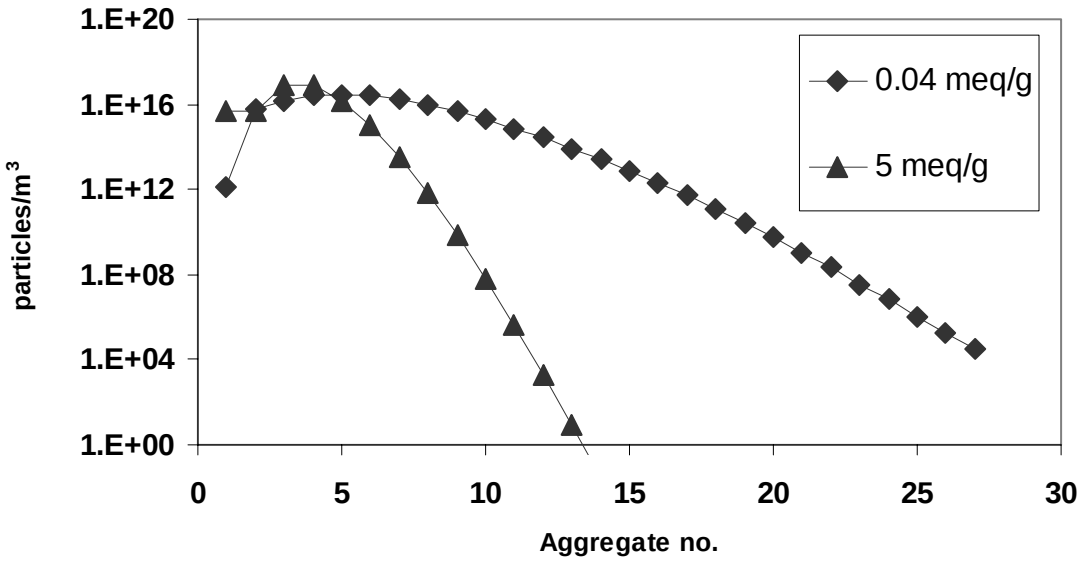

Figure 10: The effect of monomer charge; Monomer mass = 500, I=0.1, [HA]=10 ppm.

Method 2: Four Monomers

One criticism of method 1 is that it assumes that the initial population is uniform, or monodisperse. However, this is clearly not the case. Soft ionisation mass spectrometry suggests that the monomers actually have a distribution themselves, which seems to have a maximum at a mass of a few hundred, but extending to approximately 2000 (ignoring possible problems of fragmentation and ionisation suppression).

Method 2 uses a population of 4 different monomers: X_A; X_B; X_C; X_D. Aggregates, $X_{a,b,c,d}$, are allowed to form from any combination of these, where a,b,c and d are the number of X_A, X_B, X_C, and X_D in the aggregate, respectively. For any aggregate, rate constants are defined that describe the four possible aggregation steps.

$$X_{a,b,c,d} + X_A \xrightarrow{k_{fA}(a,b,c,d)} X_{a+1,b,c,d}$$

$$X_{a,b,c,d} + X_B \xrightarrow{k_{fB}(a,b,c,d)} X_{a,b+1,c,d}$$

$$X_{a,b,c,d} + X_C \xrightarrow{k_{fC}(a,b,c,d)} X_{a,b,c+1,d}$$

$$X_{a,b,c,d} + X_D \xrightarrow{k_{fD}(a,b,c,d)} X_{a,b,c,d+1}$$

where in all cases, a+b+c+d ≥ 1. Constants are also defined for the dissociations:

$$X_{a,b,c,d} \xrightarrow{k_{bA}(a,b,c,d)} X_{a-1,b,c,d} + X_A$$

where a ≥ 2, and b,c and d may take any value;

$$X_{a,b,c,d} \xrightarrow{k_{bB}(a,b,c,d)} X_{a,b-1,c,d} + X_B$$

where b ≥ 2, and a,c and d may take any value;

$$X_{a,b,c,d} \xrightarrow{k_{bC}(a,b,c,d)} X_{a,b,c-1,d} + X_C$$

where c ≥ 2, and a,b and d may take any value;

$$X_{a,b,c,d} \xrightarrow{k_{bD}(a,b,c,d)} X_{a,b,c,d-1} + X_D$$

where d ≥ 2, and a,b and c may take any value. These constants are used to calculate the changes in the concentrations of the aggregates, $N_{a,b,c,d}$, with time,

$$\begin{aligned}\frac{dN_{a,b,c,d}}{dt} = {} & k_{fA}(a-1,b,c,d)N_{a-1,b,c,d}N_A + k_{fB}(a,b-1,c,d)N_{a,b-1,c,d}N_B + \\ & k_{fC}(a,b,c-1,d)N_{a,b,c-1,d}N_C + k_{fD}(a,b,c,d-1)N_{a,b,c,d-1}N_D + \\ & k_{bA}(a+1,b,c,d)N_{a+1,b,c,d} + k_{bB}(a,b+1,c,d)N_{a,b+1,c,d} + \\ & k_{bC}(a,b,c+1,d)N_{a,b,c+1,d} + k_{bD}(a,b,c,d+1)N_{a,b,c,d+1} - \\ & N_{a,b,c,d}\left(\left[k_{fA}(a,b,c,d)N_A\right]+\left[k_{fB}(a,b,c,d)N_B\right]\right) - \\ & N_{a,b,c,d}\left(\left[k_{fC}(a,b,c,d)N_C\right]+\left[k_{fD}(a,b,c,d)N_D\right]\right) - \\ & N_{a,b,c,d}\left(k_{bA}(a,b,c,d)+k_{bB}(a,b,c,d)+k_{bC}(a,b,c,d)+k_{bD}(a,b,c,d)\right)\end{aligned} \quad (21)$$

The changes in the monomer concentrations themselves are determined by summing the positive contributions from the dissociation steps and negative contributions from the association steps for all aggregates.

Results

Figures 11 to 13 show the initial results for method 2: as for method 1, the data are plotted as number distributions, but this time all the distributions are plotted versus particle mass, since particles of the same mass may now be made up of different numbers of monomers. Figure 11 shows the effect of time upon the distribution. The most obvious difference between this result and that for method 1 (Figure 7) is that the aggregation is much faster. This is probably because of the very much large number of possible aggregation reactions that are permitted in this model compared to method 1 (compare equations 19 and 20 with 21). Also, smaller monomers are present in this system, which will have much smaller repulsive forces. The other obvious difference is that there is a definite periodic effect in this distribution that was not present for method 1. There is a pattern that repeats over a mass of 2000. This is clearly due to the mass 2000 monomer, and the separate diagonal lines represent families of aggregates with 1, 2 3 etc. mass 2000 monomers.

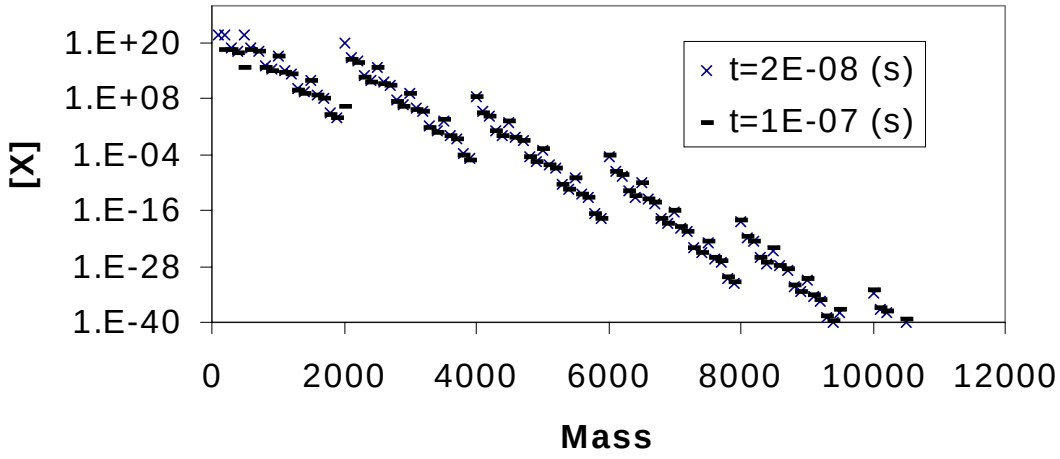

FIGURE 11: Effect of time on aggregation for I=0.1, charge = 5 meq/g and monomer masses of 100 (X_A); 200 (X_B); 500 (X_C); 2000 (X_D) and concentrations of $N_1 = 0.88x10^{22}$; $N_2 = 0.59x10^{22}$; $N_3 = 0.77x10^{22}$; $N_4 = 0.69x10^{20}$.

Figure 12 shows a comparison between the results obtained with a different set of monomers and the original result. The mass 2000 monomer has been replaced with one of 1000, and the periodic pattern seems to disappear. In fact, it has been replaced by a less obvious pattern with a period of approximately 500 instead. There has also been a shift in the position of the distribution to lower mass, similar behaviour to that observed for method 1 (Figure 9). Clearly, the large monomers, even though they have low concentrations, have a major effect on the predicted size of the aggregates. Also, there is no definite maximum for the method 2 distributions, although it is possible that the fine structure caused by the selection of the monomer set is masking any small maximum.

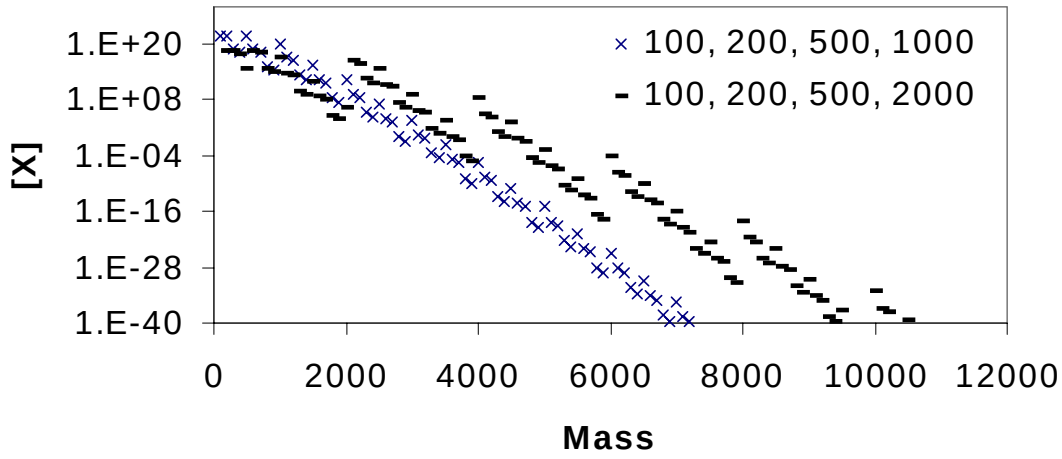

FIGURE 12: Effect of monomer population for I=0.1 and charge = 5 meq/g. Population 1: monomer masses of 100 (X_A); 200 (X_B); 500 (X_C); 2000 (X_D) and concentrations of $N_1 = 0.88x10^{22}$; $N_2 = 0.59x10^{22}$; $N_3 = 0.77x10^{22}$; $N_4 = 0.69x10^{20}$. Population 2: monomer masses of 100 (X_A); 200 (X_B); 500 (X_C); 1000 (X_D) and concentrations of $N_1 = 0.88x10^{22}$; $N_2 = 0.59x10^{22}$; $N_3 = 0.77x10^{22}$; $N_4 = 0.14x10^{21}$.

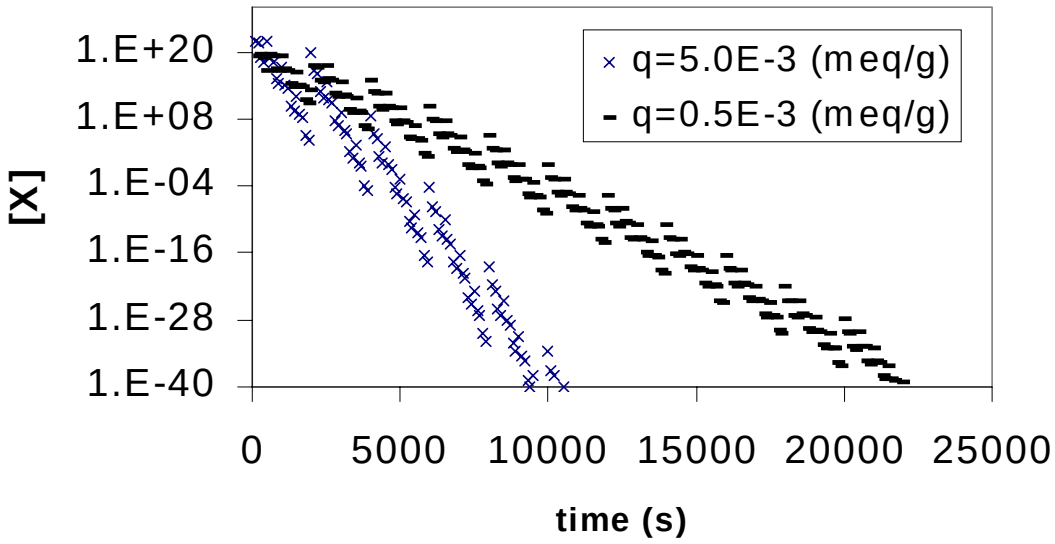

FIGURE 13: Effect of charge on aggregation for a monomer set of 100, 200, 500, 2000. monomer masses of 100 (X_A); 200 (X_B); 500 (X_C); 2000 (X_D) and concentrations of $N_1 = 0.88x10^{22}$; $N_2 = 0.59x10^{22}$; $N_3 = 0.77x10^{22}$; $N_4 = 0.69x10^{20}$.

Figure 13 shows the result of a change in charge density on the population distribution. The monomer masses and starting concentrations are the same as for Figure 11. The same qualitative effect is shown here as was predicted by method 1. There is a general shift to aggregates of higher mass, although there remain significant concentrations of smaller material. Again, this is the same general behaviour that has been observed in experiment (Bryan et al 2001a,b).

Conclusions

A model has been developed that is able to calculate the rate constants for the association and dissociation of humic like molecules, and then calculate the mass distributions that would result. The magnitudes and distribution of rates strongly suggest that association/ dissociation is not **directly** responsible for the non-exchangeable binding of metal ions. However, the model does suggest that aggregation of small humic like molecules to produce aggregates should take place. Two methods, involving one and four monomers have been tested, and both predict aggregation. The model behaviour is qualitatively similar to real humic behaviour, in particular the effect of a reduction in charge density, which results in a shift to larger mass aggregates, whilst significant concentrations of the smaller species are maintained. The most significant difference between the model prediction and real data is that the model predicted aggregates are much smaller, by roughly an order of magnitude. A major limitation of the model (both methods) is that it is constrained to aggregation reactions that involve addition of monomers either to themselves or existing aggregates; aggregates are not permitted to aggregate. The result is that a long series of separate steps would be required to produce very large material, whereas in reality, there would be no such restriction. This may be the reason for the discrepancy between model and real humic species. This work has shown that self-association is possible, and in fact, should be expected. However, it does not prove that the large species that exist in solution must be aggregates and not true macromolecules.

References

Bartschat, B.M., Cabaniss, S.E. and Morel, F.M.M. Oligoelectrolyte model for cation binding by humic substances. *Environmental Science and Technology*, 1992, *26*, 284-294.

Benedetti, M.F., Van Riemsdijk, W.H. and Koopal, L.K. Humic substances considered as a heterogeneous donnan gel phase. *Environmental Science and Technology*, 1996, *30*, 1805-1813.

Bryan N.D., Robinson V.J., Livens F.R., Hesketh N.H., Jones M.N.and Lead J.R. Metal-humic interactions: A random structural modelling approach. *Geochimica et Cosmochimica. Acta,* 1997, **61**, 805-820.

Bryan N.D., Jones D.M., Appleton M., Livens F.R., Jones M.N., Warwick P., King S.J.and Hall A., A Physicochemical Model of Metal-Humate Interactions. *Physical Chemistry Chemical Physics*, 2000, 2, 1291-1300.

Bryan N.D., Jones M.N., Birkett J. and Livens F.R. The Application of a New Method of Analysis of Ultracentrifugation Data to the Aggregation of a Humic Acid by Cupric Ions. *Analytica Chimica Acta,* 2001a, 437, 281-289.

Bryan N.D., Jones M.N., Birkett J. and Livens F.R. Aggregation of Humic Substances by Metal Ions Measured by Ultracentrifugation. *Analytica Chimica Acta,* 2001b, 437, 291-308.

Bryan N.D., Jones D.M., Keepax R. Warwick P., Stephens S., Higgo J.J.W. An Experimental and Modelling Study of Metal Ion/Humate Non-Exchangeable Binding.
2003, HUPA project 1st Technical Progress Report.

Buurman P., van Lagen B., Piccolo A. Increase in stability against thermal oxidation of soil humic substances as a result of self association. *Organic Geochemistry*, 2002, 33(3), 367-381.

Choppin, G.R.. Humics and radionuclide migration. *Radiochimica Acta*, 1988, *44/45*, 23-28.

Clapp C.E. and Hayes M.H.B. Sizes and shapes of humic substances. *Soil Science*, 1999, 164(11), 777-789.

Conte, P. and Piccolo, A. Conformational arrangement of dissolved humic substances. Influence of solution composition on association of humic molecules. *Environmental Science and Technology*, 1999, *33*, 1682-1690.

Halim M., Conte P., Piccolo A. Potential availability of heavy metals to phytoextraction from contaminated soils induced by exogenous humic substances. *Chemosphere*, 2003, 52(1), 265-275.

Hayes, M.H.B. and Swift, R.S. The chemistry of soil organic colloids. In Greenland, D.J. and Hayes, M.H.B. (eds.) *The Chemistry of Soil Constituents*, 1978, (179-320), Wiley, London.

Hayes, M.H.B. and Swift, R.S. Genesis, isolation, composition and structures of soil humic substances. In de Boodt, M.F., Hayes, M.H.B. and Herbillon, A. (eds.) *Soil Colloids and Their Association in Aggregates*, 1990, (245-305), Plenum, New York.

Hiemenz P.C. and Rajagopalan R. *Principles of Colloid and Surface Chemistry*, 3rd edn.,1997, Marcel-Dekker, New York.

Hogg, R., Healy, T.W. and Fuerstenau, D.W. Mutual coagulation of colloidal dispersions. *Trans. Faraday Soc.*, 1966, *62*, 1638-1651.

Jones M.N. and Bryan N.D. Colloidal properties of humic substances. *Advances in Colloid and Interface Science*, 1998, 78, 1-48.

Keepax R.E., Jones D.M., Pepper S.E. and Bryan N.D. The effects of humic substances on radioactivity in the environment. in Keith-Roach M. and Livens F.R. (eds.) *Microbes and Radionuclides*, 2002, (pp 143- 177), Elsevier, Amsterdam.

King S.J., Warwick P., Hall A. and Bryan N.D. The dissociation kinetics of dissolved metal-humic complexes. *Physical Chemistry Chemical Physics*, 2001, 3, 2080-2085.

Piccolo A. The supramolecular structure of humic substances: A novel understanding of humus chemistry and implications in soil science. *Advances in Agronomy*, 2002, 75, 57-134.

Piccolo, A. New insights on the conformational structure of humic substances as revealed by size exclusion chromatography. In Drozd, J., Gonet, S.S., Senesi, N. and Weber, J. (eds.) *The Role of Humic Substances in Ecosystems and in Environmental Protection,* 1997, *IHSS, Wroclaw, Poland.*

Piccolo, A., Nardi, S. and Concheri, G. Macromolecular changes of humic substances induced by interaction with organic acids. *European Journal of soil science*, 1996, *47*, 319-328.

Reemtsma T. and These A. On-line coupling of size exclusion chromatography with electrospray ionization-tandem mass spectrometry for the analysis of aquatic fulvic and humic acids. *Analytical Chemistry*, 2003, 75(6), 1500-1507.

Schulton, H.R. and Schnitzer, M. A state of the art structural concept for humic substances. *Naturwissenschaften*, 1993, *80*, 29-30.

Stenson A.C., Landing W.M., Marshall A.G., Cooper W.T. Ionization and fragmentation of humic substances in electrospray ionization Fourier transform-ion cyclotron resonance mass spectrometry, *Analytical Chemistry*, 2002, 74(17), 4397-4409.

Swift R.S. Macromolecular properties of soil humic substances: Fact, fiction, and opinion. *Soil Science*, 1999, 164(11), 790-802.

Tanford, C. *Physical Chemistry of Macromolecules.* 1961 John Wiley and Sons Inc.

Wershaw R.L. Model for humus in soils and sediments *Environmental Science and technology*, 1993, 27, 814-816.

Wershaw, R.L. A new model for humic materials and their interactions with hydrophobic chemicals in soil-water or sediment-water systems. *Journal of Contaminant Hydrology*, 1986, *1*, 29-45.

Wiese, G.R. and Healy, T.W. Effect of Size on Colloid Stability. *Trans. Faraday Soc.*, 1970, *66*, 490-499.

Yates L.M. and von Wandruszka, R. Effects of pH and metals on the surface tension of aqueous humic materials. *Soil Science Society Of America Journal*, 1999, 63(6), 1645-1649.

Annex 16

Modelling the Transport of Actinide Elements in the North-Eastern Irish Sea

O. J. Marsden, L. Abrahamsen, C. Gent, N. D. Bryan and F. R. Livens

University of Manchester, Manchester, U.K.

Modelling the Transport of Actinide Elements in the North-Eastern Irish Sea.

O. J. Marsden, L. Abrahamsen, C. Gent, N. D. Bryan and F. R. Livens

University of Manchester, Manchester, U.K.

Introduction

The industrial scale exploitation of nuclear fission has led to the production of a range of artificial isotopes and elements, including fission products such as ^{90}Sr, ^{99}Tc and ^{137}Cs and transuranium elements such as Np, Pu and Am. The geochemical behaviour of these is of interest because of the need to assess the radiological impacts of releases into the environment, but there are relatively few localities worldwide where these elements are present in sufficient quantity to allow detailed study. The authorised low level effluent discharges from the BNFL nuclear fuel reprocessing plant at Sellafield in North Western England into the Irish Sea have led to the labelling of nearby sediments with a range of isotopes, and it is possible to use this locality to explore the transport and geochemistry of these elements. (Cundy *et al*., 2002; Ridgway & Shimmield, 2002; Thomson *et al*., 2002).

Construction of the Sellafield site began in 1947, initially to support the UK nuclear weapons programme, and discharges of low level effluents to sea commenced in 1952. There are complete records of activity discharged for many of the most important constituents of the effluents, such as ^{137}Cs, Pu-α, ^{241}Pu or ^{241}Am, partial records for other constituents such as ^{99}Tc or ^{237}Np and essentially no information on radiologically minor but potentially useful species such as ^{236}U (Gray *et al*., 1995). In addition, the separate components, ^{238}Pu and $^{239,240}Pu$, which comprise Pu-α, have been measured separately since 1978 and sediment core data have been used to reconstruct the historical discharge of ^{238}Pu from 1952 (Kershaw *et al*., 1990). As the functions of the Sellafield site have changed over time, from weapons-related activities to the reprocessing of civilian fuel, and as the burnup of the plant feedstocks has increased and effluent treatment improved, so the elemental and isotopic composition of the effluent discharges have also changed (Wilson, 1996). In general, discharges increased through the 1960s to reach maxima in the 1970s, before decreasing substantially in the first half of the 1980s. The ^{137}Cs peak discharge was over 5000 TBq yr^{-1} and that of total Pu over 50 TBq yr^{-1}. Discharge levels since the mid-1980s have been trivial by comparison with the peak years.

Discharge is via a pipeline direct into the Irish Sea. On release, the radionuclides primarily become associated with fine, suspended material to differing degrees, depending on their particle-reactivity. More detailed descriptions of relevant aspects of actinide speciation and particle reactivity can be found in Pentreath (1988), Clark *et al*. (1995) or Morris *et al*. (2000). As a result, all the actinides are significantly particle-associated, although solution transport is proportionately more important for those with relatively low K_d values; for example, Cs^+, NpO_2^+ or UO_2^{2+}.

The eastern Irish Sea basin is generally quite shallow, typically only 30 m deep, and as a result of tidal movement and currents, the fine-grained particles with their associated radionuclides are focused into a belt of muds and muddy sediments (the “mud patch”) which lies parallel to the coast (Hetherington, 1976; Pentreath *et al.*, 1984; Kershaw *et al.*, 1992; MacKenzie *et al.*, 1994).

With time, some of the particulates have been redistributed by tidal processes or storm events and deposit in the intertidal areas of local estuaries, particularly the River Esk (Hetherington, 1978; Aston & Stanners, 1981; MacKenzie *et al.*, 1994), but also the Wyre, 60 km south (Aston and Stanners 1981) and in the Solway Firth to the north (Jones *et al.*, 1984). The intertidal sediments of the Esk estuary have been studied here.

Actinide Experimental Data

30 cm deep sediment cores (20 x 20 cm in area) were collected over a number of years from the intertidal saltmarshes of the Esk Estuary The concentrations of a suite of actinides and other radioisotopes have been determined as a function of depth in previous studies (Marsden 2003, Marsden et al 2001, Keith-Roach *et al*. 2001, Morris *et al*. 2000).

The Model

A model was developed with the aim of matching the observed sediment profiles quantitatively to discharge histories. The model is based on the assumptions that, once discharged to sea, the radionuclides become strongly associated with suspended particles which are focused into a region of fine-grained sediment offshore, the 'Mud Patch'. Here, the radioisotopes are mixed by bioturbation and diffusion. Each year, a fraction of the surface material in the mud patch is transported onshore and accumulates in the salt marsh. Therefore, material does not move direct from the end of the Sellafield pipeline to the salt-marsh site, but first becomes incorporated into the submerged mud patch, which acts as a buffer. With time, more material enters the top of this patch, and becomes mixed with the existing material via bioturbation. Therefore, since 1952 the depth concentration profile of the mud patch has been constantly evolving. The majority of the material arriving at the Salt Marsh has been scoured from the top of the mud patch by the action of tides, waves and storms etc. Unlike the mud patch, the salt marsh site is not subject to significant biotirbation, and as the marsh accretes, the history of arrivals is conserved. Hence, there should be a direct relationship between the concentration of activity at the top of the mud patch and the material arriving at the salt marsh at any given time, and a plot of mud patch surface activity vs time should have the same shape as a plot of activity vs depth at the salt marsh.

Several authors (*e.g.* Woodhead 1988; MacKenzie *et al.*, 1998) have suggested that bioturbation in the surface sediments of the Irish Sea will produce an effect analogous to simple diffusion. In this case, Fick's Law may be used to calculate the movement of radionuclides through the mud patch: the vertical flux of material $(dx/dt)_z$ through a cross-sectional area A will be given by,

$$\left(dx/dt\right)_z = -D_z A\left(d[x]/dz\right)_z \qquad (1)$$

where D_z is the diffusion coefficient at depth z (strictly an apparent or pseudo-diffusion coefficient, since Fick's Law is used here to simulate bioturbation only; this is not a chemical diffusion coefficient), $[x]$ is the concentration of contaminant x at depth z, $(d[x]/dz)_z$ is the

concentration gradient at z and t is time. The model considers a hypothetical, homogeneous sediment column of total length z_{max}, split into N equal slices, each of depth Δz (= z_{max}/N).

Given that this mixing is due to bioturbation, it can only take place where the biota are active. Although many species may be active at shallow depths, the worm *Maxmuelleria lankesteri* is thought to be responsible for the majority of the observed mixing at moderate and greater depths (Kershaw *et al*., 1983; 1984; 1999). *M. lankesteri* is found up to 1.5 m below the sediment surface, so the model considers that mixing ceases at 1.5 m depth. The value of D_z will therefore decrease with depth. In the model, it is assumed that there is a constant diffusion coefficient in the top 10 cm of the sediment, followed by a linear decrease to zero at 1.5 m.

For each boundary, i, between slices, the model calculates the amount of material, Δx_i, which will cross that boundary:

$$\Delta x_i = -D_i A \Delta t \frac{\Delta [x]_i}{\Delta z} \qquad (2)$$

where D_i is the diffusion coefficient at boundary i, $\Delta[x]_i$ is the difference in concentration between the two slices and Δt is the length of the time step. Once all Δx_i have been calculated, the model then moves the appropriate amount of material across the boundary. This procedure is repeated for each time step, producing depth-concentration profiles with time. There is no restriction on the direction of movement (up or down), which is determined only by the sign of the concentration gradient.

It is assumed that, at any time, the radionuclide activity concentration of the newly contaminated sediment, at the top of the column, will be proportional to the activity being discharged from Sellafield at that time. The constant of proportionality is unknown, so the model uses and produces relative concentrations only. The concentrations for each step are obtained by interpolation of the discharge data, obtained from Gray *et al.* (1995). It is assumed that material will be incorporated into the top slice by the same diffusion process that controls movement across the boundaries within the column, *i.e.* determined by equation 2. Here, Δx_i will be given by the difference in concentration between the top slice and the current concentration, as obtained from the discharge data, and so the amount of "new" material entering the system may be calculated at each time step. At each time step, new material enters the column from the top (z = 0) only.

The experimental data from the mud patch and the model output profiles may be compared directly. To predict the salt marsh profiles, it is assumed that a certain (variable) depth, d, of material is resuspended, carried on shore and deposited. For each time step, the mean concentration in the slices down to depth, d, is calculated and plotted against time. This plot may be compared with the experimentally determined profile at the salt marsh.

There are two uncertain parameters: the magnitude of the diffusion coefficients and the resuspension depth *d*. Although there is agreement that bioturbation is analogous to diffusion, there is no consensus as to the correct value of the diffusion coefficient. The suggested values range from 9.5 x 10^{-8} to 5.7 x 10^{-6} $cm^{-2}s^{-1}$ (Woodhead 1988). In the case of resuspension depth, there are no published values.

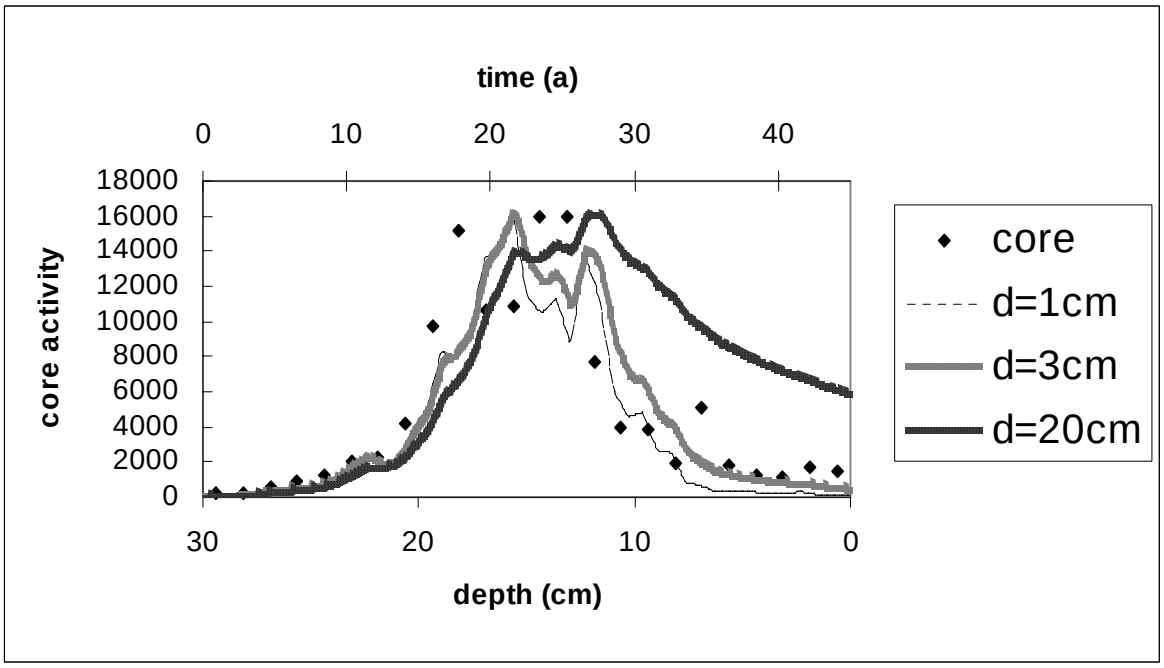

Figure 1. Measured $^{239+240}$Pu salt marsh core activity profile (Bq kg^{-1}) and model predictions (relative) for a diffusion coefficient of 9.5x10^{-8} $cm^{-2}s^{-1}$ and resuspension depths of 1 cm, 3 cm and 20 cm.

Initial calculations were performed for ^{239,240}Pu using a range of resuspension depths (*d*) from 1 to 20 cm, and diffusion coefficients at the top of the column from 9.5 x 10^{-8} to 5.7 x 10^{-6} $cm^{-2}s^{-1}$. Figure 1 shows the effect of varying resuspension depth, with constant *D* (= 9.5 x 10^{-8} $cm^{-2}s^{-1}$). The results with *d* = 1 cm most closely resemble the discharge history and those with *d* = 20 cm the least. The top of the column will always resemble the discharge most precisely, since it has been in direct contact with the "new" material, and the diffusion process will tend to homogenise adjacent regions, the rate depending on *D*. As resuspension depth increases, more old material is included and the profile diverges from the discharge history. The *d* = 20 cm profile becomes increasingly smeared with time and less like the discharge history, as there will be increasing amounts of old material included. Indeed, if the general mechanism proposed here is correct, then the salt marsh profiles should most closely match the discharge data at depth and diverge as depth decreases, regardless of the values of resuspension depth or diffusion coefficient. The *d* = 20 cm plot least resembles the profile data, which is unsurprising, since this resuspension depth is perhaps unrealistic. The more realistic *d* = 1 and 3 cm plots are very similar and, in fact, it was

found that, for any resuspension depth < 6cm, the results, and indeed the goodness of fit, were relatively insensitive to *d*.

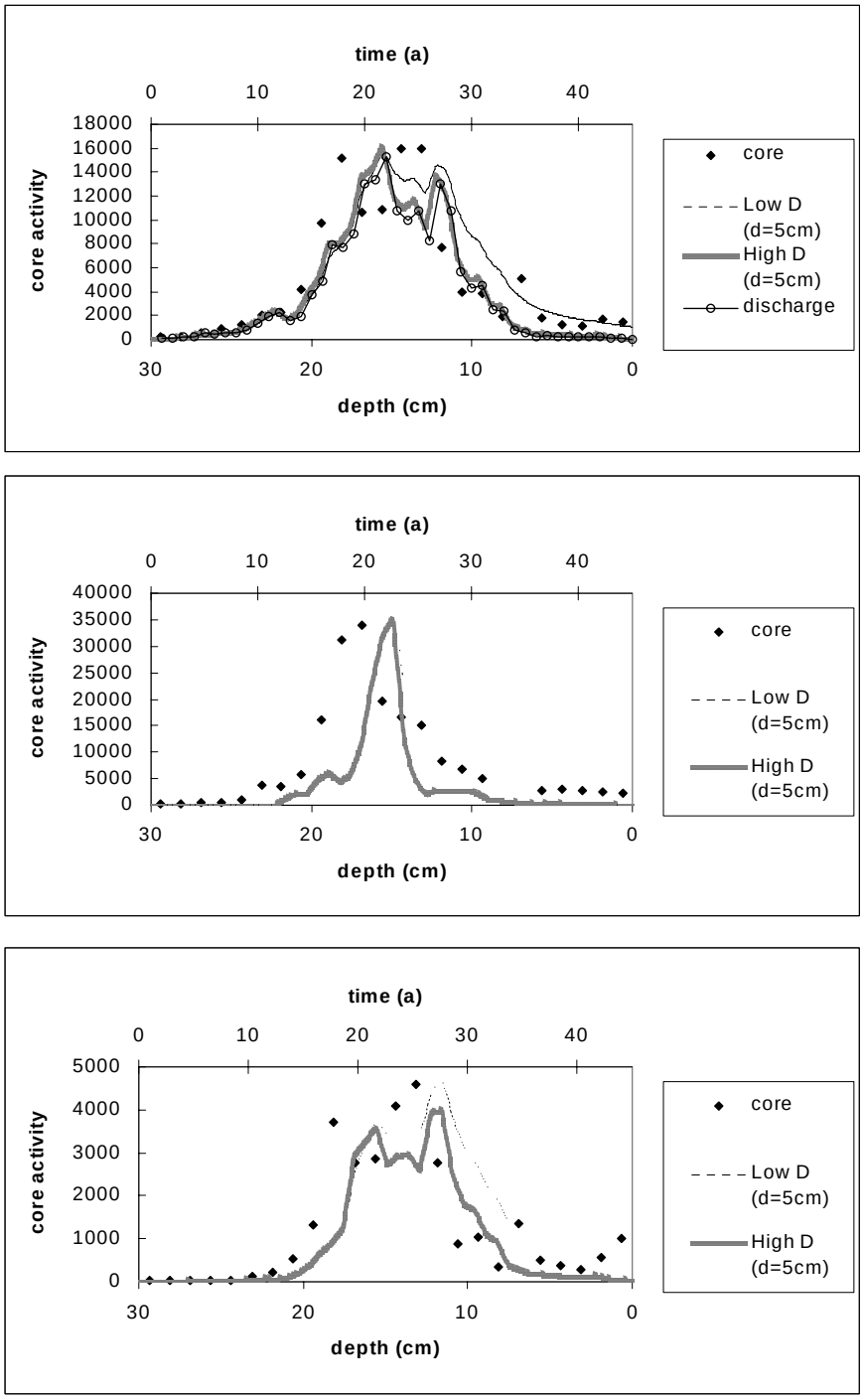

Figure 2. Sensitivity of predicted salt marsh profiles (relative activity concentrations) to diffusion coefficient (*d* = 5 cm). Results presented for (top to bottom) ^{239,240}Pu, ^{241}Am and ^{238}Pu.

Figure 2 shows the effect of diffusion coefficient on predicted salt marsh profiles for ^{239,240}Pu, ^{241}Am and ^{238}Pu respectively; in each case, d = 5 cm. For the Pu isotopes, the difference in fit does not seem very significant. However, in the case of ^{241}Am, there is a much better match to the shape with the smaller diffusion coefficient (9.5 x 10^{-8} $cm^{-2}s^{-1}$). The higher diffusion coefficient has produced the profiles that most closely resemble the discharge, because the old material quickly moves further down the column and is protected from resuspension and subsequent incorporation into the salt marsh sediment profile.

In the early 1980s, core samples were collected from the offshore mud patch and analysed for ^{239,240}Pu, ^{241}Am and ^{238}Pu (Kershaw *et al*., 1983). Figure 3 shows the relationships between these core data and model predictions for the two different diffusion coefficients (9.5 x 10^{-8} and 5.7 x 10^{-6} $cm^{-2}s^{-1}$). Figures 3a and 3b compare model and measured concentrations for ^{239,240}Pu and ^{241}Am respectively, while Figure 3c shows the ^{239,240}Pu/^{238}Pu activity ratios. In all cases, the smaller diffusion coefficient gives a much better fit than the larger. Therefore, both salt marsh and mud patch data suggest that the most appropriate value for the diffusion coefficient is very close to 9.5 x 10^{-8} $cm^{-2}s^{-1}$.

There are no published discharge data for ^{244}Cm. However, a ^{244}Cm profile at the salt marsh has been determined (Marsden 2003). Therefore, we may use the model in reverse to calculate a discharge history for ^{244}Cm, assuming that Cm is subject to the same bioturbation processes as the other isotopes, which seems reasonable. This time, a process of trial and error was used to produce a relative discharge history that, when used as input for the model (using d = 5 cm; D = 9.5 x 10^{-8} $cm^{-2}s^{-1}$) gives a result that matches most closely the measured profile data. The constructed theoretical discharge history, relative of course, is shown in Figure 4. The predicted maximum discharges in 1969 and 1974 are earlier than those real discharge maxima for the other isotopes. However, Figures 1 and 2 show that for Pu and Am, although the model gives a good fit to the shape, there is a discrepancy between the positions of the model and real maxima, approximately 3 years. There should be a similar shift here, giving adjusted maxima at 1972 and 1977, in line with the other isotopes.

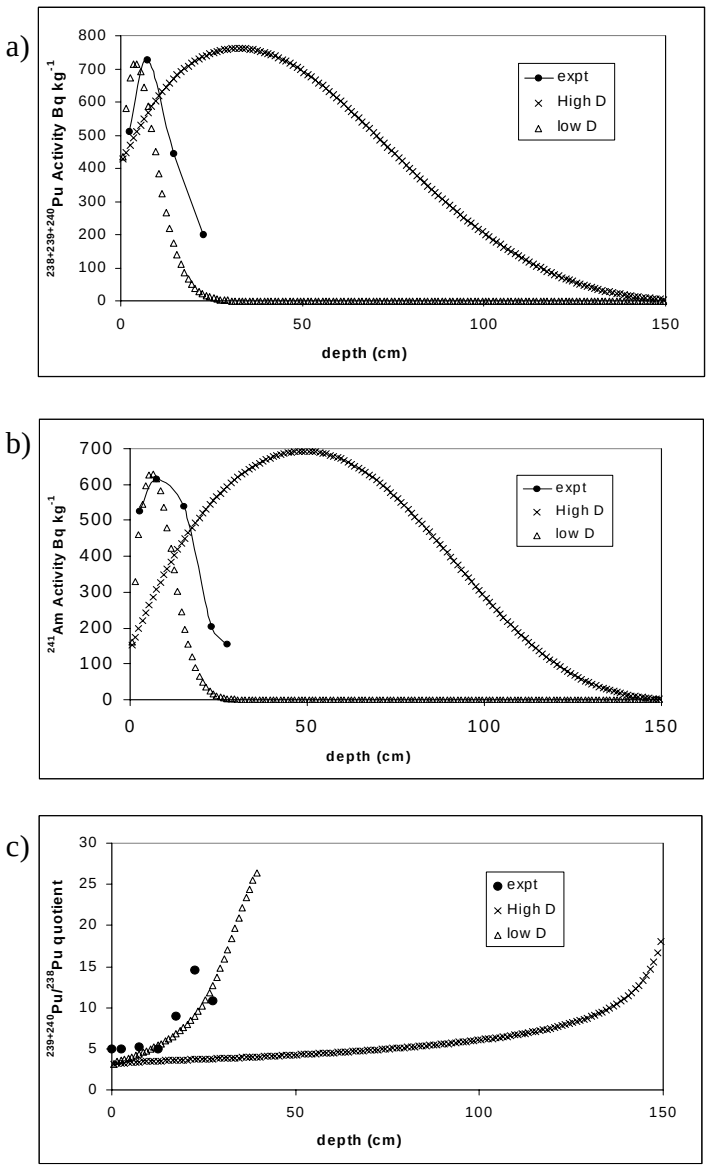

Figure 3. Modelled profile distributions in the mud patch for a) ^{238}, ^{239,240}Pu, b) ^{241}Am and c) ^{239,240}Pu/^{238}Pu activity ratio. Data presented for D = 9.5 x 10^{-8} and 5.7 x 10^{-6} $cm^{-2}s^{-1}$.

Conclusions

A model has been developed that appears to be able to simulate and predict the movement of isotopes from Sellafield within the North Eastern inshore waters of the Irish Sea. The results confirm that the movement of isotopes within the off-shore mud patch may be simulated with simple diffusion constants, which simulate bioturbation down to a depth of 1.5 m. Moreover, the 'best' value of diffusion constant is 9.5 x 10^{-8} $cm^{-2}s^{-1}$ in the top few centimetres, reducing linearly to 0 at 1.5 m.

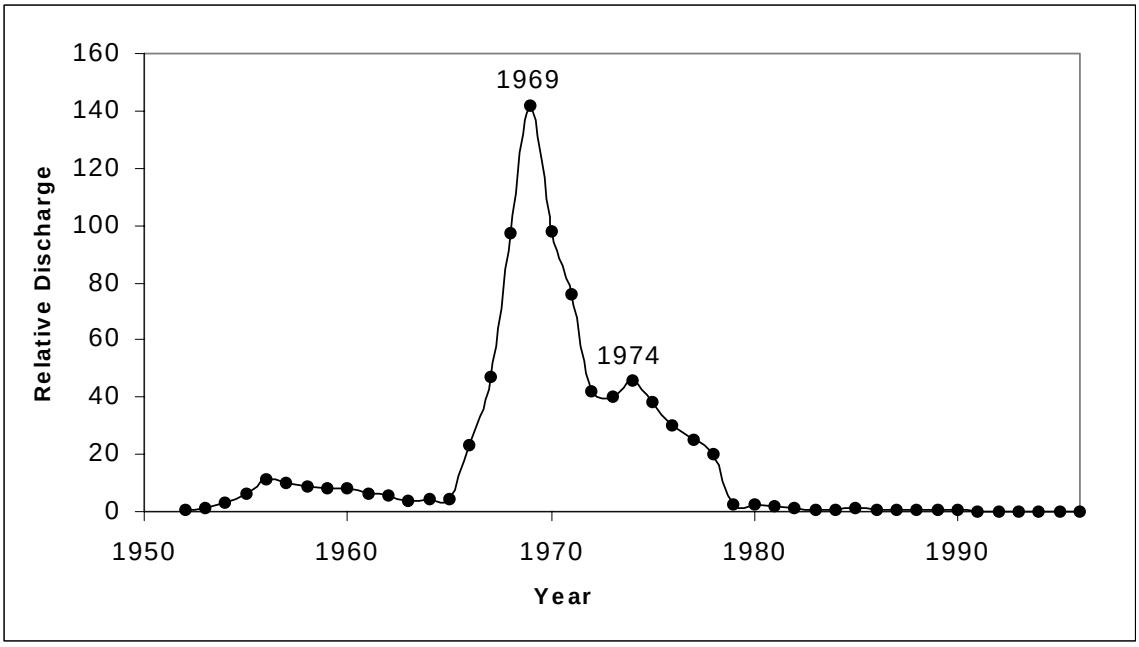

Figure 10. Predicted discharge history for ^{244}Cm

There is a definite relationship between the top few (1-6) centimetres of the model mud patch profile and the depth profiles of the same isotopes at an inter-tidal site on the Esk estuary. This is strong evidence that the mechanism for the on-shore transport of radionuclides is on reactive particulates associated with the mud patch. There is a discrepancy in the model predicted activity peaks with depth at the inter-tidal site and the real data; the origin is unclear presently. The model has been used to estimate a discharge history for ^{244}Cm.

References

Aston, S.R. and Stanners, D.A. (1981). Plutonium transport to and deposition and mobility in Irish Sea sediments. Nature, **289**, 581-582.

Clark, D.L., Hobart, D.E. and Neu, M.P. (1995). Actinide carbonate complexes and their importance in actinide environmental chemistry. Chemical Reviews, **95**, 25-48.

Cundy, A.B., Croudace, I.W., Warwick, P.E., Oh, J.-S. & Haslett, S.K. (2002). Accumulation of COGEMA-La Hague-derived reprocessing wastes in French salt marsh sediments. Environmental Science and Technology, 36, 4990-4997.

Gray, J., Jones, S.R. and Smith, A.D. (1995). Discharges to the environment from the Sellafield site 1951-1992. Journal of Radiological Protection, **2**, 99-131.

Hetherington, J.A. (1976). The behaviour of plutonium nuclides in the Irish Sea. In: Environmental toxicity of aquatic radionuclides: models and mechanisms (Miller, M.W. and Stannard, J.N. eds), Ann Arbor, Michigan, pp 81-106.

Hetherington, J.A. (1978). The uptake of plutonium nuclides by marine sediments. Marine Science Communications, **4**, 239-274.

Jones, D.G., Miller, J.M. and Roberts, P.D. (1984). The distribution of ^{137}Cs in surface intertidal sediments from the Solway Firth. Marine Pollution Bulletin, **15**, 194-197.

Keith-Roach, M.J., Day, J.P., Fifield, L.K. and Livens, F.R. (2001). Measurement of Np-237 in environmental water samples by accelerator mass spectrometry. Analyst, **126**, 58-61.

Kershaw, P.J., Swift, D.J., Pentreath, R.J. and Lovett, M.B. (1983). Plutonium redistribution by biological activity in Irish Sea sediments. Nature, **306**, 774-775.

Kershaw, P.J., Swift, D.J., Pentreath, R.J. and Lovett, M.B. (1984). The incorporation of plutonium, americium and curium into the Irish Sea seabed by biological activity. Science of the Total Environment, **40**, 61-81.

Kershaw, P.J., Woodhead, D.S., Malcolm, S.J., Allington, D.J. and Lovett, M.B. (1990). A sediment history of Sellafield discharges. Journal of Environmental Radioactivity, **12**, 201-241.

Kershaw, P.J., Pentreath, R.J., Woodhead, D.S. and Hunt, G.J. (1992). A review of radioactivity in the Irish Sea: a report prepared for the Marine Pollution Monitoring Management Group, Aquatic Environment Monitoring Report, No. 32, MAFF.

Kershaw, P.J., Denoon, D.C. and Woodhead, D.S. (1999). Observations on the redistribution of plutonium and americium in the Irish Sea sediments, 1978 to 1996: concentrations and inventories. Journal of Environmental Radioactivity, **44**, 191-221.

Marsden, O.J. Ph.D. thesis, University of Manchester (2003).

Marsden, O.J., Livens, F.R., Day, J.P., Fifield, L.K. and Goodall, P.S. (2001). Determination of U-236 in sediment samples by accelerator mass spectrometry. Analyst, **126**, 633-636.

Mackenzie, A.B., Scott, R.D., Allan, R.L., Ben Shaban, Y.A., Cook, G.T. and Pulford, I.D. (1994). Sediment radionuclide profiles: implications for mechanisms of Sellafield waste dispersal in the Irish Sea. Journal of Environmental Radioactivity, **23**, 39-69.

Mackenzie, A.B., Cook, G.T., McDonald, P. and Jones, S.R. (1998). The influence of mixing timescales and re-dissolution processes on the distribution of radionuclides in north east Irish Sea sediments. Journal of Environmental Radioactivity, **39**, 35-53.

Morris K., Butterworth J.C., and Livens F.R. (2000). Evidence for the remobilisation of Sellafield waste radionuclides in an intertidal salt marsh, west Cumbria, UK. Estuarine and Coastal Shelf Science, **51**, 613-625.

Pentreath, R.J. (1988). Sources of radionuclides in the marine environment. In: Radionuclides: a tool for oceanography (Guary, J.C., Guegueniat, P. and Pentreath, R.J., eds). Elsevier, London, pp 12-34.

Pentreath, R.J., Lovett, M.B., Jefferies, D.F., Woodhead, D.S., Talbot, J.W. and Mitchell, N. (1984). The impact on public radiation exposure of transuranium nuclides discharged in liquid wastes from fuel reprocessing at Sellafield, U.K. In: Radioactive waste management. Proc. Symp. Seattle, 1983. IAEA.

Ridgway, J. & Shimmield, G. (2002). Estuaries as repositories of historical contamination and their impact on shelf seas. Estuarine, Coastal and Shelf Science, **55**, 903-928.

Thomson, J., Dyer, F.M. & Croudace, I.W. (2002). Records of radionuclide deposition in two saltmarshes in the United Kingdom with contrasting redox and accumulation conditions. Geochimica et Cosmochimica Acta, **66**, 1011-1023.

Wilson, P.D. (1996). The nuclear fuel cycle: from ore to waste. Oxford University Press.

Woodhead, D.S. (1988). Mixing processes in the near shore marine sediments as inferred from the distributions of radionuclides discharged into the Irish Sea from BNFL, Sellafield. In: Radionuclides, a tool for oceanography (Guary, J.C., Guegueniat, P. and Pentreath, R.J., eds), Elsevier, London, pp 331-340.

Annex 17

Comparison of Dialysis, Electrophoresis, Ion Exchange and Ultrafiltration as Methods for Analysis of Complexation of Europium with Humic Acid

Benes P., Stamberg K., Mizera J. and Prochazkova S.

Czech Technical University, Department of Nuclear Chemistry,
Brehova 7, 115 19 Praha 1, Czech Republic

Comparison of Dialysis, Electrophoresis, Ion Exchange and Ultrafiltration as Methods for Analysis of Complexation of Europium with Humic Acid

Benes P., Stamberg K., Mizera J. and Prochazkova S.

Czech Technical University, Department of Nuclear Chemistry, Brehova 7, 115 19 Praha 1, Czech Republic

Abstract

Four experimental methods for determination of humate metal ion interaction were tested: equilibrium dialysis, free liquid electrophoresis, cation exchange and ultrafiltration. The system studied was europium (2.3×10^{-7} - 5×10^{-4} M, labelled with ^{152}Eu) and Aldrich humic acid (2-60 mg/L), pH 4-6, ionic strength 0.01 or 0.1($NaClO_4$), solution age 1 and 7 d. For each method, suitable experimental arrangement was found and problems or limitations were identified based on experimental results obtained under comparable conditions. Particular attention was paid to the effects of sorption of Eu and humic acid on vessel and apparatus walls, shift of equilibrium in the system and method of evaluation of results, mostly expressed as the degree of complexation (*%EuHA*). Results from dialysis, electrophoresis and ion exchange were nearly identical and these methods can yield trustworthy humate complexation data. Ultrafiltration gave incorrect data due to imperfect separation of complexed and uncomplexed Eu forms. Conclusions drawn on individual methods will contribute for judging published data obtained by the methods.

Introduction

A basic condition for obtaining reliable thermodynamic data on metal/radionuclide complexation with humic substances is the use of a well characterized method suitable for the purpose. Lack in critical assessment of experimental methods used may be the reason for frequent spread or contradiction of existing data, particularly for trace concentrations of metals, where a number of experimental difficulties can be expected. Experimental methods for complexation studies can be divided into three types:

A. Direct methods based on determination of metal humate complex after its separation from other metal species, e.g. dialysis, electrophoresis and ultrafiltration. These methods can be subject to errors due to an incomplete separation, shift of equilibrium in the system and sorption loss of metal or humic substance.

B. Direct methods without separation, based on direct measurement of complexed and/or uncomplexed metal species, for instance by ion selective electrodes or variety of spectroscopic methods. These methods are less prone to the problems mentioned above, but may have limited applicability or sensitivity.

C. Indirect methods that analyse the effect of humic substances on metal behaviour in a more complex process or system like ion exchange, solvent extraction or acidobasic titration. Potential problems here are complexity of data analysis, relying on additional input data and sometimes slow inherent shift of equilibrium.

Knowledge of the problems associated with the use of individual methods is far from sufficient, despite of rather large number of studies published (see, e.g., Weber 1988, Jones and Bryan 1998). With the aim to enhance the knowledge necessary for improving confidence in own and published results on radionuclide-humate interaction, we studied in detail the use of four methods for analysis of complexation of europium with humic acid (HA). Equilibrium dialysis, electrophoresis, ion exchange and ultrafiltration were tested. These methods belong to the most frequently used methods of type A or C mentioned above. Europium was selected as trivalent element often employed as an analogue of trivalent actinides, with a strong sorption on available surfaces. The methods were tested in their radiotracer arrangement with ^{152}Eu and the results obtained with them under similar conditions were compared.

Principles of the methods

Dialysis employs separation of uncomplexed metal M_{free} and metal humate complex MHA by diffusion through a membrane permeable only for M_{free}. Distribution of metal is studied between two solutions in reservoirs or cell compartments A and B separated by the membrane, one of them (A) containing humic acid. In equilibrium dialysis, M_{free} equilibrates between the two compartments, MHA is retained in compartment A. Then A contains MHA and M_{free} in concentrations $C_{MHA} + C_{\boldsymbol{M}}$, respectively, B contains $C_{\boldsymbol{M}}$. Degree of complexation *%MHA* can be calculated as

$$\%MHA = 100\ C_{MHA}/(C_{MHA} + C_{\boldsymbol{M}}) = 100\ (C_A - C_B)/\ C_B\ , \qquad (1)$$

where C_A, C_B are equilibrium concentrations of the metal in compartments A, B, respectively.

Three basic experimental arrangements of equilibrium dialysis have been described in the literature: equilibrium dialysis with equal (Backes and Tipping 1987) and unequal (Benes and Steinnes 1974, Weber 1988) volumes of reservoirs and equilibrium dialysis with ligand exchange (Van Loon et al. 1992, Dierckx et al. 1994, Glaus et al. 1995). All three arrangements use a surplus of indifferent electrolyte to suppress membrane (Donnan) equilibria that could cause unequal distribution of uncomplexed metal. In equilibrium dialysis with equal volumes of reservoirs (1:1), passage of M_{free} from reservoir A to reservoir B can shift equilibrium between MHA and M_{free} in the system or lead to error in determination of *%MHA* due to dilution of M_{free}. The shift or dilution are suppressed in equilibrium dialysis with unequal reservoir volumes (X:1) where the volume of reservoir A is X times larger than that of B. In this case an arrangement with floating dialysis bag (reservoir B) is often used resulting in reduced sorption loss of metal and humic substance on walls of dialysis cell (Benes et al. 1975, Shin et al. 1996, Lead et al. 1998). The sorption loss represents a principal problem when working with low metal concentrations. Another problem is the narrow analytical window of ordinary equilibrium dialysis as *%MHA* has to be in the range of 5-95% in order that it can be determined with acceptable error.

Both the problems can be solved by equilibrium dialysis with ligand exchange where a second complexing ligand L is added to the system which forms a low molecular weight complex ML_n with the metal. The complex should easily penetrate dialysis membrane, distribute equally between the reservoirs and compete with MHA complex. Formation of ML_n complex can shift the analytical window of the method to a desirable position and reduce metal sorption on dialysis cell and membrane. However, evaluation of the metal humate complexation by this method has to take into account constraints due to shift of equilibrium and requires exact knowledge of stability constant of ML_n complex. The method does not solve possible general problems in the dialysis, which are the slow attainment of dialysis equilibrium and partial passage of HA (and MHA) through the membrane. The equilibrium dialysis with ligand exchange belongs among indirect methods of metal humate complexation analysis and was not studied in this paper.

Method of electrophoresis is based on different directions or velocities of migration of metal humate complex and uncomplexed metal forms in an electric field. In this paper, method of free liquid electrophoresis (Benes and Glos 1979) is used. The method compares electrophoretic mobility of metal in solution in the presence and absence of humic substances and assumes that only negatively charged metal humates are present. Then abundance of metal humate complex can be calculated from the decrease of electrophoretic mobility towards cathode upon addition of humic substances to the solution. Further details can be found in Mizera et al. 2003 where the problems and errors of the method are discussed.

In ion exchange method, the effect of humic substances on the distribution of metal between solution and ion exchange resin is studied. Strongly acidic cation exchangers are most frequently used (see for instance Norden et al. 1993, Lead et al. 1998, Brown et al. 1999, Lenhart et al. 2000 and Gu et al. 2001). Then it is assumed that only cationic forms of metal are sorbed whereas humate complexes which are negatively charged or neutral remain in solution. For the use of the method, sorption isotherm of cationic forms of the metal on the

ion exchanger must be known for a given set of experimental conditions (pH, ionic strength, temperature). This enables calculation of equilibrium concentration of the cationic forms and, from the experimental value of distribution coefficient of metal in the presence of humic substance, also the equilibrium concentration of MHA and *%MHA*. The sorption isotherm is often assumed to be linear (Bertha and Choppin 1978, Fairhurst et al. 1995) which is, however, sometimes unjustified. The effect of sorption losses on reaction vessels remains unexplored in this method. The method is indirect in principle and involves shift of equilibrium between M_{free} and MHA due to M_{free} sorption on ion exchanger.

Principle of the ultrafiltration method is separation of M_{free} and MHA with a basic assumption that the ultrafilter quantitatively retains MHA and lets M_{free} to pass unretarded to ultrafiltrate (e.g. Caceci 1985, Leonard et al. 1994, Shin et al. 1996, Nifanteva et al. 1999). Fulfilment of this assumption is not easy as humic substances are heterogeneous in nature and can contain a large proportion of low molecular weight components, and M_{free} can be adsorbed on the ultrafilter, particularly at very low concentrations. Thus the separation has always to be carefully checked. Further problems may be associated with shift of equilibrium due to sorption of metal on the walls of ultrafiltration cell and to the cumulation of humic substances in the cell during ultrafiltration. The degree of complexation can be determined from the concentration of metal in ultrafiltrate or from the increase of concentration of metal in the solution remaining in the cell after ultrafiltration.

Experimental

Reagents, solution preparations and basic conditions of experiments

All the stock and working solutions were prepared from analytical reagents without further purification and from ultrapure water (Millipore Milli-Q 50). Humic acid (HA) was purchased from Aldrich (Na salt, tech., Lot No. 01816-054) and purified/protonated by the procedure described in Kim et al. 1990. The lyophilized product was characterized by potentiometric titration with NaOH, back titration of its mixture with excess of $Ba(OH)_2$ (proton exchange capacity PEC = 7.0 mol/kg), thermogravimetric analysis and FTIR spectroscopy (Mizera et al. 2003). It was dissolved in 0.1 M NaOH under nitrogen, adjusted to pH 6 and concentration 500 mg/L, and stored in refrigerator. A preparation of ^{152}Eu with minor admixture of ^{154}Eu was obtained from Polatom (Swierk, Poland) and had specific activity of 132 GBq/g.

Working solutions were mixed in polythene bottles from water and (in the following order) stock solutions of HA, NaOH or $HClO_4$, $NaClO_4$ and Eu^{3+} (usually labelled with ^{152}Eu) in 0.01 M $HClO_4$ to obtain required pH and composition of solution and initial concentration of HA and labelled europium. Solutions with pH 6 contained also MES at concentration 1×10^{-3} mol/L. After adjustment of pH by dropwise addition of $HClO_4$ or NaOH the solutions were stored in dark for 24 h or 7 d (pre-equilibration time), their pH was measured and, if necessary, readjusted. The sorption loss of Eu during pre-equilibration was evaluated by measurement of activity of solution aliquot at the beginning and end of pre-equilibration.

All the experiments were carried out at room temperature, 18 - 25°C. In order to allow better comparison of the methods and elucidation of their possible drawbacks, the following

basic conditions were set for the experiments: pH 4 and 6, ionic strength I = 0.01 and 0.1 (both the parameters can affect the degree of complexation and extent of sorption losses) and so called loading of HA with Eu defined as the initial Eu concentration in solution (C_{Euo}, for dialysis, electrophoresis and ultrafiltration) or equilibrium concentration of Eu in solution ($C_{Eu3+} + C_{EuHA}$, for ion exchange) divided by one third of the total proton exchange capacity of HA in the solution (C_{HAo}×PEC/3) equal to 0.01, 0.1 and 0.5 or, multiplied with 100, 1%, 10% and 50 %. It is worthwhile to note that so defined loading is not the actual loading as the total proton exchange capacity is not the actual capacity (at pH 4 and 6 only a part of exchange groups of HA is dissociated – Mizera et al. 2003) and the initial or equilibrium concentration of Eu is not the concentration of Eu bound to HA. However, so defined loading can be easily checked and still represents a useful parameter which can affect formation and properties of metal humate complexes and thus also their analysis. Finally, the two times of pre-equilibration may disclose sensitivity of a method to the strength of the bond of metal to HA or to a slow dissociation of EuHA, both possibly depending on the pre-equilibration.

Instrumentation and procedures

Activity of all samples collected in the experiments was counted in glass vials using a well-type NaI(Tl) crystal with a single-channel analyzer. Absorbance in selected samples was measured with a spectrophotometer at 254 nm.

Three experimental arrangements of equilibrium dialysis (ED) were tested. In all of them, solution A had the same initial composition as solution B except for Eu and HA that were added only to solution A. The first arrangement (ED 1:1) employed membrane SpectraPor 7 with molecular weight cut-off (MWCO) value 1 kDa and dialysis cell consisting of two equivolume (20 mL) compartments filled with 15 mL portions of solution (Benes 1967). The stirring was realized by shaking the cell along the plane of membrane held between the compartments. Activities of 1 mL samples of solutions taken in regular time intervals from both compartments through filling holes were measured. The second arrangement (ED 20:1) used a floating bag made of Visking dialysis tubing with MWCO 10-12 kDa, which was tied on both ends and filled with 10 mL of solution B. Stirring was realized by magnetic stirring of solution A in polythene bottle. Only one sample of solution B was taken after 6-14 d dialysis from the cut bag. In the third arrangement (ED > 25:1) dialysis bag was made of SpectraPor Biotech CE tubing (MWCO 500 Da, flat width 16 mm), clamped on both sides, filled with 3 mL of solution B and suspended in 230 mL solution A in a narrow polythene bottle covered with plastic foil. Two bags were placed into one bottle and the stirring was done magnetically. Solution for dialysis labelled with ^{152}Eu was prepared directly in the dialysis bottle, left to pre-equilibrate for 24 h, then two bags were placed into it and dialysis continued for 6 days. Then one bag was withdrawn, replaced by a fresh bag, opened and sampled for measurement of activity and absorbance. Dialysis was continued for another 6 days when the remaining bags were opened and sampled. 1 mL samples were also taken from solution A after its preparation and at the beginning and end of each dialysis.

The free liquid electrophoresis was studied in electrophoretic cell consisting of three parts (anodic, central, and cathodic) filled with identical solutions of stable Eu except for the central part which also contained radiotracer. From redistribution of the radiotracer caused by

migration of charged Eu species in the electric field, the cathodic and anodic mobilities of Eu were calculated (see Mizera et al. 2003 for details). The experiments were run at constant current of 2.2 mA at I = 0.1, 1 mA at I = 0.01, with corresponding voltage of 250-350 V, at room temperature, for 1 hour at I = 0.1, 2 hours at I = 0.01. Each electrophoretic experiment was carried out in duplicate.

Ion exchange method was realized in batch arrangement using strongly acidic cation exchanger Amberlite IR-120 in Na form (grain size 0.4-0.6 mm). 0.1 g of swelled and centrifuged ion exchanger was equilibrated in polythene bottle with the pre-equilibrated labelled solution containing HA at phase ratio (V/m) 500 mL/g for 90-100 h. Then the phases were separated by sedimentation and solution was sampled for determination of activity of non-adsorbed Eu. Similar experiments were carried out in the absence of HA for determination of Eu sorption isotherm.

Ultrafiltration was made in two identical stirred ultrafiltration cells (Amicon Model 8050) using two types of ultrafilters: Millipore YC 05 (cellulose acetate, MWCO 500 Da) and Millipore PLAC 04310 (regenerated cellulose, MWCO 1 kDa). The procedure used enabled detailed evaluation of Eu sorption during the ultrafiltration. First 50 mL of pre-equilibrated solution were transferred into UF cell and left to equilibrate with the cell and ultrafilter for 2h under continuous stirring. 1 mL solution samples were taken at the beginning and end of the equilibration. Their activities (a_0 and a_1) served for determination of Eu sorption loss ($a_0 - a_1$). Then ultrafiltration was conducted applying nitrogen pressure (up to 0.37 MPa) unless 10 approximately 1 mL portions of ultrafiltrate were collected in measuring glass vials. The exact volume of the portions was determined by weighing, their activities ($a_{f,i}$) indicated the course of Eu passage through ultrafilter and the sum of the activities ($\Sigma a_{f,i} = a_4$) was used for evaluation of Eu retention. The solution remaining in the cell after ultrafiltration was sampled (a_2), discarded and the cell was briefly rinsed with water. Then the cell was desorbed with 50 mL 0.1 M sodium oxalate for 2 h (desorbed activity a_3), the cell was disassembled and its lower part beneath the filter (including outlet tubing which was clamped for this purpose) was desorbed with two 5 mL portions of 1 M HCl for 15 and 60 min (activities of 1 mL portions a_5 and a_6, respectively). In order to study distribution of adsorbed Eu between the cell and ultrafilter and to check efficiency of the ultrafiter desorption, in some experiments the ultrafilter was withdrawn after the cell rinsing and its activity was measured. The same was done after desorption of reassembled cell. The measured activities were corrected to enable their comparison with total activity in the system (49 a_0).

Results of ultrafiltration were expressed as percentage of Eu retained in the cell ($\%R$), which was calculated from the activity passed through the filter

$$\%R_1 = 100 - 100\ (a_4 + 5a_5 + 5a_6) / a_1V_x \qquad (2)$$

or from the activity remaining in the cell

$$\%R_2 = 100 - 100\ [a_1V_1 - a_2(V_1 - V_f - V_x)] / a_1(V_f + V_x). \qquad (3)$$

Here V_1 , V_f and V_x are: initial volume of solution (48 mL), total volume of ultrafiltrate and volume of space below the filter, respectively.

Results and discussion

Dialysis

The first experiments were carried out using equilibrium dialysis with equal volumes of compartments (1:1). A large sorption of Eu was observed (up to 30%) both on the membrane and the cell. The increase of Eu concentration in compartment B was very slow and did not reach a steady value even after 360 h. This was probably due to the sorption of Eu on the walls of compartment B and/or slow passage of EuHA complexes through the membrane (MWCO 1 kDa). Another possible reason, slow dissociation of EuHA complexes due to shift of equilibrium in the system, is less probable as other methods indicated that the dissociation is rather rapid (Stamberg et al., this technical progress report, method of ion exchange below). Whatever is the reason, the slow establishment of equilibrium makes the arrangement tested unsuitable for the purpose.

Equilibrium dialysis with volume ratio 20:1 used reservoir B in the form of bag made of Visking cellophane. In this case the main problem was penetration of HA (and probably also EuHA) into the bag, as determined by spectrophotometric measurements at 254 nm. Establishment of dialysis equilibrium was very slow also here. Therefore further experiments were carried out with 500 Da membrane at the volume ratio 230:6. Penetration of HA through this membrane was small. From the activity and absorbance measured in the samples of solutions taken from reservoirs A and B, the following data were calculated: sorption loss (in %) of Eu (S_{Eu}) or HA (S_{HA}) and passage of Eu into the dialysis bag expressed as the ratio of the volume activity in reservoir B (dialysis bag) to the actual or initial activity in reservoir A (dialysis vessel) – B/A or B/A_0. The data are presented in Table 1 for all the conditions studied and represent results of single experiments or averages of two or three repeated experiments. In case when two data are separated by slash, the data before the slash is valid for dialysis time of 6 d, the data behind the slash is for 12 d. Their comparison indicates whether equilibrium was established or not.

The passage of Eu into the bag (B/A or B/A_0) is the main parameter needed for calculation of *%EuHA*. Its first expression (B/A) takes into account sorption losses of Eu on the dialysis vessel and the bag, the second one (B/A_0) neglects the sorption. Since the sorption losses of Eu were rather large and, consequently, significant differences between B/A and B/A_0 were found (Table 1), it is important to decide which of the values determined should be used for calculation of *%EuHA*.

As can be seen from Table 1, the values of S_{Eu} and S_{HA} depend on solution composition and age (i.e. time of pre-equilibration) in a rather similar manner, which suggests that Eu is sorbed predominantly or at least significantly as EuHA. Sorption of Eu^{3+} should be suppressed by the increase in ionic strength (Beneš and Majer 1980), which is obviously not the case. The form in which is Eu sorbed is important for evaluation of dialysis results. Significant sorption of Eu^{3+} would remove it from solution in reservoir A and diminish concentration of Eu^{3+} available for dialysis. Neglect of such sorption would result in an incorrect increase of *%EuHA* calculated from B/A_0. On the other hand, adsorbed EuHA can remain in equilibrium with Eu^{3+} in solution whose concentration in reservoir A need not be affected by EuHA sorption. Then the use of B/A_0 can represent better alternative for

calculation of *%EuHA* than the use of *B/A*, as the correction for sorption would lead to unjustified decrease of the values of *%EuHA*. The correlation between S_{Eu} and S_{HA}, particularly at 1% and 10% loading, seems to support correctness of the latter approach.

Two other findings support conclusion that the use of B/A_0 is better. First, Eu sorption equilibrium is not established in the first 7(6) days contact between solution and dialysis vessel (bag) as the sorption increases in most cases up to 13(12) days. (The apparent decrease of sorption after 7(6) days found in two cases was caused by a non-compensated averaging of repeated experiments.) Correction for the increasing Eu sorption will cause an apparent increase in Eu passage even in case when dialysis equilibrium has been established. This undoubtedly happened in all the cases when *B/A* increased with dialysis time while B/A_0 remained approximately constant (Table 1). Second, the values of *%EuHA* calculated from B/A_0 agree well with results obtained using other methods (see Table 4 below). In contrast, similar values calculated from *B/A* were unrealistically low in cases where a large difference between *B/A* and B/A_0 was found. This seems to corroborate that Eu is sorbed in dialysis cell predominantly as EuHA complexes that remain in equilibrium with Eu^{3+} in solution. Consequently, values of B/A_0 were used for further evaluation.

Table 1: Results of dialysis (10 mg/L HA, 6d/12 d experiment) as a function of loading, pH, ionic strength and age of solution – see text for explanations

Loading (%)	pH	*I*	Age (d)	S_{Eu} (%)	S_{HA} (%)	100*B/A*	100B/A_0	$Eu^{3+}{}_{eq}$ (%)
1	4	0.01	1	21.6/23.2	- /12.7	1.0/1.7	0.8/1.3	1.3±0.2
1	4	0.01	7	29.4	46.3	1.5/ -	1.1/ -	1.1±0.2
1	4	0.1	1	44.1/55.9	- /45.5	9.8/12.3	5.5/5.3	5.4±0.2
1	4	0.1	7	56.2	57.9	11.8/ -	5.1/ -	5.1±0.2
1	6	0.01	1	7.4/8.6	- /0	0.3/0.4	0.3/0.4	0.4±0.2
1	6	0.01	7	14.2	6.5	0.8/ -	0.7/ -	0.7±0.2
1	6	0.1	1	11.7/16.2	- /12.7	0.3/0.5	0.3/0.4	0.4±0.2
1	6	0.1	7	23.2	18.5	0.5/ -	0.4/ -	0.4±0.2
10	4	0.01	1	20.3/26.1	- /33.9	5.2/5.3	4.1/3.9	4.0±0.2
10	4	0.01	7	27.0	33.9	4.7/ -	3.5/ -	3.5±0.2
10	4	0.1	1	16.6/22.9	- /15.2	23.0/22.1	19.2/17.1	18.2±1.8
10	4	0.1	7	17.6	15.2	20.1/ -	16.6/ -	16.6±1.8
10	6	0.01	1	12.2/15.2	0/10.3	0.1/0.1	0.1/0.1	0.1±0.1
10	6	0.01	7	19.1	-	0.1/ -	0.1/ -	0.1±0.1
10	6	0.1	1	16.6/9.2	8.3/9.1	0.8/0.8	0.6/0.7	0.7±0.2
10	6	0.1	7	28.9	-	1.0/ -	0.7/ -	0.7±0.2
50	4	0.01	1	30.5/60.7	29.9/89.3	54.7/94.1	38.0/37.0	37.5±2.0
50	4	0.01	7	47.0	60.0	69.6/ -	36.9/ -	36.9±2.0
50	4	0.1	1	32.1/24.1	69.1/41.0	70.5/84.4	48.0/64.1	64.1±5.0
50	4	0.1	7	24.1	41.0	75.3/ -	56.8/ -	56.8±5.0
50	6	0.01	1	19.0/33.2	10.1/ -	3.2/1.3	2.6/0.9	1.8±0.2
50	6	0.01	7	23.6	18.1	3.2/ -	2.4/ -	2.4±0.2
50	6	0.1	1	35.4/46.2	14.8/32.2	24.7/33.4	15.9/14.4	15.1±1.0
50	6	0.1	7	46.2	45.8	34.4/ -	15.0/ -	15.0±1.0

Very important condition for the use of the equilibrium dialysis method is establishment of equilibrium, where the concentration of Eu^{3+} in reservoir B is the same as in reservoir A. Control experiments carried out with 8×10^{-7} M Eu at pH 4 in absence of HA have shown that Eu concentration in dialysis bag was equal to 93% of Eu concentration in dialysis vessel after 6 days and 100% after 12 days (sorption loss was only 2.8 and 5.9%, respectively).

Comparison of B/A_0 values after 6 and 12 d indicates (Table 1) that in 7 out of 12 cases these values are virtually equal, in most of other cases the values only moderately increase after 6 d. Thus the establishment of dialysis equilibrium can be assumed after 6 or 12 d and the equilibrium concentration of Eu^{3+} (in %, Eu^{3+}_{eq} in Table 1) was taken as equal to B/A_0 after 12 d or it was calculated as the average of B/A_0 values after 6 and 12 d. The error attached represents an assessed uncertainty due to measurement and other experimental errors. The loss of Eu from reservoir A caused by diffusion of Eu^{3+} into dialysis bag is mostly negligible in this respect (1.3-3.9% of Eu^{3+}_{eq}). Considering the possibility of further small increase of Eu concentration in the bag after 12 d contact and of partial sorption of Eu^{3+}, the values of *%EuHA* calculated from Eu^{3+}_{eq} data obtained must be regarded as maximum possible values.

Electrophoresis

Electrophoretic mobilities towards cathode (u_+) and anode (u_-) of Eu were measured as a function of pH (4 and 6), I (0.01 and 0.1) and initial concentration of Eu (3×10^{-8} – 1×10^{-4} M) in aqueous solutions containing 10 mg/L HA (Mizera et al. 2003). The solutions were aged for at least 1 d before the experiments. In a separate series of experiments, the effect of the aging (l h – 3 months) on the mobility of 1-2$\times10^{-5}$ M Eu at pH 4 and I = 0.01 was studied and found negligible. Values of u_+ obtained were used for calculation of *%EuHA* by means of equation

$$\%EuHA = 100\ (1 - u_+/u_0) \qquad (4)$$

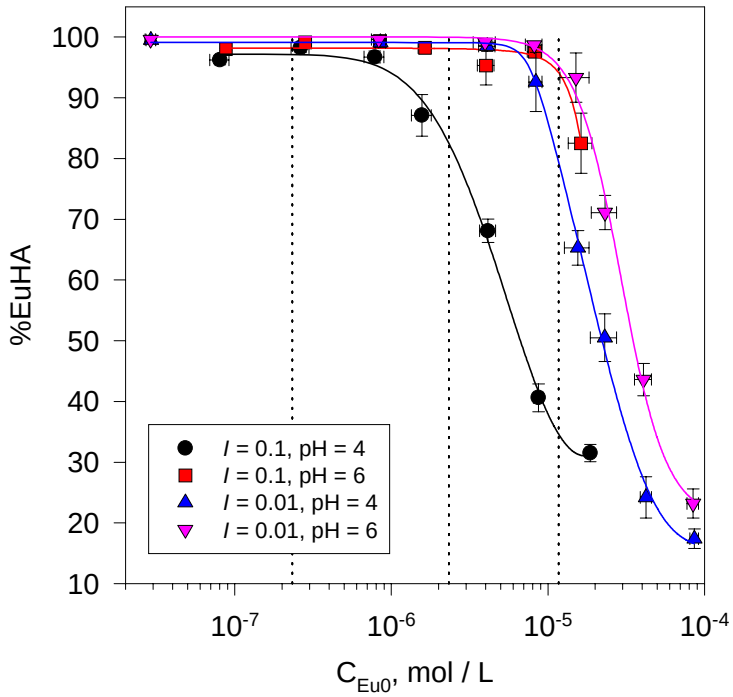

Fig.1: Percentage of Eu bound to HA determined by electrophoresis as a function of pH, ionic strength and initial concentration of Eu in aqueous solutions containing 10 mg/L HA. Vertical dashed lines denote 1%, 10% and 50% loading of HA with Eu .

where u_0 is electrophoretic mobility of Eu^{3+}, determined in absence of HA in solution of pH 3 at I = 0.01 ($u_0 = 5.74\times10^{-4}$ cm^2 V^{-1} s^{-1}) or I = 0.1 ($u_0 = 4.58\times10^{-4}$ cm^2 V^{-1} s^{-1}). The results are shown in Fig.1. The dependencies of *%EuHA* on the initial concentration of Eu were curve-fitted and the values corresponding to 1%, 10% and 50% loading were interpolated for comparison with results of the other methods (see Table 4 below). The errors attached represent estimated uncertainty due to sorption of Eu in the electrophoretic cell.The radiotracer arrangement of free-liquid electrophoresis belongs to non-invasive speciation methods (Benes and Majer 1980) as it does not disturb equilibria in solution. However, several assumptions are made when *%EuHA* is calculated using equation (4):

1) EuHA complexes are only negatively charged or neutral, 2) isotope exchange between Eu^{3+} and EuHA is slower than separation of these species by electromigration, 3) presence of other Eu forms (other complexes, pseudocolloids) can be neglected.

Whereas fulfillment of assumptions 1) and 3) represents no problem in conditions of our experiments, assumption 2) depends on kinetic stability of EuHA complexes. A higher kinetic lability could result in retardation of cathodic mobility of Eu and thus lead to specious increase of *%EuHA*. It has been shown previously (Mizera et al. 2003) that this can happen at higher loading and low pH values. Consequently, the values of *%EuHA* calculated using equation (4) represent the maximum possible abundance of EuHA complexes. The effect of kinetic lability can be assessed from the comparison of results of electrophoresis with those obtained by other methods (see below).

Ion exchange

The sorption isotherm of Eu^{3+} on the cation exchanger was determined by measurement of equilibrium concentration of Eu^{3+} in solution after contacting ion exchanger with solution of initial concentration 7.13×10^{-4} M Eu^{3+} at V/m ratio 400-2000 mL/g, pH 4 and I = 0.01 or 0.1. Two non-linear isotherms were obtained, which were numerically fitted by Langmuir equation. Parameters of Langmuir isotherm determined in this way were used in the subsequent calculations of Eu complexation with HA.

In the ion exchange method, basic problem of obtaining data on *%EuHA* for comparison with other methods is difficulty in carrying out experiments at pre-determined loading of HA with metal. Initial concentration of metal in solution decreases by up to several orders of magnitude due to metal uptake on ion exchanger. Therefore the following approach was adopted: Two series of experiments (each experiment in duplicate) were conducted for each set of conditions (pH, ionic strength, pre-equilibration time), one with fixed initial concentration of 1×10^{-5} M Eu^{3+} and varying concentration of HA (2-60 mg/L), one with fixed concentration of HA (10 mg/L) and varying concentration of Eu^{3+} (1×10^{-5}-5×10^{-4} M). The primary data obtained was equilibrium concentration of Eu in solution ($C_{Eu3+} + C_{EuHA}$). From this concentration, *%loading* was determined:

$$\%loading = 100\ (C_{Eu3+} + C_{EuHA})/\ (C_{HAo}\times\mathrm{PEC}/3). \qquad (5)$$

C_{Eu3+} and C_{EuHA} were calculated from the equilibrium concentration of Eu using balance and Langmuir equations. The resulting values served for calculation of the values of *%EuHA*. Fig. 2 illustrates typical dependence of the calculated data on the initial concentration of Eu^{3+}

for the basic set of conditions studied. Time of pre-equilibration had no significant effect on the results. It means that the pre-equilibration did not lead to formation of EuHA complexes unable of dissociation after addition of ion exchanger to the system.

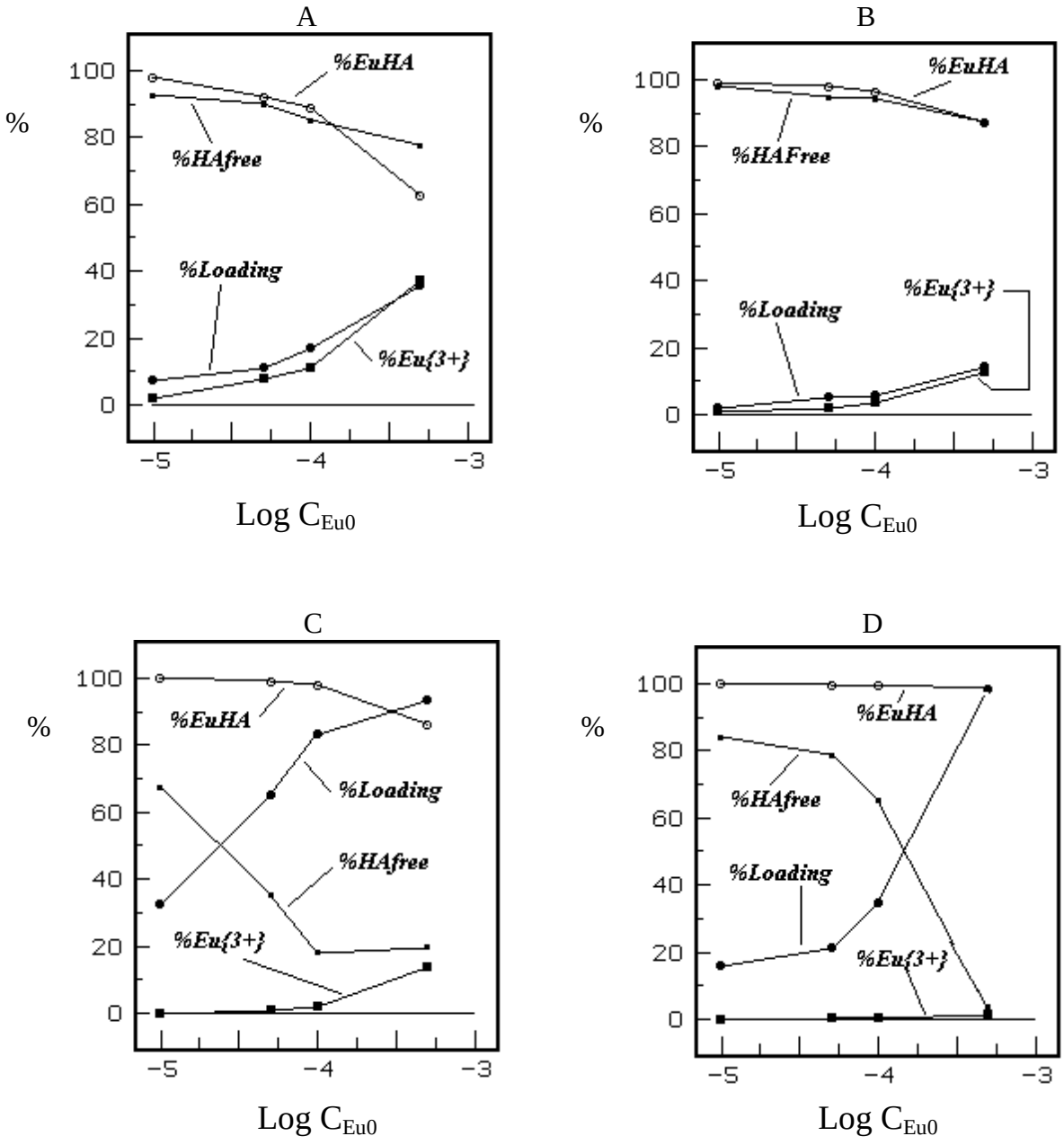

Fig. 2: Results of ion exchange experiments with 7 d old solutions containing 10 mg/L HA.
A: pH = 4, *I* = 0.1; B: pH = 4, *I* = 0.01; C: pH = 6, *I* = 0.1; D: pH=6, *I* = 0.01

As can be seen in Fig.2, the span of values of *%loading* obtained does not fulfill the requirements for comparison of *%EuHA* with other methods (1%, 10% and 50%). Therefore the missing data were calculated from stability constants of EuHA complexes derived from so called charge neutralization model (Czerwinski et al. 1994) and defined as

$$K_C = C_{EuHA} / (C_{Eu3+} \times C_{HAfree}) \qquad (6)$$

where C_{HAfree} is equilibrium concentration of free (uncomplexed) HA in solution. Values of logarithms of the constants derived from the experimental results were plotted as function of log (C_{Eu3+} + C_{EuHA}) and linear dependence was obtained (see Fig. 3):

$$\log K_C = a \times \log (C_{Eu3+} + C_{EuHA}) + b \qquad (7)$$

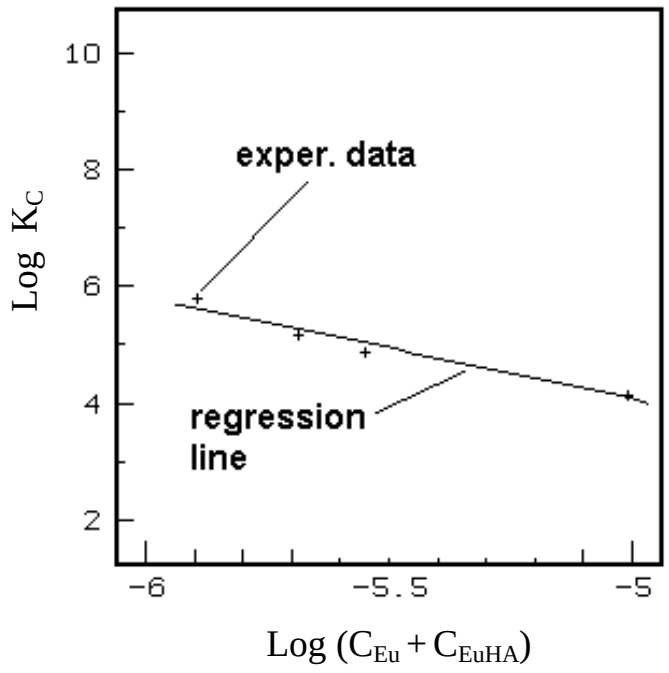

Fig. 3: Linear dependence expressed by equation (7) for pH 4 and *I* = 0.01.

Parameters *a* and *b*, together with coefficients of linear regression, characterizing the dependence for different conditions (pH, *I*) are presented in Table 2. From the values of the coefficients it follows that the linearity of the dependence is good, the worst fit was achieved in the case depicted in Fig. 3. Slope of the linear function, showing the effect of Eu concentration on K_C, increases with increasing pH and *I*.

Table 2: Parameters *a* and *b* and the values of regression coefficient *Rk* for dependence expressed by equation (7).

Conditions		Parameters		*Rk*
pH	*I*	*a*	*b*	
4	0.01	-0.957	0.314	0.41
4	0.1	-1.75	-4.67	0.98
6	0.01	-2.14	-4.50	0.90
6	0.1	-2.63	-7.79	0.92

Stability constants used for calculation of *%EuHA* were calculated from equation (7) for the values of equilibrium concentration of Eu corresponding to the desired *%loading*. C_{HAfree} was calculated from the balance of HA in solution. The calculation of stability constants in some cases involved extrapolation of validity of Eq.(7) beyond the range of experimental values for which it was determined. Accuracy of the extrapolation is unknown. Consequently, the values of *%EuHA* calculated in the described way and used for comparison (see Table 4

below) are presented here without an error. It can be only judged that the standard deviation of the values does not exceed a few percents. A better possibility of using the stability constant approach is to calculate conditions for experiments leading to desired values of *%loading* and to carry out the experiments. This approach is rather time consuming and therefore it was not used.

In all the calculations made it was assumed that no significant sorption of HA and EuHA on the walls of reaction vessel took place. Significant loss of HA and EuHA due to the sorption could lead to errors in calculation of K_C and *%EuHA*. Considering the effect of presence of ion exchanger, the sorption of EuHA would be very difficult to measure. However, comparison of the values of K_C obtained here with literature data and of the calculated *%EuHA* with results of other methods (Table 4 below) seem to indicate that the effect of such a loss was very small.

Ultrafiltration

The study of ultrafiltration aimed at verification of basic assumption of the method and at analysis of effects due to Eu sorption on the cell and ultrafilter. Therefore two ultrafilters with different MWCO and two methods of evaluation of results were compared. The experimental procedure enabled detailed analysis of Eu behaviour in the system. In order to check the efficiency of separation, parallel experiments were run with different initial concentration of Eu in presence (10 mg/L) and absence of HA, under conditions comparable to those used in the other methods. From evaluation of about 60 experiments with 1 d old solutions, the following conclusions were drawn.

Sorption losses of Eu during the equilibration of solution with cell and ultrafilter for 2 h ranged from 0 to 37.5 %, depending on pH and composition of solution. Lower losses were usually found in the presence of HA (0-12.5 %), whose dependence on pH and ionic strength was different than that in the absence of HA. This points to different mechanisms of the sorption. Eu was probably sorbed mostly as EuHA in the presence of HA and the low sorption probably did not significantly affect concentration of Eu^{3+} in solution (cf. the similar conclusion for dialysis). Thus the effect of the sorption loss need not be important.

However, desorption of Eu after ultrafiltration (measured as a_3) was in most experiments larger than the sorption loss, expressed as $a_0 - a_1$. The ratio $a_3/(a_0 - a_1)$ reached up to 10-20, increased with increasing concentration of Eu and with addition of HA. This finding shows that additional sorption of Eu can take place during ultrafiltration, which leads to a decrease in activity remaining in the cell (a_2) and thus to large errors in calculation of retention $\%R_2$ using Eq. (3). Comparison of activities of ultrafilters with the desorbed activities (a_3) indicated that Eu sorption on ultrafilters accounted only for a small part of the sorbed/desorbed activity: 1.7-20 % in absence of HA and 7-29 % in its presence.

The effect of sorption in ultrafiltration is often assessed from the change in concentration of metal/radionuclide in ultrafiltrate with increasing volume of the ultrafiltrate, when an increase in the concentration is usually atributed to a decrease in sorption of the metal/ radionuclide on ultrafilter and on cell beneath the ultrafilter, due to saturation of the corresponding surfaces. Such increase in activity was observed in a part of our experiments, whereas in other experiments a trendless variation of activity or even its pronounced decrease

was found. The decrease, which occurred only in the first 1-3 portions of the ultrafiltrate (1-3 mL), is very difficult to explain. Measurement of activity desorbed from the cell beneath the ultrafilter (a_5 and a_6) has shown that mostly less than 20 % of Eu which passed through the ultrafilter was adsorbed on the cell. Nevertheless, such measurement and efficient desorption are necessary since the activities are needed for calculation of retention using Eq. (2). Efficiency of the desorption was proved by measurement of activity of bottom part of the cell.

The sorption and desorption can cause serious problems in evaluation of ultrafiltration results. Unsatisfactory balance of activity calculated from all samples taken during ultrafiltration, which significantly deviated from expected 100 % (85-108 %) in a large part of experiments, pointed to an incomplete desorption of adsorbed Eu in some cases and to unexpected excessive desorption, probably of Eu adsorbed in preceding experiments, in other cases. These phenomena, the incomplete desorption and the "memory of cell" effect, together with the additional sorption during ultrafiltration (cf. above), manifested themselves when the retention values obtained by calculation using Eqs. (2) and (3), i.e. $\%R_1$ and $\%R_2$, were compared. In most of the experiments, $\%R_2$ was much smaller than $\%R_1$, mainly due to the last effect and concomitant decrease of a_2. When the calulation of $\%R_2$ was corrected by inclusion of special terms taking into account the additional sorption losses and the deficit of activity balance or the excessive desorption, agreement within a few percent was achieved between $\%R_1$ and $\%R_2$. For this reason, only values of $\%R_1$ were considered for further evaluation of ultrafiltration.

$\%R_1$ is less sensitive to sorption loss of Eu than $\%R_1$ but it can be affected by sorption of Eu^{3+} on ultrafilter and upper part of cell. Its apparent increase due to Eu^{3+} sorption can be approximately corrected only when HA is absent. Another source of error in the calculation of $\%R_1$ is the unexplained drop in activity of ultrafiltrate at the beginning of ultrafiltration (see above). The sometimes recommended omitting of the first portions of ultrafiltrate from the calculation of retention is not compatible with the correction for sorption used in Eq. (2). We calculated that the drop could cause a decrease in $\%R_1$ only for a few percent in some of our experiments. Furthermore, its effect can be compensated by the effect of the sorption of Eu^{3+}.

The values of $\%R_1$ obtained are presented in Table 3 for all the conditions studied and for two ultrafilters in the presence and absence of HA. They unequivocally show that Eu is strongly retained by both the ultrafilters also in absence of HA, when it can exist in solution only as Eu^{3+} or pseudocolloids formed by sorption of Eu^{3+} on colloidal or larger particles present as impurities. The retention cannot be explained as an error due to sorption of Eu^{3+} in cell since a cumulation of Eu in the solution in cell was observed (a_2 was larger than a_1) in the corresponding experiments, and the values of $\%R_2$ corrected for Eu sorption were close to $\%R_1$. At least part of Eu is retained as Eu^{3+}. This follows from the significant retention of Eu at its highest concentration, when the abundance of pseudocolloids should be low (Benes and Majer 1980), and from the fact that the retention by 500 Da ultrafilter was mostly higher than that by 1 kDa ultrafilter, although pseudocolloids should be retained quantitatively by both the ultrafilters. The possibility of retention of low molecular weight forms of Eu was corroborated by control experiments when 86 % retention of Eu by 500 Da ultrafilter and 39 % by 1 kDa ultrafilter were observed from solution of 0.1 M sodium oxalate, where Eu oxalate complexes predominated.

Table 3: Retention of Eu ($\%R_1$) in ultrafiltration of solutions containing 10 mg/mL HA (values in brackets were found in absence of HA

C_{Eu0} (M)	Filter (Da)	Conditions of experiments			
		pH 4 , I = 0.01	pH 4 , I = 0.1	pH 6 , I = 0.01	pH 6 , I = 0.1
2.3×10^{-7}	500	93.8 (92.4)	94.1 (90.9)	92.2 (94.7)	93.8 (92.6)
2.3×10^{-7}	1000	80.0 (51.7)	79.7 (37.1)	90.9 (82.7)	94.1 (82.9)
2.3×10^{-6}	500	92.3 (79.1)	88.5 (21.6)	94.6 (28.9)	88.3 (79.9)
2.3×10^{-6}	1000	64.9 (16.7)	27.9 (17.0)	73.1 (21.7)	71.4 (32.2)
1.15×10^{-5}	500	86.4 (74.0)	44.8 (75.9)	21.6 (41.8)	31.0 (44.3)
1.15×10^{-5}	1000	62.1 (11.8)	26.5 (79.4)	43.0 (44.9)	41.8 (41.4)

Retention of Eu from solutions containing 10 mg/L HA was mostly higher than that in absence of HA but, depending on conditions, the difference was not always large and even opposite relation was found at the highest concentration of Eu. The basic assumption of ultrafiltration method was not confirmed in our case and therefore $\%R_1$ found cannot be considered equal to *%EuHA*. Despite of this, the values of $\%R_1$ determined in the presence of HA using 1 kDa ultrafilter are compared in Table 4 with data on *%EuHA* obtained by the other methods. As can be seen the values are significantly lower than those of *%EuHA*, although they should be higher due to the retention of Eu^{3+}. This probably points to the passage of a part of EuHA through the ultrafilter.

In conclusion, ultrafiltration with the ultrafilters used here was not found suitable for determination of *%EuHA*. The main reason was insufficient separation of complexed and uncomplexed forms of Eu. Therefore the effect of pre-equlibratiom (ageing) of solution was not studied in this case. Nevertheless, the procedure used enabled minimalisation of some complications such as shift of equilibrium during ultrafiltration, and detailed elucidation of the effect of sorption. Some of our findings, however, still remain unexplained.

Comparison of methods

Data on *%EuHA* obtained by dialysis, electrophoresis and ion exchange, together with retention (in brackets) of Eu by ultrafiltration are compared in Table 4. The data are valid for 1 d old solutions but they can be used also for complexation in 7 d old solutions as the effect of time of pre-equilibration on *%EuHA* was found negligible. None of the methods compared is therefore affected by slowing down of dissociation of EuHA, which could be caused by ageing of the complexes. Such effect could be expected mainly in electrophoresis or ion exchange, where the kinetics of dissociation of EuHA might affect electrophoretic mobility of Eu or establishment of ion exchange equilibrium.

As can be seen from Table 4, a good agreement among the results of dialysis, electrophoresis and ion exchange methods is observed particularly when *%EuHA* is close to 100 %. With the increase of loading and the decrease in *%EuHA*, spread of the data slightly increases. Retention in ultrafiltration is, with one exception, significantly lower than the corresponding values of *%EuHA*. Following conclusions can be drawn from the comparison.

As shown in the discussion of dialysis, its results enable calculation of maximum possible values of *%EuHA*. Application of corrections for sorption of Eu^{3+} in dialysis cell and for dialysis disequilibrium, if possible and needed, would lead to decrease of calculated *%EuHA*. However, *%EuHA* values from dialysis are the same as or lower than those obtained by ion

exchange and electrophoresis. This can be regarded as confirmation that dialysis results were evaluated correctly and the method can yield reliable data on *%EuHA*.

Table 4: Comparison of *%EuHA* values obtained by dialysis (DIA), electrophoresis (EP) and ion exchange (IE) with retention of Eu (*%R_1*) in ultrafiltration (UF, in brackets) through 1 kDa ultrafilter.

Loading (%)	pH	*I*	DIA	EP	IE	UF
1	4	0.01	98.7±0.2	99.3±0.6	99.1	(80.0)
1	4	0.1	94.6±0.2	97.2±0.7	99.7	(79.7)
1	6	0.01	99.6±0.2	99.6±0.3	99.7	(90.9)
1	6	0.1	99.6±0.2	98.7±0.3	100.0	(94.1)
10	4	0.01	96.0±0.2	98.8±0.9	91.9	(64.9)
10	4	0.1	81.8±1.8	88.3±2.7	82.6	(27.9)
10	6	0.01	99.9±0.1	99.4±0.4	99.5	(73.1)
10	6	0.1	99.3±0.2	97.6±1.7	99.5	(71.4)
50	4	0.01	62.5±2.0	78.9±3.9	64.6	(62.1)
50	4	0.1	35.9±5.0	35.1±2.0	34.7	(26.5)
50	6	0.01	98.2±0.2	95.1±2.2	95.7	(43.0)
50	6	0.1	84.9±1.0	94.5±2.5	84.0	(41.8)

Similar conclusion can be drawn on electrophoresis. Calculation of *%EuHA* from cathodic mobility of Eu also leads to its maximum possible values. Suppression of the mobility due to isotopic exchange between Eu^{3+} and negatively charged EuHA complexes, which is more probable at high loading, can result in apparent increase in *%EuHA*. This probably happened at 50 % loading and pH 4, I = 0.01 or pH 6, I = 0.1, where higher values of *%EuHA* were obtained by electrophoresis than by the other methods. In other cases electrophoresis yielded comparable data, so that kinetic lability of EuHA complexes did not have any significant influence on the results.

The values of *%EuHA* presented for ion exchange were recalculated from stability constants determined using the method for a broader range of conditions. Their good agreement with data obtained by direct determination using dialysis and electrophoresis confirms that the procedure used was correct. The ion exchange method seems to be independent of strong effects of Eu sorption on reaction vessel.

Conclusions

Three methods of those tested can yield trustworthy humate complexation data, if performed and evaluated well: equilibrium dialysis with floating bag, free liquid electrophoresis and cation exchange. All three methods can be well realized in radiotracer arrangement. Basic disadvantage of the dialysis is the long time needed to achieve equilibrium. This method and electrophoresis can be affected by a sorption of uncomplexed metal on the cell, which would tend to increase the degree of complexation determined. The similar effect can be due to retardation of electrophoretic mobility of radiotracer by isotope exchange with unlabelled species. Thus the values of *%MHA* determined by both the methods represent a maximum possible degree of complexation in the system. An important issue in the use of ion exchange method is that the isotherm for the distribution of uncomplexed metal ions between solution

and ion exchanger is adequately investigated and a suitable model is used for evaluation of results.

With ultrafiltration it is difficult to find an ultrafilter capable of quantitative retention of the metal humate complex and quantitatively permeable for the uncomplexed metal. This was not achieved in the present study. Significant problems can also be due to sorption of uncomplexed metal on the cell and ultrafilter. Thus ultrafiltration based humate complexation data need to be interpreted with great caution.

Acknowledgement

This study was supported by the EC Commission under contract No. FIKW-CT-2001-00128 and by the Grant No. MSM 210000019 of the Czech Ministry of Education.

References

Benes P. (1967) "On the State of Manganese and Gold Traces in Aqueous Solutions", *J. Inorg. Nucl. Chem.* **29**, 2889.

Benes P. and Steinnes E. (1974) "In situ Dialysis for the Determination of the State of Trace Elements in Natural Waters", *Water Res*. **8**, 947.

Benes P., Steinnes E. and Gjessing E.T. (1976) "Interaction between Humus and Trace Elements in Fresh Water", *Water Res*. **10**, 711.

Benes P. and Glos J. (1979) „Radiotracer Analysis of the Physico-chemical State of Trace Elements in Aqueous Solutions .II. Electromigration Method", *J. Radioanal. Chem* .**52**, 43.

Benes P. and Majer V. (1980) „Trace Chemistry of Aqueous Solutions", Academia/Elsevier, Prague/Amsterdam.

Backes C.A. and Tipping E. (1987) „Aluminium Complexation by an Aquatic Humic Fraction Under Acidic Conditions", *Water Res.* **21**, 211.

Bertha E.L. and Choppin G.R. (1978) „Interaction of Humic and Fulvic Acids with Eu(III) and Am(III)", *J. Inorg. Nucl. Chem*. **40**, 655.

Brown G.K., MacCarthy P. and Leenheer J.A. (1999) „Simultaneous Determination of Ca,Cu,Ni,Zn and Cd Binding Strengths with Fulvic Acid Fractions by Schuberts Method", *Anal. Chim. Acta*, **402**,169.

Caceci M.S. (1985) „The Interaction of Humic Acid with Europium(III). Complexation Strength as a Function of Load and pH", *Radiochim. Acta*, **39**, 51.

Czerwinski K.R., Buckau G., Scherbaum F.J. and Kim J.I. (1994) "Complexation of the Uranyl Ion with Aquatic Humic Acid", *Radiochim. Acta*, **65**, 111.

Dierckx A., Maes A. and Vancluysen J. (1994) „Mixed Complex Formation of Eu^{3+} with Humic Acid and a Competing Ligand. *Radiochim. Acta*, **66-7**, 149.

Fairhurst A.J., Warwick P. and Richardson S. (1995) „The Influence of Humic Acid on the Adsorption of Europium onto Inorganic Colloids as a Function of pH“, *Colloids and Surfaces A. Physicochim. Eng. Aspects* **99**, 187.

Glaus M.A., Hummel W. and Van Loon L.R. (1995) „Equilibrium Dialysis - Ligand Exchange: Adaptation of the Method for Determination of Conditional Stability Constants of Radionuclide - Fulvic Acid Complexes“, *Anal. Chim. Acta*, **303**, 321.

Gu Z., Wang X., Gu X., Cheng J., Wang L., Dai L. and Cao M. (2001) „Determination of Stability Constants for Rare Earth Elements and Fulvic Acids Extracted from Different Soils“, *Talanta*, **53**, 1163.

Kim J.I., Buckau G., Li G.H., Duschner H. and Psarros N. (1990) „Characterisation of Humic and Fulvic Acids from Gorleben Groundwater“, *Fresenius J. Anal. Chem.*, **338**, 245.

Lead J.R., Hamilton-Taylor J., Peters A., Reiner S. and Tipping E. (1998) „Europium Binding by Fulvic Acids“, *Anal. Chim. Acta*, **369**, 171.

Lenhart J.J., Honeyman B.D., Cabaniss S.E. and MacCarthy P. (2000) „Uranium(VI) Complexation with Citric, Humic and Fulvic Acids“, *Radiochim. Acta*, **88**, 345.

Leonard K.S., Harvey B.R., Woodhead R.J., Brooks T. and McCubbin D. (1994) „Assessment of an Ultrafiltration Technique for the Fractionation of Radionuclides Associated with Humic Material“, *J.Radioanal. Nucl. Chem. Art.*, **181**, 309.

Mizera J., Benes P. and Masnerova G. (2003) „Electrophoretic Determination of the Degree of Eu Complexation by Humic Acid: Analysis and Assessment of Experimental Error“. In: Buckau G. (Editor) “Humic Substances in Performance Assessment of Nuclear Waste Disposal: Actinide and Iodine Migration in the Far-Field (first technical progress report)”, Report FZKA 6800, Research Center Karlsruhe, April 2003, 191.

Nifanteva T.I., Shkinev V.M., Spivakov B.Ya. and Burba,P. (1999) „Membrane Filtration Studies of Aquatic Humic Substances and their Metal Species: a Concise Overview. Part 2. Evaluation of Conditional Stability Constants by Using Ultrafiltration“, *Talanta*, **48**, 257.

Norden M., Ephraim J.H. and Allard B. (1993) „The Binding of Strontium and Europium by an Aquatic Fulvic Acid. Ion Exchange Distribution and Ultrafiltration Studies“, *Talanta*, **40**, 1425.

Shin H.S., Lee B.H., Yang H.B., Yun S.S. and Moon H. (1996) „Bimodal Normal Distribution Model for Binding of Trivalent Europium by Soil Fulvic Acid“, *J. Radioanal. Nucl. Chem. Art.*, **209**, 123.

Van Loon L.R., Granacher S. and Harduf H. (1992) „Equilibrium Dialysis-Ligand Exchange - A Novel Method for Determining Conditional Stability Constants of Radionuclide-Humic Acid Complexes“, *Anal. Chim. Acta*, **268**, 235.

Weber J.H. (1988) „Binding and Transport of Metals by Humic Materials“. In: Frimmel F.H. and Christman R.F. (Editors) „Humic Substances and Their Role in the Environment“, John Viley and Sons, New York, 165.

Annex 18

Modelling of Kinetics of Complexation and Decomplexation of Eu(III) with Humic Acid

Stamberg K., Benes P, Mizera J., Vopalka D. and Prochazkova S.

Czech Technical University, Department of Nuclear Chemistry,
Brehova 7, 115 19 Prague, Czech Republic

Modelling of Kinetics of Complexation and Decomplexation of Eu(III) with Humic Acid

Stamberg K., Benes P, Mizera J., Vopalka D. and Prochazkova S.

Czech Technical University, Department of Nuclear Chemistry, Brehova 7, 115 19 Prague, Czech Republic

Abstract

The kinetics of complexation and decomplexation reactions between Eu(III) and Aldrich humic acid (HA) was investigated as a function of pH (pH 4, 5, 6, 7 and 8) in the system Amberlite IR-120(Na) – Eu(III) – HA (I = 0.1). When the complexation reaction was studied, Eu(III) labelled with ^{152,154}Eu was added to the mixture of Amberlite IR-120 + aqueous solution of HA and the concentration of Eu in solution ($=Eu\Sigma$) was measured as a function of time. In the case of decomplexation study, Amberlite IR-120 was added to the preequilibrated (appr. 80 hours) solution of Eu(III) + HA. In addition to this, sorption kinetics of Eu^{3+} on Amberlite IR-120 was determined in the absence of HA. Derivation of kinetic differential equations of the complexation/decomplexation was based on the reactions of Eu^{3+} with so-called strong (*HAS*) and weak (*HAW*) carboxylic groups of HA and on a new complexation model (Štamberg et al. 2003): $a.Eu^{3+} + HAS^{p-} \leftrightarrow Eu_aHAS^{(p-3.a)-}$, $b.Eu^{3+} + HAW^{p-} \leftrightarrow Eu_bHAW^{(p-3.b)-}$ The kinetic equations have the classical form: $dEu_aHAS/dt = k_1.[Eu]^a.[HAS] - k_2.[Eu_aHAS]$, $dEu_bHAW/dt = k_3.[Eu]^b.[HAW] - k_4.[Eu_bHAW]$ (at pH ≤ 4, only the reaction with *HAS* takes place). Kinetic model of complexation/decomplexation reactions used for the evaluation of experimental data and for the simulation calculations is based on the balance equation: $-dEu\Sigma/dt = -dEu^{3+}/dt + a.(dEu_aHAS/dt) + b.(dEu_bHAW/dt)$; dEu^{3+}/dt is substituted by the kinetic equation of sorption of Eu^{3+} on Amberlite IR-120 (the film diffusion model is used).

Introduction

The kinetics of complexation (C) and decomplexation (D) reactions between Eu^{3+} and Aldrich humic acid (HA) was investigated as a function of pH (= 4, 5, 6, 7 and 8) in the system Eu(III) – HA – Amberlite IR-120(Na), I = 0.1. Derivation of kinetic differential equations was based on the reactions of Eu^{3+} with so called strong (*HAS*, more acidic, fully dissociated at pH 4) and weak (*HAW*, less acidic, fully dissociated at pH 7) carboxylic groups of HA formulated in accordance with the our complexation model MMWM (Mean Molecular Weight Model) (Štamberg et al., 2003). Kinetic model used for the evaluation of experimental data and simulation calculations includes these differential equations in the classical form applicable for reversible reactions and the film diffusion model of sorption of Eu^{3+} on Amberlite IR-120(Na).

1 Theory – kinetic model

The complexation (and decomplexation, in the opposite direction) reactions with HAS and HAW groups, based on MMWM, can be described by Eqs. (1) and (2). Simultaneously, if cation exchanger is present, sorption of Eu^{3+} takes place (Eq. (3)).

$$a.Eu^{3+} + HAS^{n-} \Leftrightarrow Eu_aHAS^{(n-a.3)-} \quad a = 1, 2, 3,...., a_{max}, \; a_{max} = \lfloor n/3 \rfloor \qquad (1)$$

$$b.Eu^{3+} + HAW^{m-} \Leftrightarrow Eu_bHAW^{(m-b.3)-} \quad b = 1, 2, 3, ..., b_{max}, \; b_{max} = \lfloor m/3 \rfloor \qquad (2)$$

$$Eu^{3+} + 3.RNa \Leftrightarrow R_3Eu + 3.Na^{+1} \qquad (3)$$

Here the symbols denote:

a, b, a_{max}, b_{max} ... stoichiometric coefficients, the subscript *max* refers to the maximum value, i.e., to the formation of neutral complexes;

n, m ... total charge of dissociated carboxyl groups per one average molecule of HA, depending on pH (if pH ≤ 4 then m = 0 and b = 0);

R ... functional groups, $-SO_3^-$, of the strong acid cation exchangers.

The reactions (1) and (2) are regarded as reversible chemical reactions and corresponding kinetic equations (4) and (5) can be written:

$$d[Eu_aHAS^{(n-a.3)-}]/dt = k_1.[Eu^{3+}]^a.[HAS^{n-}] - k_2.[Eu_aHAS^{(n-a.3)-}] \qquad (4)$$

$$d[Eu_bHAW^{(m-b.3)-}]/dt = k_3.[Eu^{3+}]^b[HAW^{m-}] - k_4.[Eu_bHAW^{(m-b.3)-}] \qquad (5)$$

where k_1, k_2, k_3 and k_4 are the rate constants, and molar concentrations of individual components in aqueous solution at time t are given in square brackets.

The kinetic model used for the evaluation of experimental data obtained in the presence of HA and Amberlite IR-120 is based on the balance equation of sorption (6) and balance equation (7) describing the changes in total concentrations of Eu(III) species in solution, $Eu\Sigma$, in the course of C/D reactions, both in the differential:

$$d\{Eu^{3+}\}/dt = - (V/m).d[Eu^{3+}]/dt \qquad (6)$$

$$- d[Eu\Sigma]/dt = - d[Eu^{3+}]/dt + a.d[Eu_aHAS^{(n-a.3)}]/dt + b.d[Eu_bHAW^{(m-b.3)}]/dt \qquad (7)$$

(V is the volume of solution, m is the mass of Amberlite IR-120 and $\{Eu^{3+}\}$ denotes the concentration of Eu^{3+} in ion exchanger.)

In the system studied, two (Eqs. (1) and (3)) or three (Eqs. (1), (2) and (3)) reactions take place and therefore the same number of differential equations, expressing the interactions of individual reactions, are needed. First it is the differential equation (6) describing the kinetics of sorption reaction (3). On the basis of the evaluation of sorption experimental data obtained in the absence of HA, the so-called film diffusion model (8) with the equilibrium (9) and balance equations (10) and (11) are used:

$$y[3]' = \mathrm{d}[Eu^{3+}]/\mathrm{d}t = -(m/V).K_{FD}.([Eu^{3+}] - [Eu^{3+}]_{eq}) \quad (8)$$

$$[Eu^{3+}]_{eq} = \{Eu^{3+}\}/(K_L.(Q_{max} - \{Eu^{3+}\})) \quad (9)$$

$$\{Eu^{3+}\} = (V/m).([Eu]_0 - [Eu\Sigma]) + \{Eu^{3+}\}_0 = (V/m).([Eu^{3+}]_0 - [Eu^{3+}]) + \{Eu^{3+}\}_0 \quad (10)$$

$$[Eu^{3+}] = [Eu\Sigma] - a.[Eu_aHAS^{(n-a.3)-}] - b.[Eu_bHAW^{(m-b.3)-}] \quad (11)$$

where K_{FD} is the total kinetic coefficient, K_L and Q_{max} are the coefficients of Langmuir equation (9), $[\ ]_0$ and $\{\ \}_0$ are the starting concentrations at $t = 0$.

Then, in the presence of Amberlite IR-120, the kinetics of C/D reactions is described by Eqs. (12) and (13) obtained by rearrangement of Eq. (7):

$$y[1]' = -\mathrm{d}((a/(a+b)).[Eu\Sigma])/\mathrm{d}t = a.(k_1.[Eu^{3+}]^a.[HAS^{n-}] - k_2.[Eu_aHAS^{(n-a.3)-}]) - (a/(a+b)).y[3]' \quad (12)$$

$$y[2]' = -\mathrm{d}((b/(a+b)).[Eu\Sigma])/\mathrm{d}t = b.(k_3.[Eu^{3+}]^b.[HAW^{m-}] - k_4.[Eu_bHAW^{(m-b.3)}]) - (b/(a+b)).y[3]' \quad (13)$$

The concentrations of $[Eu^{3+}]$, $[HAS^{n-}]$ and $[HAW^{m-}]$ are substituted from Eqs. (11), (14) and (15), respectively:

$$[HAS^{n-}] = [HAS^{n-}]_0 - [Eu_aHAS^{(n-a.3)-}] \quad (14)$$

$$[HAW^{m-}] = [HAW^{m-}]_0 - [Eu_bHAW^{(m-b.3)-}] \quad (15)$$

If pH ≤ 4 then $b = 0$ and the system is described by differential Eqs. (8) and (12).

Numerical Runge-Kutta method of the fourth order was used to the solution of differential equations. In order to make possible evaluation of the experimental data and acquirement of the values of rate constants $k_1 - k_4$, this procedure was incorporated into a non-linear regression numerical code based on the Newton multidimensional method. Our own numerical codes were constructed for these purposes.

2 Experimental

Kinetic experiments No. 1-12 were carried out by batch method at different values of pH, contact time, t, and mass of centrifuged swollen Amberlite IR-120 in Na-form, m, see Table 1. The common conditions were: (i) ionic strength $I = 0.1$ (0.1 mol/L $NaClO_4$), (ii) solution with starting concentration of $Eu(NO_3)_3$, $[Eu]_0 = 1\text{x}10^{-5}$ mol/L labelled with $^{152,154}Eu$, (iii) concentration of HA, $m_{HA} = 10$ mg/L, (iv) initial volume of aqueous phase, $V = 0.10$ L.

When the kinetics of C-reactions were determined by means of so-called C-experiments (see Table 1), the stock solution of Eu(III) was added to the mixture of Amberlite IR-120(Na) + solution of HA and $NaClO_4$ at time $t = 0$. The solution was sampled at given time and the concentration of Eu, $[Eu\Sigma]$, was determined.

The kinetics of D-reactions (see D-experiments in Table 1) were studied in the same way, but at time $t = 0$, Amberlite IR-120(Na) was added to the preequilibrated (approx. 80 – 90 hours) solution of Eu(III) with HA (+ $NaClO_4$).

Table 1: Conditions of kinetic experiments

Exper. No.	type of experiment: C – complexation D – decomplexation	pH	mass of Amberlite IR-120, *m* (kg)	phase ratio, *V*/*m* (L/kg)
1	C	4	0.0002	500
2	D	4	0.0002	500
3	C	5	0.0002	500
4	D	5	0.0002	500
5	C	6	0.0002	500
6	D	6	0.0002	500
7	C	7	0.0005	200
8	D	7	0.0005	200
9	C	8	0.0005	200
10	D	8	0.0005	200
11	-	4	0.0002	500
12	-	7	0.0002	500

Sorption kinetics of Eu^{3+} on Amberlite IR-120(Na) in the absence of HA was also studied - see Exps. No. 11 and 12 in Table 1.
The sorption of Eu(III) on the walls of PE vials used in the kinetic studies was found negligible.

3 Results

All experimental points and calculated dependencies expressed as $([Eu\Sigma]/[Eu]_0).100$ [%] = f(*t*) are presented in Fig. 1 (C-experiments and Exp. No. 11 and 12) and Fig. 2 (D-experiments).

Sorption kinetics of Eu^{3+} on Amberlite IR-120 in the absence of HA
Results of experiments No. 11 and 12 were evaluated by means of six kinetic models differing in the type of rate-determining step of sorption process, namely: mass transfer, film diffusion, inert layer diffusion, diffusion in reacted layer and chemical reversible reaction of the first order. In this way the values of kinetic coefficients of individual models were obtained by fitting the experimental data. The quality of fitting was evaluated using statistical quantities χ^2 and *Q* (Press et al., 1989): it holds that the fit is good if $1 < \chi^2 \cong 40$ and $1 \leq Q \cong 1x10^{-5} – 1x10^{-6}$.
In accordance with the theory of ion exchange kinetics on strong acid cation exchangers (Marinsky, 1966), the film diffusion model (8) was found to be the best for both experiments No. 11 and 12. The following values of K_{FD} and quantities χ^2 and *Q* were obtained:

Exp. No 11 (pH = 4): K_{FD} = 7.82 ± 0.15 min^{-1}, χ^2 = 7.68, Q = 0.66

Exp. No 12 (pH = 7): K_{FD} = 7.66 ± 0.09 min^{-1}, χ^2 = 42.30, Q = 6.63x10^{-6}

Their arithmetic mean, K_{FD} = 7.74 min^{-1}, was used in the calculation of sorption kinetics in the absence of HA, see Figs. 1 and 4, and for the evaluation of all C/D experiments.

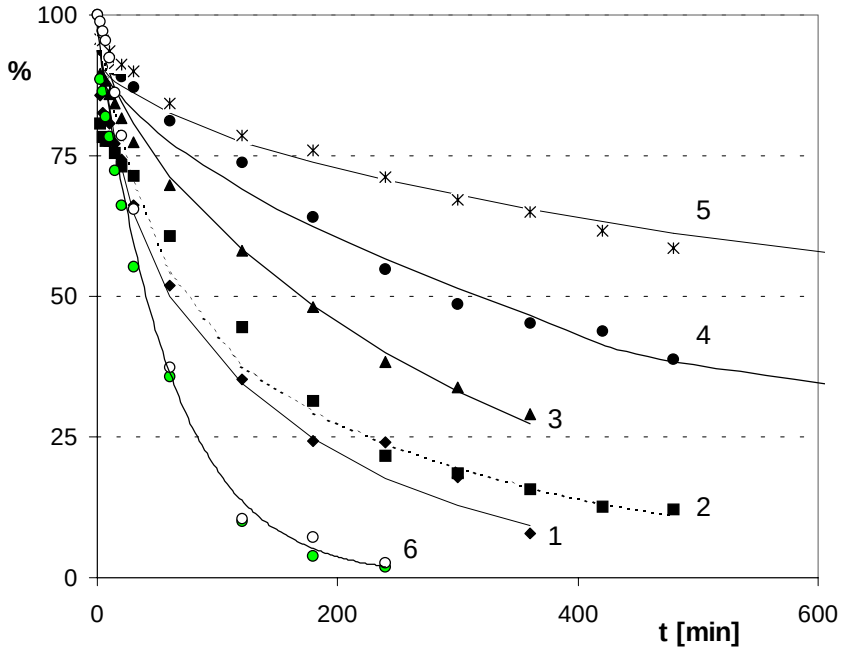

Fig. 1: Kinetics of Eu sorption, ([*EuΣ*]/[*Eu*]$_0$).100 [%] = f(*t*), under the conditions of C-experiments and in the absence of HA. 1 – Exp. No.1, 2 – Exp. No. 3, 3 – Exp. No. 5, 4 – Exp. No. 7, 5 – Exp. No. 9, 6 – Exp. No. 11 and 12 (in the absence of HA). Individual points – experimental data.

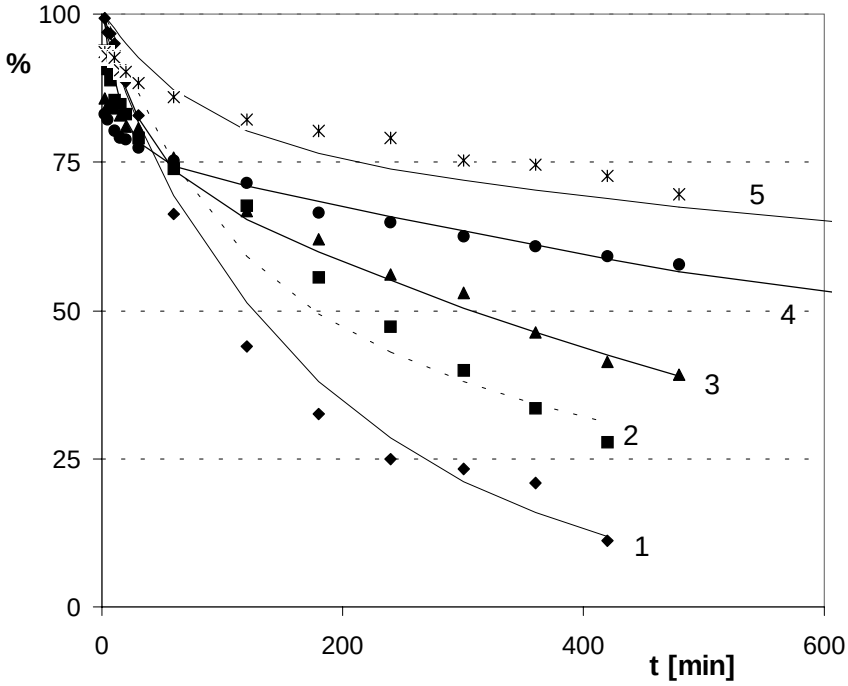

Fig. 2: Kinetics of Eu sorption, ([*EuΣ*]/[*Eu*]$_0$).100 [%] = f(*t*), under the conditions of D-experiments. 1 – Exp. No. 2, 2 – Exp. No. 4, 3 – Exp. No. 6, 4 – Exp. No. 8, 5 – Exp. No. 10. Individual points – experimental data

Kinetics of C/D reactions

Before proper evaluation of experimental data, it is necessary to determine the input data needed for the solution of differential equations, namely, the stoichiometric coefficients, *a* and *b*, and – if the data of D-experiments have to be evaluated – the concentrations of Eu species, $[Eu^{3+}]$, $[Eu_aHAS^{(n-a.3)-}]$ and $[Eu_bHAW^{(m-b.3)-}]$, in the preequilibrated solution of given pH. The data were calculated by means of the MMWM complexation model and are summarised in Table 2.

Table 2: Results of speciation calculations – concentrations of Eu species and mean values of stoichiometric coefficients for different pH.

pH	Stoichiometric coefficient		$[Eu^{3+}]$	$[Eu_aHAS]$	$[Eu_bHAW]$
	a	*b*	(mol/L)	(mol/L)	(mol/L)
4	1.03	-	4.00×10^{-6}	6.00×10^{-6}	-
5	10.00	2.74	1.09×10^{-8}	9.00×10^{-7}	3.61×10^{-7}
6	10.09	6.32	9.12×10^{-9}	9.84×10^{-7}	3.63×10^{-9}
7	10.10	7.28	1.40×10^{-8}	9.86×10^{-7}	3.75×10^{-9}
8	10.10	7.39	1.67×10^{-8}	9.86×10^{-7}	3.34×10^{-9}

Determination of rate constants k_1 to k_4 using the non-linear regression procedure was complicated by the fact, that the number of rate constants which can be determined, depended on the values of stoichiometric coefficients and therefore they were taken not only from Table 2, but also the lower values had to be used (see the guessed values of *a* and *b* in Table 3). The results are presented in Table 3 and in Fig. 3; in Table 3, the corresponding values of χ^2 and *Q* can be found, too.

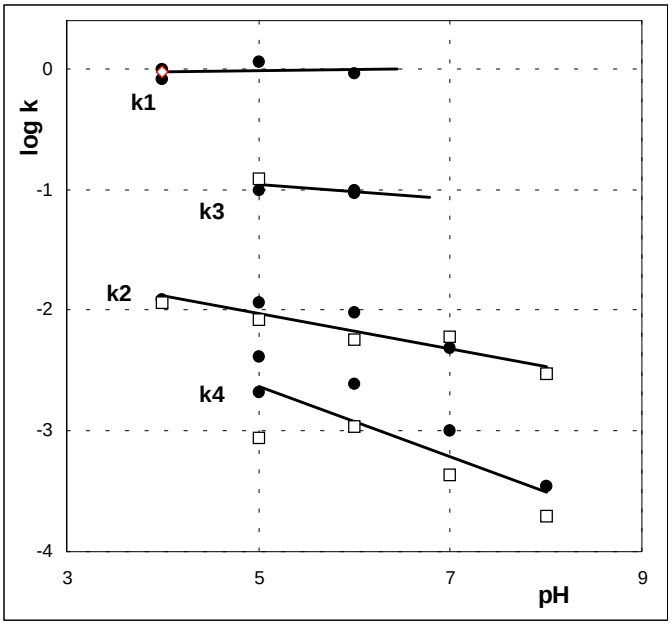

Fig. 3: The dependences of rate constants, log k_1 – log k_4, of C/D – reactions on pH. C-experiments (•), D-experiments (□), regression (—) (k_1 – $[min^{-1}mol^{-a}L^a]$, k_2 – $[min^{-1}]$, k_3 – $[min^{-1}mol^{-b}L^b]$, k_4 – $[min^{-1}]$).

From the results it can be seen that the values of k_1 and k_3, i.e. the rate constants of complexation (forward) reactions, are approximately independent of pH:

$$k_1 \approx 1\ \text{min}^{-1}.\text{mol}^{-a}.\text{L}^{a}, \quad k_3 \approx 0.1\ \text{min}^{-1}.\text{mol}^{-b}.\text{L}^{b}$$

This holds only for stoichiometric coefficients used to the regression procedure. But, if we still take the relatively high standard deviations of k_1 and k_3, the values of which express the small sensitivity, e.g., of [$Eu\Sigma$] to the changes of k_1 and k_3, then the assumption of their constancy or their standardisation in the system studied seems to be tolerable. Contrary to k_1 and k_3, the values of k_2 and k_4 are significantly pH dependent (see Fig. 3).

The values of all constants point to the higher rates of C-reactions and D-reactions on carboxylic groups HAS than on HAW and to the higher rates of C-reactions as compared with D-reactions.

The course of results of C- and D-processes, accompanied by the sorption on ion exchanger, was analyzed by simulation calculations using the determined values of rate constants. Results, shown in Figs. 4(A, B), 5(A, B, C) and 6, elucidate: (i) the kinetics of complexation of Eu^{3+} with HAS and HAW groups, (ii) the kinetics of sorption of Eu^{3+} in the presence and in the absence of HA, (iii) time-dependencies of concentrations of EuΣ, Eu^{3+} and Σ(Eu_aHAS + Eu_bHAW) in liquid phase.

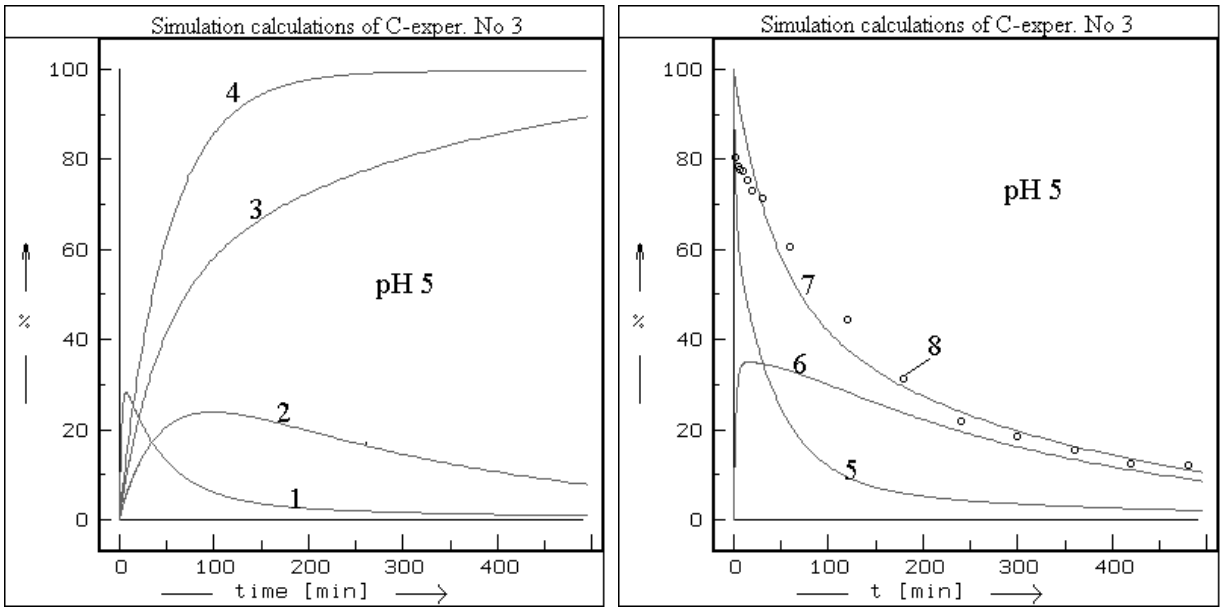

Fig. 4A: The results of simulation calculations of C-experiment No. 3. The concentration of Eu species is expressed in [%] of [Eu]$_0$. 1 – [$Eu_aHAS^{(n-a.3)-}$], 2 – [$Eu_bHAW^{(m-b.3)-}$], 3 – {Eu^{3+}} in the presence of HA, 4 – {Eu^{3+}} in the absence of HA, 5 – [Eu^{3+}], 6 - Σ([$Eu_aHAS^{(n-a.3)-}$] + [$Eu_bHAW^{(m-b.3)-}$], 7 – [$Eu\Sigma$], 8 – experimental data.

Table 3: Results of evaluation of kinetic C- and D- experiments: rate constants $k_1 - k_4$. Guessed values of stoichiometric coefficients are marked by c), and fixed initial values of kinetic coefficients by a). χ^2 and Q represents statistical quantities mentioned in the text.

Calcul. No.	Exper. No.	Type of exper.	pH	Stoichiom. coeff. a	b	$k_1 \pm \sigma$ ($min^{-1}mol^{-a}L^a$)		$k_2 \pm \sigma$ (min^{-1})		$k_3 \pm \sigma$ ($min^{-1}mol^{-b}L^b$)		$k_4 \pm \sigma$ (min^{-1})		χ^2	Q
1	1	C	4	1	-	8.27E-1	1.57E-4	1.21E-2	2.32E-6	-	-	-	-	22.0	2.08E-2
2	2	D	4	1	-	1.00 a)	-	1.15E-2	3.83E-6	-	-	-	-	15.3	2.93E-1
3	1	C	4	2 c)	-	1.00	8.12E-1	1.24E-2	3.42E-6	-	-	-	-	21.5	2.84E-2
4	2	D	4	2 c)	-	9.55E-1	7.36E-2	1.22E-2	4.22E-6	-	-	-	-	51.0	8.17E-7
5	3	C	5	2 c)	1 c)	1.13	1.2E-1	1.15E-2	3.38E-6	4E-1 ?	2.68E-1	4.11E-3	2.90E-4	12.8	3.04E-1
6	3	C	5	10	2.74	1.00 a)	-	3.10E-2	1.42E-2	8.92E-2	9.32E-3	2.10E-3	1.81E-4	19.0	8.85E-2
7	4	D	5	10	2.74	1.00 a)	-	8.46E-3	4.38E-6	1.22E-1	6.89E-3	8.83E-4	1.16E-4	12.1	3.51E-1
8	5	C	6	3 c)	2 c)	9.23E-1	9.38E-1	3.08E-3	1.22E-4	9.79E-2	5.10E-1	9.26E-3	2.60E-3	1.74	1.00
9	5	C	6	8 c)	3 c)	1.00 a)	-	7.98E-3	4.85E-6	9.33E-2	6.04E-4	1.56E-3	9.97E-7	1.79	1.00
10	5	C	6	10.10	6.32	1.00 a)	-	9.50E-3	2.45E-3	0.10 a)	-	2.45E-3	1.74E-4	2.38	1.00
11	6	D	6	10.10	6.32	1.00 a)	-	5.78E-3	1.23E-5	0.10 a)	-	1.10E-3	2.52E-6	17.0	1.97E-1
12	7	C	7	10.10	7.28	1.00 a)	-	4.80E-3	1.37E-3	0.10 a)	-	1.01E-3	3.10E-4	2.79	1.00
13	8	D	7	10.10	7.28	1.00 a)	-	6.08E-3	1.09E-5	0.10 a)	-	4.33E-4	9.37E-7	20.0	9.36E-2
14	9	C	8	10.10	7.39	1.00 a)	-	2.95E-3	6.42E-6	0.10 a)	-	3.53E-4	9.86E-7	1.53	1.00
15	10	D	8	10.10	7.39	1.00 a)	-	3.01E-3	1.83E-6	0.10 a)	-	1.96E-4	1.75E-5	3.83	1.00

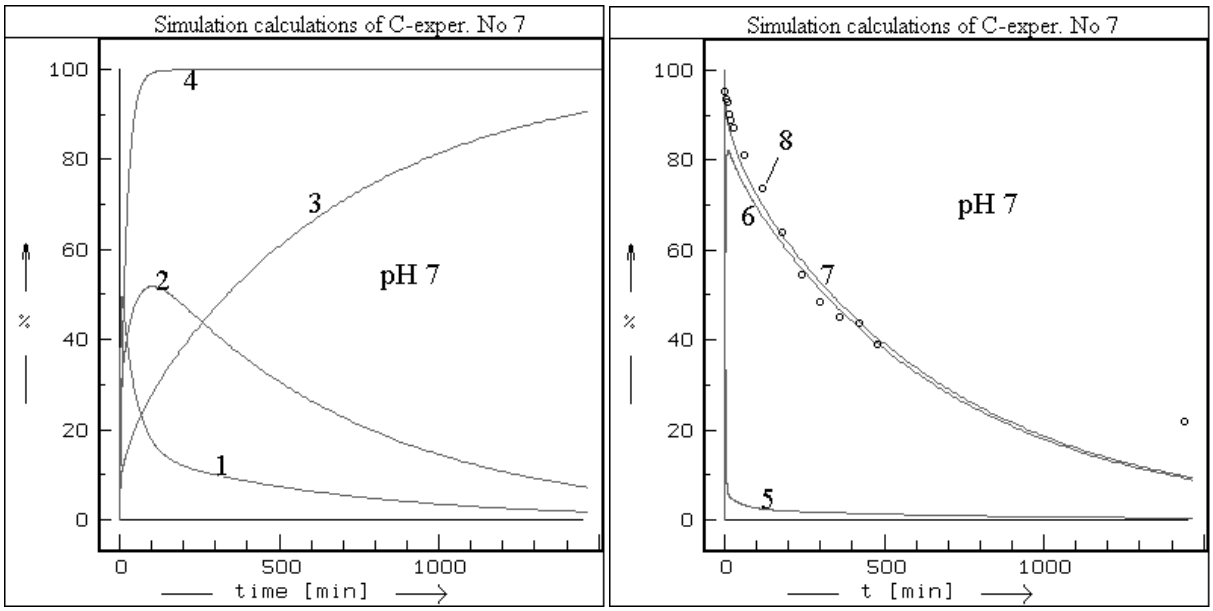

Fig. 4B: The results of simulation calculations of C-experiment No 7. The concentration of Eu species is expressed in [%] of $[Eu]_0$. 1 – $[Eu_aHAS^{(n\text{-}a.3)-}]$, 2 – $[Eu_bHAW^{(m\text{-}b.3)-}]$, 3 – $\{Eu^{3+}\}$ in the presence of HA, 4 – $\{Eu^{3+}\}$ in the absence of HA, 5 – $[Eu^{3+}]$, 6 –- $\Sigma([Eu_aHAS^{(n\text{-}a.3)-}] + [Eu_bHAW^{(m\text{-}b.3)-}]$, 7 – $[Eu\Sigma]$, 8 – experimental data.

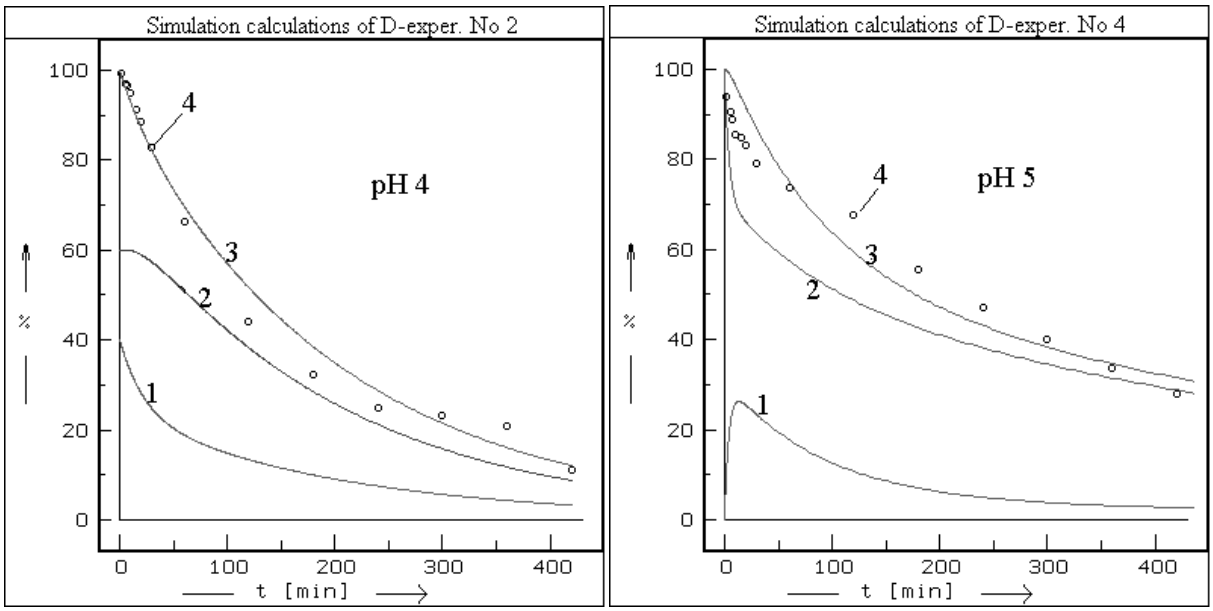

Fig. 5A: The results of simulation calculations of D-experiments No. 2 and 5 The concentration of Eu species is expressed in [%] of $[Eu]_0$. 1 – $[Eu^{3+}]$, 2 - $\Sigma([Eu_aHAS^{(n\text{-}a.3)-}] + [Eu_bHAW^{(m\text{-}b.3)-}]$ (if pH ≤ 4 then $[Eu_bHAW^{(m\text{-}b.3)-}] = 0$), 3 – $[Eu\Sigma]$, 4 – experimental data.

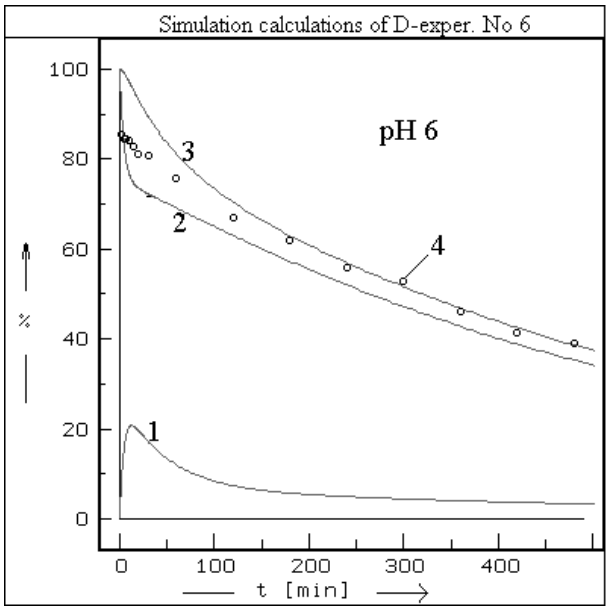

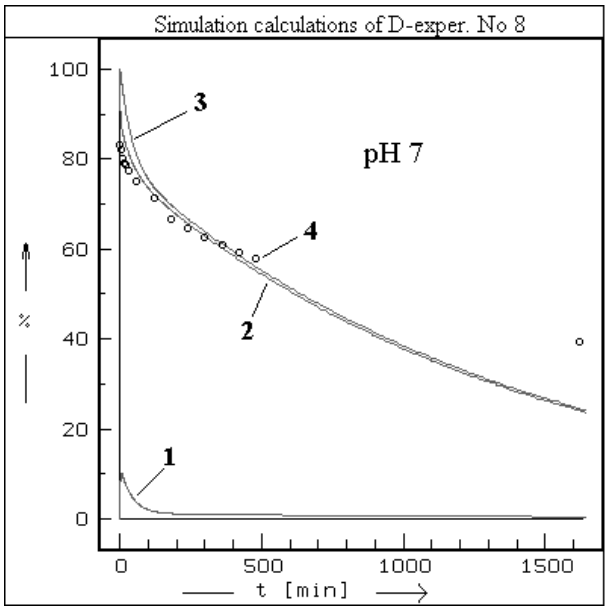

Fig. 5B: The results of simulation calculations of D-experiments No 6 and 8. The concentration of Eu species is expressed in [%] of $[Eu]_0$. 1 – $[Eu^{3+}]$, 2 - $\Sigma([Eu_aHAS^{(n\text{-}a.3)-}] + [Eu_bHAW^{(m\text{-}b.3)-}]$, 3 – $[Eu\Sigma]$, 4 – experimental data.

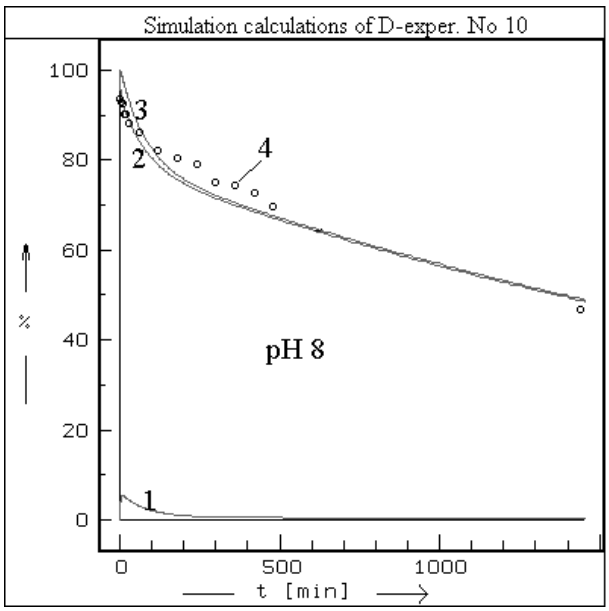

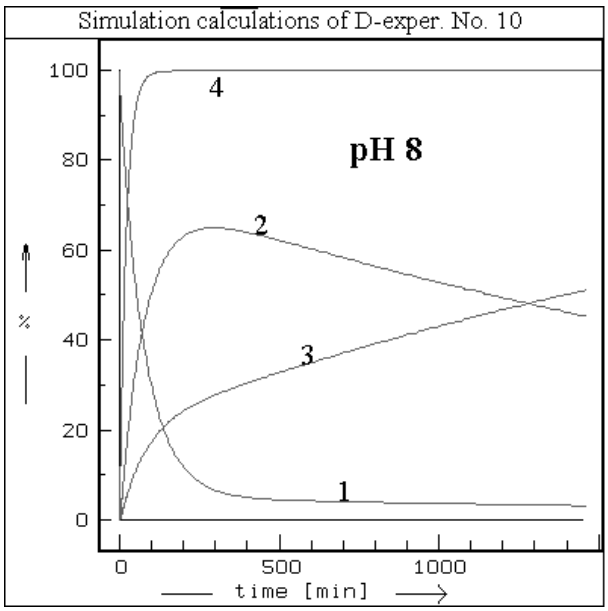

Fig. 5C: The results of simulation calculations of D-experiment No 10. The concentration is expressed in [%] of $[Eu]_0$, 1 – $[Eu^{3+}]$, 2 – $\Sigma([Eu_aHAS^{(n\text{-}a.3)-}] + [Eu_bHAW^{(m\text{-}b.3)-}])$, 3 – $[Eu\Sigma]$, 4 – experimental data.

Fig. 6: The results of simulation calculations of D-experiment No. 10. The concentration is expressed in [%] of $[Eu]_0$. 1 – $[Eu_aHAS^{(n\text{-}a.3)-}]$, 2 – $[Eu_bHAW^{(m\text{-}b.3)-}]$, 3 – $\{Eu^{3+}\}$ in the presence of HA, 4 – $\{Eu^{3+}\}$ in the absence of HA.

4 Conclusions

1. The use of ion exchange method for the study of Eu^{3+} complexation with carboxylic groups of HA is complicated by the fact that ion exchange affects the complexation process. After some time the complexation is always reversed to decomplexation – see Figs. 4A and 4B.
2. The rate constants of decomplexation, k_2 and k_4, decrease with the increasing pH while the complexation rate constants, k_1 and k_3, are virtually independent of pH – see Fig. 3.
3. The kinetics of sorption of Eu^{3+} on cation exchanger is retarded in the presence of HA. The C- and D- reactions are the rate-determining step of the sorption especially at pH ≥ 7 – see Figs. 4 – 6.
4. C- and D- reactions taking place on HAS groups are faster than those on HAW groups in the whole pH interval studied – see Figs. 4 – 6.

References

Marinsky J.A., edit. (1966) "Ion Exchange", Marcel Dekker, Inc., New York, 68.

Press W.H., Flannery B.P., Teukolsky S.A., Vetterling V.H. (1989) "Numerical Recipes in Pascal (The Art of Scientific Computation)", Cambridge University Press, Cambridge, 664.

Štamberg K., Beneš P., Mizera J., Dolanský J., Vopálka D., Chalupská K. (2003) "Modeling of metal-humate complexation based on the mean molecular weight and charge of humic substances: Application to Eu(III) humate complexes using ion exchange", *J. Radioanal. Nucl. Chem.*, **256**, 2, 329.

Annex 19

Release of americium from humic acid binding sites studied by desorption experiment using immobilized humic acid silica gel

Gyula Szabó [1], Judit Guczi [1], Tohru Miyajima [2], Horst Geckeis [3] and Robert A. Bulman [4]

[1] "Frédéric Joliot-Curie" National Research Institute for Radiobiology and Radiohygiene, PO Box 101, Budapest, H-1775, Hungary

[2] Department of Chemistry, Faculty of Science and Engineering, Saga University, 1-Honjo, Saga 840-8502, Japan

[3] Forschungszentrum Karlsruhe, Institut für Nukleare Entsorgungstechnik, 76021 Karlsruhe, Germany

[4] National Radiological Protection Board, Didcot, United Kingdom, OX11 ORQ

Release of americium from humic acid binding sites studied by desorption experiment using immobilized humic acid silica gel

Gyula Szabó[1], Judit Guczi[1], Tohru Miyajima[2], Horst Geckeis[3] and Robert A. Bulman[4]
[1]"Frédéric Joliot-Curie" National Research Institute for Radiobiology and Radiohygiene, PO Box 101, Budapest, H-1775, Hungary
[2]Department of Chemistry, Faculty of Science and Engineering, Saga University, 1-Honjo, Saga 840-8502, Japan
[3]Forschungszentrum Karlsruhe, Institut für Nukleare Entsorgung, 76021 Karlsruhe, Germany
[4]National Radiological Protection Board, Didcot, United Kingdom, OX11 ORQ

Summary

To facilitate investigations of the influence of humic acid on the migration of americium in and around nuclear waste repositories we have chemically immobilized humic on silica gels. Release of trivalent elements from humic substances has been investigated by a batch method use of the derivatized silica gel with 0.1 M $NaClO_4$ solutions at different pHs. The effect of occupation of binding sites has also been investigated. The release behavior of Am is analyzed.

Key words: humic acid, americium, release from binding site,

Introduction

Humic substances form complexes with a wide variety of metal ions and thus mediate their bioavailability, biotoxicity and transport in the biosphere. A detailed understanding of the influence of humic substances on the speciation of metal ions is beyond our reach owing to the complicated, heterogeneous and variable nature of these polydispersed, polyelectrolytic substances. Thus to predict humate-mediated movement of transuranic radionuclides through the environment, it is necessary to understand the chemistry of the interactions of transuranic elements with humic substances in fine detail.

Americium-241 is a major component of the long-lived radionuclides produced in reactors, and as such its environmental behavior has been the topic of many studies. Extensive research over the years has established that humic substances play an important role in the geochemical cycling of americium (Choppin, 1992). The effects of different experimental methods, pH, humic acids of different origin, ionic strength, and formation of mixed complexes have been studied.

However, humic acid in the environment is not confined to the aqueous phase, often adsorbing to inorganic surfaces and colloids. Investigations with actinide and lanthanide ions, and transition metal ions verify the humic coating of these surfaces is an important component in metal ion sorption. From these studies pH and ionic strength are important terms in describing the sorption-desorption of metal ions to humic-coated surfaces, similar to results from aqueous

complexation studies. From an investigation of the literature it can be seen that binding-sorption processes have been investigated in details, but release-desorption or binding reversibility data are rare. Consequently an improved understands of the release-desorption process and a larger database for modeling can be achieved.

Experimental

Materials and methods

Silica gel (Polygoprep Si-300, 20 μm, BET surface area 100 m^2/g) was obtained from Macherey-Nagel. Humic acid was purchased from Aldrich Chemical Co. Ltd. and purified by the method of Kim et al., 1990. 3-Aminopropyltriethoxysilane and 1-(3-Dimethylaminopropyl)-3-ethylcarbodiimide hydrochloride were purchased from Aldrich Chemical Co. Ltd. Humic acid was immobilized on silica gel (SiO_2-HA) by using previously described procedure (Szabo et al., 1992; Bulman et al., 1997, Koopal et al., 1998. The specific surface area of the prepared solid phase was determined by BET method and are given in Table 1. C, H and N analyses of HA-SiO_2 were conducted on an automatic CHNS-O analyzer (see Table 1). The IR spectra of the prepared silica gel was recorded using a NICOLET 5PC FT-IR Spectrometer. ^{241}Am was determined by liquid scintillation (LC) counting in a Packard Tri-Carb 2550 liquid scintillation counter. The proton exchange capacity of the immobilized HA was determined by potentiometric titration (Table 1).

Stock solutions of Nd(III) were prepared by dissolving $Nd(NO_3)_3$ in 0.1 mol l^{-1} $NaClO_4$ and diluted as needed to concentrations 10^{-6} - 2 10^{-3} mol l^{-1} with 2-morpholine-ethane sulfonic acid (MES) or 4-pyridineethane sulfonic acid (PES) buffer (10^{-3} mol l^{-1}). Kim et al., 1989 and Buckau et al., 1992 have shown that these buffers does not alter the complexation of Am(III) by humic substances.

Binding/Sorption experiment

The binding of Am-Nd by the immobilized humic acid was examined at pH 4, 5 and 6 in 0.1 M $NaClO_4$ containing 1-200 x 10^{-6} mol l^{-1} concentration of Am-Nd by batch method. Accurately weighed quantities of the gels, typically about 100 mg, were added to the buffered (pH 4-6) 0.1 mol l^{-1} $NaClO_4$ solutions containing of different concentrations of Nd spiked with ^{241}Am (300 Bq; (2.34 $\cdot 10^{-9}$ g; 9,6 $\cdot 10^{-12}$ mol). The resulting suspensions were shaken at room temperature for 48 h. The concentrations of Nd-Am in a clarified aliquot, which was collected by centrifugation, were measured by LC. The amount of nuclides bound by the solid phases was calculated and the isotherms were plotted. The maximal binding capacity (B_{max}) of SiO_2-HA was calculated from the one site binding isotherms:

$$q = B_{max}K'[M^{z+}] / (1 + K'[M^{z+}]) \qquad (1)$$

where q is the amount of M^{z+} bound and B_{max} is the maximum binding capacity. The free concentration of M^{z+} is presented as $[M^{z+}]$. The symbol K' is an association constant often referred to as the binding strength.

Releasing/desorption experiment

Desorption was conducted following sorption. Seven different sorbed Am-Nd concentrations were used for each pH. At the end of 48 h sorption, nine-tenths of the supernatant of each sample was replaced by the same volume of 0.1 M NaClO4 whose pH had been adjusted to that samples. The suspensions were shaked for 48 h. Following the same procedure as for sorption, the samples were centrifuged and the activity measured. The desorption step was repeated eight times. The concentration of Am-Nd retained by the gel in the suspension after each desorption step was calculated according to the following equation:

$$q_i = q_{i-1} - (C_i - C_{i-1}/10)/W \qquad (2)$$

where q_i is the concentration of Am-Nd remaining on the gel at the end of ith desorption step (μmol/g); q_{i-1} is the concentration of Am-Nd remaining on the gel at the end of (i-1)th desorption step (μmol/g); C_i is Am-Nd concentration in the solution at the end of the ith step (μmol/L); C_{i-1} is Am-Nd concentration in the solution at the end of the (i-1)th desorption step (μmol/L), and W is the solid concentration in the suspension (g/L).

Results

The characteristics of the prepared silica gel are shown in Table 1. From C, H, and N analyses of SiO_2-HA it has been established that the gel has average humic substances contents of 19.3 mg g^{-1} solid matter. The extensive coating of humic substances on the derivatized silica gels will minimize the areas for interaction of ^{241}Am(III) by any silanol binding sites remaining on the silica gel. In addition, Bulman and Szabo, 1991, studies have demonstrated only slight uptake of ^{241}Am(III) species by un-derivatized silica gels.

On the basis of the well recognized analogue chemistry of Nd(III) for Am(III) (Moeller, 1970) it is likely that the complexing capacity measured of SiO_2-HA for Nd(III) will be quite similar to their complexing capacity for Am(III).

Determination of maximal binding capacity (B_{max}) of humic acid immobilized on silica gel

Typical binding isotherms (solid phase concentration vs. liquid phase concentration in equilibrium) of Am-Nd(III) by SiO_2-HA at different pH values in 0.1 mol l^{-1} $NaClO_4$ are presented on Fig. 1. The complexation of Am-Nd(III) by humic acid immobilized on solid support leads to an increase of metal binding on the surface until the saturation of the complexing sites occurs under the experimental conditions. From these binding isotherms it has been possible to calculate, see Table 1, the maximal binding capacity B_{max} (expressed in mol g^{-1} solid phase) using equation 1. As seen in Table 1 and Fig. 1., B_{max} increases with increasing pH (4 to 6). This increase with pH is likely to result from an increase in the number of ionized carboxylic binding sites. A similar phenomenon has been reported by Cacei, 1985, Kim et al., 1991 and Moulin et al., 1992.

Table 1. Characteristics of the used SiO_2-HA

	SiO_2-HA
Substrate content (mg g^{-1})	19.3 ± 1.2
Proton exchange capacity (meq/g solid matter)	0.0673
Maximal bindig capacity (μmol g^{-1}):	
at pH 4	14.81 ± 1.02
at pH 5	16.25 ± 0.78
at pH 6	18.39 ± 0.94
BET surface area[a] (m^2 g^{-1})	74 ± 8

[a]The surface area of the parent silica gel is 100 m^2 g^{-1}

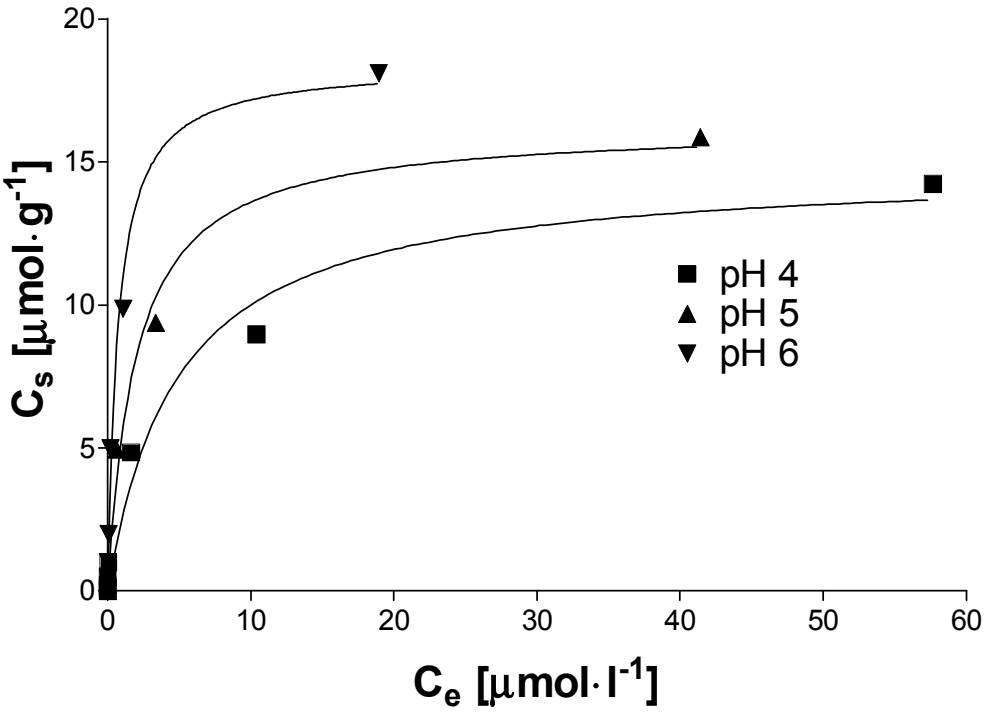

Figure 1. Binding isotherm of SiO_2-HA for Am-Nd(III) in 0.1 mol l^{-1} $NaClO_4$ at pHs 4, 5 and 6.

Release of Am from humic acid binding sites

To understand the release behaviour of Am from humic acid, we chose seven different loaded humic acids ranging from 0.5 to 98 % at pH 4-6 to conduct desorption experiments as described previously. Here a new method is suggested, which is the step-by–step batch experiment modeling Am removal from the binding site of HA. The results are given in Figure 2-4

at pH 4, 5 and 6 respectively.

The release of Am from the binding sites at different pHs exibits several marked differences: principally the release of Am from HA increases with either increase pH or higher metal loading. From an investigation of the highly loaded HA, it can be concluded that there is a minimum of two binding sites on HA. In case of low loaded HA the amount of release of Am is determined by the stability constant of Am-humate. Suprisingly high desorption was obtained in case of 96% loaded Am-humate, 49%, 23% and 12% at pH 4, 5 and 6 respectively. This study shows that Am could be mobilized easily from HA by changing pH. It is also evident that the release of Am from HA depends on the occupation of the binding sites.

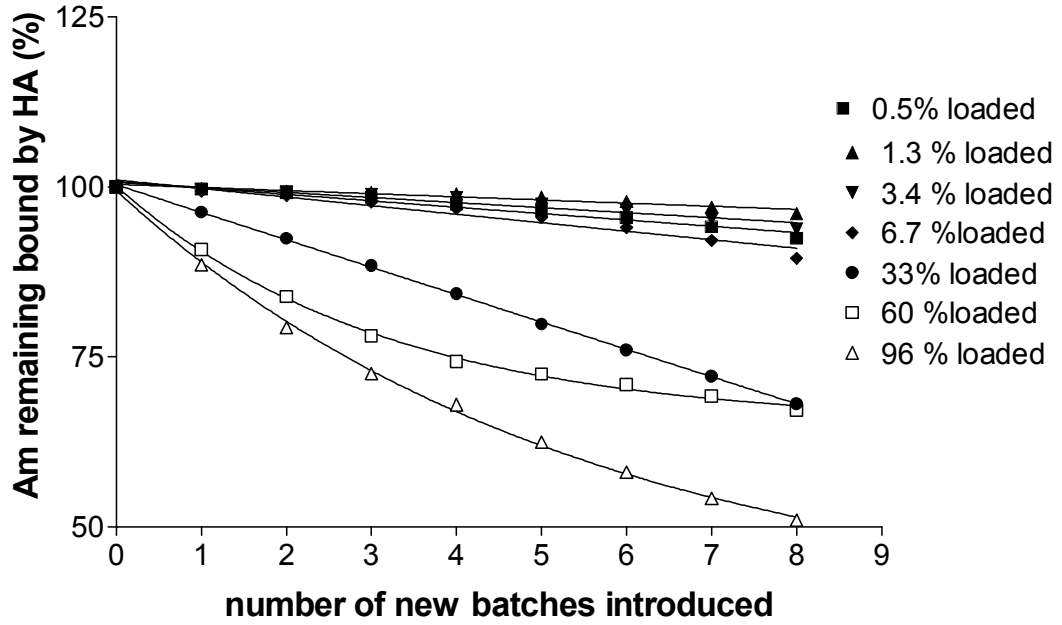

Figure 2. Release of Am(III) from humic acid binding sites at pH 4 with 0. M $NaClO_4$

Acknowledgments

This work was supported by either European Commission, EC Contract No. FIKW-CT-2001-00128 or Hungarian-Japanase bilateral cooperation, JAP-12/98.

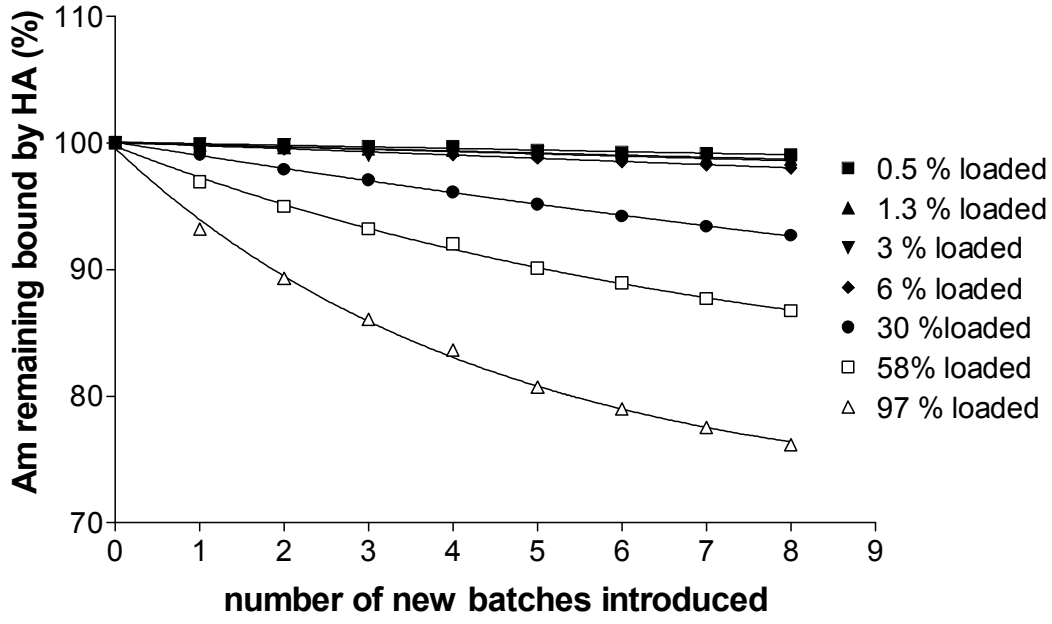

Figure 3. Release of Am(III) from humic acid binding sites at pH 5 with 0. M $NaClO_4$

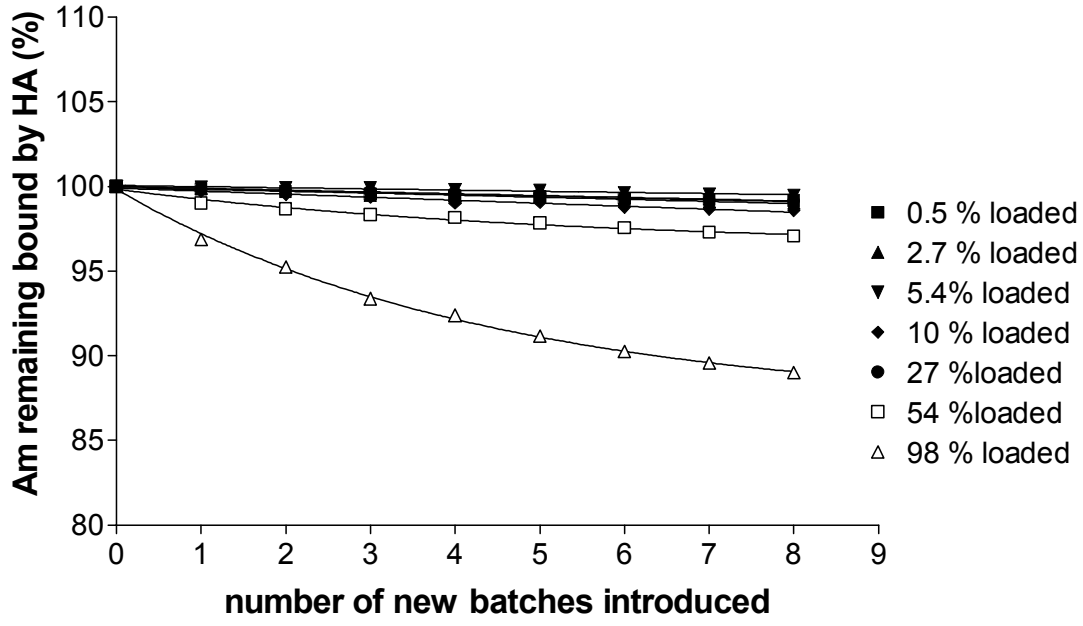

Figure 4. Release of Am(III) from humic acid binding sites at pH 6 with 0. M $NaClO_4$

Literature

Buckau, G., Kim, J.I., Klenze, R., Rhee, D.S., Wimmer, H.
A comparative spectroscopic study of the fulvate complexation of trivalent transuranium ions, *Radiochimica Acta*, 57, **105** (1992)

Bulman, R. A., Szabó, Gy.
Investigations of the interactions of transuranic radionuclides with humic and fulvic acids immobilized on silica gel. *Lect. Notes Earth Sci.* **33**: 329 (1991).

Bulman, R.A., Szabó, Gy., Clayton, R.F., Clayton C.R.
Investigation of the uptake of transuranic radionuclides by humic and fulvic acids chemically immobilized on silica gel and their competitive release by complexing agents, *Waste Management*, **17** (1997) 191

Caceci, M.
The interaction of humic acid with Eu(III). Complexation strength as a function of load and pH. *Radiochimica Acta,* **39**, 51 (1985)

Choppin, G.R.: The role of natural organics in radionuclide migration in natural aquifer system. *Radiochimica. Acta*, **58/59**, 113 (1992)

Kim, J.I., Buckau, G., Bryant, E., Klenze, R.
Complexation of americium(III) with humic acid. *Radiochimica Acta*, **48**, 135 (1989)

Kim, J.I., Rhee, D., Buckau, G.
Complexation of Am(III) with humic acids of different origin. *Radiochimica Acta*, **52/53**, 49 (1991)

Koopal, L.K., Yang, Y., Minnaard, A.J., Theunissen, P.L.M., Van Riemsdijk, W.H.
Chemical immobilisation of humic acid on silica, *Colloid Surfaces A: Physicochem. Eng. Aspects*, **141** (1998) 385-395

Moeller, T.
Periodicity and the lanthanides and actinides. *J. Chem. Educ*., **47**, 417 (1970)

Moulin, V., Tits, J., Moulin, C., Decambox, P., Mauchien, P., de Ruty, O.
Complexation behaviour of humic substances towards actinides and lanthanides studied by Time-Resolved Laser-Induced Spectrofluorometry. *Radiochimica Acta*, **58/59**, 121 (1992)

Szabo, Gy., Farkas, Gy., Bulman, R.A.
Evaluation of silica-humate and alumina-humate HPLC stationary phases for estimation of the adsorption coefficient, K_{OC}, of soil for some aromatics, *Chemosphere,* **24** (1992) 403-412

Annex 20

Preliminary results for preparation and characterisation of immobilised humic acid on silicon wafer

Gyula Szabó [1], Judit Guczi [1], Judit Telegdi [2] and Ioannis Pashalidis [3]

[1] "Frédéric Joliot-Curie" National Research Institute for Radiobiology and Radiohygiene, PO Box 101, Budapest, H-1775, Hungary

[2] Department of Surface Modification and Nanostructures, IC CRC Hungarian Academy of Sciences, H-1025 Budapest, Hungary

[3] University of Cyprus, Department of Chemistry, 2016 Nicosia, Cyprus

Preliminary results for preparation and characterisation of immobilised humic acid on silicon wafer

Gyula Szabó[1], Judit Guczi[1], Judit Telegdi[2] and Ioannis Pashalidis[3]
[1]"Frédéric Joliot-Curie" National Research Institute for Radiobiology and Radiohygiene, PO Box 101, Budapest, H-1775, Hungary
[2] Department of Surface Modification and Nanostructures, IC CRC Hungarian Academy of Sciences, H-1025 Budapest, Hungary
[3]University of Cyprus, Department of Chemistry, 2016 Nicosia, Cyprus

Abstract
To facilitate understanding the chemistry of the interactions of radionuclides with humic acid (HA) in microscopic scale, we have immobilized humic acid on silicon wafers. In this communication, we present a simple protocol to immobilise humic acid on silicon wafer surface. A trifunctional silane reagent 3-aminopropyltrimethoxysilane (APTES) was used to modify the surface of silicon wafers and appeared to be able to strongly attached soluble humic acid through their carboxylic groups to solid support. Humic acid, anchored in a following incubation step, were proved to be able to bind Am(III).

Key words: humic acid, silicon wafer, americium, atomic force microscopy

Introduction
Humic substances are among the most widely occurring natural organic products on the earth's surface. It has been recognized for sometime that humic materials have a major role in the transport and sorption of metal ions in the environment. Additions to our understanding of the structure and the nature of metal-ion binding sites of humate are still a laudable goal even though there have already been many investigations of the nature of the binding of metal ions, particularly those of the transuranic ions. The chemistry of the interactions of radionuclides with humic acid (HA) needs to be understood in details so that humate-mediated migration of radionuclides through the environment can be predicted. To achieve such a data in microscopic scale, several detective techniques, such as atomic force microscopy (AFM), chemical force microscopy (CFM), nuclear microprobe analysis (NMA) and X-ray photoelectron spectroscopy (XPS) can be used to measure intermolecular forces and to visualize the surface morphology.

The main aim of this work was to provide humic material with specific properties in order to study with different spectroscopic techniques, the complexation behaviour of surface bound humic acid in microscopic scale. Namely, humic acid has been immobilised on silicon wafers in order to mimic surface bound humic substances in natural aquatic systems.

Experimental
Materials
3-aminotriethoxysilane, hydrogen peroxide, hydrochloric acid, ammonium hydroxide, toluene, sodium acetate and N-(3-dimethylaminopropyl)-N'-ethyl-carbodiimide hydrochloride

(EDC) were purchased from Aldrich. The purified and characterised Aldrich humic acid was obtained from Technical University of Prague. ^{241}Am was obtained from AEA Technology. Silicon wafer polished on one side was purchased from Plano GmbH. The silicon wafers were cut into pieces of approximately 1 cm by 2 cm before cleaning and modifying. The remaining chemicals were obtained from commercial sources and were used without purification.

Apparatus

Atomic force microscope (NanoScope III, Digital Instrument, USA) was used in contact mode for imaging silicon wafer samples with and without modification. In the image processing only auto-flattening was used. The radioactivity of ^{241}Am bound on the silicon wafers was determined by gamma-ray spectrometer NK-350 with a NaI(Tl) scintillator an NZ-138 well-type detector shield (GAMMA, Hungary).

Immobilization procedure

The chemical procedure for preparation of immobilized humic acid on silicon wafer based on Unger 1978, Szabó et al., 1992; Koopal et al., 1998 and Wei et al., 2000 work. Illustration of the procedure is showed in Figure 1. The process was performed as follows: (i) degreased ultrasonically in chloroform, rinsed with water; (ii) activated-oxidized in alkaline solution (1:1:5, v/v, NH_4OH:H_2O_2:H_2O) for 5 min and 5 times water rinse; (iii) activated-oxidized in acidic solution (1:1:5, v/v, HCl:H_2O_2:H_2O) for 5 min and 5 times water and methanol rinse, designated "activated" and stored for later comparison with the modified wafers; (iv) silanised by immersing in 1% APTES/toluene solution for 2 h; (v) curing for 20 h under vacuum at 130 ^{0}C; immobilization of HA in alkaline –alcoholic solution and water rinse; (vi) end-capping of remaining NH_2 groups in acetate solution at pH 10 with EDC for 4 h, washing and heating at 110 ^{0}C. The final product was stored on air.

Calculation of quantity of HA immobilized on wafer

The quantity of HA immobilized on wafer was determined thorough Am(III) sorption investigation. The cleaned, amino-modified and immobilized HA wafers were loaded with Am(III) from 0.01 M $NaClO_4$ at pH 6 for 24 h. After loading the wafers were washed with distilled water and measured in gamma spectrometer to determine the surface-bound americium. The quantity of immobilized HA on wafers was calculated use of Kim and Cherwinski (1996) idea. Namely, loading capacity (LC) of HA for metal ion can be expressed as:

$$LC = \frac{z(M^{z+})}{(PEC)(HA)}$$

where

z is the charge of the complexing metal ion

(M^{z+}) is the maximal amount of metal ion complexed by HA (mol/wafer)

(PEC) is the proton exchange capacity of HA (eq/g HA)

(HA) is the quantity of HA (g/wafer).

Rearrange that equation to calculate the quantity of HA on the surface

$$(HA) = \frac{z(M^{z+})}{(PEC)(LC)}$$

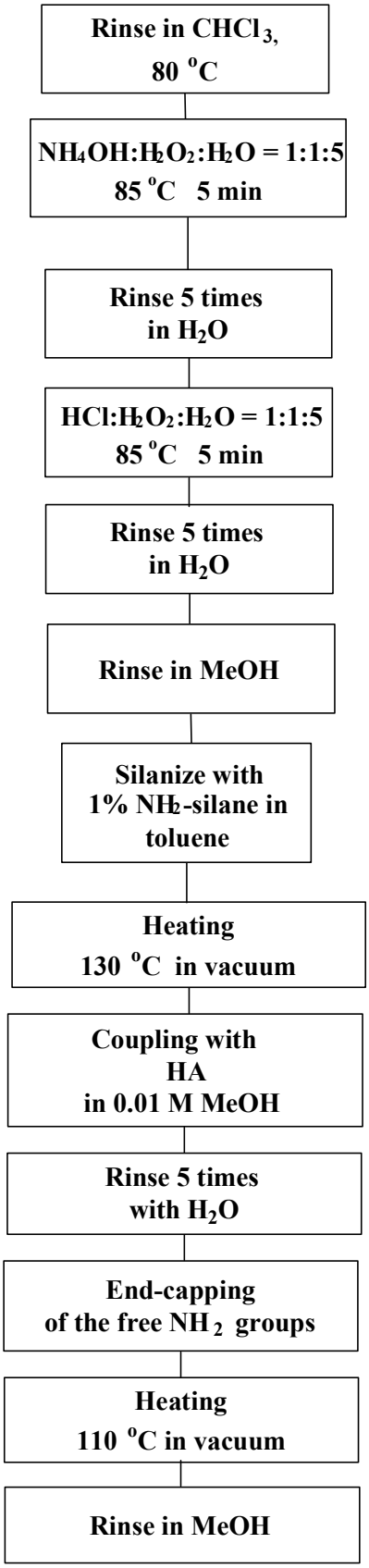

Figure 1. Flow diagram of the preparation of the immobilized humic acid on silicon wafer

Results

Wafer samples with identical reaction history were examined by AFM in contact mode. Images of the activated, amino-silylated and HA immobilized wafer surfaces taken in height mode (xy=2x2μm; z=6nm) are shown in Fig 2-4. 3D visualization facilitates the comparison of morphologies of pre-treated and original wafer samples as shown in Fig. 5.

The activated wafer surface was clean (Fig. 2.) with a surface roughness (RMS) of 0.274 nm. The RMS value of the silylated wafer sample was 0.520 nm, about double so high as the RMS roughness (0.274 nm) of the underlying native surface sample (Fig 3.). The surface of silanized silicon-wafer is fully covered by small, bell-shaped precipitates whose diameters are in the range of 3-5 nm as the section analysis shows. The application of humic acid resulted in a smoother surface (Fig. 4) than was noticed on the silanized silicon wafer. The roughness (RMS) is 0.371 nm. The morphology of HA surface covered by hemi-spherical particles is converted into an irregular surface topography. Instead of small bell-shaped precipitates with average diameter of 2.4 nm (which covered the surface uniformly) in this case on the surface there are bigger products with an average diameter of 2.8 nm sporadically.

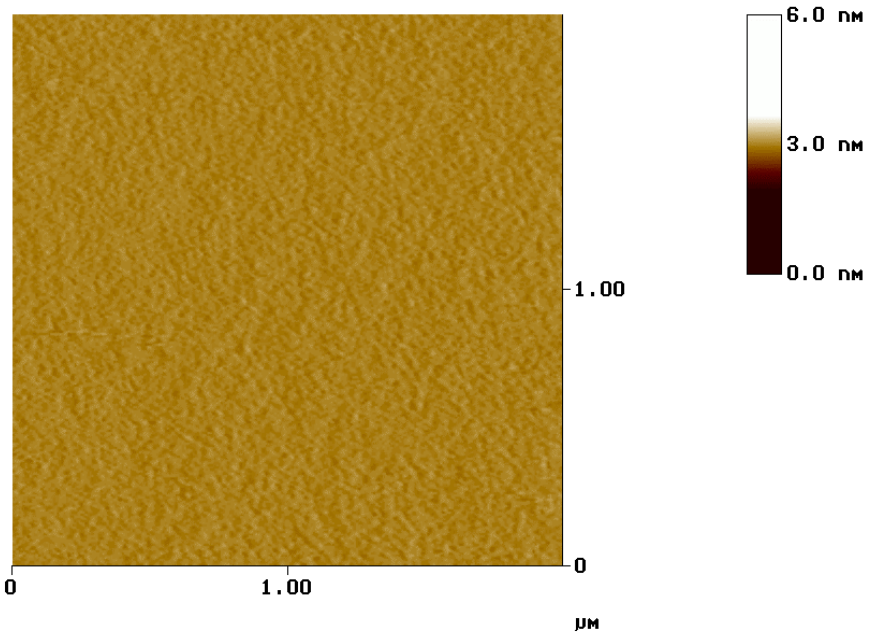

Figure 2. 2D AFM image of activated silicon wafer

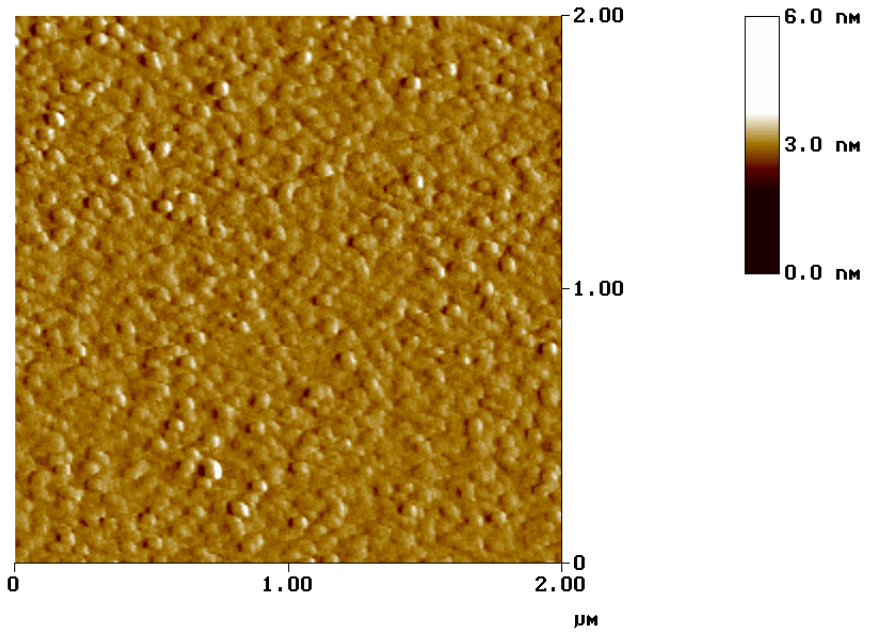

Figure 3. 2D AFM image of amino-silanized silicon wafer

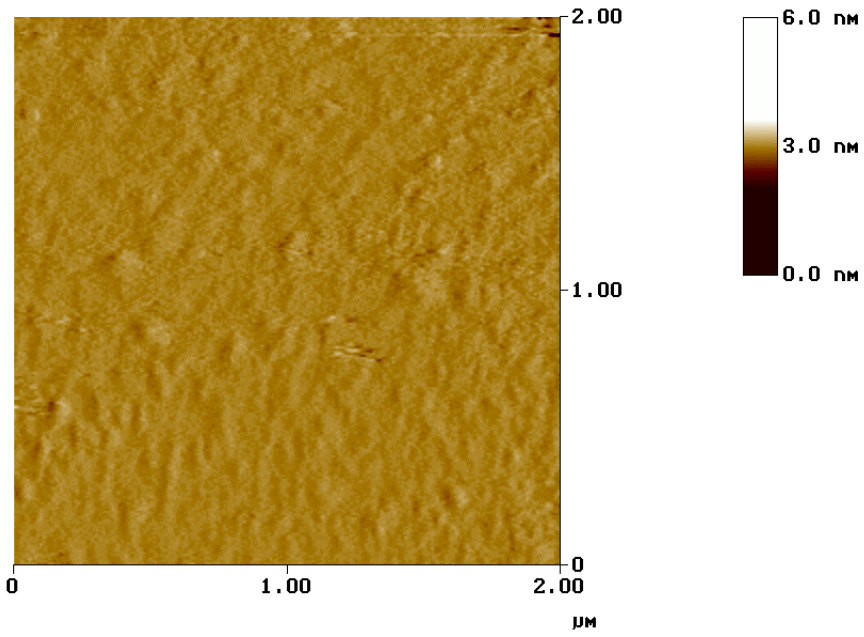

Figure 4. 2D AFM image of HA immobilized HA on silicon wafer

Activated silicon wafer

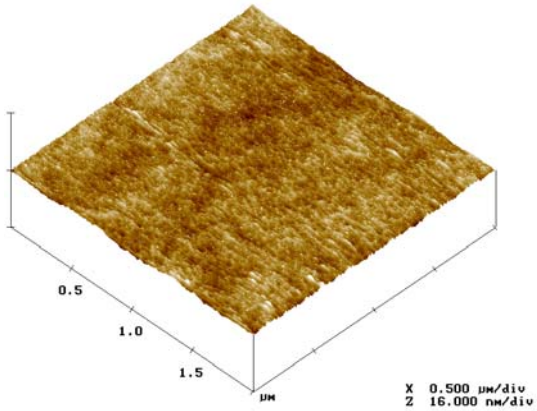

Amino silanized silicon wafer

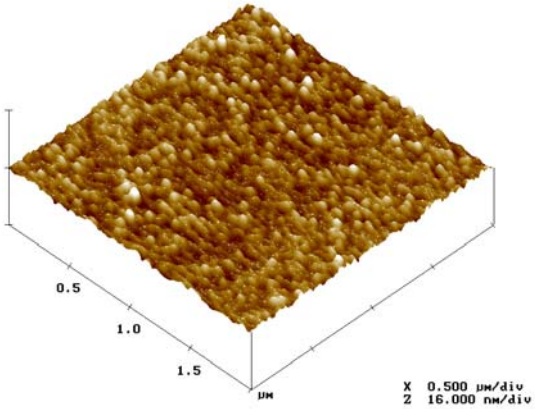

Immobilised HA on silicon-wafer

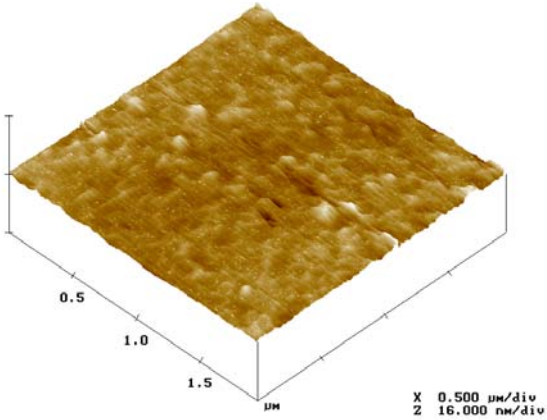

Figure 5. 3D AFM image of silicon wafer samples.

The quantity of HA immobilized on wafer was determined thorough Am(III) sorption investigation in 0.01 M $NaClO_4$ at pH 6 (Fig. 6.). From Fig. 6. It can be concluded that the HA immobilized on silicon wafer binds more Am (III) than either silanised or activated silicon wafer. To calculate the amount of HA immobilized on the silicon wafer, loading capacity equations were used with an assumption that LC is 0.8 for HA at pH 6. Substituting the PEC (5.4 mmol/g) and the measured Am (specific activity: 3.062 10^{13} Bq/mol) activity (22.3 Bq/wafer) into the equation we have got that the amount of immobilized HA on the surface is 5.1 10^{-10} g/wafer (1,3 10^{-10} g/cm^2).

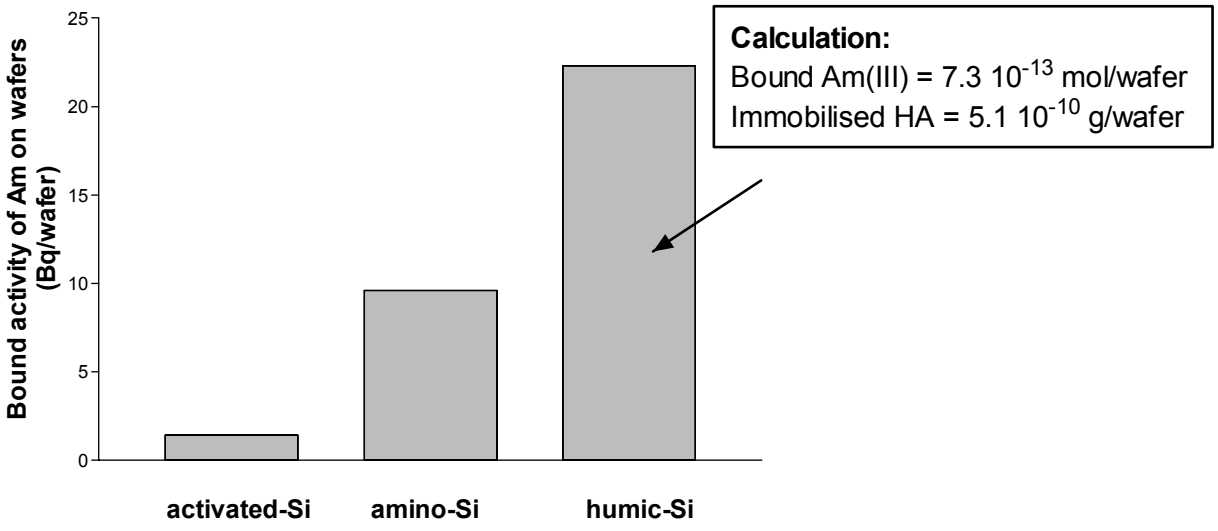

Figure 6. Binding of Am(III) on different silicon wafers at pH 6 in 0.01 M $NaClO_4$

Acknowledgments

This work was supported by European Commission, EC Contract No. FIKW-CT-2001-00128.

Literature

Kim, J.I., Czerwinski, K.R.,
Complexation of metal ions with humic acid: Metal ion charge neutralization model, *Radiochimica Acta*, **73** (1996) 5-10

Koopal, L.K., Yang, Y., Minnaard, A.J., Theunissen, P.L.M., Van Riemsdijk, W.H.
Chemical immobilisation of humic acid on silica, *Colloid Surfaces A: Physicochem. Eng. Aspectts*, **141** (1998) 385-395

Szabo, Gy., Farkas, Gy., Bulman, R.A.
Evaluation of silica-humate and alumina-humate HPLC stationary phases for estimation of the adsorption coefficient, K_{OC}, of soil for some aromatics, *Chemosphere,* **24** (1992) 403-412

Unger, K.K.
Porous Silica: Journal of Chromatography Library **Vol 16**. Elsevier, Amsterdam 1978

Wei, Z.Q., Wang, C., Zhu, C.F., Zhou, C.Q., Xu. B., Bai, C.L.
Study on single-bond interaction between amino-terminated organosilane self-assembled monolayers by atomic force microscopy, Surface Science 459 (2000) 401-412

Annex 21

U(VI) Mono-Hydroxo Humate Complexation

Pashalidis I.

University of Cyprus, P.O. Box 20537, 1678 Nikosia, Cyprus

U(VI) Mono-Hydroxo Humate Complexation

Pashalidis I.

University of Cyprus, P.O. Box 20537, 1678 Nikosia, Cyprus

Abstract

The complexation of the uranyl ion with humic acid is investigated. Excess amounts of U(VI) is used and the concentration of the humic acid complex is determined by solubility enhancement over the solid phase. pH is varied between 7.5 to 7.9 in 0.1 M $NaClO_4$ under normal atmosphere and room temperature. The $U(OH)^+$ concentration is determined from the U(VI) solubility between pH 4.45 and 8.62 in absence of humic acid. The effective humate ligand concentration (EHLC) is used as described in (Buckau 2004). Only a limited range of data can be used for determination of the complexation constant because of flocculation or sorption of the humic acid upon progressive complexation. Analysis of the complex formation dependency with pH shows that the dominant interacting species in the concerned pH range are either $UO_2(OH)^+$ or $(UO_2)_3(OH)_5^+$. The complexation constant is evaluated to be logß = 6.20 ± 0.02 if presence of $(UO_2)_3(OH)_5^+$ is not regarded. Including the latter species and assuming that the interacting species is still the mono-hydroxo ion, the stability constant becomes about 0.6 log units higher. Interaction with the $(UO_2)_3(OH)_5^+$ ion is not considered, despite such a complex cannot be entirely excluded. The complexation constant has about same number as found for the humate complexation of the non-hydrolyzed uranyl ion, or significantly higher if the UO_2OH^+ ion concentration is deduced under regard of coexistence of the $(UO_2)_3(OH)_5^+$ ion. Consequently, the hydrolysis of the non-complexed uranyl ion shows basically the same or a higher complexation constant as the hydrolysis of the humate complex. This indicates that the humate complex does not occupy several coordination places of the uranyl ion. The same or higher numbers found for the humate complexation strength of the hydrolyzed and non-hydrolyzed uranyl ion, with the nominal charge of +1 and +2, respectively, indicates that the hydroxyl ion may be involved in the complex stabilization. Final evaluation of data will require direct determination of species involved.

pspasch@ucy.ac.cy

Introduction

Humic and fulvic acids complex actinide ions. Ternary complexes with hydroxo or carbonate ions are also formed. In the present work, the concentration of the reacting uranyl mono-hydroxo ion and the humate complex is determined from thermodynamic solubility data and the solubility enhancement due to humate complex formation. The interpretation of humate complexation data depends on assumptions made with respect to the complexation process. Direct measurement of the humate ligand concentration is difficult in the hydrolyzing range of strongly complexing highly charged actinide ions. A suggestion for a consistent description of the effective humate ligand concentration, including the pH neutral range, is given in Buckau 2004. The humate ligand concentration as given in that work is used for interpretation of the present data.

Experimental

The solubility of U(VI) is studied in 0.1 M $NaClO_4$. U(VI) solutions were prepared by dissolution of $UO_2(NO_3)$ $6H_2O$ (Merck Co) in aqueous 0.1 M $NaClO_4$. $UO_2(OH)_2$(s) was prepared by evaporation of a U(VI) solution at pH 3 under normal atmospheric conditions at 25 ºC. The yellow precipitate was separated from the solution washed with bidestilled water, dried and characterized by UV-Vis, FTIR spectroscopy and x ray difraction (Guiner method). For solubilty studies $UO_2(OH)_2$ solid was conducted with pure 0.1 M $NaClO_4$ solutions or $NaClO_4$ solutions containing 0.1 g/L humic acid. Humic acid solutions were prepared from humic acid isolated from Gorleben groundwater (Gohy-573), purified and characterized as described elsewhere (Kim et. al 1990).

Solubility measurements were carried out in 0.1 M $NaClO_4$ under normal atmospheric conditions at 25 ºC. pH was varied by addition of 0.1 M NaOH or 0.1 M $HClO_4$, respectively. Following three days equilibration time pH was measured by using a glass electrode (Ross type, Orion Co) and the analytical U(VI) concentration in solution was determined spectrophotometrically (Cary 5, Varian Co) by means of arsenazo III according to a method described elsewhere (Savvin 1961) and by Inductively Coupled Plasma-Atomic Emmision Spectroscopy (Lamda 40, Perkin Elmer Co). The molar extinction coefficient for the U(VI)-Arsenazo(III) complex at 650 nm was estimated to be 61000 ± 1500 L $mol^{-1}cm^{-1}$.

Results and discussion

The solubility of U(VI) as a function of pH is shown in Fig. 1 (data given in Table 1). The solubility data are fitted with hydroxo and carbonate species, resulting in the constants given in Table 2. The data are in an acceptable range (Reiller 2004). In Fig. 2, the resulting relative distribution of different uranyl species is shown. In the pH range of interest, charge neutral and negative species are dominant. For the purpose of humic acid complexation, the cationic species UO_2^{2+} and $UO_2(OH)^+$ could be considered. As seen in Fig. 3, the concentration of the uranyl mono-hydroxo ion is more than two orders of magnitude higher than that of the uranyl ion, and as shown below, in this pH range the hydrolysis species dominates the humic acid interaction and not the non-hydrolyzed uranyl ion. The important numbers for the present

work thus are (i) the solubility of U(VI) in absence of humic acid, and (ii) the concentration the $UO_2(OH)^+$ ion, both in the pH range where the humic acid induced solubility enhancement is studied (pH 7.5 – 7.9). These data form the basis for evaluation of the humic acid complex concentration by solubility enhancement and the concentration of the complex forming uranyl mono-hydroxo ion. As further discussed below, alternatively the data may be evaluated by regard also of the (3,5) species ($(UO_2)_3(OH)_5^+$). In this case the postulated concentration of the (1,1) species (UO_2OH^+) is lower and both (1,1) and (3,5) are in similar species concentrations (NEA-TDB). In principle, one could also consider complexation between humic acid and the (3,5) species. Such a complex, however, is not considered in this paper.

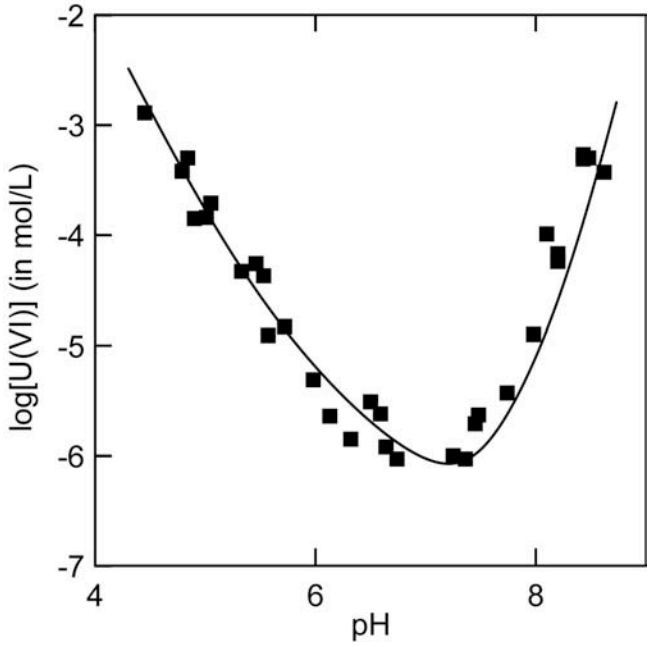

Fig. 1: Solubility of U(VI) over $UO_2(OH)_2$ solid phase as a function of pH in 0.1 $NaClO_4$ under normal atmosphere. Experimental data are given in Table 1 and the fitted curve with associated constants is given in Table 2.

Table 1: Solubility of U(VI) over $UO_2(OH)_2$ solid phase as a function of pH in 0.1 M $NaClO_4$ under normal atmosphere (pCO_2=-3.5).

pH	log[U(VI)]	pH	log[U(VI)]	pH	log[U(VI)]	pH	log[U(VI)]
4.45	-2.89	5.53	-4.37	6.64	-5.92	8.10	-3.99
4.79	-3.42	5.57	-4.91	6.74	-6.03	8.20	-4.24
4.84	-3.30	5.72	-4.83	7.25	-6.00	8.20	-4.17
4.90	-3.85	5.98	-5.31	7.36	-6.03	8.43	-3.27
5.01	-3.84	6.13	-5.64	7.45	-5.71	8.43	-3.31
5.05	-3.71	6.32	-5.85	7.48	-5.63	8.48	-3.30
5.33	-4.33	6.50	-5.51	7.74	-5.43	8.62	-3.43
5.46	-4.26	6.59	-5.62	7.98	-4.90		

Table 2: Solubility product, carbonate complexation constants and hydrolysis constants for the UO_2^{2+} ion. Solubility product refers to amorphous $UO_2(OH)_2$(s).

$logK_{sp}$	logß					
	110	120	101	102	103	
-21.7 (± 0.3)	8.3 (± 0.2)	14.9 (± 0.3)	8.5 (± 0.3)	15.1 (± 0.3)	19.5 (± 0.1)	This work
-22.18 ±0.09*	8.8	16.2	8.4	17.0	22.5	Reiller 2004

Mean value for results from Kramer 1992, Meinrath 1993. Meinrath 1996 and Kato 1996. Other values in this line from Reiller 2004.

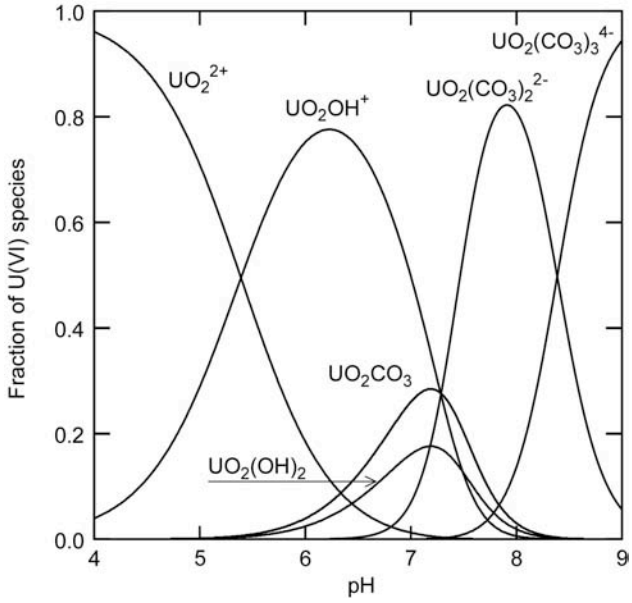

Fig. 2: Uranyl ion pecies distribution from solubility data deduced from data shown in Fig. 1 and Table 1.

The effective humate ligand concentration ([EHLC]) is used as described in (Buckau 2004) and is shown in Fig. 3. It increases only slightly with increasing pH in the range investigated. The concentration of U(VI) in presence of 100 mg/L humic acid is also shown. Starting at pH 7.9, a considerably solubility enhancement is seen compared to the solubility without addition of humic acid. As expected from the increase in the concentrations of ions considered for humic acid complexation with decreasing pH, also the solubility enhancement in presence of humic acid increases. Below pH 7.6, however, a relative drop in the U(VI) concentration is observed. Simultaneously, flocculation or sorbtion of humic acid on the uranium solid phase is visually observed. The decrease in solubility enhancement below pH 7.6, therefore, is not regarded for calculation of the U(VI) humic acid complexation constant (see below).

The complexation behavior is evaluated based on data deduced from the results shown in Fig. 3. The individual experimental data for different pH values are given in Table 3, i.e. the total uranium concentration including solubility enhancement from humic acid complexation ($[U]_{tot}$), the calculated concentration of the uranyl mono-hydroxo ion ($[UO_2(OH)^+]$), the EHLC (from Buckau 2004) and the concentration of uranium complex (as the solubility

enhancement in presence of humic acid). Evaluation based on complexation with the uranyl ion (UO_2^{2+}) results in a pH dependent stability constant much higher than found in the non-hydrolyzing range. Furthermore, the concentration of such a complex should increase by two orders of magnitude per unit decrease in pH. This is not the case (Fig. 3). Consequently, data are evaluated for the interaction with the uranyl mono-hydroxo ion ($UO_2(OH)^+$). In Table 3, the resulting complexation constants and "degrees of ligand loading" are given for the individual pH values investigated.

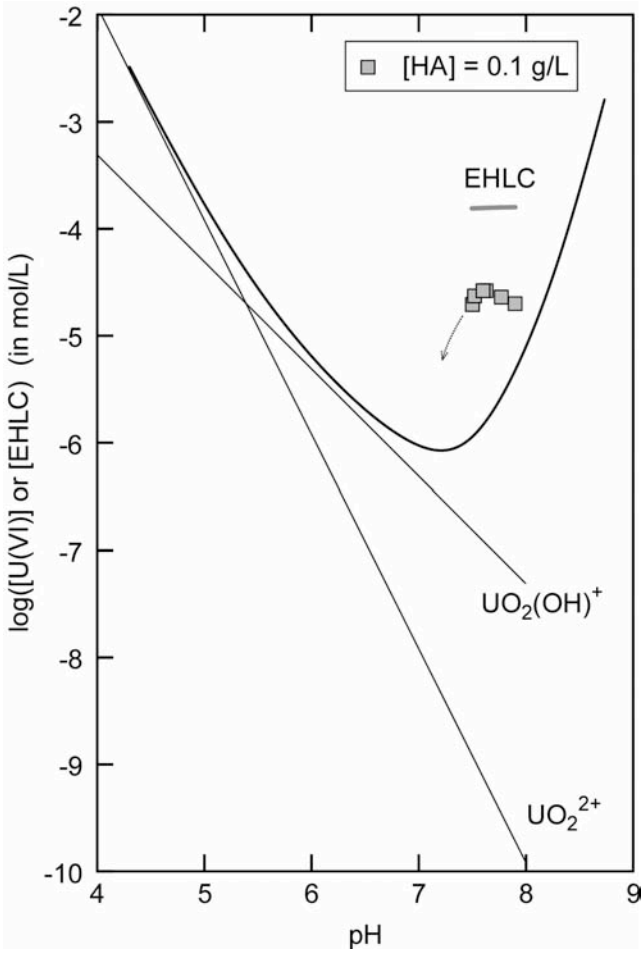

Fig. 3: Concentrations of relevant uranyl species calculated by the data from Table 1, solubility curve without addition of humic acid, enhanced uranium solubility in presence of 0.1 g/L humic acid and effective humic acid ligand concentration from (Buckau 2004). In these calculations no polynuclear species are regarded.

As mentioned above, below pH 7.6 humic acid flocculates/sorbes on the U(VI) solid phase. This is reflected in the variation of logß and the degree of ligand loading with U(VI) as shown in Fig. 4. In the absence of a solid phase, flocculation of the humate complex by the trivalent actinide ion Am^{3+} is not observed until the loading of the humate ligand approaches ligand saturation. This indicates that in the presence of the U(VI) solid phase, sorption is the reason for decrease of humic acid in solution. Evaluation of the stability constant (disregarding values at pH 7.50 and 7.52) results in logß = 6.20 ± 0.02 (L/mol).

Table 3: Data from the uranyl humate complexation study at different pH values: The measured total U(VI) concentration, the uranyl mono-hydroxo ion concentration calculated from thermodynamic data (cf. Table 2), the effective humate ligand concentration (EHLC) (from Buckau 2004) and the uranium(VI) humate concentration by the difference between total measured concentration and sum of ionic species from thermodynamic data (Table 2) (solubility enhancement in presence of humic acid). From these data, the individual complexation constants and fractions of EHLC complexed with U(VI) ("loading") are calculated. Data at pH 7.50 and 7.52 are affected by sorption/flocculation of humic acid.

pH	$\log[U]_{tot}$ (in mol/L)	$\log[UO_2(OH)^+]$ (in mol/L)	log[EHLC] (in mol/L)	log[U-HA] (in mol/L)	logß (in L/mol)	U-HA/EHLC
7.50	-4.71	-6.81	-3.81	-4.74	*5.94*	*0.12*
7.52	-4.63	-6.83	-3.82	-4.66	*6.05*	*0.14*
7.60	-4.58	-6.91	-3.81	-4.61	6.18	0.16
7.63	-4.58	-6.94	-3.81	-4.61	6.21	0.16
7.77	-4.64	-7.01	-3.80	-4.70	6.17	0.13
7.90	-4.70	-7.21	-3.80	-4.83	6.22	0.09

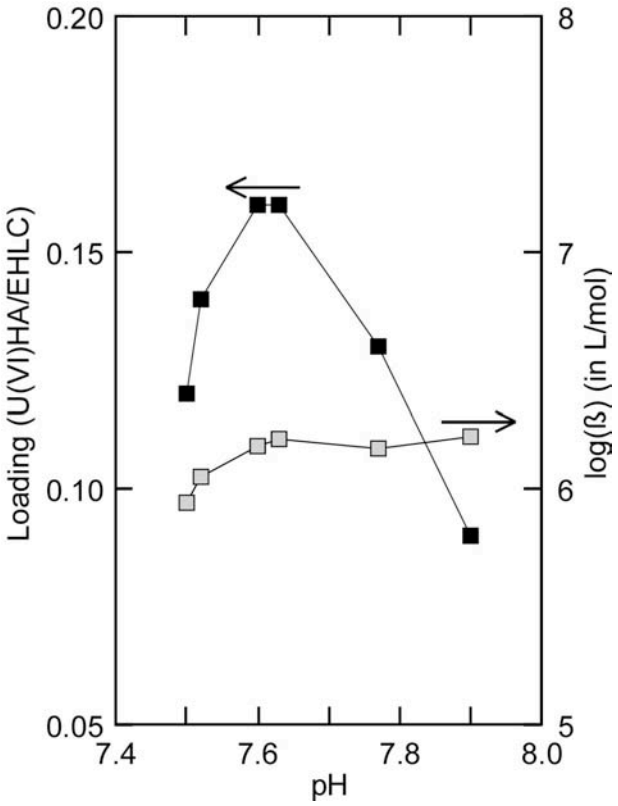

Fig. 4: Complexation constant and degree of humate ligand loading as a function of pH (data from Table 3). The data below pH 7.6 are effected by loss of humic acid in solution with increasing ligand loading as also visually observed during the experiment.

In Fig. 5, the species distribution is shown for conditions comparable to those used in Fig. 2, however in the presence of 100 mg/L humic acid. It is found that the two humic acid complexes of the uranyl ion regarded dominate the species distribution up to a pH of about 8. At higher pH values the anionic di- and tri-carbonate species become dominant.

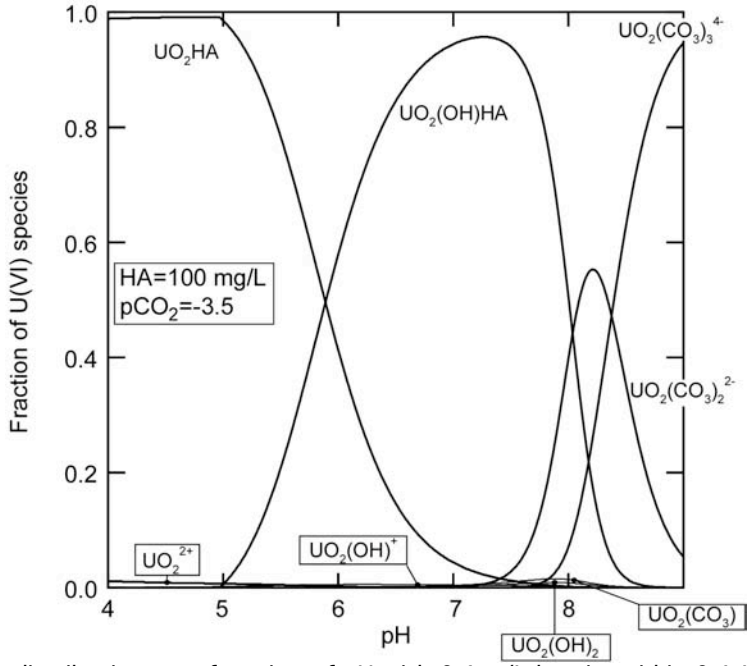

Fig. 5: U(VI) species distribution as a function of pH with 0.1 g/L humic acid in 0.1 $NaClO_4$ under normal atmosphere. The regarded humic acid complexes UO_2HA and $UO_2(OH)HA$ dominate the species distribution up to pH of about 8.

In Fig. 6a, the stability constant for the uranyl mono-hydroxo humate complex is shown in context with the two different routes for obtaining this complex, starting with the non-complexed uranyl ion. Given that the complexation strengths of the humate ligand with both the hydrolyzed and the non-hydrolyzed uranyl ions are basically indistinguishable, the hydrolysis of the uranyl humate complex is deduced to be of the same strength as the hydrolysis of the non-complexed uranyl ion. Somewhat different number are obtained if the coexistence of $(UO_2)_3(OH)_5^+$ species are regarded (cf. NEA-TDB). Evaluation of solubility data with this species regarded results in a decrease in concentration of the $UO_2(OH)^+$ of about 0.6 logarithmic units. Still assuming that the mono-hydroxo species is the dominant humate complex, this leads to a corresponding increase in the stability constant of about 0.6 logarithmic units. The results from such an evaluation are shown in Fig. 6b.

As a first approach one would expect the humate complexation constant for the uranyl mono-hydroxo complex to be weaker than that of the non-hydrolyzed uranyl ion. The same is the case for comparison of the hydrolysis of the uranyl humate complex compared to that of the non-complexed uranyl ion. In Fig. 7, the stepwise hydrolysis constants for the uranyl ion (data in Table 4) are compared with the hydrolysis of the uranyl humate complex (cf. Figs. 6a-b). Looking at the stepwise hydrolysis constants, the expected decrease is found for progressive occupation/charge compensation with an increasing number of charged ligands replacing hydration water in the equatorial plane of the uranyl ion. Especially the third stepwise hydrolysis constant is very weak reflecting the formation of a negative complex.

As already mentioned above, in the case of hydrolysis of the humic acid complex, the hydrolysis constant is of the same strength as the first hydrolysis constant of the non-complexed uranyl ion. Depending on the type of complex with the carboxylic functional groups of humic acid, one could rather expect a lower number, especially for subsequent hydrolysis

after bidentate binding or binding with several carboxylic functional groups of the humic acid. A final conclusion on the nature of the humic acid metal ion complexation is not possible from this study, but it could indicate a limited number of complexing groups and a limited coordination number. On the other hand, humic acid has a large density of oxygen functional groups in addition to the proton exchanging ones (Buckau 2004). Enhancement of the binding via hydrogen bonds of the hydroxo group entering to form the ternary complex could also be possible. A final conclusion will require thorough comparison with other ternary humate complexes and spectroscopic data.

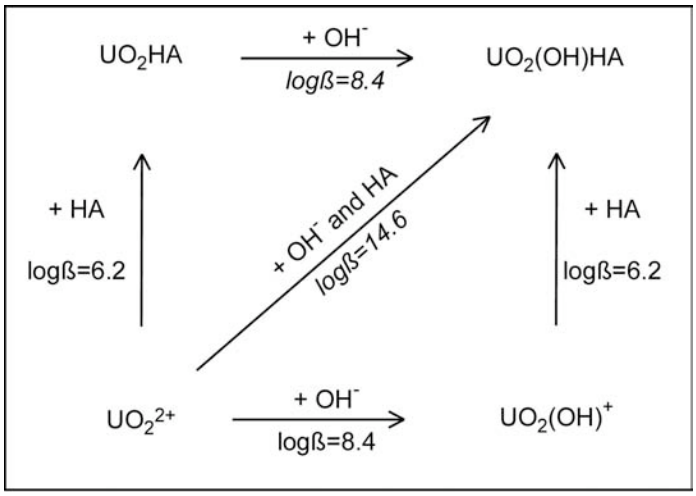

Fig. 6a: Stability constants for the different routes from the non-complexed uranyl ion to the uranyl mono-hydroxo humate complex. Hydrolysis of the uranyl humate complex is deduced from the other data. Data used originate from the use of only mono-nuclear species in the evaluation. Regard of the polynuclear species $(UO_2)_3(OH)_5^+$ is shown in Fig 6b.

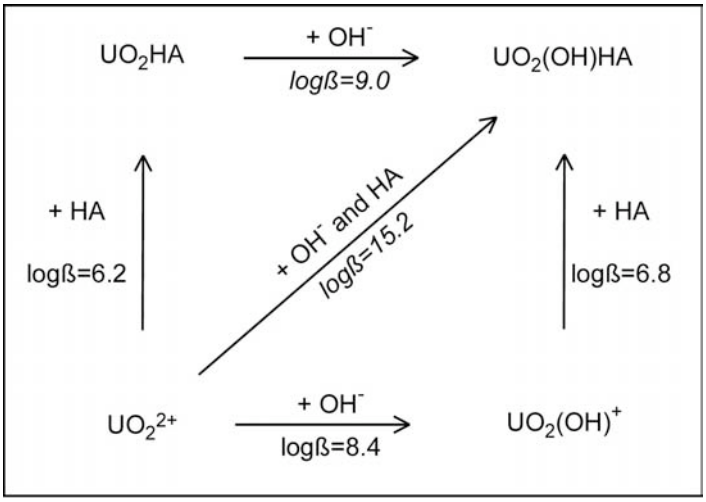

Fig. 6b: Stability constants for the different routes from the non-complexed uranyl ion to the uranyl mono-hydroxo humate complex. Hydrolysis of the uranyl humate complex is deduced from the other data. The concentration of $UO_2(OH)^+$ is calculated under the assumption of coexistence of $(UO_2)_3(OH)_5^+$ for evaluation of solubility data. The calculated concentration of the uranayl mono-hydroxo species is about 0.6 log units lower and the calculated stability constant correspondingly about 0.6 log units higher. Results without regard of the polynuclear species $(UO_2)_3(OH)_5^+$ is shown in Fig 6a.

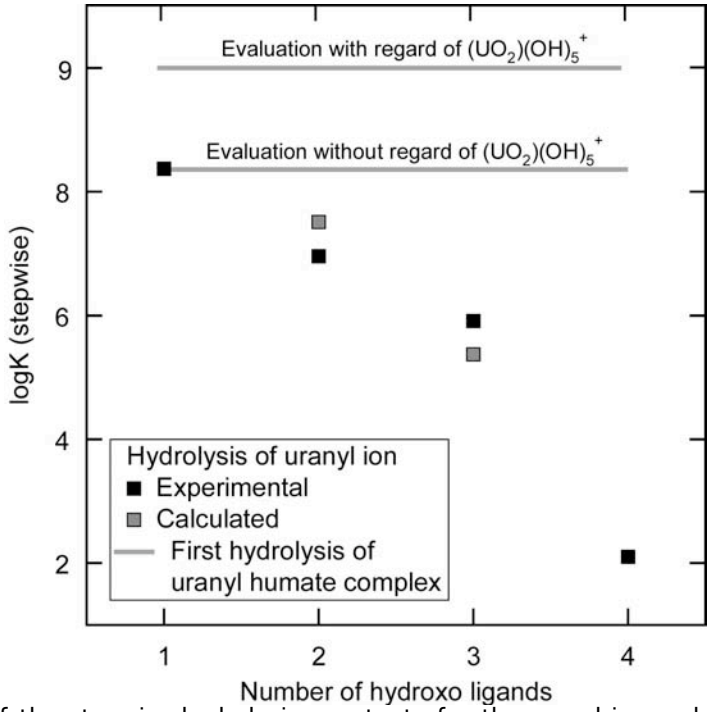

Fig. 7: Comparison of the stepwise hydrolysis constants for the uranyl ion and the hydrolysis of the uranyl humate complex. For data evaluation without regard of $(UO_2)_3(OH)_5^+$, hydrolysis of the humate complexed uranyl ion does not deviate significantly from hydrolysis of the non-complexed zranyl ion. If $(UO_2)_3(OH)_5^+$ is regarded for data evaluation, the corresponding hydrolysis constant of the uranyl humate complex becomes significantly stronger than for the first hydrolysis of the non-complexed uranyl ion.

Table 4: Hydrolysis of Uranyl ion.

Species	logß (cumulative)				logK(stepwise)	
	Exp. Data (Zero IS)	Model[1)] (Zero IS)	Exp. data (0.1 M[2)])	Model[1)] (0.1 M[2)])	Exp. Data (0.1 M[2)])	Model[1)] (0.1 M[2)])
1,1	8.75	8.75	8.37	8.37	8.37	8.37
1,2	15.85	16.48	15.25	15.88	6.88	7.51
1,3	21.75	21.84	21.16	21.25	5.91	5.37
1,4	23.6	21.3	23.2	20.9	2.1	(-0.31)[3)]

1: NCRM (Neck Charge Repulsion Model) Calculated for maximum distance, i.e. 180, 120 and 90 degree angle for 2, 3 and 4 hydroxo ligands, respectively.
2: $NaClO_4$
3: Value too low because permutation of yl- oxygen axis not regarded.

Summary and conclusions

The hexavalent uranyl ion forms strong complexes with humic acid in the non-hydrolyzing range. In this study it is shown that also strong ternary complexes are formed in the pH neutral range. Data show the existence of humic acid complexes with the first hydrolysis species. Alternatively one could consider complexation with the $(UO)_3(OH)_5^+$ ion. The complex most probably formed is found to be UO_2(OH)HA. The stepwise stability constant for humate complexation of the uranyl mono-hydroxo ion is shown to have a complexation constant of logß = 6.2, the same complexation constant as found for the humate complexation of the non-complexed uranyl ion. Comparison of the stepwise hydrolysis constants for the

non-complexed uranyl ion and the uranyl humate complex shows that both processes have interaction constants of logß = 8.4. Regarding presence of, but not complexation with, the $(UO)_3(OH)_5^+$ ion, the uranyl mono-hydroxo complexation constant becomes increased by about 0.6 log units. The results indicate that the humate complex of the uranyl ion does not occupy a large number of coordination sites and does not lead to a charge neutralization of the uranyl ion. Another possible impact could be enhancement of the complexation strength by hydrogen bonding to neighboring oxygen functional groups of the humic acid. Further studies are required in order to resolve the exact coordination of the humate complexes of the uranyl and the mono-hydroxo uranyl ions.

References

Buckau G. (2004) "Approach for physico-chemical interpretation of An(III) and An(VI) humate complexation", Annex 3, same report.

Kato Y., Kimura T., Yoshida Z. and Nitani N. (1996) "Solid-liquid phase equilibria of Np(VI) and U(VI) under controlled CO_2 partial pressure", ", *Radiochimica Acta*, **74**, 21.

Kim J.I., Buckau G., Li G.H., Duschner H., Psarros N. (1990) "Characterization of Humic and Fulvic Acids from Gorleben Groundwater", *Fresenius J. Anal. Chem.*, **338**, 245.

Kramer-Schnabel U., Bischoff H., Xi R.H. and Marx G. (1992) "Solubility products and complex formation equilibria in the systems uranyl hydroxide and uranyl carbonate at 25°C and I=0.1 M", ", *Radiochimica Acta*, **56**, 183.

Meinrath G. and Kimura T. (1993) "Behavior of U(VI) solids under conditions of natural aquatic systems", ", *Inorg. Chim. Acta*, **204**, 79.

Meinrath G., Kato Y., Kimura T. and Yoshoda Z. (1996) "Solid-aqueous phase equilibria of uranium(VI) under ambient conditions", ", *Radiochimica Acta*, **75**, 159.

NEA-TDB (2003) "Update on the Chemical Thermodynamics of Uranium, Neptunium, Plutonium, Americium and Technetium, Volume 5. Thermochemical database of the OECD-NEA (Organization for Economic Co-operation and Development - Nuclear Energy Agency).

Reiller P. (2004) "Prognosticating the humic complexation for redox sensitive actinides through analogy, using the charge neutralization model", Annex 11, same report.

Savvin, S. B. (1961) "Analytical use of arsenazo III - Determination of thorium, zirconium, uranium and rare earth elements", *Talanta*, **8**, 673

Annex 22

Initial studies on temperature impact of humic acid

Pashalidis I. [1], Colocassidou C. [1], Costa C.N. [1], Efstathiou A.M. [1] and Buckau G. [2]

1) University of Cyprus, P.O. Box 20537, 1678 Nikosia, Cyprus

2) Institut für Nukleare Entsorgung, Forschungszentrum Karlsruhe, P.O. Box 3640, 76021 Karlsruhe, Germany

Initial studies on temperature impact of humic acid

Pashalidis I.[1]*, Colocassidou C. [1], Costa C.N. [1], Efstathiou A.M. [1] and Buckau G.[2]

1) University of Cyprus, P.O. Box 20537, 1678 Nikosia, Cyprus
2) Institut für Nukleare Entsorgung, Forschungszentrum Karlsruhe, P.O. Box 3640, 76021 Karlsruhe, Germany

Abstract

The impact of temperature on the stability of the humic acid Gohy-573(HA) is studied. The studies are made both in order to add general knowledge about humic acid but also in order to provide the basis for experimental setup of studies, and judgment of published data, on the metal ion humate complexation as a function of temperature. Methods applied are mass spectroscopy as a function of temperature elevation up to 240 °C, and UV/Vis spectroscopy. Mass spectroscopy is conducted under inertgas atmosphere in order to avoid burning with air oxygen. UV/Vis spectra are measured after storage of humic acid solution (pH=6.0, I=0.1 M $NaClO_4$) at temperatures up to 95 °C. The reversibility of changes is also studied by UV/Vis spectroscopy after subsequent storage at room temperature. Already at 50 °C release of water is observed from dried humic acid with a peak around 60°C. A second large water release is found with the maximum around 100 °C. Above 100 °C also carbon dioxide is released, followed by release of carbon monoxide above 130 °C. The carbon monoxide and dioxide releases show two distinct maxima at around 180 and 210 °C. The UV/Vis spectra show an increase in the absorption towards short wavelengths with increasing temperature and storage time. Already at 60 °C, considerable changes occur after storage for one week. At 95 °C the change in the spectral feature after 24 h is in the order of that found for 1 week storage at 80 °C. After storage at elevated temperatures, the changes in the spectra remain even after 1 week of storage at room temperature. Release of water, carbon monoxide and carbon dioxide at high temperature is certainly related to oxidation with the high oxygen inventory in humic acid. The nature of the water release and changes in the UV/Vis spectra at lower temperature is not fully clear. Further experiments, including complexation properties, fluorescence spectroscopy and IR-reflection spectroscopy at elevated temperature are under consideration.

*pspasch@ucy.ac.cy

Introduction

Humic and fulvic acids consist mainly of carbon, oxygen and hydrogen. In addition small varying quantities of nitrogen and sulfur are found. Disregarding the latter, the sum formula is approximately $CO_{0.5}H$ (Buckau 2004). The thermal stability of humic acid is of interest for general understanding of the nature of humic acid. Furthermore, deduction of thermodynamic data (ΔH and ΔS) requires studies over a temperature interval. In this context, response of humic acid to elevated temperature needs to be known. For these reasons, initial studies on the response of humic acid to thermal treatment are conducted. The release of water, carbon monoxide and carbon dioxide of humic acid in response to temperature elevation under inert-gas atmosphere is studied by mass spectroscopy. Furthermore, the change in UV/Vis spectra of dissolved humic acid is studied at different temperatures and storage times, including reversibility by subsequent storage at room temperature.

Experimental

The humic acid Gohy-573(HA) is used. The groundwater is isolated from 140 m depth in the Gorleben aquifer system. The humic acid originates from microbiologically mediated conversion of Miocene brown coal sand under simultaneous reduction of sulfate dissolving from the underlying Gorleben salt dome. Details on origin, preparation and characteristic properties of this humic acid can be found in (Artinger et al. 2000, Buckau et al. 2000a, Buckau et al. 2000b, Kim et al. 1990). Mass spectroscopic quantification of water, carbon dioxide and carbon monoxide released from humic acid under temperature elevation up to 240 °C under inertgas is done by a setup described in Costa et al. 2000. The temperature-programmed desorption (TPD) experiments were conducted in a specially designed flow-system with a humic acid sample amount of 150 mg. The temperature of the reactor was increased from 25°C to 240°C, using a thermal gradient of 15 °C/min. He was used as a carrier gas for released gases. Analysis of the gas effluent stream from the reactor was done by online quadrupole mass spectrometer (Omnistar, Balzers) equipped with a fast response inlet capillary/leak valve (SVI 050, Balzers) and data acquisition systems. The analyzer response was calibrated against standard mixtures. The mass numbers (*m/z*) 15, 28, 44 and 46 were used for NH_3, CO, CO_2 and NO_2 quantification, respectively. Prior to temperature elevation and effluent gas analysis, the samples were pretreated and the sample chamber cleaned by He flow for 30min at 25°C.

UV/Vis spectroscopy is conducted with solutions of 12 mg/L humic acid at pH 6.0 (10^{-3} mol/L MES buffer) in 0.1 M $NaClO_4$. Solutions are kept in water bath for storage at different temperatures (±0.1 °C).

Results and discussion

In Fig. 1, the release of water, carbon dioxide and carbon monoxide is shown as a function of temperature elevation up to 240 °C. Release peaks can be identified at five different tem-

peratures (cf. Fig. 1). The release of water, carbon dioxide and carbon monoxide at temperatures above 100 °C can be related to oxidation with the humic acid oxygen inventory. The amount of oxygen would be sufficient for oxidation of basically the whole hydrogen inventory if no other reactions would occur. This, however, is not the case. An indication for exhaustion of the oxygen inventory is the progressive generation of carbon monoxide above about 140 °C. At around 240 °C, the decomposition process ceases, and one may expect a residue of thermally stable hydrocarbon. Comparison with UV/Vis spectroscopy results (below) leads to the conclusion that the second release of water with a peak around 100 °C is an irreversible process with combustion of hydrogen with the humic acid oxygen inventory resulting in the formation of water. The main question arising from the results shown in Fig. 1 is to which extent the first release of water with a peak around 60 °C is a reversible or irreversible process, i.e. a release of structurally bound hydration water or the result of chemical conversion of the humic acid.

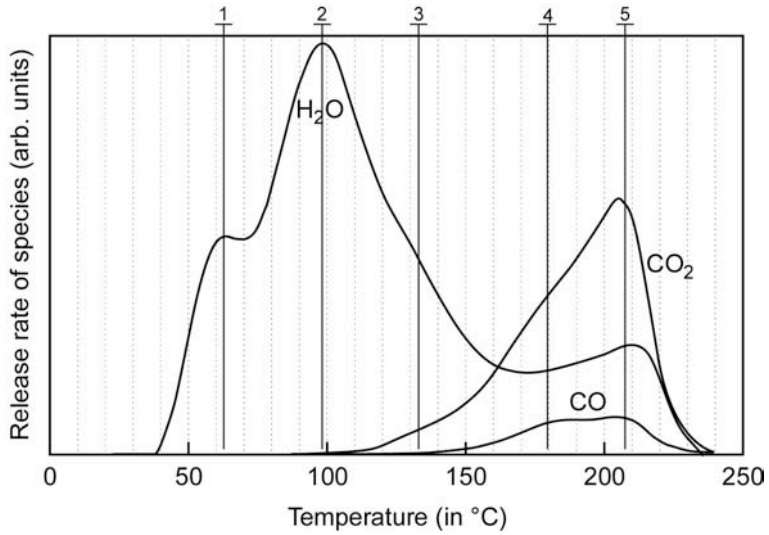

Fig. 1: Release of water, carbon dioxide and carbon monoxide monitored by mass spectrometry upon thermal treatment of Goh-573(HA) under inertgas atmosphere.

The UV/Vis absorption of humic acid solution after 24 h at room temperature (25 °C), 80 °C and 95 °C is shown in Fig. 2. The difference between the room temperature spectrum and the spectrum at 80 °C is small but significant and well reproducible. At 95 °C, the spectrum shows a considerable change with strong increase towards shorter wavelengths. The UV/Vis spectra of humic and fulvic acids are basically featureless. They show a nearly exponential increase in absorption towards shorter wavelengths (Fig. 3). Plotting the logarithm of the absorption against the wavelength, the deviation in the characteristics of the UV/Vis absorption with the changes at 95 °C becomes emphasized (Fig. 3).

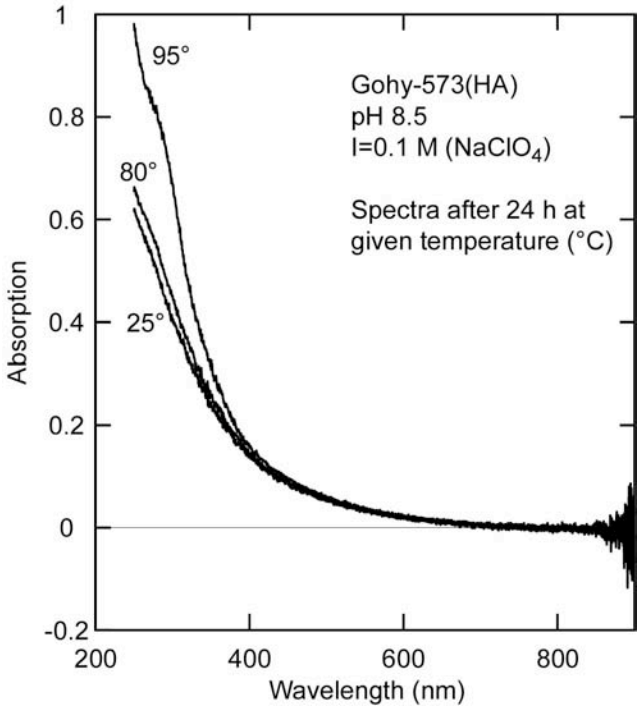

Fig. 2: UV/Vis spectra of Gohy-573(HA) solution after storage at different temperatures for 24 hours.

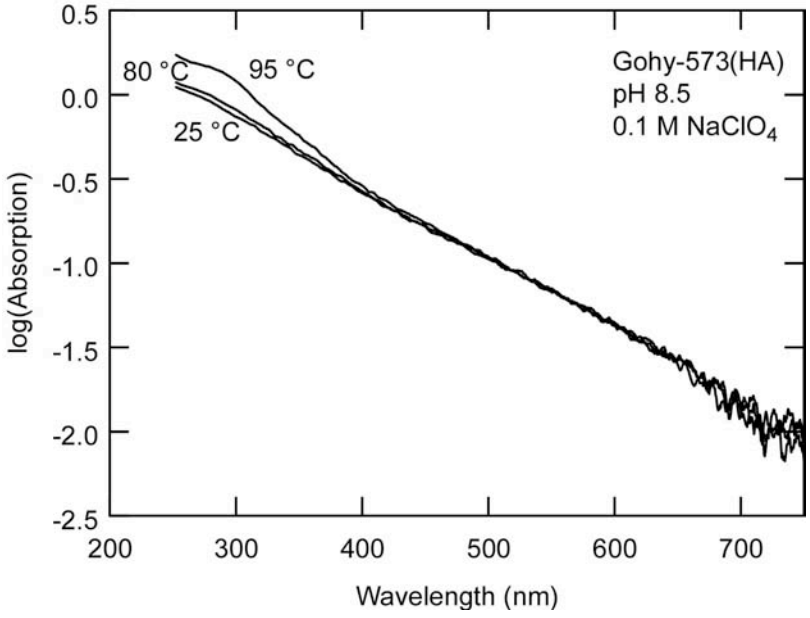

Fig. 3: Logarithm of UV/Vis absorption of Gohy-573(HA) solution after storage at different temperatures for 24 hours (cf. Fig. 2).

In Fig. 4, the impact of storage time at elevated temperature is shown. At 60 °C, basically no change is seen after 24 h (not shown). After one week, however, the spectrum has changed in comparable magnitude with a storage at 80 °C for 24 h. Similarly, the change in the spectrum at 80 °C after one week storage time is comparable to that after 24 h storage time at 95 °C. This shows that rearrangements take place already at 60 °C, however, the kinetics is relatively slow compared to higher temperatures.

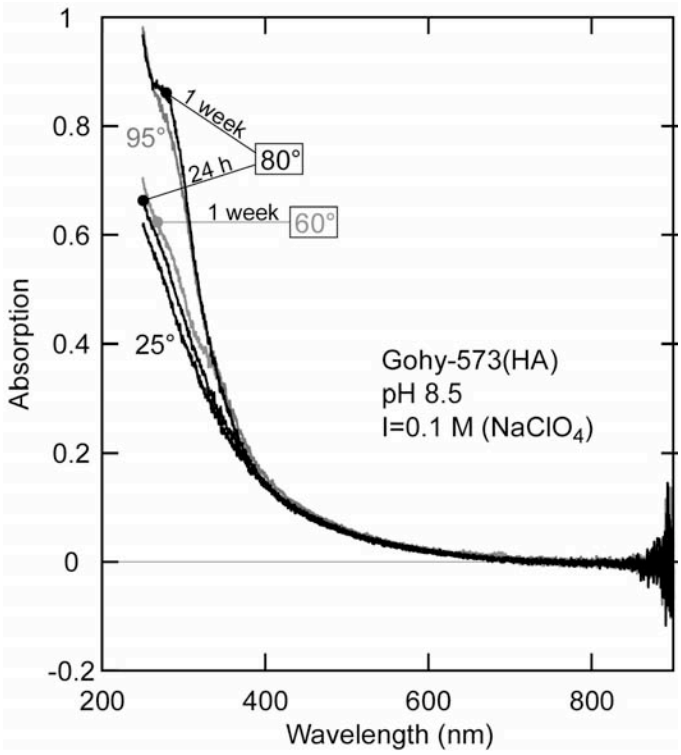

Fig. 4: UV/Vis spectra of Gohy-573(HA) as given in Fig. 1 (24 h storage time). In addition, influence of 1 week storage time at 60 and 80 °C.

The reversibility was investigated by bringing samples down to room temperature (25 °C) after the storage at elevated temperatures. In no case the original spectra were obtained but the spectra remained unchanged (therefore no spectra shown). This includes storage at 25 °C for as long as one week of the sample kept at 80 °C for 24 h.

Summary and conclusions

Above 40 °C, release of water is observed with the dry humic acid sample. To which extent this release with a peak at around 60 °C is associated with structural changes or only release of structurally bound water remains open. A second large water release with the maximum around 100 °C appears to be associated with combustion of backbone hydrogen and oxygen followed by decomposition above 100 °C under the release of carbon dioxide and finally carbon monoxide above around 140 °C. The UV/Vis spectroscopic study shows that rearrangement of dissolved humic acid takes place already at 60 °C. With increasing temperature the expected increase in conversion velocity is found. The changes are “irreversible” within the time scales investigated, i.e. up to one week of subsequent storage at room temperature.

The results are of preliminary nature. With respect to investigations of the temperature dependency of metal ion humate complexation, it shows the need to be aware of possible changes in the humic acid structure already at 60 °C. From a more generic point of view further studies are required, including the response to changes in pH (especially high pH) and follow up of decomposition of solid samples by IR spectroscopy. The use of fluorescence spectroscopy as a very sensitive indicator to structural changes is also considered.

References

Artinger R., Buckau G., Geyer S., Wolf M., Kim J.I., Fritz P. "Characterization of Groundwater Humic Substances: Influence of Sedimentary Organic Carbon", *Applied Geochemistry*, **15/1**, 2000, 97-116.

Buckau G., Artinger R., Fritz P., Geyer S., Kim J.I., Wolf M. (2000a) "Origin and Mobility of Humic Colloids in the Gorleben Aquifer System", *Applied Geochemistry*, **15/2**, 171-9.

Buckau G., Artinger R., Geyer S., Wolf M., Kim J.I., Fritz P. (2000b) "Groundwater in-situ Generation of Aquatic Humic and Fulvic Acids and the Mineralization of Sedimentary Organic Carbon", *Applied Geochemistry*, 15/6, 819-32.

Buckau G. (2004) "Approach for Physico-Chemical Interpretation of An(III) and An(VI) Humate Complexation.", Annex 3, same report.

Costa, C.N., Anastasiadou, T., and Efstathiou, A.M., *J. Catal.* **194**, 250 (2000).

Kim J.I., Buckau G., Li G.H., Duschner H., Psarros N. (1990) "Characterization of Humic and Fulvic Acids from Gorleben Groundwater", Fresenius J. Anal. Chem., **338**, 245.

Annex 23

Complexation properties of Humic and Fulvic Acids extracted from Callovo-Oxfordian and Opalinus Clay

Francis Claret, Thorsten Schäfer, Thomas Rabung, Andreas Bauer, Manfred Wolf* and Gunnar Buckau

Forschungszentrum Karlsruhe, Institut für Nukleare Entsorgung, D-76021 Karlsruhe, Germany

***GSF-National Research Center for Environment and Health, Institute of Groundwater Ecology, D-85764 Neuherberg, Germany**

Complexation properties of Humic and Fulvic Acids extracted from Callovo-Oxfordian and Opalinus Clay

Francis Claret, Thorsten Schäfer, Thomas Rabung, Andreas Bauer, Manfred Wolf* and Gunnar Buckau

Forschungszentrum Karlsruhe, Institut für Nukleare Entsorgung, D-76021 Karlsruhe, Germany
*GSF-National Research Center for Environment and Health, Institute of Groundwater Ecology, D-85764 Neuherberg, Germany

Abstract

Clay is foreseen both as back-fill material and host rock for nuclear waste disposal. It contains organic matter that can be released and form dissolved organic matter (DOC). Part of this DOC consists of humic and fulvic acids. Humic substances in natural water are present in the form of humic colloids, consisting of the organic entities, associated mineral structures and complexed metal ions. These humic colloids can play a major role in the radionuclide migration in natural aquifer systems (Choppin 1992). Cement may be present in a nuclear waste repository as a waste form or as part of engineered structures. In case of water intrusion, cement dissolution will, amongst others, lead to high pH values (initial pH>13). On a short time scale, a minor fraction (few percent) of the clay organic matter is dissolved. With prolonged contact time with alkaline solution, the hydrophobic clay organic matter becomes chemically converted and a large portion (up to around 50 % after about 1.5 years) is forming hydrophilic humic and fulvic acids (Claret *et al*, 2003). In this paper, humic and fulvic acids initially released from Callovo-Oxfordian and Opalinus Clay under near-field high pH conditions are quantified and characterized. Furthermore, their complexation with Cm^{3+} is investigated. The humic and fulvic acids are characterized by Asymmetrical Flow Field-Flow Fractionation (AFFFF) and Near Edge X-ray Absorption Fine Structure (NEXAFS) spectroscopy. The complexation with the Cm^{3+} ion is studied by Time Resolved Laser Fluorescence Spectroscopy (TRFLS).

Methods and results

Clay samples origin and extraction of humic and fulvic acids

Callovo-Oxfordian clay samples from three different depths from the boreholes EST 104 samples (447, 494, 516 m below surface) and one Opalinus shale sample (579.19-579.45 m) are studied. The origin of the clay organic matter, identified by biomarkers, in the Oxfordian series (447 m depth) is mainly of terrestrial origin, whereas organic carbon in the Callovian (494-516 m) series is mainly of marine origin (Landais *et al,* 1999). The organic matter present in the Opalinus clay formation is of a mixed terrestrial marine origin (Mazurek *et al,* 2002).

The total organic carbon (TOC) concentration in the Bure clay is ~1.3 wt% (independent of depth) whereas only < 0.4 wt% is found in the Opalinus clay sample (Taubald *et al,* 2000; Claret *et al,* 2002). Humic and fulvic acids are extracted using slightly modified International Humic Substances Society protocol. The different amounts extracted are given in Table 1. No humic acid was found in the Opalinus clay sample.

Table 1: Total organic carbon (TOC) in clay samples and the fraction of TOC extracted as humic acid (HA) and fulvic acid (FA).

Sample*	TOC (weight %)	HA or FA (% of TOC)	Sample*	TOC (weight %)	HA or FA (% of TOC)
447 HA / FA	1.4	5.2 / 1.3	516 HA / FA	1.4	7.1 / 0.5
494 HA / FA	1.4	5.2 / 1.2	OPA FA	0.4	1.1

*447, 494 and 516: Respective depths of samples from the Bure site. “OPA FA”: fulvic acid extracted from Opalinus clay.

Characterization of humic and fulvic acids

UV/VIS

The UV/Vis spectra of the samples are shown in Fig. 1 (left part). The absorption is normalized to the DOC content. The large differences in this “specific absorption” reflect differences in the humic substances. It also, however, reflects the presence of non-absorbing organic compounds (cf. below). In the right part of Fig. 1, the spectra are scaled and grouped for similar absorption behavior. The figure shows that the humic and fulvic acids form different groups, however, all humic acids show very similar spectral form. The same is true for the different fulvic acids.

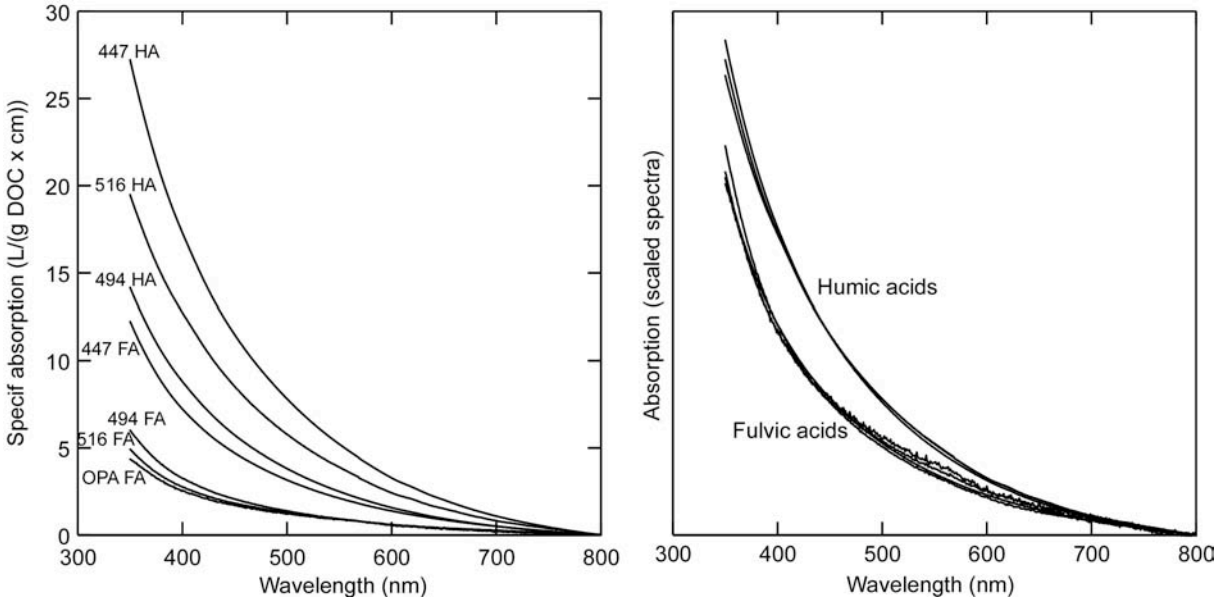

Fig. 1: UV/Vis spectroscopy of humic and fulvic acid samples, normalized to the DOC concentration (left part) and scaled to comparable magnitudes for comparison of spectral features(right part).

The fulvic acids 494 FA, 516 FA and OPA FA, however, show very low specific absorptions. Given that the relative absorption curve shapes are so similar for all fulvic acids of the present study (cf. Fig. 1, lower part), the low specific absorption may indicate the presence of non-absorbing organic constituents. In order to clarify this issue, asymmetrical flow field-flow fractionation was applied.

Asymmetrical Flow Field-Flow Fractionation

Fulvic acids are characterized by the size distribution at pH 9.1 in 0.005 mol/L Tris buffer. The size distribution of the sample 447 m from the Bure site shows the typical features of fulvic acid (Fig. 2). The other Bure samples of marine origin, contrary to the sample from 447 m depth of terrestrial origin, show a bi-modal distribution. The first peak with the smaller particles agrees with fulvic acid in general and also with the fulvic acid from the fulvic acid from 447 m depth (terrestrial origin). The second peak shows larger particles that of atypical size for fulvic acid. The same bi-modal distribution is found for the fulvic acid from the Opalinus clay.

The results support the indications from UV/Vis spectroscopy, namely that, with exception for 447 FA, there are additional components in the fulvic acid samples. These components are obviously of organic nature (lowering the specific UV/Vis absortion) and are larger in size. Aiming at identifying the nature of the samples, they were also characterized by STXM.

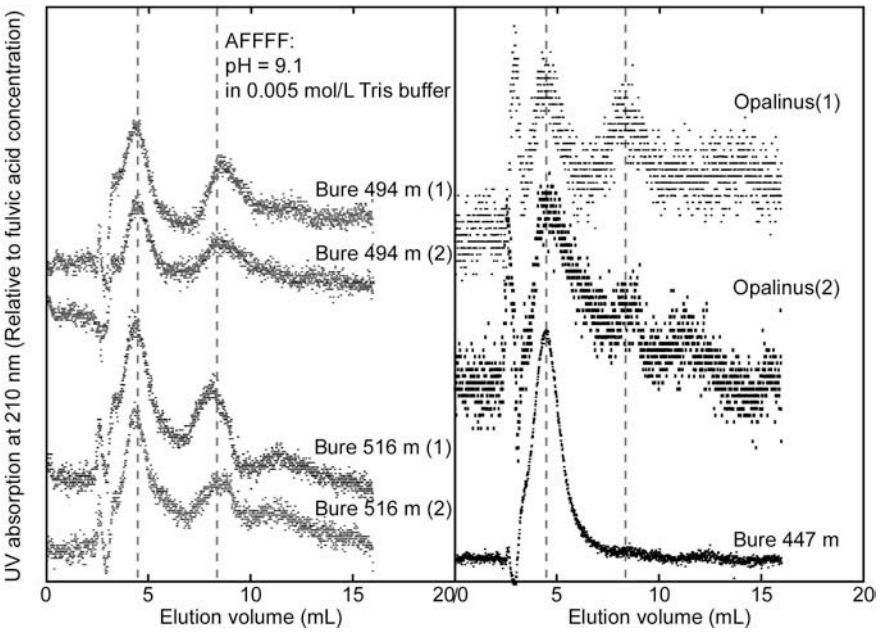

Fig. 2: AFFFF of fulvic acid samples (parallel samples).

NEXAFS

NEXAFS spectra were obtained using Scanning transmission X-ray microscopy (STXM) performed at the beam line X1A (NSLS) operated by the State University of New York at Stony Brook. The principle of the method is described in (Jacobsen *et al,* 1991). For the comparison all NEXAFS spectra were baseline corrected and normalised prior to peak fitting. The spectra were then de-convoluted following the protocol described in (Schafer *et al,* 2003). The resulting distribution of carbon in different functional groups is given in Table 2.

Table 2: Distribution of carbon as different functional groups determined by NEXAFS.

	% carbon in functional structures					
Sample*	Quinone	Aromatic	Phenol	Aliphatic	Carboxyl	Carbonyl
447 HA	9.7	19	15.5	16.3	25.7	13.9
494 HA	5.9	16.8	11.9	17.7	30.8	17.0
516 HA	6.9	19.3	13.5	18.3	26.7	15.4
447 FA	7.8	19.1	13.9	18.1	28.3	13.6
494 FA	7.6	15.4	11.7	17.9	30.3	17.1
516 FA	2.2	7.3	4.4	26.5	38.9	20.7
OPA FA	0	9.7	0	28.9	39	22.4

*447, 494 and 516: Respective depths of samples from the Bure site. “OPA FA”: fulvic acid extracted from Opalinus clay.

In all samples, the largest individual peak is from carboxylic groups. This peak area is also bigger for fulvic acids compared to the humic acids. The composition of humic material is related to the originating material and history (Rice *et al,* 1991). The humic acids show no strong trend with the differences in origin. For the fulvic acids, however, aliphatic, carboxyl

and carbonyl functional group increase with depth, with a corresponding decrease in the other groups. This reflects differences in marine and terrestrial originating organic material (Flaig 1972; Nissenbaum *et al,* 1972). The Opalinus fulvic acid has a comparably low content of oxygen containing functional groups. This reflects the history of this sample, namely higher burial temperature compared to the Bure samples (80°C instead of 40°C (Landais *et al,* 1999; Mazurek *et al,* 2002)) which may lead to deoxygenation processes and possibly also polymerisation.

Complexation behavior

The complexation behavior was studied using Time Resolved Fluorescence Spectroscopy (TRFLS). By this method metal ion speciation can be done with respect to both emission band shape and fluorescence decay behavior. Investigations were conducted at 5.7<pH< 6 to avoid metal ion hydrolysis and thus restrict the number of species involved to the humate/fulvate complex and the non-complexed Cm^{3+} ion. In addition, results can be readily compared to of published data. The Cm concentration in the humic acid samples was 0.2 μmol/L, whereas 0.1 μmol/L was used for fulvic acid samples. The emission spectra show the characteristic shape of humate and fulvate curium complexes with peak maximum around 600 nm, compared to 593.8 nm for the non-complexed Cm^{3+} ion. (Fig. 3) (Czerwinski *et al,* 1996; Kim *et al,* 1996). The Cm(III) fluorescence shows a shift from 593.8 nm of the non-complexed Cm^{3+} ion to about 600 nm for the humic and fulvic acid complexes (Fig. 3). Whereas for humic acid all Cm(III) is complexing, for fulvic acid free Cm(III) aqua ion is still present . Therefore, the relative peak areas of the two species in the different spectra are evaluated by peak deconvolution (Table 3). Quantification of the two respective Cm(III) species is done by estimating the relative fluorescence intensity of the fulvate complex to be a factor of four higher than that of the non-complexed Cm^{3+} ion (Buckau *et al,* 1992) (Table 3). The total fulvate ligand concentration in the individual samples is calculated using a complexation constant of 5.86 L/mol (Buckau *et al,* 1992). Finally, based on a proton exchange capacity of 6 meq/g fulvic acid and a carbon content of 45 %, the loading capacity is calculated (Buckau *et al,* 1992). In the latter calculation it is assumed, that all the dissolved organic carbon is fulvic acid. As can be seen from these numbers, the DOC normalized fulvic acid ligand concentration decreases with increasing depth of the samples and is also very low in the OPA FA sample. The Cm(III) loading capacity expected for fulvic acid at the concerned pH and ionic strength is between about 50 and 63 % (Kim *et al,* 1996). The number found for the 447 FA is exactly in the expected range. Contrary to this, the numbers for the other samples are too low.

The question arising is: What is the nature and role of the organic matter co-extracted with fulvic acid of marine origin, lacking the humic matter typical absorption in the visible range, appearing in the form of larger particles (from AFFFF) and with a different carbon functionality distribution (especially high aliphatic content)? The specific absorptions at 300

and 400 nm and the Cm fulvic acid ligand concentrations, both normalized to the carbon (DOC) concentration of the respective samples, are plotted against each other in Fig. 4.

Table 3: Cm(III) complexation results with fulvic acid samples at pH 5.6 – 6 in 0.2 mol/L $NaClO_4$.

Sample	DOC1) (mg C/L)	Cm3+ (rel. peak area) (%)	CmFA (rel. peak area)	Cm3+ (10-8 mol/L)	CmFA (10-8 mol/L)	FA(tot)2) (10-6 mol/L)	LC3)
447 FA	8.7	0.075	0.925	2.45	7.55	4.54	58.0
494 FA	8.7	0.17	0.83	4.50	5.50	1.83	23.3
516 FA	10.4	0.32	0.68	6.53	3.47	0.805	8.6
OPA FA	6.6	0.45	0.55	7.66	2.34	0.466	7.9

1) DOC: Dissolved Organic Carbon; 2) Calculated with a complexation constant of 5.85 (L/mol);
3) LC: Loading Capacity, calculated for an assumed FA proton exchange capacity of 6 meq/g FA

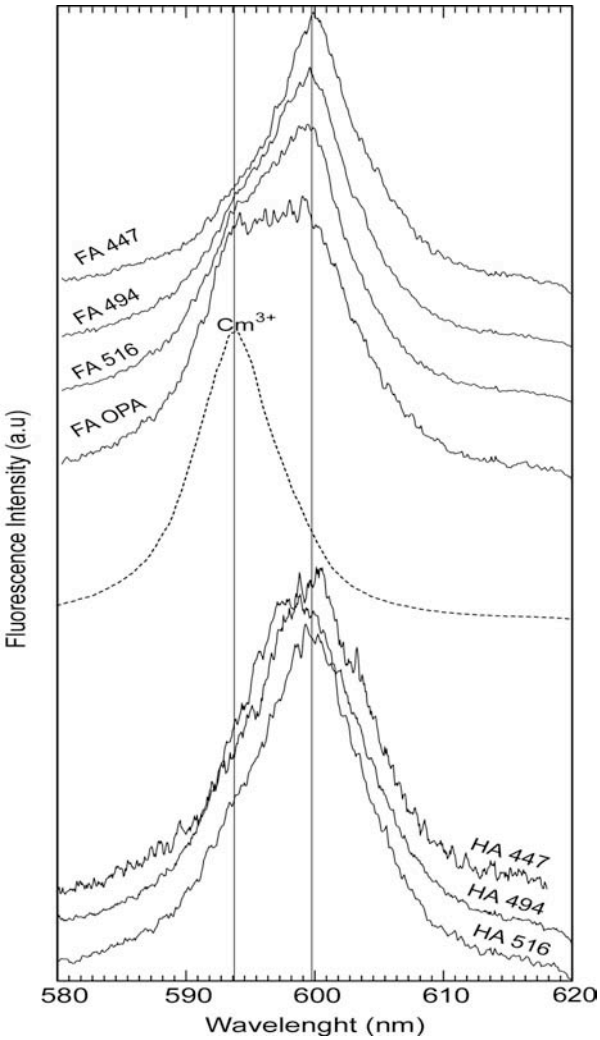

Fig. 3: Fluorescence spectra of Cm(III) with the different humic and fulvic acids. Vertical lines represent the positions of the two components humic/fulvic complex and the non-complexed Cm^{3+} ion (cf. reference spectrum).

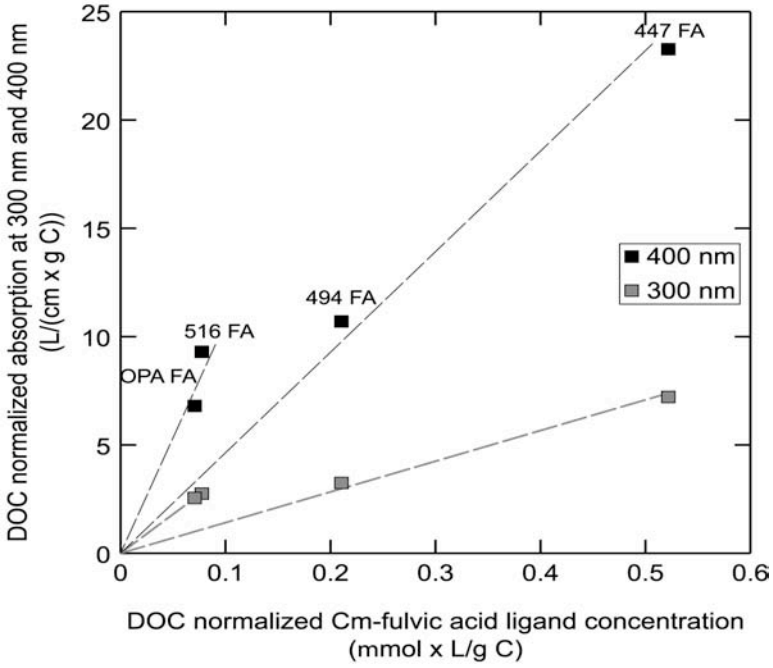

Fig. 4: Specific absorption at 300 and 400 nm of the fulvic acids plotted against the specific Cm-fulvic ligand concentration.

In both cases, the specific absorption at 300 and 400 nm correlate with the total Cm fulvate ligand concentration. The data allow for zero ligand concentration at zero absorption. Two groups of fulvic acids can be observed (447 and 494 FA and 516 and OPA FA). They , however, show distinct differences in the magnitude of the correlation. This shows that the observed complexing function is directly related to the fraction of the organic material that absorb in the visible range. The difference is that the specific absorption of the complexing 516 FA and OPA fulvic acid fraction is higher, or alternatively, the observed complexing function is lower. The latter deserves special attention. For this reason the composition of carbon functionalities of the different fulvic acids is shown in Fig. 5 as a function of the Cm fulvate ligand concentration observed by TRLFS.

As seen in Fig. 5, the structural composition of the two fulvic acids 447 FA and 494 FA is relatively similar, with a trend towards a lower content of chromophoric quinone-type, C=C bonds and phenolic structures. In the 516 FA and OPA FA, the content of these chromophoric constituents is significantly lower. This is especially true for the OPA FA that has also experienced higher burial temperatures. It therefore appears as if the distinctly different correlations between the Cm fulvate concentration as observed by TRLFS in the fulvic acids of terrestrial origin and those of marine influence (516 FA and OPA FA) is related to the more efficient energy transfer from chromophoric groups with the former ones. To which extent the high content of carboxylic groups not adjacent to non-aromatic/chromophoric groups do not contribute to complexation or is simply not observed by TRLFS cannot be

determined from the present data. This would require additional studies, preferentially also by other speciation methods and with larger quantities of fulvic acids.

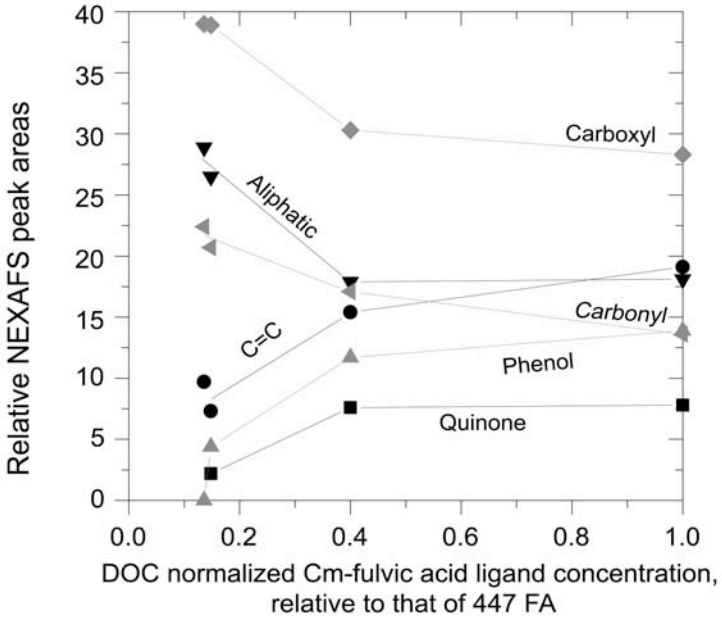

Fig. 5: Relative NEXAFS peak areas for different carbon functionalities plotted against the DOC normalized fulvic acid ligand concentration from Cm(III) complexation study, relative to that of the fulvic acid 447 FA. The guiding lines make use of the average values for the MHM 516 FA of marine origin and the opalinus clay originating fulvic acid OPA FA.

Summary and outlook

Up to about 8 % of clay organic matter that can be rapidly released (standard IHSS protocol conditions) as humic and/or fulvic acid from Callovo-Oxfordian argillite or Opalinus clay under conditions potentially relevant for water intrusion in a clay nuclear waste repository. Characterization shows that especially in the Callovo-Oxfordian original features of the organic matter, reflecting terrestrial and marine origin, are preserved in the humic and fulvic acids. Fulvic acid influenced by marine origin shows a separate size peak, atypical for fulvic acid of terrestrial origin. It also shows a low content of chromophoric carbon functionalities. Cm(III) is complexed by both the humic and fulvic acids. The method used for the complexation studies results in a complexation behavior for the fulvic acids of terrestrial origin as reported in the literature. The fulvic acid derived from marine influenced sediments show a less efficient complexation. This may, however, also be the result of lower energy transfer efficiency with decreasing content of chromophoric groups. In the latter case, the method used would underestimate the complexation behavior and thus underestimate the potential impact on radionuclide migration. The present study is made with total fulvic acid amounts in the µg range. Verification of the exact complexation behavior of the 494, 516 and

OPA FA would require larger amounts of material not presently available and preferentially, application of complementary speciation methods.

Acknowledgements

The results presented in the present paper were collected during a work supported by a Marie Curie fellowship of the European Commission programme "Nuclear Fission" under the contract number FIKW-CT2002-50509. ANDRA and NAGRA are also acknowledged for making respectively the MHM site clay and the Opalinus Clay from Benken samples available. We are grateful for beamtime allotment by BNL/NSLS. Spectromicroscopic data were collected using the X1-A1 STXM developed by the group of Janos Kirz and Chris Jacobsen at SUNY Stony Brook, with support from the Office of Biological and Environmental Research, U.S. DoE under contract DE-FG02-89ER60858, and from the NSF under grant DBI-9605045. The zone plates were developed by Steve Spector and Chris Jacobsen of Stony Brook and Don Tennant of Lucent technologies Bell Labs with support from the NSF under grant ECS-9510499.

References

Buckau, G., Kim, J. I., Klenze, R., Rhee, D. S. and Wimmer, H. (1992) A comparative Spectroscopy Study of the Fulvate Complexation of Trivalent Transuraniums Ions. *Radiochimica Acta*, **57**, 105-111.

Choppin, G. R. (1992) The Role of Natural Organics in Radionuclide Migration in Natural Aquifer Systems. *Radiochimica Acta*, **58-9**, 113-120.

Claret, F., Bauer, A., Schafer, T., Griffault, L. and Lanson, B. (2002) Experimental investigation of the interaction of clays with high-pH solutions: A case study from the Callovo-Oxfordian formation, Meuse-Haute Marne underground laboratory (France). *Clays and Clay Minerals*, **50**, 633-646.

Claret, F., Schafer, T., Bauer, A. and Buckau, G. (2003) Generation of humic and fulvic acid from Callovo- Oxfordian clay under high alkaline conditions. *Science of the Total Environment*, **317**, 189-200.

Czerwinski, K. R., Kim, J. I., Rhee, D. S. and Buckau, G. (1996) Complexation of trivalent actinide ions (Am^{3+}, Cm^{3+}) with humic acid: The effect of ionic strength. *Radiochimica Acta*, **72**, 179-187.

Flaig, W. (1972) Biochemical factors in coal formation. Pp. in: *Advances in Organic Geochemistry* (H. R. Von Gaertner and H. Wehner), Pergamon Press, Oxford

Jacobsen, C., Williams, S., Anderson, E., Browne, M. T., Buckley, C. J., Kern, D., Kirz, J., Rivers, M. and Zhang, X. (1991) Diffraction-limited imaging in a scanning transmission x-ray microscope. *Optics Communications*, **86**, 351--364.

Kim, J. I. and Czerwinski, K. R. (1996) Complexation of metal ions with humic acid: Metal ion charge neutralization model. *Radiochimica Acta*, **73**, 5-10.

Landais, P. and Elie, M. (1999) Utilisation de la géochimie organique pour la détermination du paléoenvironnement et de la paléothermicité dans le Callovo-Oxfordien du site de l´Est de la france. Etude de l´Est du bassin de Paris, Edition EDP Sciences, 35-61.

Mazurek, M., Elie, M., Hurford, A., Leu, W. and Gautschi, A. (2002) Burial History of Opanilus Clay. Proceeding of the international Conference *Clays in natural and engineered barriers for radioactive waste confinement.*, *Reims*, pp. 101-102.

Nissenbaum, A. and Kaplan, I. R. (1972) Chemical and isotopic evidence for the in situ origin of marine humic substances. *Limnol. Oceanogr.*, **17**, 570-582.

Rice, J. A. and Maccarthy, P. (1991) Statistical Evaluation of the Elemental Composition of Humic Substances. *Organic Geochemistry*, **17**, 635-648.

Schafer, T., Hertkorn, N., Artinger, R., Claret, F. and Bauer, A. (2003) Functional group analysis of natural organic colloids and clay association kinetics using C(1s) spectromicroscopy. *Journal de Physique IV*, **104**, 409-412.

Taubald, H., Bauer, A., Schafer, T., Geckeis, H., Satir, M. and Kim, J. I. (2000) Experimental investigation of the effect of high-pH solutions on the Opalinus Shale and the Hammerschmiede Smectite. *Clay Minerals*, **35**, 515-524.